



Petrology of Early Proterozoic Granitoids in the Halls Creek Mobile Zone, Northern Australia

By

Masatsugu Ogasawara

B.Eng. in Mining Geology (Akita University),
M.Eng. in Mining Geology (Akita University)

A thesis submitted in partial fulfilment of the
requirements for the degree of
Doctor of Philosophy

University of Adelaide
Adelaide

1996

TABLE OF CONTENTS

TABLE OF CONTENTS	i
LIST OF TABLES	ix
LIST OF FIGURES.....	xiii
SUMMARY	xxi
STATEMENT OF ORIGINALITY.....	xxv
ACKNOWLEDGEMENTS	xxvi
CHAPTER 1. INTRODUCTION	1
1.1. Aim of Thesis.....	1
1.2. Field Work and Method of Study.....	1
1.3. Previous Investigation	3
1.4. Regional Geological Setting	6
1.5. Definition of Terms	10
1.5.1. Classification and Nomenclature of Granitoids	10
1.5.2. Nomenclature of Granitoid Bodies.....	10
1.5.3. Enclaves in Granitoids.....	11
CHAPTER 2. GEOLOGY AND STRUCTURE	12
2.1. Introduction	12
2.2. Geology of Sally Downs Bore Area.....	16
2.2.1. General.....	16
2.2.2. Tickalara Metamorphics	16
2.2.2.1. Pelitic and psammo-pelitic schists and gneisses	17
2.2.2.2. Carbonate rocks with associated calc-silicate rocks.....	17
2.2.2.3. Amphibolites	18
2.2.3. Fine Grained Tonalitic Rocks	19
2.2.4. Meta-gabbro.....	19

2.2.5. Eastern Leucocratic Granitoids Suite.....	20
2.2.6. Dougalls Granitoid Suite.....	21
2.2.7. Ord River Tonalite Suite.....	22
2.2.8. Western Porphyritic Granite	23
2.2.9. Meta-dolerite.....	24
2.2.10. Central Leucocratic Granite	25
2.2.11. Hornblendite and Mela-gabbro.....	25
2.2.12. Sally Downs Tonalite.....	26
2.2.12.1. General	26
2.2.12.2. Xenoliths of country rock in the Sally Downs Tonalite	28
2.2.12.3. Mafic microgranular enclaves in the Sally Downs Tonalite.....	30
2.2.12.4. Syn-plutonic basic dyke in the Sally Downs Tonalite	31
2.2.13. Granite Dyke in the Sally Downs Tonalite.....	33
2.3. Structural Relationships in the Sally Downs Bore Area.....	33
2.3.1. Introduction	33
2.3.2. Review and Discussion of the Interpretation of the Structures in the Granitoids.....	34
2.3.3. Structural Map and Structural Subarea of the Sally Downs	39
2.3.4. Eastern Part of the Sally Downs Bore Area	40
2.3.5. Central Part of the Sally Downs Bore Area.....	41
2.3.6. Western Part of the Sally Downs Bore Area	42
2.3.7. Sally Downs Tonalite.....	43
2.3.8. Faulting	45
2.3.9. Summary	46
2.4. Geology and Structure of Sophie Downs Granitoid.....	47
2.4.1. General.....	47
2.4.2. Sophie Downs Granitoid	49
2.5. Geology of Supplementary Sampling Localities in the Halls.....	50

2.5.1. Turkey Creek Area.....	50
2.5.2. Mabel Hill Tonalite	53
2.5.3. Springvale area.....	54
2.5.4. Whitewater Volcanics.....	55
2.6. Lamboo Complex in the King Leopold Mobile Zone	56
2.7. Regional Structure and Gravity Data.....	59
2.7.1. Regional Structure	59
2.7.2. Gravity Anomalies and Their Implications.....	60

CHAPTER 3. PETROLOGY (PART 1): PETROLOGY OF THE
ROCKS FROM THE SALLY DOWNS BORE AREA

EXCLUDING THE SALLY DOWNS TONALITE.....	63
3.1. Introduction	63
3.2. Tickalara Metamorphics and Fine Grained Tonalitic Rocks	63
3.2.1. Pelitic and Psammo-pelitic Schists and Gneisses.....	63
3.2.2. Amphibolite	67
3.2.3. Fine Grained Tonalitic Rocks	71
3.3. Meta-gabbro.....	72
3.3.1. Petrography	72
3.3.2. Geochemistry	73
3.4. Eastern Leucocratic Granitoid Suite.....	74
3.4.1. Petrography	74
3.4.2. Mineral Chemistry	76
3.4.3. Geochemistry	77
3.4.4. Origin of Garnets in the Eastern Leucocratic Granitoid	81
3.5. Dougalls Granitoid Suite.....	84
3.5.1. Petrography	84
3.5.2. Mineral Chemistry	86
3.5.3. Geochemistry	88

3.6. Ord River Tonalite Suite	93
3.6.1. Petrography	94
3.6.2. Mineral Chemistry	95
3.6.3. Geochemistry	96
3.7. Western Porphyritic Granite.....	99
3.7.1. Petrography	99
3.7.2. Mineral Chemistry	100
3.7.3. Geochemistry	101
3.8. Meta-dolerite.....	102
3.8.1. Petrography	102
3.8.2. Mineral Chemistry	103
3.8.3. Geochemistry	104
3.9. Central Leucocratic Granite.....	105
3.9.1. Petrography and Mineral Chemistry	105
3.9.2. Geochemistry	106
3.10. Hornblendite and Mela-gabbro	107
3.10.1. Petrography.....	107
3.10.2. Mineral Chemistry	109
3.10.3. Geochemistry.....	111

**CHAPTER 4. PETROLOGY (PART 2): PETROLOGY OF THE
SALLY DOWNS TONALITE AND THE RELATED**

ROCKS	115
4.1. Introduction	115
4.2. Petrography and Mineral Chemistry of the Sally Downs	116
4.2.1. Petrography	116
4.2.2. Mineral Chemistry	117
4.3. Geochemistry of the Sally Downs Tonalite	119
4.3.1. Major elements	120

4.3.2. Trace elements.....	121
4.4. Areal Chemical Variation in the Sally Downs Tonalite.....	124
4.4.1. Local Chemical Variability	124
4.4.2. Areal Chemical Variation in the Sally Downs Tonalite.....	126
4.5. Discussion on the Petrology of the Sally Downs Tonalite.....	132
4.5.1. Fractionation Crystallization Model of the Sally Downs Tonalite.....	132
4.5.2. Trace Elements in Minerals.....	135
4.6. Petrology of Mafic Microgranular Enclaves and Syn-plutonic Dyke.....	138
4.6.1. Petrography	139
4.6.2. Mineral chemistry.....	139
4.6.3. Geochemistry	140
4.6.4. Origin of Mafic Microgranular Enclaves in the Sally Downs Tonalite.....	142
4.7. Petrology of Tonalites from Mabel Hill and the Main Body of the Mabel Downs Granitoid Suite.....	144
4.7.1. Petrography	144
4.7.2. Geochemistry	145
 CHAPTER 5. PETROLOGY (PART 3): PETROLOGY OF THE SOPHIE DOWNS GRANITOID, BOW RIVER GRANITOID, GRANITOIDS FROM THE KING LEOPOLD MOBILE ZONE, AND WHITEWATER VOLCANICS	
5.1. Introduction	147
5.2. Sophie Downs Granitoid.....	147
5.2.1. Petrography and Mineral Chemistry	147
5.2.2. Geochemistry	149
5.2.3. Areal Chemical Variation in the Sophie Downs Granitoid	152

5.3. Bow River Granitoid and Granitoids from the King Leopold	
Mobile Zone	153
5.3.1. Petrography	154
5.3.2. Geochemistry	156
5.4. Whitewater Volcanics.....	160
5.4.1. Petrography	160
5.4.2. Geochemistry	161

CHAPTER 6. GEOCHRONOLOGY AND ISOTOPE

GEOCHEMISTRY	162
6.1. Introduction	162
6.2. Sally Downs Tonalite	164
6.3. Sophie Downs Granitoid.....	165
6.4. Dougalls Granitoid Suite.....	166
6.5. Ord River Tonalite Suite	167
6.6. Eastern Leucocratic Granitoid.....	168
6.7. Western Porphyritic Granite.....	168
6.8. Tickalara Metamorphics	168
6.9. Hornblendite	169
6.10. Discussion of the Geochronological Results.....	169
6.11. Sr Isotope Geochemistry.....	172
6.12. Nd Isotope Geochemistry.....	174
6.13. Comparison of Geochronological Data of Early Proterozoic	
Rocks in Northern Australia.....	180

CHAPTER 7. GENERAL RESUME AND COMPARISON WITH

OTHER EARLY PROTEROZOIC GRANITOIDS.....	184
7.1. Introduction	184
7.2. Tonalite-trondhjemite.....	186

7.3. A-type granitoid.....	190
7.4. High K ₂ O granitoids and volcanics	191
CHAPTER 8. PETROGENESIS OF GRANITOIDS IN THE	
HALLS CREEK MOBILE ZONE.....	196
8.1. Introduction.....	196
8.2. Constraints on granitoid petrogenesis provided by the present crustal structure of North Australian Province.....	196
8.3. Eastern Leucocratic Granitoid.....	199
8.4. Tonalite and Trondhjemite.....	203
8.5. High K ₂ O Granitoids	212
8.6. The Sophie Downs Granitoid	219
8.7. Summary of Petrogenesis of Granitoids in the Halls Creek Mobile Zone	226
CHAPTER 9. IMPLICATIONS OF THE GRANITOIDS	
PETROGENESIS FOR THE EARLY PROTEROZOIC	
OROGENY IN THE HALLS CREEK MOBILE ZONE	229
9.1. Tectonic models for Proterozoic Orogenies.....	229
9.2. Supercontinents and the Early Proterozoic orogens	235
9.3. Model for the evolution of the Halls Creek Mobile Zone.....	238
CHAPTER 10. CONCLUSIONS	
	246
REFERENCES	251
APPENDIX 1. SAMPLE CATALOGUE.....	290
APPENDIX 2. MODAL COMPOSITION OF GRANITOIDS	291

APPENDIX 3. MAJOR AND TRACE ELEMENT	
ANALYTICAL TECHNIQUES.....	292
A3.1. Pulverising Techniques for Whole Rock Chemical Analysis.....	292
A3.2. Major Element Analytical Techniques	292
A3.3. FeO Determination Technique and Results	293
A3.4. Fluorine Determination Technique and Results.....	293
A3.5. Trace Element Analytical Techniques.....	294
APPENDIX 4. RESULTS OF MAJOR AND TRACE ELEMENT	
ANALYSIS OF GRANITIDS.....	296
APPENDIX 5. EXPERIMENTAL TECHNIQUE AND	
RESULTS OF RARE EARTH ELEMENT ANALYSIS	298
APPENDIX 6. EXPERIMENTAL TECHNIQUE OF SR	
ISOTOPE ANALYSIS.....	300
APPENDIX 7. EXPERIMENTAL TECHNIQUE OF	
ELECTRON MICROPROBE ANALYSIS	302
APPENDIX 8. CHEMICAL COMPOSITION OF MINERALS	304

Plate-1. Geological map of the Sally Downs Bore Area

Plate-2. Structural map of the Sally Downs Bore Area

(Plate-1 and -2 in the back pocket)

LIST OF TABLES	Follows page
Table 2-1. Development of structure in the granitoid.....	36
Table 3-1. Chemical compositions of the Tickalara Metamorphics (1).....	65
Table 3-2. Chemical compositions of the Tickalara Metamorphics (2).....	65
Table 3-3. Representative chemical compositions of minerals from amphibolite	68
Table 3-4. Chemical compositions of amphibolite	69
Table 3-5. Representative chemical compositions of minerals from meta-gabbro.....	73
Table 3-6. Chemical composition of meta-gabbro	73
Table 3-7. Representative chemical compositions of minerals from the Eastern Leucocratic Granitoid	76
Table 3-8. Representative chemical compositions of minerals from the Dougalls Granitoid Suite	87
Table 3-9. Representative chemical compositions of minerals from the Ord River Tonalite Suite	95
Table 3-10. Representative chemical compositions of minerals from meta-dolerite.....	103
Table 3-11. Chemical compositions of meta-dolerite	104
Table 3-12. Representative chemical compositions of minerals from hornblendite and mela-gabblo	109
Table 3-13. Two pyroxene geothermometry for hornblendite.....	110
Table 3-14. Chemical compositions of mela-gabbro and hornblendite	111
Table 3-15. Petrogenetic models of mela-gabbro and hornblendite by least squares mixing of major elements	112
Table 4-1. Modal compositions of the Sally Downs Tonalite	116

Table 4-2. Chemical mode of sample 51706 from the Sally Downs Tonalite.....	116
Table 4-3. Representative chemical compositions of hornblende and biotite from the Sally Downs Tonalite, Mafic microgranular enclaves, and Syn-plutonic basic dyke.....	117
Table 4-4. Chemical compositions of allanite, epidote, and sphene from the Sally Downs Tonalite	119
Table 4-5. Average chemical composition of the Sally Downs Tonalite	120
Table 4-6. Local chemical variability within the Sally Downs Tonalite	125
Table 4-7. Fractional crystallization models of the Sally Downs Tonalite by least squares mixing of major elements	132
Table 4-8. Summary of distribution coefficient of rare earth element, used in the model calculation.....	135
Table 4-9. Chemical compositions of mafic microgranular enclaves and syn-plutonic basic dyke in the Sally Downs Tonalite	141
Table 5-1. Representative chemical compositions of biotite from sample 30706 of the Sophie Downs Granitoid	148
Table 5-2. Average chemical composition of the Sophie Downs Granitoid	149
Table 5-3. Chemical composition of Whitewater Volcanics.....	161
Table 6-1. Rb-Sr isotopic results.....	164
Table 6-2. Regression of Rb-Sr data.....	164
Table 6-3. Sm-Nd and Rb-Sr isotopic parameters	174
Table 7-1. Summary of petrological and geochemical characteristics of granitoids in the Halls Creek Mobile Zone.....	184

Table 7-2. Summary of geochemical data for A-type granites and related volcanics	190
Table 7-3. Chemical characteristics of high K granites and volcanics from selected examples.....	192
Table A1-1. Sample catalogue.....	290
Table A2-1. Modal compositions of granitoids	291
Table A3-1. Instrumental settings of X-ray fluorescence spectrometer for major element analysis.....	295
Table A3-2. Major elements analyses of standard samples by x- ray fluorescence spectrometry.....	295
Table A3-3. Results of FeO determination	295
Table A3-4. Results of Fluorine determination.....	295
Table A3-5. Instrumental settings of X-ray fluorescence spectrometer for trace element analysis	295
Table A3-6. X-ray fluorescence analysis of Rb and Sr on sample 51706, for the examination of precision of the analysis	295
Table A3-7. Trace elements analysis of standard samples by x-ray fluorescence spectrometry.....	295
Table A4-1. Chemical compositions of Fine Grained Tonalitic Rocks.....	297
Table A4-2. Chemical compositions of the Eastern Leucocratic Granitoid	297
Table A4-3. Chemical compositions of the Dougalls Granitoid Suite	297
Table A4-4. Chemical compositions of the Ord River Tonalite Suite	297
Table A4-5. Chemical compositions of the Western Porphyritic Granite and the Central Leucocratic Granite	297

Table A4-6(A). Chemical compositions of the Sally Downs Tonalite (grid samples).....	297
Table A4-6(B). Chemical compositions of the Sally Downs Tonalite (samples for chemical variability examination and geochronology).....	297
Table A4-6(C). Chemical compositions of the Sally Downs Tonalite (samples for initial examination).....	297
Table A4-7. Chemical compositions of the Mabel Hill Tonalite and a tonalite from the main body of the Mabel Downs Granitoid Suite	297
Table A4-8. Chemical compositions of the Sophie Downs Granitoid	297
Table A4-9. Chemical compositions of the Bow River Granitoid.....	297
Table A4-10. Chemical compositions of granitoids from the King Leopold Mobile Zone	297
Table A4-11. Chemical compositions of miscellaneous granitoids from the Sally Downs Bore area.....	297
Table A5-1. Rare earth element analysis of USGS standard sample SCo-1.....	299
Table A5-2. Results of rare earth element analysis by isotope dilution mass spectrometry.....	299
Table A7-1. Instrumental conditions of electron microprobe anaalysis.....	303
Table A7-2. Instrumental conditions of electron microprobe for rare earth element analysis.....	303
Table A7-3. Electron microprobe analysis of rare earth element on Durango Apatite Standard	303
Table A8-1. Results of electron microprobe analysis (Microfiches in the back pocket)	

LIST OF FIGURES	Follows page
Fig. 1-1. Outline of tectonic units of the Kimberley region.....	1
Fig. 1-2. Locality map of East Kimberleys.....	1
Fig. 1-3. Archaean-Middle Proterozoic regional tectonic provinces of Australia.....	7
Fig. 2-1. Diagrammatic relation of rock units in the Halls Creek Mobile Zone.....	12
Fig. 2-2. Simplified geological map of the Halls Creek Mobile Zone.....	13
Fig. 2-3. Geology of the Sally Downs Bore area.....	16
Fig. 2-4. Distribution of carbonate rock units in the Sally Downs Bore area.....	17
Fig. 2-5. Field geological photographs.....	20
Fig. 2-6. Field geological photographs.....	22
Fig. 2-7. Geology around the hornblendite in the central part of the Sally Downs Bore area.....	25
Fig. 2-8. Field geological photographs.....	26
Fig. 2-9. Field geological photographs.....	29
Fig. 2-10. Field geological photographs.....	30
Fig. 2-11. Field geological photographs.....	31
Fig. 2-12. Field geological photographs.....	31
Fig. 2-13. Stereo plots of structural data for the Sally Downs Bore area.....	39
Fig. 2-14. Field geological photographs.....	41
Fig. 2-15. Degree of preferred orientation in the Sally Downs Tonalite.....	44
Fig. 2-16. Diagrammatic time relationships of tectonic and igneous events in the Sally Downs Bore area.....	47
Fig. 2-17. Geology of the Sophie Downs Granitoid.....	47

Fig. 2-18. Field geological photographs.....	48
Fig. 2-19. Field geological photographs.....	50
Fig. 2-20. Geology of the Turkey Creek area and sample localities.....	51
Fig. 2-21. Geology of the Mabel Hill and Springvale sample localities.....	53
Fig. 2-22. Detailed geology of the Springvale area and sample localities.....	54
Fig. 2-23. Field geological photographs.....	54
Fig. 2-24. Time relationships of crystallization of igneous rocks in the King Leopold Mobile Zone	56
Fig. 2-25. Geology of central part of the King Leopold Mobile Zone.....	58
Fig. 2-26. Landsat image of the Halls Creek Mobile Zone.....	59
Fig. 2-27. Gravity map of the Halls Creek Mobile Zone	60
Fig. 3-1. Photomicrographs of Tickalara Metamorphics, fine grained tonalitic rocks, and meta-gabbro	64
Fig. 3-2. Sample locality map for samples of the Tickalara Metamorphics, Fine grained tonalitic rocks, Western Porphyritic Granite, and Central Leucocratic Granite in the Sally Downs Bore area.....	65
Fig. 3-3. Na ₂ O-CaO-K ₂ O diagram of Tickalara Metamorphics.....	66
Fig. 3-4. An-Ab-Or plot of plagioclase from amphibolite.....	68
Fig. 3-5. Sample locality map for mafic rocks in the Sally Downs Bore area	69
Fig. 3-6. FeO*/MgO-SiO ₂ and FeO*/MgO-FeO plots of amphibolite.....	69
Fig. 3-7. Modal Quartz-Alkali feldspar-Plagioclase diagram for granitoids	71

Fig. 3-8. Photomicrographs of the Eastern Leucocratic Granitoid and Dougalls Granitoid.....	74
Fig. 3-9. Biotite and garnet composition plot from the Eastern Leucocratic Granitoid.....	76
Fig. 3-10. Sample locality map for the Eastern Leucocratic Granitoid.....	77
Fig. 3-11. Major element variation diagram of the Eastern Leucocratic Granitoid.....	77
Fig. 3-12. Na ₂ O-K ₂ O and Na ₂ O-K ₂ O-CaO plot of the Eastern Leucocratic Granitoid.....	78
Fig. 3-13. Trace element variation diagram of the Eastern Leucocratic Granitoid.....	78
Fig. 3-14. Chondrite normalized REE plot of Eastern Leucocratic Granitoid.....	80
Fig. 3-15. Distribution coefficients of rare earth elements for typical minerals.....	80
Fig. 3-16. Plagioclase and pyroxene plots of the Dougalls Granitoid Suite.....	86
Fig. 3-17. Sample locality map for the Dougalls Granitoid Suite	88
Fig. 3-18. Major element variation diagram of Dougalls Granitoid Suite.....	89
Fig. 3-19. Na ₂ O-K ₂ O and normative Qz-Ab-Or plots of the Dougalls Granitoid Suite	90
Fig. 3-20. Trace element variation diagram of the Dougalls Granitoid Suite.....	91
Fig. 3-21. Rb-K ₂ O and chondrite normalized Y-Ce/Y plots of the Dougalls Granitoid Suite	91
Fig. 3-22. Chondrite normalized REE plot and tonalite (21902) normalized REE plot of Dougalls Granitoid Suite samples.....	92

Fig. 3-23. Photomicrographs of the Ord River Tonalite Suite, Western Porphyritic Granite, and Central Leucocratic Granite.....	93
Fig. 3-24. Sample locality map for the Ord River Tonalite Suite	96
Fig. 3-25. Major element variation diagram of Ord River Tonalite Suite.....	96
Fig. 3-26. Trace element variation diagram of Ord River Tonalite Suite.....	97
Fig. 3-27. Chondrite normalized REE plot of Ord River Tonalite Suite	98
Fig. 3-28. Biotite and Feldspar plot of Western Porphyritic Granite.....	100
Fig. 3-29. Major element variation diagram of Western Porphyritic Granite and Central Leucocratic Granite	101
Fig. 3-30. Normative Qz-Ab-Or plot of Western Porphyritic Granite and Central Leucocratic Granite.....	101
Fig. 3-31. Chondrite normalized REE plot of Western Porphyritic Granite and Central Leucocratic Granite	101
Fig. 3-32. Photomicrographs of meta-dolerite and hornblendite.....	102
Fig. 3-33. Composition of pyroxenes from meta-dolerites	103
Fig. 3-34. FeO*/MgO-SiO ₂ , FeO*/MgO-FeO plots and AFM diagram of meta-dolerite.....	104
Fig. 3-35. Chondrite normalized REE plot of meta-dolerite.....	105
Fig. 3-36. Chondrite normalized REE plot of hornblendites	113
Fig. 4-1. Sample locality map of Sally Downs Tonalite.....	115
Fig. 4-2. Photomicrographs of the Sally Downs Tonalite, mafic microgranular enclaves, and syn-plutonic basic dyke.....	116

Fig. 4-3. Compositions of hornblende, biotite, and plagioclase from the Sally Downs Tonalite and from mafic microgranular enclaves.....	117
Fig. 4-4. Photomicrographs of allanite, epidote, and sphene in the Sally Downs Tonalite.....	118
Fig. 4-5. Chondrite normalized REE pattern of accessory minerals from the Sally Downs Tonalite.....	119
Fig. 4-6. Histogram of SiO ₂ contents and mol Al ₂ O ₃ /CaO+Na ₂ O +K ₂ O of samples from the Sally Downs Tonalite.....	120
Fig. 4-7. Major element variation diagram of Sally Downs Tonalite.....	120
Fig. 4-8. Na ₂ O-K ₂ O and Na ₂ O-K ₂ O-CaO plots of the Sally Downs Tonalite.....	121
Fig. 4-9. AFM diagram and normative Qz-Ab-Or plot of the Sally Downs Tonalite.....	121
Fig. 4-10. Trace element variation diagram of Sally Downs Tonalite (A).....	121
Fig. 4-11. Trace element variation diagram of Sally Downs Tonalite (B).....	121
Fig. 4-12. Chondrite normalized REE pattern of the Sally Downs Tonalite.....	124
Fig. 4-13. Areal geochemical variation within the Sally Downs Tonalite.....	126
Fig. 4-14. Model of intrusive mechanism.....	132
Fig. 4-15. Estimated amounts of fractionated phase of the Sally Downs Tonalite.....	135
Fig. 4-16. Rock budget of REE in sample, 51706, from the Sally Downs Tonalite.....	136
Fig. 4-17. Estimated REE composition of minerals.....	136

Fig. 4-18. REE patterns, normalized to tonalite (50801).....	137
Fig. 4-19. REE Kd values of hornblende	138
Fig. 4-20. Sample locality map for mafic microgranular enclaves, syn-plutonic basic dyke, and granite dyke in the Sally Downs Tonalite pluton.....	139
Fig. 4-21. Major element variation diagram of Mabel Hill Tonalite, a sample from the main body of the Mable Downs Granitoid, and mafic microgranular enclaves in the Sally Downs Tonalite.....	141
Fig. 5-1. Sample locality map of the Sophie Downs Granitoid.....	147
Fig. 5-2. Photomicrographs of the Sophie Downs Granitoid	148
Fig. 5-3. Compositions of feldspar and biotite from the Sophie Downs Granitoid.....	149
Fig. 5-4. Major element variation diagram of the Sophie Downs Granitoid.....	149
Fig. 5-5. Mol. $\text{Na}_2\text{O}+\text{K}_2\text{O}/\text{Al}_2\text{O}_3$ - Mol. $\text{Al}_2\text{O}_3/\text{CaO}+\text{Na}_2\text{O}+\text{K}_2\text{O}$ plot and $\text{Na}_2\text{O}-\text{K}_2\text{O}$ plot of the Sophie Downs Granitoid	149
Fig. 5-6. Mol $\text{Na}_2\text{O}+\text{K}_2\text{O}/\text{Al}_2\text{O}_3$ - SiO_2 plot and normative Q- Ab-Or diagram of the Sophie Downs Granitoid.....	150
Fig. 5-7. Trace element variation diagram of the Sophie Downs Granitoid.....	151
Fig. 5-8. Chondrite normalized REE patterns of the Sophie Downs Granitoid.....	151
Fig. 5-9. Ga- Al_2O_3 and $(\text{Zr}+\text{Nb}+\text{Ce}+\text{Y}) - (10000*\text{Ga}/\text{Al})$ plots of the Sophie Downs Granitoid	151
Fig. 5-10. Areal geochemical variation in the Sophie Downs Granitoid.....	152

Fig. 5-11. Photomicrographs of the Bow River Granitoid, granitoids from the King Leopold Mobile Zone, and Whitewater Volcanics	154
Fig. 5-12. Major element variation diagram of Bow River Granitoid, granitoids from the King Leopold Mobile Zone, and Whitewater Volcanics	157
Fig. 5-13. Trace element variation diagram of Bow River Granitoid, granitoids from the King Leopold Mobile Zone, and Whitewater Volcanics	157
Fig. 5-14. Chondrite normalized REE pattern of Bow River Granitoid and Whitewater Volcanics	158
Fig. 6-1. Rb-Sr isochron for the Sally Downs Tonalite.....	164
Fig. 6-2. Rb-Sr isochron for the Sophie Downs Granitoid	166
Fig. 6-3. Rb-Sr isochron for the Dougalls Granitoid	167
Fig. 6-4. Rb-Sr isochron for the Ord River Tonalite.....	167
Fig. 6-5. Rb-Sr isochron for the Tickalara Metamorphics.....	169
Fig. 6-6. ϵNd - ϵSr diagram	174
Fig. 6-7. $^{147}\text{Sm}/^{144}\text{Nd}$ versus age of source material.....	177
Fig. 7-1. SiO_2 - K_2O plot of granitoids from the Halls Creek Mobile Zone	184
Fig. 7-2. Primordial mantle normalized plot of granitoids from the Halls Creek Mobile Zone	185
Fig. 7-3. Y-Sr/Y plot of granitoids from the Halls Creek Mobile Zone	186
Fig. 8-1. P-wave velocity models of North Australian Craton and southeastern Australia.....	196
Fig. 8-2. Fractional crystallization models for the Eastern Leucocratic Granitoid.....	200

Fig. 8-3. Composite P-T diagram for water-saturated andesitic composition, showing crystallization paths of tonalites.	203
Fig. 8-4. Petrogenetic examination of tonalitic rocks on composite P-T diagrams for tholeiitic composition with 5 % of added water and for dehydration melting of amphibolite.	206
Fig. 8-5. Cooling paths of the high K ₂ O granitoid (type I) magmas.....	214
Fig. 8-6. Composite P-T diagrams for tholeiite composition showing possible source condition of high K ₂ O granitoid (type I) magmas.	215
Fig. 8-7. Petrogenetic model for high K ₂ O granite (type II).....	218
Fig. 8-8. P-T conditions for the formation of the A-type Sophie Downs Granitoid magma by fractionation from a basaltic magma.....	226
Fig. 8-9. P-T of source regions of the Early Proterozoic granitoid magmas of the Halls Creek Mobile Zone.....	226
Fig. 9-1. Simplified model of supercontinental cycle.....	232
Fig. 9-2. Proterozoic and Phanerozoic supercontinents and orogenies.....	235
Fig. 9-3. Configuration of early Late Proterozoic supercontinent Rodinia and location of Early Proterozoic orogens.	235
Fig. 9-4. Schematic illustration of evolution of Halls Creek Mobile Zone.....	238

Errata

p. 13, second to last line of 1st paragraph: should be "predominant" instead of "prediminant".

Fig. 2-1 (also Figs. 2-3, 3-2, 3-5, 3-10, 3-17, 3-24, 4-20) "Tikalara" should be "Tickalara".

Fig. 2-5 caption, A and B: should be "coloured" instead of "colored".

Fig. 2-9 caption, A: should be "hammer in 'centre right' " instead of 'centre left'.

p. 34, paragraph 3, line 9: should be "the" instead of "th".

p. 48, paragraph 3, line 7: should be "granitoid" instead of "gnanitoid".

Fig. 2-19 caption, B: should be "The large prominent ridge traversing the Sophie Downs Granitoid.....depicted in Fig. 2-17".

Fig. 2-20 caption: should be "Geology.....localities (modified.....Plumb (1968))."

Fig. 2-21 caption: should be "Geology.....localities, modified.....roads."

Fig. 2-25 caption: should be "Geology.....Mobile Zone, modified from Gellatly et al. (1974).
.....in the map."

p. 70, second to last line of second to last paragraph: "(Beccalura et al., 1973)" should be "(Beccaluva et al., 1979)".

The complete reference (omitted from list of references in thesis) is "Beccaluva, L., Ohnenstetter, D., and Ohnenstetter, M., 1979. Geochemical discrimination between ocean-floor and island-arc tholeiites- application to some ophiolites. Can. Jour. Earth Sci., 16, 1874-1882."

Fig. 3-7 caption: "ME: Mafic maicrogranular....." should be "ME: Mafic microgranular....."

p. 106, last line: "Porpyritic" should be "Porphyritic".

p. 121, omit first sentence.

Fig. 4-9B: add "Solid arrow: gabbro-trondhjemite trend, dashed arrow: common calc-alkaline trend, after Barker and Arth (1976)".

P. 122, line 1: "780ppm " should be " 928ppm".

Fig. 4-21, caption, 2nd line: "Mable" should be "Mabel"

P. 150, 2nd line, and References: "Loiseller" should be "Loiselle"

p. 150, paragraph 3, line 3: "metaaluminous" should be "metaluminous"

Fig. 5-10 (2) H. Zr: " ≥ 200 ppm" should be " < 200 ppm" and " > 200 ppm" should be " ≥ 200 ppm".

p. 157, lines 1 and 2: $\text{Al}_2\text{O}_3/\text{CaO}+\text{Na}_2\text{O}+\text{K}_2\text{O}$ ratio for S-types is > 1.1 , according to Chappell and White (1992).

THESIS SUMMARY

The Halls Creek Mobile Zone in the Kimberley region, Western Australia, contains various types of Early Proterozoic granitoids. The petrogenesis of the granitoids is examined to provide constraints on the nature and style of the Early Proterozoic orogeny in the area.

Integrated field, petrographic, geochemical, and Sr isotopic studies of the granitoids have been performed in four areas in the Halls Creek Mobile Zone. The areas have been primarily selected to study the Mabel Downs Granitoid (Sally Downs Bore area and Turkey Creek area in the central part of the mobile zone), the Bow River Granitoid (Springvale area in the western part of the mobile zone), and the Sophie Downs Granite (Sophie Downs area in the southeastern part of the mobile zone). As it has become clear that the Sally Downs Bore area contains varieties of granitoid in addition to the Mabel Downs Granitoid, detailed study has been conducted in the Sally Downs Bore area to establish a frame work of the granitoid activity in the Halls Creek Mobile Zone.

Six granitoid suites have been recognized in the Sally Downs Bore area.

(1) The Eastern Leucocratic Granite is a garnet bearing leucocratic granite and is interpreted as a highly fractionated granitoid derived from a low Al tonalite. The granitoid is characterized by high SiO₂ (average 76.0%).

(2) The Dougalls Granitoids Suite comprises tonalite and trondhjemite. Orthopyroxene is found in some of the tonalite.

(3) The Ord River Tonalite Suite includes biotite tonalite. Only minor relict hornblende crystals are found.

(4) The Western Porphyritic Granite is a coarse grained, porphyritic augen-textured biotite granite. It is mildly peraluminous, and is characterized by a high concentration of K₂O, Rb, Zr.

(5) The Central Leucocratic Granite is a fine to medium grained biotite granite and is mildly peraluminous. It has a moderate level of Sr and a negative Eu anomaly, indicating a role of plagioclase in the magma residue or in the fractionated phase. Although the granite is characterized by high K₂O (3.77-4.89 %), it has a low Y concentration (3.6-16.4 ppm) and high Sr/Y ratio.

(6) The Sally Downs Tonalite is the youngest granitoid in the area, and is a part of the Mabel Downs Granitoid Suite. Geochemical variation within the tonalite pluton is mainly ascribed to crystal fractionation during intrusion. Hornblende and plagioclase fractionation explains most of the variation found in the tonalite pluton. Rb-Sr whole rock data suggest an emplacement age of 1833 ± 43 Ma with an initial $^{87}\text{Sr}/^{86}\text{Sr}$ ratio of 0.70292 ± 0.00015 . The low initial $^{87}\text{Sr}/^{86}\text{Sr}$ ratio precludes a significant contribution of older crustal materials at any stage of its evolution.

The tonalites and trondhjemite of suites 2,3, and 6 above, have low K₂O, Rb, and Y contents and high Sr contents. Geochemical features suggest that the tonalites and trondhjemite can be classified as high Al types. The tonalite magmas are considered likely to have been derived from the partial melting of subducted oceanic crust leaving a residue consisting of garnet and pyroxene (\pm hornblende). It is inferred that a subducted oceanic slab, situated between what are now the Kimberley block and North Australian block, was sufficiently hot, presumably young at the time of the subduction, to be able to generate tonalitic magma by dehydration melting.

The Bow River Granitoid is a mildly peraluminous and K₂O rich granitoid, and is enriched in Rb and Y, similar to typical granitoids of the Barramundi igneous association of the North Australian block. The Bow River Granitoid magma could have been generated by partial melting of

mafic lower crust leaving a residue containing plagioclase and pyroxene. The magma may have had some interaction with sedimentary rocks of the Early Proterozoic Halls Creek Group to increase the alumina saturation level.

The Sophie Downs Granitoid is an alkali-feldspar granite, intruded into a high crustal level, before deposition of the Saunders Creek Formation of the Halls Creek Group. It has A-type characteristics, showing a high Ga/Al ratio, and a high concentration of Rb, Ce, Y, Zr, Nb, and F. The data indicate that the granitoid magma is derived by crystal fractionation from basaltic magma generated in a rift environment.

Petrogenetic examination of the granitoids suggests that Early Proterozoic tectonic setting of the Halls Creek Mobile Zone was followed by:

(1) initial rifting of continental crust and generation of A-type Sophie Downs Granitoid magma.

(2) tectonic transition from rifting to convergent tectonism resulting in a change in the type of granitoid magmatism; convergent tectonism included

i) subduction of oceanic crust resulting in three stages of partial melting of subducting slab to generate tonalitic magmas.

ii) generation of a large volume of K₂O rich granitoid magma in the lower crust leaving a residue of plagioclase and pyroxene. The heat to induce the partial melting of the mafic lower crust may have been derived from newly underplated mafic magma in the lower crust.

iii) generation of a low Al tonalitic magma and other granitoid magmas by partial melting of mafic and intermediate igneous rocks in the crust. The heat to induced the partial melting was derived by intrusion of mafic magma into the crust.

Although ensialic orogeny is postulated by the majority of workers for most of the Early Proterozoic provinces in the North Australian block, including the Halls Creek Mobile Zone, the results of the present study strongly suggest that tectonics relating initial rifting and subsequent subduction of oceanic crust operated in the Halls Creek Mobile Zone during the Early Proterozoic.

This thesis contains no material which has been accepted for the award of any other degree or diploma in any university, and to the best of my knowledge and belief, contains no copy or paraphrase of material previously published or written by another person, except where due reference is made in the text of the thesis.

DATED 3/8/96 SIGNED

NAME: MASATSUGU OGASAWARA COURSE: Doctor of Philosophy

I give consent to this copy of my thesis, when deposited in the University Libraries, being available for photocopying and loan.

SIGNATURE:

DATE: 25/8/1996

ACKNOWLEDGMENTS

This project was supervised by Dr. R.L. Oliver, to whom I am grateful for his continual encouragement and helpful advice. I would like to express my deep acknowledgment of his critical assessment of the draft of the thesis.

The project was suggested by Professor R.W.R. Rutland and was initially supervised by Dr. R.W. Nesbitt.

I thank Drs. J. Foden and S.S. Sun for providing technical instruction for isotope dilution mass spectrometry analysis of rare earth elements and for valuable discussions on geochemistry and igneous petrology. Rb-Sr isotopic work was possible with the support of Dr. L.P. Black of BMR (now Australian Geological Survey Organization) and with permission from the Research School of Earth Science, ANU to use their facility.

Technical support by John Stanley, K.R. Turnbull and P.J. McDuire of the Geology Department of the University of Adelaide was invaluable. Much of the electron probe analysis was facilitated by B.J. Griffin of the Electron Optical Center of the University of Adelaide.

Discussions with Steve Hancock, Rosemary Allen, Mark Fanning, Koya Suto were helpful.

Many thanks to Collin Codner of the Sally Malay Prospect of Australian Anglo American Company for his generous support in the field.

I thank Dr. M.T. McCulloch of ANU for including two specimens from this project in his regional Nd isotopic study. Nd isotopic data analyzed by him provided additional constraints on the petrogenesis.

Drs. T.J. Griffin and I.M. Tyler of Geological Survey of Western Australia revealed to me their newly found unconformity between the

Sophie Downs Granitoid and Saunders Creek Formation in the field. I appreciated the opportunity to examine the new evidence which helped establish the tectonic evolution of the Halls Creek Mobile Zone.

I thank my wife Mio for assisting me in the field and for initial typing of the draft.

To my two sons, Masaki and Tsuguki, and a daughter, Miki, thanks for helping me to keep a perspective and thank you for your sacrifices.

I thank my parents, Masami and Sueko, and parents in law, Hidetoshi and Yayoi Soma, for providing assistance, especially while Mio and I were in Adelaide.

Again thanks to all for their support.

The research on which this thesis is based was funded by a University Research Grant Scholarship.



CHAPTER 1. INTRODUCTION

1.1. Aim of Thesis

The granitoid is one of the major component of the continental crust. Therefore, the generation of the granitoid magma and its emplacement processes are important factors for the development of the continental crust. As the granitoid shows considerable variations in petrological and geochemical characteristics, it is necessary to obtain the characteristics before establishing a petrogenetic model for any granitoid body. The thesis is principally concerned with an petrological and geochemical examinations of the Early Proterozoic granitoids in the Halls Creek Mobile Zone, northern Australia (Fig. 1-1). The present study includes detailed investigations of a fractionation and emplacement processes of granitoid magmas in the Halls Creek Mobile Zone. The petrogenetic models of the granitoids in the Halls Creek Mobile Zone are presented based on the examination. It was expected to be able to provide information on the nature and tectonic style of the Early Proterozoic orogeny and on the formation of the continental crust.

1.2. Field Work and Method of Study

The project involves sampling based on detailed mapping of the Early Proterozoic Lamboo Complex and the Halls Creek Group (for definition, see later). Two main areas have been selected for detailed work.

One is the Sally Downs Bore area (Fig. 1-2), about 90km north of the Halls Creek. The area extends about 13 km from the Ord River in the north to near the White Rock Bore and Melon Patch Bore in the south, and from Sally Downs Bore in the west 12km to Dougalls Bore in the east. This area has been selected in order to study the Mabel Downs Granodiorite, although the main body of the Mabel Downs Granodiorite

Fig. 1-1. Outline of tectonic units of the Kimberley region

Major tectonic units are from Bureau of Mineral Resources (1976).

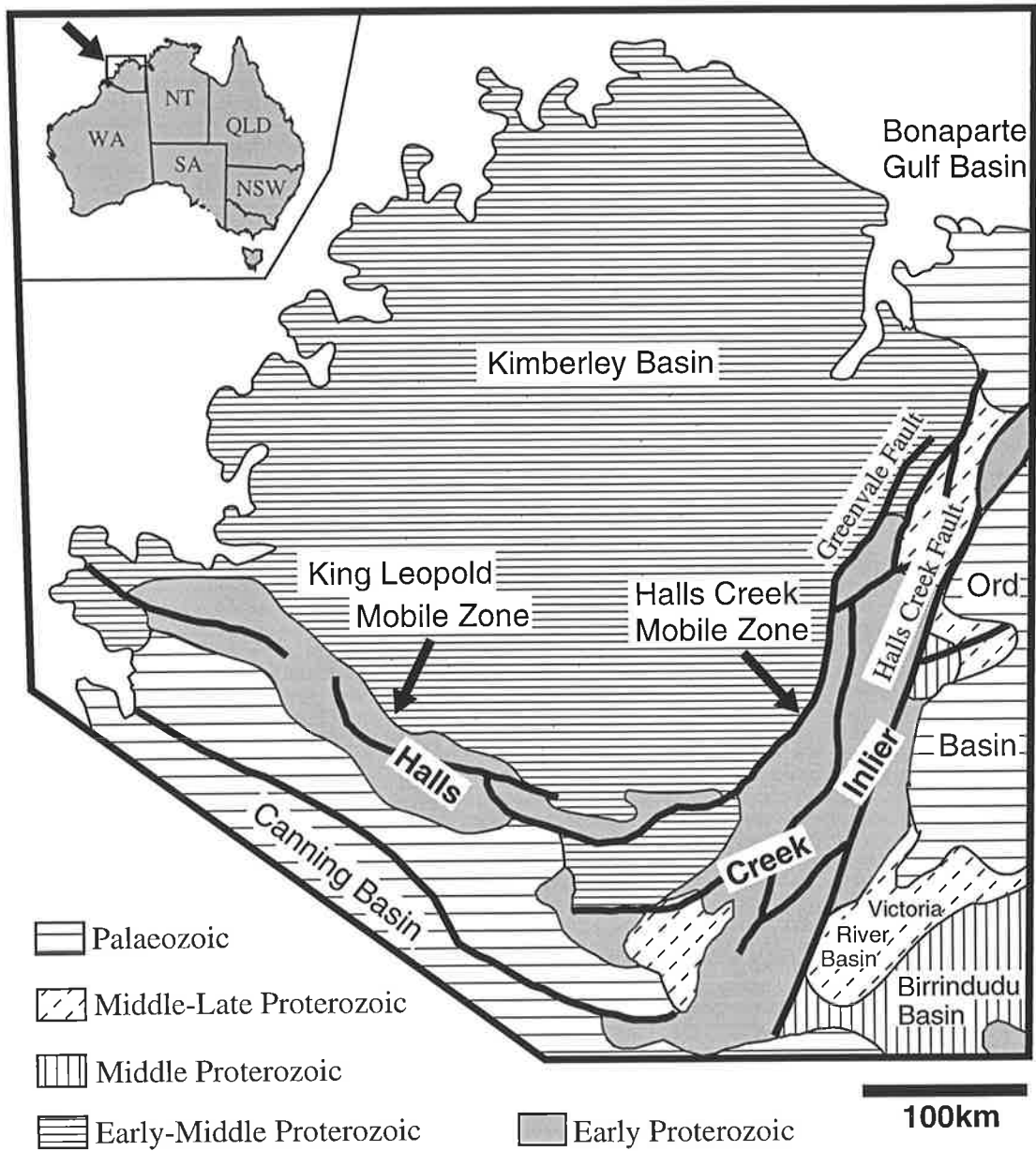


Fig. 1-2. Locality map of East Kimberleys

Names of major locations in the East Kimberleys are indicated.

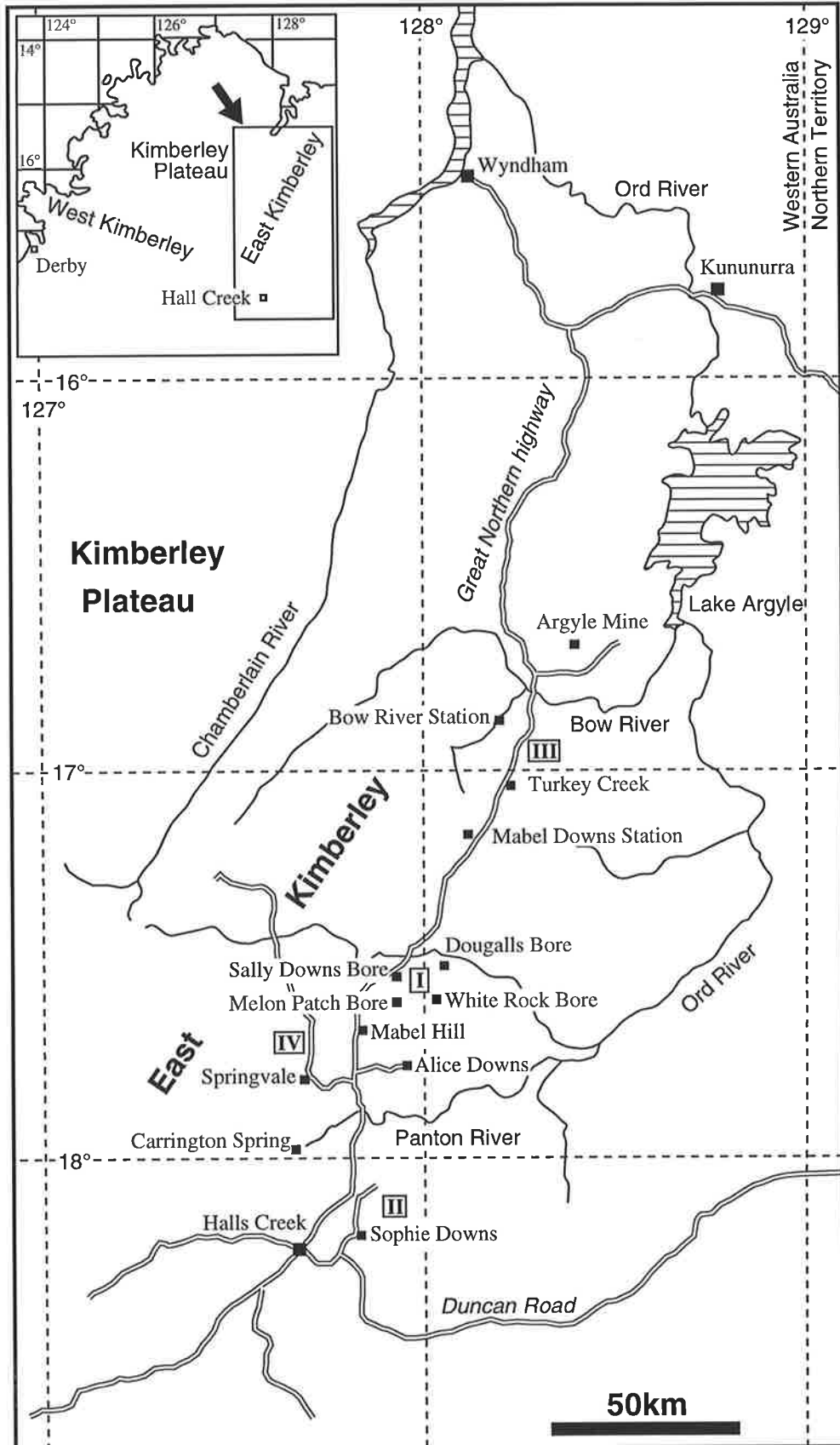
Studied areas are marked with Roman numerals.

I: Sally Downs Bore area

II: Sophie Downs area

III: Turkey Creek area

IV: Springvale area



crops out 4km north of the area of investigation, and extends further to the north for more than 80km to the Bow River. The more extensive occurrence has not been studied because of the likelihood that it represents a composite body. Instead, the more limited outcrop of the Mabel Downs Granodiorite in the Sally Downs Bore area has been investigated, as mentioned.

The other detailed study area is situated near the Sophie Downs Homestead where the Sophie Downs Granite is present in the Halls Creek Group. This area is 30km east of Halls Creek township (Fig. 1-2).

Samples were taken from four additional areas within the Halls Creek Mobile Zone to enable the petrology and geochemistry of type rock suites of the Lamboo Complex to be examined in the laboratory.

Reconnaissance sampling was conducted in the King Leopold Mobile Zone of the West Kimberleys (Fig. 1-1).

A total of 30 weeks was spent in the field from the middle of July to the end of September in 1978 and from early May to the end of September in 1979.

The areas are reached by tracks within distances of 50km from the Great Northern Highway which links Perth and Darwin and passes through the middle of the region (Fig. 1-2).

Samples have been petrographically examined, and the chemical composition of minerals also obtained by electron microprobe analysis to aid petrographic description.

From field observations and petrographic investigations, some 280 samples were selected for whole rock geochemical analysis. Ten major elements and fifteen trace elements were determined in these samples by X-ray fluorescence spectrometry. Rare earth element analysis of twenty three samples has been made by isotope dilution mass spectrometry. An Sr isotope investigation was carried out at the BMR isotope laboratory in

the Research School of Earth Science, Australian National University for dating and isotope geochemistry. Details of sample preparation and analytical techniques are described in Appendix 3, 5, 6, and 7.

These results were used to model the petrogenesis of the studied rocks.

1.3. Previous Investigation

The earliest work in the Kimberley region, northern part of Western Australia, was that by Hardman (1884, 1885) who outlined the geology of this area as seen during his two expeditions. Although the area which he examined was restricted to the eastern part of Halls Creek Mobile Zone (Fig. 1-1) and the southern part of King Leopold Mobile Zone, he recognized the major rock types of the area. After his finding of alluvial gold in the East Kimberleys during his second expedition (Hardman, 1885), gold mining was carried out around Halls Creek (Fig. 1-2). Subsequently, various explorations were performed in the Kimberley region in the early twentieth century.

Matheson and Guppy (1949) mapped the Precambrian rocks near Halls Creek. The term Lamboo Complex was first used for granites, gneisses, and undigested remnants of metasediments of the area. Metasediments were assigned to the Halls Creek Group, and basic lavas were labeled the McClintock Greenstones.

Traves (1955) made a geological reconnaissance of the Ord and Victoria River Basin region (Fig. 1-1), as a member of the Land Research and Regional Survey unit of the Commonwealth Scientific and Industrial Research Organization. Most of the Halls Creek Mobile Zone was included in the work.

Systematic mapping on the scale of 1:250,000 in the Kimberley region was carried out by the BMR and the Geological Survey of Western

Australia (GSWA), during 1962-67. The maps which are relevant to the present study are Dixon Range (Dow and Gemuts, 1967), Lansdowne (Gellatly and Derrick, 1967), Gordon Downs (Gemuts and Smith, 1968), Lissadell (Plumb, 1968), Mount Ramsay (Roberts et al. 1968), and Lennard River (Derrick and Playford, 1973). Subsequently, a comprehensive description of the Precambrian geology of the Lennard River sheet area was presented by Gellatly et al. (1974), and of the geology of the Lansdowne sheet area by Gellatly et al. (1975). Dow and Gemuts (1969) synthesized the geology of the East Kimberleys, and Gemuts (1971) described the Lamboo Complex in detail.

During the joint mapping project by the BMR and GSWA, isotopic ages were determined by Bofinger (1967). These isotopic ages were re-examined by Page (1976) and Page et al. (1984). Page and Hancock (1988) presented three zircon U-Pb ages of the rocks from the Halls Creek Mobile Zone.

Thom (1975) summarized the Precambrian geology of the Kimberley region. Plumb and Derrick (1975) reviewed the Proterozoic geology from the Kimberley to Mount Isa. Plumb and Gemuts (1976) summarized the geology of the Kimberley region in an Excursion guide for the IGC (Sydney). Plumb (1979a), and Plumb et al. (1981) described and discussed the regional Precambrian geology of northern Australia. Plumb et al. (1985) summarized the Proterozoic geology of the East Kimberleys. Griffin (1989) discussed the structure and lithology of the King Leopold Mobile Zone, and proposed the use of Hooper Complex for the crystalline complex in the King Leopold Mobile Zone. Griffin and Grey (1990a) and Griffin and Grey (1990b) reviewed the early Proterozoic geology of the Halls Creek Mobile Zone and King Leopold Mobile Zone and the early to middle Proterozoic sedimentary cover rocks in the Kimberley Basin, respectively. Griffin and Tyler

(1992) presented a summary of field work of GSWA-BMR joint re-mapping project in the Kimberley region. Blake and Hoatson (1993) described field relationships between granite, gabbro, and migmatite of the Lamboo Complex and discussed the origin of the migmatite.

Detailed studies of specific aspects of the ultrabasic-basic intrusives of the Lamboo Complex have been made by Wilkinson et al. (1975), Hamlyn (1975, 1977, 1980), Hamlyn and Keays (1979), Thornett (1980), Mathison and Hamlyn (1987), and Sun et al. (1991).

Structural descriptions of the Kimberley region were presented by Hancock and Rutland (1984), Page and Hancock (1988), Griffin and Myers (1988), White and Muir (1989), and Tyler and Griffin (1990).

Geochemistry of the granitoids of the Halls Creek Mobile Zone was described by Ogasawara (1988), as a part of present study. Sheppard et al. (1995) reported geochemistry of felsic igneous rocks from the southern Halls Creek Mobile Zone.

Sun et al. (1986) presented Nd and Sr isotopic data of mafic and ultramafic rocks in the Halls Creek Mobile Zone and of alkaline rocks in the Kimberley region, and discussed the isotopic evolution of the Kimberley region. McCulloch (1987) presented and summarized Nd isotopic data from Precambrian rocks of the Australian continent, including Nd isotopic analyses of two specimens collected during the present study. The latter are re-examined with new Sr isotopic data in Chapter 6.

Subsequent to the finding of diamond bearing lamproites and kimberlites in the Kimberley region, geochemical and isotopic information from these rocks has been presented (Jaques et al., 1984; Jaques et al., 1986; Nelson et al., 1986; Jaques et al., 1990), and geochemical characteristics of the subcontinental lithosphere of the

Kimberley region were discussed in the light of the petrogenesis of diamond bearing rocks (Nelson et al., 1986; Jaques et al., 1990).

1.4. Regional Geological Setting

Regional tectonic units in northern Australia are briefly described, and the tectonic setting of the Halls Creek Inlier in relation to other tectonic units is summarized in this section.

Three types of tectonic unit are used in the Tectonic Map of Australia and New Guinea (G.S.A., 1971). These are orogenic provinces, transitional domains, and platform covers; these units are characterized by different forms of tectonism, viz. orogenic tectonism, transitional tectonism, and cratonic tectonism, respectively.

The present exposure of a tectonic unit is largely controlled by later cratonic tectonisms. Therefore, even though, the tectonic unit is separated by later platform covers, it may be continuous underneath. Hence broadly contemporaneous domains, or sedimentary basins of similar tectonic history and style, are grouped into the same tectonic unit (G.S.A., 1971).

Orogenic tectonism is an intense tectonism involving the development and deformation of orthogeosynclines or metamorphic and igneous complexes prior to cratonization (G.S.A., 1971).

Transitional tectonism is a late to post-orogenic development associated with cratonization, and it is transitional in time, place, and style between orogenic and cratonic tectonisms (G.S.A., 1971).

Cratonic tectonism involves the deposition of platform covers and deformation of platform covers and basement. Its deposits overlie the immediately preceding orogenic provinces, and associated transitional domains, and spread across older orogenic provinces and platform covers (G.S.A., 1971).

Although the transitional tectonism is obvious in some areas, it may not be clearly distinguished from the orogenic tectonism in other areas. Indeed Rutland (1976, 1981) classified regional tectonics in terms of tectonic units of the platform basement and cover, or orogenic province and platform cover. In the present work, the transitional domains are included in the orogenic provinces, whereas the term transitional tectonism is still used to describe its characteristic tectonism.

Most of exposed basement areas are referred to as "inliers" instead of blocks, or geocynclines, or provinces (Plumb, 1979a). A part of the inlier can be described as a zone. Thus regional orogenic tectonic units are classified under the terms, province, inlier, and zone.

The orogenic units in northern Australia used in this study, are largely based on the work of Plumb et al. (1981) and Rutland (1981). They are shown in Fig. 1-3 and are as follows:

1. Archaean Orogenic Provinces

- Rum Jungle Complex (Inlier)

- Nanambu Complex (Inlier)

- Others

2. North Australian Orogenic Province (Early Proterozoic)

- Halls Creek Inlier

- a) Halls Creek Orogenic Zone

- b) King Leopold Orogenic Zone

- Arnhem Inlier

- Pine Creek Inlier

- Tenant Creek Inlier

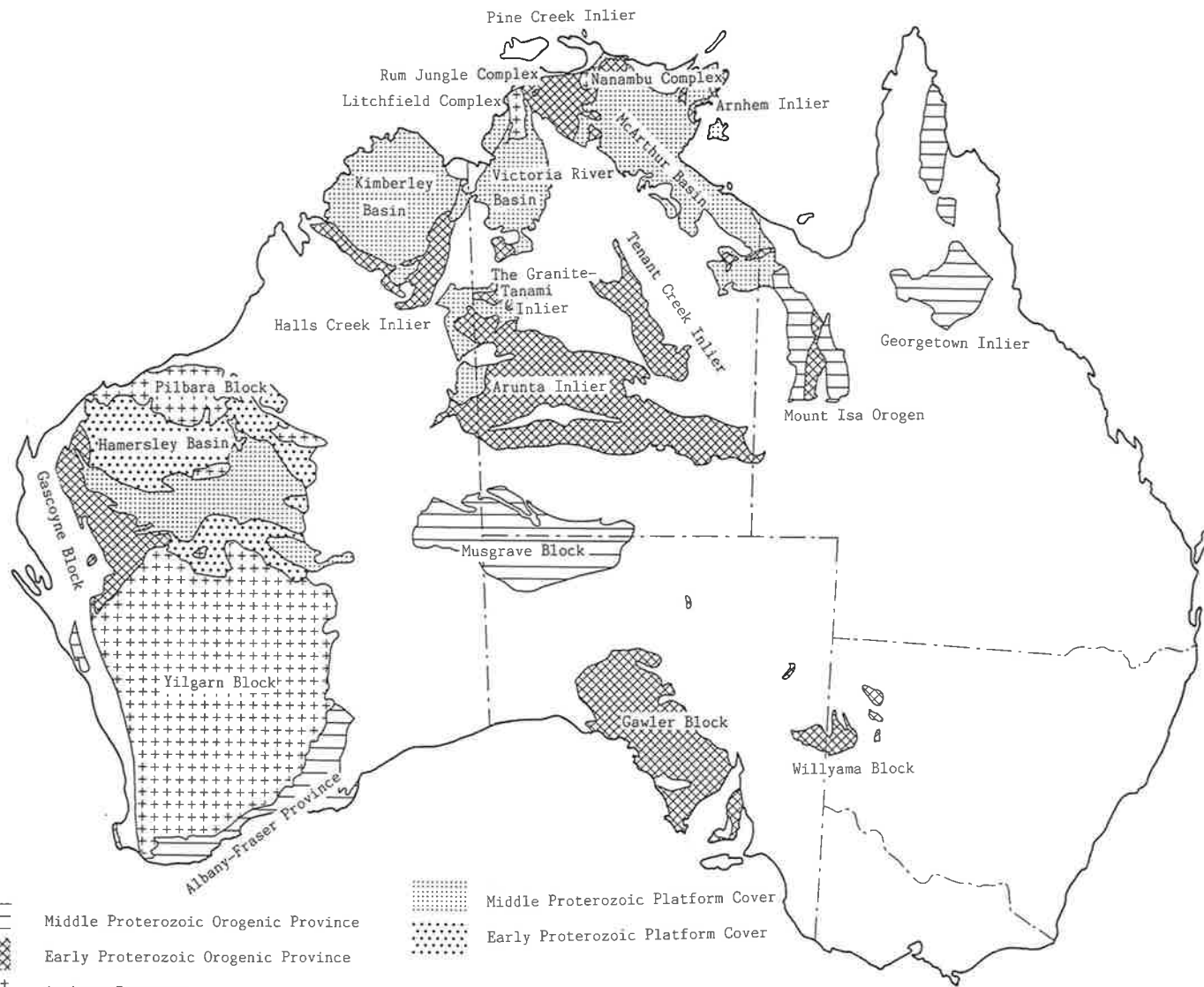
- The Granites-Tanami Inlier

- Others

3. Central Australian Orogenic Province (Early to Middle Proterozoic)

Fig. 1-3. Archaean-Middle Proterozoic regional tectonic provinces of
Australia.

Definitions of orogenic province and platform cover areas are based on
Plumb et al. (1981); see text for details. Boundaries of tectonic provinces
are from Bureau of Mineral Resources (1979).



——— Middle Proterozoic Orogenic Province
 ——— Middle Proterozoic Orogenic Province
 [Cross-hatch] Early Proterozoic Orogenic Province
 ++++ Archean Basement
 ++++ Archean Basement
 ++++ Archean Basement

[Dotted] Middle Proterozoic Platform Cover
 [Stippled] Early Proterozoic Platform Cover

Mount Isa Inlier

Others

The Halls Creek Orogenic Zone is part of the Halls Creek Inlier, and is exposed within the Halls Creek Mobile Zone. The term Halls Creek Mobile Zone indicates a linear zone of repeated localized deformation; it was tectonically active from at least the Early Proterozoic to the end of the Palaeozoic (Plumb and Derrick, 1976, and Plumb and Gemuts, 1976). However the Halls Creek Orogenic Zone represents the area which is characterized by the Early Proterozoic orogenic and transitional tectonisms. Similarly, the relationship between King Leopold Orogenic Zone and King Leopold Mobile Zone can be described as above.

Plumb et al. (1981) defined two subprovinces in the North Australian Orogenic Province, viz. the older McClintock Subprovince and the younger Palmerston Subprovince. The McClintock Subprovince consists of rocks of the Halls Creek and Arnhem Inliers, pelitic gneisses in the Tenant Creek Inlier, and several other rocks. Plumb et al. (1981) considered that these were metamorphosed at about 1950-1900 Ma and the Palmerston Subprovince (Pine Creek, Arunta, the Granite-Tanami inliers) underwent metamorphism at about 1840-1800 Ma. However, an extensive review by Page (1988) does not support this age difference between the orogenic events of the two subprovinces.

Etheridge M. A. et al. (1987) indicated that the Early Proterozoic terranes of northern Australia were affected by an essentially isochronous orogenic event between about 1850 and 1880 Ma, and defined this event the Barramundi orogeny. Page (1988) supported this conclusion based on geochronological evidence. Therefore, the North Australian Orogenic Province can be described as the area characterized by the Barramundi orogeny.

The Halls Creek Mobile Zone (Traves, 1955) is situated in the east Kimberley region of northeast Western Australia (Fig. 1-1 and 1-2). It lies between latitudes 16° and 19°S and longitudes 127° and 128°30'E. The Halls Creek Mobile Zone extends NNE-SSW for a distance of 350km from near Kununura to south of Halls Creek, and is 50 to 80km wide. Traves (1955) continued the mobile zone to the Litchfield Complex of Northern Territory (Fig. 1-3), but Sweet et al. (1974) defined a Fitzmaurice Mobile Zone for the northern part of the Halls Creek Mobile Zone of Traves (1955). According to Sweet's definition the Halls Creek Mobile Zone is restricted to the region south of the Fitzmaurice Mobile Zone. Yet another possibility is suggested by Plumb (1979a), viz. that the Halls Creek Mobile Zone continues to the north beneath the Bonaparte Gulf Basin as indicated by offshore structural data and gravity trends.

The NW-SE trending King Leopold Mobile Zone (Traves, 1955) which joins the southern end of the Halls Creek Mobile Zone (Fig. 1-1), is 350km long and 50km wide.

The Halls Creek and King Leopold Mobile Zones comprise the Halls Creek Inlier (Plumb, 1979a), as now exposed. The inlier consists of rocks of the Halls Creek Group and Lamboo Complex of Early Proterozoic age (see Fig. 2-1).

To the southeast of the Halls Creek Mobile Zone, The Granites-Tanami Inlier is exposed (Fig. 1-3). The Tanami Complex of The Granites-Tanami Inlier is correlated with the Halls Creek Group by Blake et al. (1975). East of the Halls Creek Mobile Zone are the Middle Proterozoic Birrindudu Basin, Victoria River Basin, and Palaeozoic Ord Basin (Fig. 1-1). The Halls Creek Mobile Zone and the King Leopold Mobile Zone are bounded to the south by the Phanerozoic Canning Basin. West of the Halls Creek Mobile Zone is the late Early Proterozoic Kimberley Basin (Fig. 1-1). Relatively undeformed rocks of the

Kimberley Basin unconformably overlies the rocks of the Halls Creek Inlier.

The western margin of the Halls Creek Mobile Zone is separated from the Kimberley Basin mainly by the Greenvale Fault (Fig. 1-1). The northern part of the eastern margin of the zone is mainly bounded by the Halls Creek Fault, but the southern part of the margin is unconformably overlain by younger rocks.

1.5. Definition of Terms

1.5.1. Classification and Nomenclature of Granitoids

Classification and nomenclature of plutonic rocks presented in Streckeisen (1976) are used in this thesis. The classification is based on modal mineralogy. The term granite used here has a broad meaning, including monzogranite and syenogranite (Streckeisen, 1976). Trondhjemite is applied to light colored tonalites which have the content of mafic and related minerals less than 10 %.

1.5.2. Nomenclature of Granitoid Bodies

As granitoid bodies generally form a large scale mass, several terms were used to describe that, e.g., batholith and pluton. In this thesis, the following nomenclature of granitoid bodies is used

Granitoid body: a small unit of granitoids derived from same magma. Any shape of granitoid body is included, e.g., sheet-like bodies.

Pluton: a large mass of granitoids derived from a magma.

Suite: a granitoid suite is defined when a number of granitoid plutons and bodies are considered to have been derived from a unique magma type (White and Chappell, 1983).

Batholith: the term, batholith, is applied to any large granitoid mass whose exposure exceeds five hundreds square kilometers, and it may contain granitoids derived from several different magma sources.

1.5.3. Enclaves in Granitoids

Granitoids commonly contain pieces of different materials within those. Didier (1973) and Didier and Barbarin (1991) proposed a nomenclature to describe these materials. Didier (1973) recommended the use of enclave for a piece of foreign material enclosed within an igneous rock, and inclusion for a piece of foreign material enclosed within a crystal. The various types of enclaves are classified by Didier and Barbarin (1991) into followings, xenolith, xenocryst, surmicaceous enclave, schlieren, felsic microgranular enclave, mafic microgranular enclave, and cumulate enclave. Definition of the terms used in this thesis is based on Didier and Barbarin (1991), and is given as follows:

Mafic microgranular enclave: mafic microgranular enclaves, typically dioritic to tonalitic in composition, containing more mafic minerals than the host granitoid. They have relatively fine grained igneous microstructures (Vernon, 1984). Several terms, viz. autoliths, mafic inclusions, microgranitoid enclaves and cognate xenolith, have been used by other workers to describe those, but mafic microgranular enclave is used in this thesis.

Schlieren: enclave of elongated form with ill-defined boundaries.

Xenolith: exogenous enclave, typically a rock fragment of country rock.

CHAPTER 2. GEOLOGY AND STRUCTURE

2.1. Introduction

The field relationships and structural features of the Early Proterozoic Halls Creek Group and Lamboo Complex in the studied area are described and discussed in this chapter.

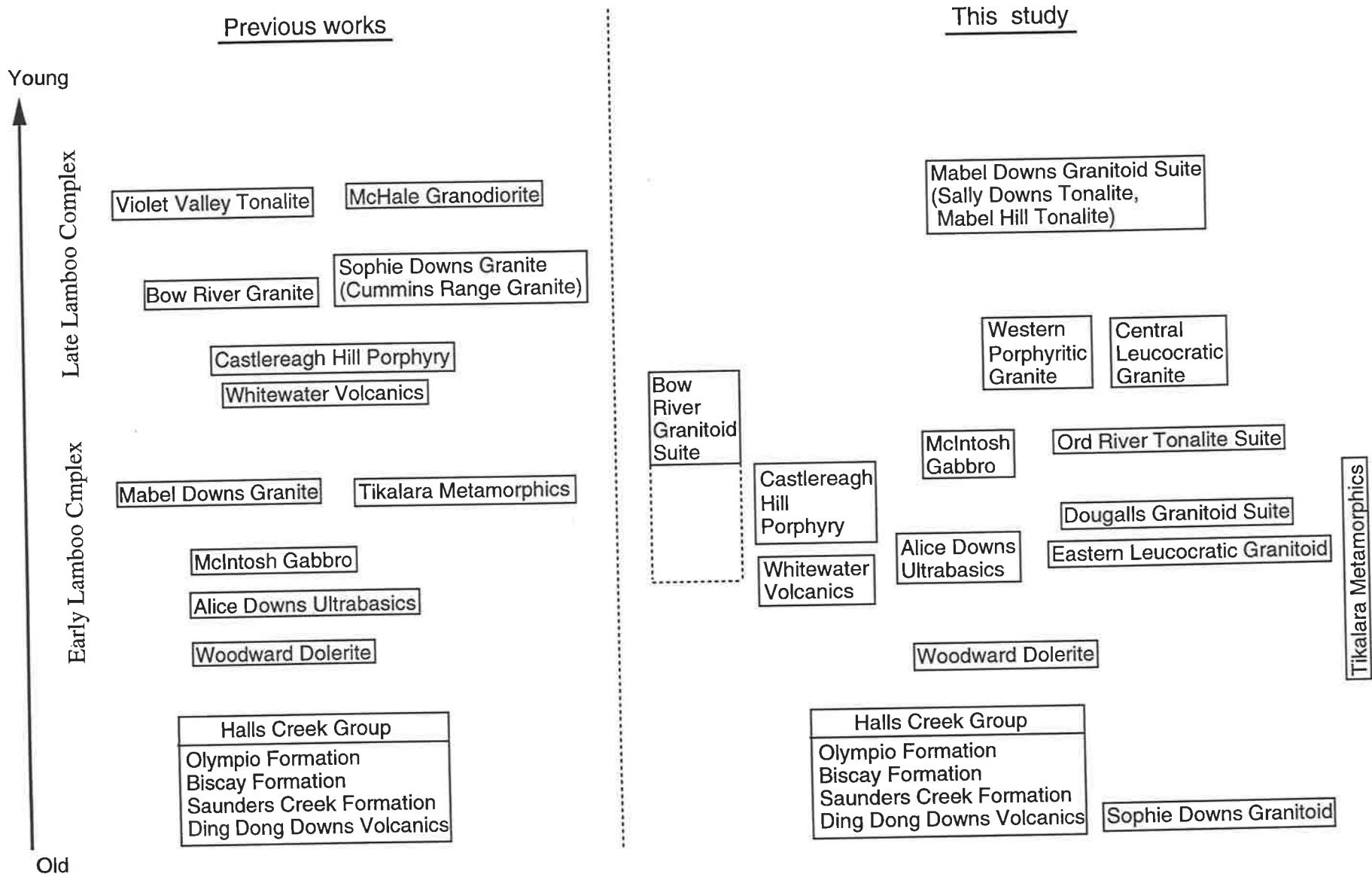
The definition of the Lamboo Complex has been changed several times since its initial introduction by Matheson and Guppy (1949). The name Lamboo Complex was used by Traves (1955) for only the granitic rocks, and the term Halls Creek Metamorphics for all metasediments and volcanics of the Halls Creek Mobile Zone. Later, Dow and Gemuts (1969) defined the Lamboo Complex as comprising basic to acidic intrusive rocks and high grade metamorphics. The latter are thought to be the highly metamorphosed equivalents of the Halls Creek Group which, less modified, consists of unmetamorphosed and low grade metasediments and volcanics.

Gellatly et al. (1974) added the Whitewater Volcanics to the Lamboo Complex from their observation in the King Leopold Mobile Zone. In this thesis the definition of the Lamboo Complex according to Gellatly et al. (1974) is used.

The Halls Creek Group has been subdivided into four formations (Fig. 2-1); definitions and detailed descriptions of the formations are presented by Dow and Gemuts (1969). The basal Ding Dong Downs Volcanics are exposed only in the Saunders Creek Dome, 15 km east of the Sophie Downs study area. This formation is composed of basic volcanic rocks and intercalated sediments (Dow and Gemuts, 1969). The Saunders Creek Formation, which is mainly quartz sandstone, was deposited on the Ding Dong Downs Volcanics under shallow-water condition. Part of the Saunders Creek Formation is in contact with the northern end of the Sophie Downs Granite within the Sophie Downs study

Fig. 2-1. Diagrammatic relation of rock units in the Halls Creek Mobile Zone.

Previous works are from Gemuts (1971) and Gellatly et al. (1974). Time relationship of rock units used in this study are modified after Sheppard et al. (1995) and Page and Sun (1994).

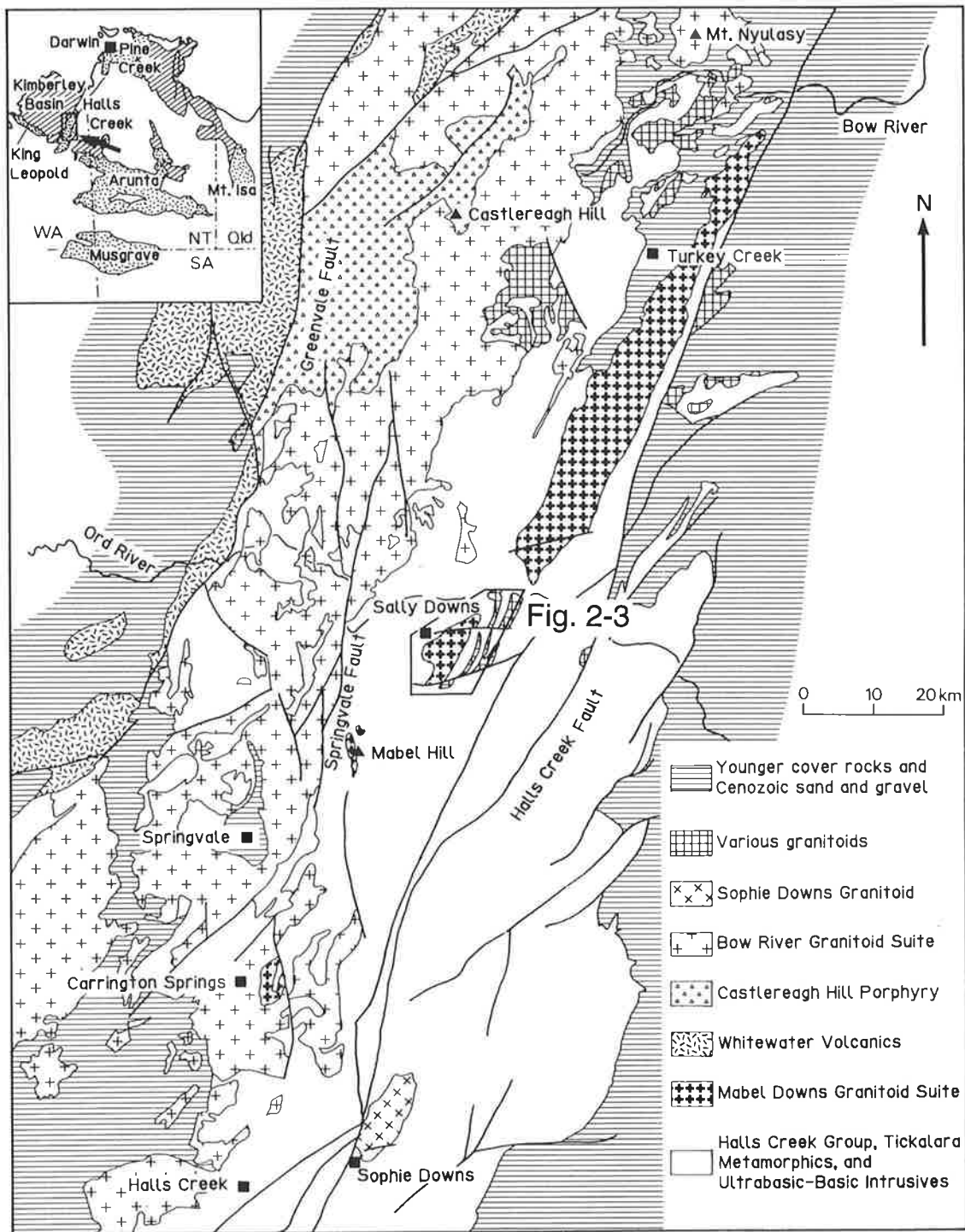


area, and where the formation unconformably overlies the granite (T. Griffin (1992) personal communication). The formation is well exposed around the Saunders Creek Dome and in the Cummins Range (Dow and Gemuts, 1969). The Biscay Formation, which overlies the Saunders Creek Formation, consists of thick basic and acidic volcanic rocks and interbedded greywacke and siltstone with carbonate layers. The Olympio Formation, at the top of the Halls Creek Group, is predominant subgreywacke with subsidiary siltstone, shale, and conglomerate.

The high-grade metamorphic rocks in the Lamboo Complex are called the Tickalara Metamorphics (Dow and Gemuts, 1969), and they occur mainly between the Halls Creek Fault and the Springvale Fault (Fig. 2-2). Some of the metamorphics can be correlated with part of the less metamorphosed Halls Creek Group, thus a boundary between them becomes obscure. However, some high-grade gneisses and migmatitic gneisses can still not be identified as belonging to the Halls Creek Group. Nevertheless all the high-grade metamorphic rocks in the Halls Creek Mobile Zone are classified as Tickalara Metamorphics. The boundary separating these from the Halls Creek Group, established by Gemuts (1971), is retained. The grade of metamorphism increases from the south to the north reaching granulite facies near Turkey Creek (Gemuts, 1971). In the Sally Downs Bore area, the Tickalara Metamorphics, which are predominantly basic metamorphic rocks with several distinct horizons of carbonate rocks and pelitic schists, can be correlated with part of the Biscay Formation of the Halls Creek Group from the similarity of their lithologies.

The Woodward Dolerite, Alice Downs Ultrabasics and McIntosh Gabbro are basic to ultrabasic intrusive rocks of the early Lamboo Complex. The McIntosh Gabbro consists of a number of differentiated

Fig. 2-2. Simplified geological map of the Halls Creek Mobile Zone
Modified after Bureau of Mineral Resources (1967)



basic intrusions. Some of them form large elliptical sill-like bodies, such as the McIntosh Sill and Toby Sill (Gemuts, 1971).

The term Mabel Downs Granodiorite has been used by Gemuts (1971) for the gneissic igneous intrusions which extend in a belt from 25km north of Halls Creek northward to the Bow River (Fig. 2-2). It is considered by Dow and Gemuts (1969) that the granodiorite formed by partial melting of the Tickalara Metamorphics. The Mabel Downs Granodiorite is not a single pluton, but consists of a number of granitoid plutons, and is referred to in this thesis as the Mabel Downs Granitoid Suite. The main body of the suite extends from just north of the Ord River 80km northward to the Bow River and has a width of 6 to 9km. Three small bodies of the suite are exposed south of the Ord River, near Sally Downs Bore, Mabel Hill, and Carington Spring. Several granitoids near Dougalls Bore and Black Rock Anticline, and orthopyroxene bearing granodiorites near Turkey Creek, have been grouped with the Mabel Downs Granodiorite by Dow and Gemuts (1969); their relationship to the main body of the suite will be discussed later.

Dow and Gemuts (1969) and Gellatly et al. (1974) defined post-tectonic or late-tectonic acid igneous rock group which includes the Bow River Granite, Sophie Downs Granite, Violet Valley Tonalite, McHale Granodiorite, Castlereagh Hill Porphyry, and Whitewater Volcanics. However, new U-Pb age determinations of samples from the granites and volcanics (Page and Sun, 1994) do not agree that the all units can be grouped into the post-tectonic or late-tectonic group. Therefore, the post-tectonic or late-tectonic group is not used in this thesis.

The Whitewater Volcanics (see Fig. 2-1) comprise andesitic to rhyolitic ashflow tuffs and lavas, and unconformably lie on the Halls Creek Group (Dow and Gemuts, 1969). The volcanics crop out along the western margin of the Halls Creek Mobile Zone (Fig. 2-2).

Castlereagh Hill Porphyry intrudes the Whitewater Volcanics, and is present in the northwest of the mobile zone (Dow and Gemuts, 1969).

The Bow River Granitoid Suite (Bow River Granite of Dow and Gemuts, 1969) includes a variety of granitoids ranging from granite to granodiorite. The granitoids are coarse grained, and commonly have porphyritic feldspars. These granitoids occur on the western side of the Halls Creek Mobile Zone, and comprise a large batholith 300km long 20 to 40km wide (Fig. 2-2). They intrude the Whitewater volcanics, and Castlereagh Hill Porphyry (Plumb and Gemuts, 1976). The granitoids, volcanics, and porphyry are believed by Dow and Gemuts (1969) to be cogenetic.

The granitoids which occur in the cores of anticlines or domes on the eastern margin of the Halls Creek Mobile Zone were initially grouped as Sophie Downs Granite by Dow and Gemuts (1969). In the present study, however, only the single granitoid pluton in the Sophie Downs Dome (Fig. 2-2) is called by this name, and five other small plutons in the Cummins Range are now referred to as the Cummins Range Granite.

The Violet Valley Tonalite and McHale Granodiorite are considered to be the youngest granitoids in the mobile zone, but have not been studied in the present work. The Violet Valley Tonalite intrudes the Tickalara Metamorphics, Mabel Downs Granitoid Suite, and Bow River Granitoid Suite, and crops out in two areas, viz. northwest of Mabel Downs Station and 80km to the west of Halls Creek (Gemuts, 1971). The McHale Granodiorite occurs to the east of the Halls Creek Fault in the Osmond Range (Dow and Gemuts, 1969).

The detailed geology and structural relationships of the rock suites for each of the areas which are investigated in the present study, are described in the following sections.

2.2. Geology of Sally Downs Bore Area

2.2.1. General

A geological map of the area is presented in Plate 1 and Fig. 2-3.

The area is occupied by the Tickalara Metamorphics and a variety of intrusive rocks of the Lamboo Complex. All the names of the igneous bodies in the area are used here for the first time (Fig. 2-1) as the bodies have so far been undifferentiated from granitic gneiss of the Tickalara Metamorphics, or Mabel Downs Granodiorite, or Bow River Granite. Some of the smaller igneous bodies have a complex distribution among the other rocks and are not regionally mappable.

In the western part of the Sally Downs Bore area, the metamorphics, Ord River Tonalite Suite, meta-dolerite, and Central Leucocratic Granite are shown as one complex in the geological map (Fig. 2-3 and Plate 1). Only carbonate rocks of the metamorphics are shown separately on the map, because of their distinct appearance in the field and good continuity throughout the studied area.

The Sally Downs Bore area is characterized by the presence of large amounts of tonalite-trondhjemitic rocks comprising three suites. The older tonalite-trondhjemitic suites are the Dougalls Granitoid Suite and the Ord River Tonalite Suite. A younger suite without trondhjemitic variation is the Sally Downs Tonalite, which is regarded as part of the Mabel Downs Granitoid Suite.

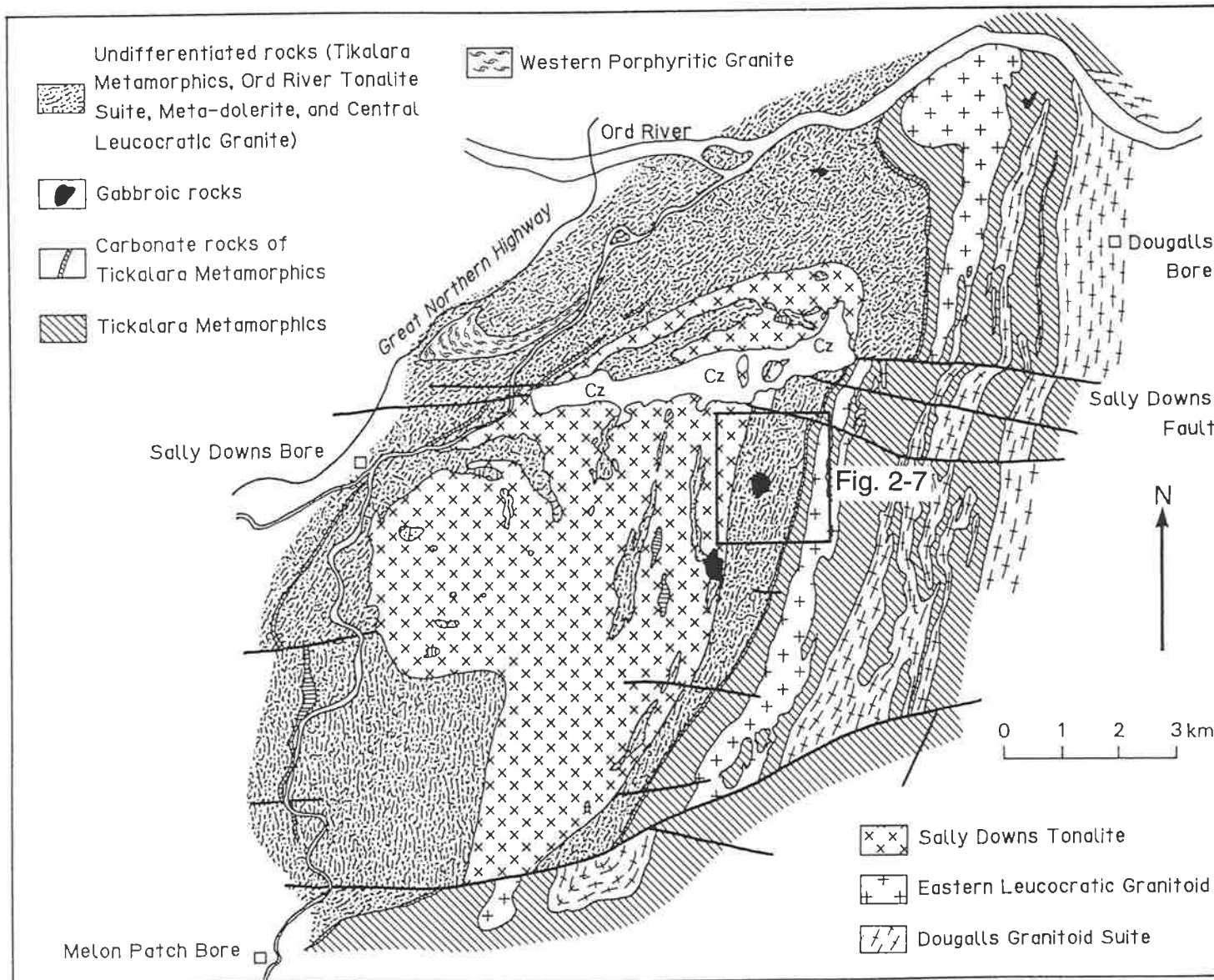
Less significant amounts of other types of granitoid, such as the Eastern Leucocratic Granitoid, and gabbroic rocks occur among them.

2.2.2. Tickalara Metamorphics

In the Sally Downs Bore area, the Tickalara Metamorphics consist of amphibolites, pelitic and psammo-pelitic schists and gneisses, and

Fig. 2-3. Geology of the Sally Downs Bore area

Cz indicates area covered by Cenozoic sand, soil, and gravels.



carbonate rocks. The amphibolite is the most predominant rock type among them.

The scarcity of younging directions apparent in the metamorphics means that no inference of stratigraphy or order of superposition was possible. Only the carbonate units suggest an original stratigraphy, through these also may be repeated by folding.

2.2.2.1. Pelitic and psammo-pelitic schists and gneisses

Pelitic and psammo-pelitic schists and gneisses are widespread throughout the area as thin layers within the amphibolites and granitoids. Thickness of each unit of the schists and gneisses varies from several tens of centimeters to 250 meters. Within these units there is considerable variation from quartzofeldspathic schists and gneisses to micaceous schists. Major constituent minerals of the rocks are biotite, feldspars, and quartz.

Garnet porphyroblasts up to 15mm in diameter and fibrolitic sillimanite are visible in many hand specimens. Cordierite is commonly present in the pelitic rocks of the central and the northern part of the area. Orthopyroxene was found in one sample of garnet biotite gneiss.

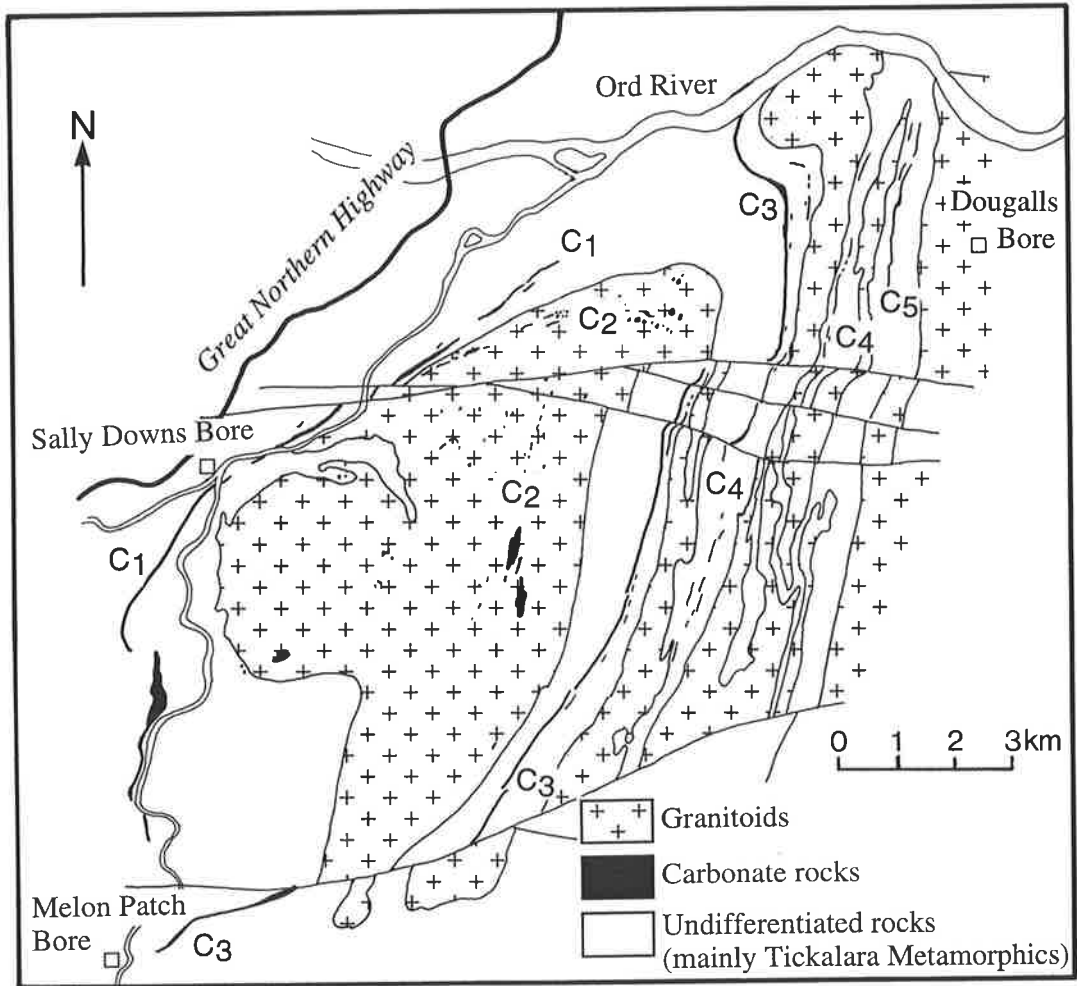
2.2.2.2. Carbonate rocks with associated calc-silicate rocks

Six major carbonate rock units have been recognized in the area. Each unit has been numbered from C₁ to C₅ (Figs. 2-3 and 2-4) without any stratigraphic implication.

The C₁ carbonate unit occurs to the west of the Sally Downs Tonalite, and is 4 to 10 meters thick. It can be traced for more than 12km. The C₂ unit is more discontinuous and comprises, in part, strings of carbonate rock xenoliths in the Sally Downs Tonalite. The C₃ unit is situated between the Sally Downs Tonalite and the Eastern Leucocratic

Fig. 2-4. Distribution of carbonate rock units in the Sally Downs Bore area

Carbonate rock units of the Tickalara Metamorphics can be traced for considerable distance in the mapped area, showing original stratigraphic horizons. Each carbonate rock unit has been numbered from C₁ to C₅, from west to east.



Granitoids. It extends for more than 15km from the Ord River to the Melon Patch Bore. It is likely to continue further south to the outcrop of a carbonate rock east of Mabel Hill (Fig. 2-2). The unit is noticeable because of its high topographic relief; it stands up to 40 meters higher than the surrounding area. The thickness of the unit varies from 5 to 50 meters. Several discontinuous carbonate rock outcrops, near the main horizon, are included in the unit. The C4 carbonate which occurs to the east of the Eastern Leucocratic Granitoid, is 2 to 50 meters thick. The C5 unit which consists of several thin carbonate rocks is recognized only to the west of the Dougalls Bore.

The carbonate rocks are white coarse grained marbles containing varying amounts of fine to medium grained disseminated silicate minerals. Most of the silicate minerals are dark green clinopyroxene, pale green epidote, or reddish brown garnet.

Clinopyroxene and epidote occur also in greenish brown calc-silicate lenses representing boudinaged originally more silica-rich layers within the limestone.

2.2.2.3. Amphibolites

The amphibolites crop out mainly in the east of the Sally Downs Bore Area. Near Dougalls Bore, they are medium grained, and have equigranular texture, whereas, in the southeast, the rocks show more obvious schistosity defined by the orientation of amphibole crystals.

Hornblende, plagioclase and clinopyroxene are the most common minerals in these rocks. The amphibolites are predominantly greenish black due to the abundance of hornblende crystals, but bands of calc-amphibolite which are light green also are present. The bands are rich in clinopyroxene, are 5 to 20 centimeters thick, and the boundaries between these and the host amphibolite are sharp. Such bands might suggest that

some of the amphibolites are derived from basic tuff which is intercalated with more calcareous basic tuff representing possible mixing with a limy sediment. Medium grained well foliated, garnet-clinopyroxene amphibolites are also present in the area. They are more closely associated with the calc-silicate rocks.

The deformed quartz veins, 1 to 3mm wide, are common in the amphibolites and are usually parallel to the schistosity.

2.2.3. Fine Grained Tonalitic Rocks

Minor amounts of fine grained rocks of tonalitic composition are found to the north of the Sally Downs Tonalite. They are dark gray, foliated, fine grained rocks and occur as inclusions in the Ord River Tonalite Suite or are interlayered with it. They consist largely of plagioclase, quartz, biotite and/or hornblende, and show variable texture in hand specimen. One variety has small lenticular aggregates of medium grained hornblende, constituting 5 to 10% of the rock. Another variety has plagioclase crystals up to 1.2 cm long in the fine grained matrix, suggesting the possibility of a original porphyritic texture. The rock may be a metamorphosed volcanic rock of intermediate composition, although the alternative possibility that it is originally a sedimentary rock or fine grained intrusive of tonalitic composition, can not be excluded.

2.2.4. Meta-gabbro

Meta-gabbro is found about 3km northwest of Dougalls Bore as a small lenticular body, surrounded by amphibolite (Plate 1 and Fig. 2-3). The rock consists of medium grained amphibole and orthopyroxene, is dark green and shows a foliation which is manifested by the preferred orientation of the amphibole. No other occurrence of meta-gabbro is observed in the Sally Downs Bore area.

2.2.5. Eastern Leucocratic Granitoids Suite

This suite includes a variety of leucocratic granitoids which occur to the east of the C₃ carbonate unit (Fig. 2-3 and Fig. 2-4). The light yellowish rocky outcrops of the granitoids, without much vegetation on them, make a distinct high ridge which continues from the Ord River to the Melon Patch Fault (Fig. 2-5A). The Eastern Leucocratic Granitoids intrude the amphibolites and metasediments of the Tickalara Metamorphics.

The main body which crops out about 200m east of the C₃ carbonate unit is 500 to 800m wide at the southern part. The northern end of the body is elliptical in shape, as the result of multiple deformation, and is terminated by the Ord River. Several thin lenticular bodies of granitoid are present east of the main body.

The granitoids vary in texture and mineralogy. Three main types of granitoids are recognized, gradational to each other within the main body.

Type I granitoid of the Eastern Leucocratic Granitoid Suite is a coarse to medium grained pink leucocratic granite which contains up to 7% garnet as fine to medium grained rounded crystals. Fine grained biotite is present as strongly stretched aggregates. Plagioclase is medium to coarse grained, and dark to light gray. Iron oxide is also common in the rocks. The coarse grained varieties of the granite show a pegmatitic appearance.

Type II granitoid is a strongly foliated medium grained granite. The rock resembles the trondhjemite of the Dougalls Suite (see below) in hand specimen, but differs from it by the presence of K-feldspar and minor garnet. More mafic minerals are present in this than in type I granitoid. The granite occurs mainly in the southern part of the main body.

Fig. 2-5. Field geological photographs; the Eastern Leucocratic Granitoid and Dougalls Granitoids.

A. Rocky outcrops (light colored hill) of the Eastern Leucocratic Granitoid in the Tickalara Metamorphics are clearly visible. Carbonate rock horizons of the metamorphics are light colored in the foothill of the granitoid hill. 7km east of the Sally Downs Bore, looking east.

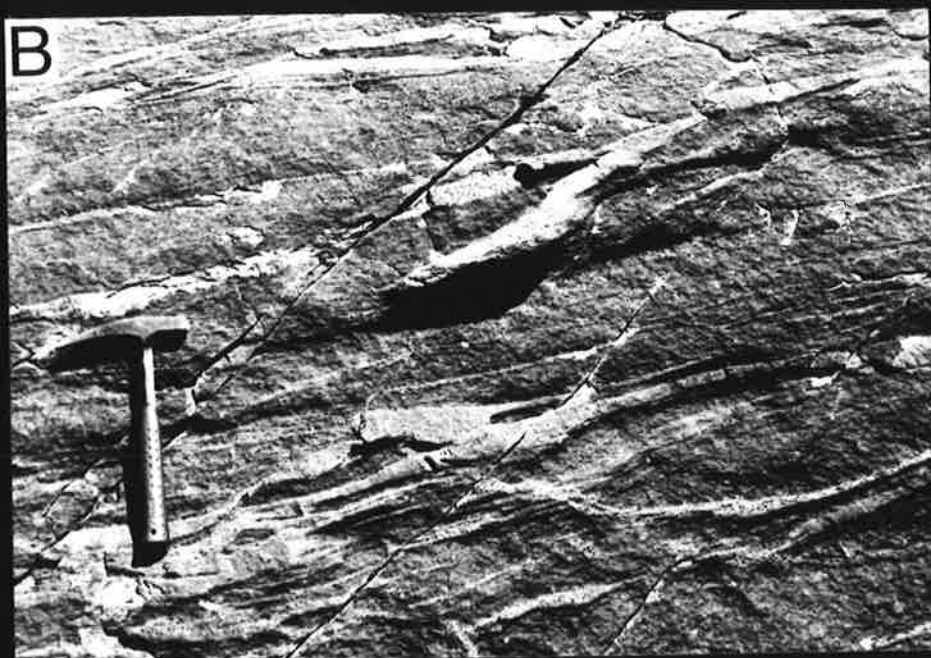
B. Trondhjemite (light colored) and tonalite (dark colored) of the Dougalls Granitoid Suite. Small veins of the trondhjemite are found in some locations, but it is present as a large homogeneous body in the southern part of the eastern Sally Downs Bore area. Length of the hammer is 33 cm.

C. Tonalite of the Dougalls Granitoid Suite intruded into amphibolite; both rock units have been deformed, presumably by D₂. Same hammer as in photograph B. was used for scale.

A



B



C



Type III granitoid is a foliated medium to coarse grained leucocratic granite characterized by the presence of unusually dark colored plagioclase. Although the plagioclase of the other two types of granitoid is similar in composition, it is not as dark in color as in this type. The granite has minor amounts of K-feldspar, and some of the rocks are classified as a trondhjemite.

2.2.6. Dougalls Granitoid Suite

The Dougalls Granitoid Suite in the Sally Downs Bore area includes two types of granitoids, viz. tonalite and trondhjemite. Variable amounts of orthopyroxene are present in most of the tonalite. The tonalite is coarse grained, foliated, and commonly dark gray to brownish dark gray with vitreous luster in hand specimen. Dark gray plagioclase is medium to coarse grained. Orthopyroxene is light amber color, and medium grained. Biotite is the most abundant mafic minerals in this rock. Minor hornblende is present, but it is a major constituent in the rocks which do not have orthopyroxene.

Three bodies of the tonalite are recognized to the north of the Sally Downs Fault within the Tickalara Metamorphics (Plate 1 and Fig. 2-3). The western body is 5km by 0.5km, and extends in a northerly direction. The southern end of it has been cut by the Sally Downs Fault, but it continues to the south of the fault with one kilometer right lateral apparent horizontal displacement. The tonalite body has two large amphibolite xenoliths in it and is cut by the several mylonite zones trending east-west.

A very thin sheet-like central tonalite body, is 30 to 50m wide, and is associated with several similar thin tonalitic veins.

The eastern body crops out near Dougalls Bore (Plate 1 and Fig. 2-3), and extends in a northerly direction. The eastern margin of this body

has not been demarcated in the field, but its width is at least two kilometers. Many large amphibolite blocks are enclosed within the tonalite, but are not shown on the map (Plate 1 and Fig. 2-3).

All three tonalites are commonly cut by pegmatite veins which have dark gray plagioclase.

Near the Dougalls Bore, a medium grained massive garnet and orthopyroxene bearing tonalitic rock is found with no obvious contact relations. It may be a granulite facies metamorphic rock of intermediate composition, but is included with the tonalites here.

Four major bodies of tonalite have been mapped south of the Sally Downs Fault. Minor relict orthopyroxene is present in the rocks. They still have a dark colored appearance in the field, but not much vitreous luster (Fig. 2-5C). In this area, the geology becomes complicated by the intrusions of trondhjemite.

The trondhjemite is medium grained, and foliated, and it intrudes the tonalite subparallel to its foliation (Fig. 2-5B). Mafic minerals of the trondhjemite are fine to medium grained biotite, modally ranging from 5 to 10%. Plagioclase is medium grained and dark gray. The trondhjemites become the predominant rock toward the south of the Sally Downs Bore area.

2.2.7. Ord River Tonalite Suite

This suite consists of two types of tonalite, coarse grained biotite tonalite (type I) and medium grained biotite tonalite (type II). The main body of the type I tonalite occurs in the northern part of the Sally Downs Bore area, with a northeast trend. Less continuous thin gneissic tonalite bodies around the Sally Downs Tonalite are also included in this unit. Good exposures of the type I tonalite are found along the Ord River and its tributaries (Fig. 2-6A).

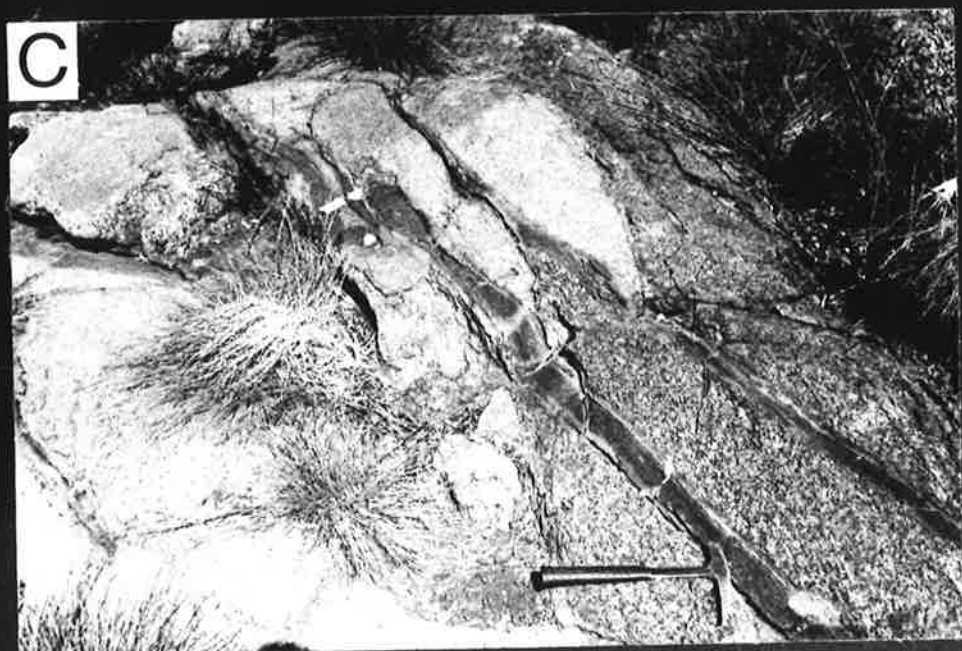
Fig. 2-6. Field geological photographs; the Ord River Tonalite Suite and Western Porphyritic Granite.

A. Type I tonalite of the Ord River Tonalite Suite in the river bed of the Ord River. Strong foliation and layering are visible.

Scale: diameter of the lens cap is 5 cm.

B. Type II tonalite of the Ord River Tonalite Suite is cut by pegmatite veins which contain garnet. Scale: length of the hammer is 33 cm

C. Granite and leucocratic granite of the Western Porphyritic Granite. Leucocratic granite is the left half of the photograph. Boundary of the two granitoids is displaced by fractures which are occupied by mylonitized micro-granodioritic dykes. Scale: length of the hammer is 33 cm.



The type I tonalitic rocks have a foliated medium to coarse grained texture with plagioclase, quartz, biotite as the major constituents.

The plagioclase is characteristically dark gray with variable grain size up to 8mm in length. The fine to medium grained biotite is commonly present as aggregates of 5 to 10mm diameter. Subsidiary hornblende is recognized in some rocks.

Pale yellowish green epidote is common; a few minor small black metamictic grains of allanite may be found.

The contact relationships of the main body to the other rocks are not obvious because of its concordant relationship to the country rocks, but the relationship between small tonalite bodies and other rocks suggests the type I tonalite of the Ord River Tonalite Suite is older than the meta-dolerite. The tonalites are cut by pegmatite veins which have dark gray plagioclase similar to that of the tonalite.

The medium grained tonalite (type II) is a leucocratic equigranular rock, consisting essentially of quartz, plagioclase, and biotite. Small amounts of garnet are found near pegmatite veins which themselves also contain garnet (Fig. 2-6B). The type II tonalite commonly encloses, migmatitically, bodies of the Fine Grained Tonalitic Rocks. The type II tonalite intrudes the type I tonalite of the suite, but is older than the meta-dolerite.

2.2.8. Western Porphyritic Granite

Coarse grained, porphyritic, augen-textured granites are present in the northwest of the Sally Downs Bore area, 2.5km to the northeast of the Sally Downs Bore (Fig. 2-3). The granites are described as the Bow River Granitoid in the Dixon Range 1:250,000 sheet (Dow and Gemuts, 1967). Although these granites have a similar appearance to the Bow River Granitoid, no direct relationship between them is known.

The granites crop out in an arch-shaped body, 3.5km long and up to 1km wide (Fig. 2-3). Several separated bodies are also present to the northwest of the Great Northern Highway. The granites conformably intrude the pelitic gneisses and amphibolites of the Tickalara Metamorphics and tonalites of the Ord River Suite.

Two varieties of granite, viz. granite and leucocratic granite, are found in the bodies (Fig. 2-6C). The leucocratic granite intrudes the granite.

The granite includes lenticular xenoliths of basic rocks, which are derived from the country rocks. The granites are cut by a mylonitic micro-granodiorite "dyke" along faults (Fig. 2-6C). Subsequently these rocks have been intruded by a thin aplitic granite.

2.2.9. Meta-dolerite

Meta-dolerite is a massive to weakly foliated fine grained basic rock which occurs only to the west of the C3 carbonate unit. The thin lenticular or sheet-like shape of the bodies is controlled by the Central Leucocratic Granite which intrudes them in the form of a number of concordant sheets. The width of the meta-dolerite varies from a few tens centimeters to several hundreds of meters. Fine grained acicular amphibole and plagioclase are the only minerals visible in hand specimen. However under the microscope, orthopyroxene is commonly present as relict crystals.

Small lenses of a light grey less metamorphosed medium grained dolerite is rarely present in the core of the bodies. However coarse grained metamorphic hornblende is occasionally found in the rock. Plagioclase, orthopyroxene, clinopyroxene, and amphibole are the major minerals in the rocks.

2.2.10. Central Leucocratic Granite

This leucocratic granite intrudes the Tickalara Metamorphics, the Ord River Tonalite Suite, and the meta-dolerite around the Sally Downs Tonalite, and also is present in the Sally Downs Tonalite as xenoliths together with other older rocks. The sheet-like bodies of the granite are mainly concordant with the surrounding rocks, and the thickness of the bodies varies from several meters to 200 meters.

The granite is foliated and fine to medium grained. The mafic mineral is fine grained biotite which commonly occurs as thin aggregates 10mm long. The feldspars are mostly fine to medium grained.

2.2.11. Hornblendite and Mela-gabbro

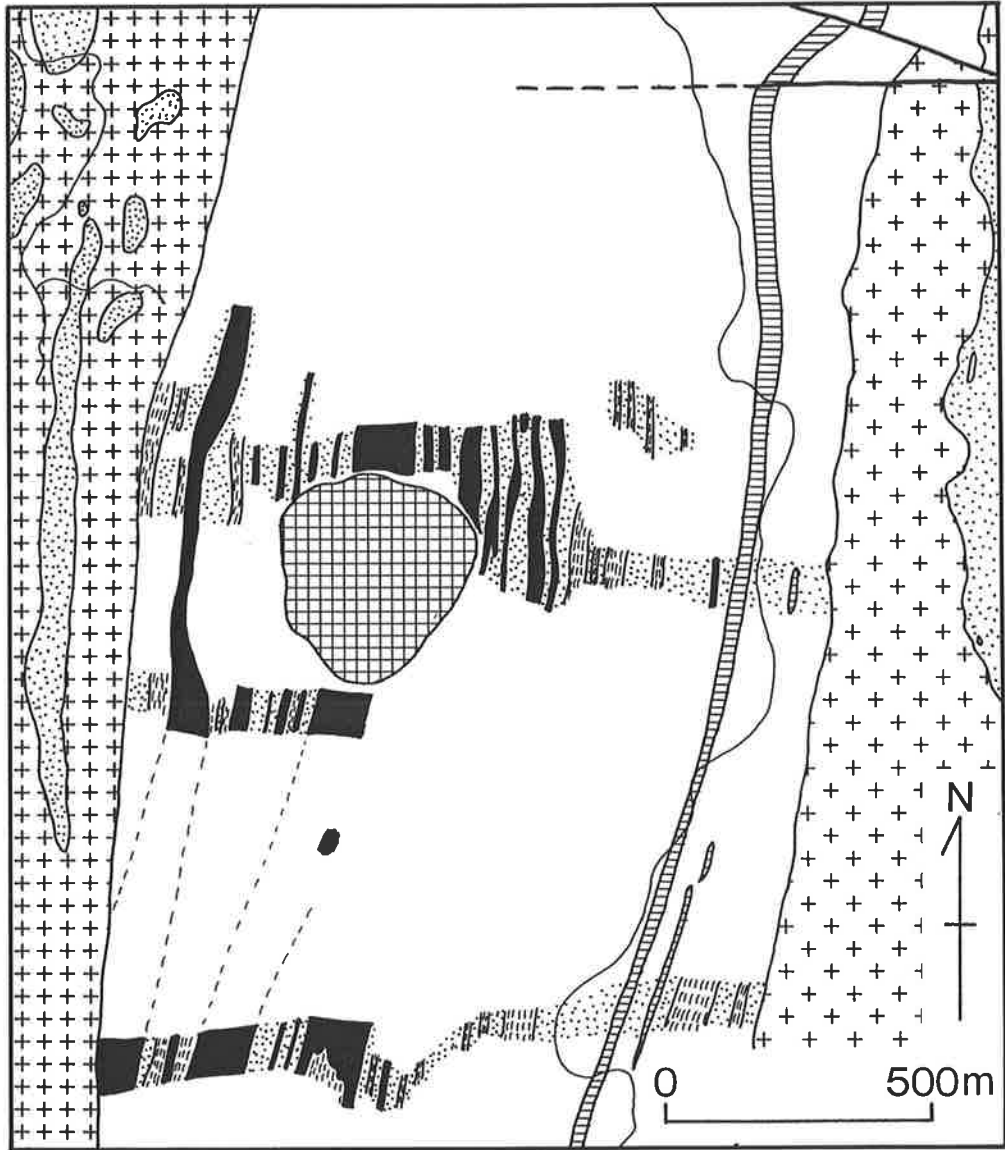
The rocks vary in composition from hornblende mela-gabbro to olivine-pyroxene hornblendite, consisting of various ratios and combinations of such chief constituents as olivine, pyroxenes, hornblende, plagioclase, and quartz.


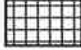

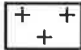
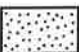


Two small olivine-pyroxene hornblendite bodies are found in the central part of the Sally Downs Bore area within the Tickalara Metamorphics and some granitoids (Fig. 2-3 and Plate 1). The southern body, which has a circular shape of 200m diameter, is situated to the south of the Sally Downs Fault between the Sally Downs Tonalite and the C3 carbonate unit. A smaller body which is 100m in diameter, is present to the north of the Sally Downs Tonalite.

Although no outcrop showing a contact relationship between the hornblendite and its surrounding rocks was observed, field mapping around the bodies suggests that the hornblendite intruded the Tickalara Metamorphics, Ord River Tonalite Suite, meta-dolerite, and Central Leucocratic Granite (Fig. 2-7).

Fig. 2-7. Geology around the hornblendite in the central part of the Sally
Downs Bore area

Interlayered occurrence of the Tickalara Metamorphics and the Central Leucocratic Granitoid is shown on the map. Tonalites of the Ord River Tonalite Suite and the meta-dolerite are not shown in the map, but are present within the interlayered complex, making a further complication for mapping. Hornblendite obviously cuts the interlayered structure, indicating that it intruded later than the Central Leucocratic Granite.



- | | | | |
|---|-----------------------------|---|-------------------------------|
|  | Sally Downs Tonalite |  | Hornblendite |
|  | Central Leucocratic Granite |  | Eastern Leucocratic Granitoid |
|  | Amphibolite |  | Carbonate rocks |
|  | Gneiss and schist | | |

The olivine-pyroxene hornblendite has a massive poikilitic texture, and is greenish black in outcrop. The oikocrysts of hornblende, up to 2.5cm in length, make up a large proportion of the rock. Variable amounts of fine to medium grained olivine, orthopyroxene, and clinopyroxene are enclosed in the hornblende.

Seven mela-gabbro and hornblendite bodies are present in the Sally Downs Tonalite as xenoliths.

Two types of the mela-gabbro, viz. olivine-orthopyroxene mela-gabbro and hornblende mela-gabbro, are found.

The hornblende mela-gabbro has coarse grained hornblende in a pale green matrix of fine grained clinopyroxene, hornblende, plagioclase, and quartz.

2.2.12. Sally Downs Tonalite

2.2.12.1. General

The Sally Downs Tonalite, is a new name for a small pluton of the Mabel Downs Granitoid Suite. It occurs in the central to southwestern parts of the Sally Downs Bore area (Fig. 2-3). The pluton is 12km long, and 2.5 to 6km wide with a north-northeasterly prolongation. The central portion of the pluton bulges westward. The pluton is well exposed in a low to moderately high rocky hill (Fig. 2-8A, B, and C), enabling a detailed field observation and sampling to be made.

The southern end of the pluton is truncated by the east-west trending Melon Patch Fault; south of the fault the displaced fragment of the pluton could not be located. The Sally Downs Fault divides the pluton into two parts; a main block and a smaller northern block.

Contacts of the pluton tend to be concordant with foliation in the country rock and in the pluton. However, a slight discordance between the margin of pluton and the trend of foliation in the country rock on the

Fig. 2-8. Field geological photographs; the Sally Downs Tonalite

A. Typical rocky exposure of the Sally Downs Tonalite

Photograph was taken 4 km east of the Sally Downs Bore, south of the track connecting the Sally Downs Bore and the Dougalls Bore. Looking to south.

B. Eastern Boundary of the Sally Downs Tonalite

Rocky hill extending from center to right of the photograph is the Sally Downs Tonalite. The area of the Tickalara Metamorphics, mainly amphibolite and gneiss, is in the lower left of the photograph, showing different topography and vegetation. Photograph was taken at the southeastern margin of the Sally Downs Tonalite pluton.

C. Areal photograph of the central part of the Sally Downs Tonalite pluton. Looking south. Upper left is southeastern margin of the pluton. White blocks are xenolithic blocks consisting of carbonate rocks.



eastern margin is manifested by their convergence southwards (Plate 1). The northwestern margin of the northern block shows evidence of movement along the contact in the form of shear zones several centimeters wide parallel to the contact.

East-west trending shear zones, which are several centimeters to several tens of centimeters wide, are present in the southern part of the pluton; dislocation is clearly manifest along some of them. Major creeks run commonly along the shear zones.

The tonalite is a weakly to moderately foliated coarse grained rock, consisting mainly of hornblende, biotite, plagioclase, and quartz. Minor amounts of epidote and rare allanite also are present. In the west of the pluton reddish brown sphene, one to two millimeters in diameter, is visible in handspecimens.

Compositionally the pluton varies from hornblende-rich basic tonalite to hornblende-free biotite tonalite. The hornblende-free biotite tonalite is commonly found in the west of the pluton. No internal contact relationship is found, though it may be present in the western part of the pluton.

Although there is the large scale compositional variation in the pluton, the tonalite is homogeneous on an outcrop scale, except for compositional layering, mafic microgranular enclaves, and xenoliths. The mafic microgranular enclaves and xenoliths are ubiquitous but the compositional layering is found only occasionally in the northern and eastern parts of the pluton. The layering is manifested by different amounts of mafic minerals, and different grain size. The thickness of the layers varies from two centimeters to 20 centimeters.

A number of epidote veins, a few millimeters wide, are found in the tonalite. Only two granite dykes cut the tonalite in the south of the body.

2.2.12.2. Xenoliths of country rock in the Sally Downs Tonalite

Numerous xenoliths and screens of country rock are present in the pluton (Fig. 2-3 and Plate 1). Generally, xenoliths of basic rocks and carbonate rocks are obvious in the field (Fig 2-8C), because of their different composition and appearance compared with the host tonalite.

A large screen of country rock, 2.5km long and 400m wide, is found in the northern block (Fig. 2-3 and Plate 1). It is composed of the Tickalara Metamorphics, the Ord River Tonalite Suite, meta-dolerite, and the Central Leucocratic Granite. Many carbonate rocks of the Tickalara Metamorphics also occur in the screen, as well as in the tonalite, as small xenoliths. At least one traceable horizon of the carbonate rocks is recognized along the northern edge of the screen.

A large number of the screens and xenoliths, which range from several centimeters to 3km in length, are present in the eastern part of the main body. These include two large carbonate xenoliths, both about 800m long, which are found in high white prominent outcrops. In the west of the main body, four large xenoliths are found. An arch-shape embayment of the country rock is present in the northwest of the main body. It is 2.5km long and 400m wide, and is composed of granitoids, metasediments, and meta-dolerite. In the southern part of the pluton, only rare small xenoliths are observed.

The shape of the xenoliths in general is largely controlled by the original lithological layering or schistosity, and even original lithology can be traced from one xenolith to another (Fig. 2-3 and Plate 1). Such a relationship between xenoliths in the granitoid is called "Ghost stratigraphy or structure" (Pitcher, 1970), and similar relationships are well described in the Thorr pluton of Donegal, Ireland (Pitcher and Berger, 1972).

Boundaries between xenoliths of meta-dolerite and the host tonalite are commonly sharp (Fig. 2-9A). Occasionally the boundaries are emphasized by a thin quartzo-feldspathic fringe; quartzo-feldspathic veins which penetrate the xenolith are connected to these (Fig. 2-9B and C); the veins do not extend further into the host tonalite. These quartz-feldspathic fringes and veins are thought to possibly represent a late phase activity of the tonalite intrusion, at a stage when the magma had crystallized most of its mafic minerals and plagioclase but interstitial quartz-feldspathic liquid is still present. Movement of a xenolith relative to the host tonalite, or development of a crack in the xenoliths at this stage, might facilitate the squeezing out the quartz-feldspathic liquid from the tonalite and its injection into a space, such as contact between xenolith and host, or fractures.

Most of the meta-dolerite xenoliths are angular in shape. Elongated xenoliths have the long axis aligned parallel to the foliation of the tonalite (Fig. 2-9A). Initial brittle fracturing of the meta-dolerite into small pieces is thought to have taken place.

Xenoliths of metasediments and granitoids in contrast have a lenticular shape. These were more ductile than the meta-dolerite during intrusion of the tonalite.

The sharp boundaries between the xenoliths and the tonalite implies that reaction between them was insignificant, indicating that the tonalite magma is not derived by in situ anatexis, or granitization.

The arch-shaped embayment of country rock in the tonalite (Fig. 2-3), and a similarity of the lithology of the xenoliths to the nearby country rock, however, indicates that these incorporated bodies did not move far relative to their original position.

The rejection of the in situ anatexis hypothesis despite the closeness of the xenoliths to the original position suggest that a restite model (White

Fig. 2-9. Field geological photographs; xenoliths of meta-dolerite in the Sally Downs Tonalite.

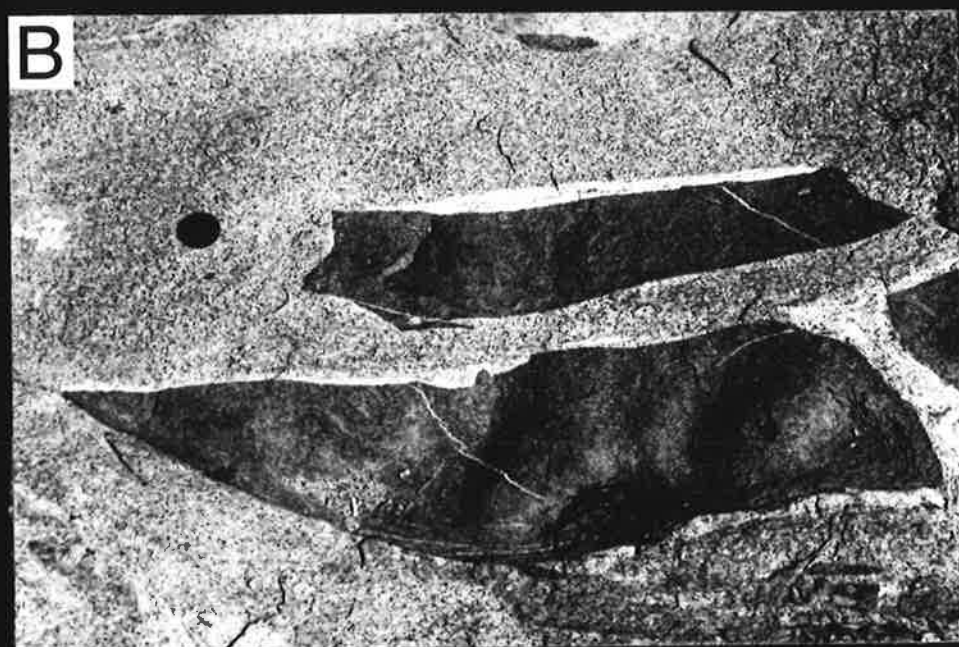
A. Meta-dolerite xenolith swarm in the Sally Downs Tonalite. Photograph is taken 6 km east of the Sally Downs Bore. The photograph depicts the location of sample 51505, which is shown in Fig. 3-5.

A hammer in the center left of the photograph is 33 cm long.

B. Boundaries between the meta-dolerite xenoliths and the tonalite are emphasized by a thin quartzo-feldspathic fringe to the xenoliths. Enlarged photograph of central part of photograph A.

Scale: diameter of a lens cap is 5 cm.

C. Meta-dolerite xenolith and quartzo-feldspathic fringe. A quartzo-feldspathic vein, penetrating the meta-dolerite xenolith is connected to the fringe. The xenolith and host tonalite are cut by slightly younger tonalite vein. Photograph was taken at the same location as photograph A. Scale: 5 cm long.



and Chappell, 1977) for the origin of the xenoliths is not valid here. The restite model postulates that xenoliths represent the residuum of partial melting or anatexis, and these are incorporated in to the melt, and together mobilized and transported from a source region (White and Chappell, 1977). White et al. (1974) also show an example of xenoliths of country rock in a granite, which are restricted to the immediate vicinity of a contact and which are distinct from restite. In the Sally Downs Tonalite, the xenoliths of the country rock are scattered throughout the pluton such as one might expect in a mobilized anatectic granite. The abundance of xenoliths, however, is taken to indicate that the present erosional level of the pluton is very close to a roof or floor of the pluton. The presence of large screens and xenoliths is likely to be the expression of an irregularly shaped top or bottom of the pluton.

This irregularity can be explained, at least in part, by local passive stoping (Pitcher, 1970). However, it does not mean that the entire volume of the pluton is created by the stoping mechanism.

Simultaneous intrusions of two tonalite sheets may also create a screen of the country rock, as in the northern block of the pluton.

2.2.12.3. Mafic microgranular enclaves in the Sally Downs Tonalite

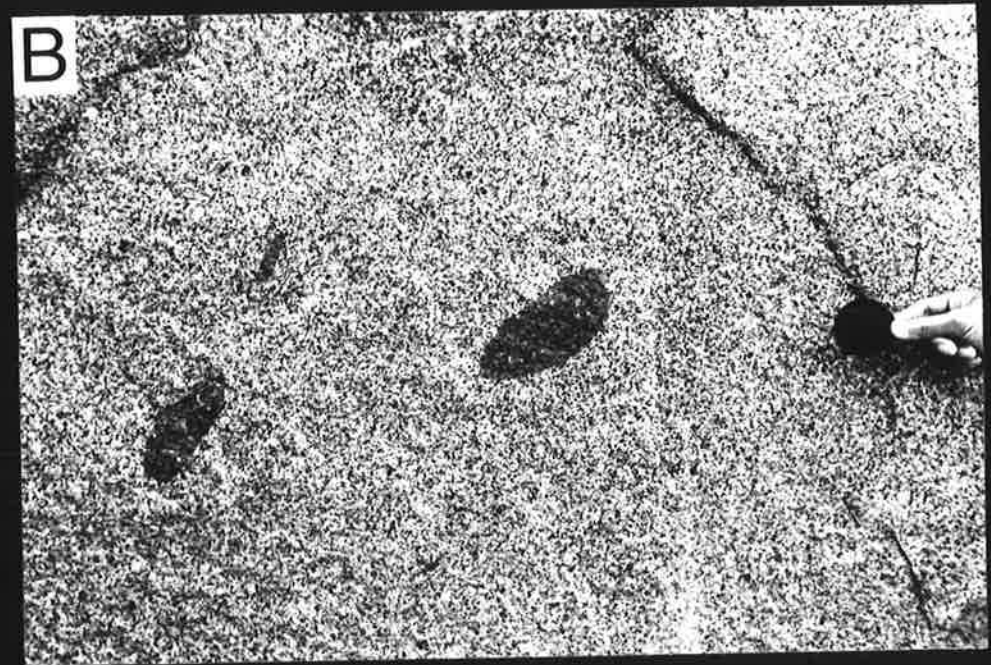
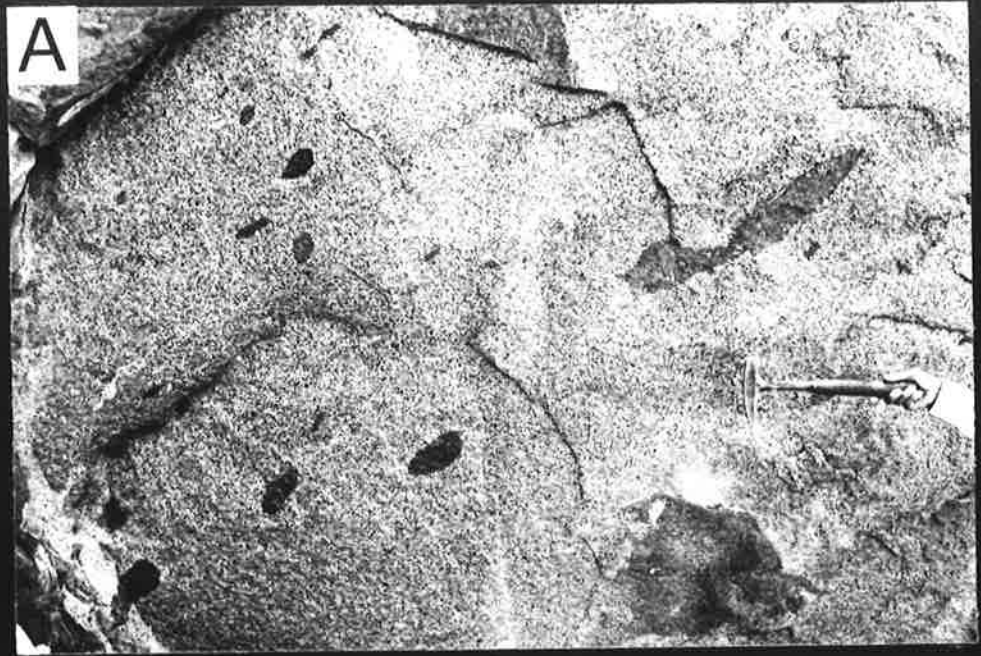
The pluton is characterized by the ubiquitous presence of mafic microgranular enclaves which are generally fine grained and quartz dioritic in composition (Fig. 2-10A and B). The shape of the mafic microgranular enclaves varies from circular to lenticular. The mafic microgranular enclaves are significantly elongated near the margin of the pluton. The size of the enclaves ranges from several centimeters to one meter long for lenticular varieties, and several meters long for the elongated types. Occasionally, large blocks of the mafic microgranular enclave are found (Fig. 2-10C).

Fig. 2-10. Field geological photographs; mafic microgranular enclaves in the Sally Downs Tonalite

A. Typical mafic microgranular enclaves. Size of the typical enclaves ranges from several cm to 10 cm. Scale: length of a hammer is 33 cm.

B. Enlarged photograph of A, showing typical slightly elongated enclaves. Margins of the enclaves are not sharp. Scale: diameter of lens cap is 4.5cm.

C. Large blocks of mafic microgranular enclave.
Scale: length of a hammer is 33 cm.



Most of the mafic microgranular enclaves are melanocratic rocks consisting of fine to medium grained hornblende, biotite, plagioclase, and minor quartz; coarse grained plagioclase phenocrysts are occasionally present.

The margins of the mafic microgranular enclaves (Fig. 2-10B) are not sharp compared to those of the meta-dolerite xenolith (Fig. 2-9B).

The mafic microgranular enclaves generally occur sporadically within the tonalite, but swarms of the enclaves are present in some places. In the northwest margin of the pluton, a two meter wide inclusion swarm is found (Fig. 2-11 A). Within the swarm, the shape and composition of the mafic microgranular enclaves vary, and on these bases can be grouped into three types. One type of mafic microgranular enclaves is lenticular with a long to short axis ratio about 4:1 (Fig. 2-11 C), and minor plagioclase phenocrysts. The second type is a tabular enclave with long to short axis ratio of 15:1 (Fig. 2-11 B). Enclaves of this type have many plagioclase phenocrysts. The third type is a thin layer of mafic rock whose long to short axis ratio is about 50:1 (Fig. 2-11 A and C). It appears that the mafic microgranular enclaves are more elongated near the margin of the swarms. It is likely that the wide range in the length to breadth ratio of the enclaves within the swarm results from different physical properties of the enclaves, rather than locally different stresses.

The orientation of the mafic microgranular enclaves are mostly parallel to the orientation of the swarms. Those orientations are parallel to the mineral orientation of the host tonalite.

2.2.12.4. Syn-plutonic basic dyke in the Sally Downs Tonalite

A type of basic rock found in the northern part of the main block of the tonalite pluton (see Fig. 3-20 for location) has intrusive relationships with the tonalite which are somewhat enigmatic (Fig. 2-12 A). The basic

Fig. 2-11. Field geological photographs; a swarm of mafic microgranular enclaves in the Sally Downs Tonalite

A. A swarm of mafic microgranular enclaves. The location of the enclave swarm is 5.5 km northeast of the Sally Downs Bore, along the northwestern margin of the northern block of the Sally Downs pluton. Variable size and aspect ratio of the enclaves are observed within the swarm. Looking to north. Scale: length of a hammer is 33 cm.

B. Tabular mafic microgranular enclaves and strongly elongated mafic microgranular enclaves in the swarm. Close up photograph of central part of the photograph A. Looking to south. See text for discussion of the shape of the enclaves. Scale is 5 cm long.

C. Lenticular mafic microgranular enclave in the swarm. Close up photograph of lower left part of the photograph A. Looking to northeast. Scale is 5 cm long.

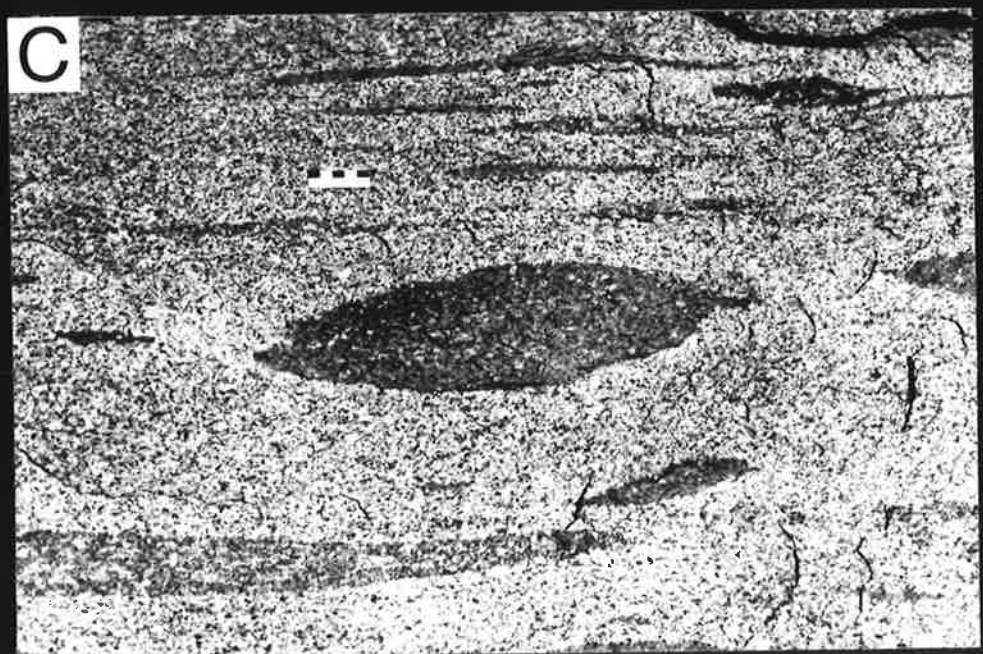
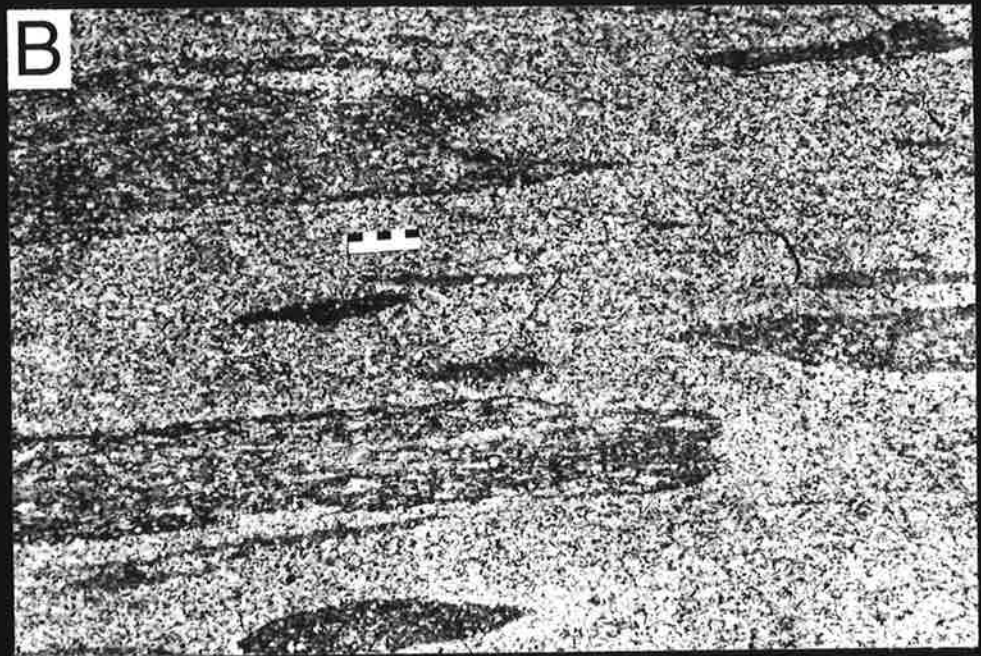
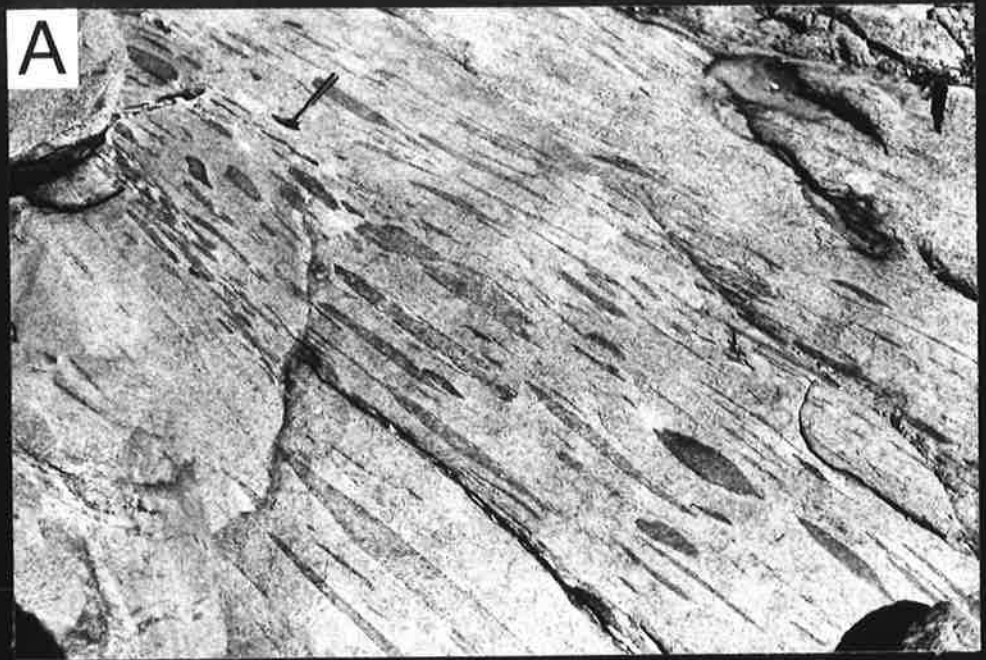


Fig. 2-12. Field geological photographs; syn-plutonic basic dyke in the
Sally Downs Tonalite

A. Outcrop of syn-plutonic basic dyke in the Sally Downs Tonalite

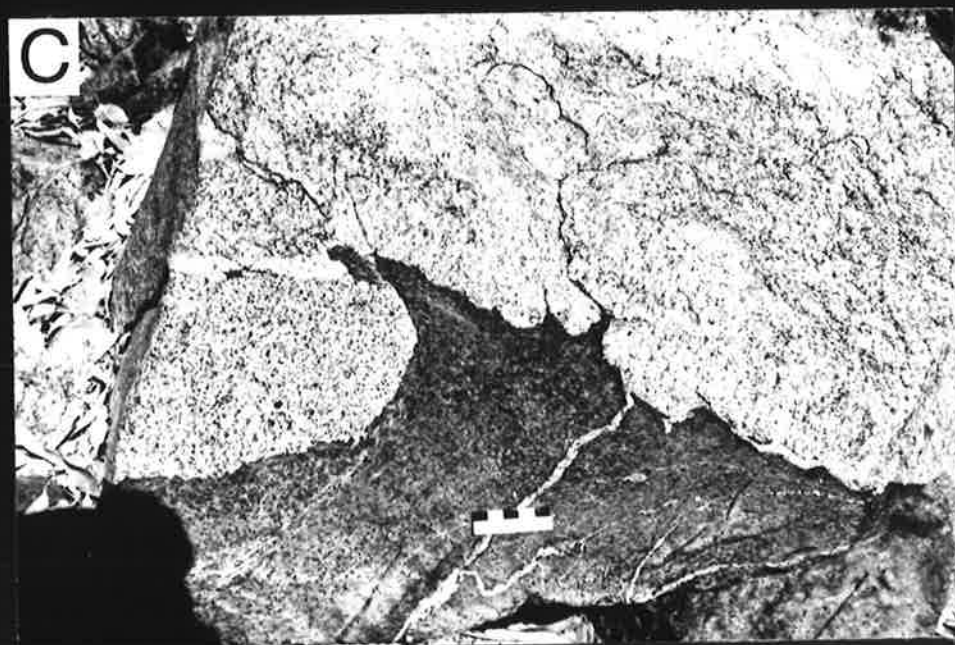
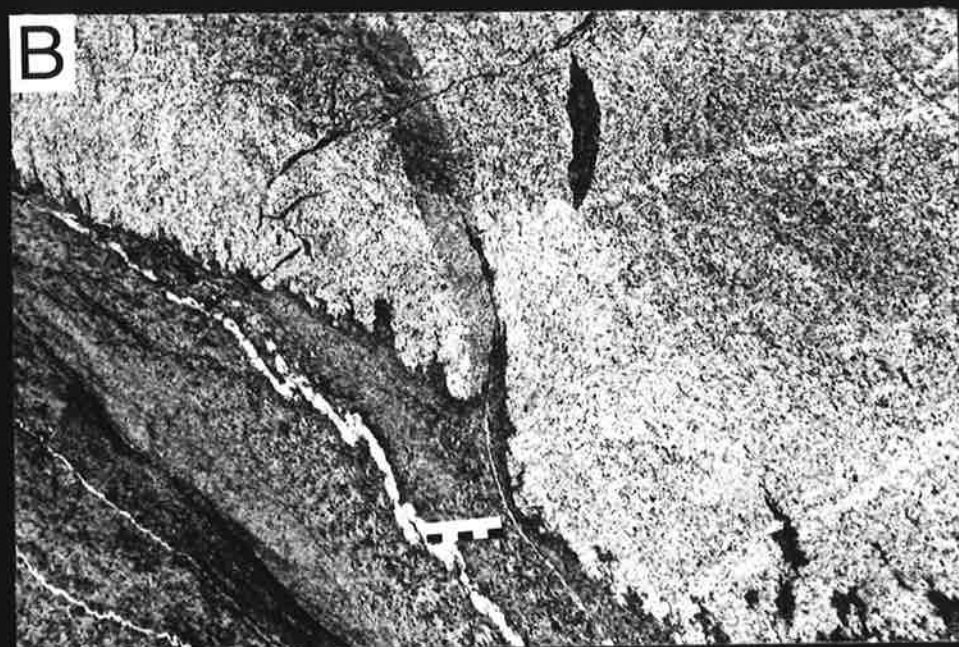
Scale: length of a hammer is 33 cm.

B. Close up of central part of photograph A. Syn-plutonic basic dyke intruded into the tonalite. Contact between the dyke and tonalite is typically "saw toothed".

Scale is 5 cm long.

C. Contact relationship between the syn-plutonic basic dyke and the tonalite. The syn-plutonic basic dyke is back-veined by the host tonalite. See tonalite vein cutting basic dyke near the scale.

Scale is 5 cm long.



rock is fine grained, and amphibole-rich. Coarse grained rims against the tonalite, about one centimeter wide, are present in places. These may be the result of reaction between the basic rocks and the host tonalite. The basic rock is several meters wide and less than ten meters long; the long dimension lies oblique to the foliation in the tonalite and in places appears to cut some of the mafic microgranular enclaves at right angles (Fig. 2-12 B). The evidence suggests that the basic rock intruded the tonalite. However, the basic rock is also "back-veined" by the host tonalite (Fig. 2-12 C). The veins in the basic rock are quartzo-feldspathic, but contain rare hornblende crystals. The veins are continuous into the tonalite.

The above relationships suggested that the basic rock intruded the tonalite at a stage when the tonalite was solid enough to be fractured and allow intrusion of the basic rock but warm enough and fluid enough to be capable of "back-veining" into the basic rock, or when the tonalitic magma was largely crystallized but still had some interstitial low temperature liquid of quartz-plagioclase peritectic composition.

The contact between the basic rock and the host tonalite is typically "saw toothed" (Fig. 2-12 B), manifesting the development of foliation in the tonalite. This is an indication that the foliation is at least partly developed after the emplacement or incorporation of the syn-plutonic basic dyke.

If a basic magma has been present during or shortly after the emplacement of the tonalite, the relationship between the basic magma and tonalite has important implications for the petrogenesis of the host tonalite. Alternatively it is possible that the basic dykes represent remobilized, or partially melted, older basic rocks, such as amphibolite of the Tickalara Metamorphics, or meta-dolerite, but this is not considered so likely.

2.2.13. Granite Dyke in the Sally Downs Tonalite

A thin granite dyke, up to two meters wide, intrudes the Sally Downs Tonalite in the south of the pluton (see location in Fig. 3-20), and it also cuts the Central Leucocratic Granite. The granite dyke is apparently the youngest granitoid in the Sally Downs Bore area.

It is a medium grained, leucocratic, biotite granite. The petrology and geochemistry of the granite have been examined in this study. However, no further detail discussion is given in this thesis, as it has limited occurrences. The whole rock geochemistry of the granite is listed in Table A4-11.

A similar granite is found 700m further south, associated with a pegmatite.

2.3. Structural Relationships in the Sally Downs Bore Area

2.3.1. Introduction

Lithologies and intrusive relationships have been presented above. It is also essential to understand time relationships between deformations, and igneous activities and metamorphisms, and these are now described.

Dow and Gemuts (1969) described two episodes of intense deformation resulting in tightly folded Tickalara Metamorphics and Halls Creek Group. They considered that the second deformation episode coincided with the major period of metamorphism. However, as a result of the present work, three regional deformations are recognized in the Sally Downs Bore area. Intrusion of the Sally Downs Tonalite postdated those deformations. Subsequent faulting followed the intrusion of the tonalite.

Because the area is dominated by granitoid bodies, many of the structural data have been obtained from these granitoids. Hence, a brief review and discussion of the interpretation of the structural elements

found within the granitoids is given before a description of the structural relationships of the area.

2.3.2. Review and Discussion of the Interpretation of the Structures in the Granitoids

Granitoid plutons commonly show preferred orientation of a variety of components (see further, below), and there is still much controversy with regard to their interpretation (e.g. Pitcher, 1979; Paterson et al., 1989; Paterson et al., 1991). In the circum-Pacific region (especially in U.S.A.), such an internal structure of the Mesozoic plutons is often understood as a magmatic flow structure, and is used as an indication of the intrusive mechanism (Cloos, 1932; Compton, 1955; Lipman, 1963; MaColl, 1964). Such a point of view was discussed in Balk's classic volume (Balk, 1937). On the other hand, in regions where Precambrian granitoids and gneisses are exposed, the structure of the granitoids is often described as having been caused by regional deformation. Multiple deformations commonly have taken place in such regions, thus it may not be possible to distinguish easily an original flow structure, if any, from a structure resulting from later deformations.

Possible origins of structure in granitoids and their time relationships to a cooling history are discussed, and criteria to distinguish them are considered.

Regional deformation is an obvious possible cause of the development of the structure in the granitoids. Magmatic flow is an alternative possibility (Balk, 1937), although not much information on the physical properties of granitoid magmas during intrusion is available. Intrusion-induced deformation, named by Pitcher (1979), results from the injection of a magma, and involves the outward and upward expansion of the country rock and of the granitoid itself, like a balloon. The

mechanism has been recognized by a number of workers (e.g. Martin, 1953; Akaad, 1956; Davis, 1963; Nelson and Sylvester, 1971; White, 1973; Gastil, 1979; Holder, 1979). The intrusion-induced deformation can be divided into two types, I (internal) type and E (external) type. When the deformation of the structure in a granitoid pluton is caused directly by an injection of its own magma, or a consanguineous magma intruded essentially synchronously in the same pluton, the mechanism is classified as I type intrusion-induced deformation. On the other hand, the deformation of a granitoid pluton by another magma body is an E type intrusion-induced deformation, a concept that was suggested by Gastil (1979).

Paterson et al. (1989 and 1991) reviewed the criteria for the identification of magmatic and tectonic foliations in granitoids, and they concluded that foliations in granitoids can form by magmatic flow, submagmatic flow, high-temperature solid-state deformation and moderate- to low-temperature solid-state deformation. Although the classification of the foliation-forming mechanisms is based on the physical criteria of foliations, a consideration of origin of the flow and deformation of the granitoids is also important to understand the significance of the foliations in the granitoids with relation to the regional tectonics. The submagmatic flow and high-temperature solid-state deformation could be found during the intrusion-induced deformation.

The history of the emplacement and cooling of a granitoid pluton is considered in three stages to facilitate the understanding of its physical properties in relation to the country rocks. Stage 1 of the granitoid emplacement is up to the time the liquid magma has solidified completely. Stage 2 is a period which starts from the end of stage 1 and continues until the pluton has finally cooled to a regional geothermal temperature. Stage 3 follows stage 2; no significant thermal difference between the

granitoid and country rocks exists. Hibbard (1987) described the deformation of incompletely crystallized magma systems, and showed that slightly different deformation styles were related to the difference in crystal/melt ratio in the stage 1.

Table 2-1 shows combinations of the above mechanisms and timing, and possible structural patterns within a pluton in relation to the structure of the country rocks, and to the overall trend of the contact of the pluton.

In the granitoids, structures are defined by preferred orientations of the following elements:

minerals (e.g. biotite, hornblende, feldspars)

mafic microgranular enclaves

mafic clots or aggregates

schlieren

xenoliths of country rocks.

The preferred orientations of the minerals and mafic microgranular enclaves are frequently observed, but orientations of schlieren may show some discordance to that of the other elements.

The regional deformation would create a penetrative foliation, hence the structural pattern in a pluton is likely to be basically conformable to the country rocks. However, there may be some differences which are caused by different physical properties of the pluton and country rocks. When a regional deformation takes place during stage 1 of the pluton (R1 structure of Table 2-1), the pluton can be called a syn-tectonic granitoid with regard to the regional deformation. Similarly, if the pluton is subjected to the deformation during stage 2 (R2) or 3 (R3), it is called a pre-tectonic granitoid. Therefore the structure of a post-tectonic granitoid must be due to some other mechanism, e.g. intrusion-induced deformation or magmatic flow.

Table 2-1. Development of structure in the granitoid

MECHANISM		STAGE OF EMPLACEMENT OF GRANITOID MAGMA		
		Stage 1 (Liquid magma or crystal mush)	Stage 2	Stage 3 (Cooled to regional geothermal level)
		Solidus		
Regional deformation		R1 (C, n)	R2 (C, n)	R3 (C, n)
Intrusion- induced deformation	I type	I1 (N, P or n)	I2 (N, P or n)	I3 (N, P or n)
	E type	E1 (C or N, n)	E2 (C or N, n)	E3 (C, n)
Magmatic flow		F1 (N, P)	F2 (N, P)	F3 (N, P)

1. Structural relationship between a pluton and the country rock.

C ; conformable (foliations and lineations of the pluton and country rock show same orientation)

N ; not necessarily conformable

2. Angular relationship between foliation within a pluton and trend of the contact

P ; conformable (foliation in the pluton is parallel to the contact of the pluton)

n ; not necessarily conformable

Comments

R1 ; Crystallized during regional deformation (syn-tectonic)

R2 ; Regional deformation after crystallization of granitoid magma, but the granitoid is still warmer than country rocks. Thus the granitoid deforms more easily.

R3 ; Regional deformation after the cooling of granitoid to regional geothermal level, no significant structural difference between granitoid and country rock

I1 ; Deformed by continuous injection of magma of the same pluton.

I2 ; Cooled to lower than the solidus temperature then deformed by magma itself or by lower temperature melt of same magma (more acidic magma)

I3 ; May not be possible. In the case of a mantled gneiss dome it may be a possible mechanism but it needs a special high thermal gradient in the pluton.

E1 ; Deformed by the second intrusion during the stage 1.

E2 ; Intrusion-induced deformation after solidification but the pluton is still warm some degree. A second pluton which imposed the foliation may be derived from completely different magma.

E3 ; Intrusion-induced deformation after cooling the granitoid.

F1 ; Flow of magma which is liquid or liquid with minerals.

F2 ; Granitoid may flow.

F3 ; Same as F2.

The situations I3, F2, and F3 of Table 2-1 are unlikely to develop structures in the granitoid, except in the case of a mantled gneiss dome (Eskola, 1949), or due to other special conditions.

Foliation in a granitoid, caused by the E type intrusion-induced deformation, will be conformable with that in the country rocks, a relationship similar to that due to regional deformation. Examination of the structural pattern in and near the initial granitoid will give information with regard to the position of a second pluton which imposed the foliation on the granitoid and country rocks. For example a concentric pattern may be present around the second pluton. In such a case, it may be possible to distinguish E type intrusion-induced deformation from regional deformation.

The regional deformation and E type intrusion-induced deformation will affect a pluton which already has a structure, so an overprinting may result. Indeed within the same stage the effect of any mechanism may be present in association with the effect of another mechanism. For example, I type or E type intrusion-induced deformation may be combined with the local effect of magmatic flow, or with regional deformation on a broader scale.

Structural patterns resulting from I type intrusion-induced deformation differ due to a range in ductility contrast between the pluton and country rocks. The relationships are discussed by Berger and Pitcher (1970). If the ductility of the pluton is greater than that of the country rock, the pattern will be conformable to the shape of the contact. If the ductility contrast is low, a cross-cutting fabric will occur. Holder (1979) studied in detail the process of deformation in and around the Ardara pluton in Donegal, Ireland. The pluton was earlier described by Akaad (1956). Holder (1979) determined variation of finite strain within the pluton by measuring shapes of contained xenoliths. The deformation

process and emplacement mechanism were quantitatively modeled by applying Ramsay's balloon model (Holder, 1979).

The magmatic flow causes a structural pattern conformable to the shape of the contact to be developed. Some of the criteria which Balk (1937) uses to distinguish his primary structure from secondary ones may be still applicable, viz. that for the primary structures, the strike and dip of the foliation may locally vary over short distances, and the foliation planes wrap around xenoliths.

Lineations also are found in a granitoid which is produced by either deformation or magmatic flow. However, depending on the physical state of the magma, the magmatic flow will produce lineations either parallel or perpendicular to the flow (Berger and Pitcher, 1970). Unless its physical state is known, their significance remains questionable.

The degree of preferred orientation may vary in the granitoid pluton. Commonly, it increases progressively toward the margin of the pluton. Such a variation can be produced by either the intrusion-induced deformation or magmatic flow, but not by regional deformation if the granitoid is reasonably homogeneous.

Petrographic observations of the structural elements provide additional information. As mentioned by Pitcher (1979), the weak orientations of minerals and schlieren can indicate an early stage of viscous flow without plastic deformation during crystallization. The main criterion of magmatic flow suggested by Paterson et al. (1989) is the preferred orientation of primary igneous minerals that show no evidence of plastic deformation or recrystallization, either of the aligned crystals or of interstitial minerals. Paterson et al. (1989) suggested that this criterion is strongest where the oriented mineral is euhedral K-feldspar or plagioclase because feldspars generally do not grow as euhedral crystals in unmelted metamorphic rocks.

The preferred orientation of aggregates of small mafic minerals in a granitoid may suggest that deformation was associated with recrystallization in the rocks.

Hence, an examination of the structural pattern in and around a granitoid pluton, assisted by petrographical study, will give possible mechanisms for its development, and the time relationship between intrusion and deformation events.

2.3.3. Structural Map and Structural Subarea of the Sally Downs

Bore Area

The planar and linear structural features in the area have been mapped and are presented in Plate 2.

The mapped area has been divided into 14 subareas (Fig. 2-13) based on structural styles and lithological associations. These subareas were defined to facilitate description and analysis of the structural features.

Three eastern subareas, E₁, E₂, and E₃, comprise the following rock suites; Tickalara Metamorphics, Dougalls Granitoid Suite, and Eastern Leucocratic Granitoid Suite.

Three central subareas, A₁, A₂, and A₃, are situated between the Sally Downs Tonalite pluton and C3 carbonate unit. These subareas consist, essentially, of the Tickalara Metamorphics, Ord River Tonalite Suite, and Central Leucocratic Granite.

Three western subareas, W₁, W₂, and W₃, are the areas to the northwest and west of the Sally Downs Tonalite pluton. A similar lithological association to that of the central subareas is present in these areas, though subarea W₁ includes also the Western Porphyritic Granite.

The Sally Downs Tonalite pluton, the largest rock unit in the Sally Downs Bore area, has been divided into five structural subareas. Subarea T₁ corresponds to the northern block of the pluton. Subarea T₂ is an

Fig. 2-13. Stereo plots of structural data for the Sally Downs Bore area

(1). Subareas of plotted structural data in the Sally Downs Bore area.

Thick lines are boundaries of subareas. Names of subareas are indicated.

Major granitoids are indicated with gray.

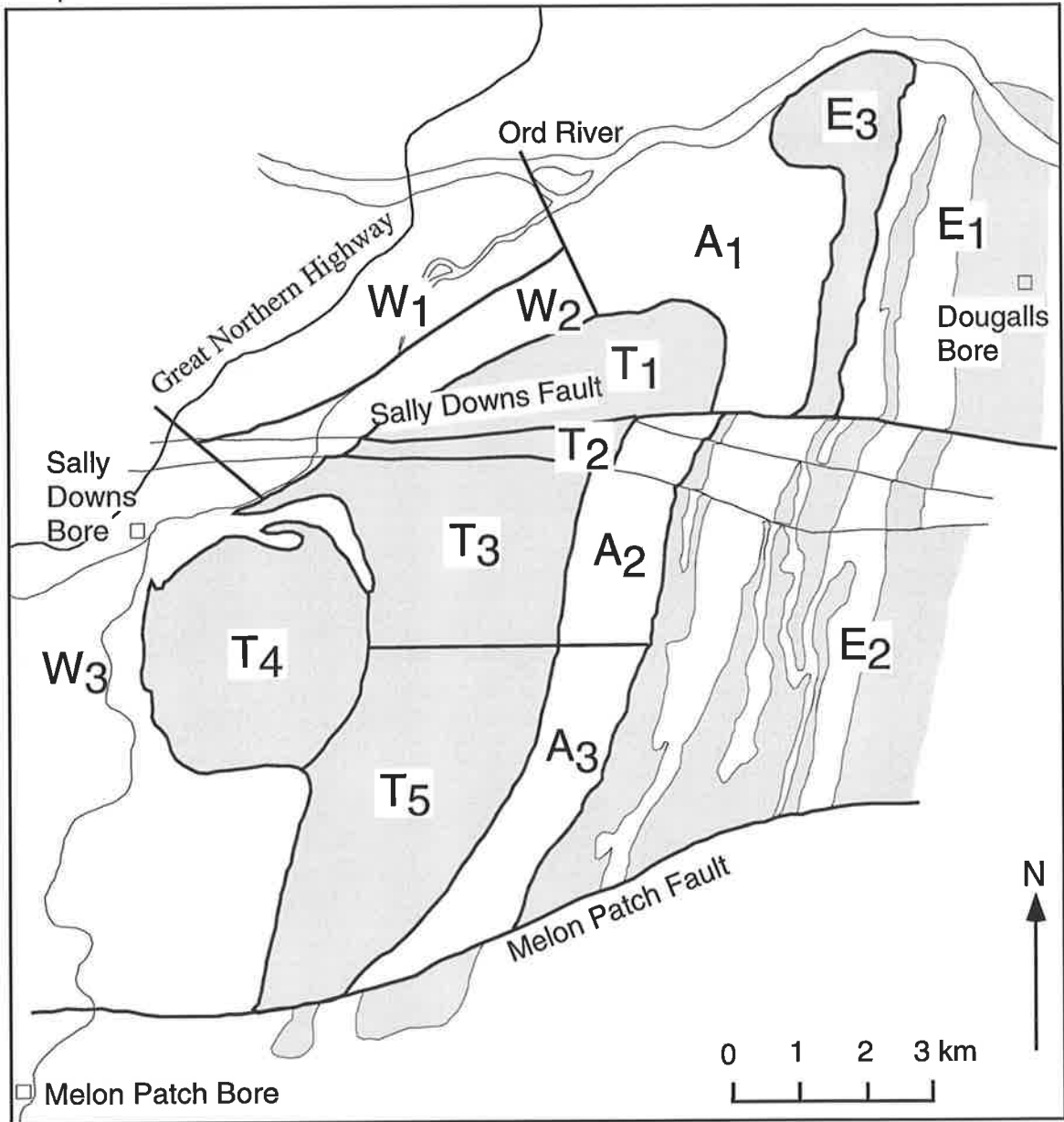
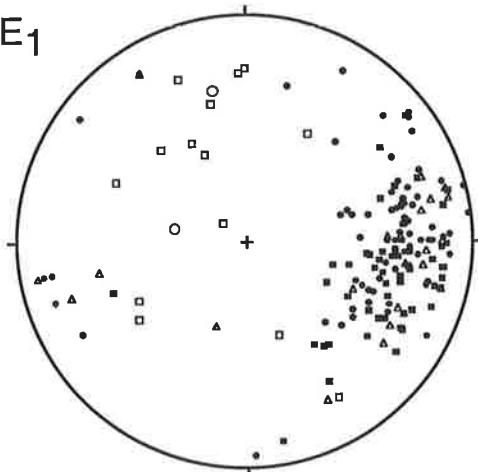


Fig. 2-13 (2). Stereo plots of the structural data for subareas E₁, E₂, E₃, A₁, A₂, and A₃.

Stereo plot: equal area projection (Schmidt projection)

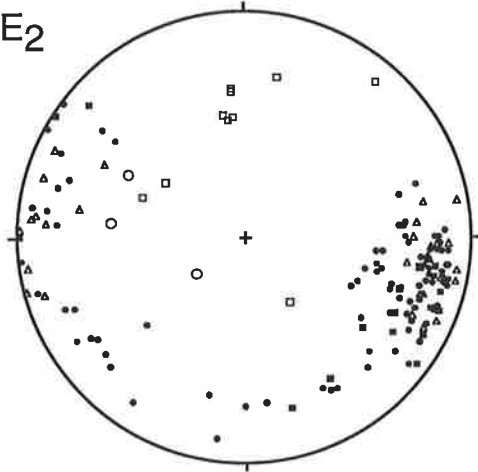
S-Gr is foliation in the granitoids. N is number of plotted data.

A. E₁



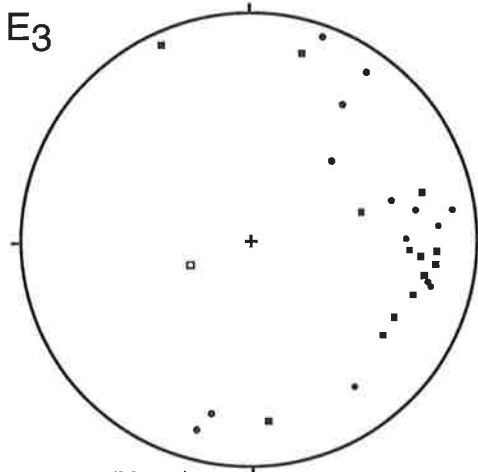
▪:S0(N=55) ▲:S-Gr(N=23)
 •:S1(N=69)
 ◻:L1(N=14) ○:L2(N=2)

B. E₂



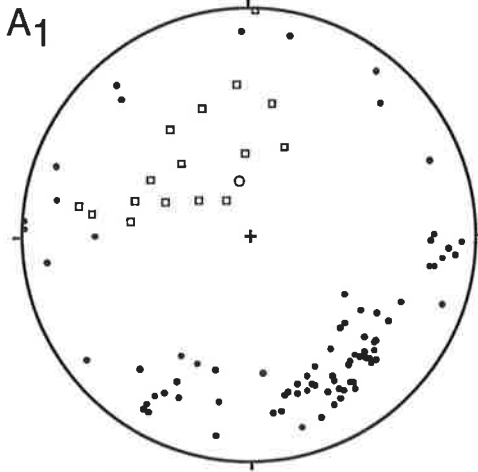
▪:S0(N=19) ▲:S-Gr(N=32)
 •:S1(N=85)
 ◻:L1(N=10) ○:L2(N=3)

C. E₃



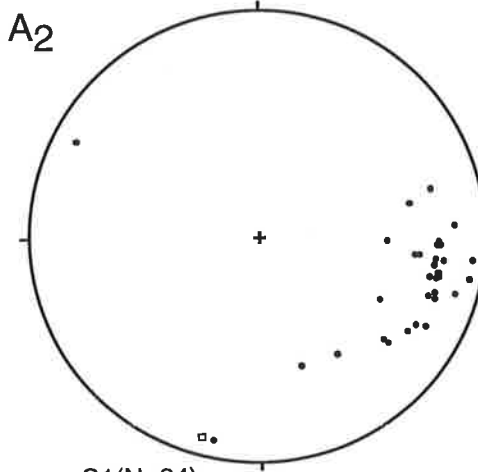
▪:S0(N=13)
 •:S1(N=14)
 ◻:L1(N=1)

D. A₁



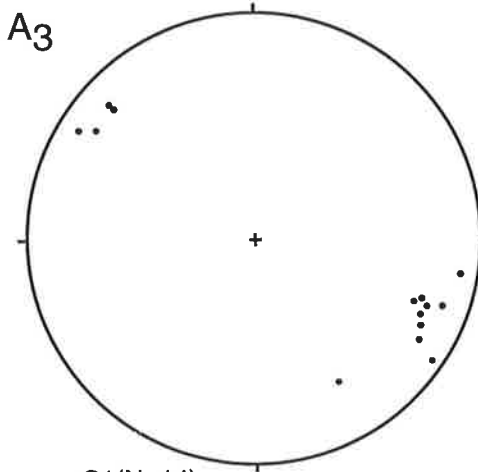
•:S1(N=84)
 ◻:L1(N=16) ○:L2(N=1)

E. A₂



•:S1(N=34)
 ◻:L1(N=1)

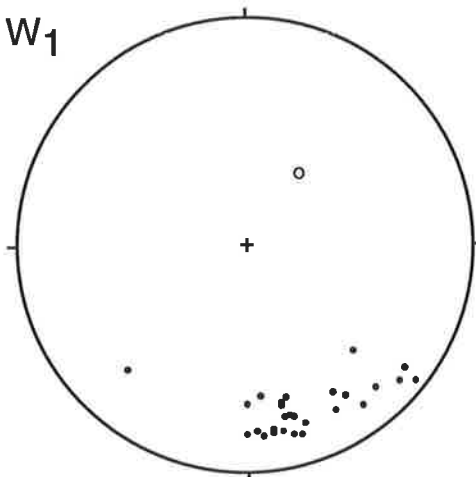
F. A₃



•:S1(N=14)

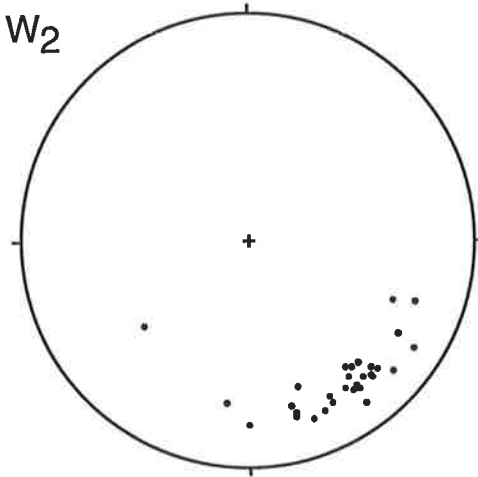
Fig. 2-13 (3). Stereo plots of the structural data for subareas W₁, W₂, and W₃.

G. W_1



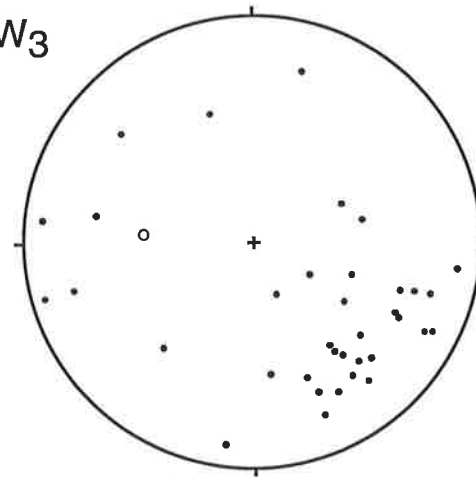
•:S1(N=27)
○:L2(N=1)

H. W_2



•:S(N=30)

I. W_3

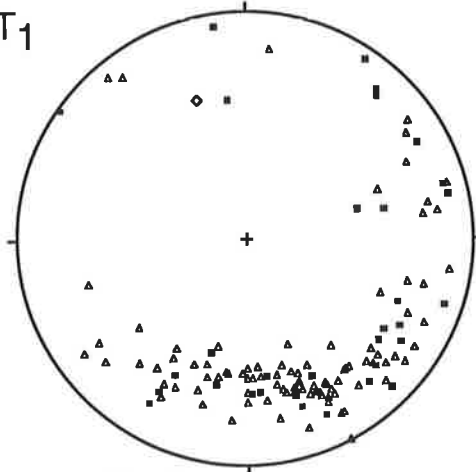


•:S1(N=36)
○:L2(N=1)

Fig. 2-13 (4). Stereo plots of the structural data for subareas T1, T2, T3, T4, and T5.

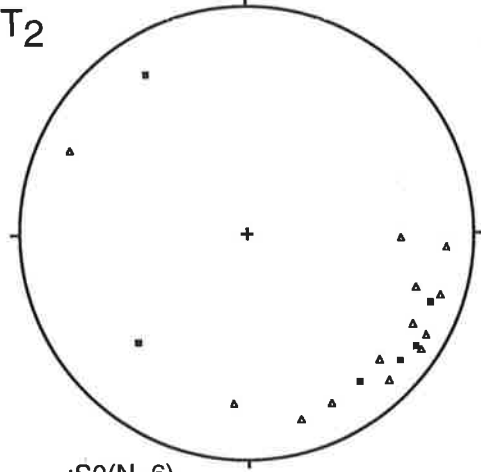
S-Gr and L-Gr are foliations and lineations, respectively, in the Sally Downs Tonalite. S0 is foliation or layering of the xenoliths in the Sally Downs Tonalite.

J. T₁



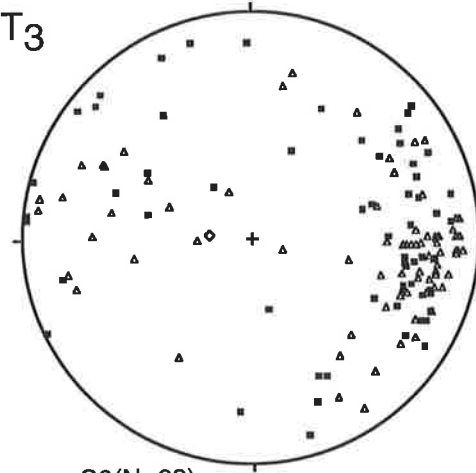
■:S0(N=30)
▲:S-Gr(N=93)
◆:L-Gr(N=1)

K. T₂



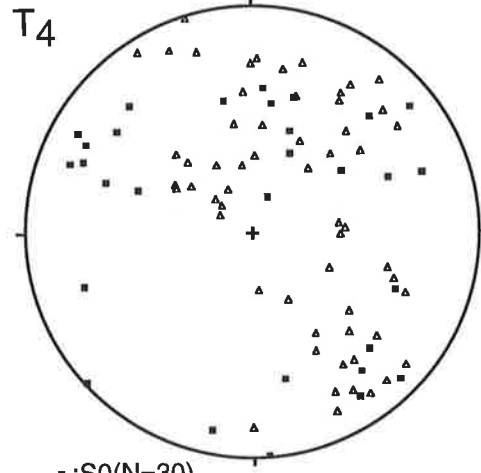
■:S0(N=6)
▲:S-Gr(N=13)

L. T₃



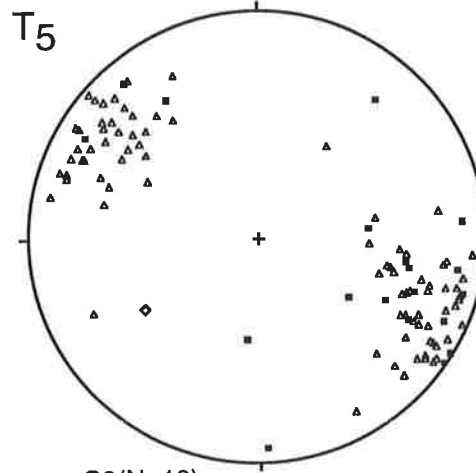
■:S0(N=63)
▲:S-Gr(N=76)
◆:L-Gr(N=1)

M. T₄



■:S0(N=30)
▲:S-Gr(N=58)

N. T₅



■:S0(N=19)
▲:S-Gr(N=86)
◆:L-Gr(N=1)

area along the Sally Downs Fault. This area is excluded from analysis in association with other subareas because the structures are influenced by the fault. Subareas T3, T4, and T5 are northern, western, and southern parts of the main body, respectively, south of the Sally Downs Fault (Fig. 2-13).

Stereographic projections of the structural elements for each subarea are shown in Fig. 2-13. The stereographic projections are equal area projections (Schmidt nets).

2.3.4. Eastern Part of the Sally Downs Bore Area

The lithological boundaries (S₀) and penetrative schistosity (S₁) characterize the Tickalara Metamorphics of the eastern subareas. F₁ folding event is indicated by mesoscopic scale isoclinal and intrafolial folds.

In the Eastern Leucocratic Granitoid Suite, a strong and streaky foliation, manifested by elongated aggregates of biotite, is characteristically present. The foliation is conformable to the foliation in the country rocks, and at the eastern margin of the northern end of the granitoid body, an angular relationship of the foliation to the contact of the granitoid was found. Therefore regional deformation is most likely to be the origin of the foliation in the granitoid. Because the foliation is folded by F₂ and F₃, the deformation is D₁. Hence the granitoid was emplaced pre-D₁ or syn-D₁.

The Dougalls Granitoid Suite has similar structural features to those of the Eastern Leucocratic Granitoid Suite. Thus the granitoid suite is considered to be pre-D₁ or syn-D₁.

In subarea E₁, the orientations of S₁ show only a small spread, striking north-south and dipping 50-70° west. F₂ folds plunge about 45° towards 320-330°.

In subarea E2, mesoscopic F2 folds are quite common in the amphibolite, plunging 60° towards the north. The regional orientation of S1 is similar to that in subarea E1, but shows local variation due to F2 folding. Quartz veins are commonly present in the amphibolites, and they are deformed by D1.

The principal feature of subarea E3 is the occurrence of macroscopic folds of two generations, viz. F2 and F3. The isoclinal F2 folds plunge at 70° toward 250° on the northern limb of the major F3 fold. The F3 fold is reclined and plunges 55° towards the north. The axial surface of the fold trends north-northeast. No penetrative schistosity parallel to the F2 or F3 axial planes is apparent.

Along the western side of the carbonate unit C3, a folded fault is assumed. The boundaries between subarea E3 and A1, E2 and A2, and E2 and A3 are made to coincide with this fault. An indication of the presence of this fault is a discordance of S0 and S1 between the A1 subarea and the hinge zone of an F2 fold in the E3 subarea. The F2 fold plunges southwest in the E3 subarea, but F2 fold plunge in the subarea A1 shows different orientation. In addition, quite different lithological associations in the respective subareas suggests a structural discontinuity. It appears from the above that the faulting took place after the F2 folding and the fault has been folded by an F3 fold.

2.3.5. Central Part of the Sally Downs Bore Area

The Tickalara Metamorphics, fine grained tonalitic rocks, and Ord River Tonalite Suite display S1 schistosity which is layer parallel and penetrative. F1 isoclinal folds are occasionally found in the Tickalara Metamorphics (Fig. 2-14A). F2 folds are generally open and plunge at 40° toward 350° on the southern limb of the F3 fold and 40-60° toward 280-300° on the northwestern limb. Mineral lineation, manifested by

Fig. 2-14. Field geological photographs; structural elements.

A. Folds in the Tickalara Metamorphics.

Folds in pelitic gneiss of the metamorphics at location 3.5 km west-southwest of the Dougalls Bore. F₁ isoclinal folds are refolded by F₂, which has a vertical axial plane in the photograph.

Scale is 5 cm long.

B. Strongly deformed Ord River Tonalite.

Photograph was taken 3.5 km northeast of the Sally Downs Bore.

Scale: a ball point pen in the lower center is 14 cm.

C. Close up of the central part of Photograph B., showing streaky compositional foliation in the Ord River Tonalite and the mafic enclave.

Scale: a ball point pen in the lower center is 14 cm.



preferred orientation of sillimanite and biotite, is parallel to the axes of the F₂ folding. However the F₂ fold event did not impose any penetrative schistosity in the rocks.

Meta-dolerite is generally massive, but a weak foliation is occasionally present. This weak foliation is considered to be a result of D₃, because it is unlikely to have resulted from the D₂ which is associated with an upper amphibolite facies metamorphism.

The intrusion of the Central Leucocratic Granite is later than that of the meta-dolerite though foliation of the granite is stronger than the parallel weak foliation of the meta-dolerite. The different intensity of the preferred orientation of minerals in the meta-dolerite and the granite is attributed to the different physical properties of the two rocks during deformation.

Two episodes of aplitic veining have been found in this area. The veins of the first episode have been folded by D₂ and those of the second one by D₃.

The major F₃ fold plunges 55° towards the north. Poles of S₀ and S₁ in this area show the effect of the F₃ folding (Fig. 2-13).

In subarea A₂, similar structural styles to those in the A₁ area are found. S₁ trends north to north-north-east and dips steeply west. At the southern end of the A₂ subarea, S₁ swings to the northeast.

The hornblendite body in subarea A₂, shows no schistosity and obviously cuts all structures. Therefore it is considered that the hornblendite was emplaced after the D₃ event.

2.3.6. Western Part of the Sally Downs Bore Area

This area is to the northwest and west of the Sally Downs Tonalite (Fig. 2-13). Lithological associations and structural styles are generally similar to those in the central part. In addition, however, the area

includes the Western Porphyritic Granite. The timing of the intrusion of this granite has not been clearly ascertained by previous workers. This granite was originally assigned to the Bow River Granite by Gemuts (1971). However structural relationships suggest that the granite was deformed by either D₁ or D₂. It is tentatively regarded as a syn- or pre-D₂ granite.

Between the Western Porphyritic Granite and the Sally Downs Tonalite, a strong foliation is developed in the tonalitic rocks of the Ord River Tonalite Suite and metasediments (Fig. 2-14B and C). These extensively deformed rocks could indicate the presence of a ductile deformed zone, oriented NE-SW direction.

The carbonate unit C₁ represents an S₀ surface, and the S₀ surface is generally parallel to the S₁ penetrative schistosity.

In subarea W₁, mesoscopic isoclinal F₂ folds in the pelitic gneiss plunge at 58° towards 37°. Axial plane schistosity is manifested by the parallelism of sillimanite. A mesoscopic fold in the migmatitic Ord River Tonalite Suite also plunges in the same direction.

In subarea W₃, a small number of measurements of the structural elements do not provide much information.

2.3.7. Sally Downs Tonalite

Foliation which is defined by the parallel orientation of minerals, such as hornblende, biotite, and plagioclase, is commonly observed in the Sally Downs Tonalite pluton. Alignment of lenticular mafic microgranular enclaves is generally parallel to the foliation defined by the minerals, therefore the lenticular mafic microgranular enclaves were also utilized to measure the foliation. Measurements of both structural elements have been presented in Plate 2.

The degree of the preferred orientation varies within the pluton. Fig. 2-15 shows the degree of preferred orientation of minerals in the Sally Down Tonalite, which is based on the field estimation. It is weak in the central and western part of the tonalite pluton, and it becomes strong near the eastern margin of the pluton. The foliation is totally lacking in some rocks. From this evidence, an interpretation of intrusion-induced deformation or magmatic flow is preferred for the origin of the structure in the Sally Downs Tonalite.

Linear preferred orientation of hornblende and biotite is found in some localities.

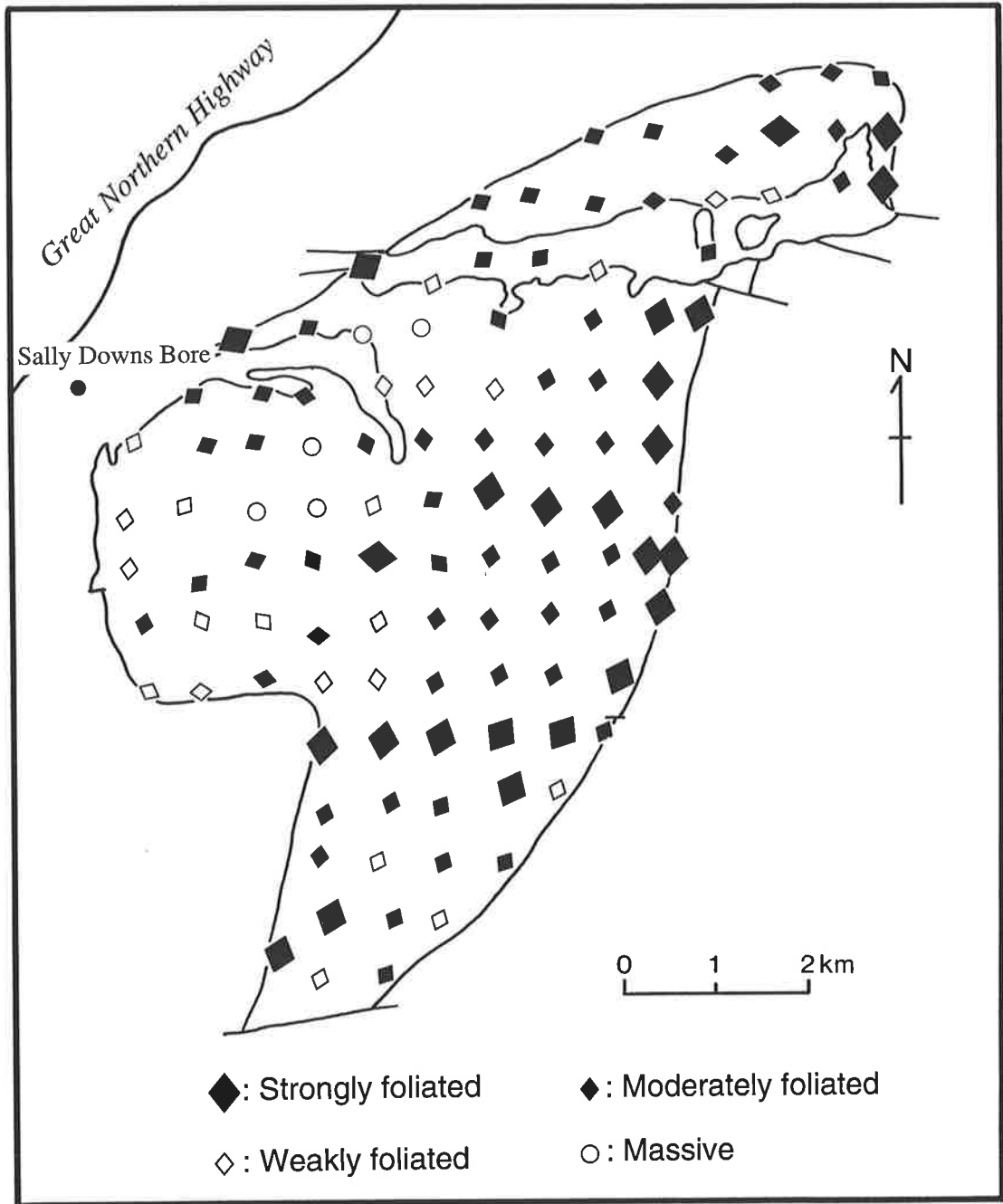
In subarea T₁, foliation follows the shape of the pluton, dips outward in the northwest of the subarea, and inward along the eastern margin. The features of the foliation are basically similar to S₁ in the country rocks. On a stereo diagram (Fig. 2-13), the poles of the foliation are concentrated in the vicinity of 85°/030°.

The poles of S₀ and S₁ in the xenoliths within the Sally Downs Tonalite show a similar distribution to the foliation of the tonalite and its country rocks.

In subarea T₂, orientations of the foliation are not easily ascertained because of dislocation and possibly rotation by the Sally Downs Fault and also poor outcrops in the subarea. However the limited observations suggest that the structural features are continuous from subarea T₁ to T₃ through subarea T₂.

In subarea T₃, maximal density of poles occurs at 25°/100° and consequently the general attitude of the foliation is steeply dipping to the west. In the western part of the subarea, an elongated basin structure is inferred from the structural data. In the southern part of the basin structure, dips of the foliation become very shallow. These data could

Fig. 2-15. Degree of preferred orientation in the Sally Downs Tonalite. Size of the plotted symbol indicates degree of the preferred orientation. Direction of long axis of plotted symbols (diamond) indicates approximate direction of foliation.



imply that the cores of one of the local surges of magma is situated in the area.

In subarea T4, foliations dip outward at between 30° and 70° near the contact of the pluton, and trends parallel to the contact. However within the Sally Downs Tonalite pluton, direction and amplitude of the dip vary significantly. This may be a result of multiple intrusions of the same magma, viz. an early phase of tonalite which partly solidified and was cut by a late phase of the magma. In subarea T4 the concentric pattern of the foliation suggests one such intrusion center of tonalitic magma.

The stereo diagram of subarea T5 (Fig. 2-13) shows that the foliations have a northeast trend and dip steeply either northwest or southeast.

2.3.8. Faulting

Two major faults are present in the Sally Downs Bore area. These are the Sally Downs Fault and the Melon Patch Fault. Faulting took place after the intrusion of the Sally Downs Tonalite. Some other east-west trending faults in the southern part of the area may have been active prior to the intrusion of the tonalite. However, any faulting that took place early in the sequence of geological events is likely to be obscured by later deformations.

A significant change in lithology and structural characteristics from the eastern part to the central part of the Sally Downs Bore area is considered to be the result of early dislocation (pre-F3).

A. Sally Downs Fault

To the east of the Sally Downs Tonalite, correlation of carbonate units, and of the Eastern Leucocratic Granitoid, across the fault suggest a right-lateral displacement with a 1.5km horizontal component. However,

to the west of the Sally Downs Tonalite, the magnitude of the horizontal displacement decreases to only 200m. It is also clearly shown by the outline of the Sally Downs Tonalite pluton. The western margin of the pluton does not show much dislocation, whereas the eastern margin has a large dislocation. To the west of the pluton, the fault intersects lithological boundaries and foliation at a shallow angle, but is nearly normal to them east of the pluton. Thus the apparent dip of the boundaries and foliation on the fault plane is shallow to the west, but steep to the east of the pluton. If the movement of the fault was not only horizontal but also vertical, the discrepancy of the horizontal displacements along the fault can be explained. In this case the northern block of the fault would have been moved 2.5km upward and 2.1km eastward relative to the southern block. The sense of the faulting is in accord with the lithological observations, orthopyroxene bearing tonalite is much more prevalent in the northern block, and also the metamorphic grade of the Tickalara Metamorphics increases regionally towards the north (Gemuts, 1971).

B. Melon Patch Fault

The magnitude and sense of movement of the Melon Patch Fault can be inferred from the correlation of carbonate units C₁ and C₃ across the fault (Fig. 2-4). The C₃ unit continues southward to the carbonate rocks just east of the Melon Patch Bore. The C₁ unit is correlated with some of the scattered carbonate rocks west of the Melon Patch Bore, and with a carbonate unit 3km east of the Great Northern Highway. Thus the fault is right-lateral with a 3km horizontal displacement.

2.3.9. Summary

Time relationships of tectonic events and the igneous activities in the Sally Downs Bore area are diagrammatically summarized in Fig. 2-16.

Field relations of the meta-gabbro suggest initial basic igneous activity in the area after deposition of the Halls Creek Group (Tickalara Metamorphics) before D₁.

The Dougalls Granitoid Suite and the Ord River Tonalite Suite are manifestations of the first tonalite-trondhjemite plutonism which took place before or during D₁. The emplacement of the Eastern Leucocratic Granitoid is considered to be earlier than the intrusion of the tonalite-trondhjemite.

After the D₂ deformation, a second basic igneous event took place, resulting in the emplacement of a number of sheets of the meta-dolerite. Syn-D₃ granite, viz. the Central Leucocratic Granite, followed this event.

The D₃ deformation completed a sequence of folding in the area, and was responsible for the large scale structures. After the deformation, several bodies of hornblende were emplaced, followed by the intrusion of the Sally Downs Tonalite which locally induced deformation around and in the tonalite itself.

Small dykes of biotite granite in the Sally Downs Tonalite represent final igneous activity in the area.

Faulting is the last obvious tectonic event in the area.

2.4. Geology and Structure of Sophie Downs Granitoid

2.4.1. General

The Sophie Downs Granitoid is present north of the Sophie Downs homestead, 30km to the east of the Halls Creek (Figs. 2-2). The granitoid pluton is an elliptical shape elongated NNE-SSW; it is 15km long and 5km wide (Fig. 2-17). The western half of the the pluton is exposed as

Fig. 2-16. Diagrammatic time relationships of tectonic and igneous events in the Sally Downs Bore area

Timing of intrusion of plutonic rocks is presented in relation to deformation and metamorphism

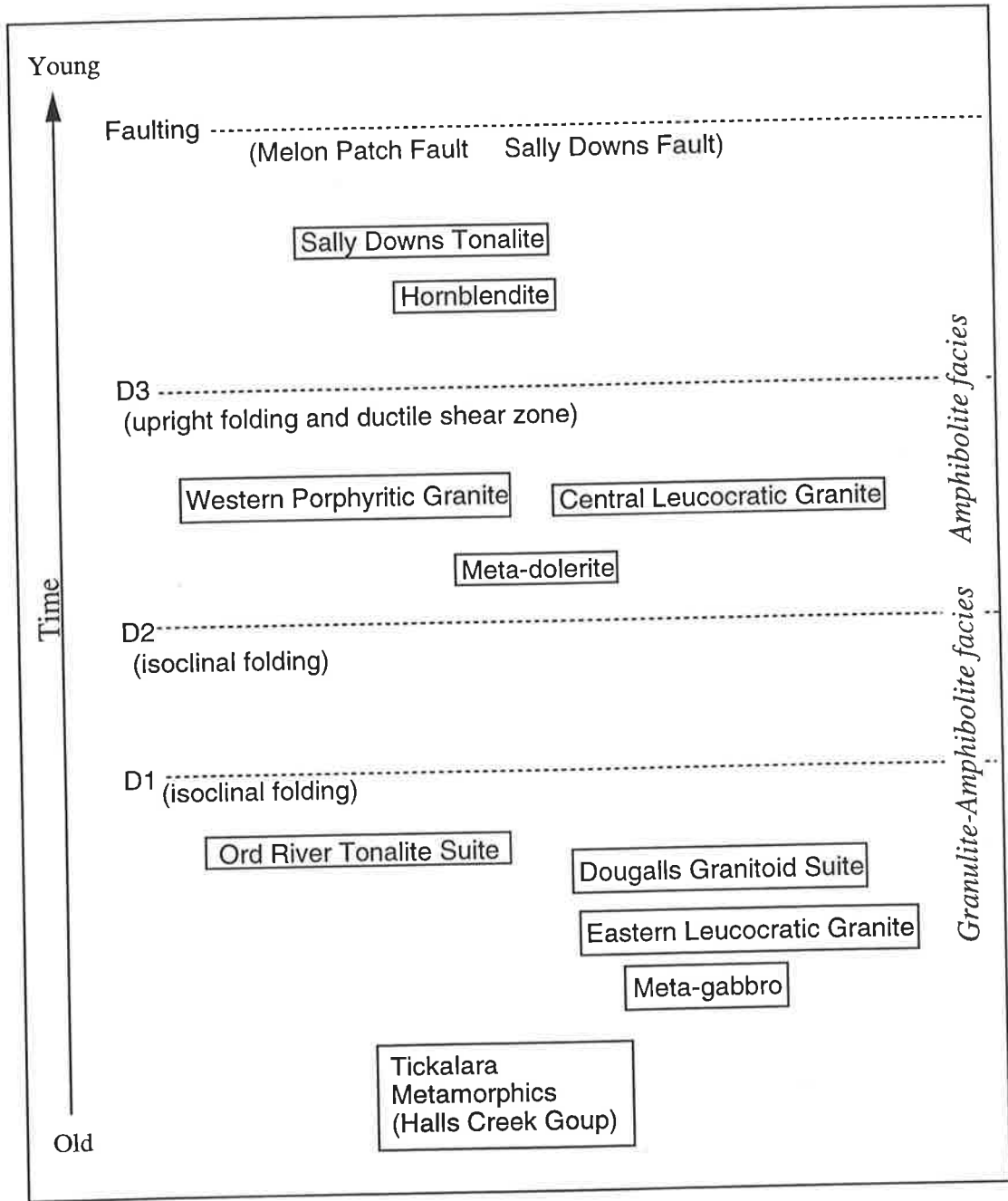






Fig. 2-17. Geology of the Sophie Downs Granitoid

The solid line labelled Q is a quartz vein. See location of the Sophie Downs Granitoid in Fig. 2-2.



-  Biscay Formation and Olympic Formation
-  Saunders Creek Formation
-  Sophie Downs Granitoid
-  Xenoliths (Ding Dong Downs Volcanics) in the Sophie Downs Granitoid

scattered low lying outcrops, and the eastern half forms somewhat high terrain (Fig. 2-18A and B, respectively).

The Sophie Downs Granitoid is regarded as a late intrusive of the Lamboo Complex (Dow and Gemuts, 1969), similar to the Bow River Granitoid Suite. Gemuts (1971) suggests that the Sophie Downs Granitoid may be genetically related to the Bow River Granitoid Suite. However, a recent finding of unconformity between the Sophie Downs Granitoids and the Saunders Creek Formation (T. Griffin (1992) pers. comm.: Griffin and Tyler, 1992) indicates that the granitoids is older than the most of the part of the Halls Creek Formation. This also suggests that the Sophie Downs Granitoid is the oldest granitoid in the Halls Creek Mobile Zone.

The granitoid is unconformably overlain by the Saunders Creek Formation on the northern margin of the pluton. Contact with the Biscay Formation along the central and southern margins is considered as fault. However, in southern part the pluton, the granitoid with similar composition to the Sophie Downs Granitoid intruded a quartz-sericite schist of the Biscay Formation (Fig. 2-18C). This evidence indicates that presence of a second granitoid activity in the Sophie Downs Dome. The Halls Creek Group bedding and early schistosity is domed around the granitoid. Rocks of the Halls Creek Group younger than Biscay Formation (i.e., Olympio Formation) are not present in the core of the structure.

The Saunders Creek Formation in the Sophie Downs area is 230m thick and comprises quartz pebble conglomerate, quartz sandstone, and pelitic schist. The conglomerate contains boulders derived from the Sophie Downs Granitoid. The formation is overlain by the Biscay Formation; consisting of basic volcanic rocks, followed by pelitic schist, quartz-sericite schist, and carbonate rocks.

Fig. 2-18. Field geological photographs; Sophie Downs Granitoid (1)

A. Typical exposure of the Sophie Downs Granitoid in the western part of the granitoid body. Photograph was taken 11 km northeast of the Sophie Downs Homestead.

B. Areal photograph of eastern part of the Sophie Downs Granitoid. Looking to east, showing rocky hill. The prominent ridge in the central part of the photograph is a quartz vein.

C. Contact relationship between the Sophie Downs Granitoid and quartz-sericite schist, presumably acidic volcanics of the Ding Dong Down Volcanics. Sharp contact is shown. Schistosity in the quartz-sericite schist is clearly truncated by the Sophie Downs Granitoid. Photograph was taken 1.4 km east of the Sophie Downs Homestead. Scale is 5 cm long. Vertical dark bar in the center of photograph is the shadow of a branch of a tree.



2.4.2. Sophie Downs Granitoid

The Sophie Downs Granitoid pluton is composed of coarse to fine grained alkali-feldspar granite. The term alkali-feldspar microgranite may be appropriate for a very fine grained variety which is predominant in the western half of the pluton. The grain size of this variety is indicative of a high level pluton, emplaced into shallow crustal depths, and cooled rapidly. However, in the eastern half of the pluton, medium to coarse grained rocks are common. Grain size distribution thus requires faster cooling in the western part of the pluton than the eastern part, or two discrete surges of magma.

The alkali-feldspar granite consists of equal amounts of quartz, albite, and K-feldspar, together with minor biotite, muscovite, and opaque minerals. Fluorite is found occasionally, visible in hand specimens. An unusual rock which is made up of less K-feldspar than the typical alkali-feldspar granite of the Sophie Downs pluton occurs near a large quartz vein. The anomalous mineral composition may be a result of extensive metasomatism by the hydrothermal solution from which was formed the quartz vein.

A large number of xenoliths are scattered throughout the pluton. The size of the xenoliths varies from a few centimeters to 600 meters long. The xenoliths consist of sericite schist, crenulated biotite schist, and amphibolite; all are derived from the Ding Dong Downs Formation. Directions of crenulation cleavage plane of crenulated biotite schist xenoliths are randomly orientated between the xenoliths, suggesting that the intrusion postdates the crenulation. Long axes of large elongated xenoliths indicate the presence of weak concentric structure within the pluton (Fig. 2-17). The center of the concentric structure may suggest core of the surge of the granitic magma.

The granitoid itself is generally massive or weakly foliated. The weak foliation is manifested by the preferred orientation of biotite, muscovite, and, occasionally, by trains of opaque minerals. However, a strong mylonitic schistosity and lineation is found in several localities.

The foliation generally trends northeast and dips 60° to the east. It is parallel to the long axis of the Sophie Downs Dome, and sub-parallel to the Halls Creek Fault. Therefore, the foliation may be a result of tectonism which created the dome structure, and/or caused by movement on the Halls Creek Fault.

Small aplite dykes intrude the alkali-feldspar microgranite in the central part of the pluton (Fig. 2-19A).

Numerous quartz veins are found in the pluton, especially in the south. In the eastern part of the pluton, a large quartz vein which is 8km long and 20m wide forms a prominent ridge and dominates the topography in the area (Fig. 2-19B).

Brecciated granitoid which occurs in the north of the pluton is thought to be a type of intrusive breccia (Fig. 2-19C). Brecciation might have been caused by a pressure built up by the boiling of fluid in the final stages of emplacement, as proposed for some high level intrusives by Burnham and Ohmoto (1980).

2.5. Geology of Supplementary Sampling Localities in the Halls Creek Mobile Zone

2.5.1. Turkey Creek Area

Sampling has been carried out near Turkey Creek (Fig. 2-2 and 2-20), 60km northeast of the Sally Downs Bore, in the north of the Halls Creek Mobile Zone. The basic purpose of this sampling was to examine the main body of the Mabel Downs Granitoid Suite, and an

Fig. 2-19. Field geological photographs; Sophie Downs Granitoid (2)

A. Aplite vein in the Sophie Downs Granitoid

Aplite veins are found in the central part of the granitoid body. Small dislocations are observed cutting the aplite veins.

Scale: diameter of lens cap is 5 cm.

B. The large prominent ridge traveling in the Sophie Downs Granitoid is the quartz vein (20 m wide and 8 km long), depicted in Fig. 2-17B.

C. Brecciated Sophie Downs Granitoid at the northern margin of the granitoid body.

Scale: length of a hammer is 33 cm.



orthopyroxene bearing granodiorite. In addition, a specimen of Bow River Granitoid was taken from north of the Bow River.

The granulite facies metamorphic grade is attained in the Turkey Creek area, and is the highest grade outcropping in the East Kimberleys, according to Gemuts (1971). Small bodies of igneous intrusions in the region add to the complexity of the geology.

A. Mabel Downs Granitoid Suite

The site from which specimen (52006) was taken is 4km southeast of Turkey Creek (Fig. 2-20), and situated on the northern margin of the main body of the Mabel Downs Granitoid Suite. It was selected because an Sr isotope analysis of the rock from this locality has been presented by Bofinger (1967). Thus major and trace element data from the present work can be combined with Bofinger's Sr isotope result, and comparisons of Rb and Sr concentrations also can be made.

The rock at this site is a coarse grained biotite hornblende tonalite. Minor allanite and epidote are present in the rock. The tonalite has lenticular hornblende rich mafic microgranular enclaves.

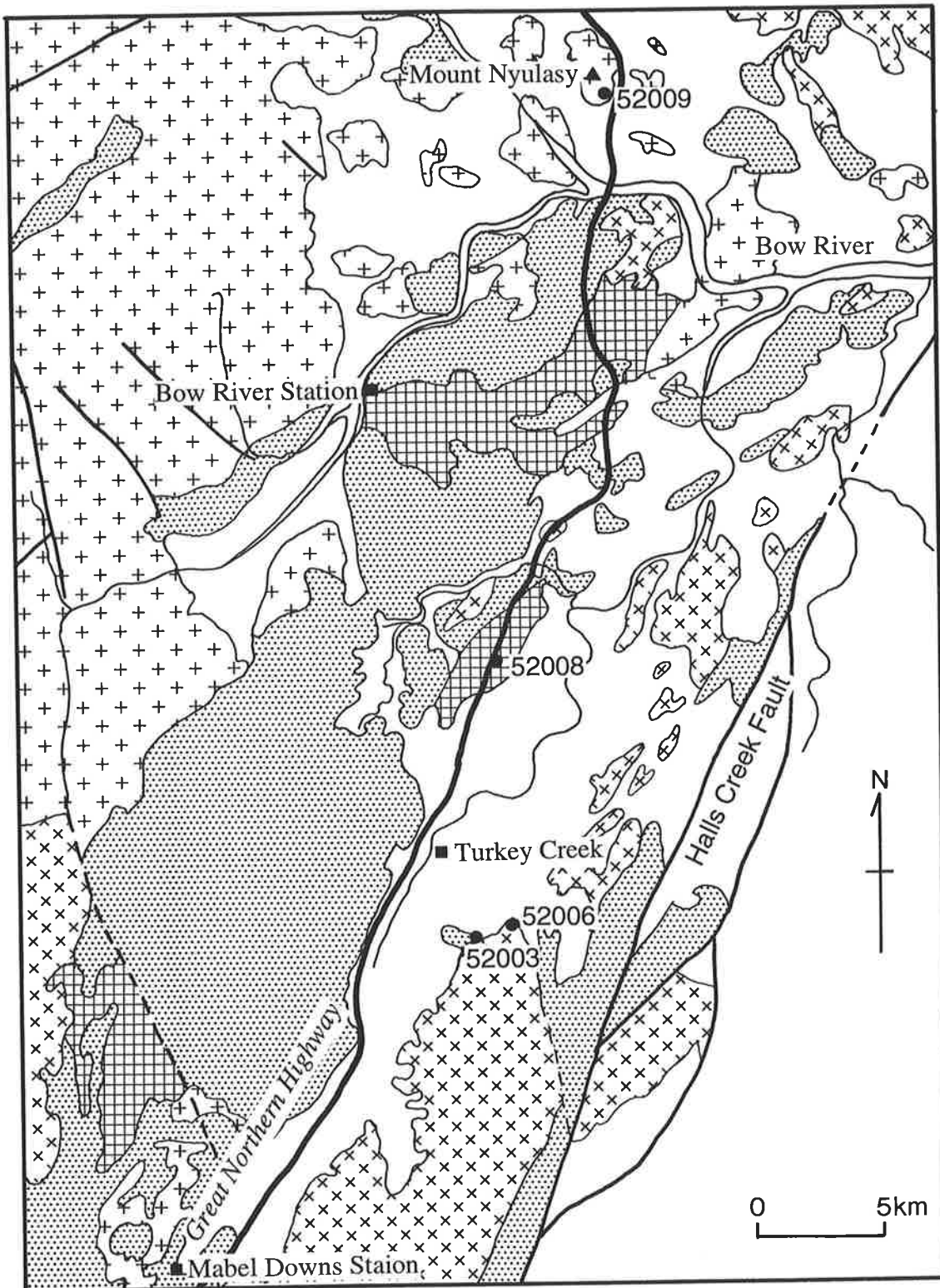
The mineralogy and outcrop appearance of this tonalite resemble occurrences of the Sally Downs Tonalite.


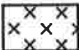
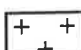

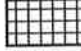
B. Gneissic Tonalite

Gneissic tonalite (52003) has been collected from a point 1km southwest of the previous outcrop (Fig. 2-20). The rock is a medium grained biotite tonalite; it apparently predates the emplacement of the main body of the Mabel Downs Granitoid Suite.

C. Orthopyroxene bearing Tonalite

Fig. 2-20. Geology of the Turkey Creek area and sample localities
Modified from Dow and Gemuts (1967) and Plumb (1968).



- | | | | |
|---|----------------------------------|---|--|
|  | Younger cover rocks |  | Mabel Downs Granitoid |
|  | Bow River Granitoid |  | Tickalara Metamorphics and Ultrabasic-basic intrusives |
|  | Orthopyroxene bearing Granitoids | | |

Three orthopyroxene bearing granodiorite bodies have been described by Gemuts (1971) to the north and southwest of Turkey Creek (Fig. 2-20). The largest body is 7km by 7km near the Bow River Homestead, and a small lenticular mass crops out 5km south of the largest body. A triangular shaped 15km by 3km body is situated to the northwest of Mabel Downs Station (Gemuts, 1971).

A specimen (52008) was collected from the second body along the Great Northern Highway. The rock is a coarse grained tonalite, dark brown in handspecimen. It is composed of biotite, orthopyroxene, and brown quartz and feldspar. Orthopyroxene is generally not evident in the handspecimen.

Gemuts (1971) described the orthopyroxene bearing granitoid as part of the Mabel Downs Granodiorite. However, because there is no orthopyroxene bearing granitoid in the main body of the Mabel Downs Granitoid Suite and no evidence of transition between them, it is felt unnecessary to group them together.

The characteristic presence of orthopyroxene in the granitoid from near Turkey Creek and in the tonalite from the Dougalls Granitoid Suite, suggests that these rocks can be correlated. Therefore, it is concluded that the orthopyroxene bearing granitoid must be excluded from the Mabel Downs Granitoid Suite, but included in the Dougalls Granitoid Suite which is older than the Sally Downs Tonalite, a correlative of the main body of Mabel Downs Granitoid Suite to the south of Ord River. The occurrence of similar orthopyroxene bearing granodiorite from the north of the Springvale Homestead (see section 2.5.3.) suggests that the suite has a distribution of some considerable extent.

D. Bow River Granitoid

A sample (52009) of the Bow River Granitoid was taken from Mount Nyulasy (Fig. 2-20), 15km northeast of the Bow River Homestead.

The rock is a massive, coarse grained granite, and consists of biotite, ovoid quartz, pale green epidotized plagioclase, and K-feldspar.

2.5.2. Mabel Hill Tonalite

Mabel Hill Tonalite is a new name for a small tonalite body of the Mabel Downs Granitoid Suite near Mabel Hill (Fig. 2-21). The tonalite body is 6km long, 2km wide and elongated in a north-south direction. A tiny body to the northeast of the tonalite may be a part of the tonalite.

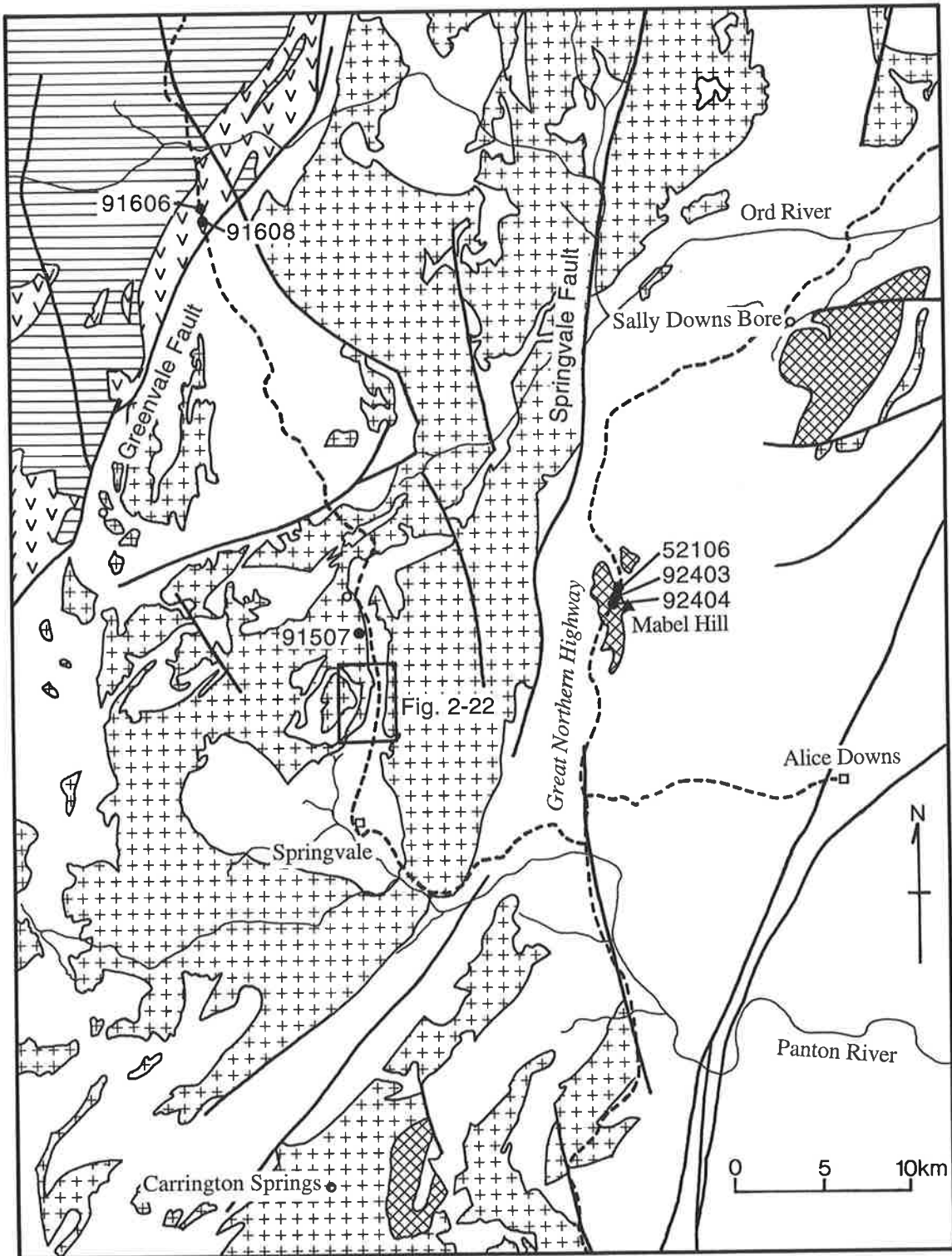
Samples were collected along the Great Northern Highway in the middle of the body. The rock is a foliated, coarse grained hornblende-biotite tonalite. Minor epidote and allanite are present. The tonalite is very similar to an acidic part of the Sally Downs Tonalite.



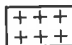
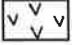


Outcrop of the Mabel Hill Tonalite is very small compared with the Sally Downs Tonalite pluton of the Mabel Downs Granitoid Suite. Indeed, extent of outcrop of the suite decreases toward the south. This could be a manifestation of the outcrop areas representing different levels within the suite; hence only shallow portions of the granitoid close to its roof are exposed now in the south; thus the granitoid appears small in area and is expected to have a large portion of the body underneath. This interpretation is consistent with an increase in metamorphic grade from south to north, indicating exposure of a deeper crustal portion in the north.

Alternatively, the igneous activity of the Mabel Downs Granitoid Suite is less significant in the southern part of the area.

The granitoids of the Mabel Downs Suite are present in a narrow zone trending NNE from the Bow River to Mabel Hill; the southern

Fig. 2-21. Geology of the Mabel Hill and Springvale sample localities
Modified from Dow and Gemuts (1967). Dashed lines are roads.



- | | |
|--|--|
|  Sedimentary rocks of Kimberley Basin |  Mabel Downs Granitoid |
|  Bow River Granitoid |  Whitewater Volcanics |
|  Undifferentiated Granitoids |  Halls Creek Group, Tickalara Metamorphics, and Ultrabasic-basic intrusives |

extension of the zone can be traced to the east of Carington Spring, 30km south of the Mabel Hill Tonalite body (Gemuts, 1971).

2.5.3. Springvale area

A small area, 20km north of Springvale Homestead, has been selected primarily to examine the Bow River Granitoid Suite (Fig. 2-21 and Fig. 2-22). It is in the middle of a batholith of the granitoid suite, and is situated near large xenoliths of Tickalara Metamorphics. Large gabbroic bodies, viz. Toby sill and a gabbro body of the Springvale, are present in this area.

The area is littered with bouldery tors (Fig. 2-23A)- typical Bow River Granitoid topography.

A. Tickalara Metamorphics

The metamorphic rocks are fine grained psammitic and pelitic gneisses which have been migmatized to a variable degree.

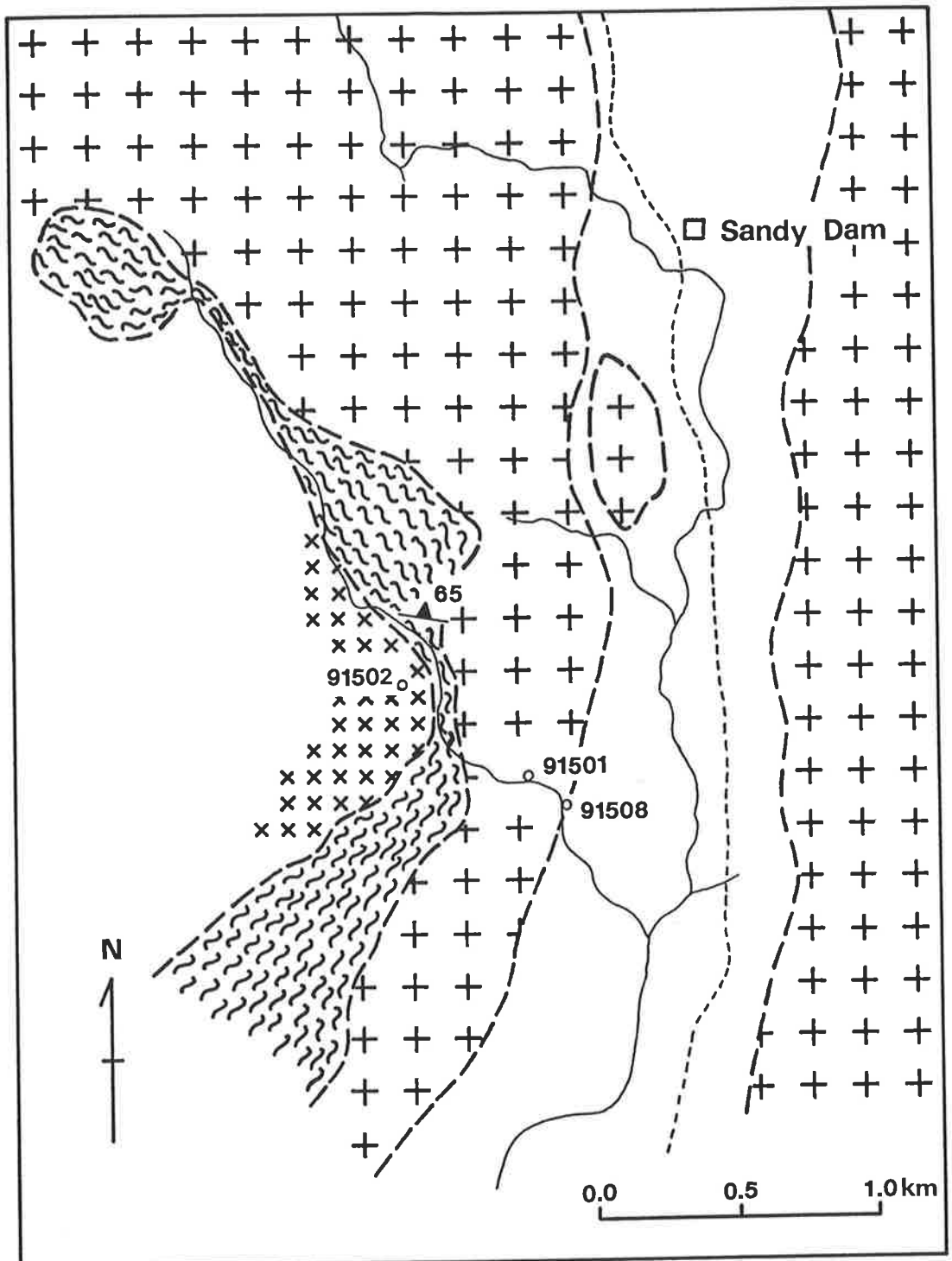
B. Orthopyroxene bearing granodiorite

Orthopyroxene bearing granodiorite was found to the west of the gneisses (Fig. 2-22). It is the southernmost occurrence of orthopyroxene bearing granitoid in the Halls Creek Mobile Zone.

The granodiorite is coarse grained and weakly foliated. It consists of light brown quartz and feldspar, biotite, and a small amount of orthopyroxene. Although no contact relationship has been observed, it is likely that the granodiorite intruded the metamorphic rocks, then both were intruded by the Bow River Granitoid Suite and brought to their present position as a large xenolith.

The granodiorite can be correlated with part of the Dougalls Granitoid Suite which contains orthopyroxene.

Fig. 2-22. Detailed geology of the Springvale area and sample localities
See Fig. 2-21 for location of the area. The dashed line is a road.






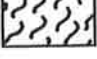
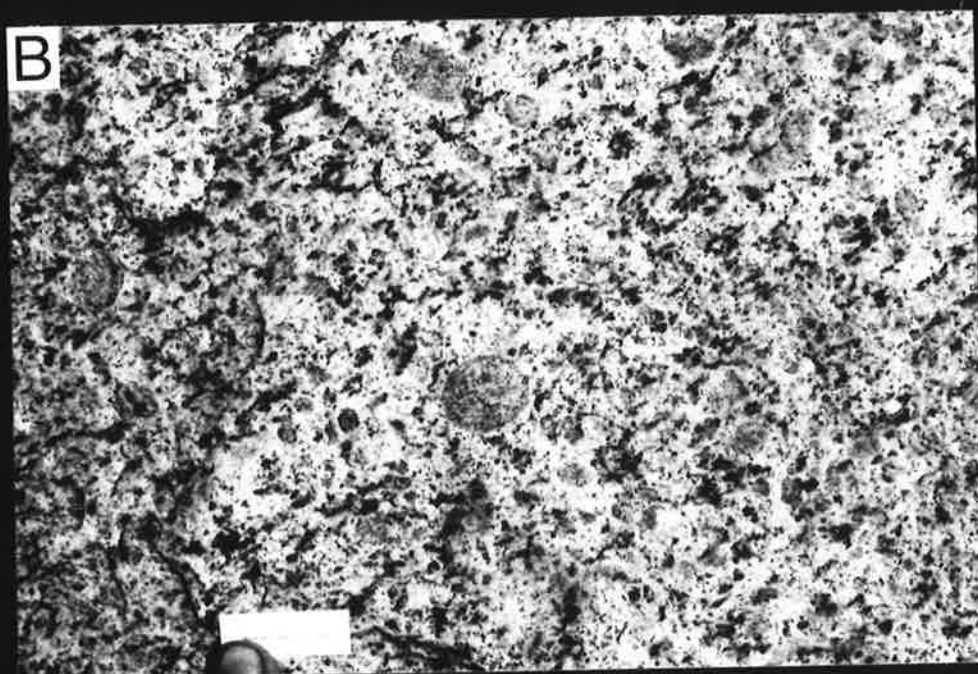
- | | |
|--|---|
|  Cenozoic sand and gravel |  Bow River Granitoid |
|  Orthopyroxene bearing granodiorite |  Gneiss and migmatite |

Fig. 2-23. Field geological photographs; Bow River Granitoids

A. Typical exposure of the Bow River Granitoid. The area is littered with bouldery tors.

B. Type II Bow River Granitoid. Large rounded crystals are quartz, K-feldspar, and epidotized plagioclase. Scale: 2 cm.

C. Type I Bow River Granitoid. Large rounded K-feldspar comprises about 40 % of the rock. Scale: diameter of lens cap is 5 cm.



C. Bow River Granitoid Suite

Two types of granitoid have been found in the Bow River Granitoid Suite of this area.

Type I Bow River Granitoid (Fig. 2-23C) is a coarse grained, porphyritic granite and is widely exposed in the area. Large rounded K-feldspars, up to 2.5cm in diameter, comprise about 40% of the rock. Medium grained biotite and a small amount of muscovite are present. Type I granitoid has rare xenoliths of gneissic granodiorite which may be an earlier phase of the granitoid suite or a completely different granitoid.

Type II Bow River Granitoid (Fig. 2-23B) occurs to a smaller extent than type I, and type II granitoid is intruded by type I. Type II granitoid is a medium grained granite; it has large phenocrysts of rounded quartz, K-feldspar, and epidotized plagioclase.

2.5.4. Whitewater Volcanics

The Whitewater Volcanics which comprise ashflow tuffs and lavas ranging from andesite to rhyolite, unconformably overlie the Halls Creek Group, but are intruded by the Castlereagh Hill Porphyry and Bow River Granitoid (Dow and Gemuts, 1969). The volcanics occur mainly west of the Greenvale Fault in the East Kimberleys, separating the Halls Creek Group and Lamboo Complex from younger sedimentary rocks of the Kimberley Basin.

The area where the volcanics were examined is situated 38km north-northwest of the Springvale Homestead (Fig. 2-21). The volcanics are exposed in a narrow belt, 2 to 4km wide, along the Greenvale Fault. The Whitewater Volcanics consist of pale green rhyolitic ashflow tuffs and reddish brown porphyritic rhyodacite. A welded texture is well preserved in the ashflow tuffs.

A small number of specimens were collected from the area for petrography and geochemistry.

2.6. Lamboo Complex in the King Leopold Mobile Zone

As well as occurring in the Halls Creek Mobile Zone the Lamboo Complex is well exposed in the King Leopold Mobile Zone (Fig. 1-1), trending northwest to west-northwest. As mentioned in Chapter 1, the crystalline complex in the King Leopold Mobile Zone was named the Hooper Complex by Griffin (1989). The Hooper Complex includes the Lamboo Complex and an upper part of the Halls Creek Group. An examination of the Lamboo Complex in the King Leopold Mobile Zone should provide further constraints on the petrogenesis of the igneous rocks of the complex. A brief review of the Lamboo Complex in the mobile zone, and comparisons of the complex in the two mobile zones are presented. Descriptions of rocks from the Lamboo Complex which have been studied in the present work are also included here.

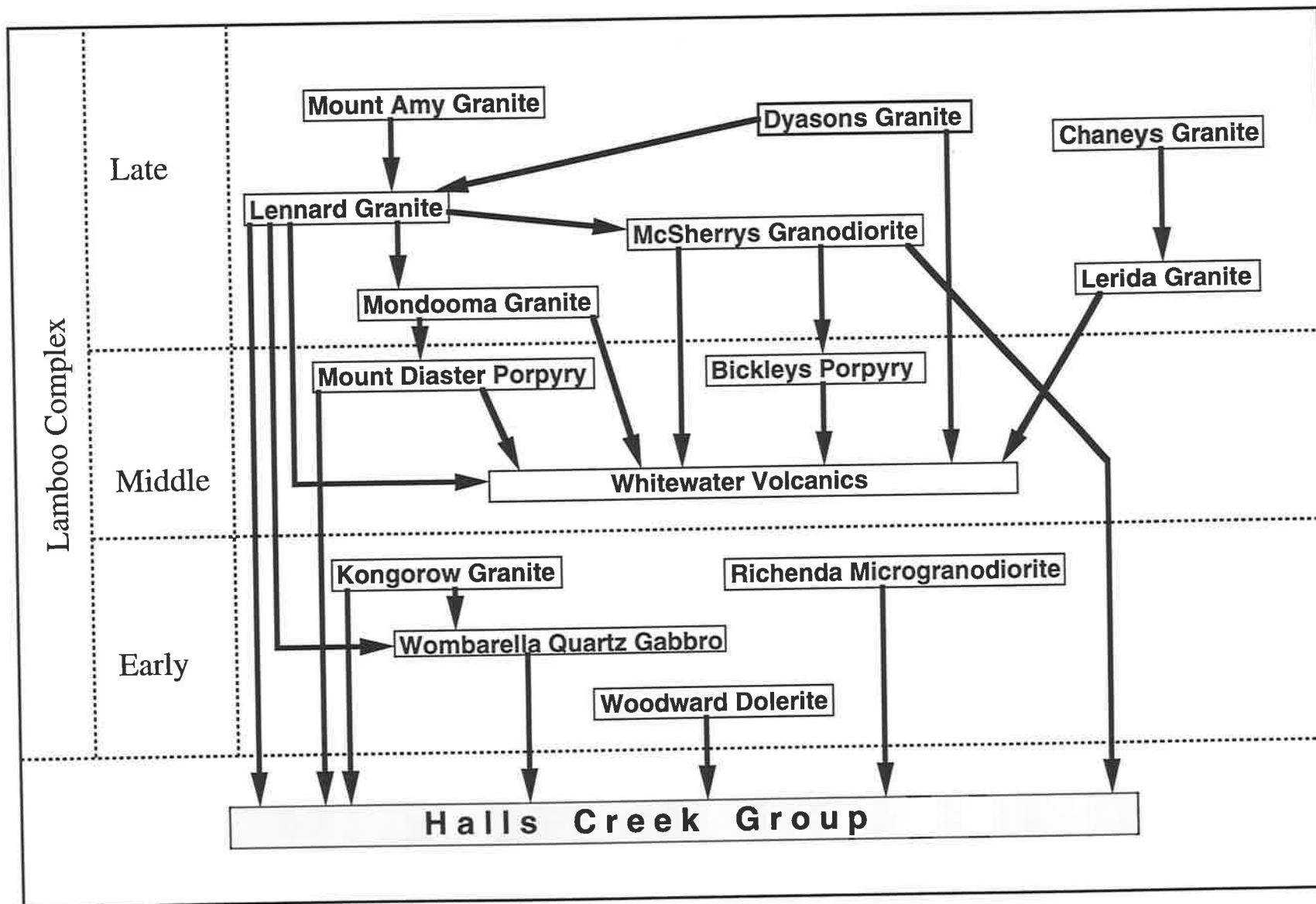
The Lamboo Complex in the King Leopold Mobile Zone is described by Gellatly et al. (1974), Gellatly et al. (1975), and Griffin and Grey (1990).

The Halls Creek Group occurs in the central and southwestern part of the mobile zone, among granitoids of the Lamboo Complex; it comprises greywacke, shale, siltstone and minor acid volcanics which have been strongly folded, and metamorphosed to greenschist and almandine-amphibolite facies assemblages (Gellatly et al., 1974). These rocks of the Halls Creek Group can be assigned to the Olympio Formation, i.e. the upper part of the Halls Creek Group.

Contact relationships of igneous rocks of the Lamboo Complex in the Lennard 1/250,000 sheet area of the King Leopold Mobile Zone are diagrammatically summarized in Fig. 2-24 based on the study by Gellatly et

Fig. 2-24. Time relationships of crystallization of igneous rocks in the
King Leopold Mobile Zone

Arrows indicate intrusive relationships. A rock unit pointed by an arrow head is intruded by a rock unit at the origin of the arrow. Construction of this diagram is based on a study by Gellatly et al. (1974).



al. (1974). The early, middle, and late Lamboo Complexes were defined using time relationship against the Whitewater Volcanics which is the middle of the complex.

The early Complex in the King Leopold Mobile Zone comprises two basic intrusives and two granitoids (Fig. 2-24). The Wombarella Quartz "Gabbro" is composed of biotite-orthopyroxene quartz gabbro, quartz norite, and tonalite. Some tonalite contains orthopyroxene (Gellatly et al., 1974). The Wombarella Quartz "Gabbro" is correlated with the McIntosh Gabbro in the Halls Creek Mobile Zone by Plumb and Gemuts (1976), but the orthopyroxene bearing tonalite of the Wombarella Quartz "Gabbro" may be comparable to similar rocks in the Dougalls Granitoid Suite.

The extrusion of the Whitewater Volcanics was followed by intrusion of porphyries which are believed to be comagmatic with the volcanics.

The presence of a large number of post-Whitewater Volcanics granitoid bodies in the King Leopold Mobile Zone may imply that more complex and more extended igneous activity took place in the region than in the Halls Creek Mobile Zone (Plumb and Gemuts, 1976). However, it is more likely that more detailed field observations are able to identify more granitoid bodies and more igneous activities in the King Leopold Mobile Zone. In the Halls Creek Mobile Zone, most of post-Whitewater Volcanics granitoids are simply grouped into the Bow River Granitoid Suite. A detailed study of the Bow River Granitoid Suite should reveal multiple igneous intrusions within the suite, similar to those in the King Leopold Mobile Zone.

Emplacement of granodiorite and tonalite, such as McSherrys Granodiorite, after the eruption of the Whitewater Volcanics and before the intrusion of the Lennard Granite are recorded in the King Leopold

Mobile Zone (Gellatly et al., 1974). The Bow River Granitoid and Lennard Granite and related granite form large batholiths in both the Halls Creek and King Leopold Mobile Zones.

In the King Leopold Mobile Zone, specimens were collected from the Richenda Granodiorite, McSherrys Granodiorite, and Dyasons Granite (Fig. 2-24).

A. Richenda Granodiorite

The largest body of the Richenda Granodiorite (Richenda Microgranodiorite of Gellatly et al. (1974)) was examined 4km to the northwest of the Colemans Camp (Fig. 2-25).

The granodiorite body has a roughly circular shape 4km in diameter. It is a medium grained biotite granodiorite, and is generally massive. Locally a schistosity caused by shearing is apparent. Dark bluish gray rhyolite occurs in the western part of the body. Phenocrysts of quartz and biotite are evident. The presence of the rhyolitic variety suggests that the Richenda Granodiorite is a high level intrusive. Therefore it is likely to be a member of the late Lamboo Complex.

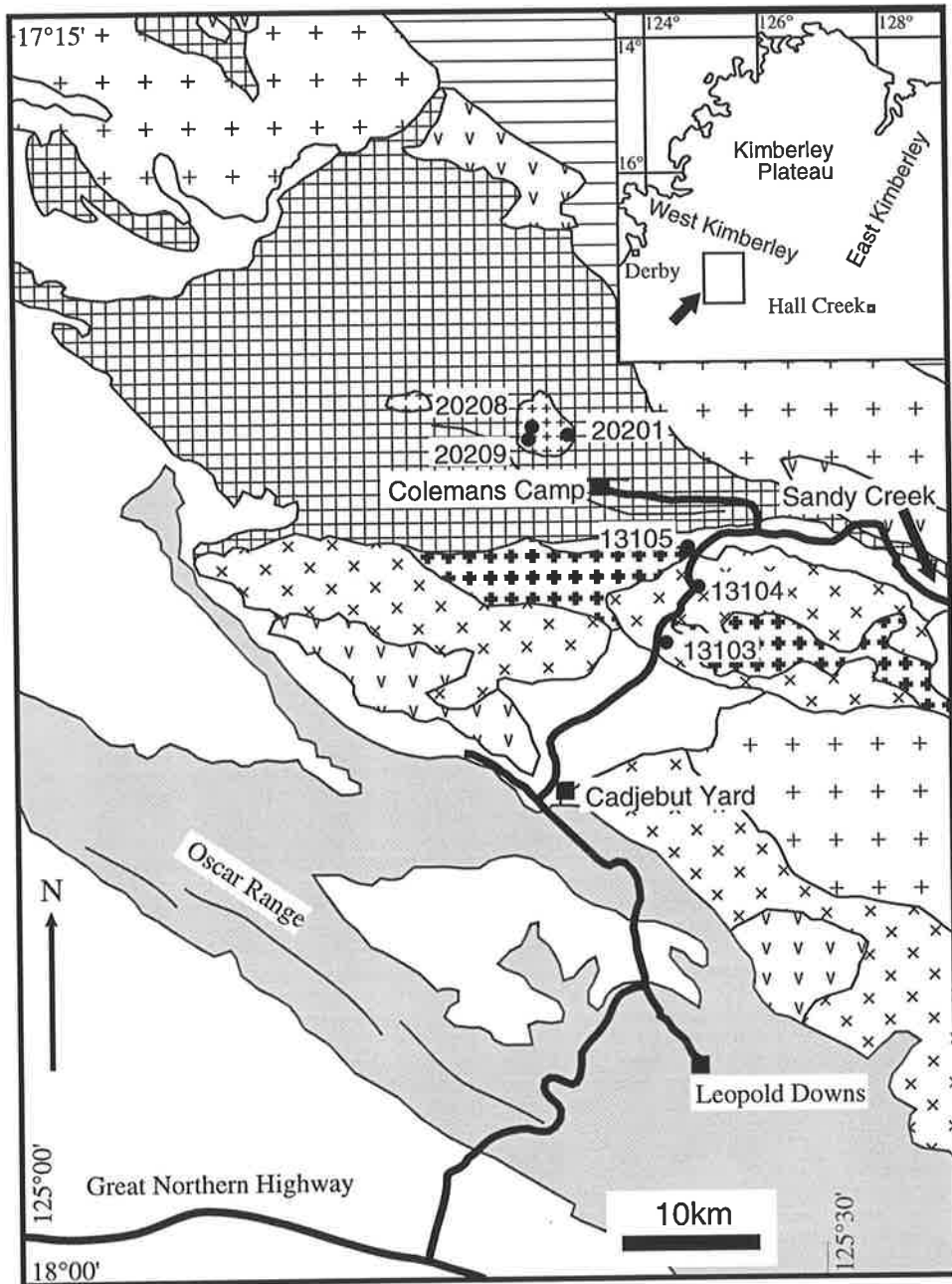
B. McSherrys Granodiorite



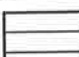

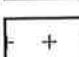
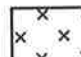
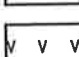

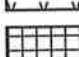
Specimens were collected along the track from Cadjebut Yard to Colemans Camp (Fig. 2-25). The rocks are coarse grained hornblende-biotite granodiorite, and are strongly foliated. A large number of lenticular mafic microgranular enclaves are present.

C. Dyasons Granite

A specimen was collected 7km to the southeast of the Colemans Camp. It is a medium grained biotite granodiorite. Very strong foliation in the rock could be related to the Sandy Creek Shear Zone (Fig. 2-25).

Fig. 2-25. Geology of central part of the King Leopold Mobile Zone
Geological map modified from Gellatly et al. (1974). Sample localities
are indicated in the map.



- | | | | |
|---|--------------------------|---|----------------------------|
|  | Cenozoic sand and gravel |  | Palaeozoic |
|  | Kimberley Group |  | Dyasons Granite |
|  | Lennard Granite |  | McSherrys Granodiorite |
|  | Whitewater Volcanics |  | Richenda Microgranodiorite |
|  | Halls Creek Group | | |

2.7. Regional Structure and Gravity Data

2.7.1. Regional Structure

Two mobile zones, the Halls Creek Mobile Zone and the King Leopold Mobile Zone, form the basic regional structure in the Kimberley area.

The north-northeast trend of the Halls Creek Mobile Zone is manifested by faults which have similar trend to it, such as Halls Creek Fault, Springvale Fault, and Greenvale Fault (Fig. 2-2). However, these faults show a slightly oblique relationship to the axial trend of the Mabel Downs Granitoid Suite. The trend of the suite is considered to be parallel to the major trend of Early Proterozoic orogenic activity, that is of the Halls Creek Orogenic Zone, which is thus divergent from the trend of the Halls Creek Mobile Zone, manifested by the faults.

In the Halls Creek Mobile Zone (Fig. 2-2), north-northeast trending faults show left-lateral strike-slip displacements (Plumb and Gemuts, 1976). North-northwest trending faults also show left-lateral displacement, and lineaments parallel to these faults are obvious in the Landsat image (Fig. 2-26). However east-west trending minor faults, such as the Sally Downs Fault and Melon Patch Fault in the Sally Downs Bore area, suggest right-lateral displacement. The displacement patterns can be explained as the result of left-lateral movement along the Halls Creek Mobile Zone (Rod, 1966). The total cumulative left-lateral displacement across the Halls Creek Mobile Zone is considered to be at least 110km by Plumb and Gemuts (1976). However, Hancock and Rutland (1984) suggested much smaller displacement, viz. about 30km by the correlation of their D3 structures across the Halls Creek and Woodward Faults. The left-lateral movement along those faults took place after D3 phase of deformation of Hancock and Rutland (1984), and

Fig. 2-26. Landsat image of the Halls Creek Mobile Zone

Band 5 image of the MSS sensor of Landsat is used. Part of two scenes, Path 114/ Row 072 and Path 114/ Row 073, are shown. An image taken in winter of the southern hemisphere was selected to avoid any cloud cover; this season is dry in the studied area. The images were taken on 28th June, 1980. The combined image shows broad structural and lithological variety in the area.

128°

17°

18°



50 km

possibly in Late Proterozoic to Early Paleozoic (Dow and Gemuts, 1969). Although the major displacement took place after D3, the faults may have originated in the Early Proterozoic or even earlier in the tectonic history (Hancock and Rutland, 1984; White and Muir, 1989).

On the other hand, the King Leopold Mobile Zone was deformed by reverse faulting and folding overturned towards the northeast, and was affected by only minor strike-slip faulting (Plumb and Gemuts, 1976). Deformation may be the result of displacement along the Halls Creek Mobile Zone, involving movement of the western block (Kimberley block) to the south (Plumb and Gemuts, 1976).

2.7.2. Gravity Anomalies and Their Implications

The gravity map was examined to obtain information on the subsurface distribution of rocks and regional structure. The striking feature of the Bouger gravity map of the region is the large positive anomaly coinciding with the Halls Creek Mobile Zone (Fig. 2-27). It has a gravity maximum 50km southwest of Turkey Creek, corresponding to the area of high grade metamorphic rocks and ultrabasic-basic intrusives.

Large negative anomalies east of the Halls Creek Mobile Zone correspond to the sedimentary basins. A positive anomaly is present to the southeast of Halls Creek over The Granites-Tanami Complex.

In the region of the Kimberley basin, the gravity picture shows no marked anomaly suggesting a simple structure.

In the Halls Creek Mobile Zone, the ultrabasic-basic plutonic bodies of the McIntosh Gabbro, such as McIntosh sill, Toby sill, and gabbro near Springvale underlie small scale positive anomalies, and could be responsible for them. Hence, similar small positive anomalies might suggest the presence of other ultrabasic-basic plutonic bodies.

Fig. 2-27. Gravity map of the Halls Creek Mobile Zone

Gravity data from following 1/500,000 Bouguer gravity maps published by Bureau of Mineral Resources.

Lissadell sheet: Bureau of Mineral Resources (1977)

Dixon Range sheet: Bureau of Mineral Resources (1978)

Gordon Downs sheet: Bureau of Mineral Resources (1978)

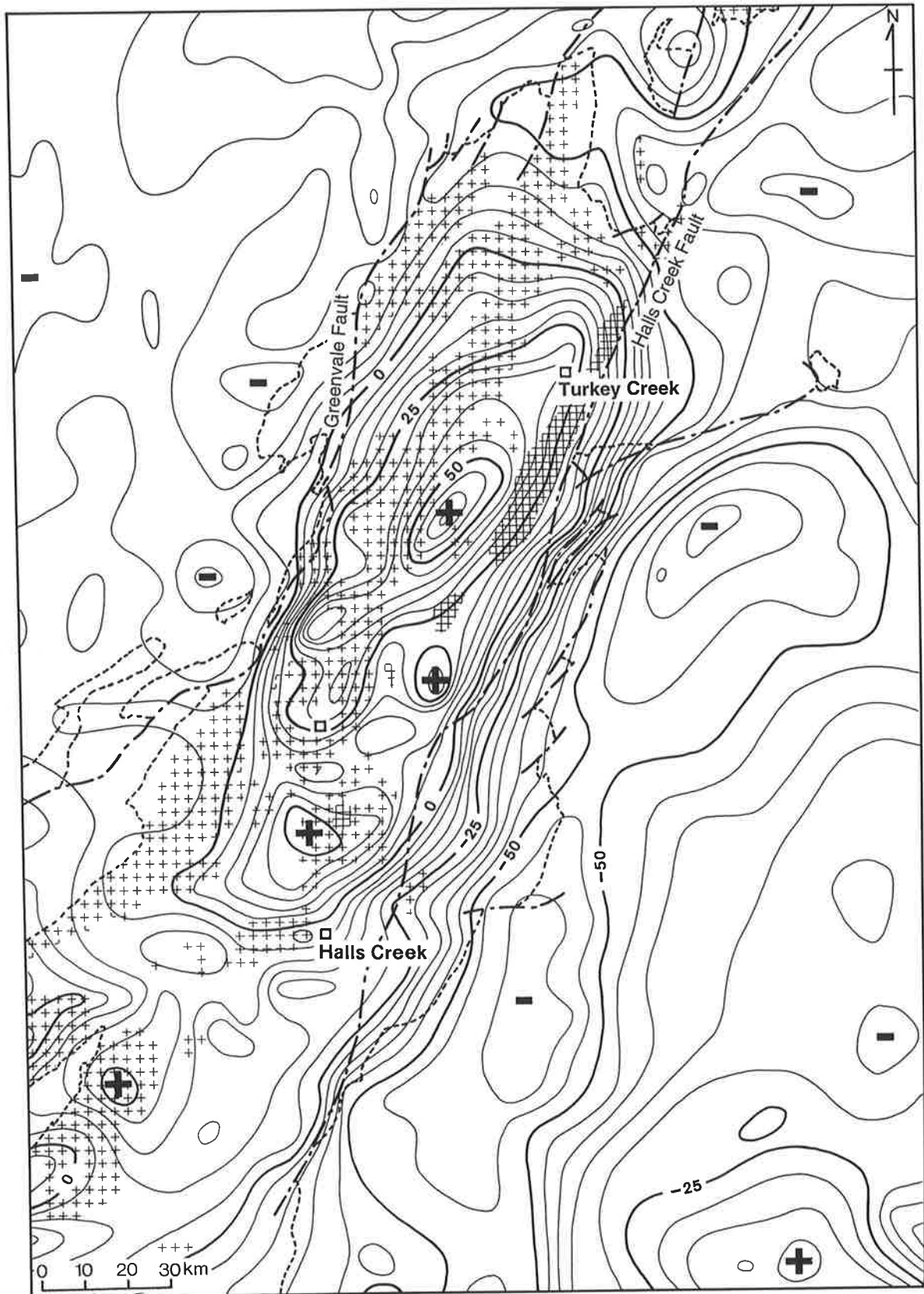
Mount Elizabeth sheet: Bureau of Mineral Resources (1977)

Lansdowne sheet: Bureau of Mineral Resources (1977)

Mount Ramsay sheet: Bureau of Mineral Resources (1977)

Gravity values are in mgal. Cross-hatch indicates exposure of Mabel Downs Granitoid Suite. Crosses indicate exposure of granitoids other than the Mabel Downs Granitoid Suite. Dashed lines are boundaries between the area of Early Proterozoic Halls Creek Group and Lamboo Complex and that of younger cover rocks. Dash dot lines are faults.

High gravity is observed in the Halls Creek Mobile Zone. See text for further discussion.



Granitoids have a relatively low specific gravity compared to basic rocks and metamorphic rocks, and may be expected to show negative Bouger anomalies. However, granitoid bodies in the area do not show obvious negative anomalies. For example, the area of the Bow River Granitoid Suite is characterized by a positive anomaly. This might indicate that the granitoid is of small volume, and rocks which have a higher specific gravity, e.g. basic igneous or high grade metamorphic rocks, are present under the granitoid. Basic igneous rocks might have provided thermal energy for the generation of a granitoid magma.

A flexure of the gravity contour to the west, over the Sophie Downs Granite, 10km east of Halls Creek, is perhaps indicative of a local negative anomaly near the granite body. The anomaly extends to the east over the Saunders Creek Dome. Therefore there may be a granitoid core under the dome similar to the Sophie Downs Dome.

From analysis of the gravity trends, Wellman (1976a, 1978) identified crustal blocks, which are in good agreement with the structural province defined by surface geology (G.S.A., 1971), and further identifiable in areas where the basement is not exposed. The north Australian block (Wellman, 1978) is bounded by the Halls Creek Mobile Zone to the west and the Arunta block to the south. Although there are covers of younger sedimentary rocks, in places, northern Australia is seen to consist of a large crustal block continuous from the Halls Creek Mobile Zone to Mount Isa, possibly with an Archaean basement.

Wellman (1978) examined the gravity anomalies across the block boundary coinciding with the Halls Creek Mobile Zone and interpreted the eastern side as the older. The interpretation implies the possible presence of an Archaean basement to Proterozoic terrain east of the Halls Creek Mobile Zone.

Wellman (1976b) calculated crustal thicknesses for Australia from gravity anomalies, and his results show that the East Kimberley region has a 35km thick crust. The thickness is a middle value within the 30-45km range of crustal thicknesses of Australia as a whole, derived by seismic survey (Dooley, 1976). However, contrasted with this interpretation, Finlayson (1987) presented larger crustal thickness for the Proterozoic North Australian Craton based on the results of refraction seismic survey, viz. 51-54km for the central part of the craton and 44-45km at the craton margins to the north and northeast. The East Kimberley region, western margin of the North Australian Craton, could have similar thickness, about 45km. The thickness of the crust in Archaean provinces is generally found to be about 35km, whereas Proterozoic crust has a significantly greater thickness of about 45km and has a high-velocity layer at the base (Durrheim and Mooney, 1991). Therefore, the crust thickness of about 45km will be likely for the East Kimberley region.

In any petrogenetic model, the current thicknesses of the crust must be considered.

CHAPTER 3. PETROLOGY (PART 1): PETROLOGY OF THE ROCKS FROM THE SALLY DOWNS BORE AREA EXCLUDING THE SALLY DOWNS TONALITE

3.1. Introduction

This chapter describes the petrology of the rocks from the Sally Downs Bore area. However, the petrology of the Sally Downs Tonalite of this area will be given in the next chapter. In the section dealing with the Dougalls Granitoids Suite, descriptions of two orthopyroxene bearing granitoid samples from the north of Turkey Creek and from north of Springvale are included. For each rock unit, petrography, mineral chemistry, and whole rock geochemistry are provided and discussed in this order. Full analytical results of mineral chemistry using electron microprobe are listed in Appendix 8.

3.2. Tickalara Metamorphics and Fine Grained Tonalitic Rocks

3.2.1. Pelitic and Psammo-pelitic Schists and Gneisses

A. Petrography

The petrography of the pelitic and psammo-pelitic schists and gneisses is briefly described. The following mineral assemblages have been recognized in the thin sections examined:

1. quartz - alkali feldspar - plagioclase - biotite - opaques
2. quartz - alkali feldspar - plagioclase - biotite - garnet - opaques
3. quartz - alkali feldspar - plagioclase - biotite - sillimanite - opaques
4. quartz - alkali feldspar - plagioclase - biotite - garnet - sillimanite - opaques
5. quartz - alkali feldspar - plagioclase - biotite - garnet - sillimanite - cordierite - opaques

6. quartz - alkali feldspar - plagioclase - biotite - garnet - orthopyroxene - orthoamphibole - opaques

7. quartz - alkali feldspar - plagioclase - biotite - muscovite - opaques

Garnet is present as pale pink porphyroblasts or xenoblasts, and commonly contains sigmoidally distributed inclusions of quartz, biotite, sillimanite, and opaques (Fig. 3-1A). Cordierite is found only in samples from the central and northern parts of the Sally Downs Bore area. It ranges in size up to 3mm, and contains inclusions of sillimanite and opaques. The rim of the cordierite is altered to pinitite. The textural relationships suggest that the biotite and sillimanite were formed before the garnet and the cordierite.

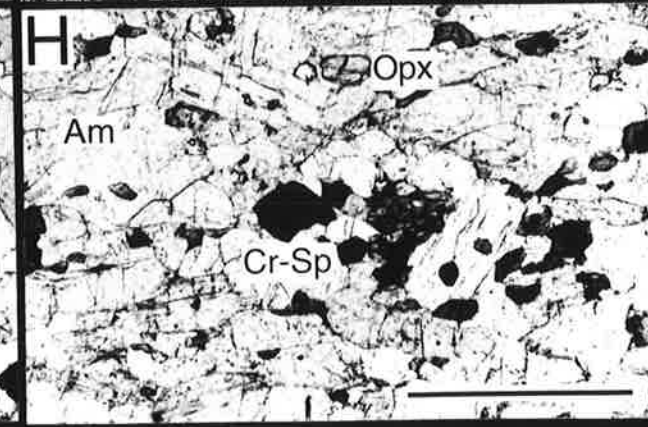
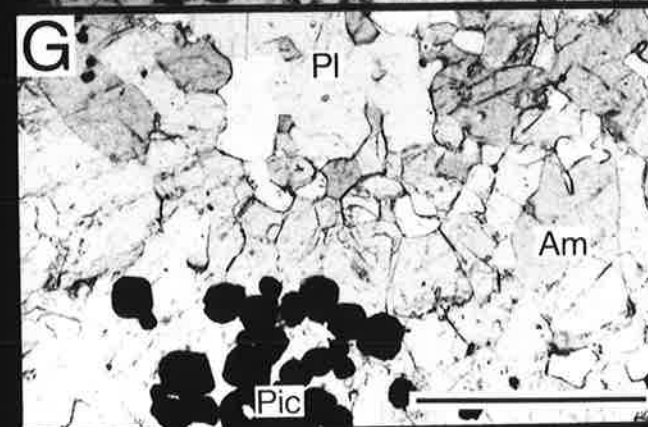
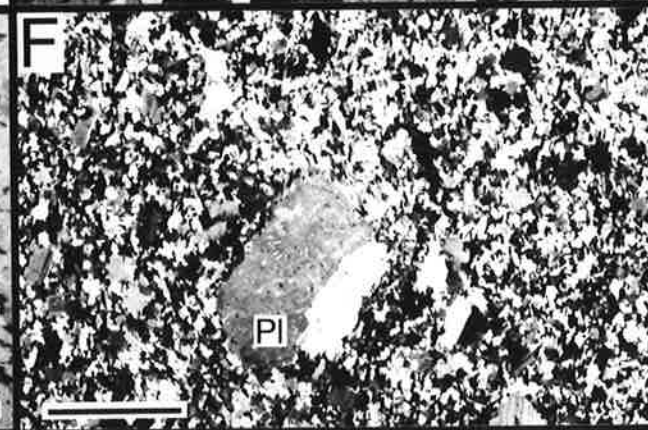
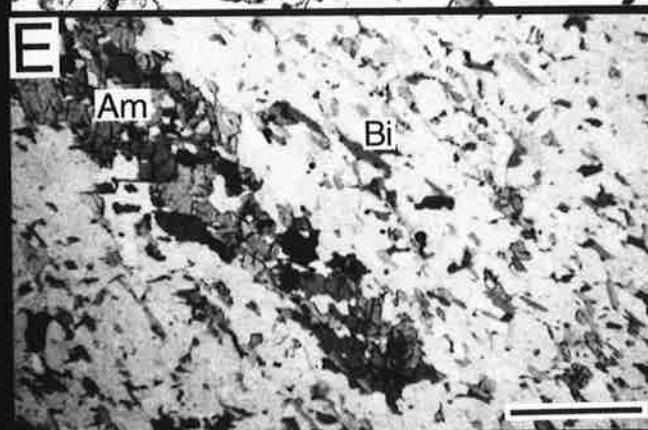
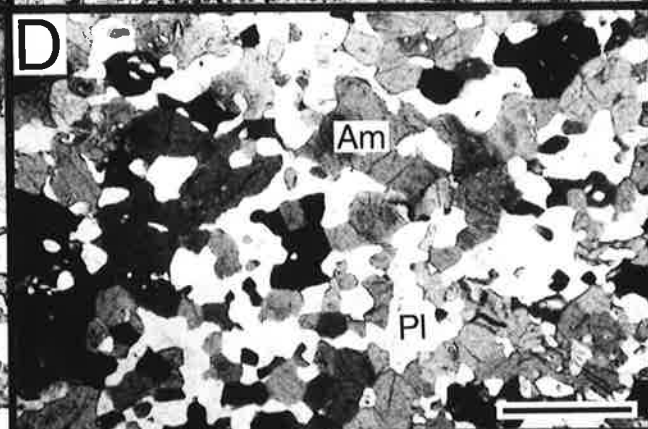
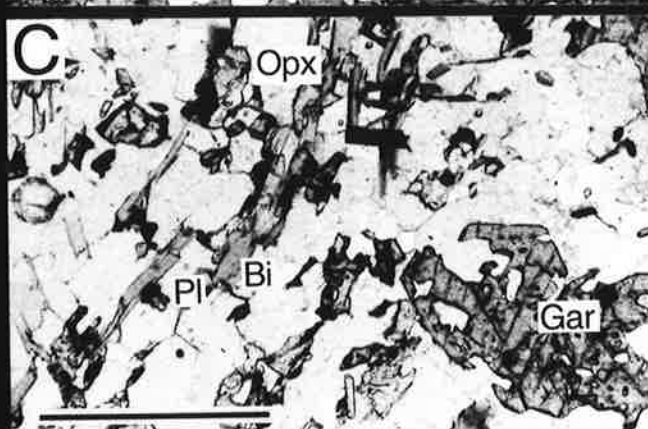
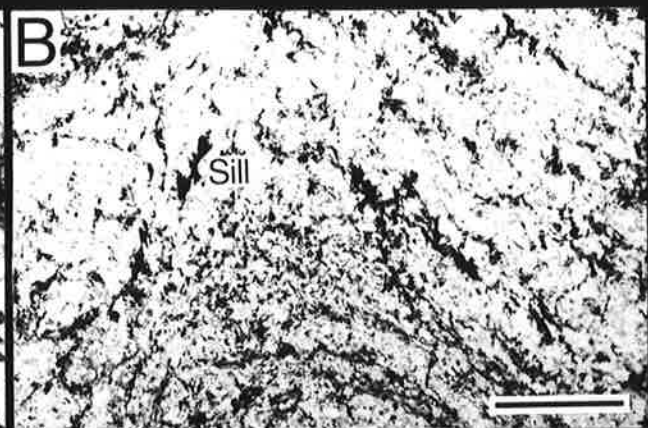
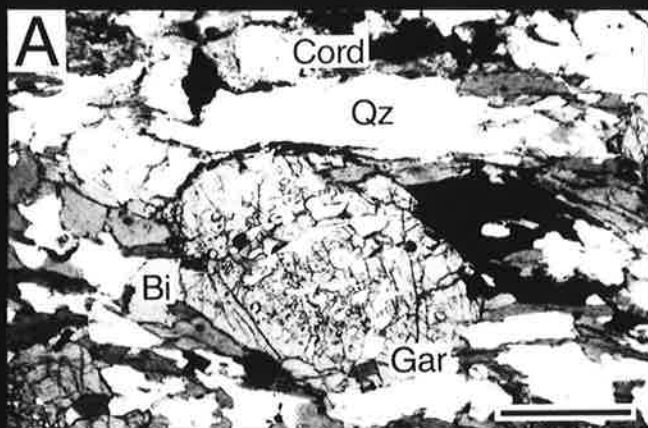
Biotite is a common mineral in the schists and gneisses, and is present as subidioblastic to idioblastic laths. The pleochroism is : α = straw yellow, β = γ = reddish brown.

Sillimanite is present as small discrete grains or as fibrolite. In the gneiss from north of the Sally Downs Bore, sillimanite has grown parallel to the axis of S₂ folds (Fig. 3-1B), suggesting crystallization of sillimanite during D₂ deformation.

Sample 40204 (sample location in Fig. 3-2) is composed of quartz, plagioclase (An 42-51), biotite, and garnet, with small amounts of orthopyroxene and orthoamphibole (Fig. 3-1C). The orthopyroxene is very small, and shows pink to blue pleochroism. Chemical composition of the orthopyroxene demonstrates that it is hypersthene with a relatively high Al₂O₃ content (Table A8-1). Small grains of the hypersthene are commonly altered to opaque minerals along the rim. Paragenesis of the orthopyroxene and the garnet is not clear but it seems that the orthopyroxene was not stable with the garnet. Pale yellow orthoamphibole is also fine grained and is possibly derived from the

Fig. 3-1. Photomicrographs of Tickalara Metamorphics, fine grained tonalitic rocks, and meta-gabbro

- A. Pelitic gneiss (21402) of the Tickalara Metamorphics. Garnet porphyroblast with inclusions of quartz. Gar: garnet, Bi: biotite, Cord: cordierite, Qz: quartz. Plane polarized light. Scale bar is 1 mm.
- B. Biotite gneiss (51005) from the north of the Sally Downs Bore. Sillimanite has grown parallel to the axial plane of S₂ folds. S₂ fold hinge is present in the center of the photograph. Sill: sillimanite. Plane polarized light. Scale bar is 10 mm.
- C. Orthopyroxene bearing biotite gneiss (40204). Opx: orthopyroxene, Gar: garnet, Bi: biotite, Pl: plagioclase. Plane polarized light. Scale bar is 1 mm.
- D. Amphibolite (21603) of the Tickalara Metamorphics. Am: amphibole, Pl: plagioclase (An 78-88). Plane polarized light. Scale bar is 1 mm.
- E. Fine grained tonalitic rocks: hornblende-biotite tonalite (11110) including elongated aggregates of hornblende. Am: amphibole (hornblende), Bi: biotite. Plane polarized light. Scale bar is 1 mm.
- F. Fine grained tonalitic rocks: plagioclase porphyritic biotite tonalite (11301). Crossed polarized light. Scale bar is 5 mm.
- G. Meta-gabbro (22101) is composed of plagioclase (pl), hornblende (Am), and picotite (Pic). Plane polarized light. Scale bar is 1 mm.
- H. Meta-gabbro (22102) is mainly composed of hornblende (Am), orthopyroxene (Opx), and green colored chromian ferroan spinel (Cr-Sp). Plane polarized light. Scale bar is 1 mm.



orthopyroxene. The orthopyroxene and the amphibole have similar chemical compositions, except lower FeO and slightly higher H₂O (estimated from values of total), Al₂O₃, CaO, and Na₂O in the amphibole than in the orthopyroxene (Table A8-1).

The presence of the orthopyroxene indicates granulite facies metamorphism, but the mineral assemblage is almost destroyed by subsequent lower grade metamorphism. Geothermometry from garnet-biotite pairs in the same rock, using the equation of Ferry and Spear (1978), yields temperatures of 680 and 776°C at 5 and 10kb, respectively. The derived temperatures are somewhat lower than the temperatures obtained from mafic granulite in the Sally Malay area (Thornett, 1981), 20km north of the studied area.

B. Geochemistry

Major element and trace element contents of the metamorphic rocks which are thought to be derived from sedimentary rocks, are listed in Table 3-1, together with major element data from the Tickalara Metamorphics (two schists and eight paragneisses) reported by Gemuts (1971). Gneisses which are considered to be derived from igneous rocks or from a mixture of igneous and sedimentary rocks are listed in Table 3-2. These are grouped as a orthogneiss member of the Tickalara Metamorphics. Locations of samples analyzed are shown in Fig. 3-2.

A study of the chemical composition of the metamorphic rocks is relevant to a consideration of the production of granitoid magmas by partial melting of the host rocks. Since the Mabel Downs Granitoid is believed to have formed by the partial melting of the Tickalara Metamorphics (Dow and Gemuts, 1969), the study provides the basis of the constraint to a petrogenesis of the granitoid.

Major elements

Fig. 3-2. Sample locality map for samples of the Tickalara
Metamorphics, Fine grained tonalitic rocks, Western
Porphyritic Granite, and Central Leucocratic Granite in the
Sally Downs Bore area.

TM: Tickalara Metamorphics, FT: Fine grained tonalitic rocks, WG:
Western Porphyritic Granite, and CG: Central Leucocratic Granite

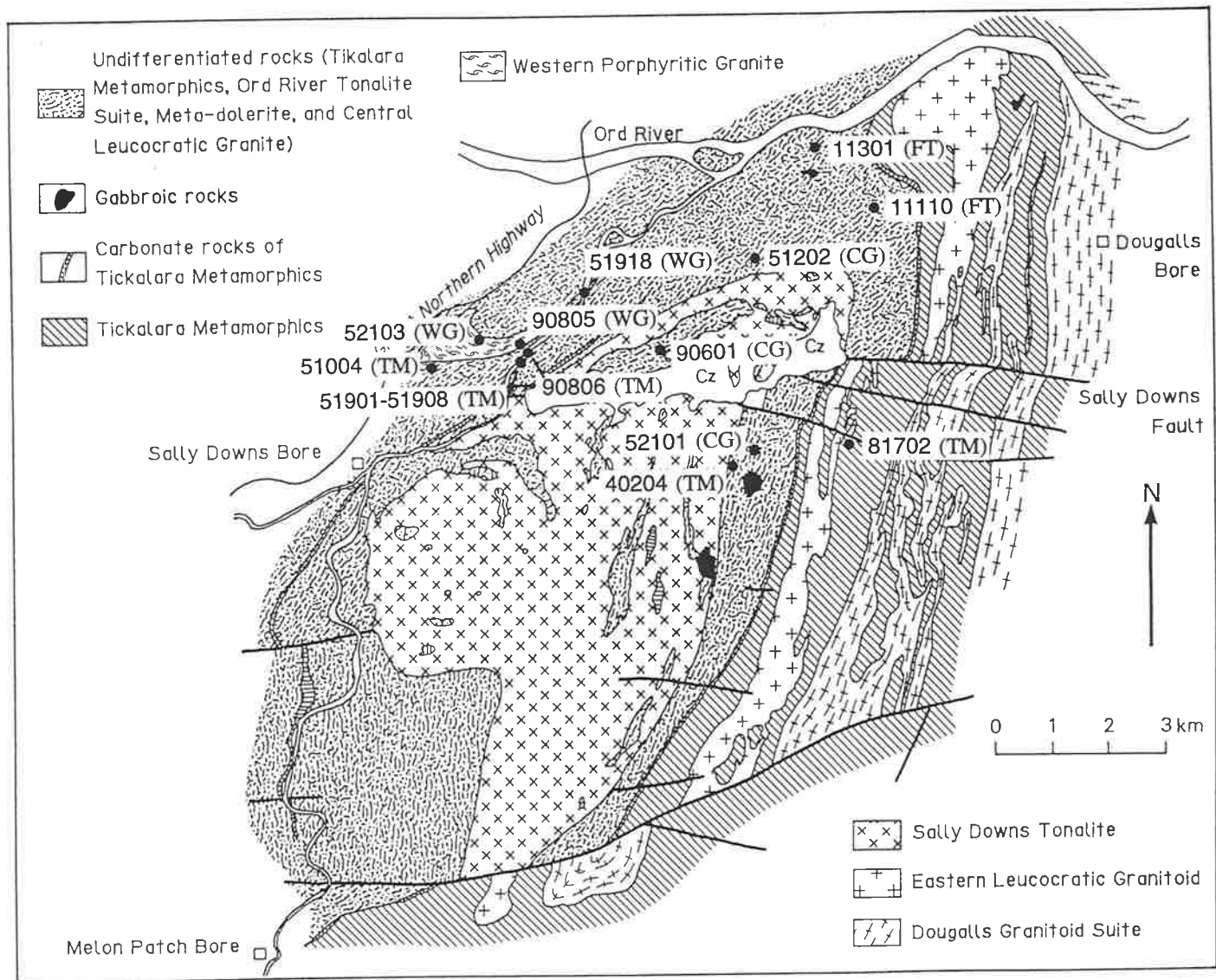


Table 3-1. Chemical compositions of the Tickalara Metamorphics (1)

Sample	51901 Gneiss	51902 Gneiss	51905 Gneiss	81702 Schist	IG1 Schist	IG2 Schist	IG3 Gneiss
SiO2 (%)	59.39	57.13	54.79	54.53	36.60	48.30	51.40
Al2O3	16.13	17.94	18.74	15.11	27.40	18.20	18.20
Fe2O3*	9.81	9.58	9.50	21.44	15.93	22.99	10.58
MnO	0.09	0.08	0.07	0.34	0.18	0.08	0.24
MgO	3.32	3.26	3.33	3.69	4.95	4.65	2.11
CaO	2.00	2.57	2.73	1.28	1.34	1.65	12.10
Na2O	1.84	2.50	2.56	2.87	0.90	1.13	0.74
K2O	4.67	4.61	4.72	2.37	3.90	2.35	2.47
TiO2	1.19	1.05	1.09	1.76	2.53	1.49	0.95
P2O5	0.03	0.03	0.04	0.05	0.15	0.05	0.08
LOI	1.17	1.00	1.10	-0.78	6.72	0.93	2.21
Total	99.64	99.75	98.67	100.66	100.60	101.82	101.08
Trace elements(ppm)							
Ba	1143	960	1078	518	-	-	-
Rb	168	166	167	104	-	-	-
Sr	205	247	266	90	-	-	-
Zr	420	330	361	167	-	-	-
Nb	23.3	23.4	24.2	12.5	-	-	-
Y	7.6	6.6	7.7	36.9	-	-	-
Sc	17.9	19.3	16.5	36.9	-	-	-
V	141	134	136	335	-	-	-
Ni	48	45	47	194	-	-	-
Th	0	0	0	5	-	-	-
Ce	97	79	97	52	-	-	-
Nd	44	35	45	18	-	-	-
Cr	180	158	174	474	-	-	-
A/CNK	1.377	1.302	1.312	1.572	3.367	2.459	0.703

Sample	IG4 Gneiss	IG5 Gneiss	IG6 Gneiss	IG7 Gneiss	IG8 Gneiss	IG9 Gneiss	IG10 Gneiss
SiO2 (%)	53.10	46.50	69.60	66.30	66.50	60.61	75.49
Al2O3	18.10	31.30	17.50	17.00	17.70	20.14	12.43
Fe2O3*	17.55	13.03	5.59	7.74	5.88	7.46	13.79
MnO	0.09	0.05	0.04	0.05	0.04	0.04	0.03
MgO	3.33	3.00	1.88	1.92	1.73	2.46	0.96
CaO	0.55	0.67	0.26	3.00	0.95	2.05	0.68
Na2O	0.30	0.89	0.11	2.24	1.35	2.08	1.01
K2O	3.66	2.35	2.94	0.55	4.46	3.83	3.88
TiO2	1.37	1.02	0.54	1.00	0.56	1.19	0.47
P2O5	0.12	0.12	0.13	0.05	0.59	0.02	0.08
LOI	0.27	1.77	1.29	0.55	0.97	0.73	1.00
Total	101.44	100.70	99.88	100.40	100.23	100.61	99.82
A/CNK	3.318	5.989	4.562	1.746	2.017	1.783	1.751

Analyses of IG1 to IG10 are from Gemuts (1971).

Fe2O3*: total Fe as Fe2O3, LOI: Loss on ignition

A/CNK: Mol. Al2O3/CaO+Na2O+K2O

Table 3-2. Chemical compositions of the Tickalara Metamorphics (2) Orthogneisses

Sample	51004	51903	51904	51907	51908	90806
Major Elements (wt%)						
SiO ₂	64.40	71.86	66.19	65.31	61.86	67.38
Al ₂ O ₃	15.92	13.28	15.59	15.82	16.47	14.51
Fe ₂ O ₃ *	6.13	3.96	5.36	6.19	7.02	6.01
MnO	0.07	0.04	0.06	0.06	0.09	0.06
MgO	1.92	1.50	1.86	2.12	2.75	1.55
CaO	4.18	2.18	3.60	2.86	5.51	3.56
Na ₂ O	3.33	3.01	3.32	3.60	1.58	3.35
K ₂ O	2.20	2.88	2.40	2.52	2.70	2.07
TiO ₂	0.86	0.49	0.60	0.69	0.79	0.72
P ₂ O ₅	0.24	0.04	0.22	0.03	0.18	0.21
LOI	0.52	0.66	0.79	0.69	0.60	0.55
Total	99.77	99.90	99.99	99.89	99.55	99.97
Trace Elements (ppm)						
Ba	1286	653	759	605	582	726
Rb	86	95	88	93	127	79
Sr	400	177	334	276	249	275
Zr	281	231	278	262	133	259
Nb	14.1	11.7	10.7	11.2	8	11.8
Y	21	7.8	20.9	10.9	18	14.6
Ce	180	67	62	79	46	160
Nd	71	31	29	38	24	59
Sc	16.9	8.5	13.5	11.3	18.1	12.4
V	79	55	64	73	117	55
Cr	30	66	24	81	38	33
Ni	14.5	18.9	14.9	24.7	31.8	13.4
Cu	22	5	7	5	7	67
Zn	73	38	61	75	78	67
Ga	N.D.	N.D.	20.2	21.6	N.D.	21
Ratios						
A/CNK	1.030	1.104	1.067	1.142	1.060	1.020
Rb/Sr	0.215	0.537	0.263	0.337	0.510	0.287
(Ce/Y) _n	23.34	23.39	8.08	19.73	6.96	29.84

Fe₂O₃*: Total Fe as Fe₂O₃

LOI: Loss on ignition

N.D.: Not determined

A/CNK: Mol. Al₂O₃/CaO+Na₂O+K₂O

(Ce/Y)_n: Chondrite normalized Ce/Y

SiO₂ contents of the schists and gneisses in Table 3-1 range widely from 36.6 to 75.49% with average value of 57.16%. High alumina and iron reflect the dominance of phyllosilicate minerals, such as mica and chlorite. A variable ratio of clays to quartz in the original sediments produces the broad spectrum of SiO₂ contents.

K₂O is moderately high, ranging from 2.35 to 4.72%, except for sample IG7 of Gemuts (1971). The Na₂O/K₂O ratio is less than 0.6 for most of the samples - a common characteristic of sedimentary rocks. When plotted on a ternary Na₂O - K₂O - CaO diagram (Fig. 3-3), the schists and gneisses lie near the K₂O corner of the diagram, and on a line representing Na₂O/CaO = 1, suggesting variation of K₂O with constant Na₂O/CaO ratio.

Mol [Al₂O₃/(CaO + Na₂O + K₂O)] ratio is more than 1.3 reflecting a peraluminous composition; an exception is sample IG3 of Gemuts (1971) - a calcareous gneiss.

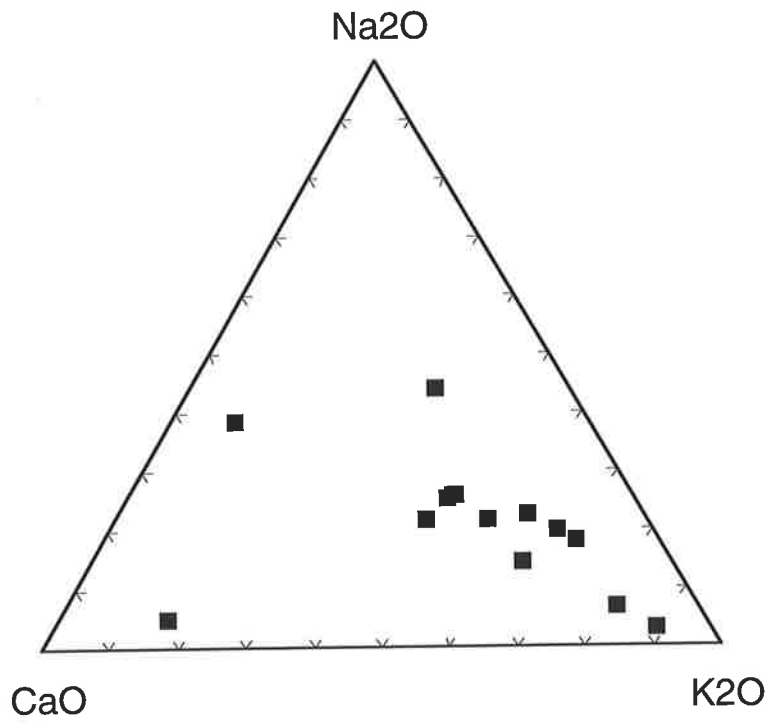
The additional four major element analyses of the schists and gneisses in the present work support the conclusion of Gemuts (1971), viz. that the rocks are similar in composition to the average shale (Clark, 1924) and greywacke (Pettijohn, 1957).

SiO₂ contents of the orthogneisses range from 61.86 to 71.86% (Table 3-2). Moderate levels of K₂O are found in the samples, ranging from 2.07 to 2.88%. Mol.[Al₂O₃/(CaO+Na₂O+K₂O)] ratios of the gneisses are less than 1.142. The ratios are clearly lower than those of the samples derived from the sedimentary rocks (Table 3-1).

Trace elements

Ba and Zr contents in the gneisses (Table 3-1) are high, ranging from 960 to 1143ppm, and from 205 to 266ppm respectively; these are slightly lower in the schist (sample 81702). Rb in the gneisses is about 167ppm. Rb depletion, a characteristic feature of granulite facies rocks

Fig. 3-3. Na₂O-CaO-K₂O diagram of Tickalara Metamorphics



(Rollinson and Windley, 1980a) is not observed. K/Rb ratios range from 190 to 235 in the metamorphic rocks.

Complete rare earth element (REE) determinations have not been made for any rocks; only the two light rare earth elements (LREE), Ce and Nd, have been analyzed. In the gneisses, Ce and Nd are high, and Y is low, suggesting a steep chondrite normalized REE pattern with LREE enrichment. The schist shows moderate LREE enrichment relative to HREE (heavy rare earth elements) estimated from the Y content. Higher Y concentration in the schist than in the gneisses may result from the presence of garnet which preferentially accommodates HREE and Y rather than LREE.

Comparing the trace element concentrations with crustal abundances, in particular post-Archaean upper crustal values (Taylor and McLennan, 1981) there are some similarities, viz. high Rb, Ba and high LREE contents (Table 3-1). However the gneisses have lower Y contents than Taylor and McLennan's values indicating depletion of HREE. Transitional metal elements, Cr, V, Sc, Ni, are generally high in the gneisses and schist compared to the post-Archaean upper crustal value (Taylor and McLennan, 1981). Values might suggest the possibility of numerous mafic rocks in the provenance. Contradicting concentrations, viz. the high Rb, Ba, LREE, Cr, V, Sc, and Ni, could be accounted for by bi-modal volcanic rocks in the source area.

Trace element contents of the orthogneisses (Table 3-2) show some similarities to the gneisses of the sedimentary rock origin from the Tickalara Metamorphics, having high levels of Ba and Zr.

3.2.2. Amphibolite

A. Petrography

The amphibolites are fine grained, and have granoblastic to nematoblastic texture (Fig. 3-1D). They have plagioclase and hornblende as major constituents. The following mineral assemblages have been recognized in the amphibolites.

1. plagioclase - hornblende - quartz - opaques
2. plagioclase - hornblende - quartz - clinopyroxene - opaques - (+ epidote)
3. plagioclase - hornblende - clinopyroxene - garnet - quartz - opaques

The garnet amphibolites are light colored rocks, having less amphibole than the amphibolite without garnet.

Plagioclase

The plagioclase is present as xenoblasts with average grain size about 0.6mm. The composition of the plagioclase ranges from An 78 to 88 in sample 21603 which is a typical example of the amphibolite (Fig. 3-4). However, in the garnet amphibolite (samples 20904 and 22105), the composition varies from An 39 to 49.

Hornblende

The hornblende (α = pale yellowish green, β = dark green, γ = bluish green) is a significant component of the rocks, constituting as much as 45%. It forms subidioblastic to xenoblastic grains ranging in size up to 1mm. $Z^{\wedge}C$ ranges from 12 to 21°.

The chemical composition and structural formula of several hornblendes are given in Table 3-3.

The hornblende in the amphibolite is magnesio-hornblende or ferro-hornblende according to the nomenclature of Leake (1968); Mg/Mg + Fe ratios from 0.478 to 0.529. Ti content of the hornblende (on the basis of 23 oxygens) varies from 0.108 to 0.147, corresponding to the content of hornblende typical of high-grade amphibolite facies (Raase, 1974).

Fig. 3-4. An-Ab-Or plot of plagioclase from amphibolite

Sample localities of amphibolites, 21603, 20904, and 22105, are shown in

Fig. 3-5.

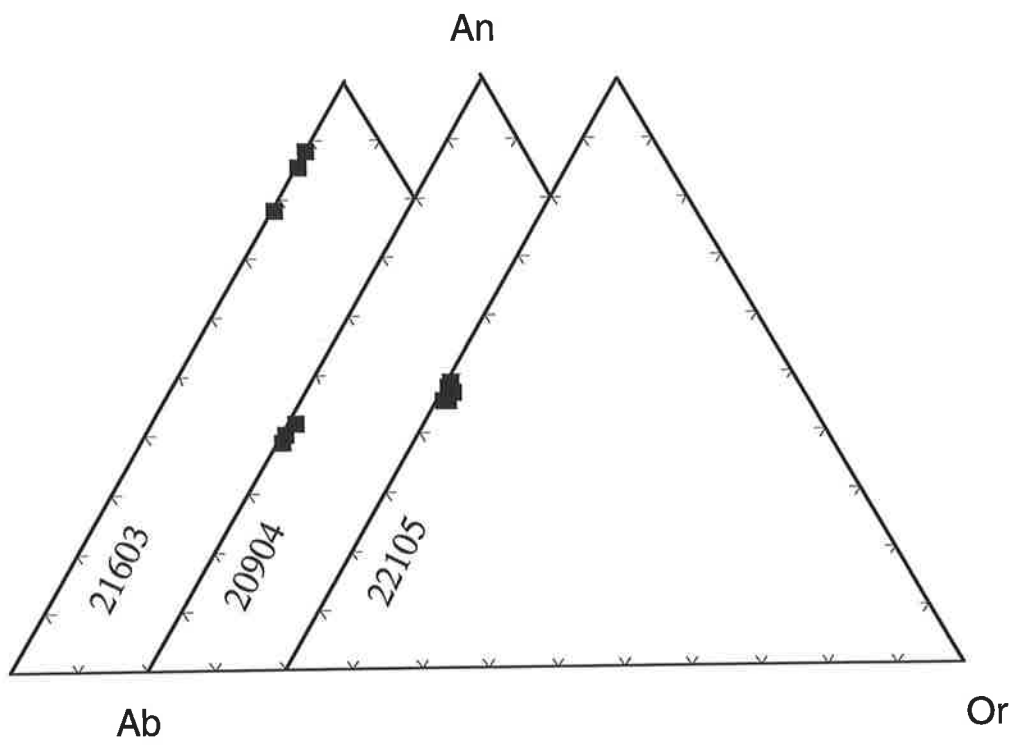


Table 3-3. Representative chemical compositions of minerals from amphibolite

Sample	Clinopyroxene			Amphibole			Garnet	
	21603	21603	22105	21603	21603	22105	22105	22105
SiO ₂ (wt%)	52.59	52.56	49.93	45.84	45.02	38.54	38.13	38.01
TiO ₂	0.11	0.19	0.12	0.99	1.25	1.19	0.00	0.05
Al ₂ O ₃	1.61	1.92	1.91	9.57	10.19	14.26	20.36	20.51
FeO*	11.94	12.31	18.67	17.51	17.62	26.66	27.23	26.17
MnO	0.31	0.36	0.57	0.28	0.18	0.23	3.99	4.01
MgO	11.84	11.82	6.16	10.69	9.89	2.49	1.38	1.32
CaO	22.00	22.03	22.03	11.53	11.94	11.51	9.72	10.21
Na ₂ O	0.45	0.40	0.37	1.29	1.53	1.01	0.00	0.05
K ₂ O	0.00	0.00	0.00	0.38	0.52	1.89	0.00	0.00
Cr ₂ O ₃	0.08	0.00	0.00	0.06	0.09	0.00	0.00	0.00
Total	100.93	101.59	99.76	98.14	98.23	97.78	100.81	100.33
Structural formula								
No.Ox.	6	6	6	23	23	23	12	12
Si	1.970	1.959	1.962	6.810	6.711	6.121	3.032	3.029
Al ^{iv}	0.030	0.041	0.038	1.190	1.289	1.879	0.000	0.000
Al ^{vi}	0.041	0.043	0.051	0.486	0.502	0.792	1.909	1.927
Ti	0.003	0.005	0.004	0.111	0.140	0.142	0.000	0.003
Fe	0.374	0.384	0.614	2.175	2.197	3.541	1.818	1.744
Mn	0.010	0.011	0.019	0.035	0.023	0.031	0.269	0.271
Mg	0.661	0.656	0.361	2.367	2.197	0.589	0.164	0.157
Ca	0.883	0.880	0.928	1.835	1.907	1.959	0.828	0.872
Na	0.033	0.029	0.028	0.372	0.442	0.311	0.000	0.008
K	0.000	0.000	0.000	0.072	0.099	0.383	0.000	0.000
Cr	0.002	0.000	0.000	0.007	0.011	0.000	0.000	0.000
Total	4.007	4.008	4.004	15.460	15.518	15.748	8.013	8.009
Mg/Mg+Fe	0.639	0.631	0.370	0.521	0.500	0.143	0.083	0.082
Ca*	0.460	0.458	0.488	0.288	0.303	0.322	-	-
Mg*	0.345	0.342	0.190	0.371	0.349	0.097	-	-
Fe*	0.195	0.200	0.323	0.341	0.349	0.582	-	-

FeO*: Total Fe as FeO

No.Ox.: Number of oxygens in structural formula

Ca*: Ca/Ca+Mg+Fe, Mg*: Mg/Ca+Mg+Fe, Fe*: Fe/Ca+Mg+Fe

In the garnet amphibolites (eg. sample number 22105), the hornblende is hastingsite or hastingsitic hornblende, with lower Mg/Mg + Fe ratios.

Clinopyroxene

The clinopyroxene is pale green to colorless, and is present as xenoblasts or subidioblasts with average grain size 0.8mm. The chemical composition of the clinopyroxene (Table 3-3) is that of salite in the amphibolite and ferrosalite in the garnet amphibolite.

Garnet

The garnet is present as pale pink idioblasts or subidioblasts, up to 1mm in size, and rich in iron and calcium (Table 3-3).

B. Geochemistry

The major and trace element contents of two amphibolites are given in Table 3-4. Sample locations are shown in Fig. 3-5.

Major elements

The silica contents show the amphibolites to be basaltic, but the values may not be truly indicative because of quartz veins which are common in the amphibolites. The obtained figures are thus maximum values only.

Although some elements may be mobile during metamorphism (Condie, 1976), the chemical data are initially treated on the assumption that the rocks preserve the original chemistry.

Total alkali contents are 1.73 and 1.55, and these are in the range of subalkalic rock in terms of boundary between alkalic and subalkalic rocks suggested by Macdonald and Katsura (1964) and Miyashiro (1978). FeO^* (total Fe as FeO)/MgO versus SiO_2 and FeO^*/MgO versus FeO values (Fig. 3-6) indicate that the rocks are tholeiites according to the discrimination boundary of Miyashiro (1974).

Table 3-4. Chemical compositions of amphibolite

Sample	21602	21603
wt(%)		
SiO ₂	49.72	50.64
Al ₂ O ₃	14.40	15.05
Fe ₂ O ₃ *	12.77	12.40
MnO	0.22	0.20
MgO	7.77	6.50
CaO	11.70	12.98
Na ₂ O	1.44	1.32
K ₂ O	0.29	0.23
TiO ₂	0.52	0.55
P ₂ O ₅	0.05	0.07
LOI	0.64	0.24
Total	99.52	100.18
Trace Elements (ppm)		
Ba	71.5	21.6
Rb	2.5	2.7
Sr	102	63
Zr	22.1	31.2
Nb	3.1	1.4
Y	13.8	16.2
Ce	7	5.1
Nd	9.4	5.8
Sc	49.8	44.1
V	278	256
Cr	295	312
Ni	98	82
Cu	324	166
Zn	94	82
FeO*/MgO	1.48	1.72

Fe₂O₃*: Total Fe as Fe₂O₃

LOI: Loss on ignition

FeO*: Total Fe as FeO

Fig. 3-5. Sample locality map for mafic rocks in the Sally Downs Bore area

MG: meta-gabbro, AM: amphibolite, MD: meta-dolerite,

UM: hornblendite and mela-gabbro (ultramafic rocks)

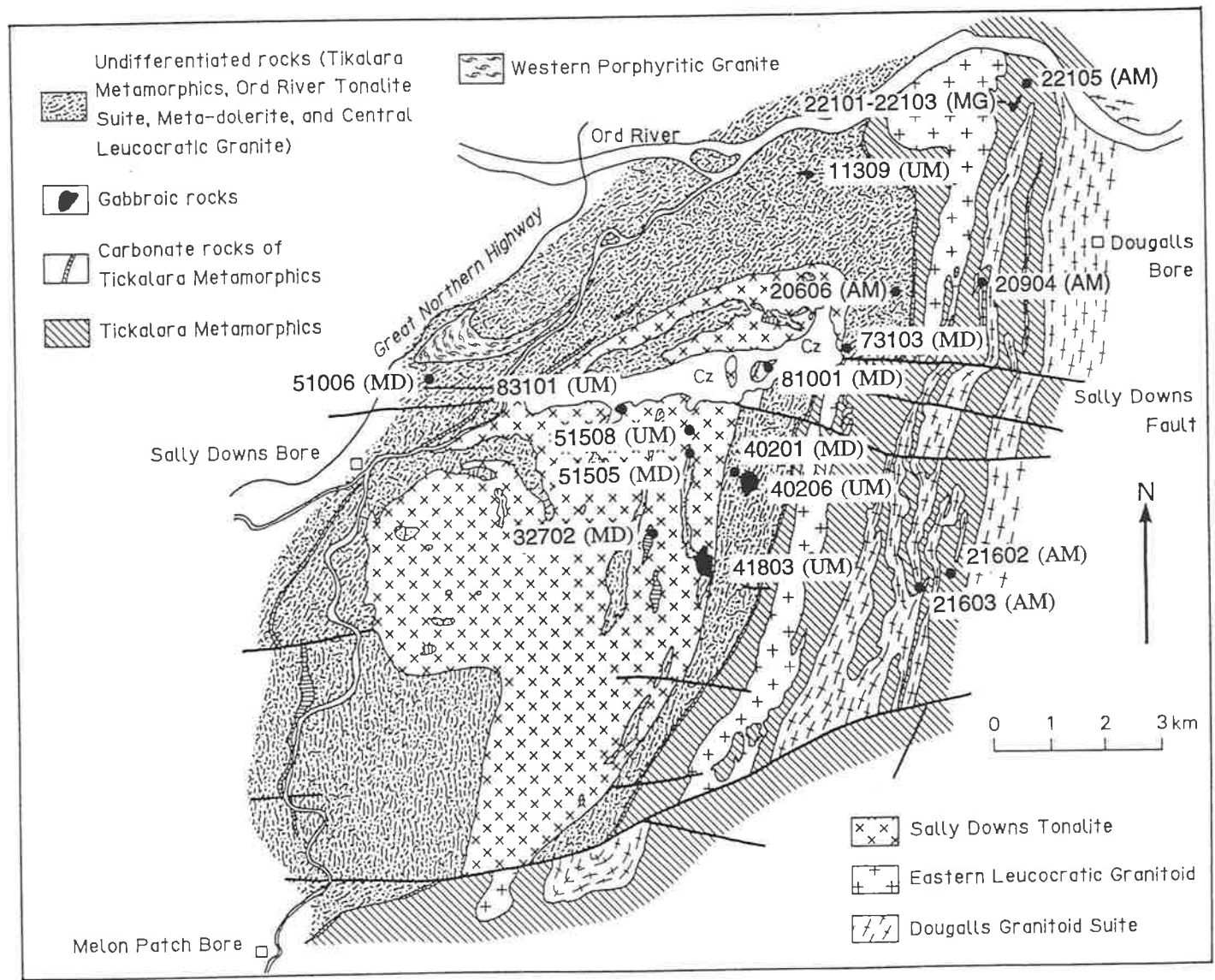


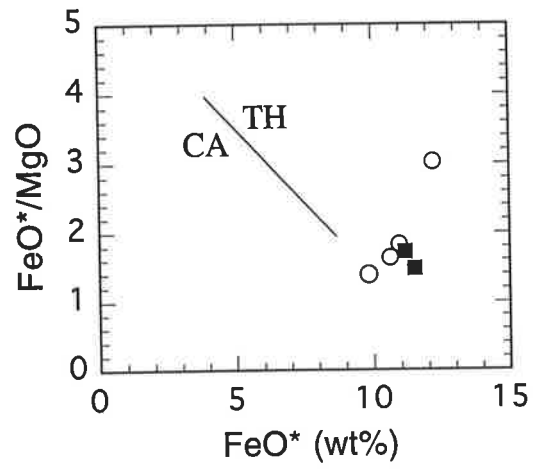
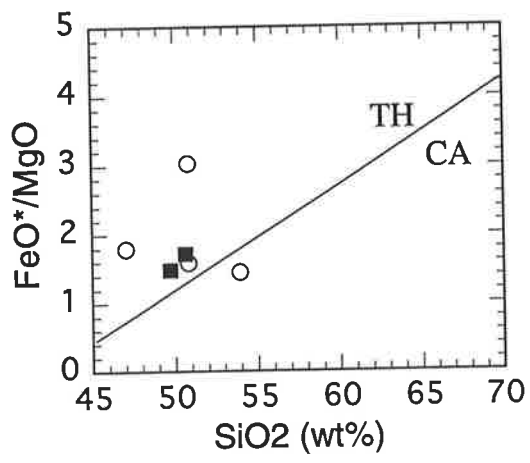
Fig. 3-6. $\text{FeO}^*/\text{MgO}-\text{SiO}_2$ and $\text{FeO}^*/\text{MgO}-\text{FeO}$ plots of amphibolite

Solid squares: present study

Open circles: data from Gemuts (1971)

FeO^* : total Fe as FeO

Tholeiite field (TH) and calcalkaline field (CA) are from Miyashiro (1978).



Major element data of four amphibolites from the Tickalara Metamorphics were presented by Gemuts (1971), and these are also considered here. They are subalkalic, and three of them plot in the tholeiite field (Fig. 3-6), though one sample, which has 54% SiO₂ is calcalkaline.

The major element data thus indicate that the amphibolites could have been derived from tholeiite.

Trace elements

Most of the trace elements are of similar value in the two samples; but Ba and Sr concentrations differ, suggesting possible element mobility. Zr and Nb, which are thought to be relatively immobile during alteration and metamorphism (Condie, 1976), are low in the rocks. The levels of HREE in the samples, suggested by their Y contents, are very low, about 3 times chondritic abundance. The close similarity to low-K tholeiites of modern island arc environments is indicated by Ti - Zr - Y discrimination (Pearce and Cann, 1973).

Vanadium is 278 and 256ppm in the samples. Ti/V ratios are 11.2 and 12.9. This ratio is high in modern mid-ocean ridge basalts (MORB) and ocean island and alkalic basalts, viz. generally more than 20, but is less than 20 in arc tholeiites, and is between 10 and 50 in back-arc basin basalts (Shervais, 1982). Hence these ratios are compatible with values from arc tholeiites or back-arc basin basalts. Ti/Cr ratio versus Ni discrimination (Beccalura et al., 1973) also suggests that the rocks are similar to the island arc tholeiite.

Therefore most of the trace element contents show that the rocks have similar characteristics to the island arc tholeiite. This is relevant to a consideration of the tectonic setting during deposition of Halls Creek Group.

3.2.3. Fine Grained Tonalitic Rocks

A. Petrography

Two samples, 11110 and 11301, are examined in detail. Sample locations are shown in Fig. 3-2. 11110 is a hornblende-biotite tonalite including elongated aggregates of medium grained hornblende (Fig. 3-1E). 11301 is plagioclase porphyritic biotite tonalite (Fig. 3-1F). They are essentially fine grained, but include medium to coarse grained hornblende or plagioclase crystals. Foliation manifested by plagioclase and biotite is apparent.

11110 is composed of plagioclase (45%), biotite (20%), hornblende (15%), and quartz (20%). The compositions are plotted on Qz-Af-Pl diagram (Fig. 3-7). Apatite, epidote, and opaque minerals are accessory. The plagioclase is subhedral; its composition ranges from An 36 to An 42 (Table A8-1), with very low Or content. Hornblende is subhedral, magnesio-hornblende as classified by Leake (1968). Biotite (α = straw yellow, β = γ = dark brown) is subhedral, with Mg/Mg+Fe 0.581-0.597 (Table A8-1).

11301 contains abundant plagioclase (45%), and lesser amounts of quartz (30%) and biotite (20%). Accessories are epidote, allanite, apatite, zircon, and opaque minerals. Small amounts of muscovite and calcite are probably secondary. Rare amphibole is mostly replaced by biotite and opaque minerals. Plagioclase is subhedral or euhedral; composition ranges from An 34 to 46, averaging An 39.6. Or content ranges from Or 0.4 to 1.7. Porphyroblastic plagioclase includes quartz, plagioclase, and biotite crystals. No compositional difference between the porphyroblastic plagioclase and matrix plagioclase is found. Biotite (α = straw yellow, β = γ = dark brown) is subhedral. Mg/Mg+Fe of the biotite ranges from 0.467 to 0.483 (Appendix 8), which is somewhat lower than that of biotite from 11110.

Fig. 3-7. Modal Quartz-Alkali feldspar-Plagioclase diagram for
granitoids

Q: quartz, A: alkali feldspar, P: plagioclase

Classification of granitoid given in the diagram is after Streckeisen
(1976).

FT: Fine grained tonalitic rocks

EG: Eastern Leucocratic Granitoid

DU: Dougalls Granitoid Suite

OR: Ord River Tonalite Suite

CG: Central Leucocratic Granite

WG: Western Porphyritic Granite

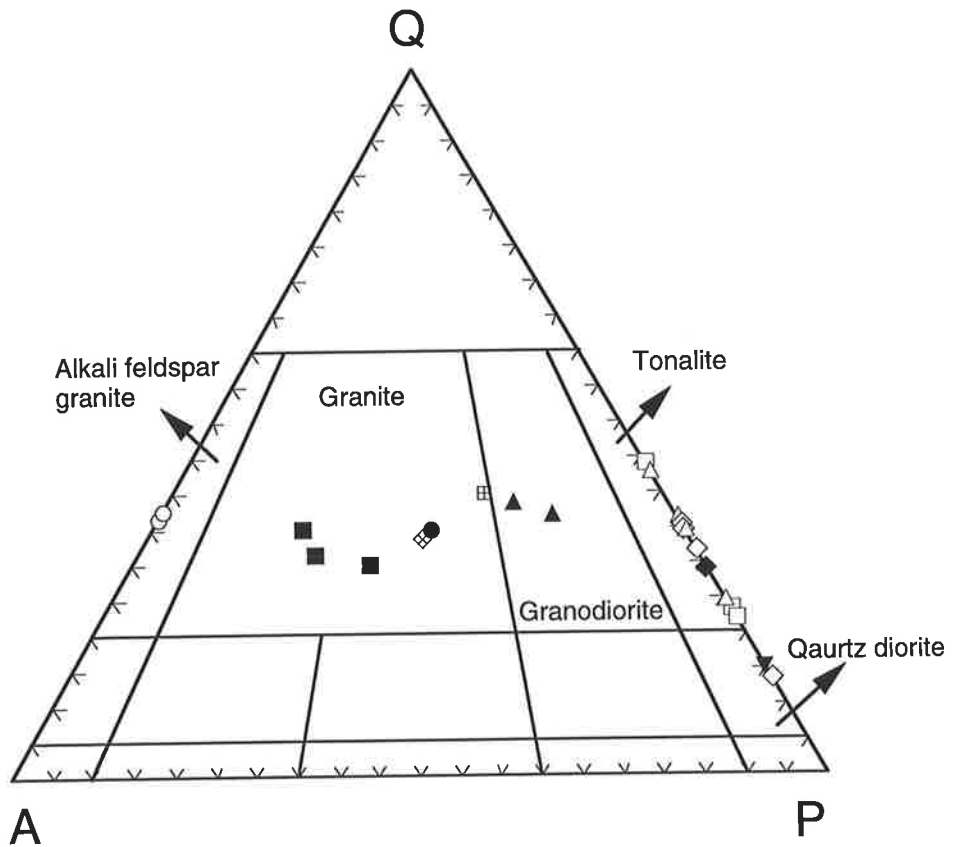
SA: Sally Downs Tonalite

ME: Mafic maicrogranular enclave in the Sally Downs Tonalite

SO: Sophie Downs Granitoid

BR: Bow River Granitoid

KL: Granitoids from the King Leopold Mobile Zone



◆ : FT

▣ : EG

◇ : DU

△ : OR

◊ : CG

● : WG

□ : SA

▼ : ME

○ : SO

■ : BR

▲ : KL

B. Geochemistry

The major and trace element data from the same samples (11110 and 11301) are listed in Table A4-1 (Appendix 4).

SiO₂ in 11110 and 11301 is 61.79 and 61.92 wt%, respectively, indicating that the rocks have intermediate composition. Sample 11110 is metaluminous, whereas 11301 is peraluminous. The Na₂O/K₂O ratio in 11110 and 11301 is 2.45 and 1.83, respectively. The lower ratio in 11301 results from higher K₂O of 11301 than in 11110.

Trace element data (Table A4-1) show that the two analyzed samples have contrasting compositions, suggesting different origins. 11110 contains high V, Cr, and Ni, and may be derived from a relatively primitive intermediate igneous rock, e.g. tonalite or andesite. However 11301 has a high concentration of Rb, Zr, Ce, and Nd. Therefore, it is likely that this rock has originated from a differentiated tonalite or possibly from sedimentary rocks.

3.3. Meta-gabbro

3.3.1. Petrography

The meta-gabbro is composed essentially of hornblende, plagioclase, spinel, and orthopyroxene. Mineral assemblages of three samples examined are:

22101; plagioclase-hornblende-picotite

22102; hornblende-orthopyroxene-chromian ferroan spinel-
plagioclase

22103; plagioclase-hornblende-orthopyroxene.

The texture of the rocks is granoblastic to nematoblastic with average grain size 0.5mm. The hornblende occurs as subidioblastic or xenoblastic grains. In sample 22101, the hornblende is clustered as

irregular shaped glomeroporphyroblastic aggregates which commonly have picotite grains in the core (Fig. 3-1G). The hornblende is pale green and its pleochroism is weak. The chemical composition of the hornblende (Table 3-5) is that of a magnesio-hornblende or tschermakitic hornblende.

The plagioclase is extremely calcic, ranging from An 97 to 98. It occurs as subidioblastic to xenoblastic grains. In sample 22101, the grain boundaries of the plagioclase are generally straight with triple junctions.

The xenoblastic grains of the orthopyroxene are slightly smaller than the amphibole, ranging up to 0.4mm. The orthopyroxene is a bronzite as revealed by electron microprobe analysis (Table 3-5) and by 2V of about 90°.

As indicated above, two types of spinel, picotite and chromian ferroan spinel, are recognized. Opaque picotite is present in sample 22101 closely associated with hornblende. It has high Fe and Cr contents (Table 3-5).

Chromian ferroan spinel is dark green and appears as small subidioblastic grains in sample 22102 (Fig. 3-1H). Zoning is manifested by color variation. Cores are richer in Cr and Fe but lower in Mg and Al (Table 3-5), relative to the rims.

3.3.2. Geochemistry

Major element and trace element contents of the meta-gabbro are presented in Table 3-6. The sample location is shown in Fig. 3-5. SiO₂ in the analyzed sample (22101) is 45.01% which approaches that in ultrabasic rocks. Although the SiO₂ content is low, Fe₂O₃* (total Fe as Fe₂O₃) and MgO are not high, being 4.89 and 8.63% respectively. High concentrations of Al₂O₃ and CaO, together with the features described above, suggest that the precursor of the meta-gabbro was rich in

Table 3-5. Representative chemical compositions of minerals from meta-gabbro

Mineral	Opx	Amphibole		Spinel			
	Sample	22102	22101	22102	22101	22102	22102
wt(%)							
SiO ₂	54.52	45.60	47.23	0.00	0.08	0.07	
TiO ₂	0.00	0.32	0.05	0.00	0.00	0.00	
Al ₂ O ₃	4.97	13.34	14.41	33.46	60.26	62.58	
FeO*	10.60	7.11	5.20	30.16	18.52	16.75	
MnO	0.21	0.09	0.19	0.34	0.15	0.07	
MgO	31.67	16.71	17.63	7.71	16.80	18.14	
CaO	0.10	11.39	11.55	0.00	0.00	0.00	
Na ₂ O	0.00	1.64	1.39	0.00	0.00	0.00	
K ₂ O	0.00	0.28	0.14	0.00	0.00	0.00	
Cr ₂ O ₃	0.00	1.11	0.07	27.08	5.05	3.15	
Total	102.07	97.59	97.86	98.75	100.86	100.76	
Structural formula							
No.Ox.	6	23	23	8	8	8	
Si	1.878	6.495	6.596	0.000	0.004	0.004	
Al iv	0.122	1.505	1.404	0.000	0.000	0.000	
Al vi	0.080	0.735	0.968	2.460	3.706	3.792	
Ti	0.000	0.034	0.005	0.000	0.000	0.000	
Fe	0.305	0.847	0.607	1.573	0.808	0.720	
Mn	0.006	0.011	0.022	0.018	0.007	0.003	
Mg	1.626	3.547	3.669	0.717	1.306	1.390	
Ca	0.004	1.738	1.728	0.000	0.000	0.000	
Na	0.000	0.453	0.376	0.000	0.000	0.000	
K	0.000	0.051	0.025	0.000	0.000	0.000	
Cr	0.000	0.125	0.008	1.335	0.208	0.128	
Total	4.021	15.541	15.410	6.102	6.039	6.036	
Mg/Mg+Fe	0.842	0.807	0.858	0.313	0.618	0.659	

FeO*: Total Fe as FeO

No.Ox.: Number of oxygens in structural formula

Table 3-6. Chemical composition of the meta-gabbro

Unit	MD	Panton Sill		McIntosh Sill			SLCI
Sample	22101	PS-A20 H17	PS-A14 H22	MS-14 M4	MS-37 M8	MS-33 M10	SLK8
wt(%)							
SiO ₂	45.01	45.00	46.72	45.95	45.37	47.51	48.03
Al ₂ O ₃	23.88	27.34	27.65	28.18	24.68	23.35	23.36
Fe ₂ O ₃ *	4.89	3.24	4.09	3.97	6.03	3.97	4.10
MnO	0.01	0.07	0.05	0.04	0.06	0.06	0.07
MgO	8.63	5.82	2.46	5.36	7.92	5.74	7.86
CaO	15.28	16.78	14.48	14.10	12.23	15.32	12.50
Na ₂ O	0.96	0.43	2.42	1.56	1.82	1.76	1.31
K ₂ O	0.14	0.04	0.16	0.07	0.07	0.05	0.74
TiO ₂	0.17	0.07	0.28	0.06	0.10	0.24	0.09
P ₂ O ₅	0.04	0.03	0.08	0.04	0.04	0.03	0.00
H ₂ O+		0.57	0.80	1.17	1.44	1.56	1.76
LOI	0.64						
Total	99.74	99.39	99.19	100.50	99.76	99.59	99.82
(ppm)							
Ba	25.9						
Rb	1.1						
Sr	143						
Zr	8.1						
Nb	1						
Y	3.2						
Sc	21.4						
V	104	41	100				
Ni	237	144	59	140	145	73	79
Nd	4.5						
Cr	5638	640	38	105	310	1020	684
Cu	139	43	45	20	40	95	
Zn	47	9	17	18	31	13	
Na ₂ O+K ₂ O	1.10	0.47	2.58	1.63	1.89	1.81	2.05
FeO*/MgO	0.51	0.50	1.50	0.67	0.69	0.62	0.47

MD: meta-gabbro, SLCI: Salt Lick Creek Layered Intrusion

Rock type and source of data:

22101: meta-gabbro: this work

PS-A20-H17: Leucocratic meta-gabbro (pl amph chl ilm): (1)

PS-A14 H22: Leucocratic meta-gabbro (pl amph cz sph ilm): (1)

MS-14-M4: Leucocratic olivine gabbro (pl ol hb cpx opx): (1)

MS-37-M8: Leucocratic olivine norite (pl ol opx hb): (1)

MS-33-M10: Leucocratic olivine gabbro (pl cpx ol opx hb): (1)

SLK8: Plagioclase-orthopyroxene mesocumulate (pl amph opx z): (2)

pl=plagioclase, amph=amphibole, chl=chlorite, ilm=ilmenite, cz=clinozoisite, z=zoisite

ol=olivine, hbl=hornblende, cpx=clinopyroxene, opx=orthopyroxene, sph=sphene

Source of data: (1)Hamlyn(1977), (2)Wilkinson et al. (1975)

Fe₂O₃*: Total Fe as Fe₂O₃ FeO*: Total Fe as FeO

LOI: Loss on ignition

plagioclase, thus possibly a leucocratic gabbro or the plagioclase cumulate phase of a basic intrusion.

Total alkali content indicates that the rock is subalkalic. High chromium content reflects the presence of the picotite.

In the Halls Creek Orogenic Zone, rocks of similar chemical composition to that of the meta-gabbro are reported by Wilkinson et al. (1975) from the Salt Lick Creek Layered Intrusion, and by Hamlyn (1977) from the Panton Sill and McIntosh Sill (Table 3-6). Comparison of the chemistry of the meta-gabbro to that of relatively unrecrystallized samples of McIntosh Sill suggest that plagioclase, olivine, and pyroxenes are major constituents of the meta-gabbro precursor.

From the geochemistry, it is concluded that the meta-gabbro is derived from a leucocratic gabbro which may represent part of the plagioclase rich cumulate phase of a basic intrusion.

3.4. Eastern Leucocratic Granitoid Suite

3.4.1. Petrography

Three types of Eastern Leucocratic Granitoid Suite are described separately.

A. Type I Granitoids

Type I granitoids of the Eastern Leucocratic Granitoid Suite are characterized by the presence of garnet (Fig. 3-8A and B). The garnets appear as rounded euhedral or subhedral grains, one to three millimeters in diameter. They are pale pink to reddish brown in thin section, and typically inclusion free. The granitoids contain quartz, plagioclase (An 12 - 17), and microcline (Or 86 - 94) as major constituents (Fig. 3-7), comprising more than 90% of the rocks (Table A2-1). Small amounts of biotite, muscovite, opaque mineral, and zircon are present. The biotite

Fig. 3-8. Photomicrographs of the Eastern Leucocratic Granitoid and
Dougalls Granitoid

A. Eastern Leucocratic Granitoid (type I).

Sample: 51603. Gar: garnet, Bi: biotite. Plane polarized light.

Scale bar is 1 mm.

B. Same as A, but under crossed polarized light.

Qz: quartz, KF: K-feldspar, Pl: plagioclase

C. Eastern Leucocratic Granitoid (type II).

Sample: 41702. Gar: garnet, Opq: opaque mineral, Bi: biotite

Plane polarized light. Scale bar is 1mm.

Type II granite is more mafic than the type I granite.

D. Same as C, but under crossed polarized light.

Pl: plagioclase, KF: K-feldspar.

E. Orthopyroxene bearing tonalite of the Dougalls Granitoid Suite

Sample: 12702. Opx: orthopyroxene, Ho: hornblende, Bi: biotite,

Opq: opaque mineral. Plane polarized light. Scale bar is 1 mm.

F. Same as E, but under crossed polarized light.

Pl: plagioclase, Qz: quartz.

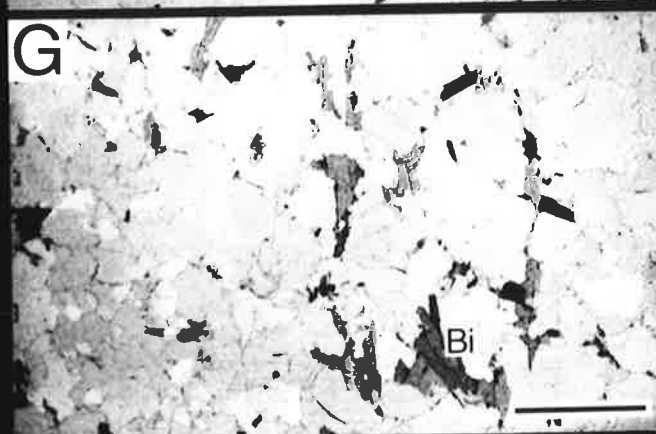
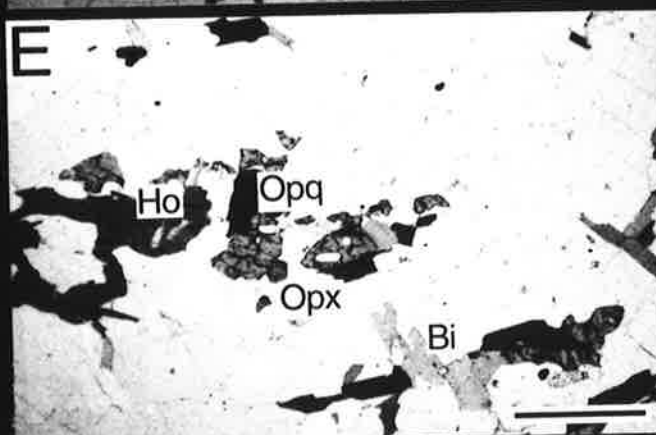
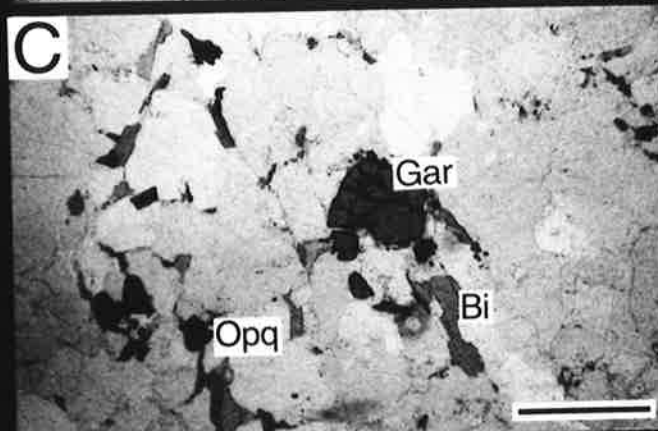
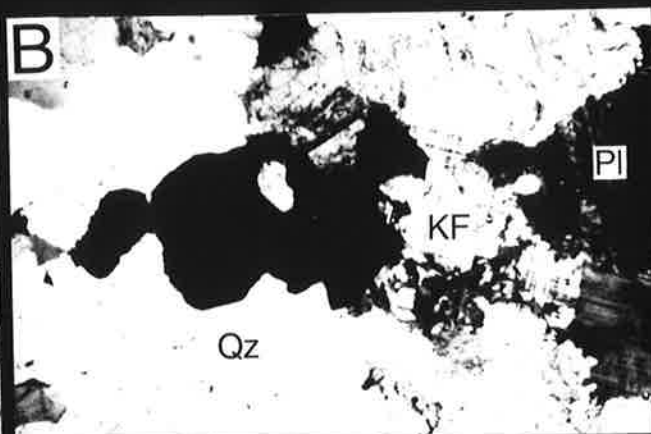
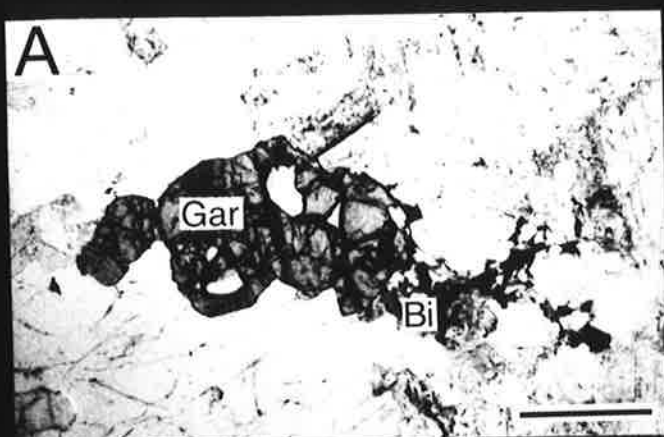
G. Trondhjemite of the Dougalls Granitoid Suite

Sample: 90301. Bi: biotite. Plane polarized light.

Scale bar is 1 mm.

H. Same as G, but under crossed polarized light.

Pl: plagioclase, Qz: quartz.



(α = yellow, β = γ = dark greenish brown) is generally subhedral, and fine to medium grained. The opaque mineral phase is ubiquitous as is the garnet.

The texture of the rocks is hypidiomorphic-granular with slight recrystallization along the grain boundaries. Myrmekite texture is observed at some plagioclase-microcline grain boundaries.

B. Type II Granitoids

The granitoids of type II are slightly more mafic than the type I granitoids, containing as much as 15% of mafic mineral. Up to 1% garnet is present also in these granitoids (Fig. 3-8C and D). Small subhedral grains are between 0.2 and 1mm in diameter. The garnets have a pale pink color in thin section, and occasionally have inclusions of quartz and perthitic feldspar.

The texture of the type II granitoids is hypidiomorphic-granular. Myrmekite texture is common. Strong foliation is manifested by parallel alignment of small flakes of biotite (α = straw yellow, β = γ = dark brown).

The type II granitoids consist of quartz, plagioclase (An 15 - 18), microcline (Or 79 - 95), biotite, muscovite, opaque minerals, zircon, apatite, allanite, and garnet.

C. Type III Granitoids

Granitoids of this type are characterized by the presence of particularly dark gray colored plagioclase. Similar gray to dark gray colored plagioclase is commonly found in charnockite, and the cause of the color is discussed by Howie (1967) and Oliver and Schultz (1968). They concluded that thin veins of iron rich material, possibly chlorite, in the plagioclase are responsible for the overall color. Under the

microscope, apart from yellowbrown to brown veins in plagioclases of the type III granitoids, the dark plagioclases are no different from normal plagioclase.

The granitoids are trondhjemite, consisting mainly of quartz and plagioclase. Rounded phenocrysts of quartz and plagioclase are present in a fine grained matrix. The texture provides evidence of extensive deformation and recrystallization.

Biotite (α = yellow, β = γ = reddish brown) occurs as elongated aggregates manifesting strong foliation. Minor muscovite and zircon are present.

3.4.2. Mineral Chemistry

A. Biotite

Representative chemical compositions of biotite from the Eastern Leucocratic Granitoids are presented in Table 3-7. Mg/(Mg+Fe+Mn) in biotites is generally low (Fig. 3-9A); in those from sample 51603 (type III) it is extremely low, approaching the pure end molecule of siderophyllite. High K₂O contents and relatively low Si (5.185- 5.511) are also characteristic. TiO₂ content ranges from 2.12 to 3.23 wt %, higher in biotites from the type I granitoid (51603 and 51607) than in those from the type II (40306 and 41702). The MnO range, from 0.08 to 0.55 wt %, is lower than that of biotites coexisting with garnets, described from other areas, whose the value is typically more than 0.75 wt % (Miller and Stoddard, 1981).

B. Garnet

Representative chemical compositions of the garnet in the granitoids are given in Table 3-7. The results show that the garnets are essentially almandine-spessartine solid solutions (Fig. 3-9B); these two end members

Table 3-7. Representative chemical compositions of minerals from the Eastern Leucocratic Granitoid

Mineral	Biotite				Garnet							
	40306	41702	51603	51607	40306	40306	40306	40306	41702	51603	51607	
	II	II	I	I	II	II	II	II	II	I	I	
Type	Core-----Rim		Core-----Rim		Core-----Rim		Core-----Rim					
SiO ₂ (wt%)	34.43	34.75	31.83	34.50	35.76	36.01	35.74	36.80	36.58	36.04	36.91	
TiO ₂	2.42	2.12	3.23	3.04	0.03	0.00	0.00	0.07	0.00	0.00	0.04	
Al ₂ O ₃	16.86	17.68	18.20	17.73	20.14	20.39	20.01	20.12	20.65	20.57	20.11	
FeO*	25.33	24.35	32.20	23.30	27.48	27.41	27.45	27.87	24.41	34.50	25.59	
MnO	0.55	0.34	0.08	0.18	9.79	9.72	9.85	9.71	15.10	5.48	11.13	
MgO	5.89	7.21	1.00	7.85	1.23	1.05	0.86	0.86	0.74	0.51	2.33	
CaO	0.00	0.00	0.00	0.00	4.52	4.48	4.28	4.20	2.92	2.66	3.25	
Na ₂ O	0.10	0.00	0.07	0.03	0.05	0.01	0.07	0.14	0.05	0.05	0.09	
K ₂ O	9.76	9.95	9.07	9.52	0.02	0.00	0.01	0.00	0.00	0.00	0.01	
Cr ₂ O ₃	0.00	0.03	0.00	0.01	0.02	0.03	0.05	0.02	0.02	0.07	0.00	
Total	95.34	96.43	95.68	96.16	99.04	99.10	98.32	99.79	100.47	99.83	99.46	
Structural formula												
No.Ox.	22	22	22	22	12	12	12	12	12	12	12	
Si	5.447	5.394	5.185	5.331	2.955	2.967	2.975	3.009	2.982	2.969	3.007	
Al iv	2.553	2.606	2.815	2.669	0.000	0.000	0.000	0.000	0.000	0.000	0.000	
Al vi	0.591	0.629	0.681	0.561	1.962	1.981	1.964	1.939	1.985	1.998	1.931	
Ti	0.288	0.247	0.396	0.353	0.002	0.000	0.000	0.004	0.000	0.000	0.002	
Fe	3.351	3.161	4.387	3.011	1.899	1.889	1.911	1.906	1.664	2.377	1.743	
Mn	0.074	0.045	0.011	0.024	0.685	0.678	0.694	0.673	1.043	0.382	0.768	
Mg	1.389	1.668	0.243	1.808	0.151	0.129	0.107	0.105	0.090	0.063	0.283	
Ca	0.000	0.000	0.000	0.000	0.400	0.396	0.382	0.368	0.255	0.235	0.284	
Na	0.031	0.000	0.022	0.009	0.008	0.002	0.011	0.022	0.008	0.000	0.014	
K	1.970	1.970	1.885	1.877	0.002	0.000	0.001	0.000	0.000	0.000	0.001	
Cr	0.000	0.004	0.000	0.001	0.001	0.002	0.003	0.001	0.001	0.005	0.000	
Total	15.693	15.724	15.625	15.643	8.066	8.043	8.048	8.027	8.029	8.029	8.033	
Mg/Mg+Fe	0.293	0.345	0.052	0.375	0.074	0.064	0.053	0.052	0.051	0.026	0.140	

FeO*: Total Fe as FeO

No.Ox.: Number of oxygens in structural formula

Fig. 3-9. Biotite and garnet composition plot from the Eastern
Leucocratic Granitoid

A. Biotite.

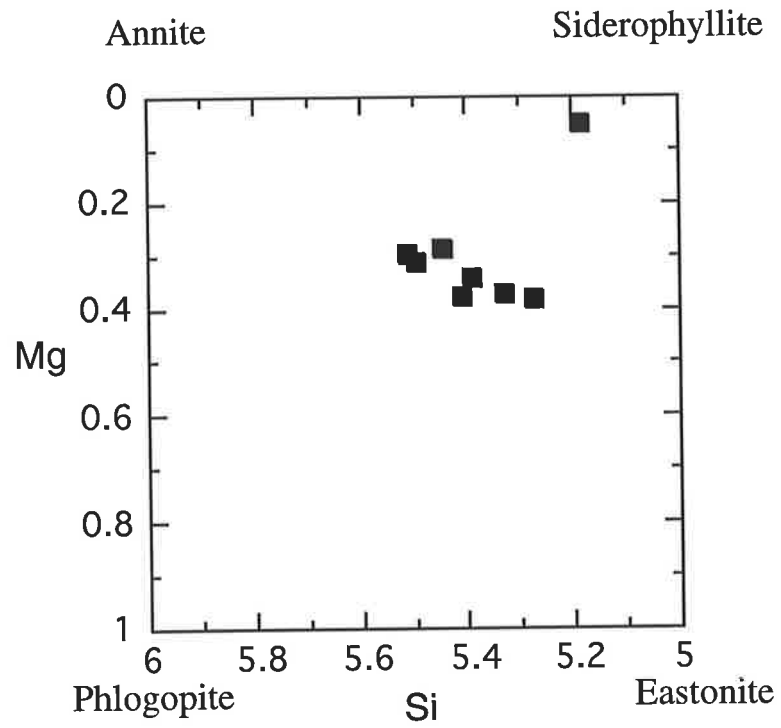
Si: Si value in the structural formula of 22 oxygens.

Mg: $Mg/Mg+Fe+Mn$

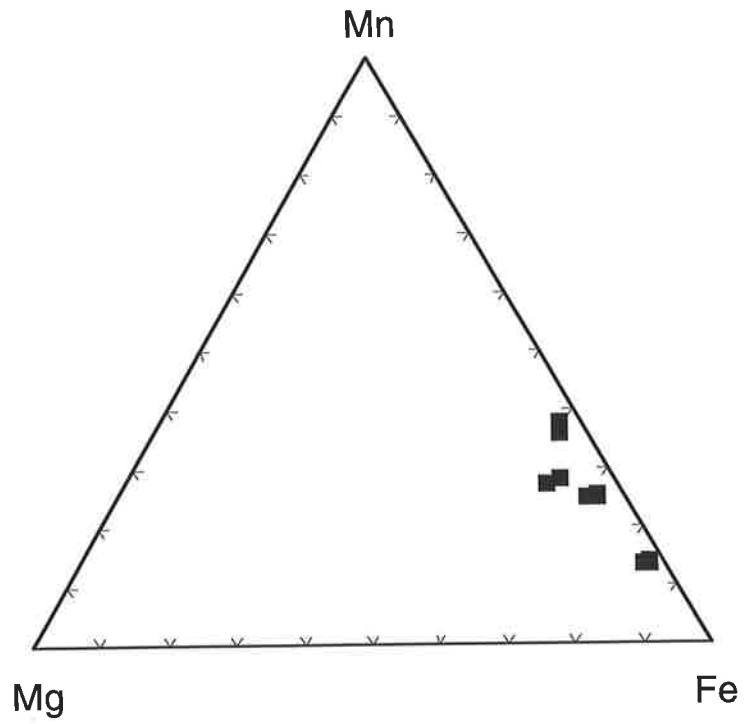
B. Garnet.

Mn, Mg, Fe: Mn, Mg, Fe values in the structural formula of 12 oxygens

A. Biotite



B. Garnet



of the garnet comprise more than 80 mole %. Spessartine content of the garnets is high, varying from 12.3 to 34.2 mole %, antithetically with the almandine content.

Analyses of core and rim, from two garnet crystals in sample 40306 (Table 3-7), indicate that zoning is weak. Similarly, Table 3-7 shows that the garnet composition is roughly uniform within a sample. However, notable compositional differences of the garnets are found between the samples analyzed, though no consistent differences between garnets from the type I and II granitoids are apparent.

3.4.3. Geochemistry

Eleven samples of the Eastern Leucocratic Granitoid are examined, and their major and trace element data are listed in Table A4-2 (Appendix 4). Sample locations are indicated in Fig. 3-10.

A. Major elements

The Eastern Leucocratic Granitoids have a limited range of SiO₂, from 74% to 78% (Table A4-2), excluding a specimen with slightly low SiO₂ (70.27%). Despite this, three types of granitoid are distinguished according to the SiO₂ content; viz. granitoids of type I have a middle value within its SiO₂ range, and type II lower and type III higher, values.

Mol. (Al₂O₃/CaO+Na₂O+K₂O) ratios range from 0.965 to 1.051 (Table A4-2). Three samples out of 11 samples analyzed are mildly peraluminous. It is interesting to point out that the garnet-bearing granitoid samples are metaluminous.

On the variation diagram (Fig. 3-11), Al₂O₃ shows a small decrease with increase of SiO₂. Because of the effect of constant sum on the Harker-type variation diagram, it is necessary to consider whether the decrease of an element with increase of SiO₂ is influenced by this effect

Fig. 3-10. Sample locality map for the Eastern Leucocratic Granitoid

(I): type I

(II): type II

(III): type III

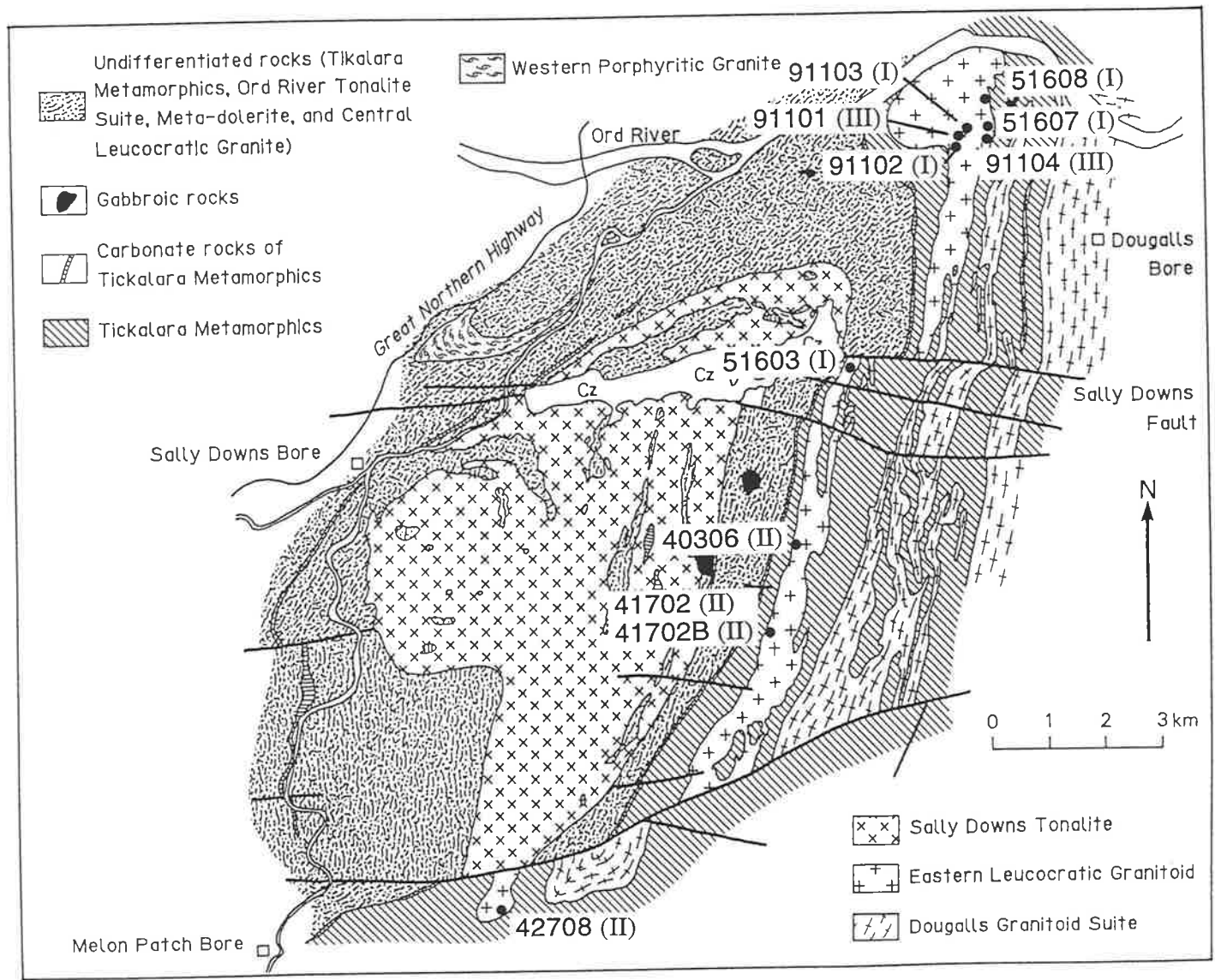


Fig. 3-11. Major element variation diagram of the Eastern Leucocratic
Granitoid

A. $\text{Al}_2\text{O}_3\text{-SiO}_2$

Reference line in the diagram shows effect of constant sum, and is drawn from a point representing 100% SiO_2 and 0% of the other element extrapolated into the diagram. Same for lines in B., C., and D. See text for details

B. $\text{Fe}_2\text{O}_3^*\text{-SiO}_2$ (total Fe as Fe_2O_3)

C. MgO-SiO_2

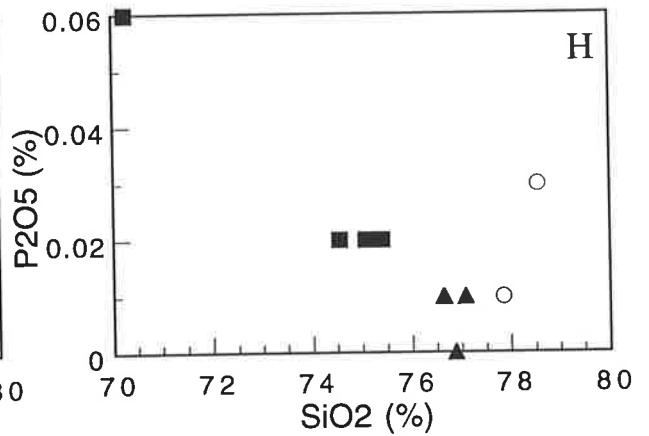
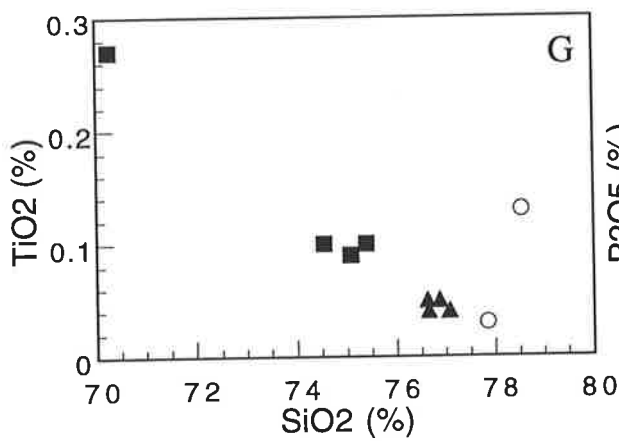
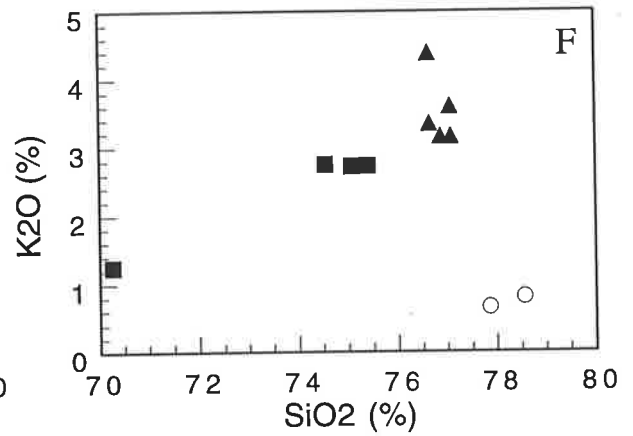
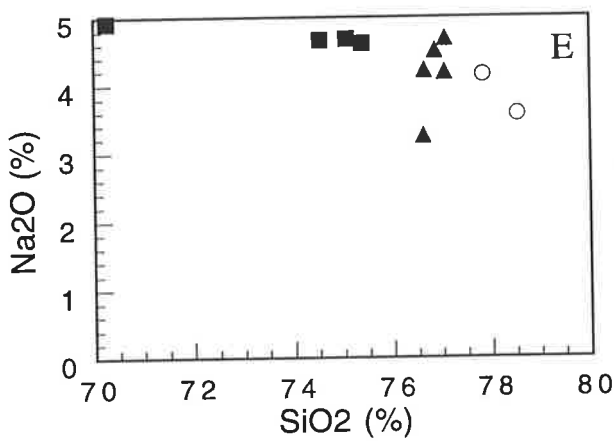
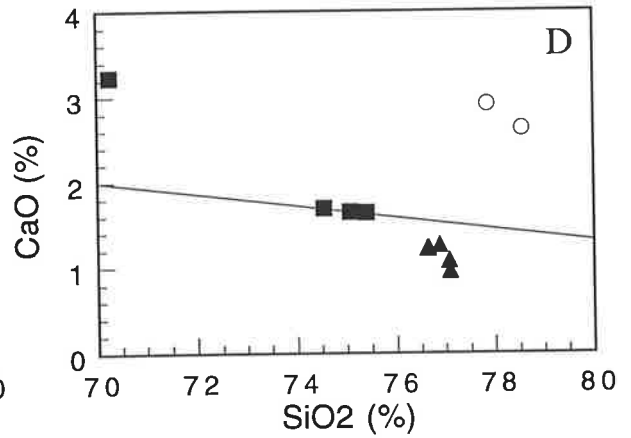
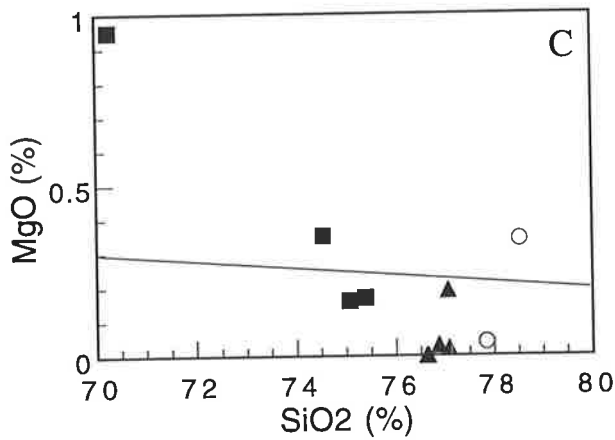
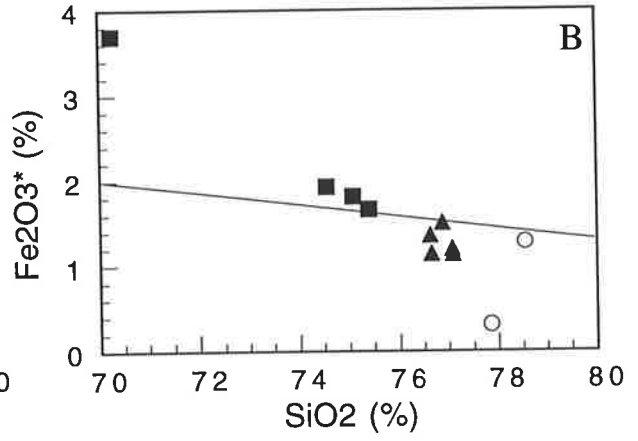
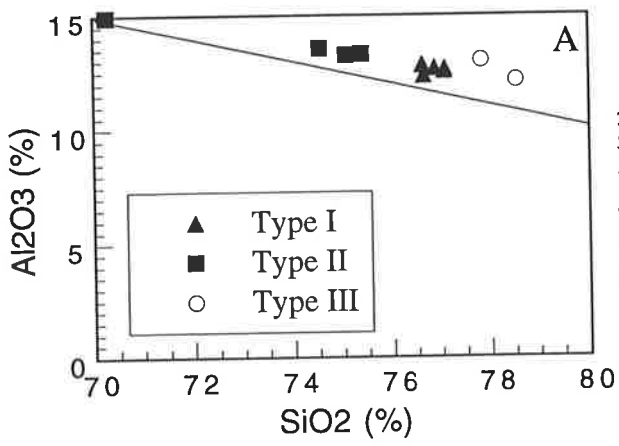
D. CaO-SiO_2

E. $\text{Na}_2\text{O-SiO}_2$

F. $\text{K}_2\text{O-SiO}_2$

G. $\text{TiO}_2\text{-SiO}_2$

H. $\text{P}_2\text{O}_5\text{-SiO}_2$



or not. To check this, reference lines are drawn from a point, representing 100% SiO₂ and 0% of the other element into the diagram (Fig. 3-11A,B,C, and D). As shown, Al₂O₃ in type II to type I granitoids decreases along the line indicating the effect of the constant sum. Fe₂O₃* decreases more than the effect of constant sum. On the CaO versus SiO₂ diagram, it is clear that the type III granitoids have a higher CaO content than the other two types, suggesting a compositional gap between them. The difference is also observed in the K₂O content, viz. the type III granitoids have very low K₂O (less than 1%). Type I granitoids may be derived from type II by fractional crystallization.

On the Na₂O versus K₂O diagram (Fig. 3-12A), type I and II granitoids show a common linear trend with total alkali content about 7.7%. However, type III granitoids occupy an area of lower total alkali with high Na₂O/K₂O ratio, resulted from a low K₂O content in the granitoids. In contrast to the K₂O concentration, a relatively high CaO content of the type III granitoids is shown in the ternary plot Na₂O - K₂O - CaO (Fig. 3-12B).

B. Trace element

Ba

Ba content in the granitoids varies considerably from 276 to 2266ppm; nevertheless, the range within each granitoid type is small as shown on Ba versus SiO₂ diagram (Fig. 3-13A). A large difference between the Ba content of type I and II granitoids contrasts with the similarity of most of the major elements in the two granitoids. A positive correlation of Ba and K₂O is significant (Fig. 3-13B), as they are potentially mobile and values are susceptible to modification during metamorphism and fluid migration. The K/Ba ratio ranges from 16 and 34.

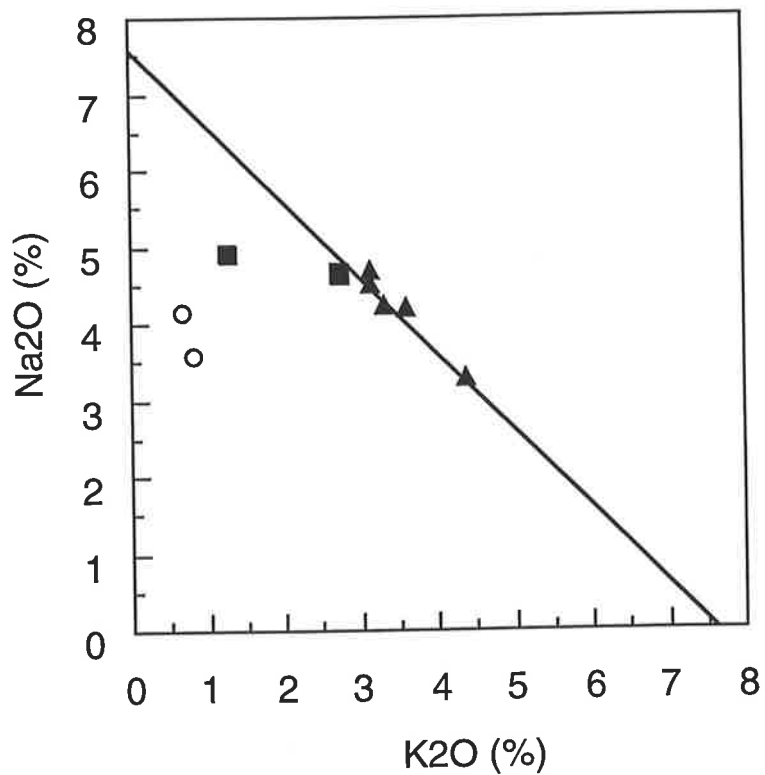
Fig. 3-12. $\text{Na}_2\text{O}-\text{K}_2\text{O}$ and $\text{Na}_2\text{O}-\text{K}_2\text{O}-\text{CaO}$ plot of the Eastern
Leucocratic Granitoid

Symbols are the same as those in Fig. 3-11.

A. $\text{Na}_2\text{O}-\text{K}_2\text{O}$

B. $\text{Na}_2\text{O}-\text{K}_2\text{O}-\text{CaO}$

A.



B.

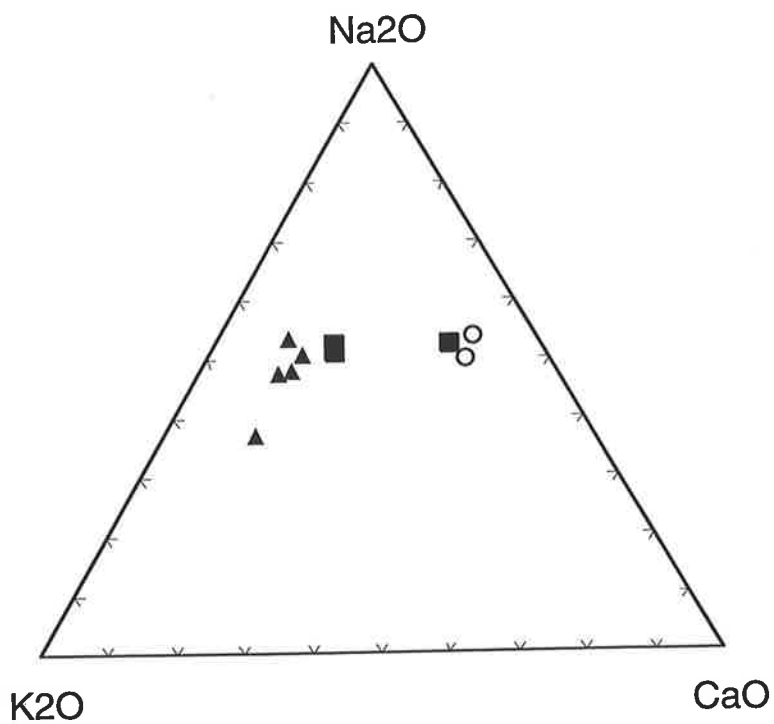


Fig. 3-13. Trace element variation diagram of the Eastern Leucocratic
Granitoid

A. Ba-SiO₂

B. K₂O-Ba

C. Rb-SiO₂

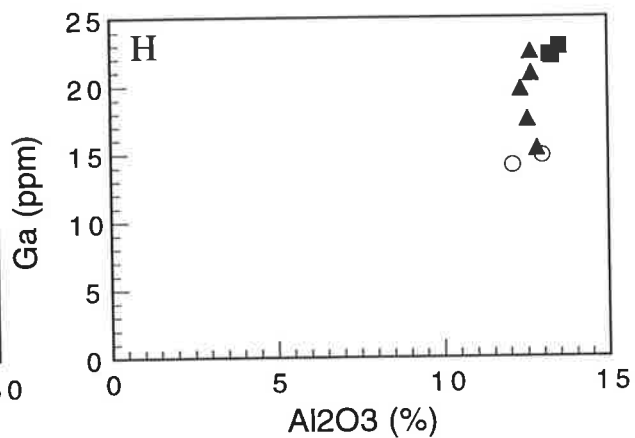
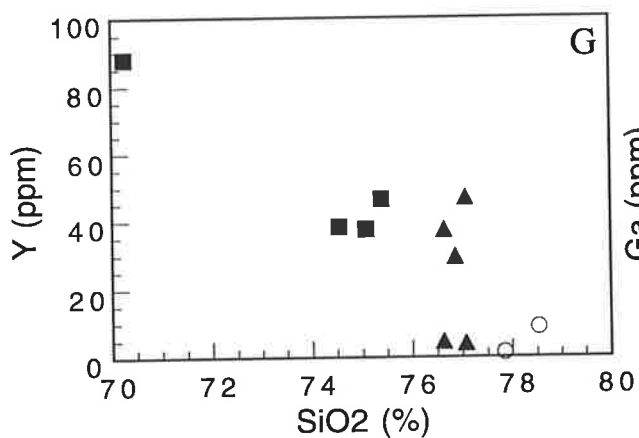
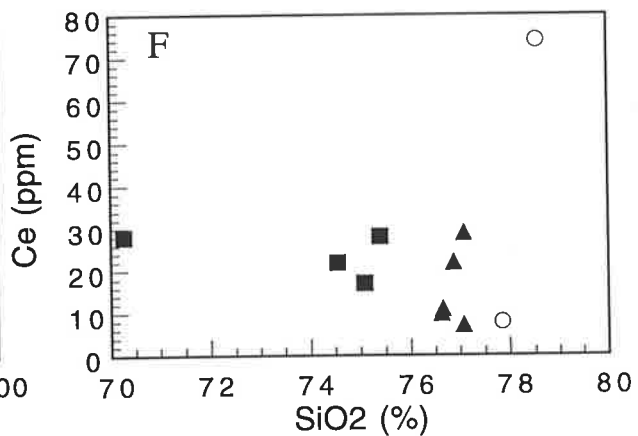
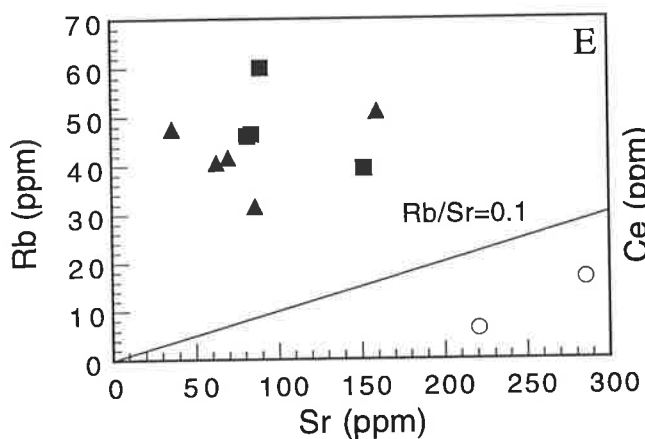
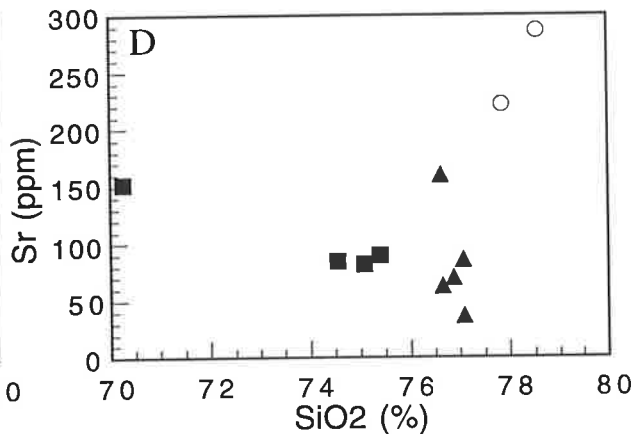
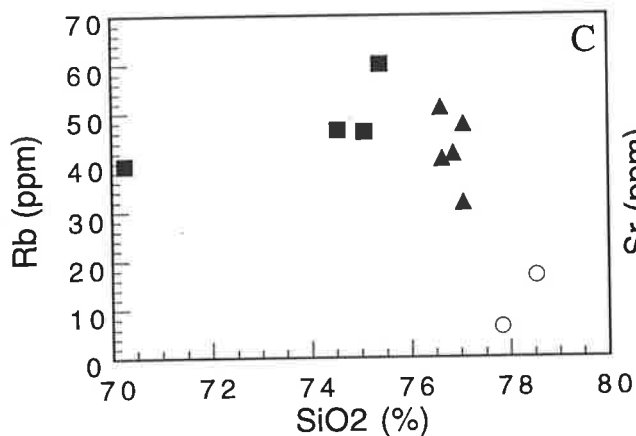
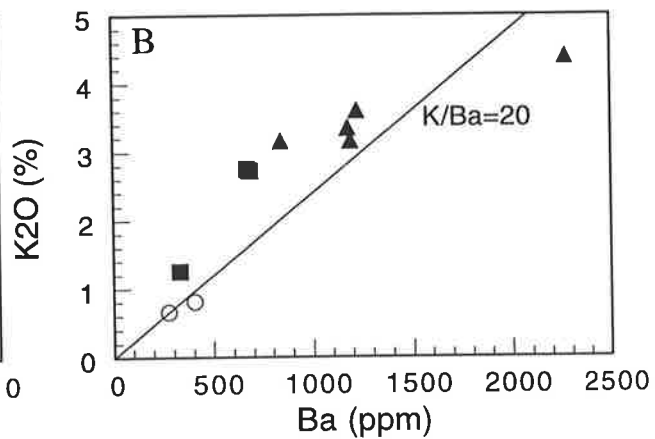
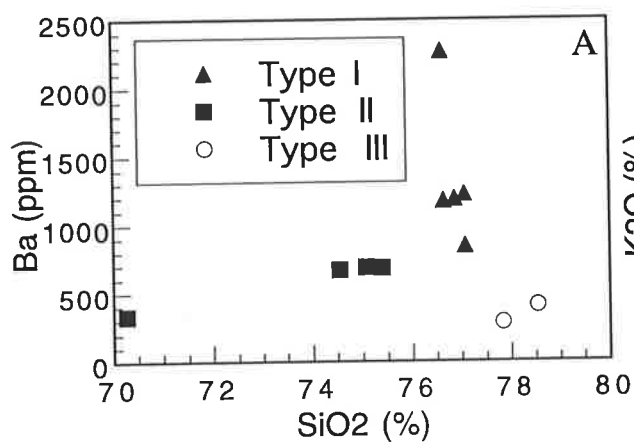
D. Sr-SiO₂

E. Rb-Sr

F. Ce-SiO₂

G. Y-SiO₂

H. Ga-Al₂O₃



Rb

The Rb content is generally low, increasing 40 to 60ppm, then decreasing from 60 to 6ppm with increase of SiO₂ content (Fig. 3-13C). Very low Rb content in the type III granitoids is characteristic. A low level of Rb is commonly found in granitoids of granulite facies rocks (e.g. Rollinson and Windley, 1980b).

Sr

Sr content in the type I granitoids ranges from 37 to 160ppm, with a mean at about 80ppm. Type II granitoids have a moderate Sr content of about 85ppm. Type III granitoids show higher Sr content than the other two types (Fig. 3-13D). Rb/Sr ratios of type I and II granitoids are between 0.26 and 1.3, but they are substantially lower in the type III granitoids, viz. less than 0.1 (Table A4-2 and Fig. 3-13E).

Y and REE

Y content varies significantly from 1.3 to 88ppm. Even in granitoids of same type, it shows considerable variation (Fig. 3-13G). With respect to the concentration of Y, the Eastern Leucocratic Granitoids can be grouped into two types, namely a low Y type (containing less than 9ppm Y) and a high Y type (containing more than 30ppm Y); the two types correspond to garnet-free and garnet-bearing granitoids, respectively. Thus the large variation may be due to the presence or absence of garnet which generally contains a high level of Y and heavy REE.

Ce is generally low, ranging from 7 to 29ppm, except in one sample from type III (Fig. 3-13F). Ce/Nd ratio is more than 1.5 - slightly higher than the ratio in chondrites (about 1.36), suggesting a slight light REE (LREE) enriched chondrite normalized pattern, at least in the LREE region. However, a high level of Y in some of the samples is not in accordance with this suggestion. In fact, a complete rare earth element

determination on a sample from type I (Table A5-2) reveals a peculiar chondrite normalized pattern (Fig. 3-14), with a concave shape, apparently depleted in the middle REE (MREE), with strong positive Eu anomaly. It is not a common pattern in any igneous rocks. Two examples of a similar pattern have been reported by Weaver et al. (1982) in an Archaean amphibolite from S.W. Greenland. Duke et al. (1992) presented similar REE patterns from granite and pegmatite of the Calamity Peak Pluton, in South Dakota.

Leucogranites showing MREE depleted chondrite normalized pattern with negative Eu anomaly are described by Zhao and Cooper (1993). They considered that the geochemical characteristics of the granite resulted from fractionation of monazite and indicated the importance of the fractionation of accessory minerals. The monazite effectively accommodates rare earth elements as indicated by their extremely high distribution coefficients (Fig. 3-15). Therefore, monazite fractionation should rapidly reduce REE (especially LREE) concentration in the magma. However, constant levels of LREE in the Eastern Leucocratic Granitoid do not indicate monazite fractionation between the samples analyzed. Furthermore, the high concentrations of HREE in the Eastern Leucocratic Granitoid are not consistent with the monazite fractionation model.

The MREE depletion and positive Eu anomaly can be achieved by apatite fractionation from a granitoid magma. The distribution coefficient values of rare earth elements between apatite and melt are shown in Fig. 3-15. Indeed, P₂O₅ content in the granitoids is very low - less than 0.02% - which may result from apatite fractionation. However, the large depletion of MREE could not be explained solely by apatite fractionation. Since the level of HREE is rather high, the apparent

Fig. 3-14. Chondrite normalized REE plot of Eastern Leucocratic
Granitoid

Sample: 51607 (type I of the Eastern Leucocratic Granitoid)

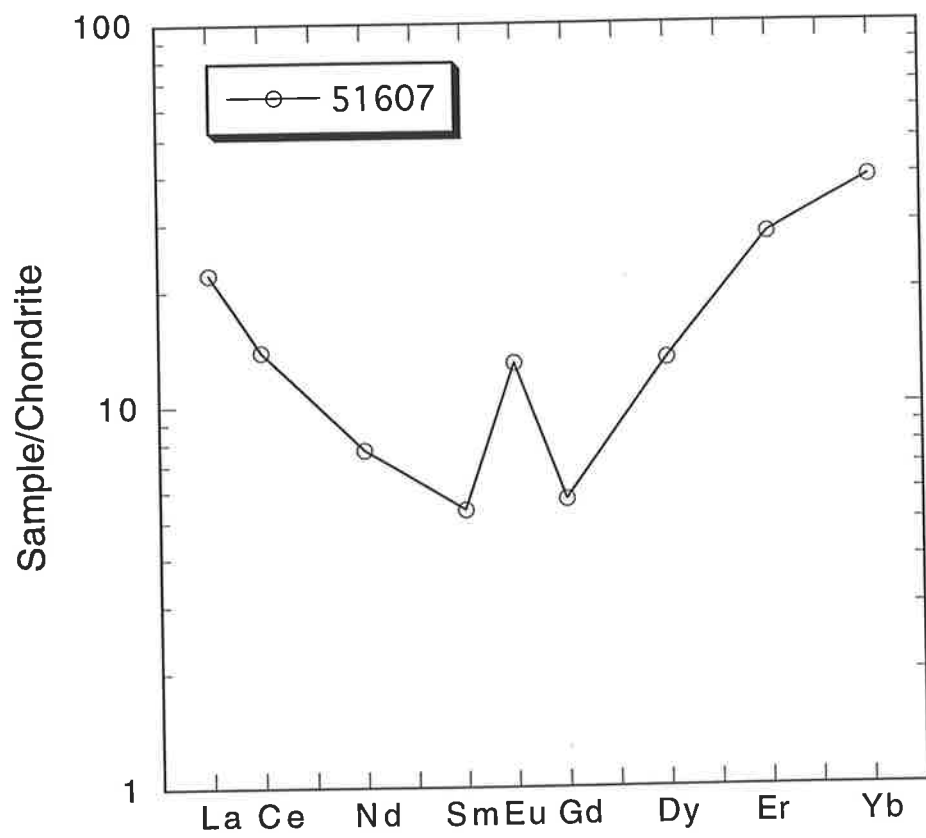


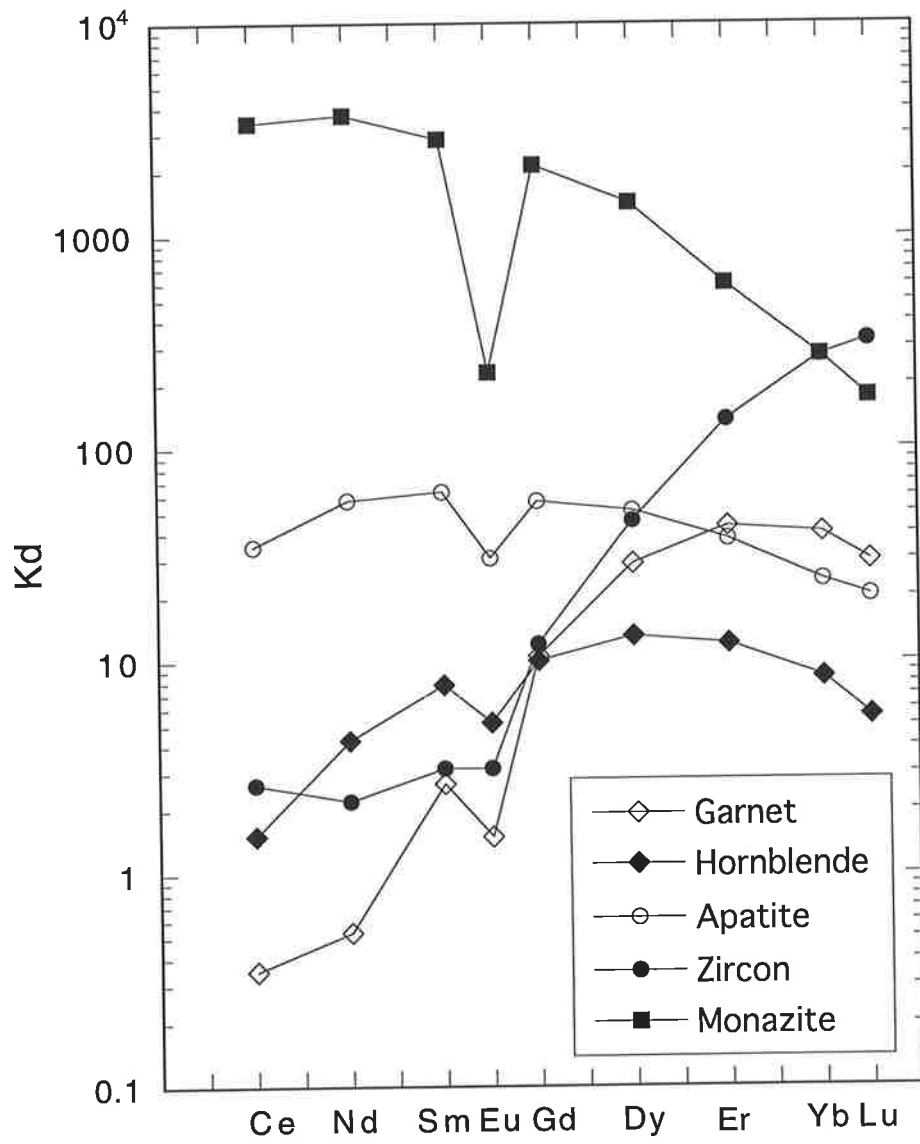
Fig. 3-15. Distribution coefficients of rare earth elements for typical minerals

Kd: mineral/melt distribution coefficients

Zircon Kd from Nagasawa (1979).

Monazite Kd from Yurimoto et al. (1990).

Kd of other minerals from Arth and Hanson (1975).



MREE depletion is merely regarded as a consequence of strong HREE enrichment.

A concentration of garnet crystals could produce the strong HREE enrichment as indicated by their high distribution coefficient values (Fig. 3-15). If garnets which generally contain high level of HREE are included in a granitoid magma as xenocrysts from the source region of the magma or country rock, they will produce the HREE enrichment. On the other hand, it is also possible that the garnet-bearing granitoid is a kind of cumulate phase in terms of garnet, concentrating most of HREE in the garnet-bearing granitoid and depleting HREE in the granitoid without garnet.

Ga

Ga content in the garnet-bearing granitoids ranges from 19.6 to 22.9 ppm (Fig. 3-13H), which is slightly higher than that in the garnet-free granitoids. This high Ga content in the garnet-bearing granitoid is likely due to the high level of Ga in the garnets, suggesting role of garnet crystals control the some of trace element compositions. $10000\text{Ga}/\text{Al}$ ratios in the garnet-bearing granitoids are high, more than 3.0 (Table A4-2). Although the Eastern Leucocratic Granitoid is not considered to be an A-type granite, the values are within the range of the A-type granites.

3.4.4. Origin of Garnets in the Eastern Leucocratic Granitoid

Garnets are occasionally found in igneous rocks. Most of the recorded occurrences of garnet are in granitoids and silicic volcanic rocks. Garnets from silicic volcanic rocks are typically rich in almandine; origin of such garnets has been discussed by Miyashiro (1955), Oliver (1956), Green and Ringwood (1968, 1972), Fitton (1972), Wood (1973), Birch and Gleadow (1974). Experimental results by Green and Ringwood (1968, 1972) indicate a high pressure (9-18kb) origin for

almandine-rich garnets in igneous rocks. However, garnets from granitoids, pegmatite, and aplite are generally rich in spessartine. Crystallization of such garnets was considered possible from an Mn-rich magma at low pressures (Miyashiro, 1955; Hall, 1965). Experimental results by Green (1977) demonstrated that spessartine-rich garnets are stable in silicic liquids to pressures as low as 3kb.

A variety of origins of garnets in granitoids has been postulated over the years and these are summarized by Miller and Stoddard (1981) and Pattison et al. (1982). The origins can be classified as follows:

(A) primary crystals crystallizing directly from the melt

A-1) high pressure phenocrysts

Green and Ringwood (1968)

A-2) low to moderate pressure crystals

Cawthorn and Brown (1976) and Abbott and Clarke (1979)

A-3) late phase stabilized by high Mn in differentiated magma

Hall (1965), Miller and Stoddard (1981), and Joyce (1973)

A-4) crystallization from a magma after its contamination with country rock

Miyashiro (1955)

(B) xenocrysts

B-1) xenocrysts brought up from near the depth of magma origin as relict source material

Pattison et al. (1982)

B-2) xenocrysts that entered the melt from country rock

Vennum and Meyer (1979)

(C) metamorphic garnets produced by metamorphism after the solidification of the granitoid magma

Garnets are present in the metamorphosed pelitic and carbonate rocks around the Eastern Leucocratic Granitoid. As the CaO content of the garnets in the granitoid is low, the xenocrystic origin of the garnets derived from the metamorphosed carbonate rock may be ruled out. Garnets in the metamorphosed pelitic rocks may have similar composition to those in the granitoid. However distribution of the pelitic rocks around the granitoid is restricted to several narrow zones, thus the widely distributed garnet crystals in the Eastern Leucocratic Granitoid should perhaps have a more widespread source.

If the garnets are xenocrysts brought up from near the depth of magma origin as relict source material, the granitoid would contain other relict xenocrysts as well. However, in the Eastern Leucocratic Granitoid, garnet is the only unusual mineral, and no other possible relict minerals, such as sillimanite, cordierite, or orthopyroxene, is found. Thus the garnets may not be derived by this mechanism.

Chemical analysis of the garnets indicates that they are almandine-spessartine solid solutions with minor contents of pyrope. Therefore they are not high pressure phenocrysts; such are typically rich in pyrope (Green and Ringwood, 1968; 1972).

Garnets commonly occur in peraluminous or corundum-normative igneous rocks (Green, 1977), however major element data of the Eastern Leucocratic Granitoid show that samples containing garnet crystals are metaluminous. Since the introduction of the aluminium into the granitoid magma by contamination would facilitate garnet crystallization, no indication of excess aluminium in the granitoid would not support the contamination model for the formation of the garnets.

Metamorphism imposed on a granitoid may produce garnets in it. However, because the Eastern Leucocratic Granitoid is metaluminous, the garnets would not readily develop as a consequence of metamorphism.

Furthermore, the peculiar REE concentration of the Eastern Leucocratic Granitoid would not be due to metamorphism alone, as the REE are relatively immobile during the metamorphism.

Thus the available evidences seem to indicate that the garnets in the Eastern Leucocratic Granitoid are primary magmatic crystals, crystallizing as either low to moderate pressure crystals or late phase crystals stabilized by high Mn in magma. Hence, the HREE enriched character of the garnet-bearing granitoid must be due to the HREE enrichment in the late stage of the magmatic differentiation, or to partly segregation of magmatic garnets in the granitoid as cumulate crystals.

3.5. Dougalls Granitoid Suite

3.5.1. Petrography

Two types of granitoid, tonalite and trondhjemite, comprise the suite in the Sally Downs Bore area. Petrographic descriptions of the two types of the granitoids are presented separately. In addition, a brief petrography of orthopyroxene-bearing granitoids from the Turkey Creek and Springvale areas is also included here, as these granitoids are considered to be a member of the Dougalls Suite.

A. Tonalite

Modal composition of the tonalite (Table A2-1) shows it consists largely of plagioclase, about 60% of the rocks. Subordinate amounts of quartz and mafic minerals, but no K-feldspar, are present (Fig. 3-7). Biotite (α = pale yellow, β = γ = reddish brown), generally the major mafic mineral in the rocks, is distributed as aggregates of small subhedral flakes, or as medium grained individual flakes with its elongation parallel to the foliation. Small amounts of hornblende (α = yellow, β = brownish

green, γ = bluish green) occur as euhedral or subhedral grains, but it is a major mafic mineral in orthopyroxene-free mafic tonalite.

Orthopyroxene is characteristically present in most of the tonalite as small anhedral grains (Fig. 3-8E and F). Shape of the orthopyroxene and replacement from its margin by biotite and opaque minerals suggest that it is a relict mineral. Weak pleochroism, pale pink to pale blue, is observed.

Pale pink garnet is found in some tonalites, as small or large subhedral grains.

Plagioclase is generally coarse grained and subhedral, and shows weak zoning. Quartz, typically medium grained, occurs as anhedral grain, and shows undulatory extinction.

Apatite, zircon, opaque are found as accessory minerals.

Texture of the tonalite are generally hypidiomorphic-granular.

B. Trondhjemite

Trondhjemite is also composed largely of plagioclase (about 60%) and quartz, but contains only small amounts of mafic minerals (Table A2-1), generally biotite and hornblende (Fig. 3-8G and H).

Biotite (α = straw yellow, β = γ = brown) and hornblende (α = yellow, β = greenish brown, γ = bluish green) occur as small subhedral grains, occasionally clustered in small aggregates. Subhedral plagioclase is medium or coarse grained. Zircon, apatite, and opaque minerals are present as accessory minerals.

C. Orthopyroxene bearing Tonalite from north of the Turkey Creek

The tonalite (52008) has hypidiomorphic-granular texture, and the modal composition (Table A2-1) shows plagioclase is a dominant phase of the rock, and orthopyroxene is next. The plagioclase is subhedral and

medium to coarse grained, up to 7mm long. Some of the grains show zoning and small K-feldspar inclusions as exsolved phase. Orthopyroxene is anhedral or subhedral and up to 4mm in size, and shows weak pleochroism, pale pink to pale blue green.

Quartz, hornblende (α = pale greenish yellow, β = greenish brown, γ = bluish green), biotite (α = pale yellow, β = γ = reddish brown) are also present in the rock. Accessory minerals are zircon and opaque minerals.

D. Orthopyroxene bearing granite from north of Springvale

The granite differs from other granitoids of the Dougalls Suite, in having considerable amounts of K-feldspar.

Equal amounts of K-feldspar and quartz are present, and plagioclase is slightly more abundant than either. K-feldspar is medium grained, with and without microcline twinning. Plagioclase is mostly subhedral, and some of the grains show zoning. Myrmekite texture developed between the feldspars.

Orthopyroxene, about 5%, is present as small anhedral grains, and has weak pleochroism (pale pink to pale green). Biotite (α = pale yellow, β = γ = reddish brown) occurs as subhedral flakes, more than the amount of orthopyroxene.

The presence of the K-feldspar may indicate the occurrence of orthopyroxene bearing granite in the Dougalls Suite, in addition to the tonalite-trondhjemitic rocks. However, because the granite is surrounded by Bow River Granitoid, the K-feldspar is possibly derived from the granitoid as a result of K-metasomatism.

3.5.2. Mineral Chemistry

A. Feldspars

Plagioclase is only feldspar in the granitoids of the Dougalls Suite, except for the sample from north of Springvale. Feldspar compositions are summarized in Fig. 3-16A, showing that the plagioclase is andesine (An30 - An50). The feldspar composition is generally more calcic in granitoids of the suite with lower SiO₂. Typically the plagioclase is normally zoned, having about An50 in the core, but weak oscillatory or reversely zoned plagioclase is also found.

The plagioclase in the granite (91502) from north of the Springvale is rather calcic (An49) compared to the other granitoids of the suite. Composition of coexisting K-feldspar is about Or92.

B. Orthopyroxene

Chemical compositions of orthopyroxene from the Dougalls Granitoid Suite are plotted on the pyroxene quadrilateral shown as Fig. 3-16B. Representative analyses are given in Table 3-8.

The orthopyroxene is of hypersthene or ferrohypersthene composition. Fig. 3-16B shows that the compositional range is small within each specimens, but is substantial from rock to rock. Variation in composition of the orthopyroxenes may be influenced by variation in whole rock chemistry, especially the FeO/MgO ratio. No obvious relationship is found between whole rock FeO*/MgO and the orthopyroxene compositions, suggesting that random oxidation states pertain between samples.

Al₂O₃ content of the orthopyroxene is generally low, ranging from 0.50 to 1.30 wt% (Table 3-8 and Table A8-1).

C. Amphibole

Amphiboles in the Dougalls Granitoid Suite are ferro-tschermakitic hornblende, ferro-hornblende or magnesio-hornblende according to

Fig. 3-16. Plagioclase and pyroxene plots of the Dougalls Granitoid Suite
A. Plagioclase An - whole rock SiO₂ value

B. Pyroxene quadrilateral plot

Solid square: 51605

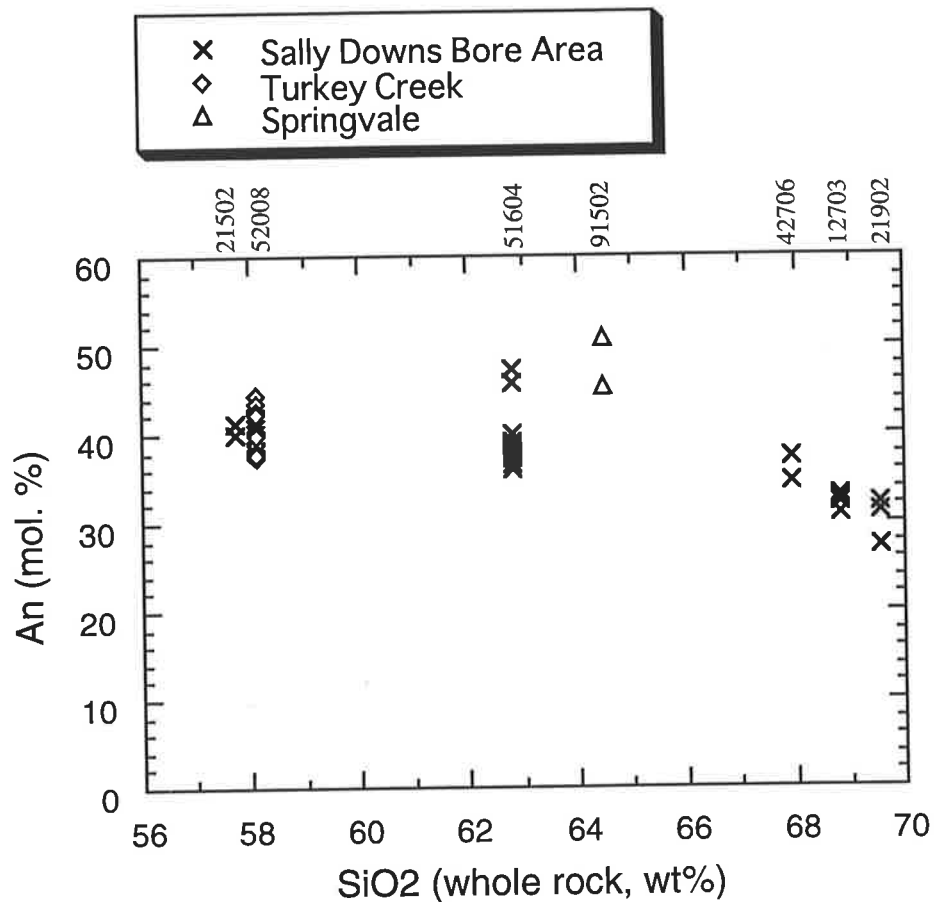
x mark: 12703

Solid triangle: 20907

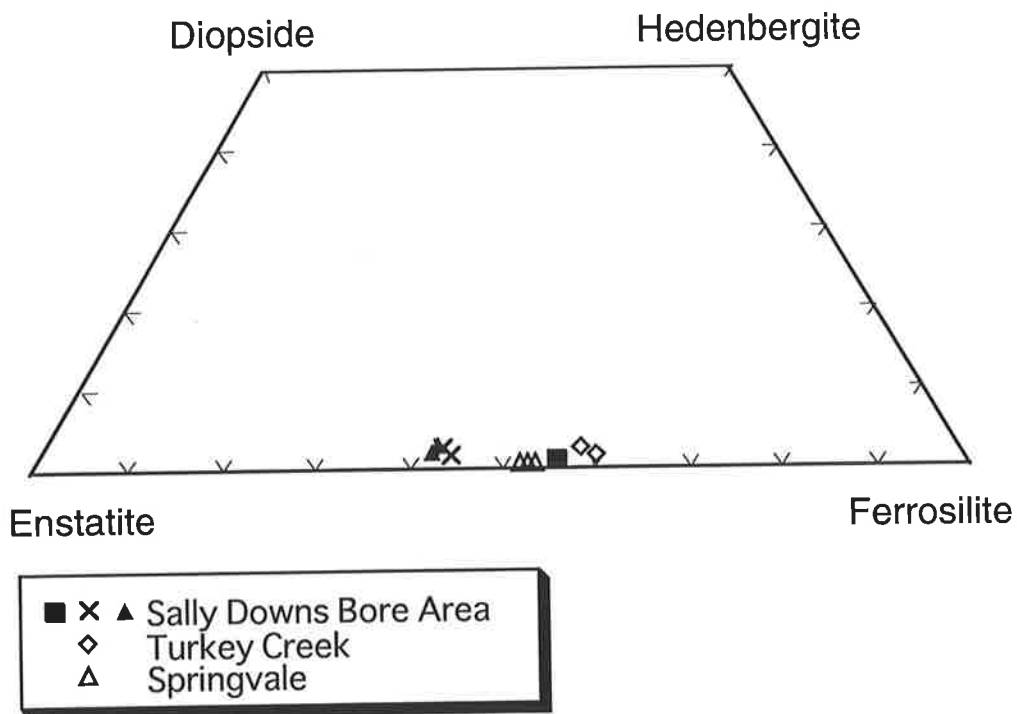
Open diamond: 52008

Open triangle: 91502

A.



B.



Leak's (1968) classification. Representative chemical compositions of amphibole are shown in Table 3-8. Amphibole Mg/(Mg + Fe) in the granitoids from the Sally Downs Bore area ranges from 0.408 to 0.516 (Table A8-1). A slightly lower Mg/(Mg + Fe) value, ranging from 0.373 to 0.401, is found in the tonalite (52008) collected north of the Turkey Creek (Table A8-1). The total Al content (Al_T = sum of tetrahedral and octahedral Al per 23 oxygens) of the amphiboles ranges from 1.88 to 2.18 (Table A8-1), except in two analyses. Experimental and empirical calibrations of the Al-in-hornblende barometer have been presented by Hammarstrom and Zen (1986), Hollister et al. (1987), Rutter et al. (1989), and Schmidt (1992). Using Schmidt's (1992) calibration, the Al content of hornblende in orthopyroxene-free trondhjemite (21502) indicates 7kb for the pressure during crystallization. The estimated pressure is considerably high. Although small differences are present between the calibrations, Al_T contents of amphiboles generally from the Dougalls Granitoid Suite indicate a pressure of solidification between 6 and 7 kb.

D. Biotite

Representative chemical compositions of biotite from the Dougalls Granitoids Suite are presented in Table 3-8. Mg/Mg+Fe in all biotites from the Dougalls Granitoids Suite ranges from 0.411 to 0.559 (Table A8-1). A slightly lower value of the ratio is found in the tonalite (52008) sampled from north of Turkey Creek. TiO₂ content of biotites is generally high, ranging from 16.4 to 4.64 % (Table A8-1). TiO₂ content of biotites from the Dougalls Granitoid Suite tends to increase from south to north in the Sally Downs Bore area.

3.5.3. Geochemistry

Major and trace element contents of the granitoids are listed in Table A4-3 (Appendix 4). Locations of samples from the Sally Downs Bore area are shown in Fig. 3-17. Those of samples from north of the Turkey Creek and from north of the Springvale are found in Fig. 2-20 and Fig. 2-22, respectively.

A. Major elements

Tonalite and trondhjemite from the Dougalls Suite range in composition from 58 to 75% SiO₂, with mean about 68%. SiO₂ content of the trondhjemite is more than 70%, and is higher than that of the tonalite.

High Na₂O/K₂O ratio and less than 1.01 of mol [Al₂O₃/(CaO + Na₂O + K₂O)] ratio of the granitoids (Table A4-3) are in accordance with distinctive chemical properties of the I-type granitoids (Chappell and White, 1974).

The major element data of the granitoids, including data from orthopyroxene bearing granitoid from north of the Turkey Creek presented by Gemuts (1971), are plotted on variation diagrams (Fig. 3-18). The tonalite and trondhjemite show linear trends on most of the diagrams, and the colinearity of the trends of the tonalite and trondhjemite implies a close genetic relationship between them.

Al₂O₃, Fe₂O₃*, MgO, CaO, and TiO₂ display a negative correlation with SiO₂ on the diagrams. Compared to the Paleozoic I-type granitoids from the Kosciusko Batholith (Hine et al., 1978), the granitoids of the Dougalls Suite have higher Al₂O₃, lower MgO, and similar values of Fe₂O₃* and TiO₂ contents.

P₂O₅ shows a small peak at about 63% SiO₂. This feature strongly suggests that variation in composition of the granitoids is due to crystal fractionation. A mixing of residium (= restite) and melt (White and

Fig. 3-17. Sample locality map for the Dougalls Granitoid Suite

P-Tn: orthopyroxene bearing tonalite

Tn: orthopyroxene free tonalite

Tr: trondjemite

Sample 51605 is collected from same location as 51604.

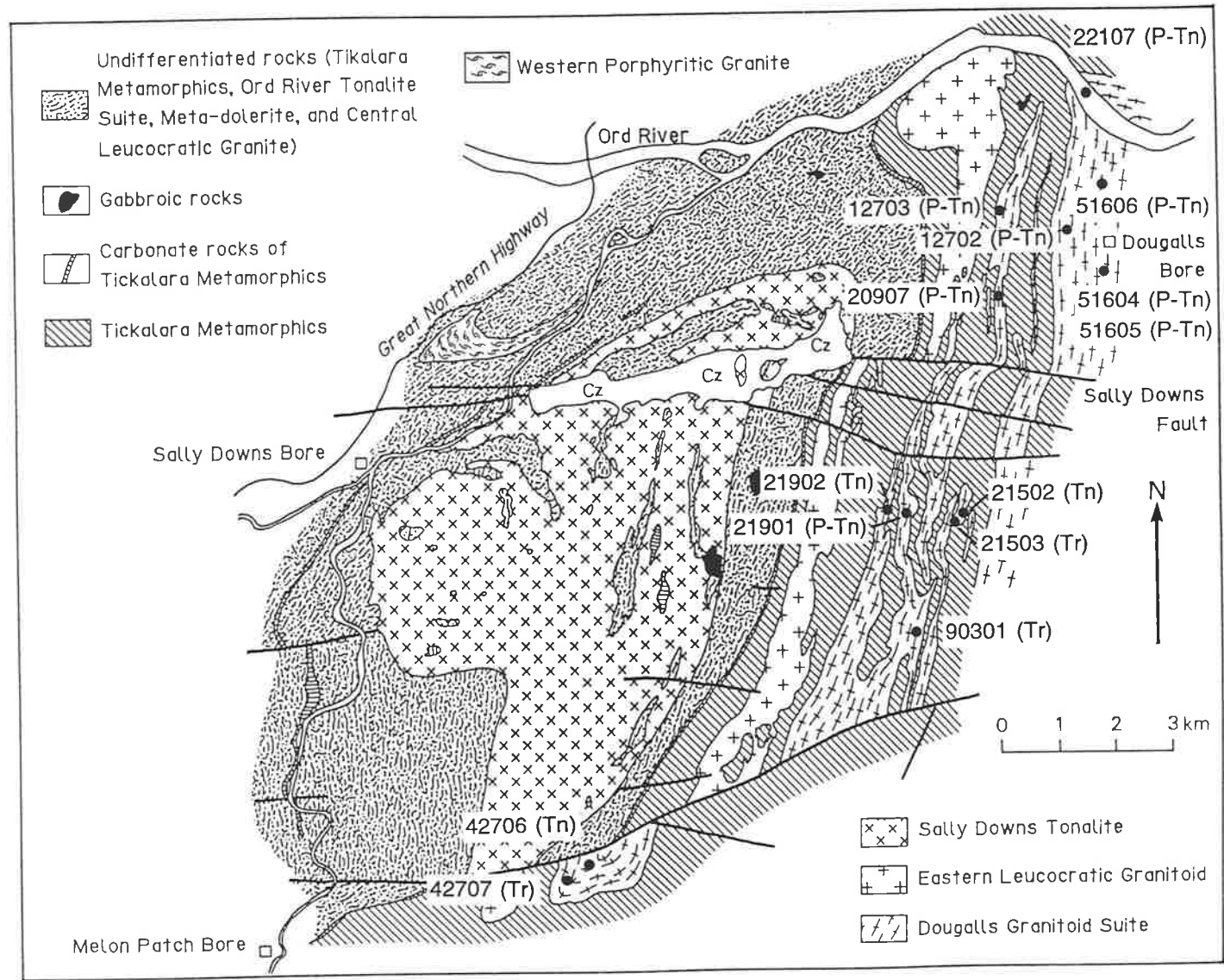


Fig. 3-18. Major element variation diagram of Dougalls Granitoid Suite

A. $\text{Al}_2\text{O}_3\text{-SiO}_2$

B. $\text{Fe}_2\text{O}_3^*\text{-SiO}_2$

C. MgO-SiO_2

D. CaO-SiO_2

E. $\text{Na}_2\text{O-SiO}_2$

F. $\text{K}_2\text{O-SiO}_2$

G. $\text{TiO}_2\text{-SiO}_2$

H. $\text{P}_2\text{O}_5\text{-SiO}_2$

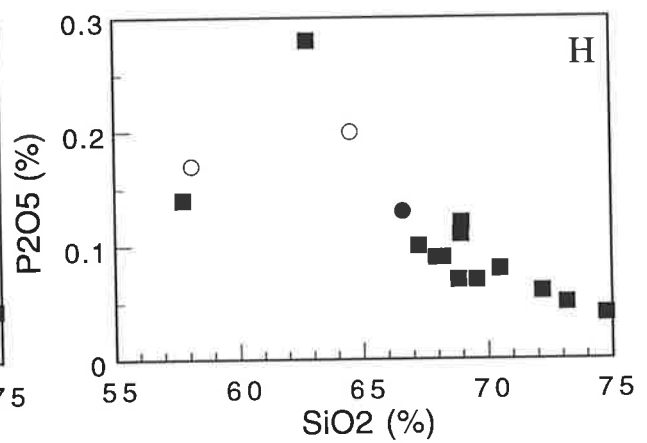
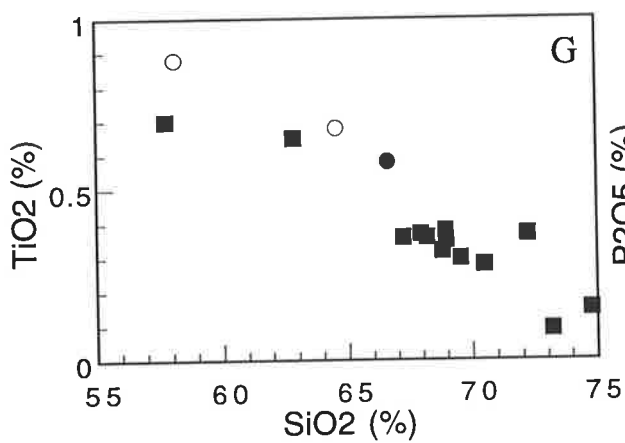
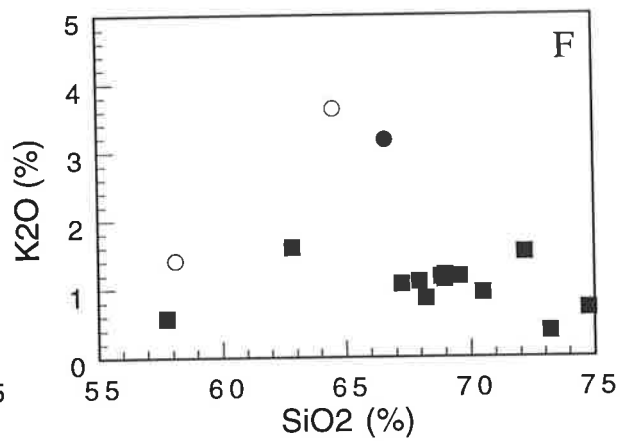
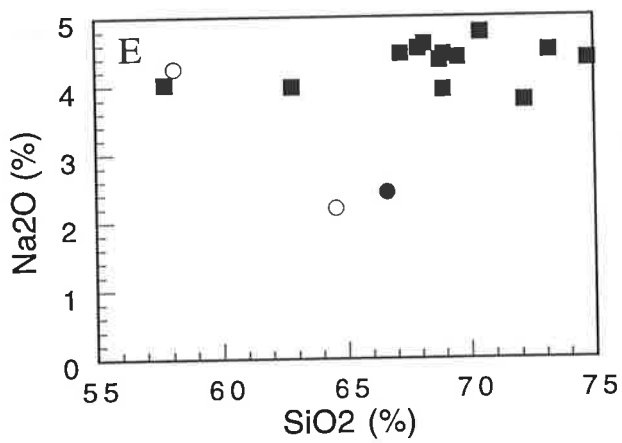
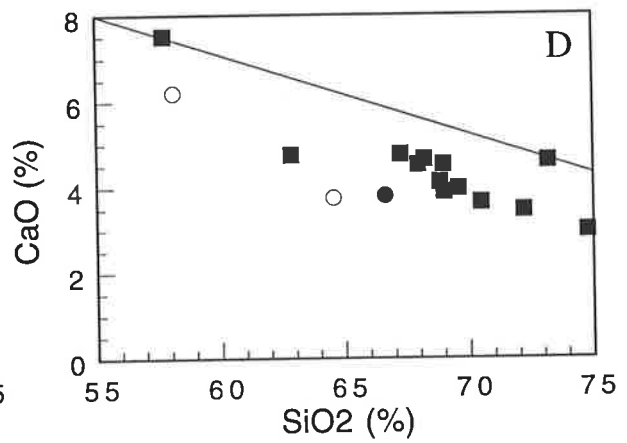
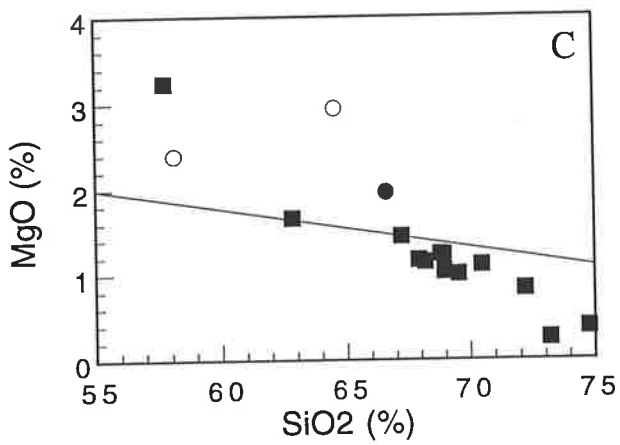
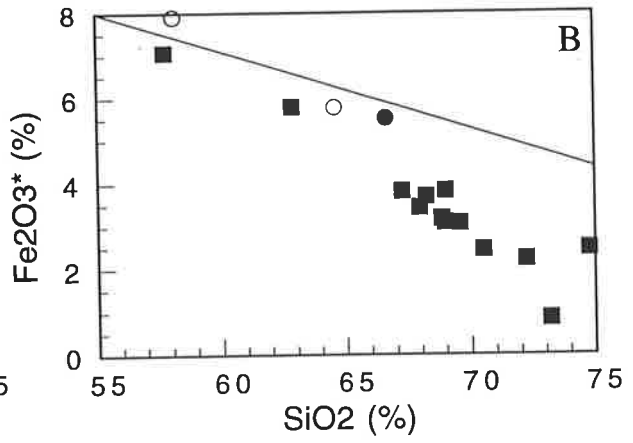
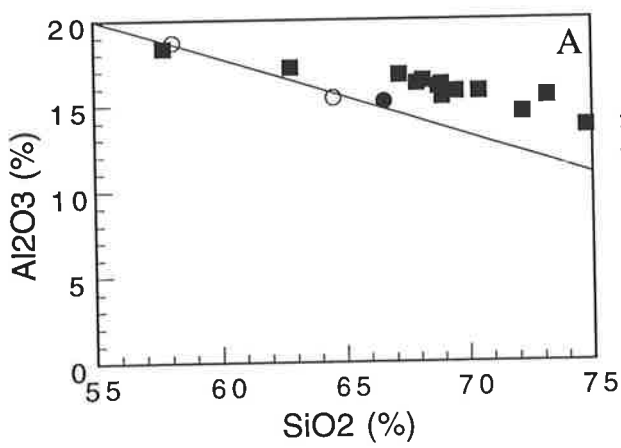
Reference lines in the diagrams A., B., C., and D., show effect of constant sum, and are drawn from a point representing 100% SiO_2 and 0% of the other element extrapolated into the diagram. See section 3.4.3 for detailed discussion of the lines.

Solid square: samples from the Sally Downs Bore area.

Open circle: granitoids of the Dougalls Suite from the area other than the Sally Downs Bore area.

Solid circle: data from Gemuts (1971).

Fe_2O_3^* : total Fe as Fe_2O_3



Chappell, 1977) can not produce the depicted curved compositional variation.

Na₂O content of the Dougalls Suite granitoids is relatively constant over the compositional range, ranging between 4 and 5%. This value is significantly higher than that in the typical I-type rocks (Hine et al., 1978).

K₂O is very low, with a tendency for slight decrease with increase in SiO₂. Most of the Dougalls granitoids are plotted in the field of tholeiitic rocks on K₂O versus SiO₂ diagram (see Fig. 7-1 for a boundary line separating the tholeiitic rocks). An Na₂O - K₂O plot (Fig. 3-19A) shows the distinct characteristics of the Dougalls Suite granitoids compared to the granitoids from Kosciusko Batholith (Hine et al., 1978), viz. low K₂O and high Na₂O of the Dougalls Granitoids.

The two samples of orthopyroxene bearing granitoids, one from north of Turkey Creek (Gemuts, 1971) and another (91502) from north of Springvale, have quite different chemical compositions from the other granitoids of the Dougalls Suite. They have higher mol [Al₂O₃ / (CaO + Na₂O + K₂O)], viz. 1.06 and 1.07, than the Dougalls Suite granitoids from the Sally Downs Bore area. This peraluminous character and the low Na₂O/K₂O ratio might suggest their classification as S-type granitoids. Most of the other elements also suggest such an affinity. Both granitoids occur in areas where Bow River Granitoid is dominant, hence modification by the Bow River Granitoid, by metasomatism or contamination, may produce S-type characteristics from an originally I-type granitoid. On the other hand, the two rock types may represent orthopyroxene bearing S-type granitoids of similar age to the tonalite and trondhjemite of the Dougalls Suite.

Fig. 3-19. Na₂O-K₂O and normative Qz-Ab-Or plots of the Dougalls
Granitoid Suite

A. Na₂O-K₂O plot

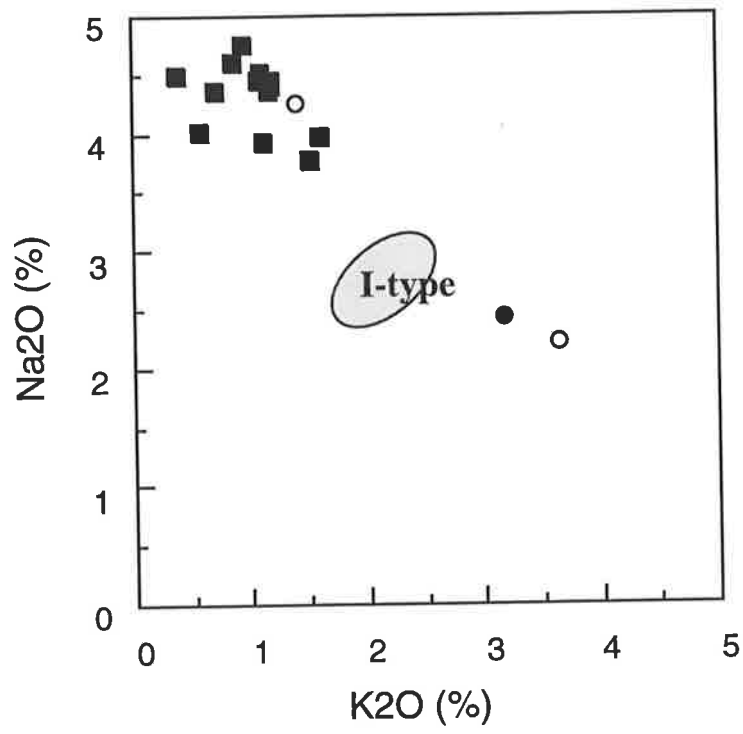
Symbols are the same as those in Fig. 3-18.

Field of typical I-type granitoids is from Hine et al. (1978).

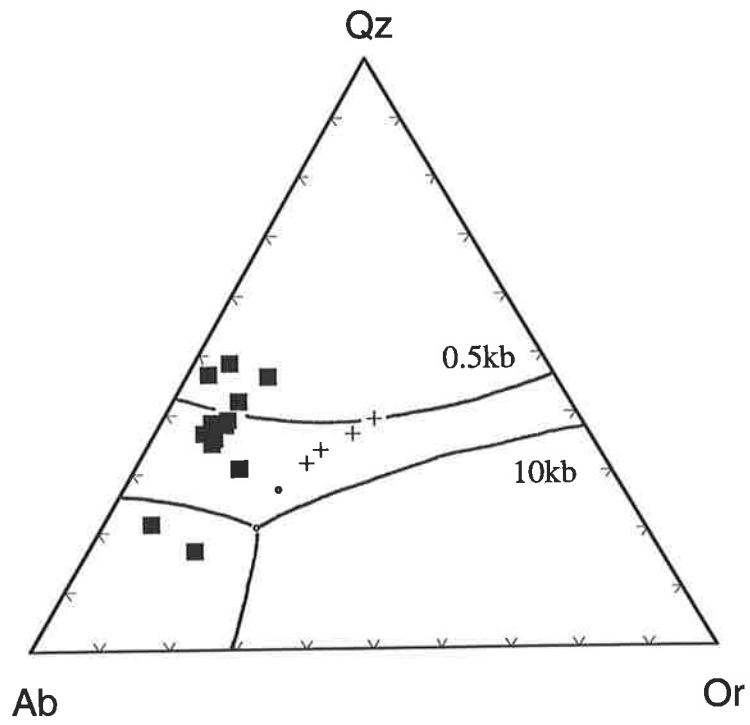
B. Qz-Ab-Or plot

Phase boundaries of the granitic system for water pressure 0.5 kb and 10 kb are shown. Crossed are minima and small open circles are eutectic points. Data from Tuttle and Bowen (1958) and Luth et al. (1964).

A.



B.



Normative Q-Ab-Or (Fig. 3-19B) for the granitoids of the Dougalls Suite plot near the gabbro-trondhjemite trend of Barker and Arth (1976), but not near the minimum melt composition of Tuttle and Bowen (1958).

B. Trace elements

Fig. 3-20 shows trace elements variations within the Dougalls Suite. As with the major elements, the trace elements also vary systematically from tonalite to trondhjemite, suggesting that the two types of granitoid are closely related by crystal fractionation.

Ba

Ba decreases from 1100ppm to 250ppm with increasing SiO₂. Because Kd's (mineral/melt distribution coefficients) of Ba for most rock-forming minerals are low, except biotite and K-feldspar (Hanson, 1978), the depletion of Ba must be due to the fractionation of one of these two minerals. Absence of K-feldspar in the tonalite and trondhjemite strongly supports the role of biotite in the depletion of Ba.

Rb

The Rb versus SiO₂ diagram shows a very similar pattern to the K₂O versus SiO₂ diagram, decreasing slightly with increasing SiO₂ (Fig. 3-20B). The Rb contents vary from 55ppm in the tonalite to 9ppm in the trondhjemite. The decrease of Rb is also accounted for by the biotite fractionation. The K₂O versus Rb diagram (Fig. 3-21A) illustrates a clear positive correlation between them, with slight increase of the K/Rb ratio from 240 to 360 with decreasing K₂O content. The change in the ratio is not easily explained, because the Kd (K/Rb) is generally high for most rock forming minerals (Hanson, 1978). Rb depletion during subsequent metamorphism which may be considered to approach granulite facies, may be responsible for the relative depletion of Rb against K₂O. Rb depletion relative to K during granulite facies

Fig. 3-20. Trace element variation diagram of the Dougalls Granitoid Suite

- A. Ba-SiO₂
- B. Rb-SiO₂
- C. Sr-SiO₂
- D. Zr-SiO₂
- E. Nb-SiO₂
- F. V-SiO₂
- G. Sc-SiO₂
- H. Y-Al₂O₃

Solid square: samples from the Sally Downs Bore area.

Open circle: granitoids of the Dougalls Suite from areas other than the Sally Downs Bore area.

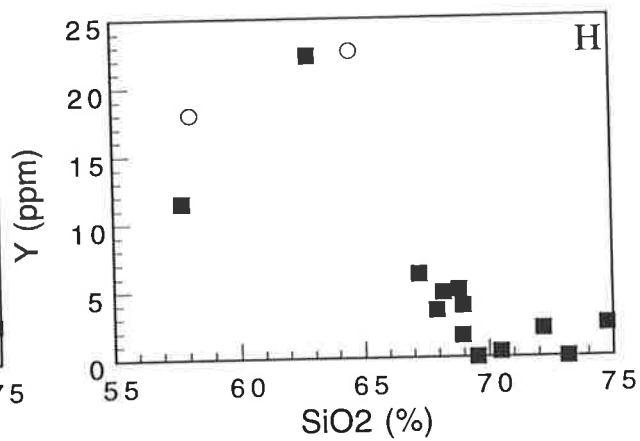
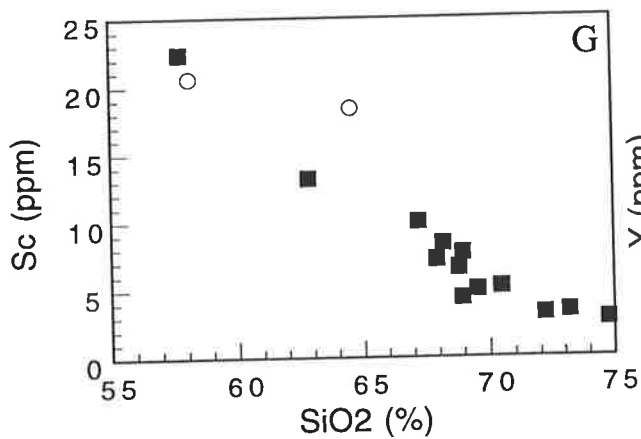
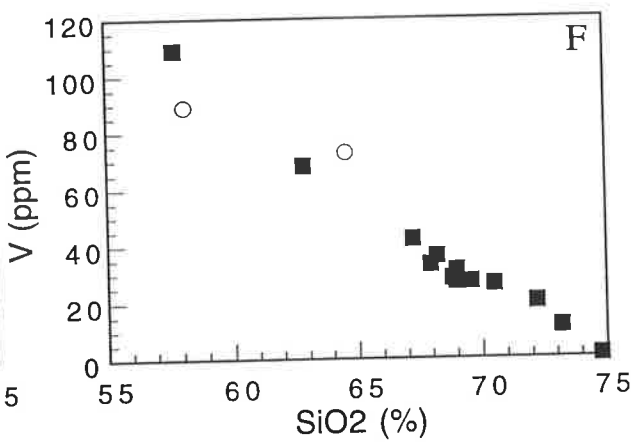
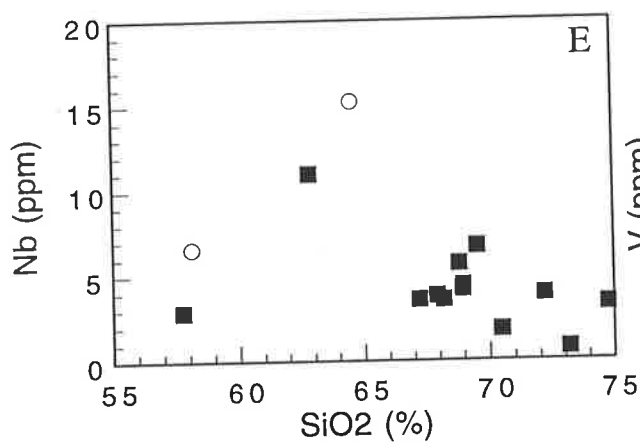
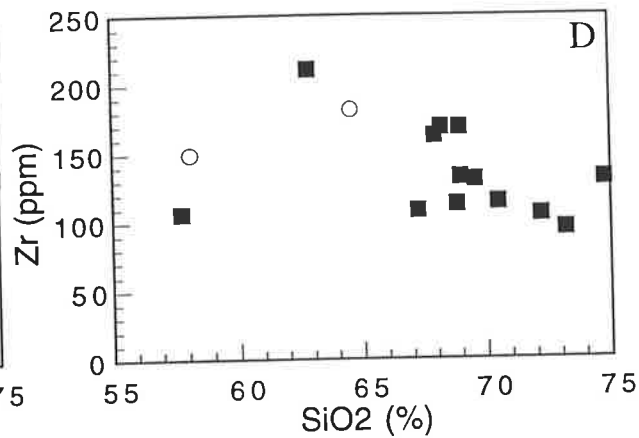
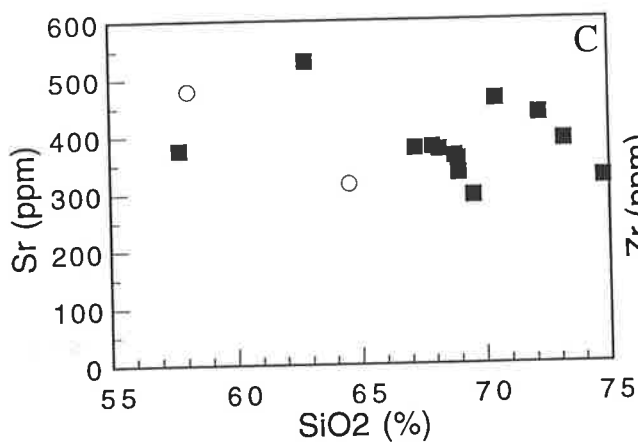
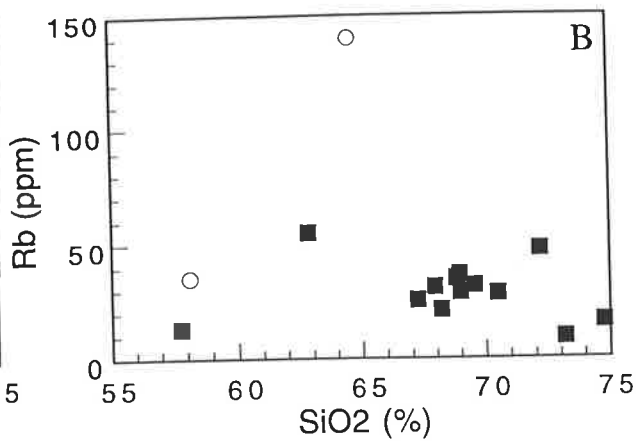
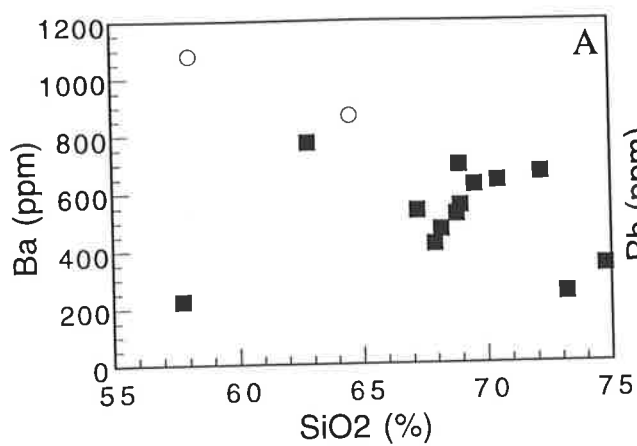


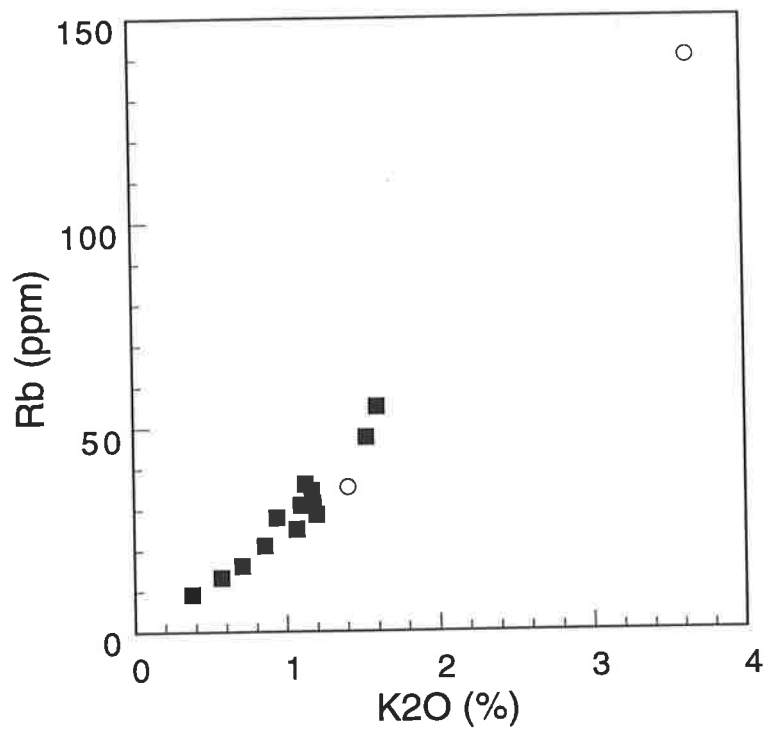
Fig. 3-21. Rb-K₂O and chondrite normalized Y-Ce/Y plots of the
Dougalls Granitoid Suite

A. Rb-K₂O

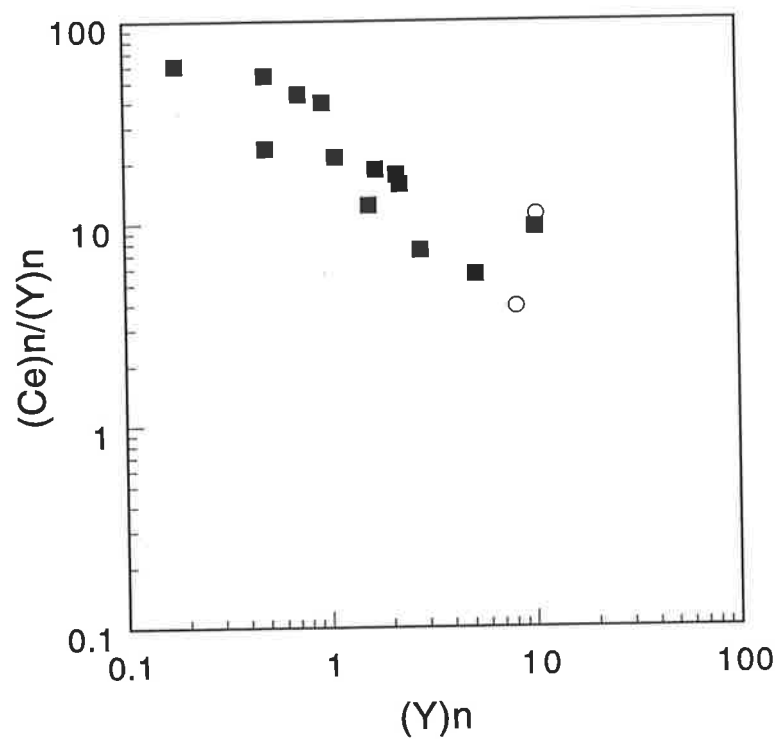
B. Chondrite normalized Y-Ce/Y plot

Symbols are the same as those in Fig. 3-20.

A.



B.



metamorphism has been described by many workers (e.g. Rollinson and Windley, 1980a).

Sr

Sr decreases from 550 to 300ppm with increase of SiO₂ (Fig. 3-20C). However, a compositional gap may be present between the tonalites and trondhjemites (samples with SiO₂ greater than 70%). Rb/Sr ratios in the tonalite and trondhjemite are very low, ranging from 0.023 to 0.107.

Zr and Nb

Plotting against SiO₂, Zr and Nb show maxima at 62% SiO₂. These trends demonstrate residual enrichments of Zr and Nb in the tonalitic melt, and subsequent depletion by fractionation of zircon. The feature supports a role of fractional crystallization to account for the variation from tonalite to trondhjemite.

V and Sc

V and Sc show strong negative correlations with SiO₂. The depletion could be the result of fractionation of pyroxene, amphibole, biotite, and magnetite.

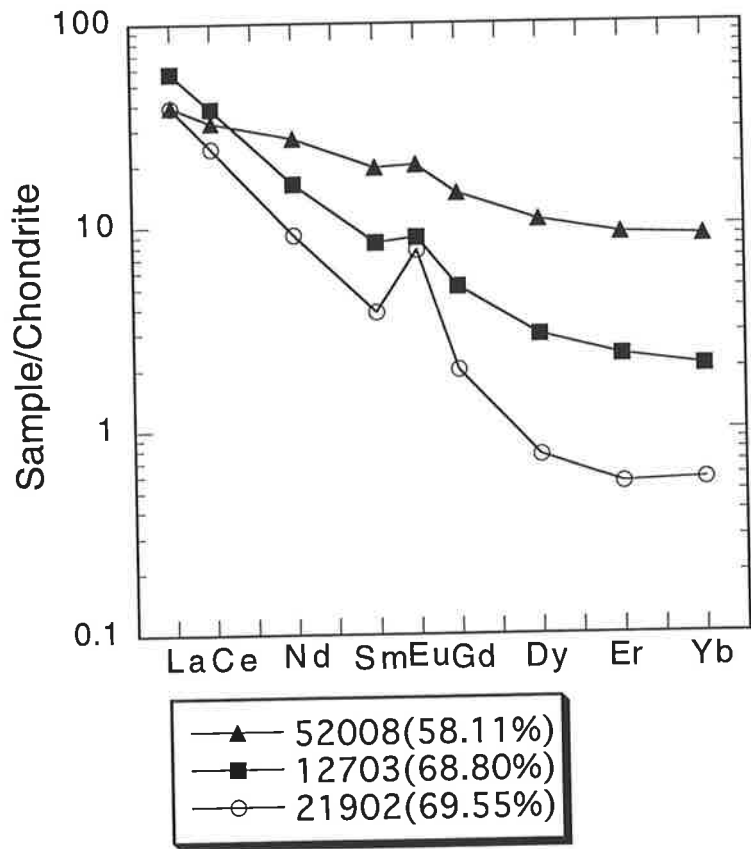
REE and Y

Chondrite normalized Ce/Y versus chondrite normalized Y (Fig. 3-21B) demonstrates that the tonalite and trondhjemite have an LREE enriched and HREE depleted fractionated pattern, with generally low and variable values of Y which indicates the level of HREE. Y decreases from about 20ppm to less than 1ppm with increasing SiO₂. Strong depletions of HREE in the trondhjemite are indicated by the very low Y value.

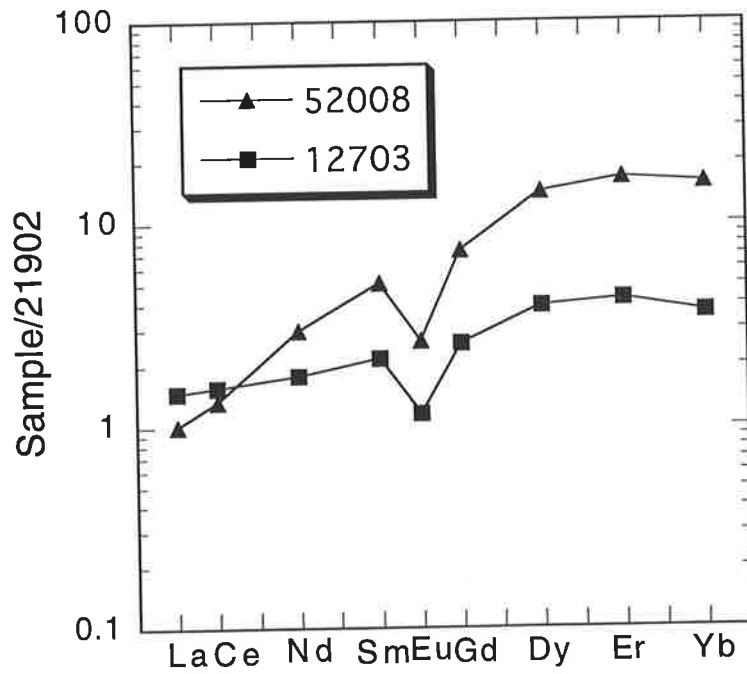
REE concentrations of three rocks from Dougalls Suite are listed in Table A5-2 (Appendix 5), and chondrite normalized patterns are presented in Fig. 3-22A. All of the rocks show a LREE enriched pattern

Fig. 3-22. Chondrite normalized REE plot and tonalite (21902)
normalized REE plot of Dougalls Granitoid Suite samples

A.



B.



with positive Eu anomaly. The positive Eu anomalies become large as SiO₂ increases. Although most of REE, except La and Ce, decrease with increasing SiO₂, marked HREE depletion with increasing SiO₂ reflects a very strongly fractionated pattern (chondrite normalized (Ce/Yb) = 42.9) in the trondhjemite (sample 21902), as suggested above.

The chondrite-normalized pattern of the trondhjemite is steep, but becomes flat in HREE region. Such a feature is common in trondhjemite from various areas (Arth et al., 1978; Compton, 1978; Tarney et al., 1979; Weaver and Tarney, 1980), and is generally considered to be the result of hornblende fractionation.

As suggested by Hanson (1980), it is advantageous, in a cogenetic sequence of rocks to normalize the REE to one of the rocks in the sequence rather than to chondrite. The trondhjemite (21902), the most fractionated sample of the three, is selected for normalizing and Fig. 3-22B shows the pattern illustrating relationships of the granitoids of the suite. HREE are reduced in the trondhjemite to about 1/15 of those in sample 52008 or 1/4 of those in sample 12703, but only small depletions from the tonalites are required to obtain the level of LREE in the trondhjemite. Therefore fractionation of some minerals which have high K_d (mineral/melt) in the HREE region and near unity in the LREE region and with negative Eu anomaly in the K_d pattern could have been responsible for the tonalite-trondhjemite REE relationships.

In fact, Fig. 3-22B indicates a pattern of relative K_d's of fractionated material; the absolute magnitude of the K_d's is dependent on the fraction removed. The evidence suggests that hornblende (see Fig. 3-15 for hornblende K_d's) is the most likely mineral fractionation of which controlled REE concentration.

3.6. Ord River Tonalite Suite

3.6.1. Petrography

A. Type I tonalite of the Ord River Tonalite Suite

This tonalite is generally coarse grained (Fig. 3-23A and B), but includes fine to medium grained crystals as a result of recrystallisation and granulation along grain boundaries. Hence, the texture is a combination of hypidiomorphic-granular and inequigranular. Foliation manifested by preferred orientation of plagioclase and biotite is apparent. Modal compositions of the tonalites are listed in Table A2-1. Data are plotted in Qz-Af-Pl diagram (Fig. 3-7). The tonalites are primarily composed of subhedral to anhedral, slightly zoned plagioclase (40 - 50%), and anhedral quartz (25-30%) which generally has undulatory extinction. Biotite (α = yellow, β = γ = yellowish brown to brown) is fine to medium grained and subhedral; it commonly forms aggregates around hornblende crystals, suggesting a replacement of hornblende by biotite. Some grains of poikilitic biotite may result from this replacement. Total biotite is 15 - 25%.

Some specimens contain subhedral to anhedral hornblende (α = yellow, β = pale green, γ = dark blue green), up to 15%. More than accessory amounts (up to 4%) of epidote are present. Accessory minerals include sphene, apatite, allanite, and zircon. Traces of carbonate and sericite are alteration products.

B. Type II tonalite of the Ord River Tonalite Suite

The type II tonalite is medium grained, hypidiomorphic-granular. It contains abundant plagioclase (50-55%) and lesser amounts of quartz (28-35%) and biotite (13-15%). Small amounts of garnet (up to 3%) are found in two samples (Fig. 3-23C and D). Accessory minerals are zircon, apatite, muscovite (probably secondary) and opaque minerals. Plagioclase is generally subhedral or anhedral; some grains are weakly

Fig. 3-23. Photomicrographs of the Ord River Tonalite Suite, Western
Porphyritic Granite, and Central Leucocratic Granite

A. Ord River Tonalite (type I)

Sample: 51303. Bi: biotite, Al: allanite. Plane polarized light.

Scale bar is 5 mm.

B. Same as A, but under crossed polarized light.

Qz: quartz, Pl: plagioclase

C. Ord River Tonalite (type II)

Sample: 11203. Bi: biotite, Gar: garnet, Pl: plagioclase.

Plane polarized light. Scale bar is 1 mm.

D. Same as C, but under crossed polarized light.

E. Western Porphyritic Granite

Sample: 90805. Bi: biotite. Plane polarized light.

Scale bar is 10 mm.

F. Same as E, but under crossed polarized light.

Qz: quartz, Pl: plagioclase, KF: K-feldspar.

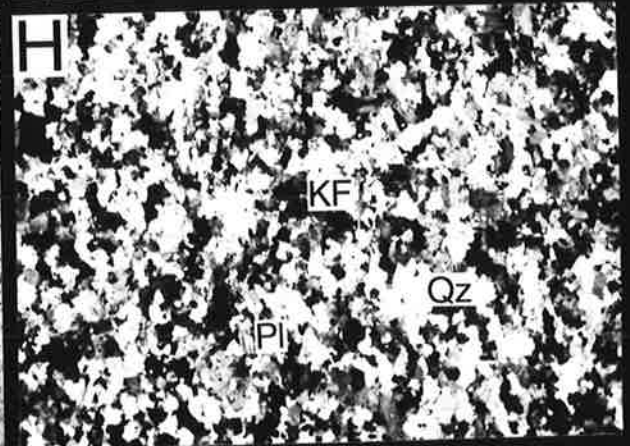
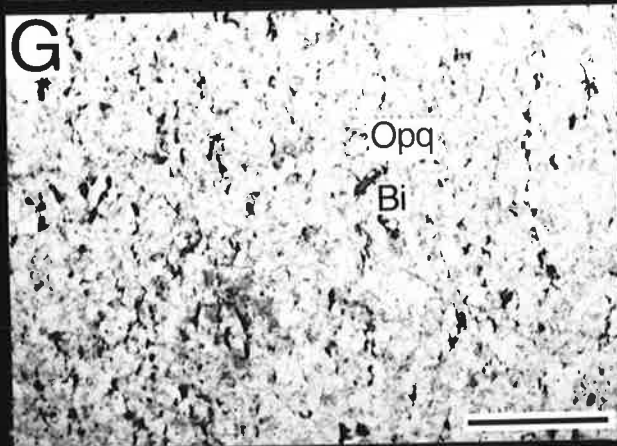
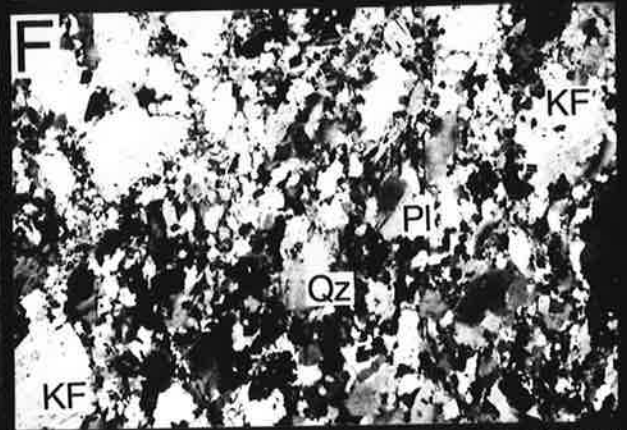
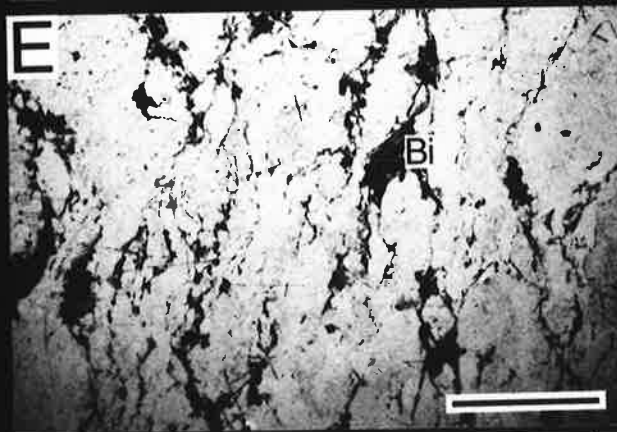
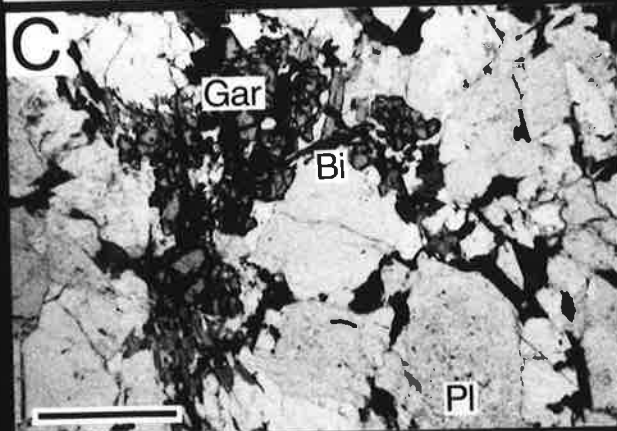
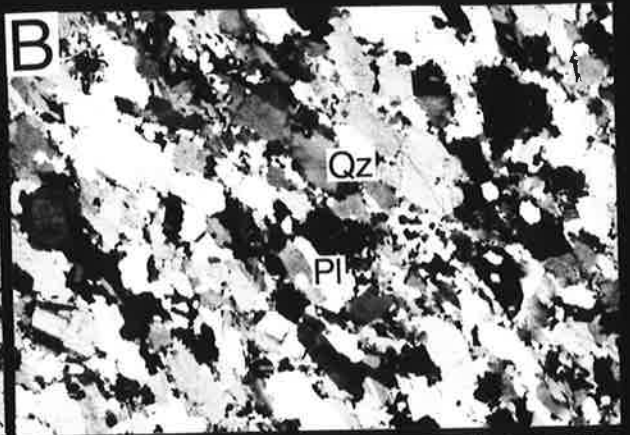
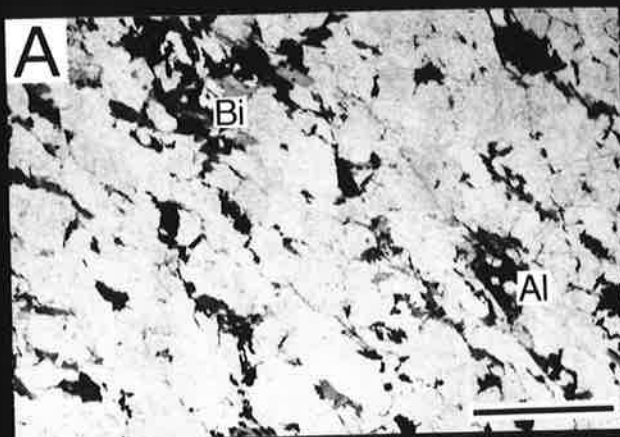
G. Central Leucocratic Granite

Sample: 52101A. Bi: biotite, Opq: opaque mineral.

Plane polarized light. Scale bar is 5 mm.

H. Same as G, but under crossed polarized light.

Qz: quartz, Pl: plagioclase, KF: K-feldspar.



zoned and some are antiperthitic. Quartz is medium to fine grained and anhedral with undulatory extinction. Biotite (α = yellow to pale brown, β = γ = brown to dark brown) averages 0.4 to 1mm in length, and is subhedral. Garnet occurs as fractured subhedral grains between 0.3 and 1.5mm in diameter, commonly in close association with biotite. The origin of the garnet is uncertain. Occurrence as primary crystal from magma, or as restite, or as xenocryst are possibilities. The restite or xenocryst origin may be difficult to ascribe to the abundant garnet crystals in near by pegmatite which intrudes the tonalite and is considered to be comagmatic in origin.

3.6.2. Mineral Chemistry

Complete chemical compositions of minerals from four samples are listed in Table A8-1. Selected data from hornblende, biotite, and garnet are presented in Table 3-9.

A. Plagioclase

Composition of plagioclase ranges from An 33 to An 42 with average An 35.6 in the type I tonalite, and from An 24 to An 35 with average An 28.7 in the type II tonalite. Small amounts of Or contents (less than 1 mol %) are found in most of plagioclases, but it is slightly higher (up to 3.1 mol %) in plagioclase which is antiperthitic.

B. Hornblende

Only two grains of hornblende have been analyzed. These are magnesio-hornblende and ferro-edenitic hornblende as classified by Leake (1968).

C. Biotite and Garnet

Table 3-9. Representative chemical compositions of minerals from the Ord River Tonalite Suite

Mineral	Garnet				Biotite				Amphibole	
	11203 Core-----Rim	11203 Rim	11203 Core-----Rim	11203 Rim	11203	11203	51302	51302	51302	51302
wt(%)										
SiO ₂	37.46	37.47	37.45	38.28	35.87	35.41	36.66	36.69	42.99	44.37
TiO ₂	0.00	0.00	0.00	0.00	1.33	2.07	2.31	2.16	1.27	1.18
Al ₂ O ₃	21.11	20.94	21.46	21.18	18.57	17.98	16.51	16.50	10.39	10.00
FeO*	33.82	34.48	34.53	32.88	21.82	22.48	19.45	19.64	18.84	17.99
MnO	4.14	3.84	4.47	2.83	0.00	0.09	0.27	0.29	0.42	0.42
MgO	1.92	1.80	1.57	3.24	8.42	7.79	11.71	11.83	9.51	10.24
CaO	1.78	1.90	1.87	1.90	0.00	0.00	0.00	0.00	11.57	11.51
Na ₂ O	0.00	0.00	0.00	0.00	0.12	0.00	0.22	0.17	1.28	1.25
K ₂ O	0.00	0.00	0.00	0.00	8.91	9.06	9.44	9.46	1.37	0.86
Cr ₂ O ₃	0.00	0.00	0.00	0.00	0.00	0.00	0.08	0.08	0.00	0.00
Total	100.23	100.43	101.35	100.31	95.00	95.88	96.65	96.82	97.64	97.82
Structural formula										
No.Ox.	12	12	12	12	22	22	22	22	23	23
Si	3.021	3.022	2.999	3.047	5.512	5.486	5.514	5.513	6.545	6.672
Al ^{iv}	0.000	0.000	0.000	0.000	2.488	2.514	2.486	2.487	1.455	1.328
Al ^{vi}	2.007	1.991	2.026	1.987	0.876	0.770	0.442	0.436	0.410	0.445
Ti	0.000	0.000	0.000	0.000	0.154	0.241	0.261	0.244	0.145	0.133
Fe	2.281	2.326	2.312	2.189	2.804	2.913	2.442	2.468	2.399	2.262
Mn	0.283	0.262	0.303	0.191	0.000	0.012	0.034	0.037	0.054	0.053
Mg	0.231	0.216	0.187	0.384	1.928	1.799	2.625	2.649	2.158	2.295
Ca	0.154	0.164	0.160	0.162	0.000	0.000	0.000	0.000	1.888	1.855
Na	0.000	0.000	0.000	0.000	0.036	0.000	0.064	0.050	0.378	0.364
K	0.000	0.000	0.000	0.000	1.747	1.791	1.811	1.814	0.266	0.165
Cr	0.000	0.000	0.000	0.000	0.000	0.000	0.010	0.010	0.000	0.000
Total	7.976	7.982	7.988	7.960	15.544	15.526	15.694	15.708	15.699	15.573
Mg/Mg+Fe	0.092	0.085	0.075	0.149	0.407	0.382	0.518	0.518	0.474	0.504
Ca*	-	-	-	-	-	-	-	-	0.293	0.289
Mg*	-	-	-	-	-	-	-	-	0.335	0.358
Fe*	-	-	-	-	-	-	-	-	0.372	0.353

FeO*: Total Fe as FeO

No.Ox.: Number of oxygens in structural formula

Ca*: Ca/Ca+Mg+Fe Mg*: Mg/Ca+Mg+Fe Fe*: Fe/Ca+Mg+Fe

Mg/Mg+Fe in biotite from the tonalites is 0.424 - 0.518; in sample (11203), which has garnet, the ratio is slightly lower, viz. 0.366 - 0.407 (Table A8-1).

The garnet in sample 11203 is almandine with small amounts of MgO and MnO. The core of the garnet is generally enriched in MgO relative to the rim. Compared to the garnet from the Eastern Leucocratic Granitoid Suite (Table 3-7), this garnet from the Ord River type II tonalite has a higher almandine (Fe) content.

Geothermometry using biotite-garnet pairs, according to the calibration of Ferry and Spear (1978), indicates temperatures of between 490 and 770°C at 5kb for the equilibration. The higher temperatures are obtained from biotite-garnet cores. The low temperatures around 500°C are obviously too low to be magmatic.

3.6.3. Geochemistry

Twelve samples of type I tonalite and six of type II tonalite of the Ord River Tonalite Suite are examined, and their major and trace element data are listed in Table A4-4. Sample locations are shown in Fig. 3-24.

A. Major elements

SiO₂ in the type I tonalite ranges from 58.4 to 66.2%, whereas type II tonalite has a limited range from 67.5 to 69.0% (Fig. 3-25). The type I tonalite is metaluminous as indicated by mol [Al₂O₃ / (CaO + Na₂O + K₂O)], less than 1.0 except for one sample (Table A4-4). However, the ratio for all of the type II tonalite samples is greater than 1.0, denoting a peraluminous character. The peraluminous nature of the type II tonalite could account for the presence of garnet in two samples. Although the type II tonalite is peraluminous, none of the ratios is greater than 1.041, so that both the type I and II granitoids are in the I-type range of

Fig. 3-24. Sample locality map for the Ord River Tonalite Suite

(I): type I of the Ord River Tonalite Suite

(II): type II of the Ord River Tonalite Suite

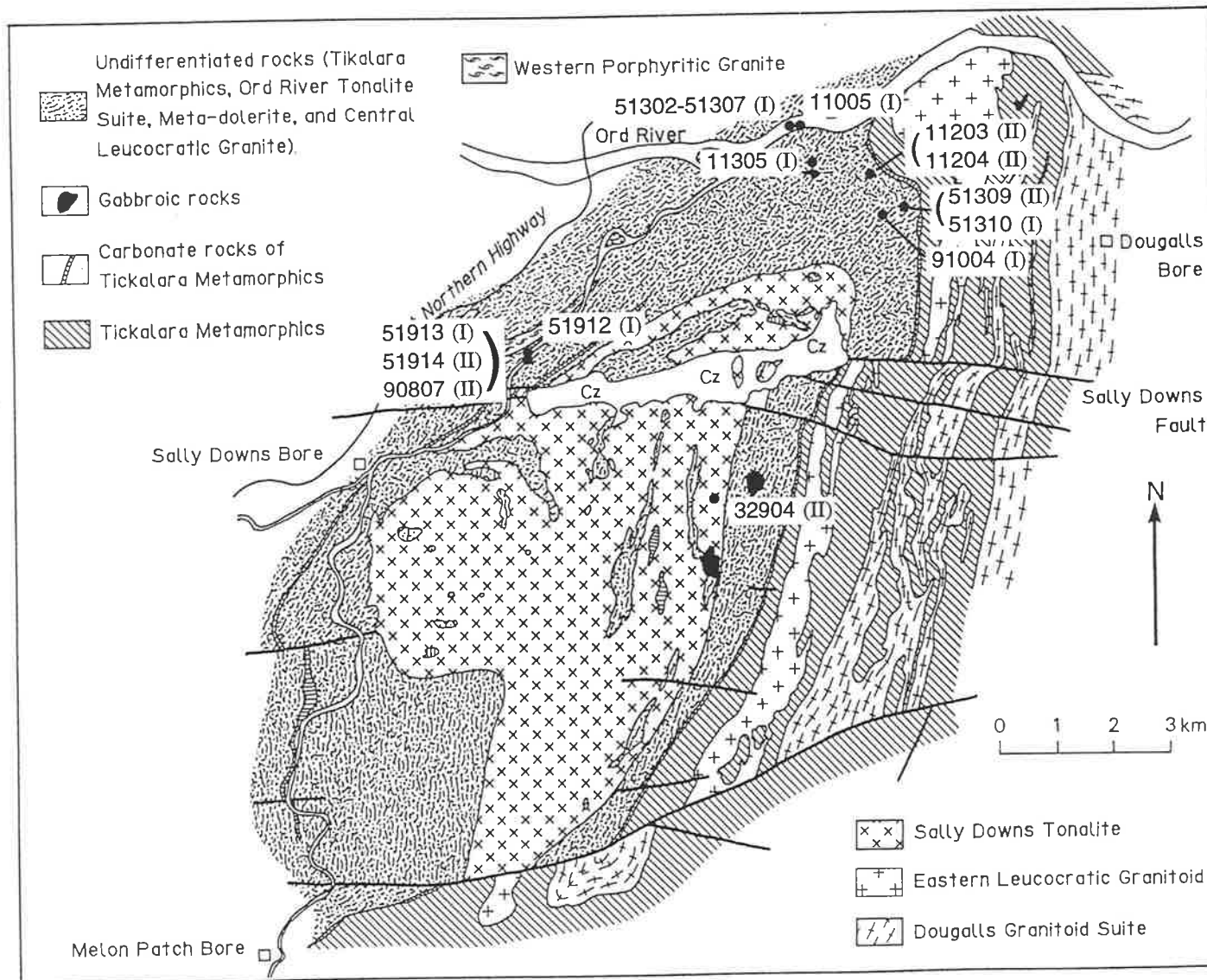


Fig. 3-25. Major element variation diagram of Ord River Tonalite Suite

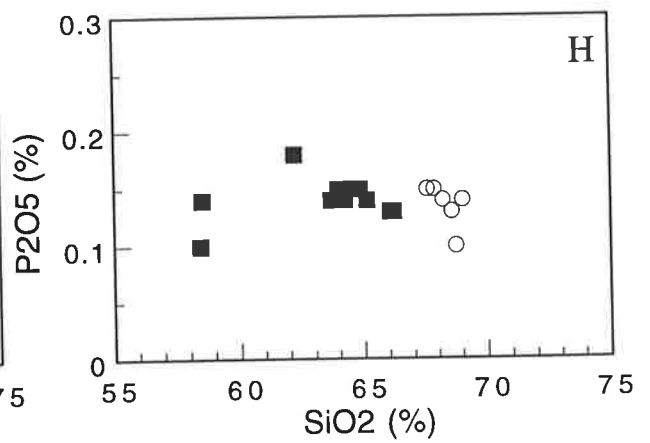
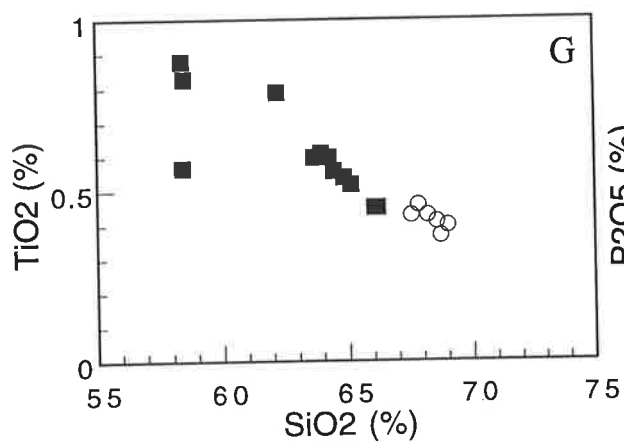
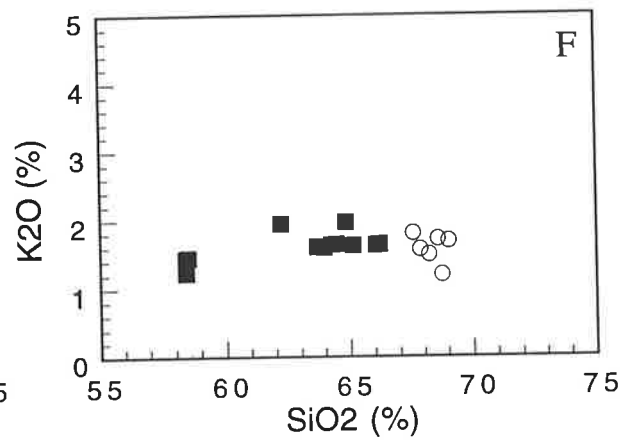
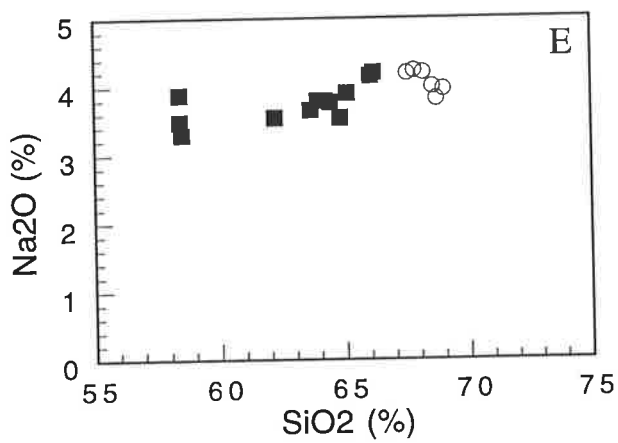
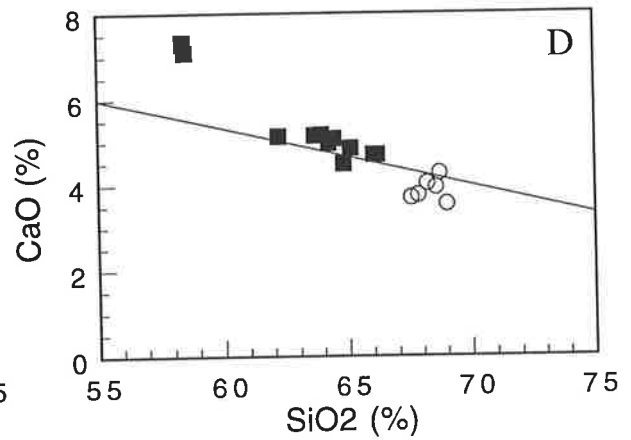
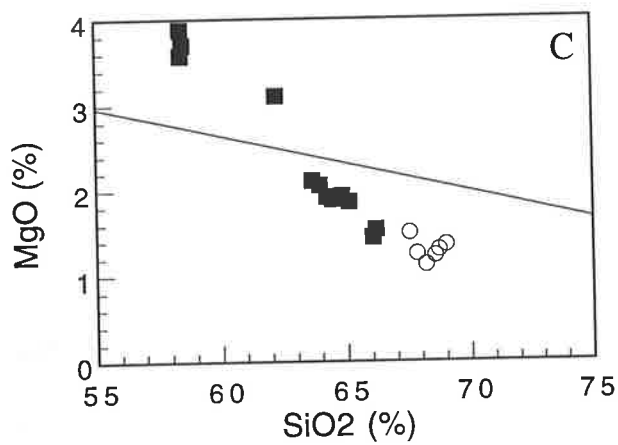
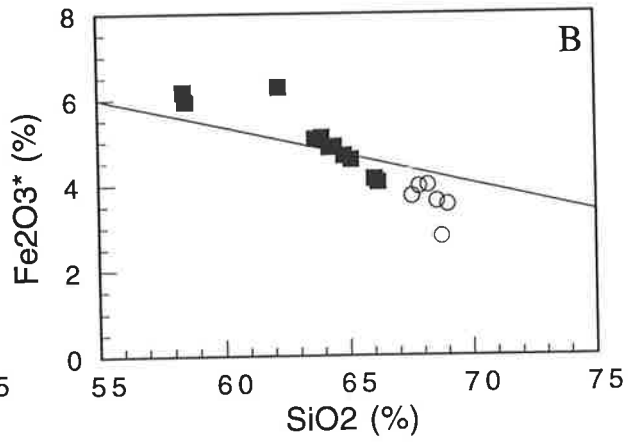
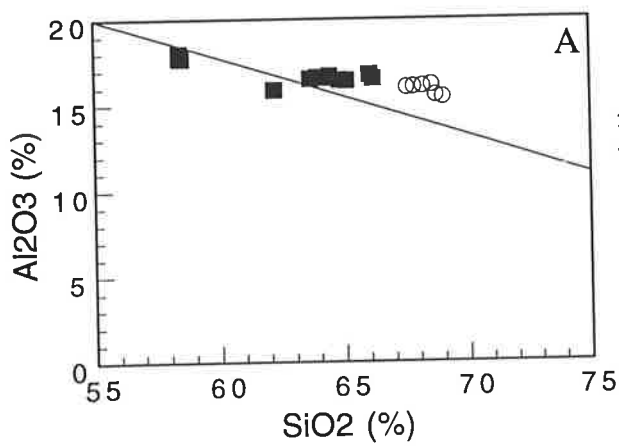
- A. $\text{Al}_2\text{O}_3\text{-SiO}_2$
- B. $\text{Fe}_2\text{O}_3^*\text{-SiO}_2$
- C. MgO-SiO_2
- D. CaO-SiO_2
- E. $\text{Na}_2\text{O-SiO}_2$
- F. $\text{K}_2\text{O-SiO}_2$
- G. $\text{TiO}_2\text{-SiO}_2$
- H. $\text{P}_2\text{O}_5\text{-SiO}_2$

Solid square: type I of the Ord River Tonalite Suite

Open circle: type II of the Ord River Tonalite Suite

Reference lines in the diagrams A., B., C., and D., show effect of constant sum, and are drawn from a point representing 100% SiO_2 and 0% of the other element extrapolated into the diagram. See section 3.4.3 for detailed discussion of the lines.

Fe_2O_3^* : total Fe as Fe_2O_3



Chappell and White (1974). High $\text{Na}_2\text{O}/\text{K}_2\text{O}$ ratios (>1.8), moreover, for the tonalites, support a geochemical affinity with the I-type granitoids.

On the variation diagram (Fig. 3-25), most of major elements change systematically with SiO_2 , suggesting a petrogenetically close relationship between the type I and type II tonalite. Al_2O_3 content is slightly higher than that of I-type granitoids from the Kosciusko Batholith (Hine et al., 1978). Fe_2O_3^* , MgO and CaO contents are similar to those of the I-type granitoids. Notable differences between the Ord River Tonalite Suite and typical I-type granitoids are found in the alkali contents, viz. higher Na_2O concentrations in the tonalite than in the I-type granitoids and lower and constant K_2O contents in the tonalite. These characteristic features are also found in the Dougalls Granitoid Suite, though the Dougalls Granitoid Suite has even lower K_2O contents than the Ord River Tonalite Suite. Slightly curved variations of Fe_2O_3^* , TiO_2 , and Na_2O versus SiO_2 (Fig. 3-25) suggest a crystal fractionation model. Constant K_2O and P_2O_5 contents preclude extensive fractionation of K_2O rich minerals and apatite. To keep the constant K_2O and P_2O_5 contents, a fractionated phase must have similar K_2O and P_2O_5 levels that of to the tonalite. Since no K-feldspar is found in the tonalite, biotite would be solely responsible for K_2O fractionation. K_2O contents (1.7%) in the tonalite would be buffered by a fractionated phase which contains 0.19 weight fraction of biotite in it, as the average K_2O content in biotite is 9%. Similarly, P_2O_5 (1.4%) in the tonalite would be buffered by a 0.03 weight fraction of apatite ($\text{P}_2\text{O}_5 = 42 \text{ wt}\%$) in the fractionated material.

B. Trace elements

Ba

Ba content ranges from 410 to 680ppm and decreases with increasing SiO₂, except for three samples which have about 300ppm Ba and the lowest SiO₂ content in the tonalite suite (Fig. 3-26). Abnormal behavior of these samples is found also with regard to some other trace elements, viz. Zr, and Y. These features may indicate that the sample should not be a member of the Ord River Tonalite Suite.

Rb and Sr

Rb broadly increases with increasing SiO₂ from 42 to 70ppm; on the other hand, Sr decreases with increasing SiO₂, from 560 to 330ppm. K/Rb ratios range from 284 to 215. The slight reduction of this ratio in the type II tonalite may be a result of hornblende fractionation. The level of Sr is comparable to that in the Dougalls Granitoid Suite, but the level of Rb is higher than that in the Dougalls Granitoid Suite. Hence, slightly higher Rb/Sr ratios (0.07 - 0.19) are found in the Ord River Tonalite Suite than in the Dougalls Suite.

Nb and Y

Nb concentrations range from 3 to 10ppm with the exception of two samples which have higher concentrations, viz. about 17ppm. Presence of garnet in these two samples may explain the abnormally high Nb concentration. However no significant difference in Y content is found between the two samples and garnet free samples. This fact precludes a xenocryst origin for the garnet in the tonalite, since the introduction of garnet in the tonalite as a xenocryst would significantly increase the Y concentration. Y largely decreases with increasing SiO₂, indicating decrease of HREE content with increasing SiO₂. The level of Y is higher than that in the Dougalls Granitoid Suite.

REE

Rare earth element (REE) concentrations (Table A5-2) of three samples from the Ord River Tonalite Suite are plotted in Fig. 3-27,

Fig. 3-26. Trace element variation diagram of Ord River Tonalite Suite

A. Ba-SiO₂

B. Rb-SiO₂

C. Sr-SiO₂

D. Rb-Sr

E. Zr-SiO₂

F. Nb-SiO₂

G. Y-SiO₂

H. V-SiO₂

Solid square: type I of the Ord River Tonalite Suite

Open circle: type II of the Ord River Tonalite Suite

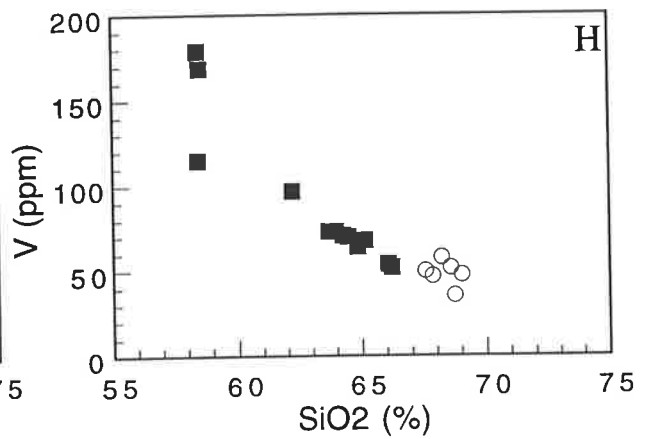
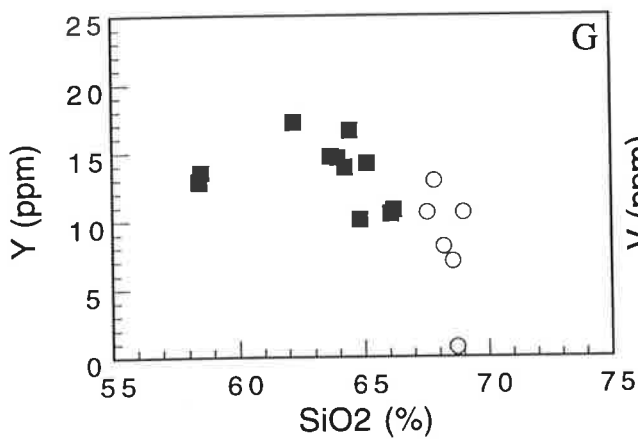
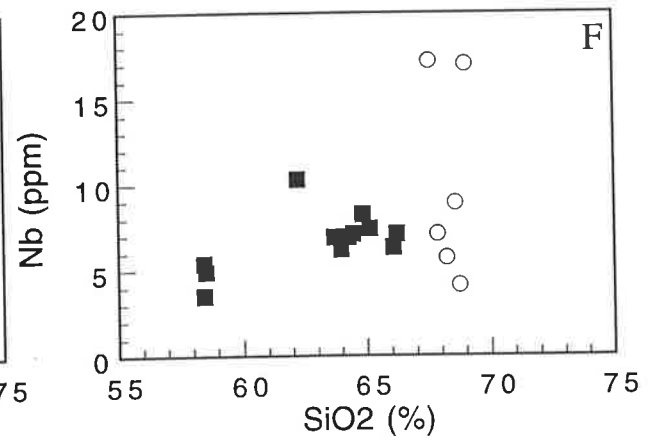
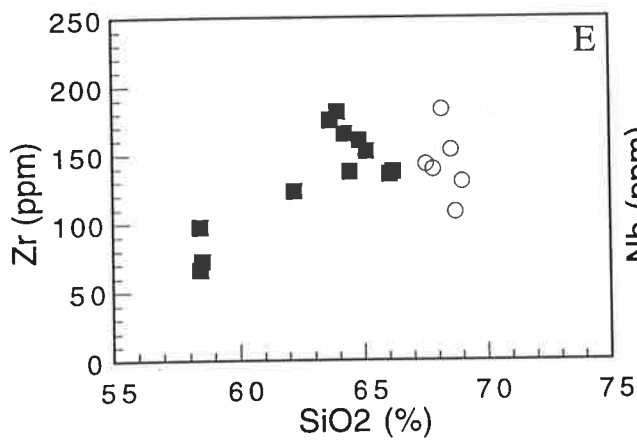
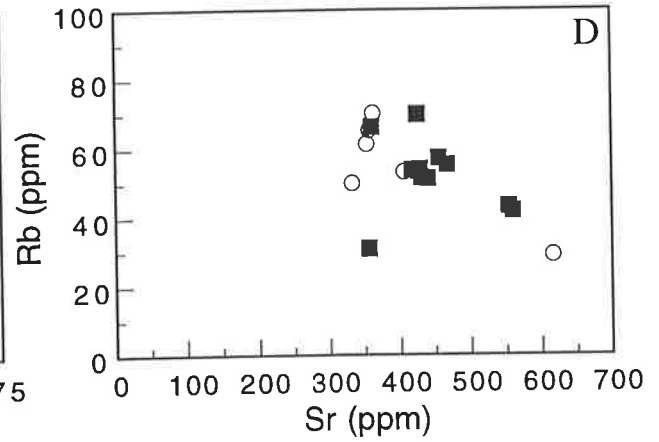
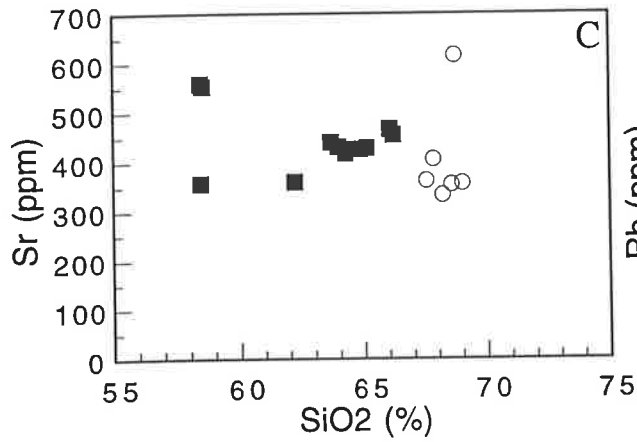
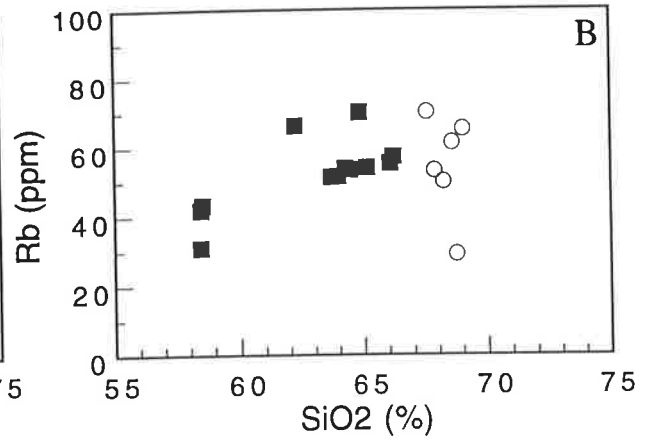
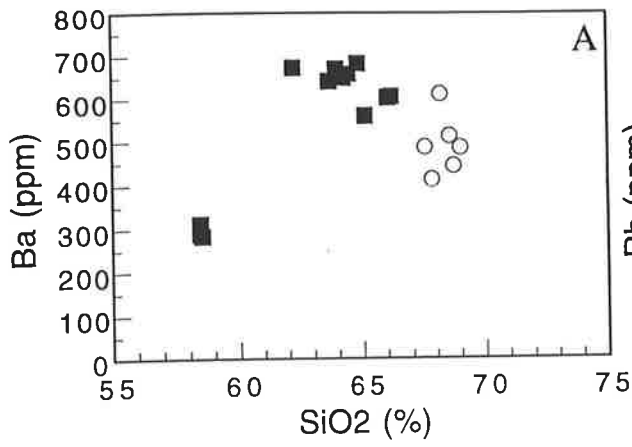
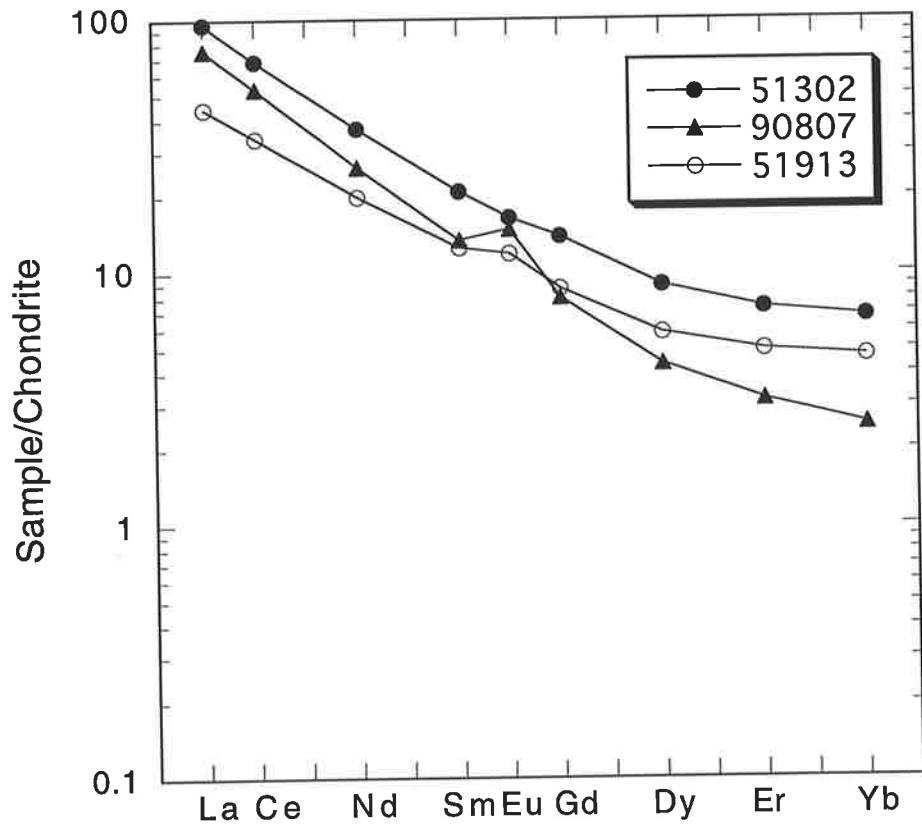


Fig. 3-27. Chondrite normalized REE plot of Ord River Tonalite Suite
Samples 51302 and 51913 are type I of the suite.
Sample 90807 is type II of the suite.



indicating LREE enriched patterns. As indicated by Y contents, HREE contents decrease with increase of SiO₂. A positive Eu anomaly is shown by the type II tonalite, suggesting possible hornblende fractionation.

3.7. Western Porphyritic Granite

3.7.1. Petrography

The Western Porphyritic Granite (Fig. 3-23E and F) is composed largely of quartz, K-feldspar, plagioclase, and biotite (Table A2-1 and Fig. 3-7). Muscovite, epidote, apatite, zircon, sphene, and opaque minerals are present as accessory minerals. Texture of the granite is characteristically inequigranular and porphyritic. Large crystals of feldspar, mostly microcline perthite but some plagioclase, are ovoidal or tabular in shape, and up to 2cm long. Strong foliation is manifested by concentrations of biotite swirling around the large feldspar grains.

Plagioclase is fine to coarse grained, commonly twinned according to albite and Carlsbad laws. Some of the large grains show weak normal zoning. Plagioclase which has twisted twin planes suggests intensive deformation. Myrmekite texture occurs at the contact of K-feldspar and plagioclase grains.

Quartz is fine to medium grained, and the medium grained crystals commonly show undulatory extinction. Some of the quartz grains are granular due to recrystallization. Deformational features can possibly be correlated with D₃.

Biotite (α = yellow, β = γ = yellowish brown to dark brown) is subhedral and medium grained, up to 3mm long, forming lenticular aggregates or thin sheets. Small subhedral muscovite is commonly present as a secondary feature, interleaved with biotite.

Apatite appears as small discrete crystals near the biotite grains, or in the plagioclase as tiny inclusions. Sphene occurs as a secondary phase

either within or in close association with biotite, and also around opaque minerals, presumably ilmenite.

3.7.2. Mineral Chemistry

A. Biotite

Chemical compositions of biotite from the Western Porphyritic Granite are given in Table A8-1. Fig. 3-28A illustrates constant Mg/(Mg + Fe + Mn) in biotite with some variation in Si value (on the basis of 22 oxygens), ranging from 5.45 to 5.60. The variation may be due largely to analytical inaccuracy of SiO₂ content. TiO₂ is between 2.3 to 2.6%. Other elements are generally constant.

B. Feldspar

Feldspar compositions from two samples of the granite are illustrated in the An-Ab-Or diagram in Fig. 3-28B. The diagram shows limited range of plagioclase composition, from An 32.4 to An 38.6 with average An 34.8 for sample 51918, and An 30.8 and An 33.1 for sample 52103. Weak normal zoning of plagioclase, from An 38.6 to An 33.5, is found in large grains.

Large grains of microcline are difficult to analyze because of perthitic lamellae, but the composition of less perthitic parts of the grains is Or 78. Small grains of microcline, probably recrystallized during deformation, have limited compositional range from Or 92 to 95. Using the equation of Whitney and Stormer (1977), the two-feldspar geothermometry suggests about 500°C at 2kb for small grains of microcline and plagioclase pairs, indicating possible deformation temperatures. In contrast, phenocrystic microcline and plagioclase pairs yield a minimum temperature of about 700°C at 2kb which is likely to be the crystallization temperature of the granite magma.

Fig. 3-28. Biotite and Feldspar plot of Western Porphyritic Granite

A. Biotite.

Si: Si value in the structural formula of 22 oxygens.

Mg: $Mg/Mg+Fe+Mn$

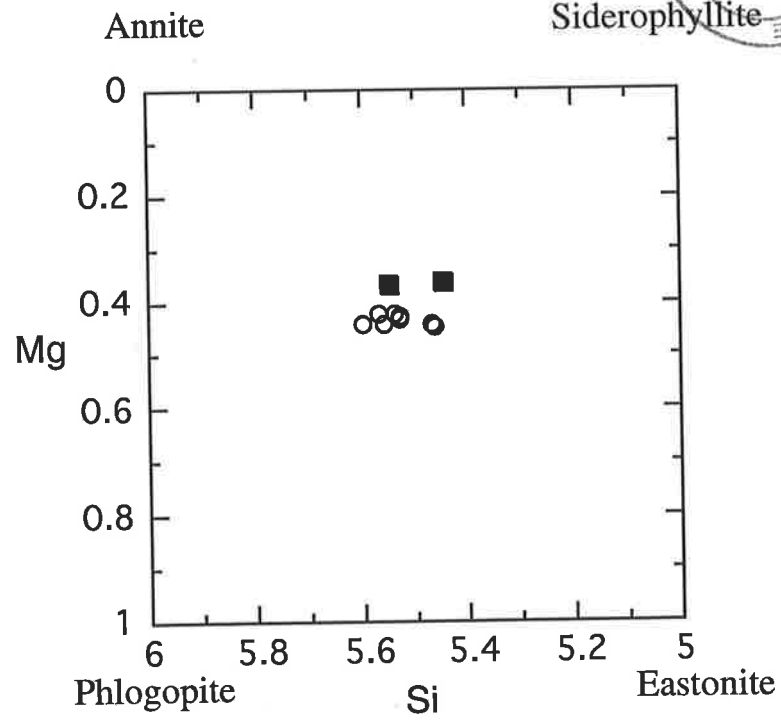
Solid square: 51918

Open circle: 52103

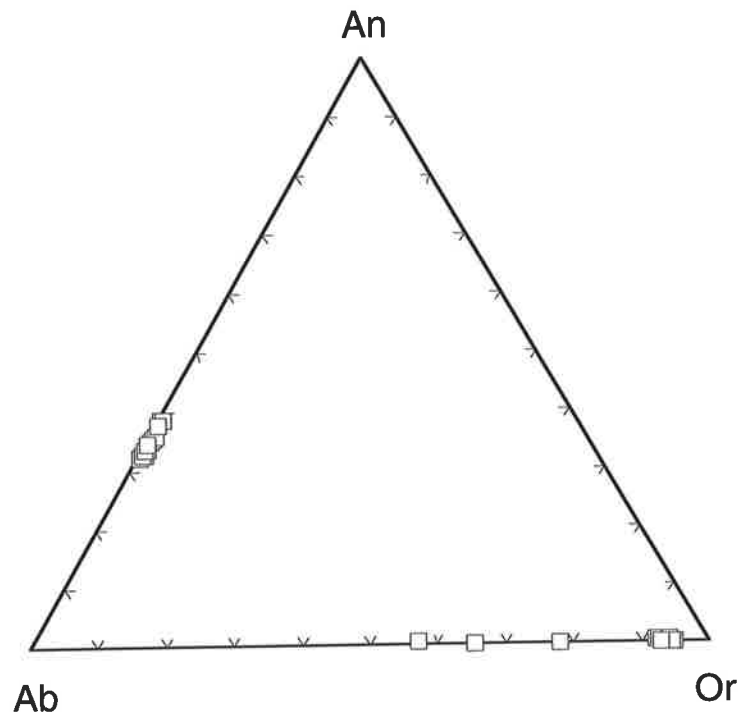
B. Feldspar composition



A.



B.



3.7.3. Geochemistry

A. Major elements

Western Porphyritic Granite analyses list in Table A4-5. Sample locations are shown in Fig. 3-2. Major element data display only small compositional variation between three analyzed samples of the granitoid.

Mol $[Al_2O_3/(CaO + Na_2O + K_2O)]$ varies from 1.030 to 1.045, which is within the range of values for I-type granitoids (Chappell and White, 1974). K_2O/Na_2O ratio is high, ranging from 1.41 to 1.70. On the major element variation diagram (Fig. 3-29), the granitoids generally display a similar compositional range to that of the S-type granitoids of the Kosciusko Batholith (Hines et al., 1979). However a subtle difference is indicated by the MgO content of the rocks, this being a lower value than in both the S- and I-type granitoids. The lower MgO value results in a slightly higher $Fe_2O_3^*/MgO$ ratio. The normative Qz-Ab-Or diagram (Fig. 3-30) shows that the granitoids plot near the minimum melt composition.

B. Trace Elements

Trace element data are presented in Table A4-5. Only a brief discussion of the data is given here.

Large ion lithophile (LIL) elements

The three analyzed samples of the granitoid contain between 780 and 1010ppm Ba, and the concentration decreases with increasing SiO_2 within the limited compositional range. Rb and Sr contents range from 114 to 173ppm and from 128 to 202ppm, respectively. Rb/Sr ratios vary from 0.564 to 1.352.

REE and Y

Fig. 3-29. Major element variation diagram of Western Porphyritic Granite and Central Leucocratic Granite

- A. $\text{Al}_2\text{O}_3\text{-SiO}_2$
- B. $\text{Fe}_2\text{O}_3^*\text{-SiO}_2$
- C. MgO-SiO_2
- D. CaO-SiO_2
- E. $\text{Na}_2\text{O-SiO}_2$
- F. $\text{K}_2\text{O-SiO}_2$
- G. $\text{TiO}_2\text{-SiO}_2$
- H. $\text{P}_2\text{O}_5\text{-SiO}_2$

Reference lines in the diagrams A., B., C., and D., show effect of constant sum, and are drawn from a point representing 100% SiO_2 and 0% of the other element extrapolated into the diagram. See section 3.4.3 for detailed discussion of the lines.

Solid square: Western Porphyritic Granite.

Open circle: Central Leucocratic Granite.

Fe_2O_3^* : total Fe as Fe_2O_3

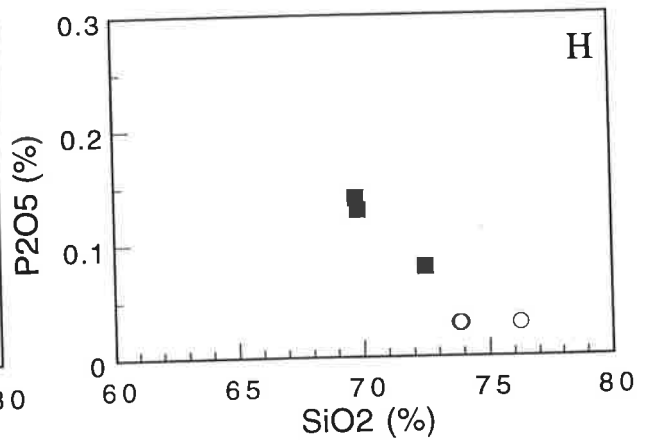
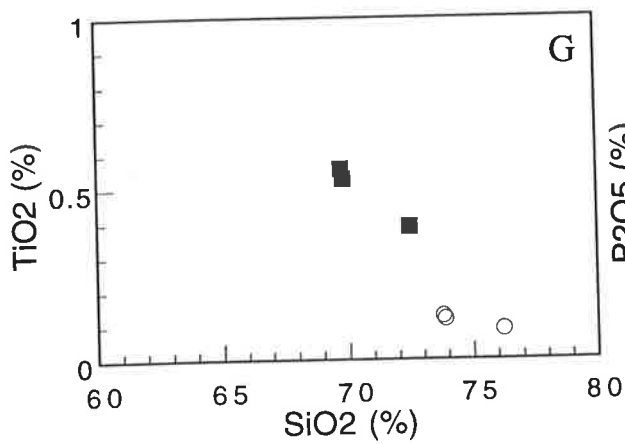
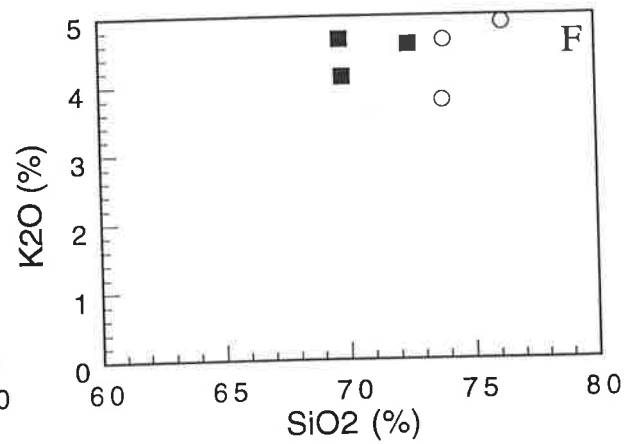
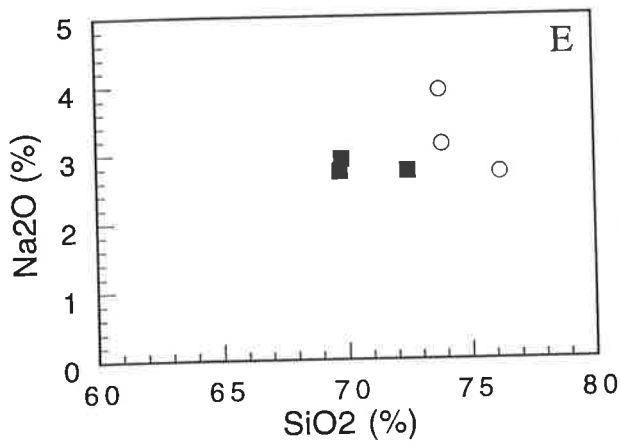
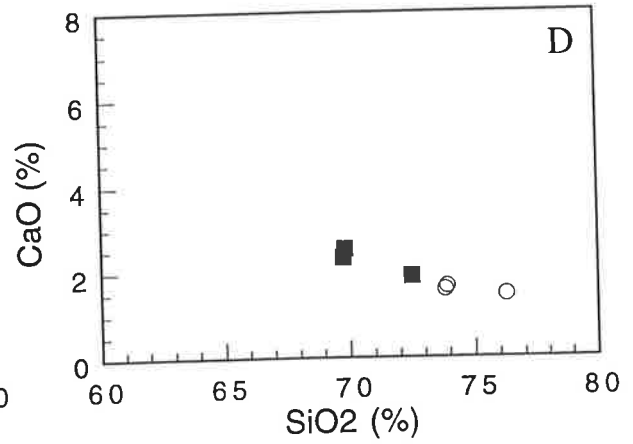
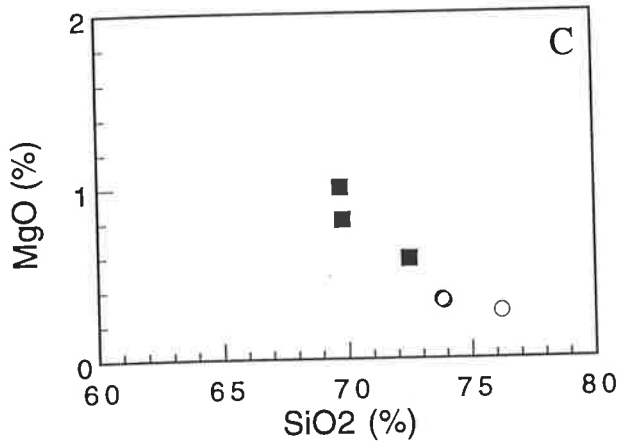
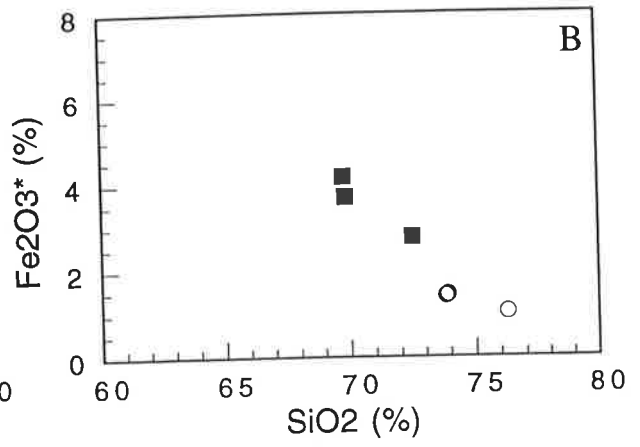
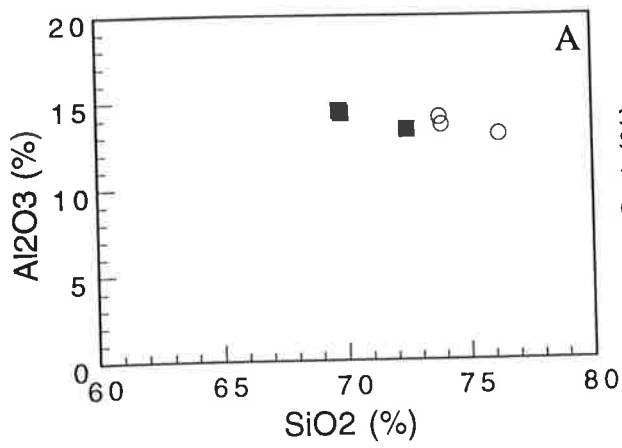
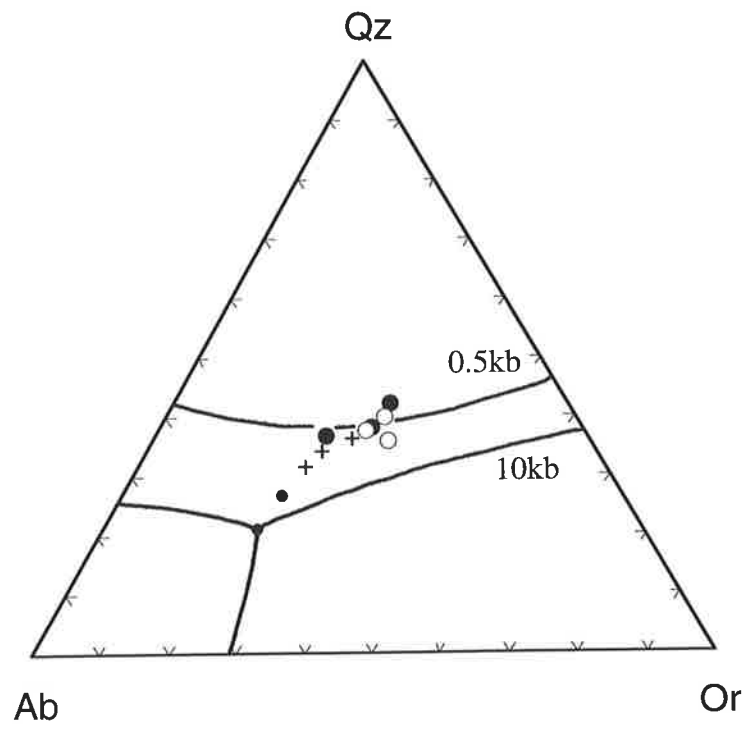


Fig. 3-30. Normative Qz-Ab-Or plot of Western Porphyritic Granite and Central Leucocratic Granite

Large solid circle: Western Porphyritic Granite.

Large open circle: Central Leucocratic Granite.

Phase boundaries of the granitic system for water pressure 0.5 kb and 10 kb are shown. Crosses are minima and small solid circles are eutectic points. Data from Tuttle and Bowen (1958) and Luth et al. (1964).



The granitoid has a high Ce and Y content. Chondrite normalized (Ce/Y) ratio of the samples, ranging from 7.7 to 14.4, suggests fractionated REE concentrations. The chondrite normalized REE pattern (Fig. 3-31) of a sample (52103) from the granitoid displays a negative Eu anomaly which suggests fractionation of plagioclase, or residual plagioclase in the source rock during partial melting.

3.8. Meta-dolerite

3.8.1. Petrography

The meta-dolerite is composed largely of plagioclase (35-55%), hornblende (15-45%), and variable amounts of two pyroxenes. Biotite (α = straw yellow, β = γ = reddish brown), opaque minerals, apatite and zircon are present as minor or accessory mineral. Since the degree of amphibolitisation is largely controlled by availability of hydrous fluids (Tarney, 1973; Beach and Tarney, 1978; Weaver and Tarney, 1981a), the extent of the metamorphism of the meta-dolerite is variable. Thus, even in a small meta-dolerite body, relatively unmetamorphosed dolerite is found in the center of the body.

Least metamorphosed rocks have subophitic texture (Fig. 3-32A and B), with some development of poikiloblastic hornblende enclosing plagioclase. Average grain size of the rocks is 0.5 to 0.8mm. The quantity of hornblende (α = pale, β = pale green, γ = greenish brown) in these rocks is low, generally less than 20%, compared with 30% pyroxene (ortho and clino).

Fine grained rocks (Fig. 3-32C and D) are extensively amphibolitised, consisting largely of hornblende (45%) and plagioclase (53%). Only trace amounts of relict orthopyroxene are recognized. Average grain size of the rocks is about 0.2mm. Small grains of

Fig. 3-31. Chondrite normalized REE plot of Western Porphyritic
Granite and Central Leucocratic Granite

52103: Western Porphyritic Granite

52101A: Central Leucocratic Granite

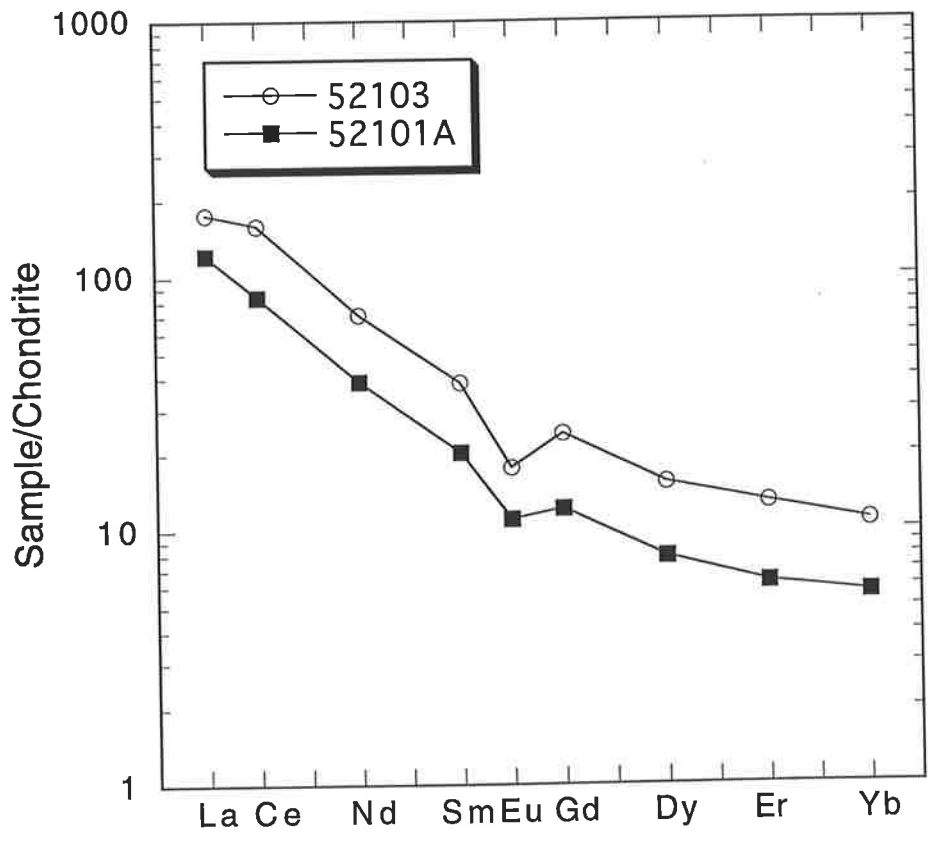


Fig. 3-32. Photomicrographs of meta-dolerite and hornblendite

A. Meta-dolerite

Sample: 73103. Opx: orthopyroxene, Cpx: clinopyroxene,
Am: amphibole (hornblende), Pl: plagioclase.

Poikiloblastic hornblende is present upper right corner.

Plane polarized light. Scale bar is 1 mm.

B. Same as A, but under crossed polarized light.

C. Meta-dolerite

Sample: 20606. Am: amphibole, Pl: plagioclase.

Plane polarized light. Scale bar is 1 mm.

D. Same as C, but under crossed polarized light.

E. Hornblendite

Sample: 11309. Ol: olivine, Opx: orthopyroxene,
Cpx: clinopyroxene, Am: amphibole.

Plane polarized light. Scale bar is 1 mm.

F. Same as E, but under crossed polarized light.

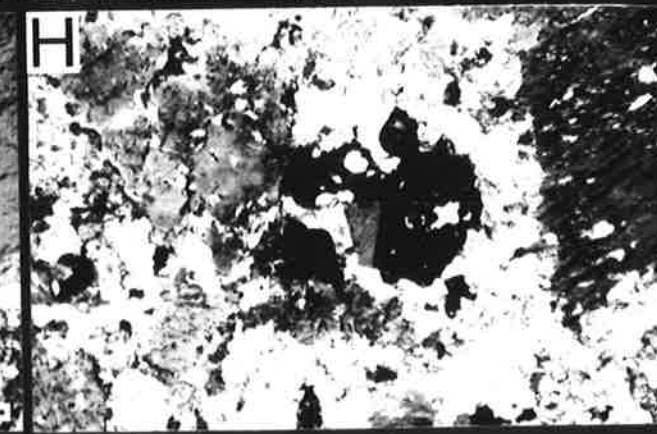
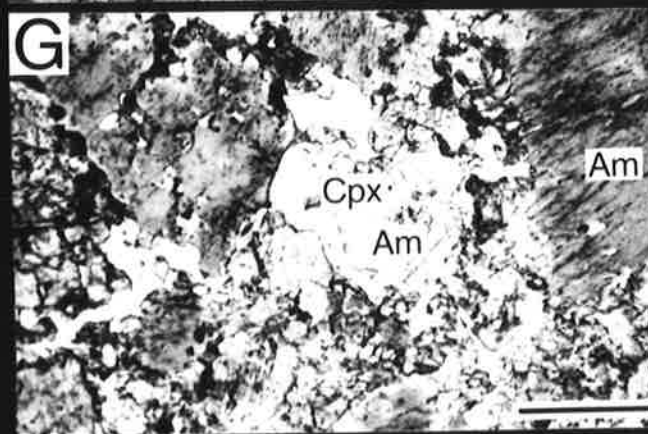
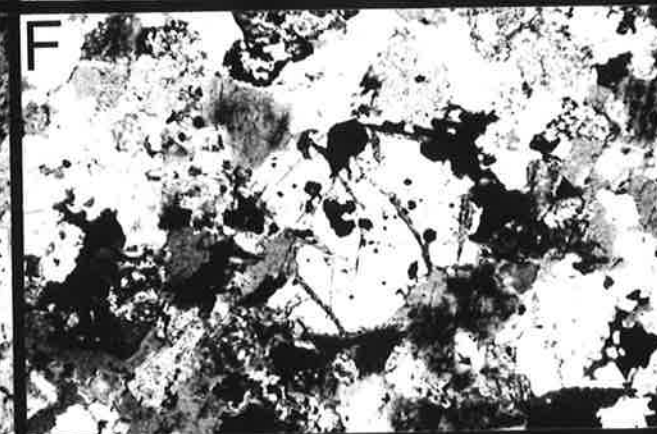
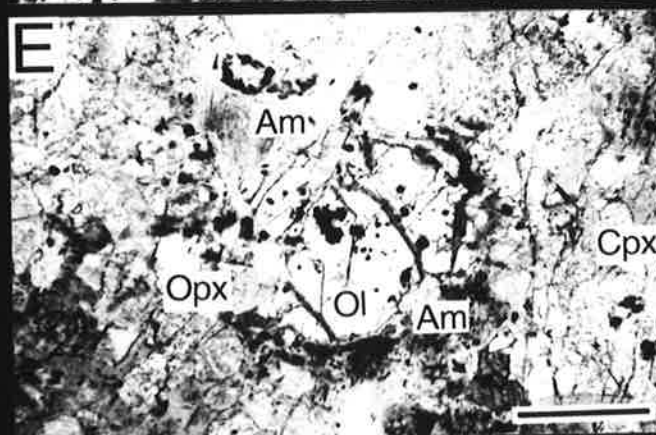
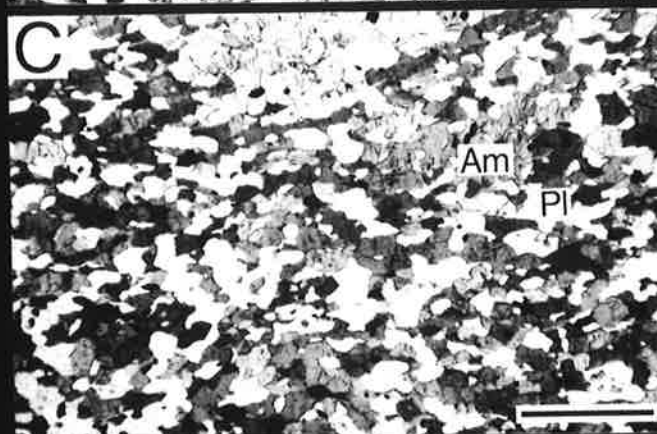
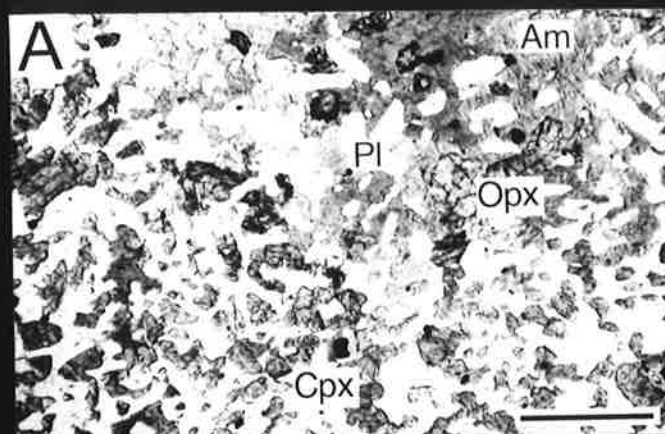
G. Hornblende mela-gabbro

Sample: 51508. Am: amphibole, Cpx: clinopyroxene.

Small crystal with high index above the Cpx symbol is a
clinopyroxene.

Plane polarized light. Scale bar is 1 mm.

H. Same as G, but under crossed polarized light.



plagioclase are aligned parallel to the elongation of the amphibole prisms. Poikiloblastic porphyroblasts of hornblende, up to 0.8mm, are present.

3.8.2. Mineral Chemistry

Chemical compositions of minerals from the meta-dolerite are listed in Table A8-1. Representative compositions are presented in Table 3-10.

A. Pyroxene

Mg/Mg + Fe in orthopyroxene is constant within each sample (Fig. 3-33), but shows slight differences between the samples. The variation is largely due to different MgO/(MgO + FeO) ratios in the respective whole rocks. Orthopyroxene contains minor amounts of Al₂O₃, MnO, CaO.

Clinopyroxene (Table 3-10) in the meta-dolerite is of salite and augite composition with Mg/Mg + Fe ratio ranging from 0.738 to 0.755. Two-pyroxene geothermometry on sample 40201 yields 901 and 951°C using the equations of Wood and Banno (1973) and Wells (1977), respectively. Slightly lower temperatures of 857 and 883°C are obtained from sample 73103. The figures from both rocks suggest subsolidus equilibration temperatures.

B. Amphibole

The amphiboles are magnesio-hornblende as classified by Leake (1968). Ti content is moderate ranging from 0.114 to 0.211 (based on 23 oxygens) with mean about 0.145 (Table 3-10 and Table A8-1).

C. Plagioclase

An content of plagioclase (Table A8-1) is high in the amphibolised samples, with an average value of 81. Plagioclase of less metamorphosed

Table 3-10. Representative chemical compositions of minerals from meta-dolerite

Sample	20606			40201			73103		
Mineral	Opx	Amph	Bi	Opx	Cpx	Amph	Opx	Cpx	Amph
wt(%)									
SiO ₂	55.09	44.59	37.28	53.36	52.91	48.29	53.66	53.21	48.75
TiO ₂	0.11	1.44	2.52	0.00	0.16	1.30	0.00	0.23	1.23
Al ₂ O ₃	1.30	11.11	16.17	0.88	1.38	8.63	0.95	1.68	8.67
FeO*	23.48	17.44	16.94	24.06	8.46	12.48	24.38	8.45	12.05
MnO	0.72	0.24	0.06	0.54	0.28	0.19	0.42	0.21	0.09
MgO	18.20	11.72	13.95	21.41	14.43	14.03	21.58	14.10	14.37
CaO	0.91	10.40	0.00	0.51	21.31	11.46	0.60	22.46	11.63
Na ₂ O	0.11	1.32	0.22	0.00	0.29	1.04	0.00	0.30	0.94
K ₂ O	0.00	0.63	9.66	0.00	0.00	0.48	0.00	0.00	0.49
Cr ₂ O ₃	0.00	0.00	0.00	0.00	0.00	0.00	0.00	0.09	0.28
Total	99.92	98.89	96.80	100.76	99.22	97.90	101.59	100.73	98.50
Structural formula									
No.Ox.	6	23	22	6	6	23	6	6	23
Si	2.052	6.571	5.529	1.985	1.979	6.990	1.981	1.965	6.996
Al ^{iv}	0.000	0.429	2.471	0.015	0.021	1.010	0.019	0.035	1.004
Al ^{vi}	0.057	0.501	0.357	0.023	0.040	0.462	0.022	0.038	0.463
Ti	0.003	0.160	0.281	0.000	0.005	0.142	0.000	0.006	0.133
Fe	0.731	2.149	2.101	0.748	0.265	1.511	0.753	0.261	1.446
Mn	0.023	0.030	0.008	0.017	0.009	0.023	0.013	0.007	0.011
Mg	1.010	2.574	3.084	1.187	0.804	3.027	1.187	0.776	3.073
Ca	0.036	1.642	0.000	0.020	0.854	1.777	0.024	0.889	1.788
Na	0.008	0.377	0.063	0.000	0.021	0.292	0.000	0.021	0.262
K	0.000	0.118	1.828	0.000	0.000	0.089	0.000	0.000	0.090
Cr	0.000	0.000	0.000	0.000	0.000	0.000	0.000	0.003	0.032
Total	3.921	15.552	15.721	3.996	3.997	15.323	3.999	4.001	15.298
Mg/Mg+Fe	0.580	0.545	0.595	0.613	0.752	0.667	0.612	0.748	0.680
Ca	0.020	0.258	0.000	0.010	0.444	0.281	0.012	0.462	0.284
Mg	0.568	0.404	0.000	0.607	0.418	0.479	0.605	0.403	0.487
Fe	0.411	0.338	0.000	0.383	0.138	0.239	0.383	0.136	0.229

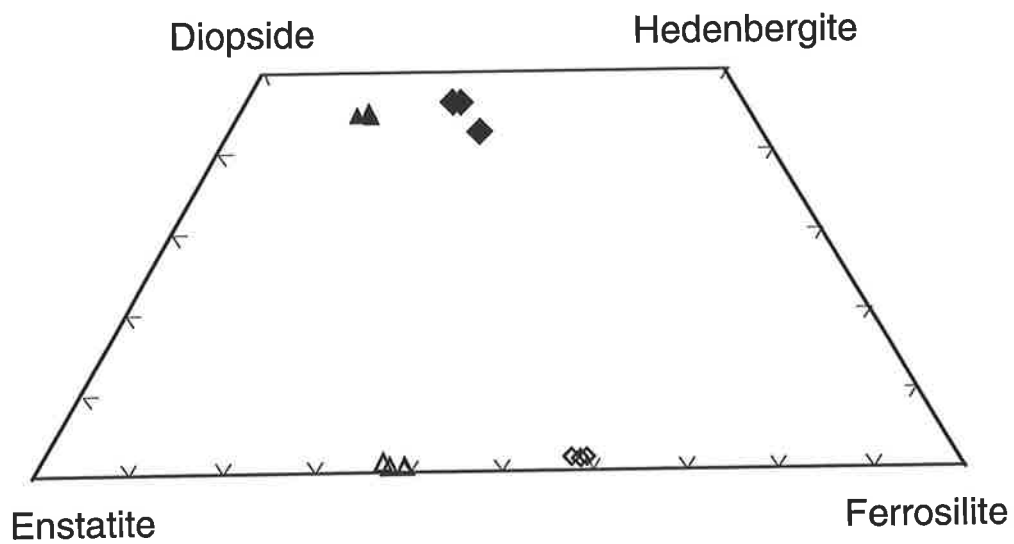
FeO*: Total Fe as FeO

Opx: Orthopyroxene, Cpx: Clinopyroxene, Amph: Amphibole, Bi: Biotite

No.Ox.: Number of oxygen in structural formula

Ca*: Ca/Ca+Mg+Fe Mg*: Mg/Ca+Mg+Fe Fe*: Fe/Ca+Mg+Fe

Fig. 3-33. Composition of pyroxenes from meta-dolerites



▲ : Clinopyroxene (40201)

◆ : Clinopyroxene (51006)

△ : Orthopyroxene (40201)

◇ : Orthopyroxene (51006)

rocks has lower An content and some of the grains show normal zoning from An 79 to 64.

3.8.3. Geochemistry

Major and trace element data of seven samples of the meta-dolerite are presented in Table 3-11. Sample locations are shown in Fig. 3-5.

A. Major elements

Three samples (20606, 32702, and 51505) are quartz normative, and the other four are slightly olivine normative. The samples have constant $\text{Na}_2\text{O} + \text{K}_2\text{O}$ contents (1.51-1.86). The levels of $\text{Na}_2\text{O} + \text{K}_2\text{O}$ are in the field of subalkalic rocks of Miyashiro (1978). However, as the alkali elements are most susceptible to mobilization during alteration and metamorphism, the levels may not show original values.

Mg-values [$(\text{Mg} / (\text{Mg} + \text{Fe})) \times 100$ atomic], calculated using ($\text{FeO} = 0.9 \times \text{FeO}^*$ (total Fe as FeO)) range from 45 to 66. Samples with high Mg-value (more than 60) may not have experienced extensive crystal fractionation, since partial melting of mantle lherzolite should yield basaltic magma with Mg-value from 70 to 74 (Perfit et al., 1980). Fe_2O_3^* (= total Fe as Fe_2O_3) content systematically increases with decreasing Mg-value, indicating iron enrichment. On an AFM diagram (Fig. 3-34C), a tholeiitic iron enrichment trend is clearly defined. Similarly, the tholeiitic character is observed in discrimination diagrams (Fig. 3-34A and B) using discrimination boundaries proposed by Miyashiro (1974).

B. Trace elements

Cr and Ni decrease with decreasing MgO, from 155 to 59ppm, and 494 to 33ppm respectively, suggesting olivine and pyroxene fractionation.

Table 3-11. Chemical compositions of meta-dolerite

Sample	20606	32702	40201	51006	51505	73103	81001
Major Elements (wt%)							
SiO ₂	49.38	52.49	49.00	46.91	47.78	49.31	48.55
Al ₂ O ₃	15.03	14.26	16.80	14.76	15.96	16.12	16.81
Fe ₂ O ₃ *	13.59	11.51	10.70	17.22	14.79	10.52	11.12
MnO	0.24	0.19	0.18	0.25	0.22	0.17	0.19
MgO	7.34	6.77	8.68	6.22	6.60	9.20	8.31
CaO	10.66	11.27	11.70	11.73	10.57	12.04	11.91
Na ₂ O	1.34	1.55	1.65	1.41	1.43	1.75	1.53
K ₂ O	0.38	0.31	0.17	0.10	0.30	0.12	0.19
TiO ₂	1.28	0.57	0.86	0.79	1.53	0.77	0.88
P ₂ O ₅	0.17	0.06	0.14	0.09	0.26	0.09	0.14
LOI	0.53	0.47	0.12	-0.09	0.48	0.03	0.54
Total	99.94	99.45	100.00	99.39	99.92	100.12	100.17
Trace Elements (ppm)							
Ba	76.8	56.4	100	48.7	130	94	62
Rb	2.6	6.9	4.7	2.7	9.6	3.8	2.5
Sr	121	80	191	99	216	112	160
Zr	95	42.9	24.4	51	95	36.7	48
Nb	7.4	3.1	3.8	4.3	8.8	3.2	3
Y	39.1	18.5	19	27.9	37.7	19.6	26
Ce	31	9.5	25	20	45	14	29
Nd	22	13.3	15	18	25	12	8
Sc	48.2	53	42.6	74.5	46.5	45.1	48
V	281	301	231	453	299	234	234
Cr	180	115	405	33	62	494	400
Ni	92	96	109	59	86	155	116
Cu	87	96	84	30	81	98	83
Zn	104	65	80	119	128	73	86

Fe₂O₃* : Total Fe as Fe₂O₃

LOI : Loss on ignition

Fig. 3-34. $\text{FeO}^*/\text{MgO}-\text{SiO}_2$, $\text{FeO}^*/\text{MgO}-\text{FeO}$ plots and AFM diagram of meta-dolerite

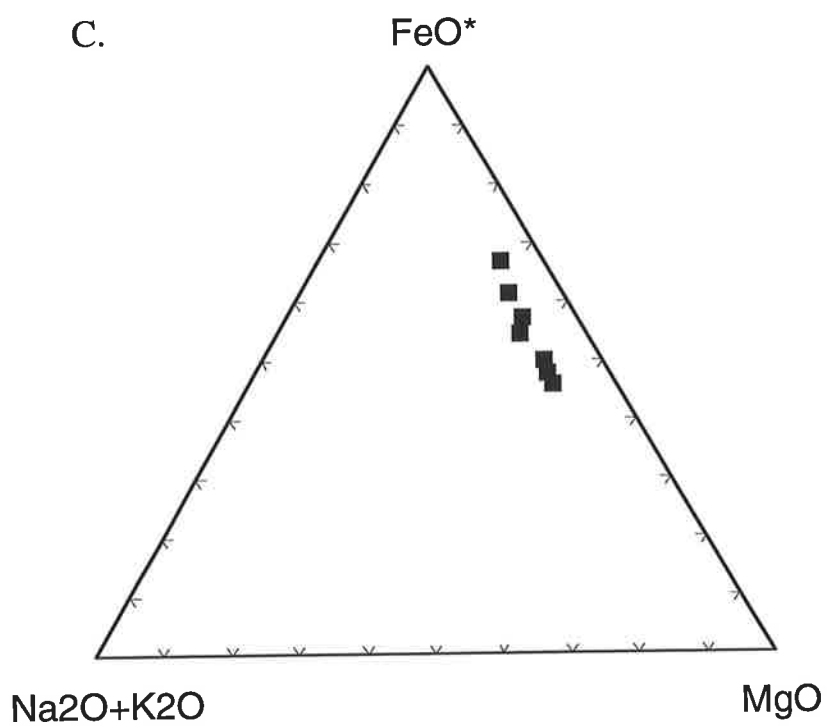
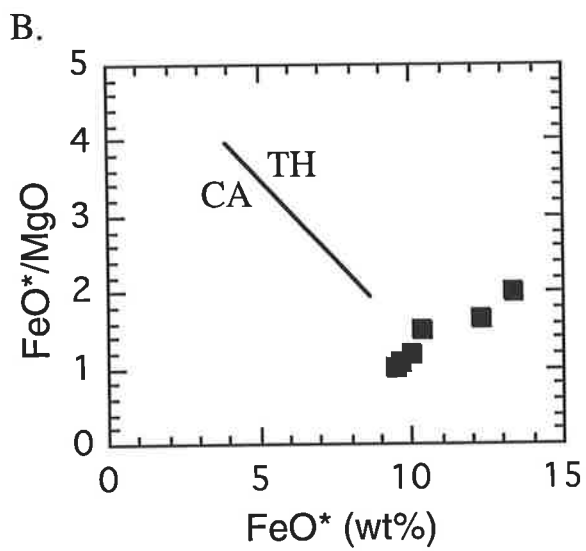
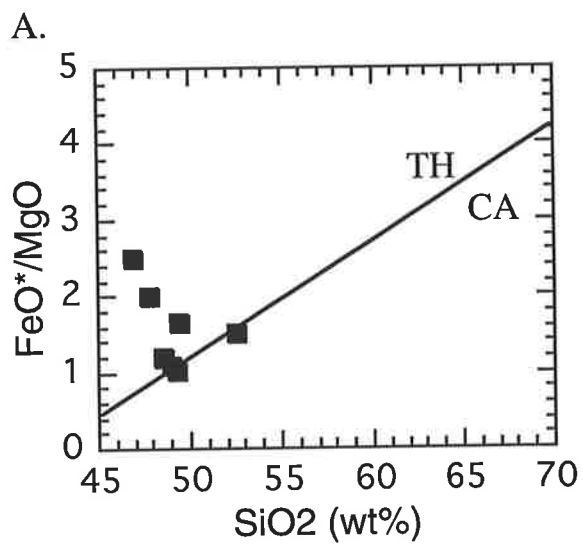
A. $\text{FeO}^*/\text{MgO}-\text{SiO}_2$ and $\text{FeO}^*/\text{MgO}-\text{FeO}$ plots

FeO^* : total Fe as FeO

Tholeiite field (TH) and calcalkaline field (CA) are from Miyashiro (1978).

B. AFM diagram

Showing Fe enrichment trend.



On the other hand, enrichment of V with decreasing MgO precludes an extensive magnetite fractionation.

Zr contents range from 24 to 95ppm and Zr/Nb ratios from 6.4 to 16. Sample 73103, which has highest Mg-value, has 36.7ppm Zr. Assuming all Zr goes into the melt and the Zr content of the source region of the meta-dolerite is 11ppm, which is the value for Archaean mantle estimated by Sun and Nesbitt (1977), about 30% partial melting of the source is required to obtain the level of Zr in the melt. Similar calculation involving Ti content indicates 27% partial melting.

Chondrite normalized (Ce/Y) ratio ranges from 1.38 to 3.03, indicating moderately fractionated REE contents. The chondrite normalized REE pattern for meta-dolerite (20606) is shown in Fig. 3-35. The pattern reveals the LREE enriched with respect to the MREE, but middle to heavy REE have rather constant values. The flat pattern in the HREE region precludes the involvement of garnet as either a residual or crystallizing phase at any stage in the dolerite evolution. A small negative Eu anomaly may suggest the involvement of plagioclase.

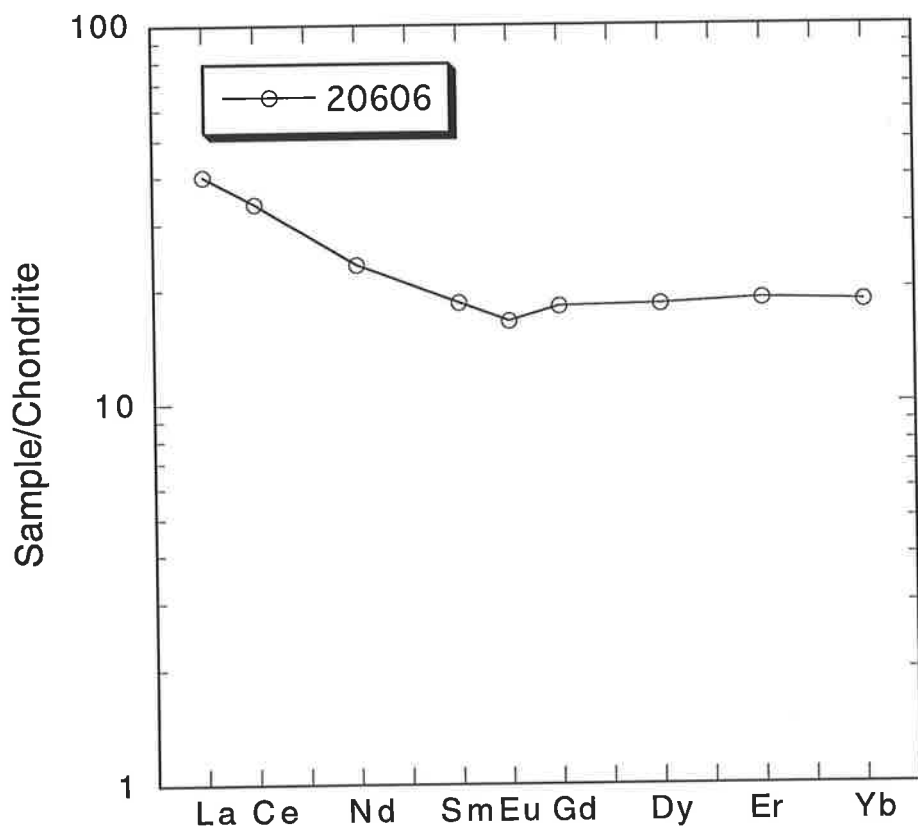
3.9. Central Leucocratic Granite

3.9.1. Petrography and Mineral Chemistry

The Central Leucocratic Granite is typically fine to medium grained and has allotriomorphic-granular to hypidiomorphic-granular textures (Fig. 3-23G and H). It is primarily composed of equal amounts of quartz, plagioclase, and K-feldspar (Fig. 3-7) and lesser amounts of biotite, muscovite, and opaque (Table A2-1). Epidote, apatite, and zircon are common accessory phases.

Biotite (α = straw yellow, β = γ = yellowish to dark brown) is generally fine grained and subhedral, and comprises about 4% by volume

Fig. 3-35. Chondrite normalized REE plot of meta-dolerite



of the granite. Chemical analysis of several biotites (Table A8-1) shows constant $Mg/Mg + Fe$ about 0.45.

Plagioclase is subhedral or anhedral and fine to medium grained. Mol An content of plagioclase ranges from 24 to 32, with less than 1 mol % of Or component (Table A8-1). K-feldspar is microcline or microcline-perthite, ranging in composition from Or 90 to Or 96. It is fine to medium grained and anhedral.

Anhedral quartz commonly shows undulatory extinction. Small flakes of muscovite may be secondary after biotite or K-feldspar.

3.9.2. Geochemistry

Major and trace element data are listed in Table A4-5. Sample locations are shown in Fig. 3-2.

A. Major elements

Major element data (Table A4-5) are plotted in Fig. 3-29 together with data of the Western Porphyritic Granite. As the mol $Al_2O_3/(CaO + Na_2O + K_2O)$ ranges from 1.03 to 1.05, the granite is peraluminous, but the ratio is slightly lower than the value of >1.09 for S-type granitoids in the Kosciusko Batholith (Hine et al., 1978). However, Al_2O_3 in the Central Leucocratic Granite is higher than that of the S-type granitoids and even slightly higher than that of the I-type granitoids (Fig. 3-29), suggesting that high values of mol $(CaO + Na_2O + K_2O)$, especially high concentrations of Na_2O and K_2O , are responsible for reducing the degree of the alumina-saturation. Two samples of the Central Leucocratic Granite show low Na_2O/K_2O ratios, but the ratio of one sample is slightly higher than unity. The general dominance of K_2O over Na_2O may imply the granite is S-type. The normative Qz-Ab-Or diagram (Fig. 3-30) shows that the granitoids plot near the minimum melt composition, similar to the Western Porphyritic Granite.

Most of the major element variations (Fig. 3-29) display a similar range to that of I-type granitoids. The evidence indicates that the Central Leucocratic Granite has transitional chemical properties between S-type and I-type.

B. Trace elements

Large ion lithophile (LIL) elements

Ba in the Central Leucocratic Granite ranges from 730 to 1150ppm, and the range is similar to that of the Western Porphyritic Granite (Table A4-5). Rb varies from 72 to 106ppm. Inverse correlation between Rb and K₂O result in a large increase of K/Rb ratio from 296 to 564 with increase of K₂O. Sr content is rather constant, about 250ppm. Rb/Sr ratios, ranging from 0.290 to 0.409, are lower than the ratios of the Western Porphyritic Granite.

Rare earth elements (REE) and Yttrium

The granite has a light REE enriched pattern with small negative Eu anomaly (Fig. 3-31). Y content of the three samples (Table A4-5) indicates that all of the rocks have a relatively low heavy REE content, viz. less than ten times chondritic abundance.

3.10. Hornblendite and Mela-gabbro

3.10.1. Petrography

As described already, two types of the mela-gabbro, viz. hornblende mela-gabbro and olivine-orthopyroxene mela-gabbro, are found. Three samples (11309, 40206, and 41802) of olivine-pyroxene hornblendite, one hornblende mela-gabbro (51508), and one olivine-orthopyroxene mela-gabbro (83101) are examined. Sample locations are given in Fig. 3-5.

A. Olivine-pyroxene hornblendite

The hornblendite (Fig. 3-32E and F) is characterized by poikilitic texture throughout. Estimated modal composition is hornblende (40-45%), clinopyroxene (25-30%), orthopyroxene (15-22%), olivine (7-15%), with trace amounts of biotite, plagioclase, and opaque minerals.

Olivine occurs as rounded small grains and is generally enclosed in orthopyroxene or directly in oikocrysts of hornblende. Olivine has inclusions of an opaque mineral, presumably spinel. Some of the olivine grains are replaced along partings by iddingsite. Orthopyroxene is subhedral and is about 1mm in diameter. Some grains are traversed by very thin lamellae. Clinopyroxene also occurs as subhedral grains mostly 1mm in diameter, including small hornblende grains but is, itself, generally included by oikocrysts of hornblende. Similar reciprocal enclosing relationships are found between orthopyroxene and clinopyroxene. Hornblende oikocrysts, up to 2.5cm long, contain most of the mafic minerals as inclusions. Biotite is present interstitially or as inclusion in the hornblende. Plagioclase is the last mineral to crystallize. The above textural relationships suggest the following crystallization sequence; olivine - orthopyroxene and clinopyroxene - biotite - hornblende - plagioclase.

B. Hornblende mela-gabbro

The hornblende mela-gabbro (Fig. 3-32G and H) is composed of hornblende (60%), clinopyroxene (26%), plagioclase (13%) and quartz (1%). Hornblende is present as both large phenocrysts, up to 1cm long, and fine grained matrix. The phenocrysts of hornblende include small crystals of plagioclase and clinopyroxene. Anhedral grains of clinopyroxene, hornblende, and plagioclase, mostly less than 0.3mm in size, comprise the matrix. Quartz is present as anhedral interstitial

grains. Along the grain boundary of the fine grained plagioclase, symplectite of plagioclase and amphibole is developed. Accessory minerals are sphene, carbonate, and opaque minerals.

C. Olivine-orthopyroxene mela-gabbro

The rock consists largely of olivine (10%), orthopyroxene (15%), clinopyroxene (40%), hornblende (7%), plagioclase (25%). Olivine is generally enclosed by pyroxenes. Pyroxenes are anhedral to subhedral, and the average grain size is 1mm. Plagioclase is present interstitially.

3.10.2. Mineral Chemistry

Chemical compositions of minerals analyzed are listed in Table A8-1. Representative compositions are summarized in Table 3-12.

A. Olivine

Olivine in the hornblendite ranges from Fo 75 to Fo 79, which is similar in composition to most olivines analyzed from the McIntosh sill (Hamlyn, 1977), the large layered basic complex exposed 20km south of the hornblendite outcrops.

Olivine Mg/(Mg + Fe) in all the samples is relatively constant (Table A8-1). Only small amounts of MnO and NiO, up to 0.34 and 0.33 wt%, respectively, are present.

B. Pyroxene

Orthopyroxene

Mg/(Mg + Fe), ranging from 0.746 to 0.807, is nearly identical to that in the olivine. No significant variation of the ratio within a sample is found. On the other hand, Ca content varies considerably from 0.012 to

Table 3-12. Representative chemical compositions of minerals from hornblendite and mela-gabbro

Mineral	Olivine		Orthopyroxene			Clinopyroxene		
	Sample	11309	40206	11309	40206	41802	11309	40206
Rock Type	Hb	Hb	Hb	Hb	Hb	Hb	Hb	Hb
SiO ₂ (wt%)	39.06	39.10	54.41	54.58	54.13	53.76	52.40	50.26
TiO ₂	0.00	0.09	0.08	0.08	0.32	0.29	0.30	0.30
Al ₂ O ₃	0.00	0.00	1.92	2.55	2.19	1.93	2.87	3.78
FeO	21.45	19.89	14.02	12.82	13.07	4.88	4.30	6.98
MnO	0.25	0.27	0.29	0.06	0.26	0.10	0.15	0.23
MgO	38.90	41.29	6.82	28.65	29.14	15.82	16.46	16.22
CaO	0.00	0.01	1.36	0.92	1.47	22.22	21.55	20.41
Na ₂ O	0.01	0.00	0.04	0.00	0.00	0.25	0.26	0.35
K ₂ O	0.02	0.01	0.00	0.00	0.01	0.02	0.02	0.00
Cr ₂ O ₃	0.06	0.00	0.07	0.17	0.24	0.18	0.33	0.73
Total	99.75	100.66	99.01	99.83	100.83	99.45	98.64	99.26
Formular Units								
No. Ox.	4	4	6	6	6	6	6	6
Si	1.012	0.998	1.968	1.944	1.921	1.974	1.937	1.874
Al ^{iv}	0.000	0.000	0.032	0.056	0.079	0.026	0.063	0.126
Al ^{vi}	0.000	0.000	0.050	0.051	0.013	0.058	0.062	0.040
Ti	0.000	0.002	0.002	0.002	0.009	0.008	0.008	0.008
Fe	0.465	0.424	0.424	0.382	0.388	0.150	0.133	0.218
Mn	0.005	0.006	0.009	0.002	0.008	0.003	0.005	0.007
Mg	1.503	1.570	1.446	1.521	1.541	0.866	0.907	0.601
Ca	0.000	0.000	0.053	0.035	0.056	0.874	0.853	0.815
Na	0.001	0.000	0.003	0.000	0.000	0.018	0.019	0.025
K	0.000	0.000	0.000	0.000	0.000	0.000	0.000	0.000
Cr	0.001	0.000	0.002	0.005	0.007	0.005	0.010	0.022
Total	2.988	3.001	3.989	3.998	4.021	3.983	3.997	4.037
Mg/Mg+Fe	0.764	0.787	0.773	0.799	0.799	0.852	0.872	0.805
Ca Ca*	-	-	0.027	0.018	0.028	0.463	0.451	0.422
Mg Na*	-	-	0.752	0.785	0.776	0.458	0.479	0.466
Fe K*	-	-	0.221	0.197	0.195	0.079	0.070	0.113

Hb: Olivine-pyroxene hornblendite

No.Ox.: Number of oxygens in structural formula

Ca Ca*: Ca/Ca+Mg+Fe for orthopyroxene and clinopyroxene

Mg Na*: Mg/Ca+Mg+Fe for orthopyroxene and clinopyroxene

Fe K*: Fe/Ca+Mg+Fe for orthopyroxene and clinopyroxene

Table 3-12. (continued)

Mineral	Amphibole				Biotite	Feldspars	
	Sample	11309	40206	41803	51508	11309	11309
Rock Type	Hb	Hb	Hb	HbGb	Hb	Hb	Hb
SiO ₂ (wt%)	45.20	44.31	41.81	47.73	39.69	57.98	62.79
TiO ₂	1.08	2.16	1.20	0.89	3.91	0.00	0.07
Al ₂ O ₃	11.61	11.82	13.90	7.91	15.69	25.70	18.01
FeO	7.55	8.09	9.90	10.25	11.31	0.02	0.04
MnO	0.07	0.00	0.10	0.18	0.00	0.00	0.00
MgO	16.17	15.95	14.53	15.58	16.93	0.01	0.01
CaO	12.15	12.33	12.14	12.49	0.00	8.19	0.02
Na ₂ O	1.96	2.02	2.24	1.01	0.10	6.27	1.34
K ₂ O	0.71	0.89	1.29	0.58	6.90	0.08	12.05
Cr ₂ O ₃	0.17	0.09	0.40	0.15	0.14	0.00	0.00
Total	96.67	97.66	97.51	96.77	94.94	98.25	94.33
Formular Units							
No. Ox.	23	23	23	23	22	32	32
Si	6.555	6.403	6.145	6.964	5.719	10.521	12.061
Al ^{iv}	1.445	1.597	1.855	1.036	2.281	0.000	0.000
Al ^{vi}	0.540	0.417	0.553	0.324	0.384	5.498	4.078
Ti	0.118	0.235	0.133	0.098	0.424	0.000	0.010
Fe	0.916	0.978	1.217	1.251	1.363	0.003	0.006
Mn	0.009	0.000	0.012	0.022	0.000	0.000	0.000
Mg	3.495	3.435	3.182	3.388	3.636	0.003	0.003
Ca	1.888	1.909	1.912	1.953	0.000	1.592	0.004
Na	0.551	0.566	0.638	0.286	0.028	2.206	0.499
K	0.131	0.164	0.242	0.108	1.268	0.019	2.953
Cr	0.019	0.010	0.046	0.017	0.047	0.000	0.000
Total	15.666	15.715	15.936	15.446	15.149	19.842	19.615
Mg/Mg+Fe	0.792	0.778	0.723	0.730	0.727	0.471	0.308
Ca Ca*	0.300	0.302	0.303	0.296	-	0.417	0.001
Mg Na*	0.555	0.543	0.504	0.514	-	0.578	0.144
Fe K*	0.145	0.155	0.193	0.190	-	0.005	0.854

Hb: Olivine-pyroxene hornblende, Hb-Gb: Hornblende mela-gabbro

No.Ox.: Number of oxygens in structural formula

Ca Ca*: Ca/Ca+Mg+Fe for amphibole and Ca/Ca+Na+K for feldspar

Mg Na*: Mg/Ca+Mg+Fe for amphibole and Na/Ca+Na+K for feldspar

Fe K*: Fe/Ca+Mg+Fe for amphibole and K/Ca+Na+K for feldspar

0.062 (cation number based on 6 oxygens). Other minor elements, Al, Mn, Cr, and Ti, also show some variation.

Clinopyroxene

Clinopyroxene in the hornblendite is homogeneous within samples in terms of $Mg/(Mg + Fe)$ (Table A8-1). Clinopyroxene $Mg/(Mg + Fe)$ in the hornblende mela-gabbro is slightly lower than that in the hornblendite.

Two-pyroxene geothermometry

The two-pyroxene geothermometer of Wood and Banno (1973) and Wells (1977) has been employed to obtain the equilibrium temperatures of pyroxenes in the hornblendite. Estimated temperatures (Table 3-13) are in the range 860-1060°C, somewhat lower than the magmatic crystallization temperature (1175°C and 1146°C) postulated for the Sally Malay mafic-ultramafic suite, exposed about 20km north of the Sally Downs Bore area, but similar to or higher than the metamorphic temperature (874°C) of the mafic granulites (Thornett, 1981). Since the hornblendite was emplaced after the peak of metamorphism, the estimated temperatures could imply subsolidus equilibration temperatures during cooling of the hornblendite. The metamorphic temperature should be lower in the Sally Downs Bore area than in the Sally Malay prospect area as the metamorphic grade increases from south to the north (Dow and Gemuts, 1969).

C. Amphibole

Amphiboles in the hornblendite are edenitic hornblende, ferroan pargasitic hornblende, pargasitic hornblende, or ferroan pargasite according to Leak's (1968) classification. However, in the hornblende mela-gabbro, they are magnesio hornblende. Amphibole $Mg/(Mg + Fe)$

Table 3-13. Two-pyroxene geothermometry for the hornblendite

Sample	T1(°C)	T2(°C)	T(°C)
	Wood and Banno (1973)	Wells(1977)	Average
11309	891	858	876
40206	959	918	939
41802	1055	1045	1050
Mafic granulite*1	846	902	874
Picrite in Sally Malay*1	1166	1184	1175
Peridotite in Sally Malay*1	1130	1162	1146

Temperature estimation using the equations by Wood and Banno (1973) and Wells (1977)

*1: Temperatures from Thornett (1981) on the mafic-ultramafic rocks from the Sally Malay area north of the Sally Downs Bore in the East Kimberley

in the hornblendite ranges from 0.711 to 0.802 (Table A8-1), which is slightly lower than the olivine and orthopyroxene values.

D. Biotite

Only hornblendite contains biotite as an accessory mineral. $Mg/(Mg + Fe)$ is similar to that in other ferromagnesian minerals. Biotites have rather high TiO_2 contents (3.3 to 4.2 wt.%), except biotites in sample 41803 (Table A8-1).

E. Feldspars

Mol An content of plagioclase in the hornblendite ranges from 35.5 to 55.5. Weak normal compositional zoning is found in tiny subhedral grain fringed by thin K-feldspar (about Or 85), suggesting enrichment of Na and K within the trapped interstitial liquid.

The plagioclase in the hornblende mela-gabbro has a similar composition.

3.10.3. Geochemistry

Major and trace element data for the hornblendite and mela-gabbro are presented in Table 3-14.

A. Major elements

All analyzed samples of the hornblendite and mela-gabbro have distinctly low Al_2O_3 contents, ranging from 5.7 to 9.1%. The low Al_2O_3 concentrations correlate with the scarcity of plagioclase, especially in the hornblendite. Because of the low Al_2O_3 contents, CaO/Al_2O_3 ratios are higher than 1.6. MgO contents in the hornblendite and olivine-orthopyroxene mela-gabbro are high, ranging from 17.3 to 20.8%. This may imply a cumulate origin for olivine and/or orthopyroxene.

Table 3-14. Chemical compositions of mela-gabbro and hornblendite

Sample	11309	40206	41803	51508	83101
Rock	Hb	Hb	Hb	HbGb	OIGb
Major Elements (wt%)					
SiO ₂	48.15	48.70	47.69	50.94	49.74
Al ₂ O ₃	5.70	4.72	6.76	9.12	7.43
Fe ₂ O ₃ *	10.22	9.85	11.75	7.76	10.37
MnO	0.16	0.16	0.19	0.16	0.17
MgO	17.92	20.82	19.03	12.19	17.28
CaO	14.88	12.48	11.87	14.69	12.91
Na ₂ O	0.99	0.84	1.01	1.09	1.13
K ₂ O	0.33	0.23	0.35	0.52	0.13
TiO ₂	0.73	0.64	0.41	0.62	0.40
P ₂ O ₅	0.14	0.02	0.07	0.23	0.05
LOI	0.66	1.10	0.45	1.70	0.29
Total	99.88	99.56	99.58	99.02	99.90
Trace Elements (ppm)					
Ba	158	75	186	493	82.3
Rb	7.1	5.2	9.2	6.4	3.4
Sr	230	125	216	630	208
Zr	65	30.9	38.8	84	19.8
Nb	4.3	1.7	1.9	4.9	1.2
Y	12.2	12.7	8.3	11.9	9.6
Ce	52	28	25	78	14
Nd	38	24	22	34	18
Sc	63	51	51	60	39.5
V	190	161	173	212	147
Cr	1876	1635	2276	995	1707
Ni	468	422	700	231	887
Cu	117	49	183	63	92
Zn	67	72	76	55	71

Hb: olivine-pyroxene hornblendite

HbGb: hornblende mela-gabbro

OIGb: olivine-orthopyroxene mela-gabbro

Fe₂O₃* : Total Fe as Fe₂O₃

LOI : Loss on ignition

However, all the hornblendite and mela-gabbro bodies, viz. xenolithic bodies in the Sally Downs Tonalite and two small stock like bodies, are rather small, up to 200m in diameter, and do not show any compositional layering. Therefore, those are not a part of the layered mafic complex. If the olivine and/or orthopyroxene in the hornblendite are cumulate, the stocks may represent a conduit to a layered complex which has already been eroded away. In this case, the whole rock chemistries indicate a mixed composition representing liquid plus cumulates.

A least squares mixing model (Wright and Doherty, 1970), deriving the composition of the hornblendite from the bulk composition of the McIntosh gabbro estimated by Hamlyn (1977) and cumulative olivine, orthopyroxene, and clinopyroxene, is presented in Table 3-15. The result suggests large amounts of cumulate consisting of clinopyroxene, orthopyroxene, and olivine; about 85% of whole rock are required to produce the chemical composition of the hornblendite. Calculated quantities of olivine and orthopyroxene are in good agreement with the modal composition of sample 40206, suggesting that most of the olivine and orthopyroxene in the sample are cumulate minerals. However the amount of calculated clinopyroxene is far in excess of the modal figure. Hence extensive reaction between clinopyroxene and melt is assumed to have formed hornblende according to this model.

On the other hand, if the hornblendite is assumed to represent a liquid composition, it is noteworthy that the major element values resemble those of basaltic komatiite (Nesbitt et al., 1979). In this case, hornblende mela-gabbro 51508 could have been obtained from the residual melt after fractionation of olivine, orthopyroxene, and clinopyroxene from the melt (Table 3-15B).

B. Trace elements

Table 3-15. Petrogenetic models of mela-gabbro and hornblendite by least squares mixing of major elements

A. Derivation of chemical composition of hornblendite (40206) from mafic liquid similar to the bulk composition of the McIntosh sill (Hamlyn, 1975) with addition of mafic cumulates consisting olivine, orthopyroxene, and clinopyroxene.

	Ol	Opx	Cpx	McIntosh	40206	Calc.	Residual
Fraction	0.1445	0.1855	0.4839	0.1588			
SiO ₂	39.10	54.58	52.40	47.55	48.70	48.68	-0.0181
TiO ₂	0.09	0.08	0.30	0.51	0.64	0.25	-0.3860
Al ₂ O ₃	0.00	2.55	2.87	18.80	4.72	4.85	0.1270
FeO*	19.89	12.82	4.30	8.50	8.87	8.68	-0.1877
MnO	0.27	0.06	0.15	0.12	0.16	0.14	-0.0182
MgO	41.29	28.65	16.46	10.60	20.82	20.93	0.1086
CaO	0.01	0.92	21.55	11.79	12.48	12.47	-0.0075
Na ₂ O	0.00	0.00	0.26	1.86	0.84	0.42	-0.4189
K ₂ O	0.01	0.00	0.02	0.06	0.23	0.02	-0.2094

Sum of (Residual)²=0.4321

B. Derivation of hornblende mela-gabbro (51508) by fractional crystallization of olivine orthopyroxene and clinopyroxene from hornblendite (40206)

	51508	Ol	Opx	Cpx	40206	Calc.	Residual
Fraction	0.3803	0.1994	0.0899	0.3176			
SiO ₂	50.94	39.10	54.58	52.40	48.70	48.72	0.0190
TiO ₂	0.62	0.09	0.08	0.30	0.64	0.36	-0.2838
Al ₂ O ₃	9.12	0.00	2.55	2.87	4.72	4.61	-0.1107
FeO*	6.98	19.89	12.82	4.30	8.87	9.17	0.2691
MnO	0.16	0.27	0.06	0.15	0.16	0.17	0.0077
MgO	12.19	41.29	28.65	16.46	20.82	20.67	-0.1470
CaO	14.69	0.01	0.92	21.55	12.48	12.52	0.0353
Na ₂ O	1.09	0.00	0.00	0.26	0.84	0.50	-0.3429
K ₂ O	0.52	0.01	0.00	0.02	0.23	0.21	-0.0239

Sum of (Residual)²=0.3067

Ol: Olivine Opx: Orthopyroxene Cpx: Clinopyroxene.

Chemical composition of those minerals are taken from results of electron probe analysis of minerals from sample 40206 (Table A8-1).

Least squares mixing methods after Wright and Doherty (1970).

FeO*: Total Fe as FeO

Sum of (Residual)²: sum of square of residuals

Ba in the hornblendite ranges from 75 to 186ppm, but the hornblende mela-gabbro contains about 500ppm Ba (Table 3-14). Part of this discrepancy can be accounted for by residual Ba enrichment in the hornblende mela-gabbro due to fractionation, according to the second model described above. If the hornblende mela-gabbro is a product by fractionation of the hornblendite (Table 3-15B), the fractionation of olivine and pyroxenes, assuming Ba mineral-melt distribution coefficients of the minerals equal to zero, increases the concentration of Ba in the mela-gabbro 2.5 times. This magnitude of Ba enrichment is in good agreement with the observed results, indicating validity of the model. Similar enrichment of Sr in the hornblende gabbro precludes fractionation of plagioclase from the liquid.

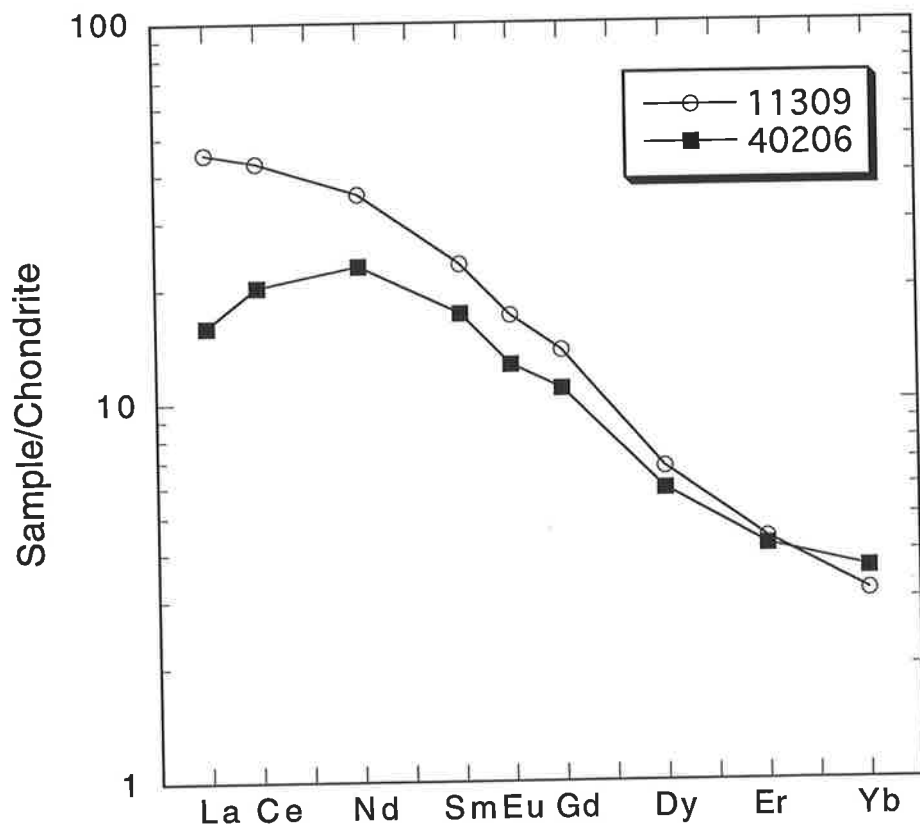
In the case of the cumulate model for hornblendite, the original concentrations of the elements in the liquid must have been high, as a simple dilution effect by the cumulate minerals reduced the concentrations.

Ni and Cr contents in the rocks range from 231 to 887ppm, and 995 to 2276ppm, respectively (Table 3-14). The high contents of these elements are compatible to both models, cumulate origin and high magnesian liquid origin.

Fig. 3-36 illustrates chondrite-normalized REE patterns of two samples from the hornblendite. Both samples have a fractionated pattern depleted in HREE with very small negative Eu anomaly. Although general LREE enrichments are observed, one of the samples (40206) shows slight depletion of La and Ce compared to Nd. The difference between the two patterns in this respect (Fig. 3-36) could be explained by fractionation of pyroxene and/or amphibole, or by more abundant cumulate pyroxene in sample 40206 than the other.

Fig. 3-36. Chondrite normalized REE plot of hornblendites

Samples, 11309 and 40206, are olivine-pyroxene hornblendites.



Because of the strong possibility that the major element characteristics of the gabbros are modified as the result of crystal accumulation, most likely of olivine and pyroxenes, absolute concentrations of the elements can not be used as primary liquid values to model petrogenesis. However, ratios of elements incompatible with the possibly cumulate minerals may be used to indicate characteristics of a primary liquid, since the ratios are not a function of the degree of mineral accumulation.

High Y/Nb ratio ranging from 2.43 to 8.00 obviously excludes an alkalic primary liquid, as alkalic rocks have a greater concentration of Nb relative to Zr or Y (Pearce and Cann, 1973). However large variation in the Ti/Zr ratio from 48 to 147 provides no clear indication of one subalkalic magma type rather than another.

CHAPTER 4. PETROLOGY (PART 2): PETROLOGY OF THE SALLY DOWNS TONALITE AND THE RELATED ROCKS

4.1. Introduction

This chapter mainly describes the petrology of the Sally Downs Tonalite which is the most voluminous rock unit in the Sally Downs Bore area. One of the objectives in studying this pluton is to facilitate the presentation of basic petrographic and geochemical data as background to a discussion of the petrogenesis of granitoids of the Mabel Downs Suite, the Sally Downs Tonalite being a member of the suite.

The Sally Downs Tonalite pluton shows a large compositional variation. Such a large compositional variation is commonly found in zoned granitoid plutons, which have been extensively studied in many areas (e.g. Bateman and Chappell, 1979; Stephens and Halliday, 1979; Perfit et al., 1980a; Tindle and Pearce, 1981). Most of the studies indicate that fractional crystallization is a likely source of the compositional variation. Hence, in order to investigate possible compositional zoning within the Sally Downs Tonalite pluton and its mechanism, a systematic sampling has been conducted.

The sampling of the tonalite for geochemical study was carried out in three stages. In the first stage of the sampling, 18 specimens of the tonalite (Table A4-6-B) have been collected along or near the track connecting Sally Downs Bore and Dougalls Bore (Fig. 4-1). Initial examination of the samples was utilized to make a further areal systematic sampling plan. In this second stage, a total of 118 samples (Table A4-6-A) - one sample from each intersection of a 600m grid over the pluton, with exception of 5 grids where two samples have been collected - have been obtained (Fig. 4-1). The samples have been used to investigate areal compositional variation and its pattern. Another 10 samples (Table A4-6-

Fig. 4-1. Sample locality map of Sally Downs Tonalite

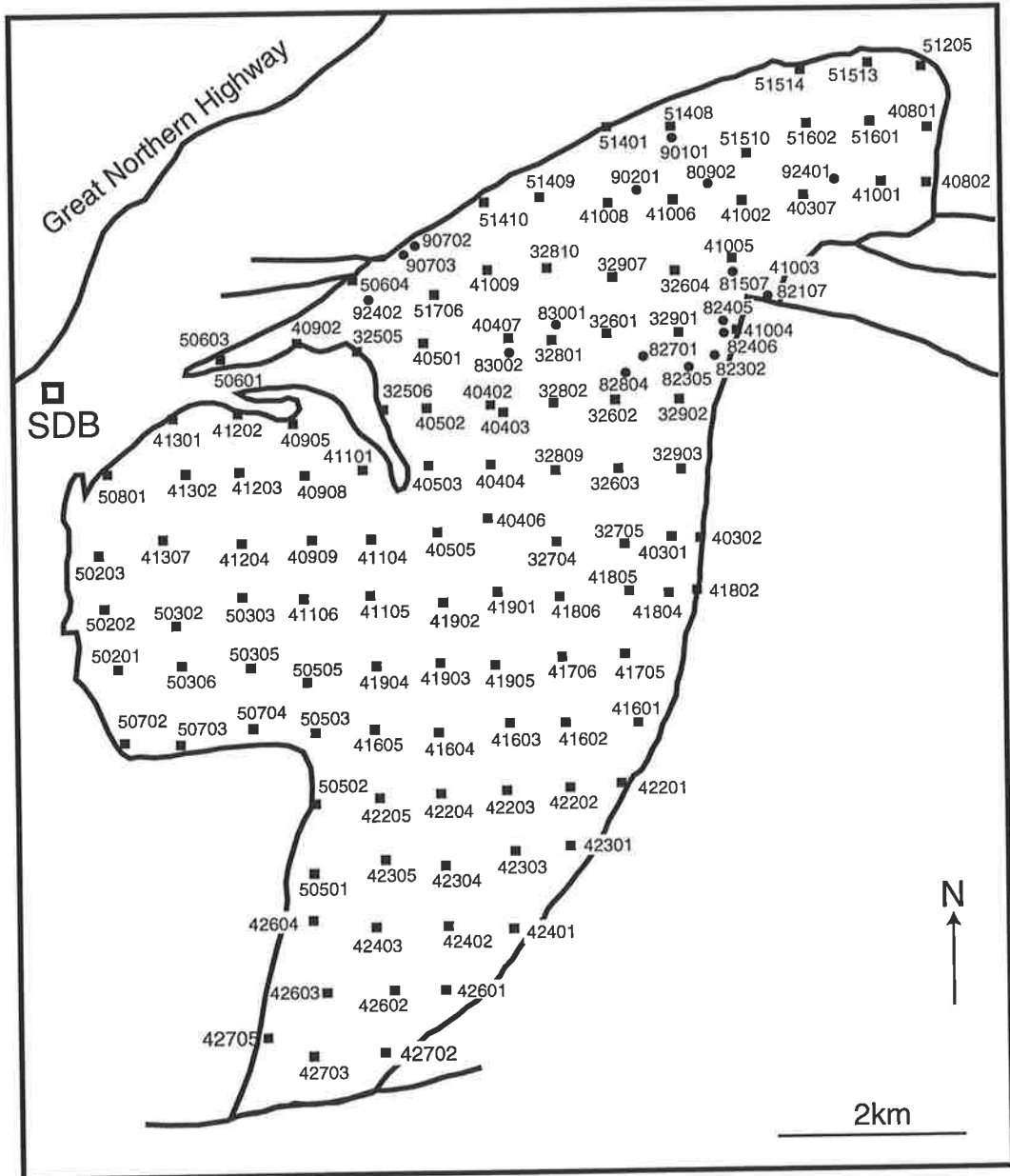
Solid circles: samples for preliminary study

Solid squares: localities for systematic sampling

Location of sample 51706 is also location of samples 51701 to 51715.

Location of sample 41001A is also location of mafic microgranular enclave sample 41001B.

SDB: Sally Downs Bore



C) have been collected in a relatively small area for examination of small scale compositional variability and for geochronological work. A total of 146 samples is geochemically examined.

Petrological descriptions of the mafic microgranular enclaves and syn-plutonic basic dyke in the Sally Downs Tonalite are included in this chapter to investigate their petrogenetical relationships to the host tonalite. In a final section of this chapter, petrography and geochemistry of tonalites from the Mabell Hill and the main body of the Mabel Downs Granitoids Suite are briefly described.

4.2. Petrography and Mineral Chemistry of the Sally Downs

Tonalite

4.2.1. Petrography

The Sally Downs Tonalite typically has a hypidiomorphic-granular texture and is coarse grained (Fig. 4-2A, B, C, and D). Slight recrystallization of quartz is found in some samples of the tonalite. The tonalite is primarily composed of plagioclase, quartz, biotite, and hornblende. Hornblende is not present in acidic varieties of the tonalite.

Modal compositions of the tonalite are presented in Table 4-1. Those are plotted on Qz-Af-Pl diagram of Fig. 3-7. A chemical mode (in weight percents) calculated from whole rock major element chemistry and actual chemical compositions of minerals in the rock using least square mixing program (Wright and Doherty, 1970) are shown in Table 4-2. The estimated chemical mode shows fairly good agreement with the modal composition which is converted from volume percents to weight percents in Table 4-2.

Plagioclase is generally subhedral and zoned; occasionally, large rectangular phenocrysts of plagioclase, up to 6mm in length, are found. Quartz is medium to coarse grained and anhedral. It has undulose

Table 4-1. Modal compositions of the Sally Downs Tonalite

Sample	42402	51706	50801	51702
Unit	SDT	SDT	SDT	MME
Quartz (%)	16.10	17.10	32.32	10.25
Plagioclase	51.21	61.30	40.77	55.42
Biotite	12.71	11.40	19.47	11.58
Hornblende	12.80	6.50	0.00	18.50
Epidote	5.04	2.90	5.97	2.50
Apatite	0.48	0.30	1.29	0.50
Opaque Minerals	1.26	0.40	0.18	1.08
Zircon	0.29	0.10	0.00	0.17
Total	99.89	100.00	100.00	100.00

SDT: Sally Downs Tonalite

MME: Mafic microgranular enclave in the Sally Downs Tonalite

Table 4-2. Chemical mode of sample 51706 from the Sally Downs Tonalite

Minerals	Mode(wt%)*1	C.M.(wt%)*2
Quartz	16.4	19.72
Plagioclase	59.3	54.49
Biotite	12	12.76
Hornblende	7.5	9.56
Epidote	3.6	2.16
Apatite	0.3	---
Zircon	0.2	0.03
Oxide	0.8	1.15
Allanite	0.01	---

*1: Modal composition in weight percent is calculated from volumetrical mode adjusting specific gravity of minerals.

*2: C.M.: Chemical mode

Chemical mode is calculated from the whole rock major element composition and chemical compositions of minerals obtained by electron probe, using a least squares mixing program (Wright and Doherty, 1970). Chemical mode of zircon is calculated from the zirconium content of the rock.

Fig. 4-2. Photomicrographs of the Sally Downs Tonalite, mafic microgranular enclaves, and syn-plutonic basic dyke

A. Sally Downs Tonalite

Sample: 51706. Ho: hornblende, Bi: biotite, Epi: epidote

Plane polarized light. Scale bar is 5 mm.

B. Same as A, but under crossed polarized light.

Pl: plagioclase, Qz: quartz

C. Sally Downs Tonalite

Sample: 32903A. Ho: hornblende, Bi: biotite, Epi: epidote

Plane polarized light. Scale bar is 5 mm.

D. Same as C, but under crossed polarized light.

Pl: plagioclase, Qz: quartz

E. Mafic microgranular enclave in the Sally Downs Tonalite

Sample: 51702. Ho: hornblende, Bi: biotite

Plane polarized light. Scale bar is 5 mm.

F. Same as E, but under crossed polarized light.

Pl: plagioclase, Qz: quartz

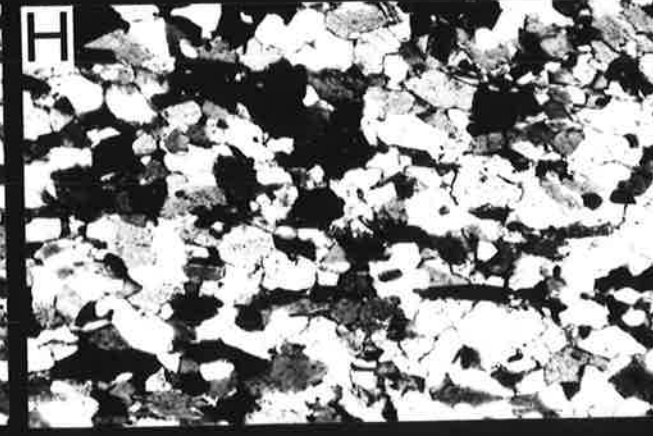
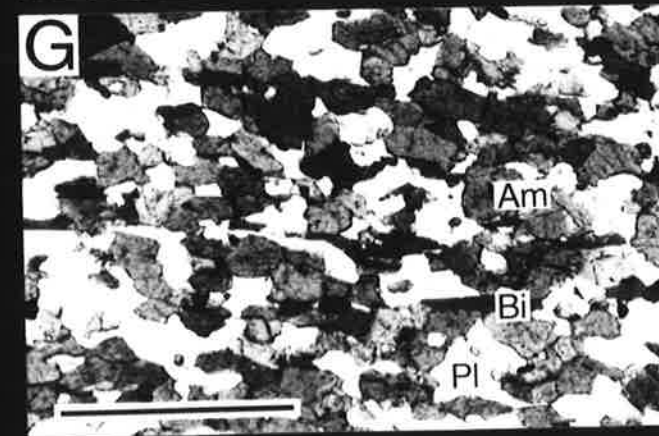
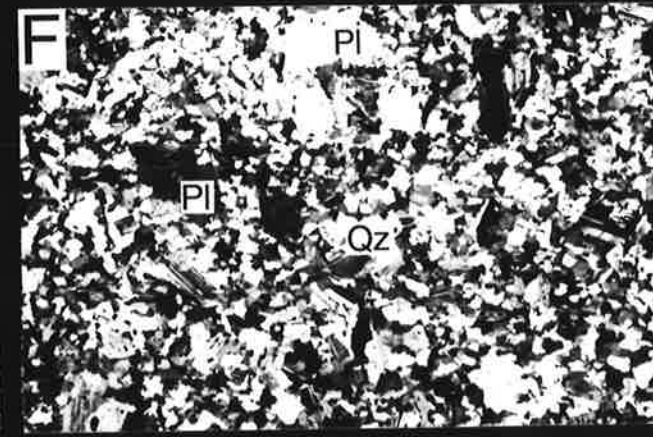
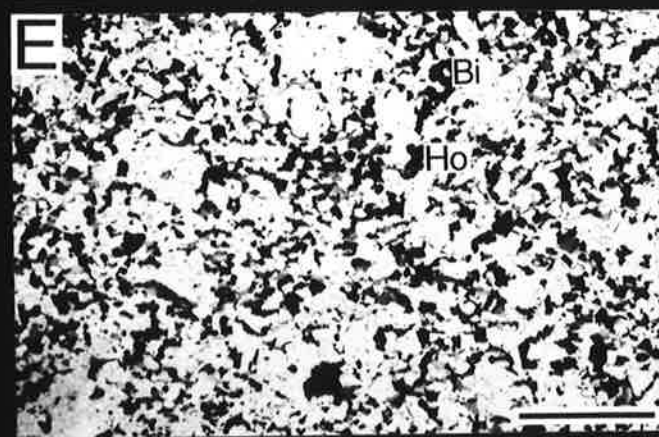
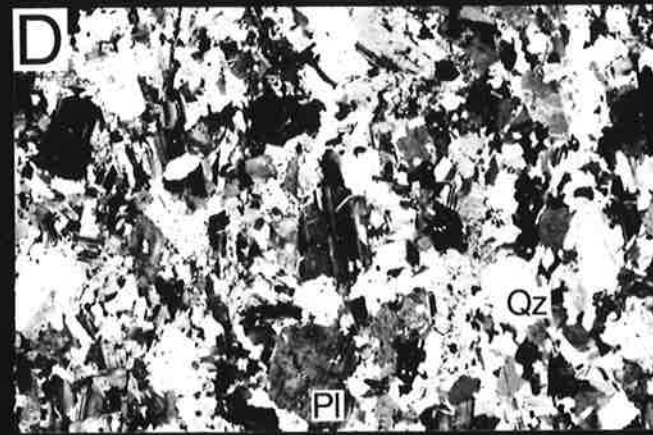
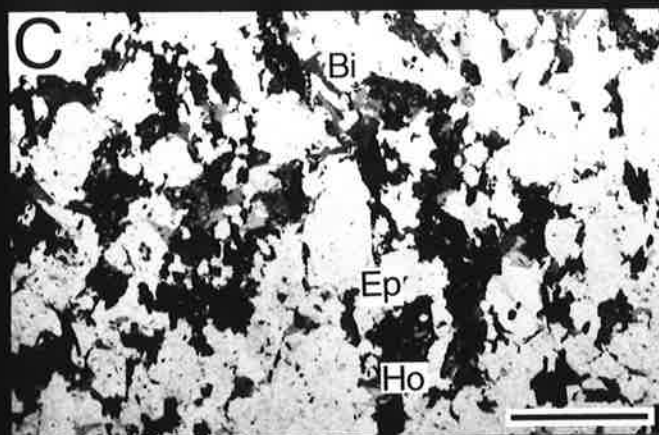
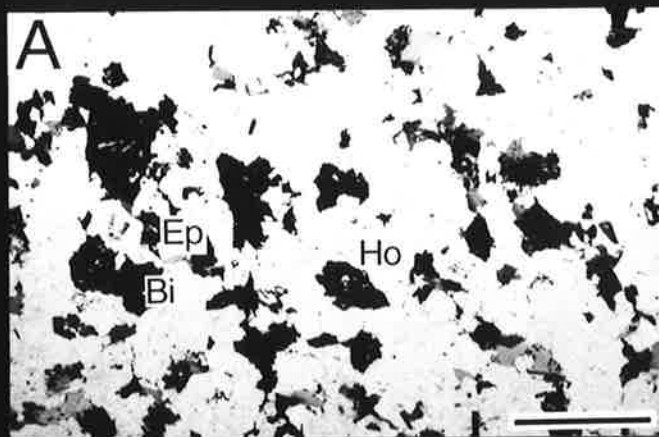
G. Syn-plutonic basic dyke from the Sally Downs pluton

Sample: 51504B. Am: amphibole, Bi: biotite, Pl: plagioclase

Biotite shows preferred orientation.

Plane polarized light. Scale bar is 1 mm.

H. Same as G, but under crossed polarized light.



extinction. Biotite (α = pale yellow, β = γ = brown) is subhedral and medium grained, average 2mm in length. Hornblende (α = pale yellow, β = γ = blue green) is medium to coarse grained and euhedral to subhedral. Accessory minerals are epidote, sphene, apatite, zircon, allanite, and opaque minerals. Textural relationships indicate hornblende and some plagioclase crystals crystallized early in the crystallization sequence.

4.2.2. Mineral Chemistry

Representative mineral compositions are presented in Table 4-3. Complete mineral composition data are listed in Table A8-1 (Appendix 8).

A. Hornblende

Most of the hornblendes in the Sally Downs Tonalite are magnesio-hornblende as classified by Leake (1968). Mg/Mg + Fe ratios of the hornblendes range from 0.548 to 0.481 (Fig. 4-3A). Hornblende with higher Mg/Mg + Fe ratios are found in low SiO₂ (56.2%) tonalite, suggesting compositional dependence of the hornblende chemistry on the whole rock chemistry.

B. Biotite

Mg/Mg + Fe ratios of biotite in the tonalite are higher than those of hornblende in the tonalite, ranging from 0.627 to 0.505 (Fig. 4-3B). TiO₂ contents of biotites increase from basic tonalite to acidic tonalite, varying from 1.55 to 2.36 weight %. However, the TiO₂ contents are significantly lower than those of the Dougalls Granitoid Suite biotites.

C. Plagioclase

Table 4-3. Representative chemical compositions of hornblende and biotite from the Sally Downs Tonalite, Mafic microgranular enclaves, and Syn-plutonic basic dyke

Unite	Sally Downs Tonalite					Mafic Micro-granular Enclaves		Syn-plutonic Basic Dyke	
	Hornblende		Biot.			Hornb.	Biot.	Hornb.	Biot.
Sample	32903A	51706	32903A	51706	50801	51702	51702	51501	51501
SiO ₂ (wt%)	44.24	43.59	37.40	36.23	36.01	44.76	37.11	44.49	38.62
TiO ₂	0.63	1.13	1.55	2.07	2.26	0.93	1.97	0.77	1.95
Al ₂ O ₃	10.79	10.43	16.75	16.58	16.69	10.61	16.82	10.43	16.70
FeO*	16.05	18.27	14.99	17.90	20.31	17.91	17.99	14.73	15.69
MnO	0.21	0.25	0.05	0.21	0.22	0.35	0.13	0.20	0.13
MgO	10.93	10.40	14.14	12.78	10.61	10.38	12.71	11.77	14.17
CaO	11.43	11.64	0.00	0.00	0.00	11.68	0.00	12.17	0.00
Na ₂ O	1.44	1.43	0.22	0.16	0.17	1.33	0.18	1.25	0.13
K ₂ O	0.69	0.82	8.98	9.48	9.35	0.81	9.33	0.49	6.96
Cr ₂ O ₃	0.07	0.10	0.11	0.04	0.05	0.01	0.00	0.23	0.10
Total	96.48	98.06	94.24	95.45	95.67	98.77	96.24	96.53	94.45
Structural formular									
No.Ox.	23	23	22	22	22	23	22	23	22
Si	6.669	6.561	5.615	5.484	5.497	6.652	5.548	6.668	5.712
Al ^{iv}	1.331	1.439	2.385	2.516	2.503	1.348	2.452	1.332	2.288
Al ^{vi}	0.587	0.411	0.580	0.443	0.501	0.511	0.513	0.511	0.624
Ti	0.071	0.128	0.175	0.236	0.259	0.104	0.222	0.087	0.217
Fe	2.024	2.300	1.882	2.266	2.593	2.226	2.249	1.846	1.941
Mn	0.027	0.032	0.006	0.027	0.028	0.044	0.016	0.025	0.016
Mg	2.456	2.333	3.164	2.883	2.414	2.299	2.832	2.629	3.124
Ca	1.846	1.877	0.000	0.000	0.000	1.860	0.000	1.955	0.000
Na	0.421	0.417	0.079	0.047	0.050	0.383	0.052	0.363	0.037
K	0.133	0.157	1.720	1.831	1.821	0.154	1.780	0.094	1.313
Cr	0.008	0.012	0.013	0.005	0.006	0.001	0.000	0.027	0.012
Total	15.573	15.668	15.620	15.737	15.674	15.582	15.664	15.538	15.284
Mg/Mg+Fe	0.548	0.504	0.627	0.560	0.482	0.508	0.557	0.587	0.617
Ca*	0.292	0.288	-----	-----	-----	0.291	-----	0.304	-----
Mg*	0.388	0.358	-----	-----	-----	0.360	-----	0.409	-----
Fe*	0.320	0.353	-----	-----	-----	0.349	-----	0.289	-----

Biot.: Biotite, Hornb.: Hornblende

FeO*: Total Fe as FeO

No.Ox.: Number of oxygens in structural formular

Ca*: Ca/Ca+Mg+Fe, Mg*: Mg/Ca+Mg+Fe, Fe*: Fe/Ca+Mg+Fe

Fig. 4-3. Compositions of hornblende, biotite, and plagioclase from the Sally Downs Tonalite and from mafic microgranular enclaves

Numbered samples are the Sally Downs Tonalite

MME: mafic microgranular enclaves

A. Hornblende Mg/Fe+Mn+Mg-Si

Mg/Fe+Mn+Mg: Fe, Mn, and Mg values from the structural formula of 23 oxygens.

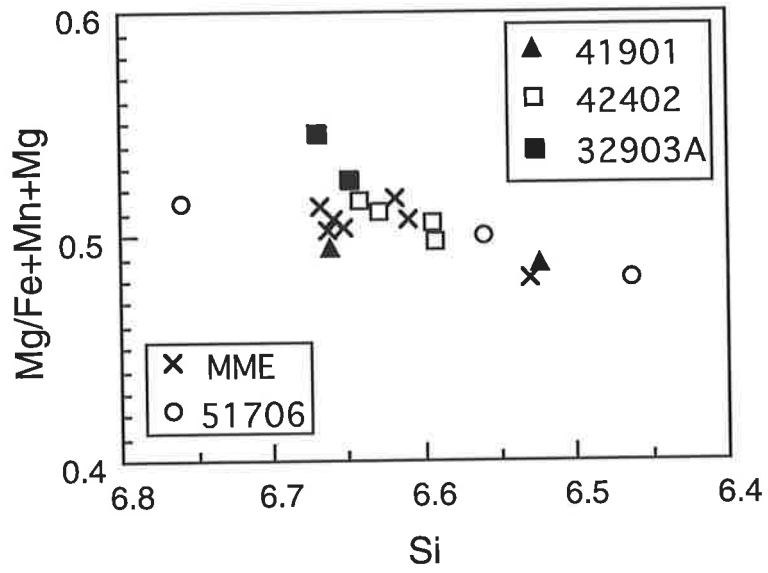
B. Biotite Mg/Fe+Mn+Mg-Si

Mg/Fe+Mn+Mg: Fe, Mn, and Mg values from the structural formula of 22 oxygens.

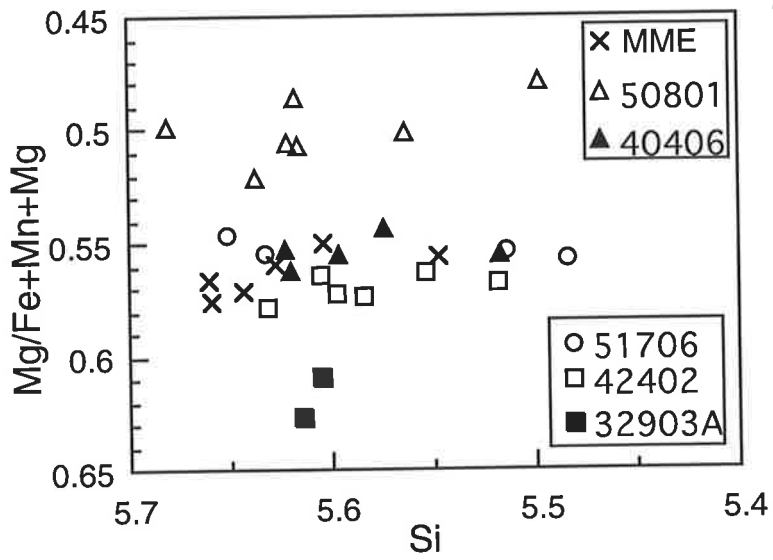
C. Plagioclase An-whole rock SiO₂

Whole rock SiO₂ values of tonalite samples are found in Table A4-6.

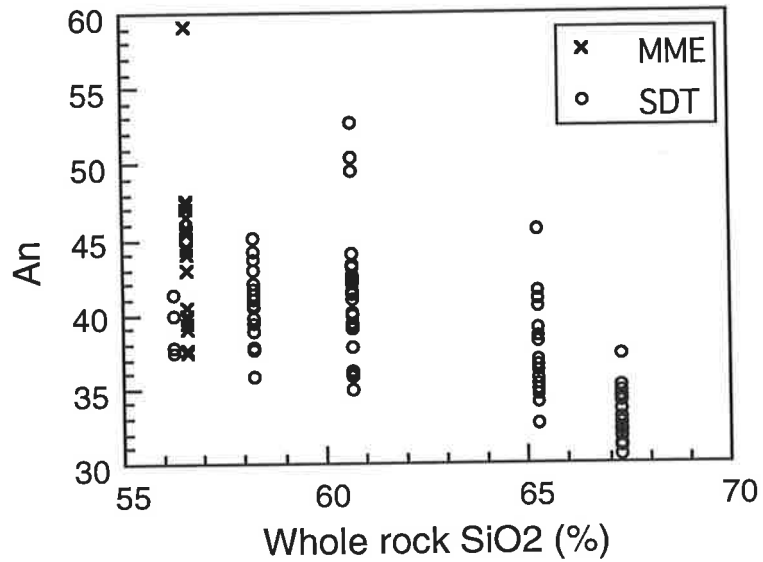
A. Hornblende



B. Biotite



C. Plagioclase



An contents of plagioclase in the Sally Downs Tonalite are presented in Table A8-1 and are summarized in Fig. 4-3C.

Considerable compositional variation is found within samples; for example, compositions of plagioclase in sample 51706 vary from An 35 to 53. Plagioclase of high An contents is generally found in a core of large zoned plagioclase crystal. Fig. 4-3 also illustrates compositional variations between samples. Consistently low Or content (typically less than 0.4) in the plagioclase reflects the low potassium abundances in the tonalite (Table A8-1).

D. Allanite

Very small amounts of allanite, generally less than 0.1% in the mode, are found in the Sally Downs Tonalite. Allanite is commonly metamict and is characterized by the presence of anastomosing cracks which radiate from it (Fig. 4-4A and B). Allanite grains are prismatic, up to 4mm in length, and may be surrounded by epidote.

Although allanite is an accessory mineral in the tonalite, it may have a significant role concerning rare earth element (REE) distribution in the tonalite, as it contains high levels of REE. Fourcade and Allegre (1981) have shown that most of the light REE in monzogranite from the Querigut complex (France) is accommodated in allanite, and pointed out the importance of allanite and other accessory minerals, such as sphene and zircon, governing trace element behavior in the granitoid petrogenesis. Similar conclusions are presented by Exley (1980), Henderson (1980), Miller and Mittlefehldt (1982), and Growmet and Silver (1983). Thus, electron microprobe analyses of the allanite from the Sally Downs Tonalite were performed to determine the REE contents. Chemical compositions of allanite from the Sally Downs Tonalite are

Fig. 4-4. Photomicrographs of allanite, epidote, and sphene in the Sally
Downs Tonalite

A. Allanite in the Sally Downs Tonalite

Sample: 51706. Al: allanite, Ho: hornblende, Epi: epidote

Radial cracks surround the allanite crystal.

Plane polarized light. Scale bar is 1 mm.

B. Same as A, but under crossed polarized light.

C. Allanite in the Sally Downs Tonalite

Sample: 51706. Al: allanite, Epi: epidote, Ho: hornblende, Bi: biotite

Pl: plagioclase

Typical euhedral allanite. Allanite has epidote rim.

Plane polarized light. Scale bar is 1 mm.

D. Same as C, but under crossed polarized light.

Central part of the allanite is metamictic.

E. Epidote in the Sally Downs Tonalite

Sample: 51706. Epi: epidote, Bi: biotite, Pl: plagioclase, Qz: quartz.

Plane polarized light. Scale bar is 1 mm.

F. Same as E, but under crossed polarized light.

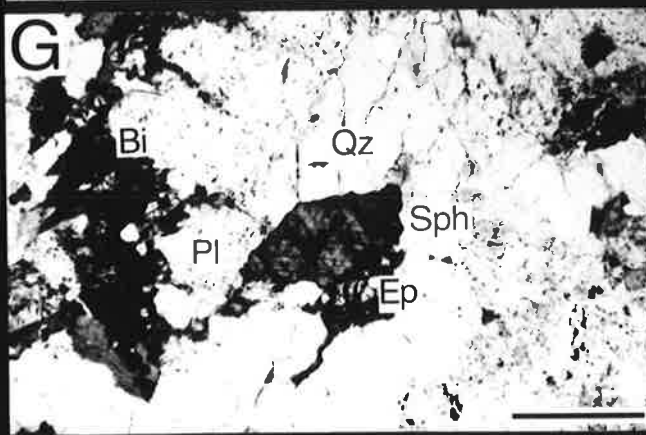
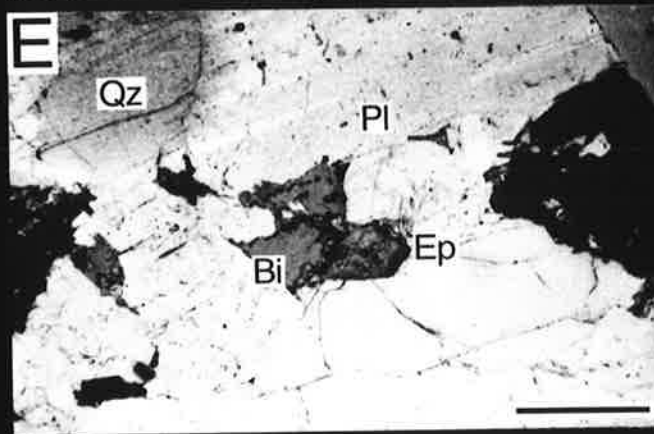
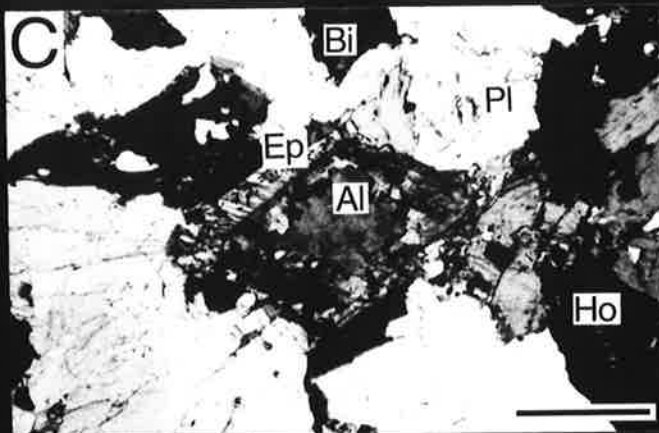
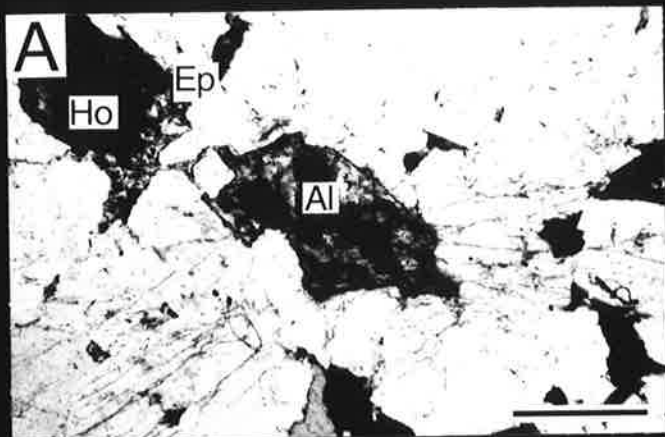
G. Sphene in the Sally Downs Tonalite

Sample: 50801. Sph: sphene, Bi: biotite, Ep: epidote, Pl: plagioclase,

Qz: quartz.

Plane polarized light. Scale bar is 1 mm.

H. Same as G, but under crossed polarized light.



presented in Table 4-4. Details of the analytical procedures are described in Appendix 7.

Table 4-4 shows the allanites to have a high light rare earth element (LREE) content. The levels are similar to those reported by Exley (1980), and Sawka et al. (1984).

Allanite with a low weight percent total (about 85%) is found in rim of grains with optically low refractive index, suggesting it is hydrated allanite. This has very low FeO and CaO. (Table 4-4)

Considerable compositional variations are observed within the grains, but no systematic rim to core variations in REE are found (Table 4-4). However, Sr and Th are consistently more enriched in the rim than in the core.

Fig. 4-5 illustrates the chondrite normalized REE pattern for representative analyses of allanite, all of them showing extensive LREE enrichment.

In addition to the allanite, sphene and epidote occur (Fig. 4-4C and D); those also are analyzed (Table 4-4 and Fig. 4-5). Sphene shows a curved chondrite normalized REE pattern with the maximum at Sm, and has a high concentration of HREE.

The significance of the high concentration of REE in these minerals is discussed in the whole rock geochemistry section (4.3.) and in the discussion of a crystallization model of the Sally Downs Tonalite (4.5.1), below.

4.3. Geochemistry of the Sally Downs Tonalite

Major and trace element data of samples from the Sally Downs Tonalite are presented in A4-6. An average chemical composition of the Sally Downs Tonalite derived from 146 analyses and chemical

Table 4-4. Chemical compositions of allanite, epidote, and sphene from the Sally Downs Tonalite

A. Sample 51706

Analysis	1	2	3	4	5	6	7	8
(wt%)	Allanite	Allanite			Allanite			Epidote
		Rim -----	Core		Rim -----	Core		
SiO ₂	32.06	37.84	45.37	31.20	38.30	32.05	31.87	37.58
TiO ₂	0.98	0.79	0.87	0.73	1.12	0.81	0.72	0.00
Al ₂ O ₃	12.34	13.58	16.26	15.13	13.50	16.16	16.03	22.62
FeO*	3.77	5.54	3.79	12.86	3.65	13.40	13.38	12.70
MnO	0.19	0.00	0.01	0.27	0.06	0.22	0.32	0.04
MgO	0.33	0.39	0.43	1.61	0.30	1.76	1.70	0.01
CaO	4.06	5.59	5.66	10.99	4.31	10.66	10.11	22.87
Na ₂ O	0.18	0.10	0.10	0.05	0.02	0.03	0.05	0.00
SrO	0.174	0.354	0.304	0.246	0.202	0.141	0.133	0.280
ThO	1.866	1.890	1.841	1.175	1.781	1.200	0.991	0.079
Y ₂ O ₃	0.023	0.014	0.016	0.052	0.017	0.016	0.014	0.006
La ₂ O ₃	2.360	4.037	2.720	3.000	6.674	6.953	6.925	0.007
Ce ₂ O ₃	22.735	10.312	6.669	6.911	12.112	11.068	11.418	0.036
Pr ₂ O ₃	0.591	0.836	0.534	0.673	1.069	0.792	0.862	0.000
Nd ₂ O ₃	1.646	2.612	1.911	2.072	2.864	2.088	2.302	0.014
Sm ₂ O ₃	0.145	0.168	0.159	0.169	0.139	0.085	0.097	0.000
Gd ₂ O ₃	0.066	0.070	0.071	0.065	0.081	0.020	0.062	0.002
Dy ₂ O ₃	0.012	0.014	0.006	0.019	0.009	0.027	0.007	0.000
Total	83.528	84.137	86.721	87.222	86.208	97.480	96.991	96.244

B. Sample 50801

Analysis	9	10	11	12	13	14	15	16	17
(wt%)	Allanite				Allanite				Sphene
	Rim -----	Core			Rim -----	Core			
SiO ₂	42.65	31.20	31.16	29.51	31.14	31.13	31.58	32.28	28.71
TiO ₂	3.16	1.18	1.14	1.11	0.88	1.04	0.67	0.62	37.06
Al ₂ O ₃	14.25	14.37	14.38	14.15	12.03	14.18	15.89	16.19	1.14
FeO*	7.44	13.96	13.91	14.30	4.68	13.89	13.27	13.67	1.08
MnO	0.28	0.43	0.41	0.33	0.07	0.36	0.38	0.34	0.10
MgO	0.48	1.82	1.78	1.94	0.33	1.66	1.30	1.29	1.01
CaO	4.06	9.92	9.88	10.02	6.63	9.88	11.47	11.50	27.08
Na ₂ O	0.22	0.07	0.04	0.07	0.01	0.04	0.04	0.04	0.00
SrO	0.268	0.137	0.133	0.126	0.447	0.120	0.137	0.150	0.090
ThO	2.687	0.981	1.054	0.899	2.288	1.139	0.850	1.166	0.000
Y ₂ O ₃	0.019	0.012	0.020	0.030	0.005	0.042	0.032	0.053	0.514
La ₂ O ₃	2.010	7.544	7.484	7.722	5.783	7.261	7.243	5.405	0.045
Ce ₂ O ₃	5.717	11.984	11.912	12.074	12.415	11.843	11.320	9.668	0.306
Pr ₂ O ₃	0.301	0.855	0.876	0.885	1.136	0.869	0.868	0.844	0.052
Nd ₂ O ₃	0.851	2.202	2.203	2.152	3.025	2.257	2.203	2.351	0.392
Sm ₂ O ₃	0.059	0.083	0.068	0.082	0.158	0.099	0.120	0.143	0.135
Gd ₂ O ₃	0.026	0.062	0.053	0.029	0.064	0.056	0.044	0.069	0.157
Dy ₂ O ₃	0.001	0.000	0.003	0.011	0.003	0.000	0.003	0.011	0.085
Total	84.479	96.810	96.506	95.440	81.094	95.866	97.420	95.790	96.956

FeO*: Total Fe as FeO

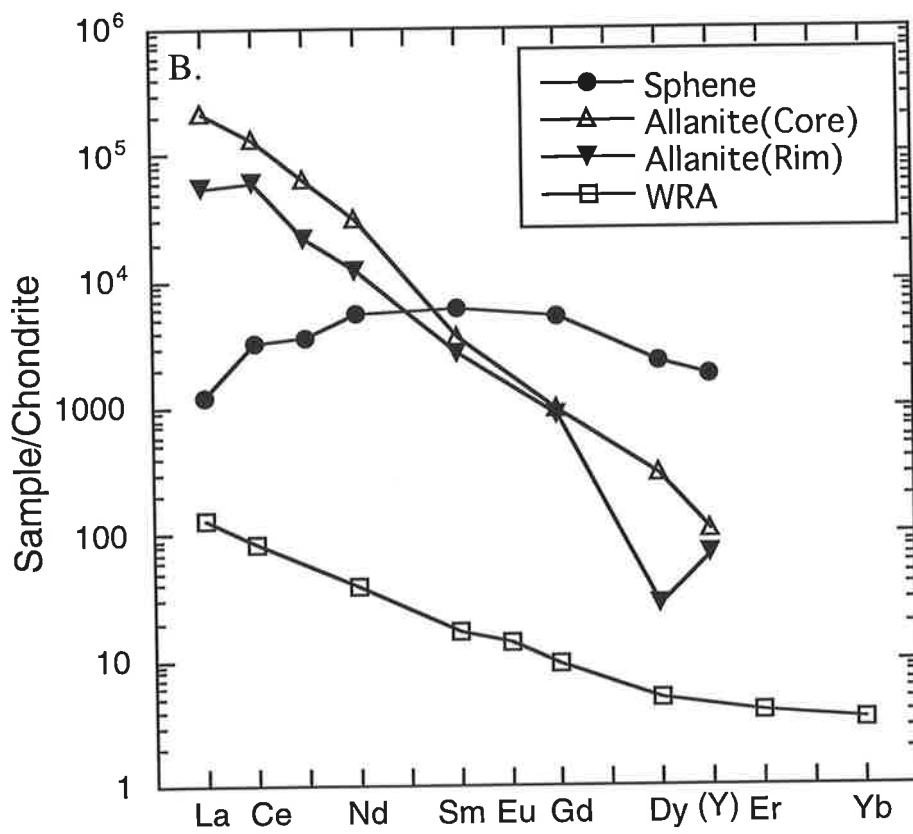
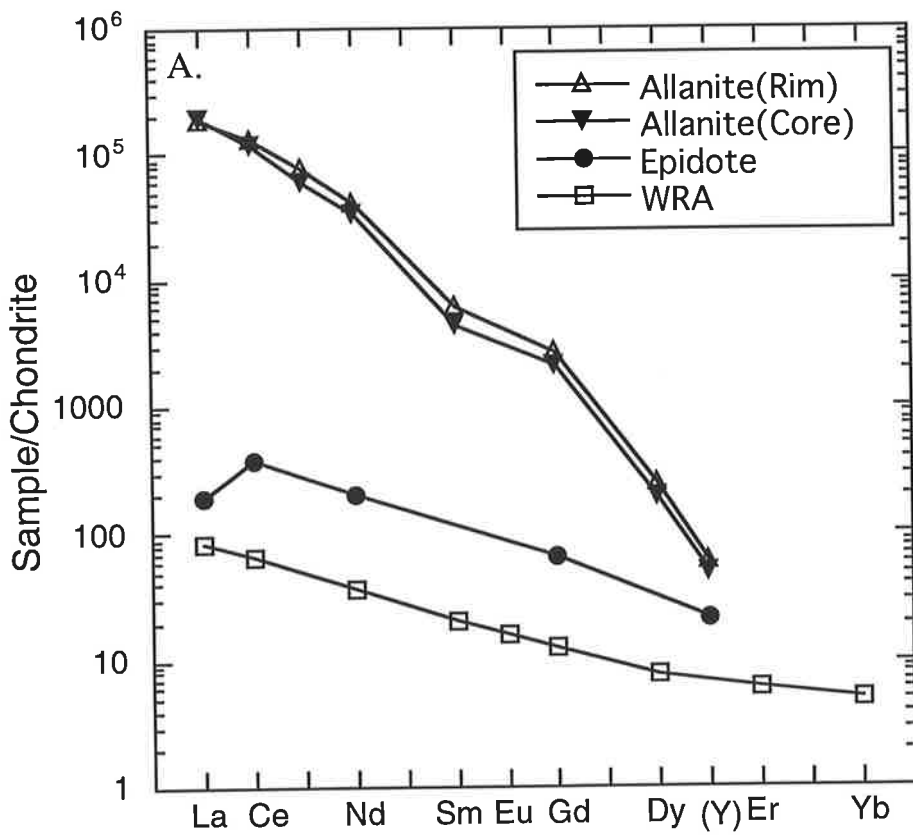
Fig. 4-5. Chondrite normalized REE pattern of accessory minerals from
the Sally Downs Tonalite

A. Tonalite sample, 51706

B. Tonalite sample, 50801

Chondrite normalized REE values of Y are plotted between Dy and Er.

WRA: whole rock REE values



compositions of three representative samples from the tonalite are shown in Table 4-5.

4.3.1. Major elements

Large variation in SiO₂ contents is found in the samples from Sally Downs Tonalite, ranging from 55.7 to 68.8% (Fig. 4-6), but the majority of the SiO₂ contents fall in the range from 59 to 62%. On the histogram (Fig. 4-6), the maximum number of samples is plotted in the SiO₂ range between 60 and 61%. The shape of the histogram is asymmetrical, having a greater tale towards the higher SiO₂ values. Table 4-5 indicates that the mean value of SiO₂ contents is 61.19%.

The tonalite is metaluminous, as mol (Al₂O₃/(CaO + Na₂O + K₂O)) ratios are less than 1.000 in all of the samples except one in which the ratio is 1.006. The average value of the ratio is 0.930 (Table 4-5). The low ratios indicate the Sally Downs Tonalite is comparable to the I-type granitoids. High Na₂O/K₂O ratios in the tonalite support this.

On the major element variation diagrams (Fig. 4-7), most of the elements show regular variation. The variations are slightly curved on the diagram, as they become less steep in the region of high SiO₂ contents (e.g. Fe₂O₃*, MgO etc.). Thus, a simple mixing of two components, e.g. high and low SiO₂ samples, could not produce the entire range of the variation. Hence, the feature suggests a fractional crystallization model for the variation rather than the restite-melt mixing model (White and Chappell, 1977). Except for Na₂O and K₂O, concentrations of elements decrease with increasing SiO₂. Fe₂O₃*, MgO, and CaO contents in particular decrease more than the effect of constant sum, indicating extensive separation of mafic and calcium rich phases from the tonalitic melt. Na₂O has a limited range of variation from 3.42 to 4.56%.

Table 4-5. Average chemical composition of the Sally Downs Tonalite

	Average	S.D.	Max.	Min.
(wt%)				
SiO ₂	61.19	2.14	68.77	55.72
Al ₂ O ₃	17.38	0.62	18.38	14.99
Fe ₂ O ₃ *	5.59	0.67	7.76	3.33
MnO	0.08	0.01	0.13	0.04
MgO	2.54	0.36	3.98	1.43
CaO	5.75	0.56	6.96	3.54
Na ₂ O	3.96	0.16	4.56	3.42
K ₂ O	1.60	0.23	3.36	1.26
TiO ₂	0.66	0.07	0.94	0.41
P ₂ O ₅	0.19	0.04	0.44	0.11
LOI	0.80	0.18	1.32	0.41
Total	99.73	0.29	100.39	99.01
(ppm)				
Ba	566	145	2087	42.9
Rb	46.3	6.9	70.9	32.3
Sr	604	69.9	954	430
Zr	134.5	13.9	171	90
Nb	6.1	1.1	10.8	3.9
Y	12.6	3.5	28.8	3.4
Ce	58.2	21.3	194	20
Nd	24	6.9	61	12
Sc	14.2	2.9	24.4	5.6
V	90	12.5	128	50
Cr	30.4	7.4	94	14
Ni	20.6	3.9	52	11
Cu	30	13.6	90	4
Zn	64.1	7.1	87	41
Ga	21.1	2	23.4	16.6
A/CNK	0.930	0.020	1.006	0.835

S.D.: Standard deviation

Fe₂O₃*: Total Fe as Fe₂O₃

A/CNK: Mol.(Al₂O₃/(CaO+Na₂O+K₂O))

Fig. 4-6. Histogram of SiO_2 contents and mol $\text{Al}_2\text{O}_3/\text{CaO}+\text{Na}_2\text{O} +\text{K}_2\text{O}$
of samples from the Sally Downs Tonalite

A. Histogram of SiO_2 contents

B. Histogram of mol $\text{Al}_2\text{O}_3/\text{CaO}+\text{Na}_2\text{O} +\text{K}_2\text{O}$ values

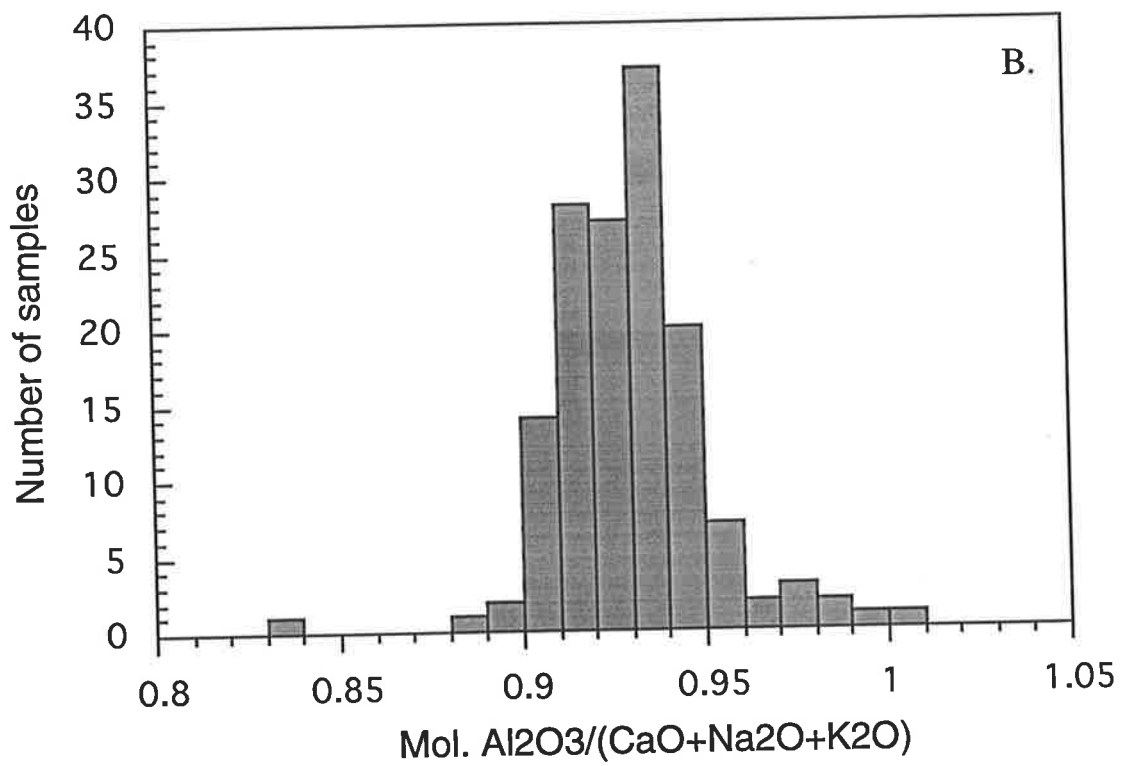
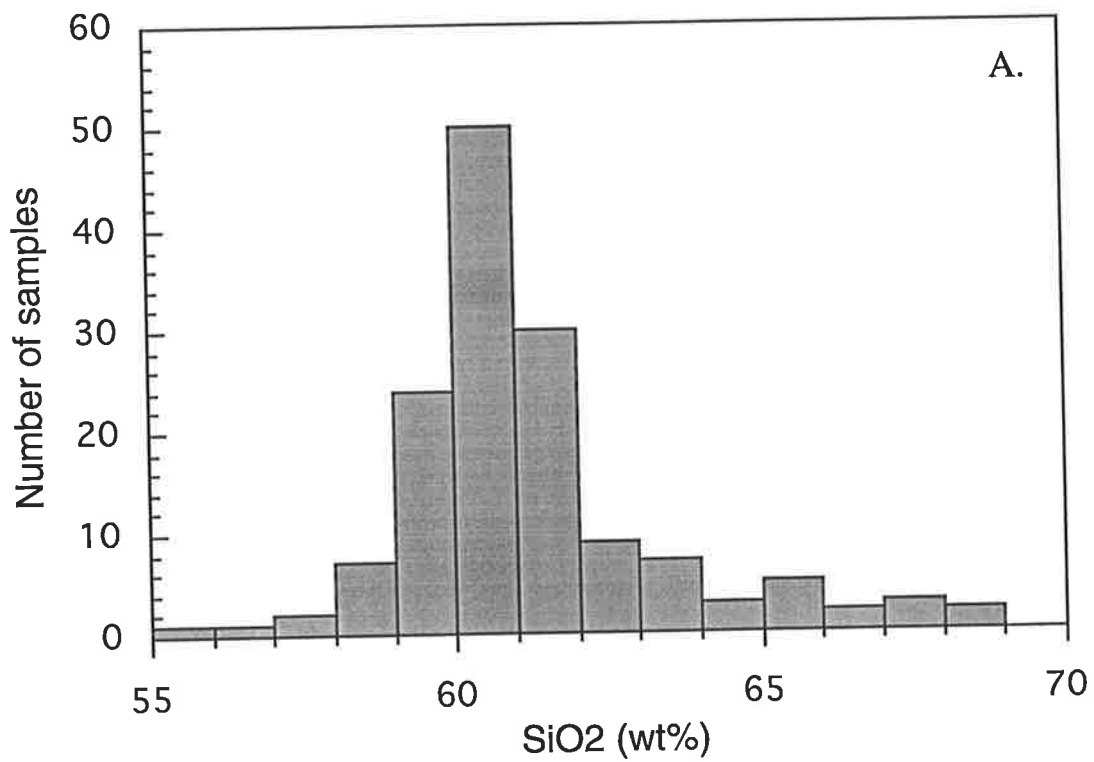
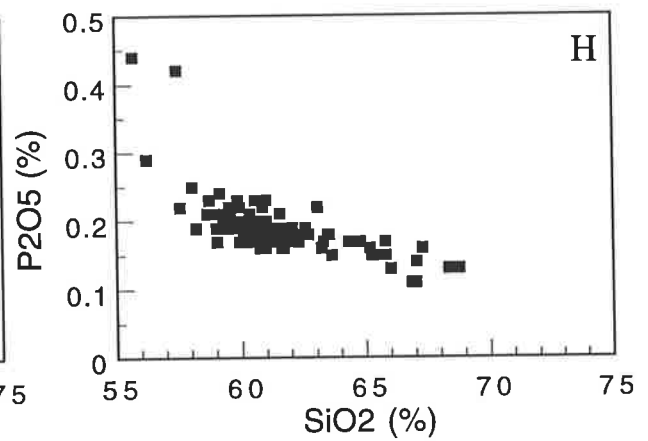
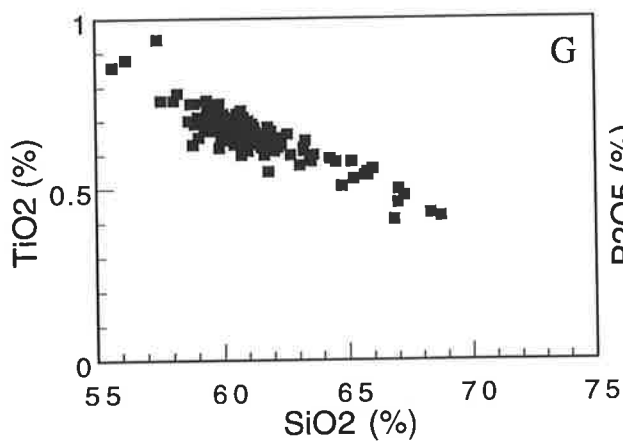
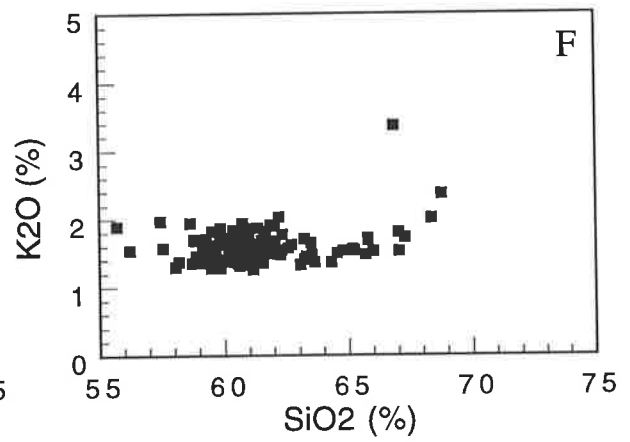
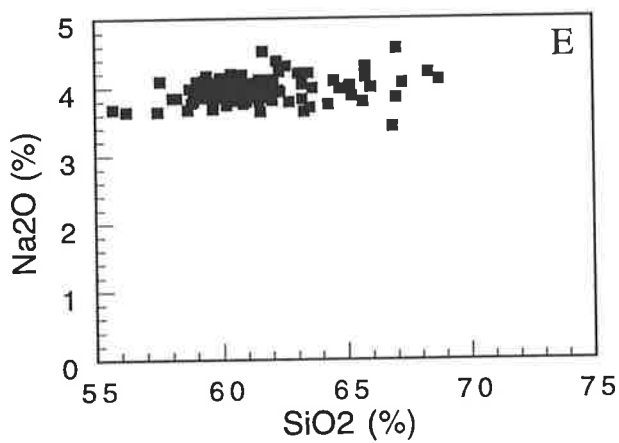
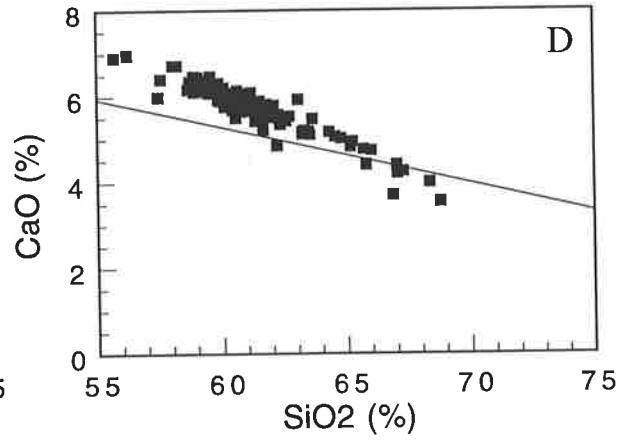
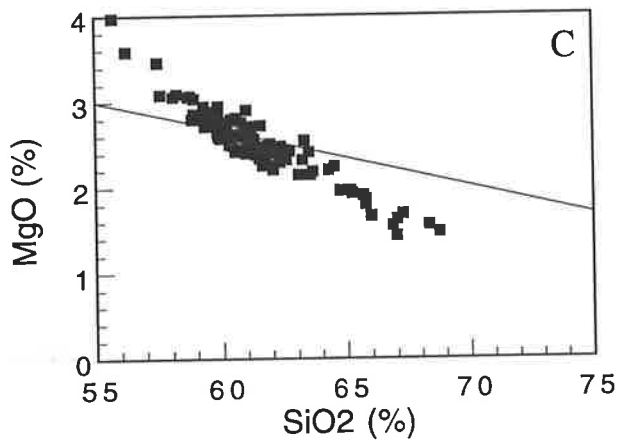
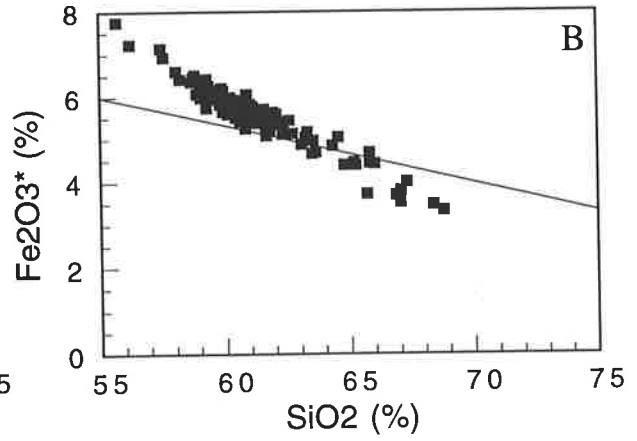
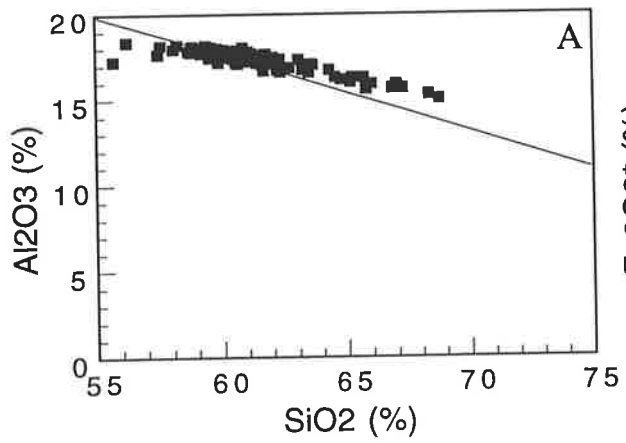


Fig. 4-7. Major element variation diagram of Sally Downs Tonalite

- A. $\text{Al}_2\text{O}_3\text{-SiO}_2$
- B. $\text{Fe}_2\text{O}_3^*\text{-SiO}_2$
- C. MgO-SiO_2
- D. CaO-SiO_2
- E. $\text{Na}_2\text{O-SiO}_2$
- F. $\text{K}_2\text{O-SiO}_2$
- G. $\text{TiO}_2\text{-SiO}_2$
- H. $\text{P}_2\text{O}_5\text{-SiO}_2$

Reference lines in the diagrams A., B., C., and D., show effect of constant sum, and are drawn from a point representing 100% SiO_2 and 0% of the other element extrapolated into the diagram. See section 3.4.3 for detailed discussion of the lines.



Although slight, increases of Na₂O and K₂O with increasing SiO₂ indicate a fractionation of low Na₂O and K₂O phases.

Most of the elements show similarity to I-type granitoids of Kosciusko Batholith rather than to S-type granitoids (Hine et al., 1978); there is even higher Na₂O and slightly lower K₂O in the Sally Downs Tonalite than in the majority of I-type granitoids (Fig. 4-8A). Fig. 4-8B shows a fractionalton from high CaO to low CaO without change of Na₂O/K₂O ratio.

Limited numbers of FeO determination of the Sally Downs Tonalite (Table A3-3) provide an average FeO/FeO*(total Fe as FeO) of 0.66. The value indicates that the tonalite is relatively oxidized. For example, the average values of the Palaeozoic I-type and S-type granites from the Lachlan Fold Belt are 0.71 and 0.84, respectively (Chappell and White, 1992). The low value of the tonalite excludes any significant involvement of sedimentary rocks in the source of the magma or in wall rock interaction of magma, as the involvement of sedimentary rocks generally reduces oxygen fugacity, therefore increases the FeO/FeO* ratio.

On the ternary (Na₂O + K₂O) - FeO* (total Fe as FeO) - MgO diagram (Fig. 4-9A), composition of the tonalite plots in the field of calc-alkaline suite. However, on the normative Q - Ab - Or plot (Fig. 4-9B), the tonalite is distinguished from the common calc-alkaline suite (Barker and Arth, 1976) by the high Ab content, reflecting the high Na₂O. The trend is similar to that linking the gabbro-tonalite-trondhjemite suites of southwest Finland (Barker and Arth, 1976).

4.3.2. Trace elements

Trace element variation diagrams are presented in Fig. 4-10 and 4-11.

Ba

Fig. 4-8. Na₂O-K₂O and Na₂O-K₂O-CaO plots of the Sally Downs

Tonalite

A. Na₂O-K₂O plot

B. Na₂O-K₂O-CaO plot

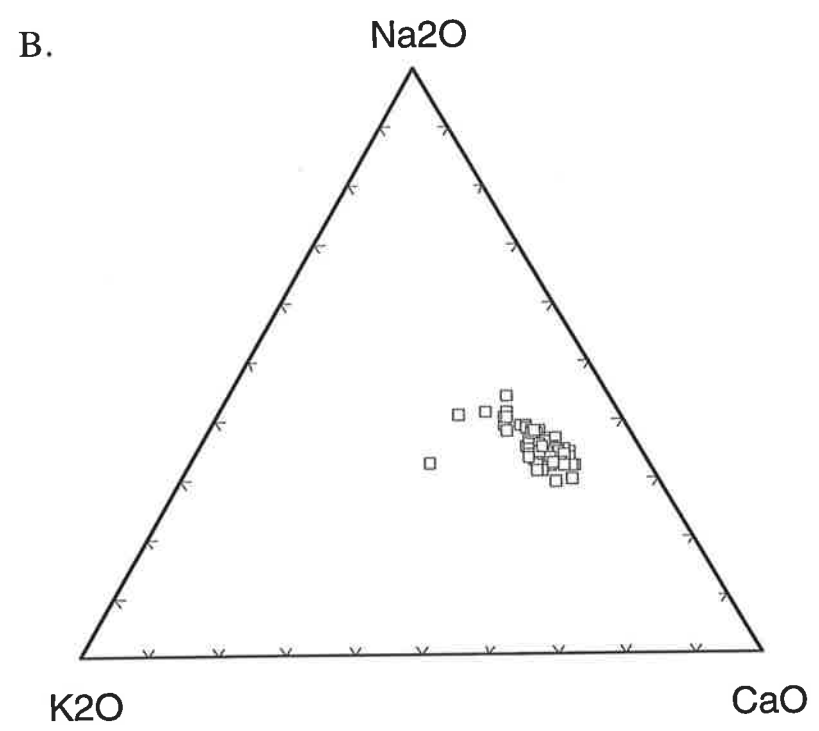
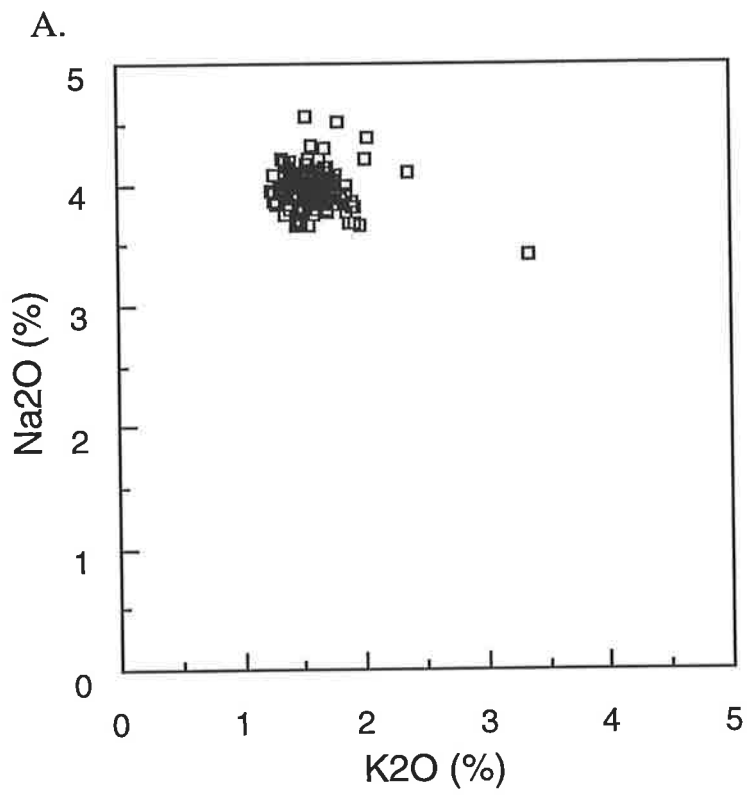


Fig. 4-9. AFM diagram and normative Qz-Ab-Or plot of the Sally
Downs Tonalite

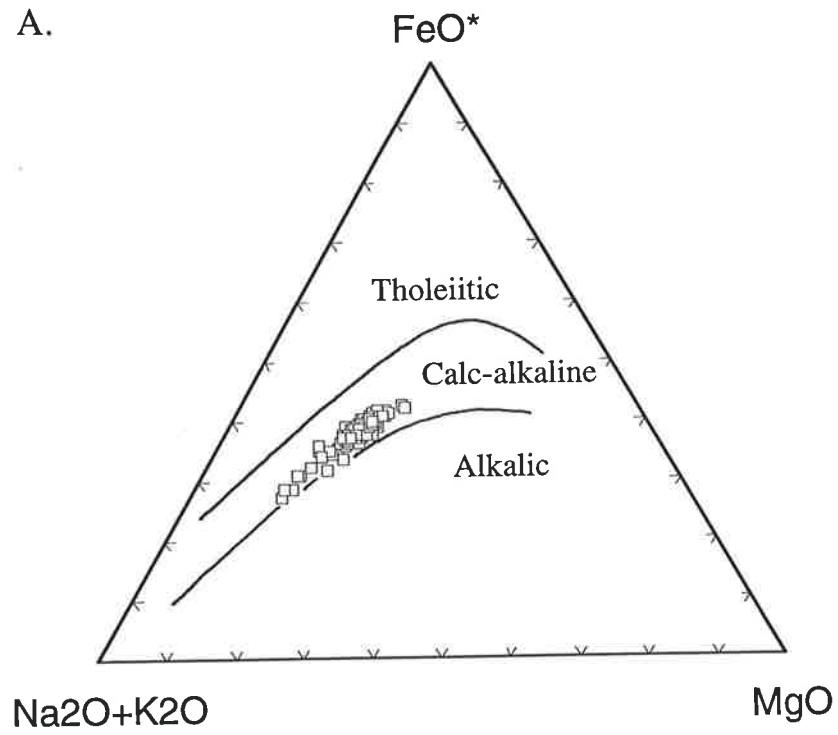
A. AFM diagram

FeO*: total Fe as FeO

B. Normative Qz-Ab-Or plot

Phase boundaries of the granitic system for water pressure 0.5 kb and 10 kb are shown. Cross symbols are minima and open circles are eutectic points. Data from Tuttle and Bowen (1958) and Luth et al. (1964).

A.



B.

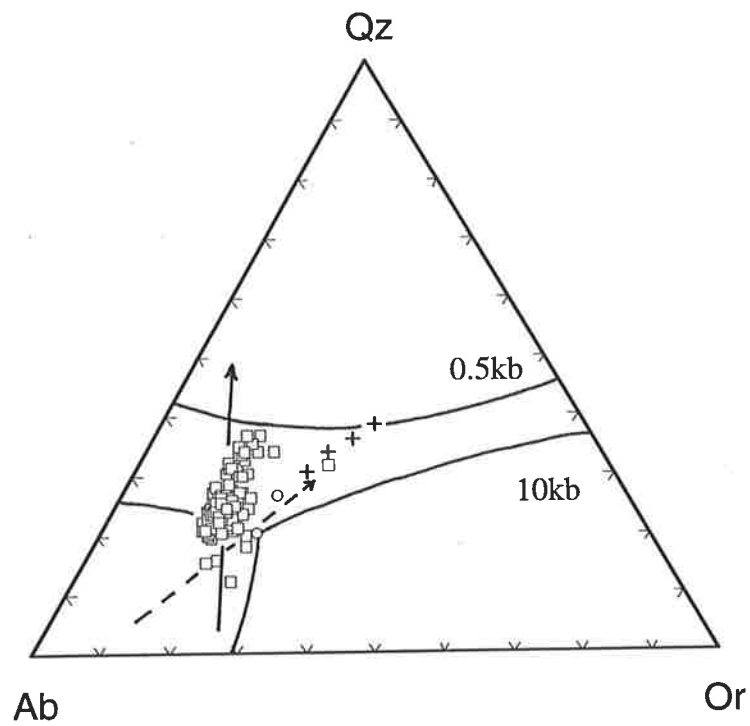


Fig. 4-10. Trace element variation diagram of Sally Downs Tonalite (A)

A. Ba-SiO₂

B. K₂O-Ba

C. Rb-SiO₂

D. K₂O-Rb

E. Sr-SiO₂

F. Rb-Sr

G. Zr-SiO₂

H. Nb-SiO₂

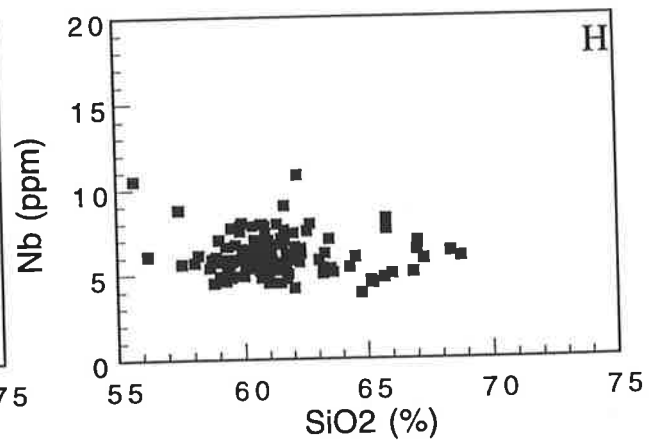
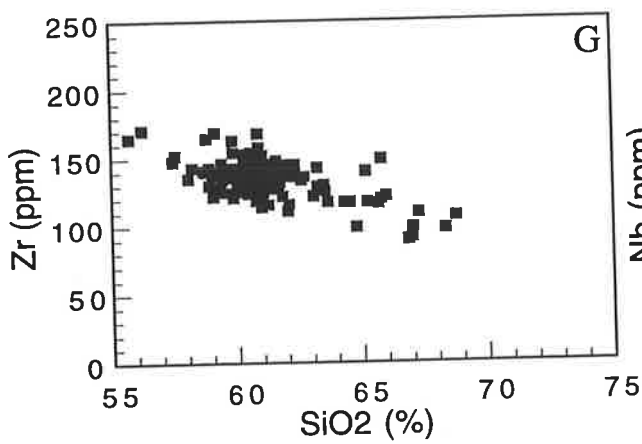
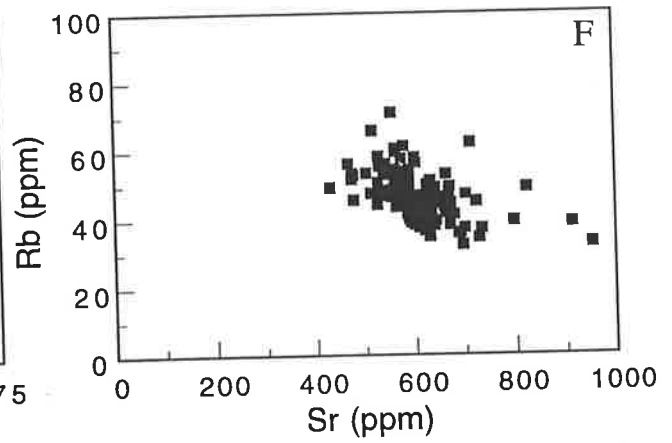
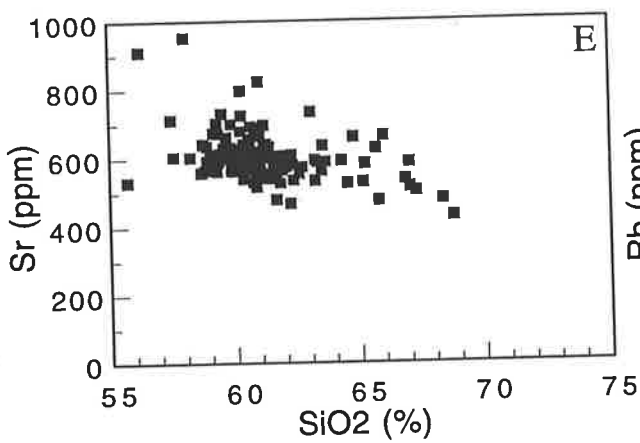
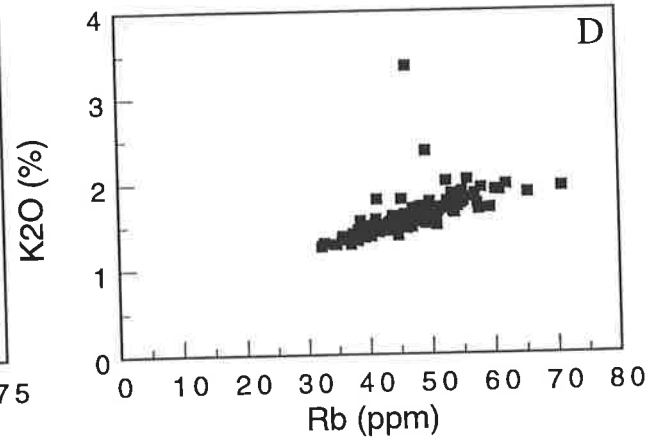
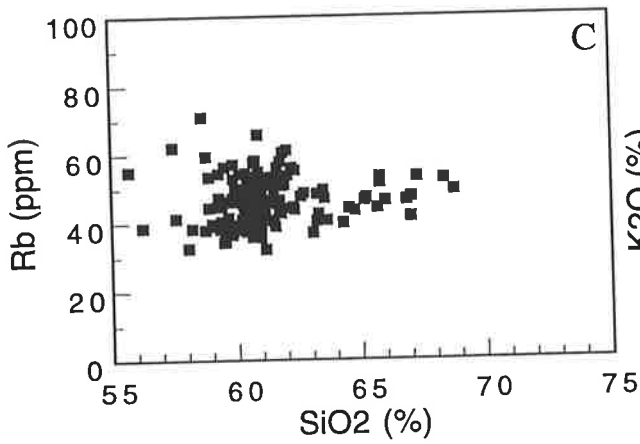
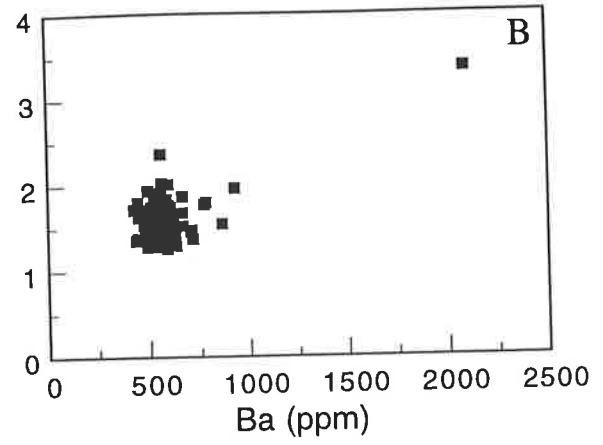
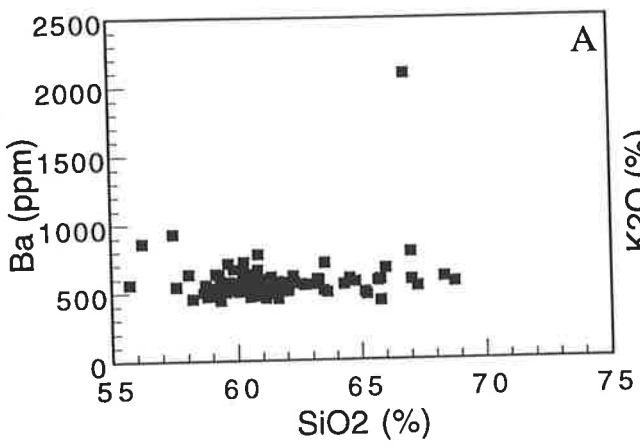


Fig. 4-11. Trace element variation diagram of Sally Downs Tonalite (B)

A. Y-SiO₂

B. Ce-SiO₂

C. Nd-SiO₂

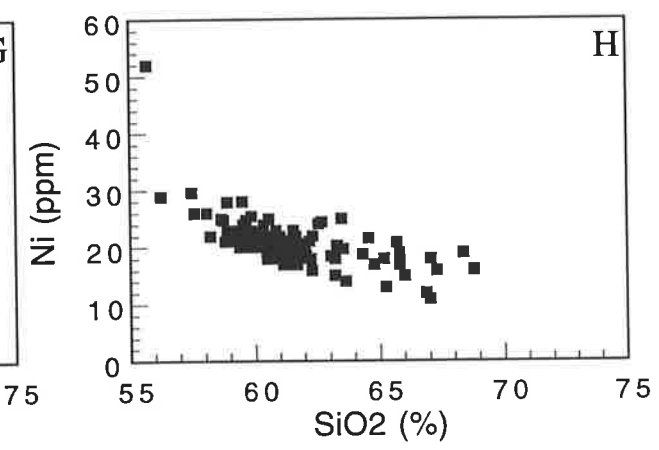
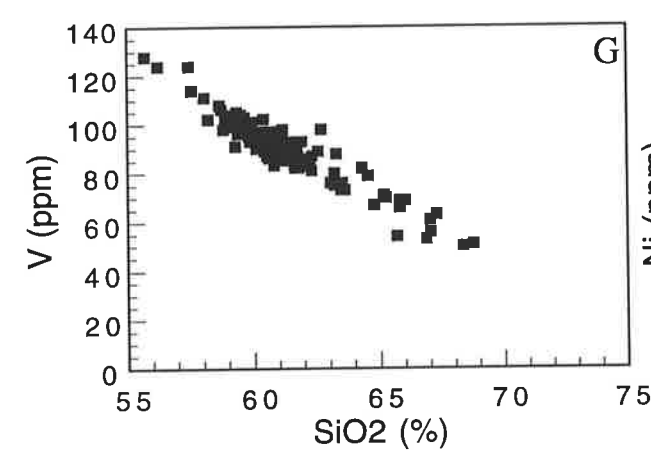
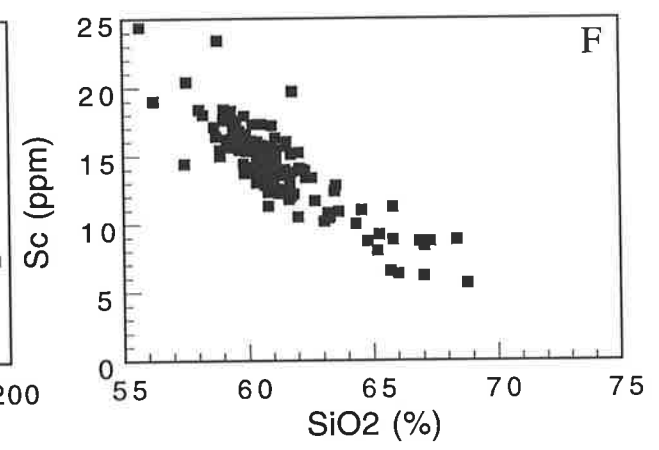
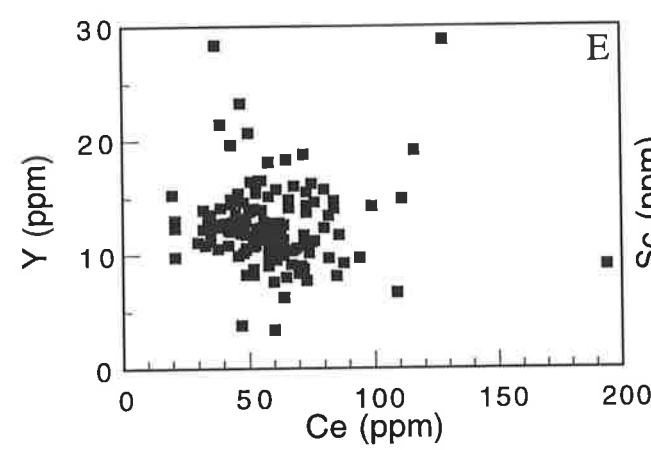
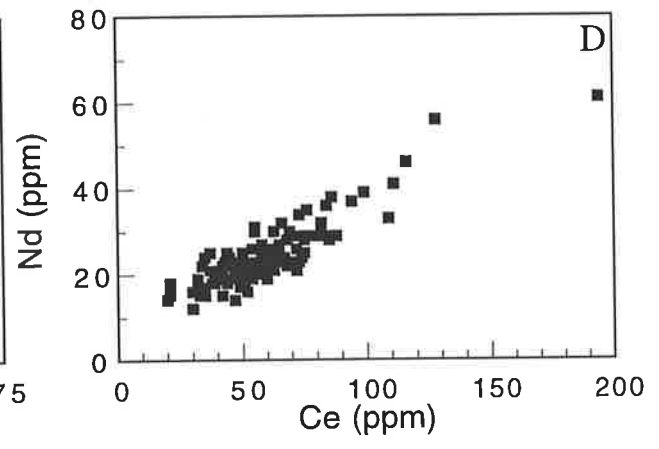
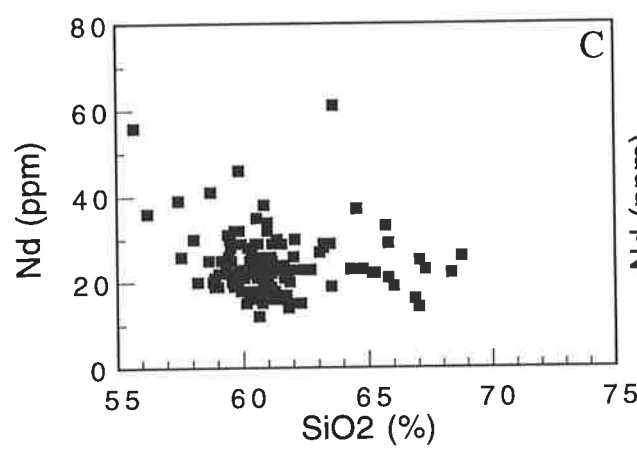
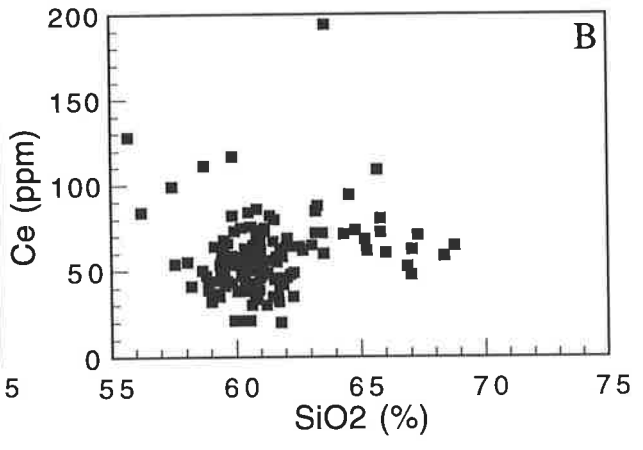
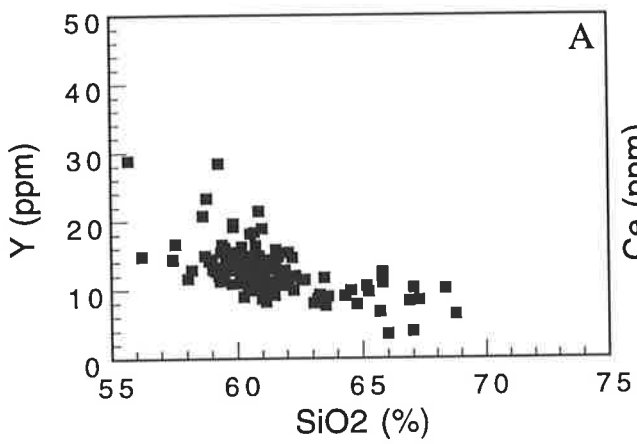
D. Nd-Ce

E. Y-Ce

F. Sc-SiO₂

G. V-SiO₂

H. Ni-SiO₂



Ba contents range from 430 to 780ppm (except one sample having 2087ppm), with average about 550ppm. No systematic correlation with SiO₂ variation is found. This feature is in contrast to the clear negative correlation between Ba and SiO₂ contents in the other two tonalite-trondhjemite suites, viz. Dougalls Granitoid Suite and Ord River Tonalite Suite, in the Sally Downs Bore area. Fig. 4-10B shows that the sample having exceptionally high Ba also contains high K₂O, with similar K/Rb ratio to the normal Sally Downs Tonalite.

Rb

Rb contents vary from 32ppm to 70ppm, and increase with increasing SiO₂ (Fig. 4-10C). The level of the Rb concentration is slightly lower than those of the Ord River Tonalite Suite, but higher than those of the Dougalls Granitoids Suite. Fig. 4-10D shows that a systematic correlation of Rb variation with K₂O, with small spread of K/Rb ratios, ranging from 350 to 200.

Sr

Sr contents decrease from 950 to 430ppm with increasing SiO₂ (Fig 4-10E), indicating a plagioclase fractionation.

Rb/Sr ratios in the Sally Downs Tonalite vary from 0.065 to 0.340 (Fig. 4-10F), and the ratios increase with increasing SiO₂. The evidence suggests the operation of fractionating plagioclase.

For a given SiO₂ percentage, the Sr contents in the Sally Downs Tonalite are slightly higher than those in the Ord River Tonalite Suite.

Zr and Nb

Concentrations of Zr range from 170 to 30ppm, showing negative correlation with SiO₂ (Fig. 4-10G). The monotonous decrease of Zr over the wide range of the tonalite composition indicates a Zr saturation in the early stage of the crystallization.

Nb contents vary from 4 to 11ppm, having a small peak at 60% SiO₂ on the variation diagram (Fig. 4-10H).

Y and REE

Y shows a clear negative correlation with SiO₂ (Fig. 4-11A) indicating depletion of heavy rare earth element (HREE) in the acidic tonalite compared with the basic tonalite. The Y contents decrease from 29 to 3.4ppm.

Ce contents vary significantly from 20 to 116ppm, but no systematic variation of the Ce contents on the diagram (Fig. 4-11B) is found. Nd also shows a similar variation (Fig.4-11C). Although analytical error is relatively large, an extensive random variation is apparent in contrast to Y. Because the tonalite contains considerable, but variable, accessory allanite, the large Ce variations could be introduced by random sampling. The allanite grains are rather large, typically 2mm long, and occasionally up to 5mm long. Thus, the presence of a grain of allanite in the sample analyzed would significantly increase the LREE content. Addition of one grain (1 x 1 x 3mm in dimension; weight 10mg, assuming of density of allanite as 3.3) of allanite (Ce₂O₃= 11%) in 100g of a sample would raise the Ce content by 11ppm (1.1 mg of Ce₂O₃(10mg x 11%) in 100g of the sample). The calculated value is about 20% of the average Ce content in the Sally Downs Tonalite. Systematic variations of Ce with Nd (Fig. 4-11D) indicate a contribution of LREE enriched phase, such as allanite, for whole rock REE compositions. A similar sampling problem involving accessory minerals is discussed by Pettingill and Patchett (1981), pointing out the importance of very large sample sizes and thorough crushing. Hence, large samples of the Sally Downs Tonalite have been crushed for REE determination.

The results of REE analysis by the isotope dilution technique are presented in Table A5-2. Chondrite normalized patterns of the analyzed

samples are shown in Fig. 4-12. The figure illustrates LREE enriched patterns for all the tonalite samples. LREE contents increase with increasing SiO₂; for example, about 70% enrichment of Ce from sample 42402 to 50801 compares with SiO₂ increase from 58.23 to 67.27 %. On the other hand, HREE contents decrease with increasing SiO₂; for example, Yb contents change from 1.11 to 0.694ppm. This contrasting behavior of LREE's and HREE's results in the patterns being pivoted about Nd; the patterns become steeper as the SiO₂ contents increase.

A small positive Eu anomaly occurs in acidic tonalite (50801), but, no significant Eu anomaly is observed in the other samples. The positive Eu anomaly may be due to hornblende fractionation.

Transition metals

All transition metals are much more concentrated in low SiO₂ tonalite than in high SiO₂ tonalite, showing a clear negative correlation with SiO₂ contents (Fig. 4-11G and H). V decreases sharply from 110 to 50ppm. Ni varies from 26ppm in the basic tonalite to 11ppm in the high SiO₂ tonalite, most of the depletion being found in tonalites with SiO₂ contents between 56 and 64%. In the tonalite with 64-68 % SiO₂, the level of Ni is roughly constant. The depletion of nickel can perhaps be accounted for by the effective accommodation of nickel in hornblende and removal of hornblende from tonalitic magma, as fractionated phase in the early stage. The constant Ni content in the tonalite with 64-68% SiO₂, can be attributed to the fact that hornblende is not crystallized from the tonalitic magma. Biotite, the only mafic mineral in the high SiO₂ tonalite, does not accommodate appreciable Ni. The Ni can be taken in opaque minerals in the high SiO₂ tonalite.

4.4. Areal Chemical Variation in the Sally Downs Tonalite

4.4.1. Local Chemical Variability

Fig. 4-12. Chondrite normalized REE pattern of the Sally Downs
Tonalite

51702 is a sample of mafic microgranular enclave in tonalite sample
numbered 51706.

SiO₂ content of the samples,

50702: 63.21%

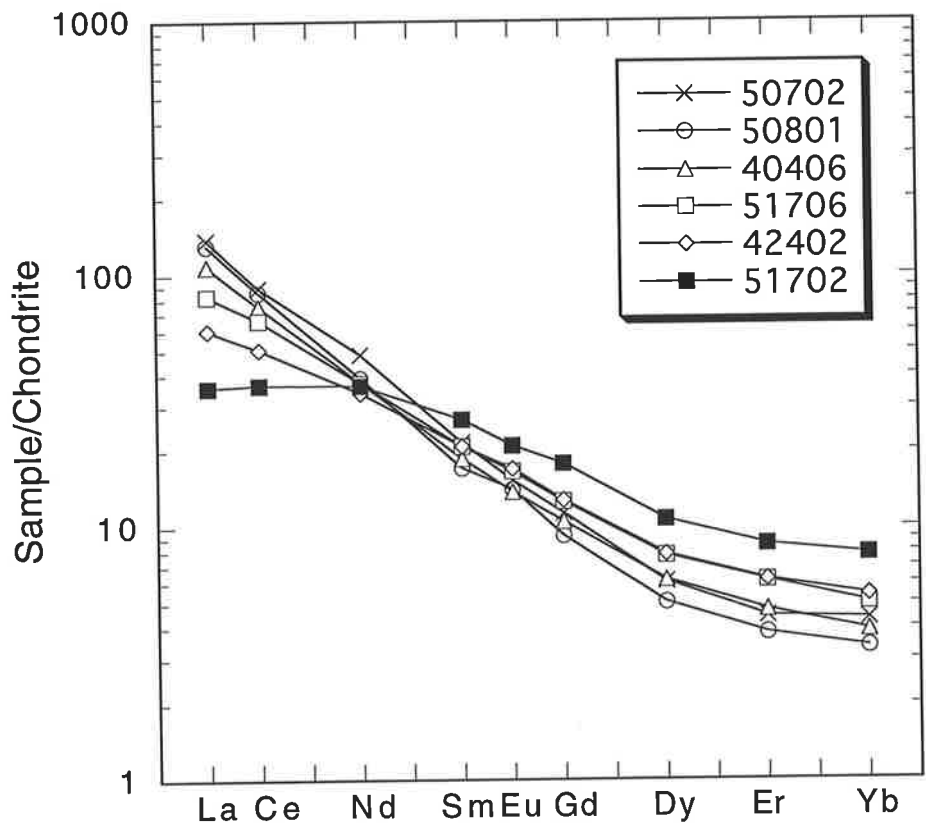
50801: 67.27%

40406: 65.25%

51706: 60.69%

42402: 58.23%

51702: 56.56%



Before the description of the areal chemical variation in the Sally Downs Tonalite, results of examination of a small scale chemical variability are presented. In order to interpret areal geochemical variation data in the Sally Downs Tonalite, it is important to know whether a significant small scale chemical variation is present or not in the tonalite body.

The chemical variability is examined in a total of 11 samples, viz. 51706 and ten extra samples collected around, and within 150m from, the sample locality of 51706. Table 4-6 shows statistical data from the analyses of these samples, indicating the degree of local chemical variability.

SiO₂ contents vary from 59.40 to 61.92%, averaging 60.74% with standard deviation 0.7 (Table 4-6). SiO₂ contents of ten samples out of eleven samples analyzed are between 60.01 and 61.92% (Table A4-6(B)). Only one sample (51709) has SiO₂ lower than 60.00%. When the sample 51709 is excluded from the statistical calculation, the standard deviation becomes smaller to 0.56. Relative standard deviation values indicate that SiO₂ and Al₂O₃ have smaller variability than the other elements (Table 4-6). The relative standard deviation, of each of the major elements except MnO, is less than 0.066, indicating homogeneity of the major components of the tonalite in the area examined. The variation of the major elements in the area examined could be largely due to analytical uncertainty, as relative error of the major element analyses is about 1%.

The relative standard deviation values of the trace elements are larger than those of the major elements, although the values of Sr, V, and Zn are low, thus permitting only small chemical variation in absolute terms of the trace elements in the area examined. As Sr is likely to be accommodated in plagioclase and V and Zn in mafic minerals or oxide minerals, a constant modal composition of the major minerals of the

Table 4-6. Local chemical variability within the Sally Downs Tonalite

	Min.	Max.	Average	S.D.	R.S.D.
Major elements (wt%)					
SiO ₂	59.40	61.92	60.79	0.704	0.012
Al ₂ O ₃	17.23	17.93	17.71	0.197	0.011
Fe ₂ O ₃ *	5.61	6.13	5.81	0.144	0.025
MnO	0.06	0.09	0.08	0.010	0.125
MgO	2.43	2.79	2.59	0.098	0.038
CaO	5.63	6.11	5.94	0.152	0.026
Na ₂ O	3.82	4.07	3.96	0.077	0.019
K ₂ O	1.39	1.68	1.51	0.099	0.066
TiO ₂	0.65	0.74	0.69	0.029	0.042
P ₂ O ₅	0.18	0.20	0.19	0.009	0.047
LOI	0.43	0.71	0.58	0.087	0.150
Trace elements (ppm)					
Ba	502	576	545	22.3	0.041
Rb	39.1	51	43.5	4.33	0.100
Sr	571	624	605	16	0.026
Zr	121	152	139	10.16	0.073
Nb	4.5	6.6	5.6	0.69	0.123
Y	10.8	13.8	12.1	0.97	0.080
Ce	32	63	51	9.12	0.179
Nd	15	23	20.1	2.42	0.120
Sc	13.6	16.3	14.9	0.81	0.054
V	90	96	93.2	2.27	0.024
Cr	25	31	29.5	1.92	0.065
Ni	18	20	19.2	0.87	0.045
Cu	22	42	33.5	5.05	0.151
Zn	62	68	65.5	1.57	0.024

Number of samples: 11

Min.: Minimum, Max.: Maximum, S.D.: Standard deviation

R.S.D.: Relative standard deviation (S.D./Average)

Fe₂O₃* = Total Fe as Fe₂O₃, LOI = Loss on ignition

tonalite in the area examined would tend to result in a small absolute variation of these trace elements. Among the trace elements, Ce has the largest relative standard deviation. As already discussed in the previous section, light REE can be effectively accommodated in allanite. Therefore the large variation in Ce content could be caused by the heterogeneous distribution of allanite in the tonalite.

Although some other trace elements have measurable chemical variation, this variation is limited for most of major and trace elements in the area examined. Therefore, it is concluded that the tonalite is homogeneous on a local scale. Hence it is assumed that the geochemistry of the tonalite within a 600m grid unit could well be represented by one sample from that unit.

4.4.2. Areal Chemical Variation in the Sally Downs Tonalite

Areal chemical variation maps of the Sally Downs Tonalite are prepared from the major and trace element data of 117 samples. Fig. 4-13 shows the areal geochemical variation of eight major elements and eight trace elements. Since most elements vary systematically with SiO₂ content, areal SiO₂ variation within the Sally Downs Tonalite pluton illustrates broadly the more detailed patterns provided by other elements. However, differences from the areal pattern are shown particularly by some elements. Characteristic features of these areal chemical variations, presented in Fig. 4-13, are discussed below.

A. SiO₂

Fig. 4-13 illustrates that four areas with more than 65% SiO₂ are present, one in the central part and one in the western central part of the pluton and other two along the northern and western margins of the pluton. Among the four areas, the high SiO₂ area in the western central

Fig. 4-13. Areal geochemical variation within the Sally Downs Tonalite
SDB: Sally Downs Bore, GNH: Great Northern Highway

Small solid squares are sample locations.

A. SiO_2

B. Al_2O_3

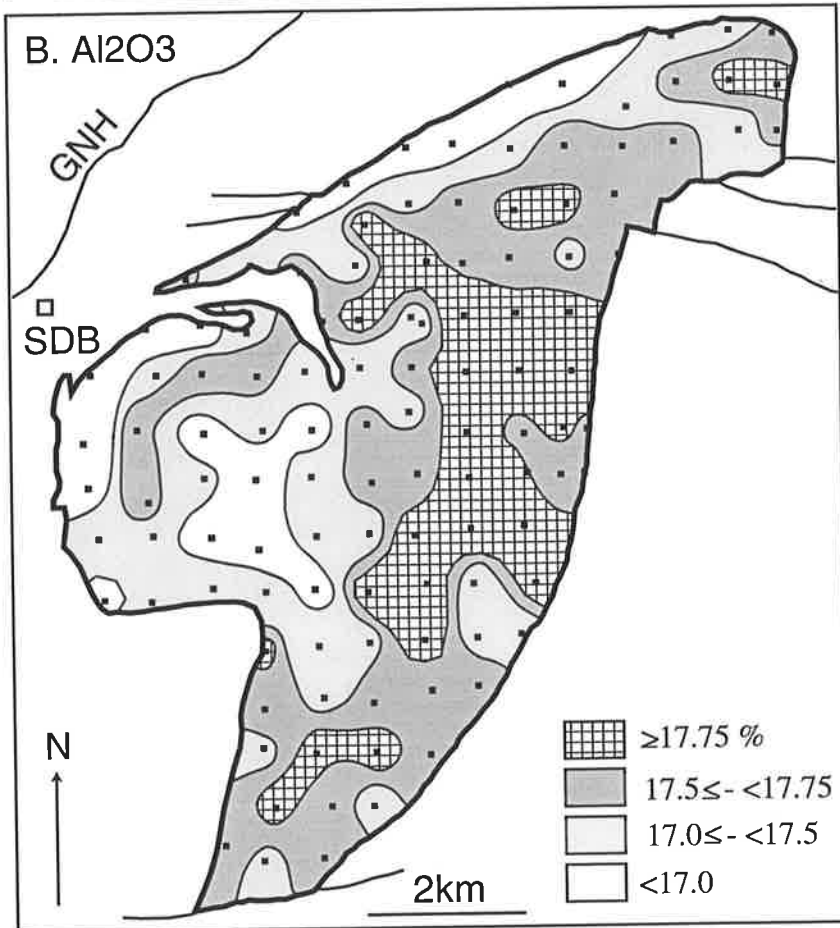
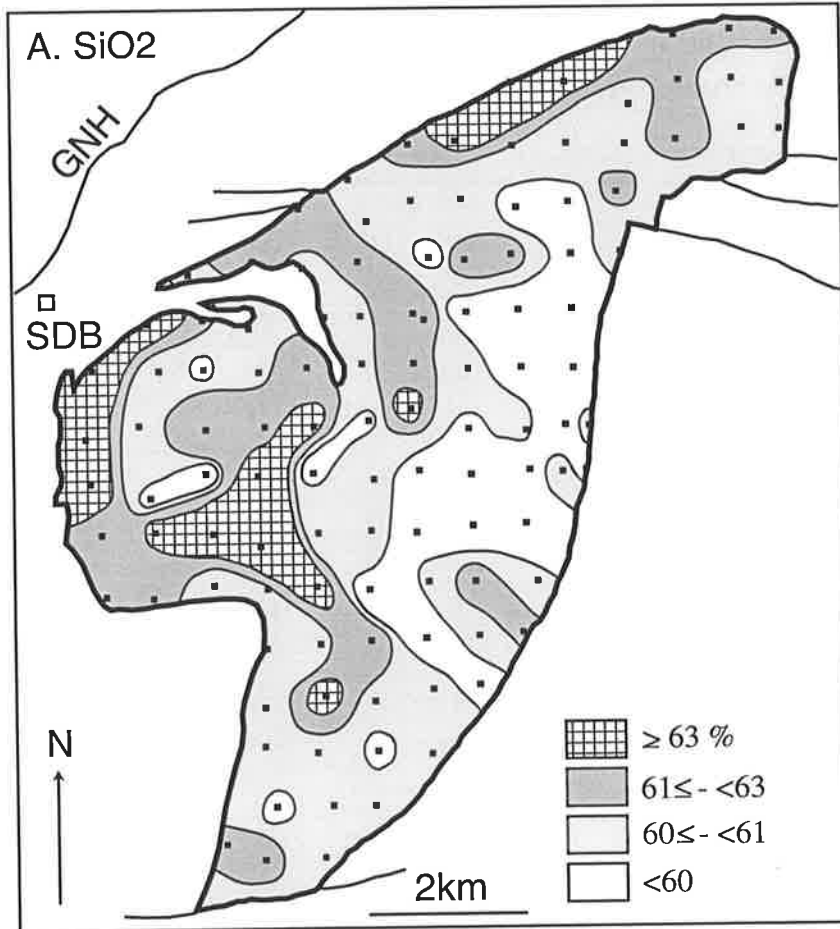


Fig. 4-13 (2). Areal geochemical variation within the Sally Downs

Tonalite

C. Fe_2O_3

D. MgO

Fig. 4-13 (2)

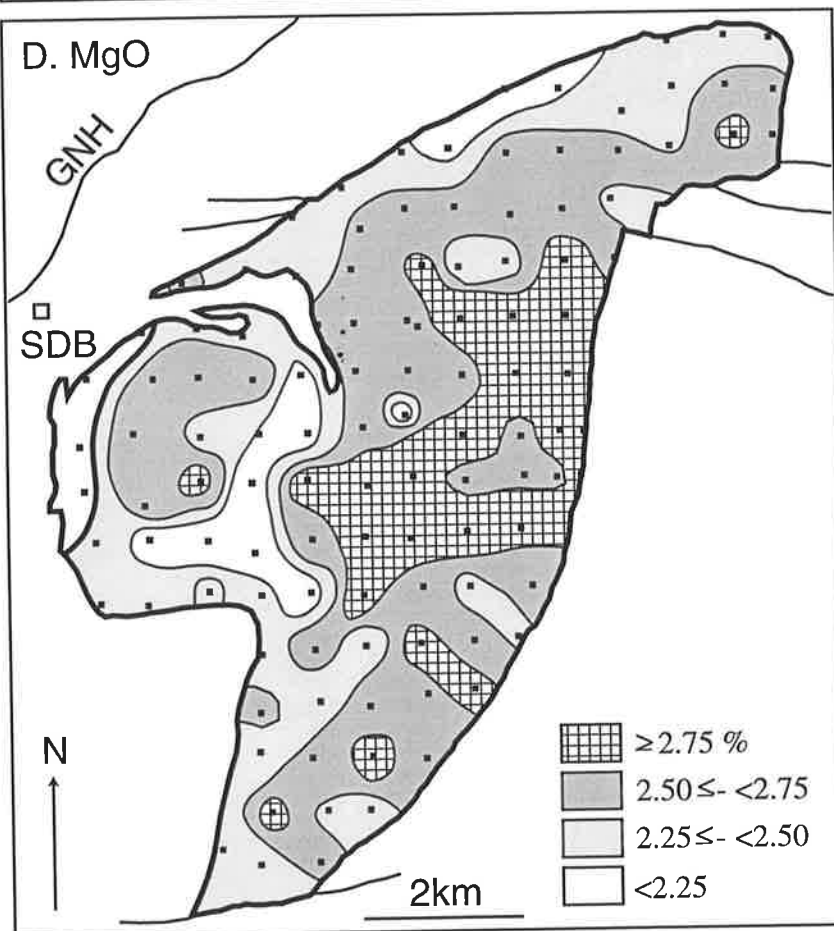
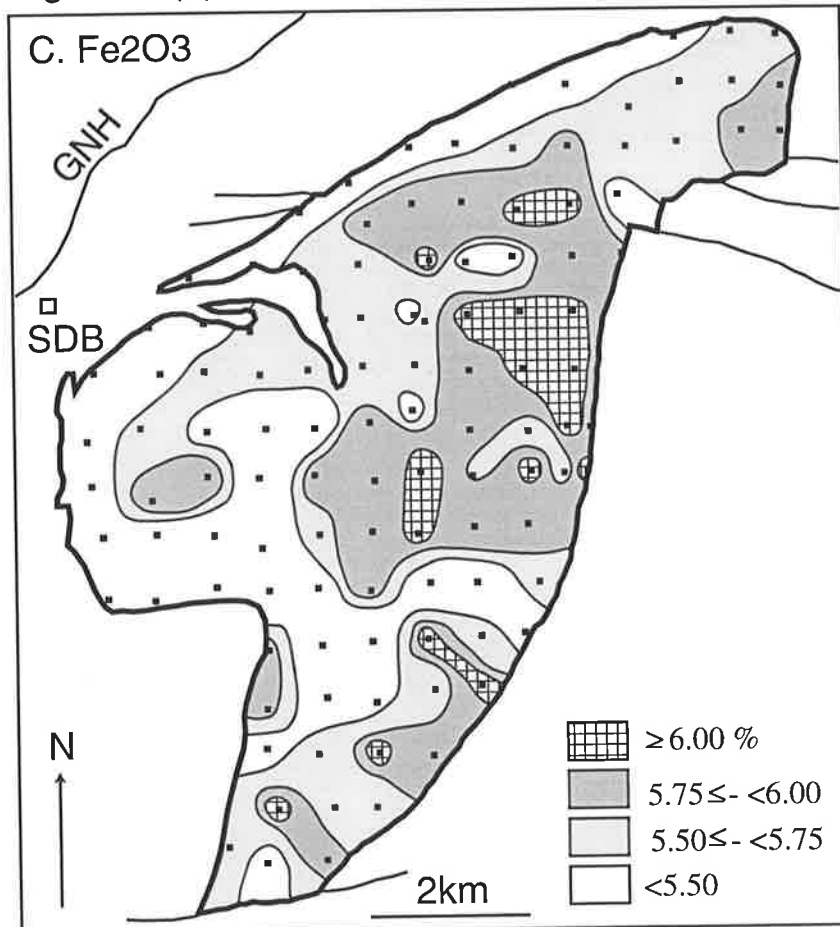


Fig. 4-13 (3). Areal geochemical variation within the Sally Downs

Tonalite

E. CaO

F. Na₂O

Fig. 4-13 (3)

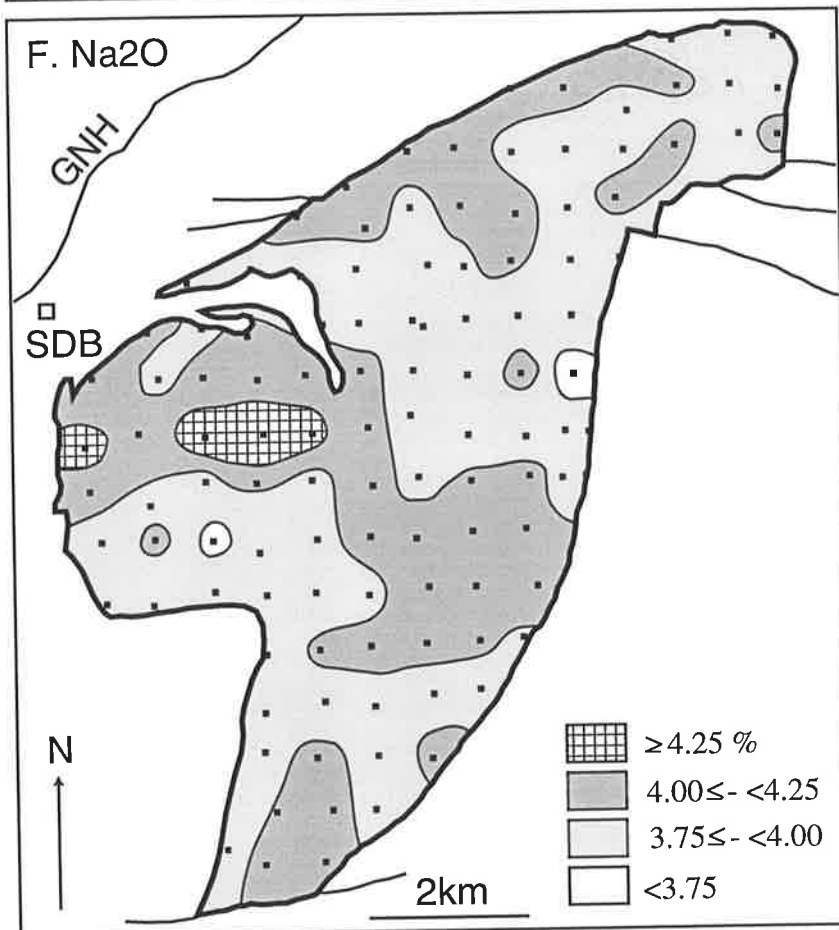
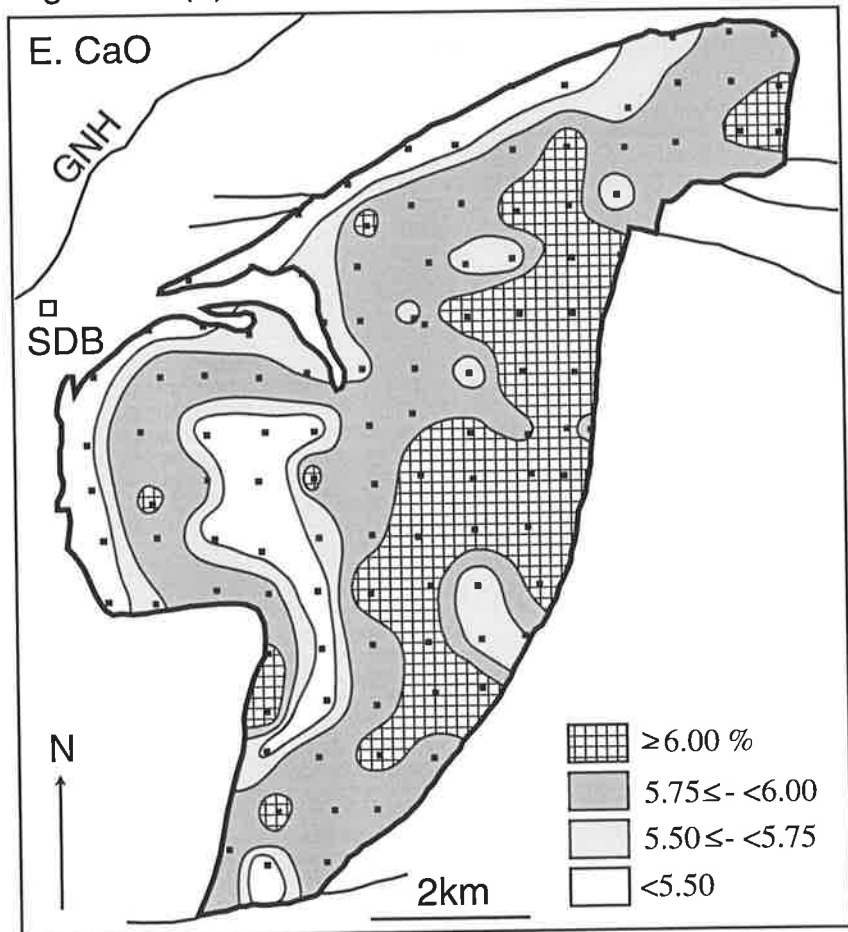


Fig. 4-13 (4). Areal geochemical variation within the Sally Downs

Tonalite

G. K_2O

H. TiO_2

Fig. 4-13 (4)

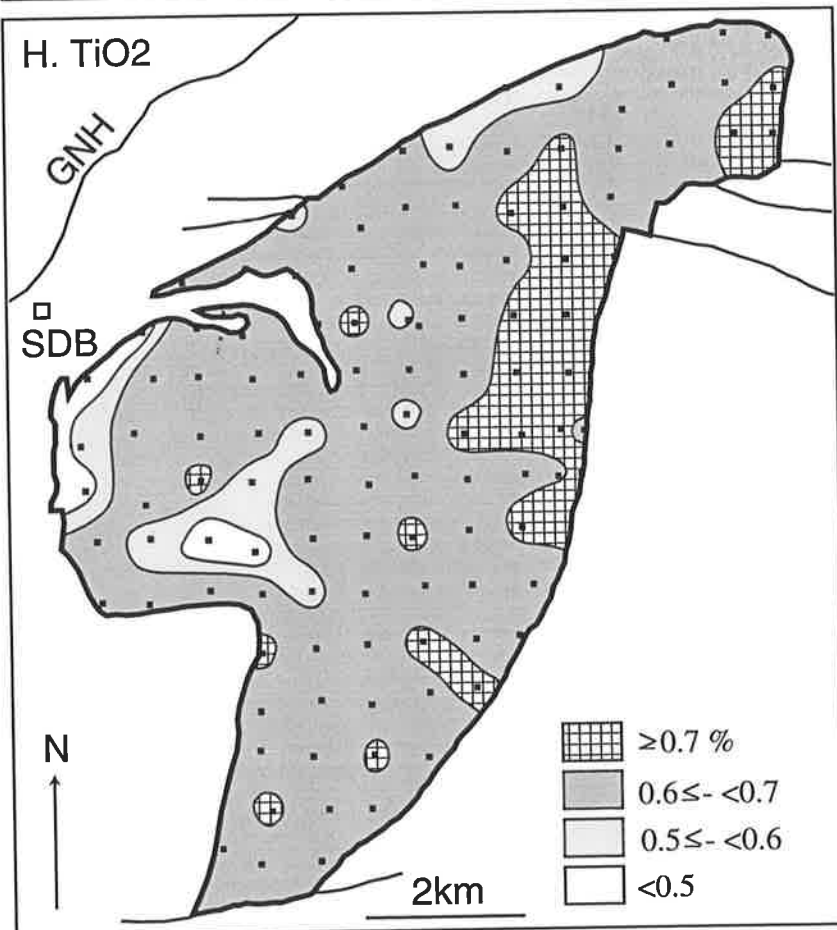
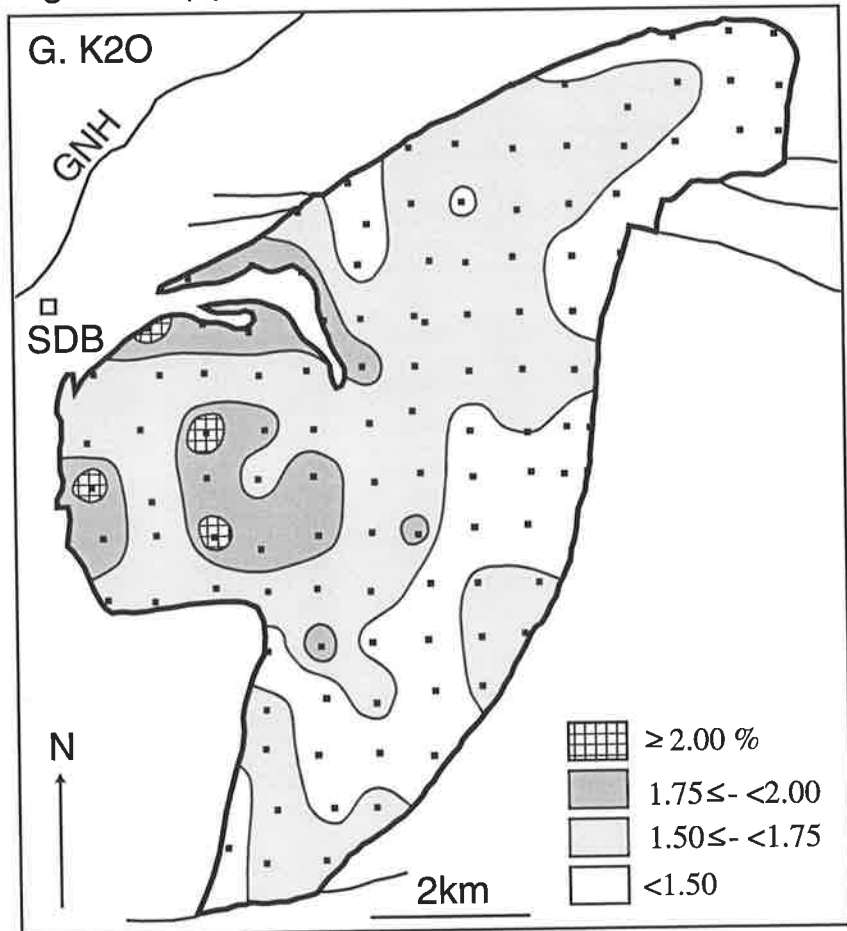


Fig. 4-13 (5). Areal geochemical variation within the Sally Downs
Tonalite

I. Ba

J. Rb

Fig. 4-13 (5)

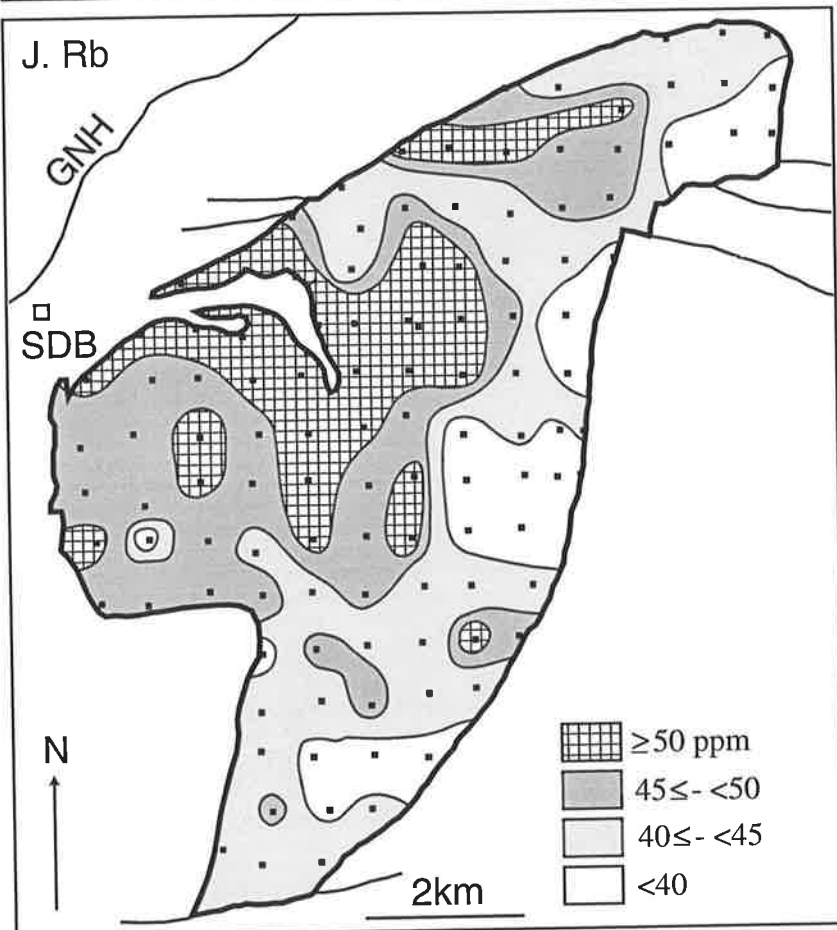
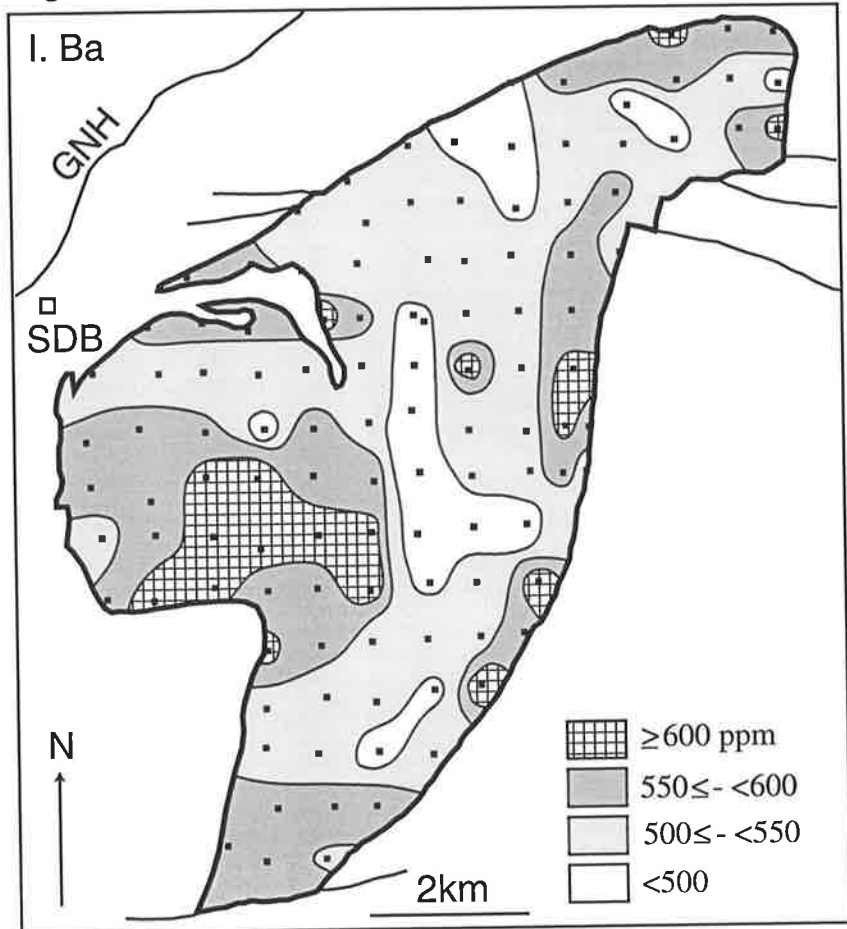


Fig. 4-13 (6). Areal geochemical variation within the Sally Downs
Tonalite

K. Sr

L. Zr

Fig. 4-13 (6)

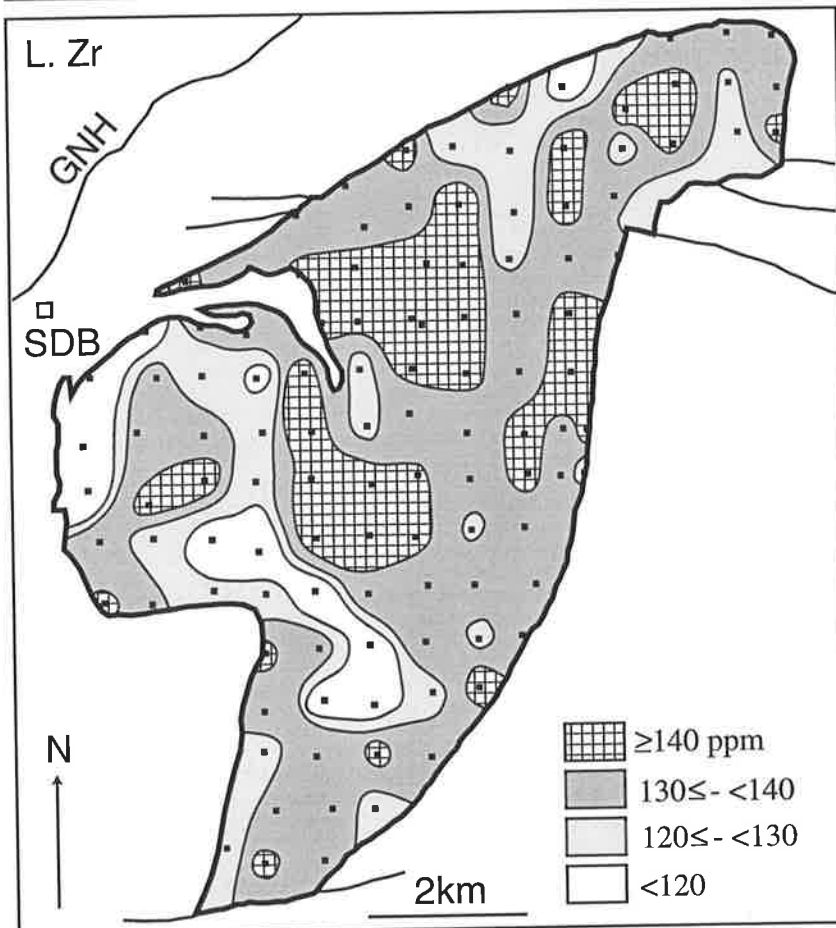
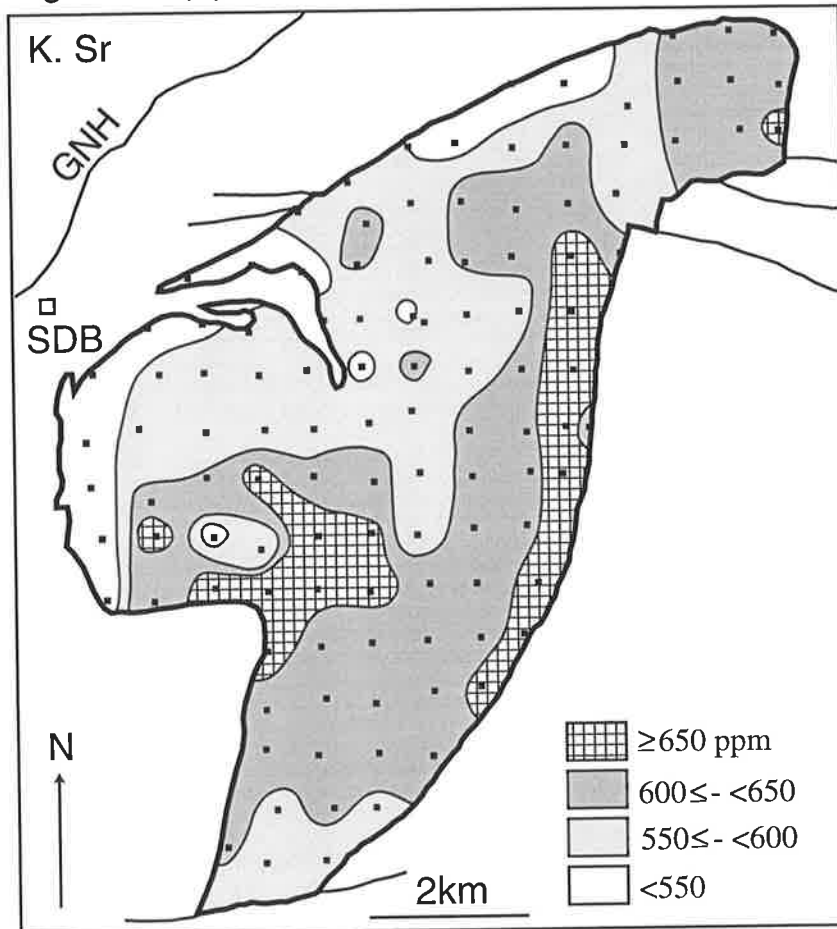


Fig. 4-13 (7). Areal geochemical variation within the Sally Downs
Tonalite

M. Nb

N. Y

Fig. 4-13 (7)

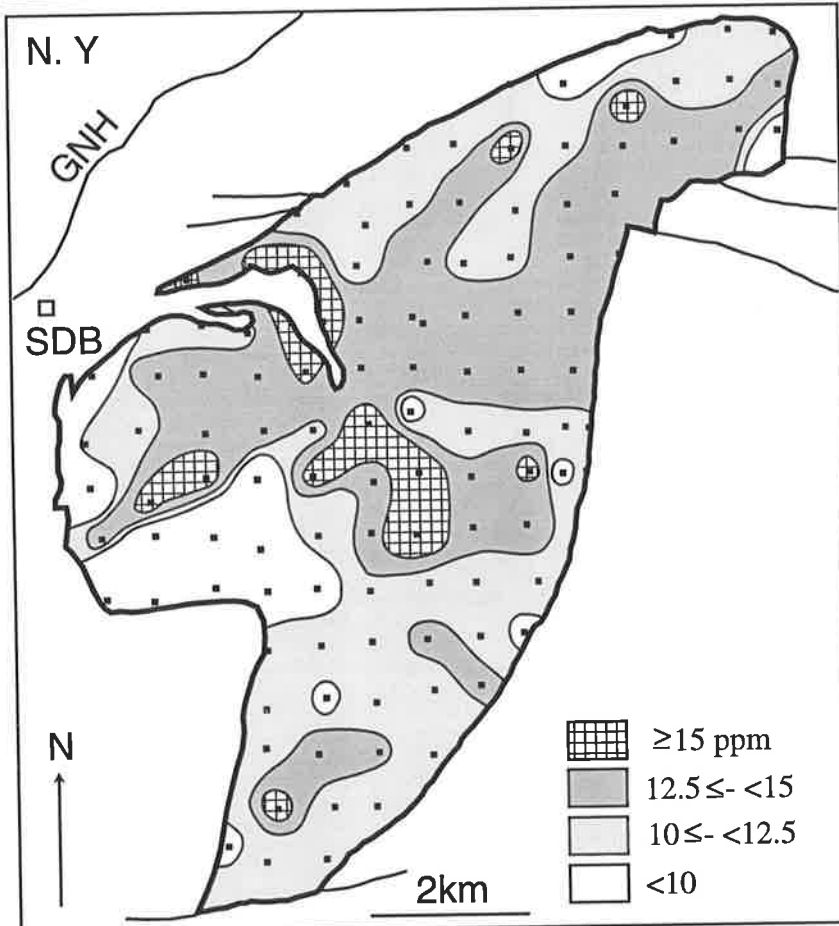
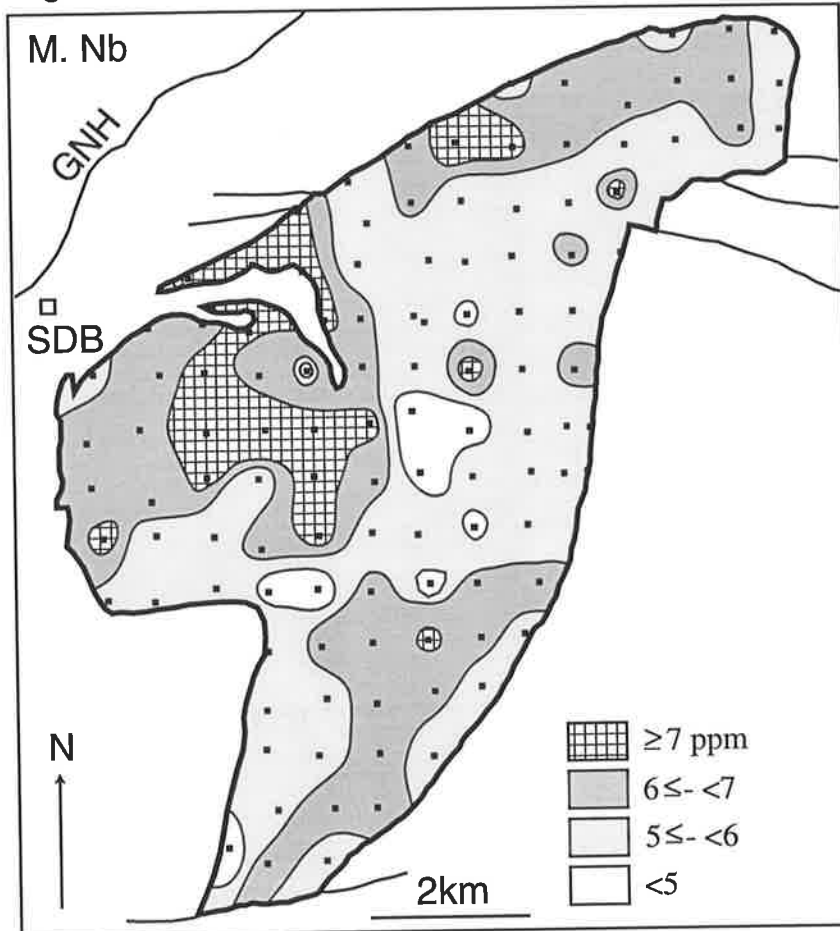
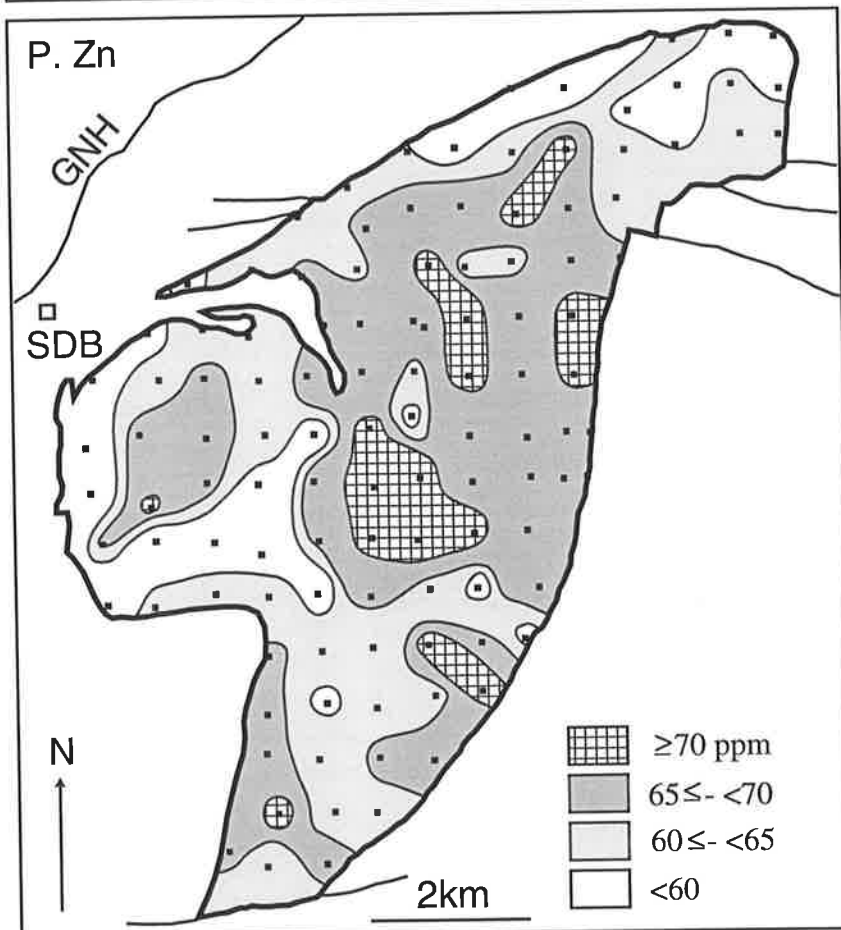
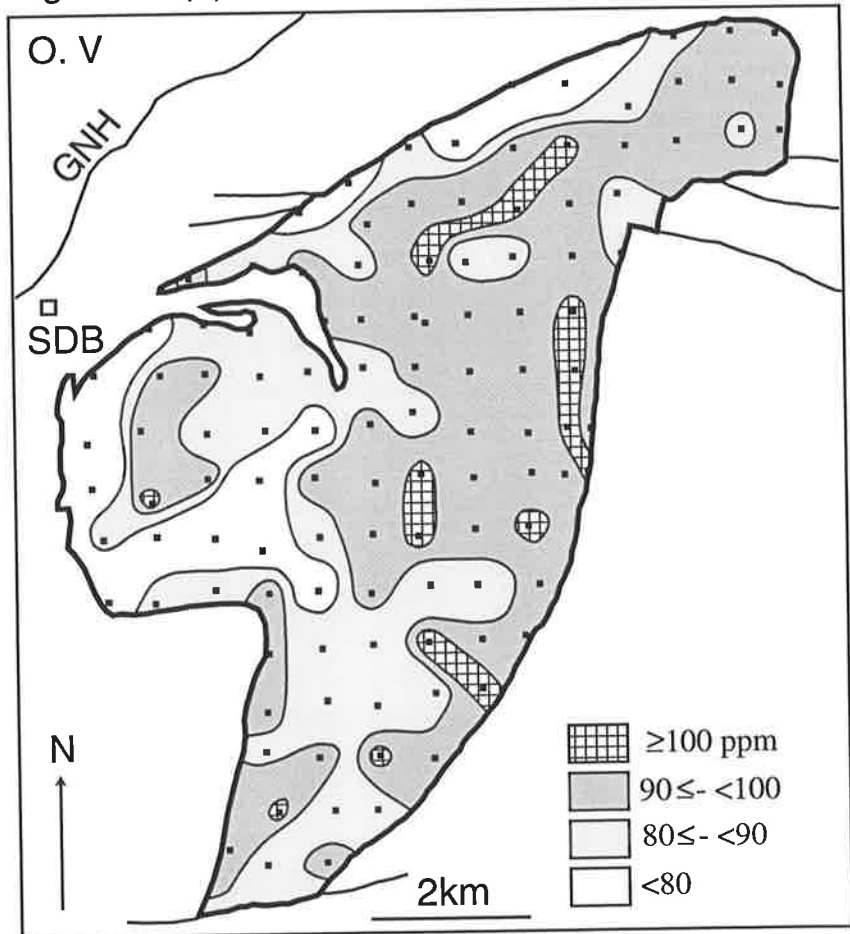


Fig. 4-13 (8). Areal geochemical variation within the Sally Downs
Tonalite

O. V

P. Zn

Fig. 4-13 (8)



part is most significant. Those areas with high SiO₂ contents could indicate locations of finally crystallized magma, as the solidus temperature of the tonalite decreases with increasing SiO₂ content (Piwinskii and Wyllie, 1968).

SiO₂ contents of the tonalite from the eastern half of the pluton are relatively homogeneous, ranging from 59 to 61%. Most of the large variations are present in the western part of the pluton. The pattern of the SiO₂ contents does not indicate an obvious concentric compositional zoning. However, except for the two areas with high SiO₂ contents along the northern and western margin of the pluton, an inward increase of SiO₂ can be discerned. This may imply weak concentric compositional zoning.

B. Al₂O₃

As Al₂O₃ decreases with increasing SiO₂, as indicated on the major element variation diagram (Fig. 4-7), the areal chemical variation of Al₂O₃ indicates a contrary concentration pattern compared with that of SiO₂. High Al₂O₃ zones are found in the eastern part of the tonalite pluton, and low Al₂O₃ rocks are present along the western margin. A weak concentric pattern centred on the low Al₂O₃ area in the western central part is similar to the areal SiO₂ variation in reverse.

C. Fe₂O₃*

The areal chemical variation pattern of Fe₂O₃* shows similarity to that of Al₂O₃, having a high concentration in the eastern part and low value centered in the western central part. Except in the northwest, high Fe₂O₃* samples are concentrated towards the margin of the pluton, constituting an iron rich marginal zone.

D. MgO

MgO has a chemical variation pattern similar to that of Fe₂O₃*. The sample with lowest MgO value is located in the center of the western central area, indicating the likely position of the finally crystallized part of the pluton at the present erosional level. In the eastern central part where most of the high MgO samples are distributed, four relatively low MgO samples concentrated within one square kilometer may represent a core of local magma convection.

E. CaO

The areal chemical variation of CaO tends to suggest concentric zoning with high CaO margin and low CaO center, though the northwestern margin has anomalously low CaO values.

F. Na₂O

The Sally Downs Tonalite pluton has a limited Na₂O range from 3.42 to 4.56%. Relatively high Na₂O samples are found in the central part and northwestern margin of the pluton. As mentioned in section 4.3.1, Na₂O generally increases with increasing SiO₂. However, the highest Na₂O zone of the central part is present 1.2km north of the high SiO₂ core of central part.

G. K₂O

K₂O variation indicates a weak concentric zoning pattern, low in the eastern and northern margin and high in the western central part and western margin. As with sodium, the pattern is largely comparable to that of SiO₂. A slightly higher than average K₂O zone margining the arch-shape tongue of country rocks east of the Sally Downs Bore might

indicate incorporation of potassium from the country rocks by the magma-wall rock interaction.

H. TiO₂

Although limited variation of TiO₂ is found in the pluton, from 0.41 to 0.94%, the areal variation shows a regular pattern similar to that of other elements such as Fe₂O₃ and MgO. A relatively high TiO₂ zone is present in the eastern part of the pluton and low TiO₂ occurs along the northwestern margin and in the western central part.

I. Ba

Fig. 4-13 indicates that Ba is enriched towards the margin of the pluton. Low SiO₂ samples from the eastern margin of the pluton have a high Ba content, though high SiO₂ samples in the western central area of the pluton also have a high Ba content. The Ba behavior is reflected in the SiO₂ vs. Ba diagram (Fig. 4-10), which shows no systematic Ba variation. Samples with relatively low Ba content were collected from the central part of the pluton. The areal variation pattern of Ba might indicate that its concentration is affected by the interaction of tonalitic magma with wall rocks.

J. Rb

The areal chemical variation pattern of Rb has similar characteristics to that of K₂O. Rb is low in the eastern and northern margin and high in the western and central part. A distinctly high Rb concentration is found margining the arch-shape tongue of country rock east of the Sally Downs Bore, similar to the distribution of K₂O.

K. Sr

As indicated by the decreasing Sr contents with increasing SiO₂ shown on the variation diagram (Fig. 4-10), the regional concentration of Sr (Fig. 4-13) is basically the reverse of that of SiO₂, though depicting similarly shaped concentration contours to those of SiO₂. The Sr and Rb areal variation patterns are similarly the reverse of each other. However, a small irregularity is found in the western central area where SiO₂ is high but Sr also is high.

L. Zr

High Zr samples are found in the eastern and central parts of the pluton. Samples with Zr less than 120 ppm were collected from the western margin and western central parts of the pluton where high SiO₂ samples also were obtained. The Zr content in the tonalitic magma is likely to be reduced by crystallization of zircon, and the low Zr samples may represent the finally solidified tonalitic magma.

M. Nb

High Nb content is found in the western part of the pluton. However, Nb has limited variation, ranging from 3.9 to 10.8 ppm, and the significance of the areal variation pattern is not clear.

N. Y

The Y content is high in the central part of the pluton. Low Y samples are found near the western and northern pluton margins. A small number of low Y samples are also found at the eastern part of the pluton where SiO₂ value is also low. This could indicate initial enrichment of Y with fractionation from relatively low Y content of magma.

O. V

Areal variation of V is similar to that of Fe_2O_3^* , having high concentration in the eastern part and low concentrations in the western central part and western and northern margins of pluton.

P. Zn

Zn also has a similar areal variation pattern to that of V and Fe_2O_3^* .

4.4.3. Summary of Areal Chemical Variation in the Sally Downs Tonalite

Areal variation of elements in the Sally Downs Tonalite can be summarized as follows,

(1) Low concentration in the eastern part, especially near the margin, and showing weak concentric zoned pattern with high concentration in the central part; SiO_2 , Na_2O , K_2O , Rb, (Nb).

(2) High concentration in the eastern part, especially a marginal zone, and showing weak concentric zoned pattern with low concentration in the central part; Al_2O_3 , Fe_2O_3^* , MgO , CaO , TiO_2 , V, Zn, Zr, (Sr).

(3) Variation pattern different from the previous two types; Ba, (Na_2O), (Sr).

Those areal variation patterns of elements in the Sally Downs Tonalite could be resulted from the fractional crystallization of tonalitic magma, the interaction of tonalitic magma with wall rocks and/or mixing of tonalitic magma and basic magma.

In the next section (4.5.1), a numerical test of the fractional crystallization model to produce the wide range of chemical composition which is found in the Sally Downs Tonalite will be presented. If fractional crystallization plays the most important part in the production

of large chemical variation in the Sally Downs Tonalite (see 4.5.1, below), the areal variation patterns can be accounted for by the following intrusive mechanism (Fig. 4-14):

(1) Tonalite magma was intruded as an elliptical shape elongated in a north-south direction (Fig. 4-14A).

(2) More input of magma into the central part produced westward expansion of the pluton inducing ductile deformation of already solidified marginal tonalite (Fig. 4-14B).

(3) Subsequent intrusion of the magma took place along the northern and western margin of the pluton (Fig. 4-14C).

At the northern margin, the magma was intruded into zones of weakness within the country rock, separating large blocks of the country rock as septa in the pluton.

4.5. Discussion on the Petrology of the Sally Downs Tonalite

4.5.1. Fractionation Crystallization Model of the Sally Downs Tonalite

In the previous sections (4.3. and 4.4.), the large compositional variations in the Sally Downs Tonalite body are outlined. From consideration of the variation diagrams, the fractional crystallization is suggested as a model for the variation. An intrusive mechanism for the tonalitic magma and its cooling history is presented above based on a study of areal chemical variations within the outcrop extent of the pluton.

In order to quantitatively evaluate the fractional crystallization model, least squares mixing calculations (Wright and Doherty, 1970) of major elements are presented in Table 4-7. Although the parental magma can be basaltic or basic tonalitic, a relatively basic tonalite, represented by sample 32903 ($\text{SiO}_2 = 57.48\%$), is assumed to be the parental tonalitic magma from which is derived acidic tonalite by fractional crystallization.

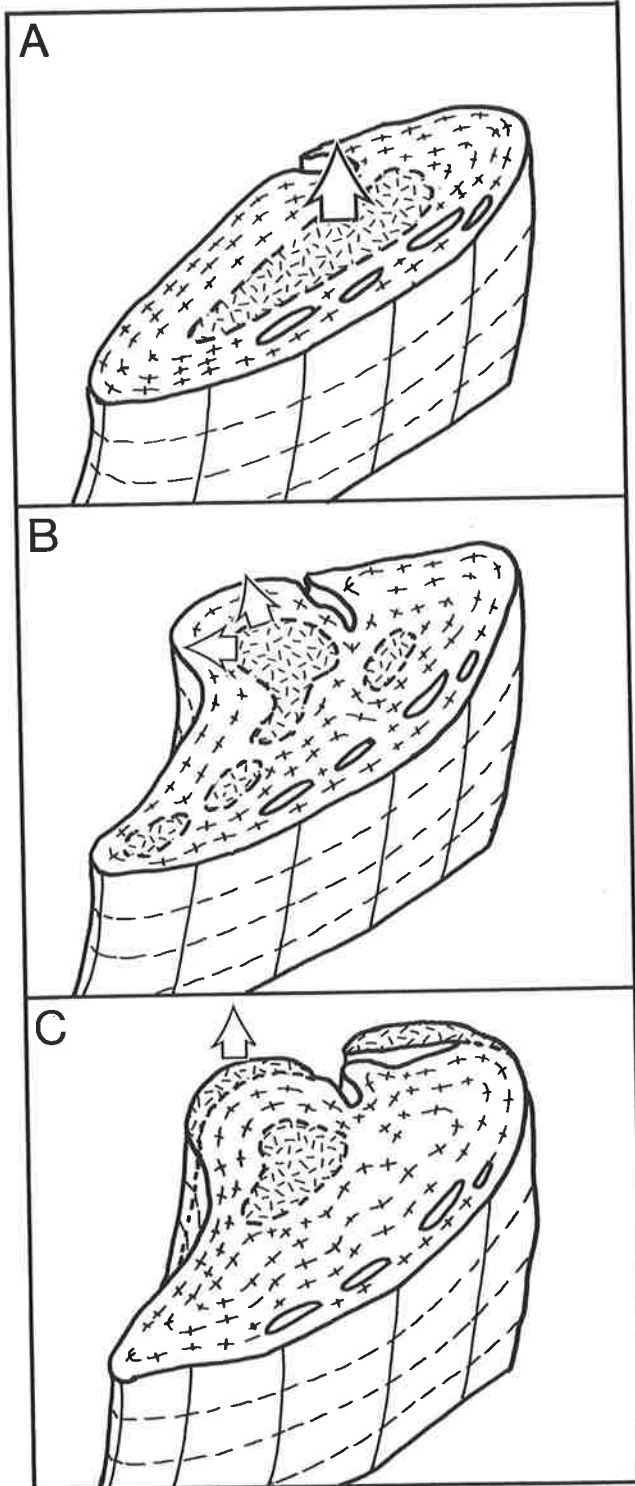
Fig. 4-14. Model of intrusive mechanism

Arrows indicate direction of magma movement.

(A) Tonalite magma was intruded as an elliptical shape elongated in a north-south direction, with inward solidification of tonalitic magma.

(B) Further input of magma into the central part produced westward expansion of the pluton inducing ductile deformation of already solidified marginal tonalite.

(C) Subsequent intrusion of the magma took place along the northern and western margin of the pluton.



Tonalitic magma
 Tonalite (solidified)

Looking from southeast

Table 4-7. Fractional crystallization models of the Sally Downs Tonalite by least squares mixing of major elements

A. Fractional crystallization model from basic tonalite (32903A) to tonalite (51706)

	Ho	Bi	Pl	Ep	Mt	Im	51706	32903A	Calc.	Residual
Fraction	0.0736	0.0625	0.1194	0.0401	-0.0006	0.0042	0.7027			
SiO2 (%)	45.45	39.73	57.61	39.21	0.00	0.00	61.48	57.48	57.48	-0.0019
TiO2	1.10	1.65	0.01	0.01	0.00	52.65	0.70	0.90	0.90	0.0000
Al2O3	10.68	17.79	26.70	24.83	0.00	0.00	18.02	18.78	18.74	-0.0372
FeO*	17.60	15.92	0.08	11.77	100.00	47.35	5.32	6.65	6.65	0.0000
MnO	0.22	0.05	0.05	0.32	0.00	0.00	0.07	0.09	0.09	0.0027
MgO	11.04	15.02	0.00	0.00	0.00	0.00	2.70	3.67	3.65	-0.0220
CaO	11.65	0.00	8.51	23.71	0.00	0.00	6.16	7.11	7.15	0.0419
Na2O	1.50	0.29	7.03	0.03	0.00	0.00	4.08	3.73	3.84	0.1061
K2O	0.75	9.54	0.03	0.03	0.00	0.00	1.47	1.58	1.69	0.1090
Sum of (Residual) ² =0.0268										

B. Fractional crystallization model from tonalite (51706) to acidic tonalite (50801)

	Ho	Bi	Pl	Ep	Mt	Im	50801	51706	Calc.	Residual
Fraction	0.0966	0.0456	0.2268	0.0246	0	0.0034	0.6059			
SiO2 (%)	44.50	37.97	58.40	38.70	0.00	0.00	68.08	61.48	61.48	-0.0039
TiO2	1.15	2.17	0.06	0.12	0.00	52.65	0.49	0.70	0.70	0.0000
Al2O3	10.65	17.38	26.24	24.17	0.00	0.00	15.85	18.02	17.97	-0.0495
FeO*	18.65	18.76	0.00	12.49	100.00	47.35	3.64	5.32	5.32	0.0000
MnO	0.26	0.22	0.04	0.18	0.00	0.00	0.06	0.07	0.09	0.0150
MgO	10.62	13.39	0.00	0.00	0.00	0.00	1.71	2.70	2.67	-0.0277
CaO	11.88	0.00	8.19	24.29	0.00	0.00	4.31	6.16	6.22	0.0551
Na2O	1.46	0.17	7.02	0.04	0.00	0.00	4.11	4.08	4.23	0.1520
K2O	0.84	9.94	0.05	0.00	0.00	0.00	1.75	1.47	1.61	0.1357
Sum of (Residual) ² =0.0480										

C. Fractional crystallization model from basic tonalite (32903A) to acidic tonalite (50801)

	Ho	Bi	Pl	Ep	Mt	Im	50801	32903A	Calc.	Residual
Fraction	0.1350	0.0931	0.2693	0.0605	0.0013	0.0071	0.4369			
SiO2 (%)	45.45	39.73	57.61	39.21	0.00	0.00	68.08	57.48	57.47	-0.0057
TiO2	1.10	1.65	0.01	0.10	0.00	52.65	0.49	0.90	0.90	0.0000
Al2O3	10.68	17.79	26.70	24.83	0.00	0.00	15.85	18.78	18.72	-0.0615
FeO*	17.60	15.92	0.08	11.77	100.00	47.35	3.64	6.65	6.65	0.0000
MnO	0.22	0.05	0.05	0.32	0.00	0.00	0.06	0.09	0.09	0.0034
MgO	11.04	15.02	0.00	0.00	0.00	0.00	1.71	3.67	3.64	-0.0329
CaO	11.65	0.00	8.51	23.71	0.00	0.00	4.31	7.11	7.18	0.0733
Na2O	1.50	0.29	7.03	0.03	0.00	0.00	4.11	3.73	3.92	0.1906
K2O	0.75	9.54	0.03	0.03	0.00	0.00	1.75	1.58	1.76	0.1844
Sum of (Residual) ² =0.0806										

Chemical compositions of minerals and rocks are recalculated to 100% total.

Ho: hornblende, Bi: biotite, Pl: plagioclase, Ep: epidote, Mt: magnetite, Im: ilmenite

Calc: calculated composition from mixing of components

FeO*: Total Fe as FeO

Sum of (Residual)²: sum of square of residuals

These calculations are presented to evaluate only compositional variations found in the Sally Downs Tonalite pluton. In the model calculation, it is assumed that the chemical compositions of the tonalite from the Sally Downs Tonalite body represent melt composition.

Model A of Table 4-7 evaluates the derivation of typical tonalite, represented by a sample 51706 ($\text{SiO}_2 = 60.69\%$, 61.48% in Table 4-7; adjusted value to make 100% total for the mixing calculation), from the parental tonalitic magma. The result suggests that plagioclase, hornblende, and biotite are major components of the fractionated phase from the parental tonalitic magma. Fractionation of these minerals from the parental magma yields approximately 70 wt% residual tonalitic magma. The fractionated phase is dioritic as indicated by the fraction of minerals in the phase.

Model B of Table 4-7 is a crystal fractionation process to produce acidic tonalite ($\text{SiO}_2 = 67.27\%$; 68.08% in Table 4-7) from the typical tonalite (51706) of the Sally Downs Tonalite body. The fractionated phase contains similar minerals to those in Model A. However, less biotite is calculated in the fractionated phase of Model B than in that of Model A. Fractionation of biotite from the tonalitic magma effectively increases the SiO_2 content of the magma, as the biotite has low SiO_2 content (38 %), but reduces the K_2O content of the magma. As a slight increase of K_2O with increasing SiO_2 is shown on the major element variation diagram (Fig. 4-7F), progressive reduction in the amount of biotite in the fractionated phase is indicated. The overall small amount of biotite in the fractionated phase has resulted in the increase of K_2O content in the magma. Hornblende is a major mafic mineral in the fractionated phase (Table 4-7). The effective removal of hornblende from the tonalitic magma explains the absence of hornblende in the acidic tonalite. Model B yields 60 wt% residual acidic tonalite magma.

Model C of Table 4-7 indicates direct derivation of acidic tonalite magma from the basic tonalite by crystal fractionation. The calculation indicates that a large amount of fractionated phase (56.3 wt%) is required to produce the residual acidic tonalite magma.

The above least squares mixing calculations of major elements to evaluate the fractional crystallization model indicates that plagioclase and hornblende are major minerals in the fractionated phase. For plutonic rocks, there are several factors which prohibit accurate calculation of petrogenetic models. These include: (1) incomplete knowledge of the composition of the magma (e.g. whether bulk chemistry of the plutonic rock represents the chemistry of the magma), (2) incomplete knowledge of the parental magma (Arth et al., 1978, Perfit et al., 1980a), (3) incomplete knowledge of the weight fraction of each rock facies, as a three dimensional description of plutonic bodies is generally difficult to make. Therefore, it is possible that other models could better explain the compositional variation of the Sally Downs Tonalite, though the fractional crystallization process presented above incorporates the basic characteristics of any likely model.

In the least squares mixing models, calculations indicate that there is a considerable amount of fractionated phase present. Such a fundamental component of the model is generally lacking in the outcrop of the tonalite, except in the form of some mafic microgranular enclaves. It could, however, be present in the lower part of the tonalitic body. The weight fraction of the fractionated phase is estimated from the chemical composition of the tonalite and the model calculation presented above. Assuming the chemical composition of the parental tonalite is similar to sample 32903, the weight fraction of the fractionated phase is calculated from the weight fraction factors estimated from those of Model A and Model C for every one percent of SiO₂ from 58 to 69 %, covering range

of SiO₂ contents found in the Sally Downs Tonalite pluton. The weight proportions of the tonalite with each one percent of SiO₂ content are obtained from 146 analytical results to examine areal geochemical variation. Although, the results represent the volumetric fraction of SiO₂ content in the Sally Downs Tonalite, assuming the specific gravity difference between basic tonalite and acidic tonalite is negligible, the volumetric fraction can be used as weight proportion figure. Fig. 4-15 shows the result of the calculation. To produce the compositional variation found in the Sally Downs Tonalite, the fractionated phase, with a dioritic composition, is 27.6 wt% of the parental tonalitic magma. The remaining 72.4 wt% solidifies as tonalite with the observed compositional variation.

4.5.2. Trace Elements in Minerals

High concentrations of certain trace elements in accessory minerals generate two problems, one being the sampling problem already discussed, and the other being the effect on the application of trace element modelling to petrogenesis.

In order to estimate the importance of accessory minerals to the trace element modelling, fractions of whole rock REE concentration in each mineral are calculated from distribution coefficients and the modal composition of sample 51706 (Table 4-1), employing a similar method to one used by Watson (1979). If all minerals are equilibrated with each other, the relative level of REE in the minerals is obtained from the solid/solid distribution coefficient. Thus the solid/solid distribution coefficients between minerals were calculated from mineral/melt distribution coefficients (Table 4-8). Then, multiplication of the relative REE level by the modal content (weight %) of each mineral yields weight fractions of REE in each mineral. The modal content of zircon is

Fig. 4-15. Estimated amounts of fractionated phase of the Sally Downs
Tonalite

Assuming the chemical composition of the parental tonalitic magma is similar to sample 32903 ($\text{SiO}_2=56.24\%$), the weight fraction of the fractionated phase is calculated for every one percent of SiO_2 from 58 to 69 %, covering the range of SiO_2 contents found in the Sally Downs Tonalite pluton. The weight proportions of the tonalite with each one percent of SiO_2 content are obtained from 146 analyses made to determine areal geochemical variation. Calculated weight fraction is indicated as relative mass of fractionated phase in this figure.

Results of calculation indicate the fractionated phase, with dioritic composition, is 27.6 wt% of the parental tonalitic magma.

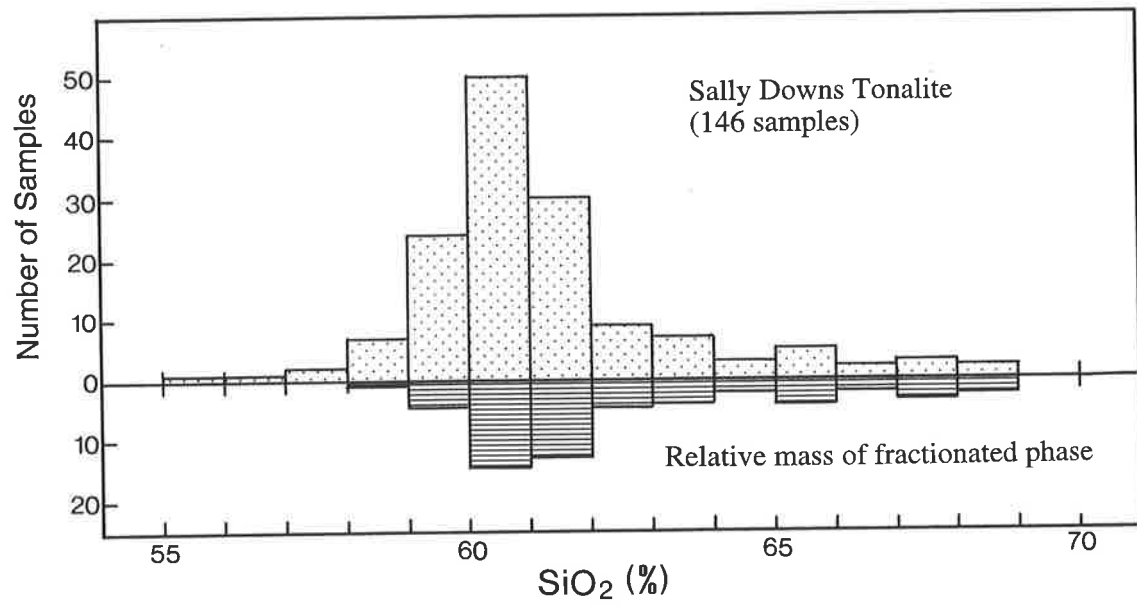


Table 4-8. Summary of distribution coefficient of rare earth element, used in the model calculation

	Hornblende	Biotite	Plagioclase	Apatite	Zircon	Allanite
Ce	0.90	0.037	0.183	34.7	2.64	635
Nd	2.80	0.044	0.173	57.1	2.20	463
Sm	3.99	0.058	0.100	62.8	3.14	205
Eu	3.44	0.145	0.814	30.4	3.14	81
Gd	5.47	0.082	0.0875	56.3	12.00	130
Yb	4.90	0.179	0.054	23.9	270.00	8.9
Ref.	1*	2*	1*	3*	3*	4*

References

- 1*: Arth and Barker (1976)
- 2*: Arth and Hanson (1975)
- 3*: Nagasawa (1970)
- 4*: Brooks et al. (1981)

estimated as 0.003% from consideration of the Zr content of the sample. Epidote is not included in the calculation, since no mineral/melt distribution coefficients are available. Thus the result may slightly overestimate REE contents in the other minerals.

Fig. 4-16 illustrates the result of the calculation, indicating the following points:

- (1) More than 40% of LREE and about 30% of HREE are accommodated in accessory minerals, although these are modally only 0.51% of total the rock.
- (2) Allanite carries about 20% of the LREE but very small amounts of HREE, while zircon holds about 20% of the HREE.
- (3) Considerable amounts of REE are present in apatite.
- (4) Hornblende is the greatest carrier of the REE, especially HREE.
- (5) More than half the Eu is present in plagioclase.

Although apatite and zircon contain large concentrations of REE, because they are present as small evenly distributed crystals, unlike allanite, no significant sampling problem is expected.

REE concentrations for each mineral can now be estimated from the above weight fraction results and whole rock REE contents. Fig. 4-17 illustrates estimated chondrite normalized REE pattern of the minerals. The level of Ce in the allanite (10^5 times of chondritic Ce; 9.5% of Ce_2O_3) is in good agreement with the microprobe result (Ce_2O_3 : 5.7-22.7%), indicating validity of the calculation used. Similar REE patterns of minerals from a quartz diorite are presented by Fourcade and Allegre (1981), although Hart and Allegre (1980) argued that a ratio of bulk concentrations cannot be calculated from the distribution coefficients. However, since the estimated REE compositions of minerals in the present work are based on the assumption that the solid/solid distribution coefficient would give ratios of bulk REE concentration between

Fig. 4-16. Rock budget of REE in sample, 51706, from the Sally Downs
Tonalite

Weight fraction of REE in each mineral is calculated from K_d values and modal composition of minerals, assuming equilibrium.

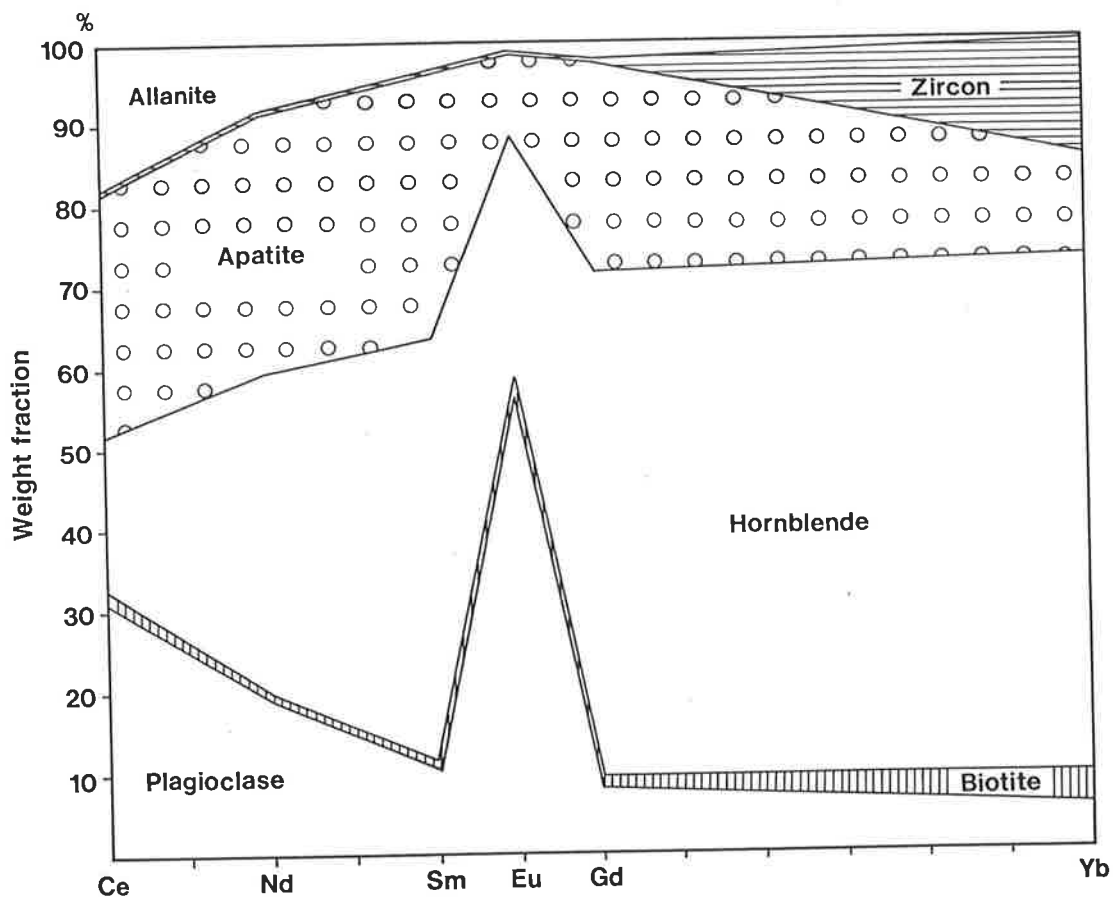
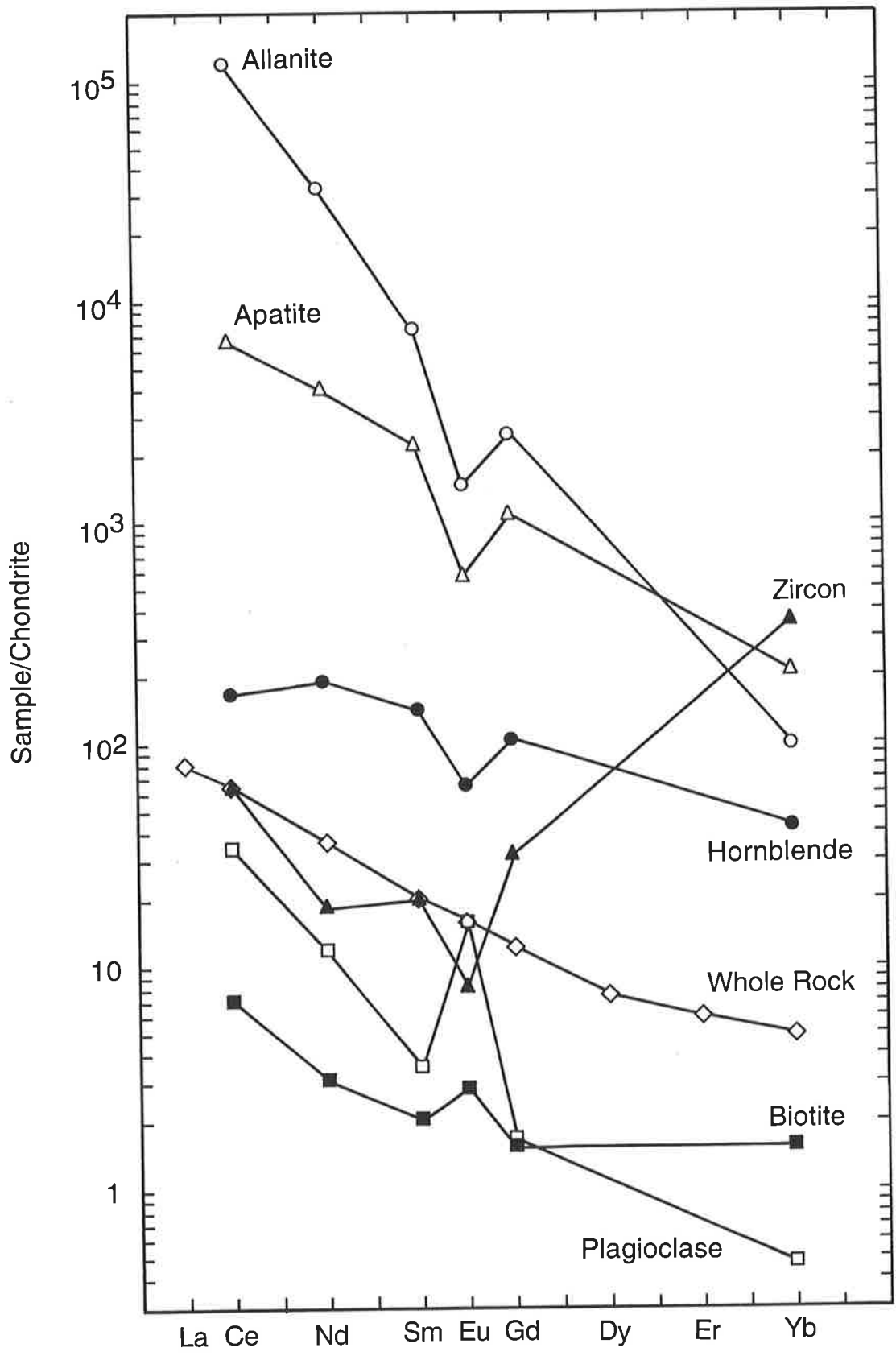


Fig. 4-17. Estimated REE composition of minerals

REE concentrations for each mineral were estimated from the weight fraction calculation of Fig. 4-16 and whole rock REE contents.

Concentration normalized to chondrite.



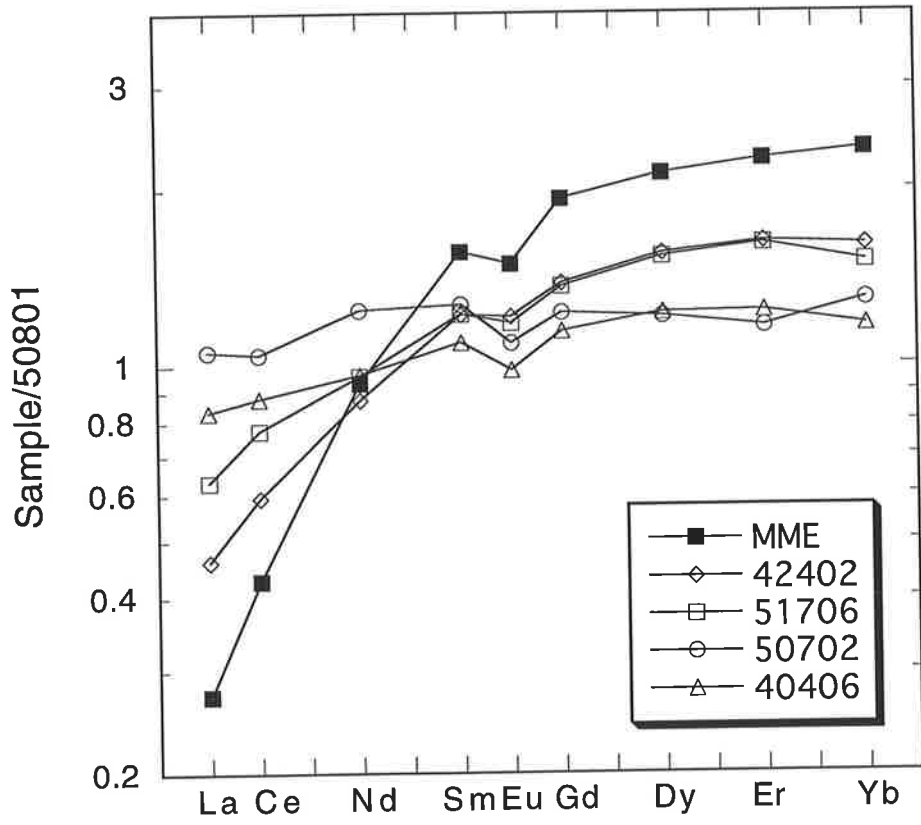
minerals, a good agreement of REE compositions of minerals between the estimated and the observed values suggests validity of the assumption in contrast to Hart and Allegre's (1980) interpretation. Although some minerals in the Sally Downs Tonalite have compositional zoning, the estimated REE composition would be an average value.

As illustrated in Fig. 4-17, most of accessory minerals have a higher REE concentration than the whole rock value, thus the fractionation of the accessory minerals should significantly decrease the bulk rock REE contents. Even small amounts of allanite as a fractionated phase would deplete the LREE (e.g., Miller and Mittlefehldt, 1982). However, in the Sally Downs Tonalite, LREE contents increase with SiO₂ increase (see earlier) and hence fractionation, thus indicating that allanite has not been a fractionated phase; instead, allanite as a late crystallization phase to accommodate LREE. Therefore, allanites are found abundantly in samples with high LREE. HREE depletion with the fractionation may be due to fractionation of either hornblende or zircon.

When REE of samples from the Sally Downs Tonalite are normalized to the acidic tonalite (50801), the normalized pattern gives an indication of the bulk solid-melt distribution coefficient of the fractionated phase. The normalization of REE data to a sample from the same suite was introduced by Hanson (1978) to obtain the distribution coefficient of the possible fractionated phase. Fig. 4-18 indicates that distribution coefficients of the fractionated phase have a value of more than one for middle and heavy REE, and less than one for LREE. Although absolute levels of the 50801-normalized value of four samples are different between samples (Fig. 4-18), the relative shapes of the normalized patterns for the samples are the same, indicating fractionation of similar phases throughout the crystallization sequence. A small negative Eu anomaly is present in the normalized patterns (Fig. 4-18).

Fig. 4-18. REE patterns, normalized to tonalite (50801)

MME: mafic microgranular enclave, sample 51702.



These patterns are very similar to those representing the mineral-melt distribution coefficient of hornblende (Fig. 4-19), indicating that hornblende is a possible fractionating phase to control REE distribution of the tonalite. Absolute values of distribution coefficients are greatly dependent on liquid composition, possibly on temperature of the liquid, and some other factors, but relative levels of distribution coefficient between one REE and another generally do not change, i.e., a shape of distribution coefficients of REE on Fig. 4-19 remains the same for any melt compositions.

As illustrated by Fig. 4-18, Nd contents stay constant for most of samples, indicating that the bulk distribution coefficient for Nd is unity during the tonalite fractionation. The hornblende Nd coefficient for the andesitic liquid (Nicholls and Harris, 1980) is close to unity; thus the removal of the hornblende with the distribution coefficients similar to those described by Nicholls and Harris (1980) could explain ranges of the REE patterns in the Sally Downs Tonalite. Furthermore if plagioclase and/or biotite accompany hornblende as fractionated phases, the bulk distribution coefficient of the hornblende would be reduced, but essentially the shape of the distribution coefficient pattern would remain the same, as the plagioclase and biotite have a low distribution coefficient with flat pattern except for Eu. Therefore, even if the hornblende coefficient for Nd is more than unity, such as found in dacite (Fig. 4-19), the bulk distribution coefficient could be reduced to unity by addition of plagioclase and/or biotite as fractionated phases. This interpretation agrees well with the fractionation model based on major element data described in section 4.5.1.

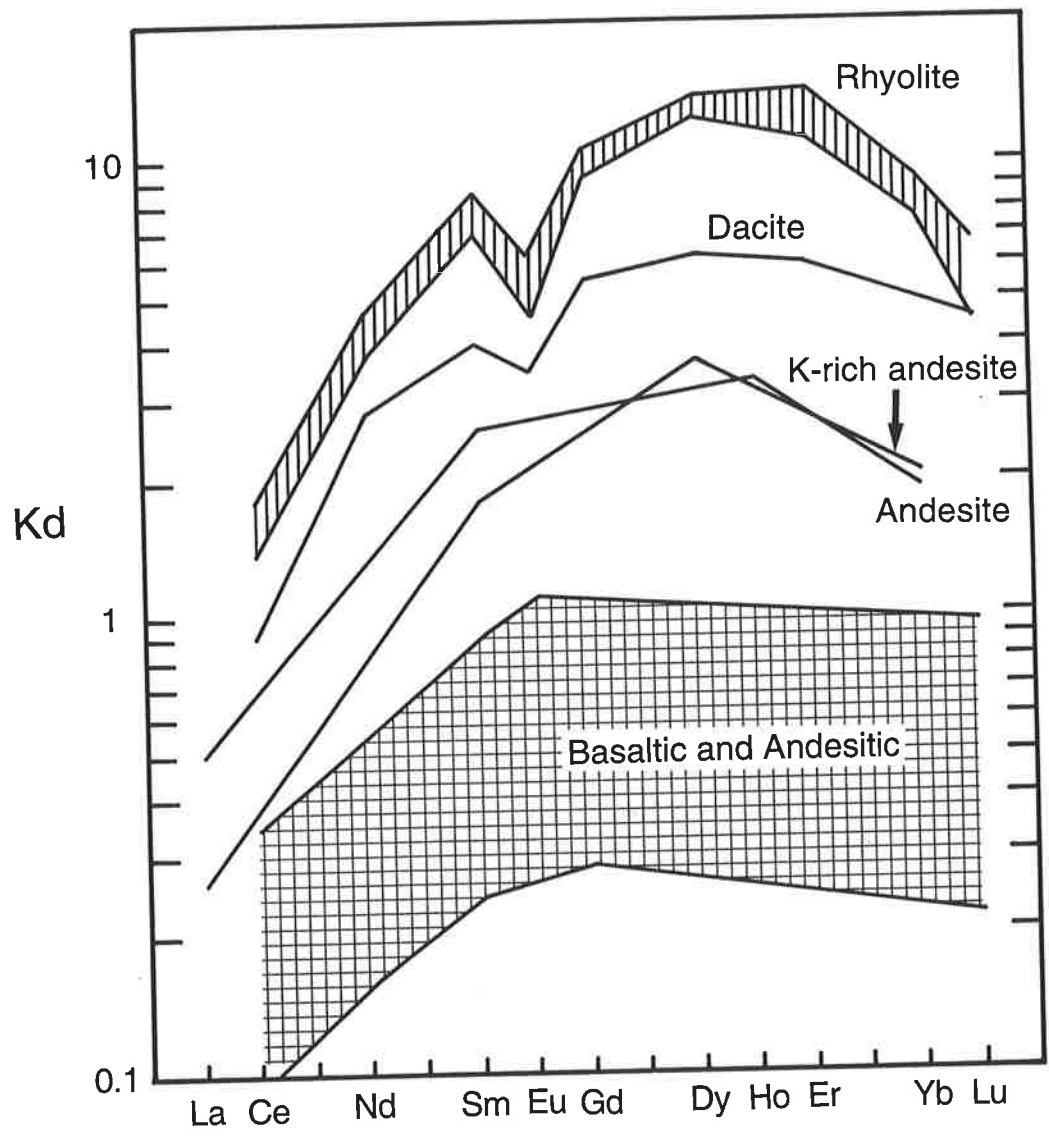
4.6. Petrology of Mafic Microgranular Enclaves and Syn-plutonic Dyke

Fig. 4-19. REE Kd values of hornblende

Hornblende Kd for dacite composition is from Arth and Barker (1976).

Kd's for andesite and K-rich andesite are from Nicholls and Harris (1980).

Kd's for other compositions are from Hanson (1980).



4.6.1. Petrography

A. Mafic Microgranular Enclaves

Mafic microgranular enclaves in the Sally Downs Tonalite are quartz diorite, consisting of similar minerals to the host tonalite, but in different proportions, viz. higher contents of mafic minerals and lower contents of quartz than the host (Table 4-1). They are typically fine grained and have hypidiomorphic granular texture (Fig. 4-2E and F). Occasionally, porphyritic plagioclase phenocrysts, up to 6mm in length, are found.

B. Syn-plutonic Basic Dyke

Fine grained amphibolite comprises the syn-plutonic basic dyke, consisting largely of blue green hornblende and plagioclase, and lesser amounts of quartz and biotite. Accessory minerals include apatite, zircon, and opaque minerals. Some of the hornblende is grouped into glomeroporphyritic aggregates (Fig. 4-2G and H), especially near the margin of the dyke.

4.6.2. Mineral chemistry

Three samples from the mafic microgranular enclaves and two samples from the syn-plutonic basic dyke are selected for electron microprobe analysis. Sample locations are given in Fig. 4-20. The chemical compositions of minerals are listed in Table A8-1, and representative chemical compositions of hornblende and biotite are given in Table 4-3.

Hornblende

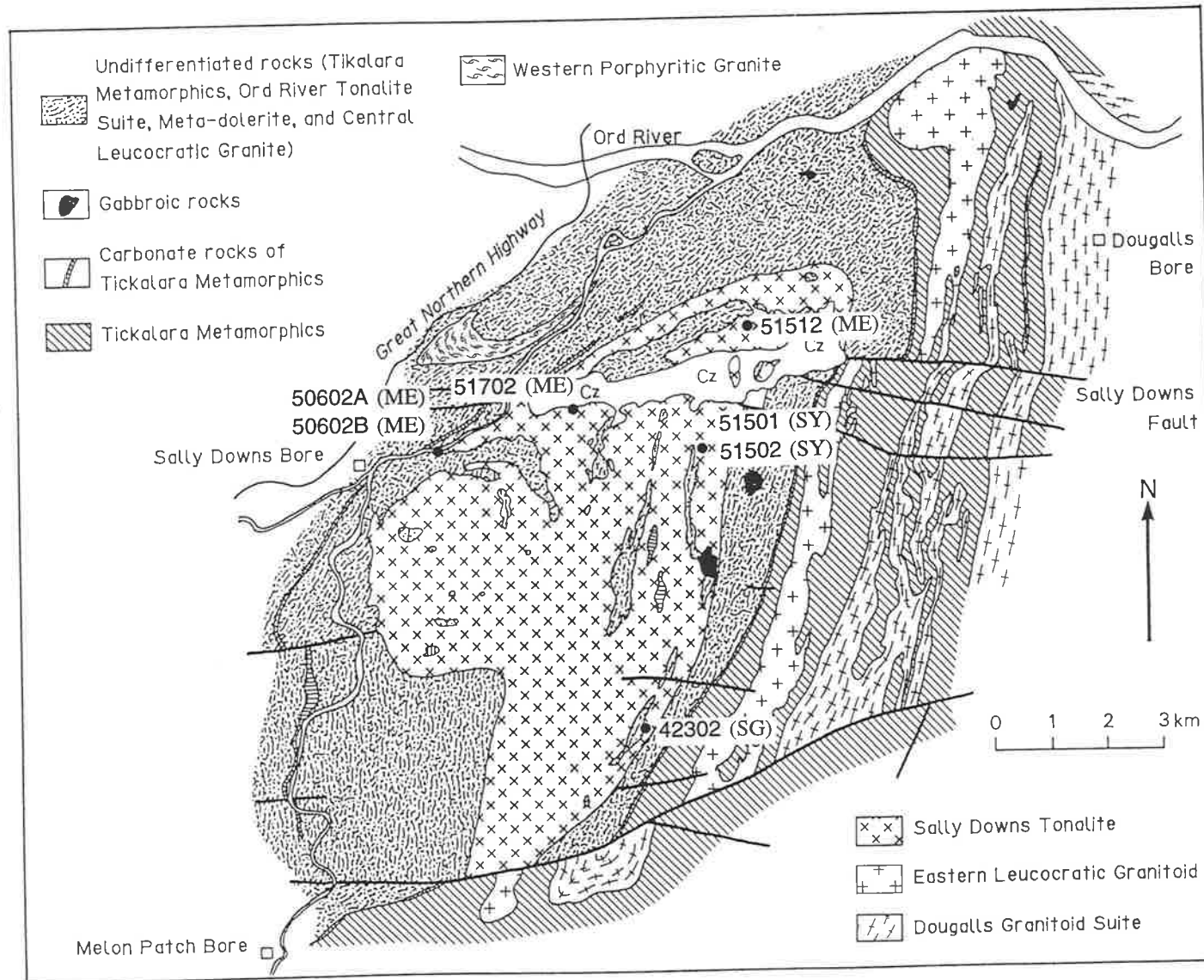
Most of the hornblende in the mafic microgranular enclaves are magnesio-hornblende or ferro-hornblende as classified by Leake (1968). Mg/Mg + Fe ratios of the hornblende range from 0.476 to 0.521. Although mafic microgranular enclaves have low SiO₂ contents (56.3 -

Fig. 4-20. Sample locality map for mafic microgranular enclaves, syn-plutonic basic dyke, and granite dyke in the Sally Downs Tonalite pluton

ME: mafic microgranular enclave

SY: syn-plutonic basic dyke

SG: granite dyke



56.6%, see section 4.6.3.) similar to that of low SiO₂ tonalite, the Mg/Mg + Fe ratios of the hornblende in the mafic microgranular enclaves are lower than those of hornblende in low SiO₂ tonalite, but similar to the Mg/Mg + Fe ratios of the hornblende in the host tonalite (Table 4-3 and see hornblende Mg/Fe + Mn + Mg in Fig. 4-3A). This feature suggests the composition of the hornblende in the mafic microgranular enclaves was largely controlled by the chemistry of the host tonalite.

The hornblende in the syn-plutonic basic dyke is magnesio-hornblende. Mg/Mg + Fe ratios of the hornblende are higher than those of the hornblende in the Sally Downs Tonalite (less than 0.550), having the average ratio 0.590.

Biotite

Mg/Mg + Fe ratios of biotite in the mafic microgranular enclaves range from 0.539 to 0.578. The ratios are not different from those of biotite in the host tonalite, thus supporting the likelihood of equilibration of mineral chemistry of the enclaves with that of the host tonalite magma. TiO₂ contents of the biotites are between 1.78 and 2.02 %.

Mg/Mg + Fe ratios of the biotite in the syn-plutonic basic dyke range from 0.599 to 0.623 with an average of 0.613.

Plagioclase

Plagioclase in the mafic microgranular enclaves are slightly more calcic than those in the host tonalite, ranging from An 37.5 to An 48 (Fig. 4-3C). Considerable compositional variation is found within samples; this reflects the presence of oscillatory zoned phenocrysts in the enclaves.

Anorthite contents in the syn-plutonic basic dyke range from An 41 to An 45, averaging An 43. The values are significantly lower than those in the meta-dolerite (generally, >An 70).

4.6.3. Geochemistry

A. Major elements

Mafic microgranular enclaves

The SiO₂ content of the mafic microgranular enclaves (Table 4-9) ranges from 56.3 to 56.6%. On the variation diagram (Fig. 4-21), most of the major elements are located in the same field as those of the host tonalite, thus supporting a comagmatic origin of the mafic microgranular enclaves and host tonalite.

Syn-plutonic basic dyke

The chemical compositions of two samples from the syn-plutonic basic dyke also are presented in Table 4-9. SiO₂ contents of the two samples are 51.05 and 51.72%. Mg-values are 60 and 62, indicating that samples have experienced only minor crystal fractionation (Perfit et al., 1980b). They are tholeiitic according to the FeO*/MgO versus SiO₂ and FeO*/MgO versus FeO* discrimination diagrams of Miyashiro (1974). There are large compositional differences between the syn-plutonic basic dyke and the host tonalite; for example, significantly low Al₂O₃ contents (14%) are found in the syn-plutonic basic dyke in comparison with that (19%) in the basic tonalite. Compared with the meta-dolerite (Table 3-10), the syn-plutonic basic dyke has lower CaO and higher Na₂O and K₂O.

B. Trace elements

Mafic microgranular enclaves

The trace element contents of the mafic microgranular enclaves are mostly similar to those in the host tonalite (Table 4-9). The chondrite normalized pattern of the mafic microgranular enclave (51702), presented in Fig. 4-12, has lower LREE and higher HREE than the host tonalite; in other words the chondrite normalized pattern of the mafic

Table 4-9. Chemical compositions of Mafic microgranular enclaves and Syn-plutonic basic dyke in the Sally Downs Tonalite

Unit	Mafic microgranular enclaves				Syn-plutonic dyke		SDT
Sample	50602A	50602B	51512	51702	51501	51502	51706
Major elements (wt%)							
SiO ₂	56.27	56.27	56.31	56.56	51.72	51.05	60.69
Al ₂ O ₃	18.06	17.93	18.37	18.35	14.25	13.94	17.79
Fe ₂ O ₃ *	7.36	7.62	7.34	7.17	11.04	11.27	5.84
MnO	0.13	0.12	0.12	0.12	0.16	0.17	0.07
MgO	3.65	3.49	3.39	3.50	7.53	8.39	2.67
CaO	6.82	6.78	6.87	7.14	9.04	9.17	6.08
Na ₂ O	4.09	4.08	4.00	3.94	2.38	2.39	4.03
K ₂ O	1.81	1.95	1.74	1.29	1.11	1.14	1.45
TiO ₂	0.90	0.94	0.84	0.85	1.12	1.12	0.69
P ₂ O ₅	0.25	0.25	0.19	0.18	0.18	0.18	0.19
LOI	0.70	0.74	0.68	0.58	0.81	0.89	0.58
Total	100.04	100.17	99.85	99.68	99.34	99.71	100.08
Trace elements (ppm)							
Ba	557	592	461	472	257	251	258
Rb	53	57	48	31.9	22.7	25.2	41.6
Sr	541	529	597	610	389	388	613
Zr	135	146	135	123	78	71	135
Nb	8.1	8.4	7.8	6.9	6.1	5.5	5.3
Y	20.7	23	26	17.9	13	13.9	11.3
Ce	56	47	26	30	46	40	54
Nd	31	32	25	22	24	23	22
Sc	20.9	22.2	24.3	25.7	27.6	29.1	15
V	124	128	119	116	196	202	94
Cr	57	58	45	47	496	624	27
Ni	31.7	33.3	29.2	29	216	235	19
Cu	113	120	90	52	56	60	36
Zn	83	85	85	82	91	91	66
Ga	N.D.	N.D.	N.D.	21.9	N.D.	N.D.	22.4
A/CNK	0.857	0.848	0.877	0.88	0.661	0.638	0.924
Rb/Sr	0.098	0.108	0.08	0.052	0.058	0.065	0.068
Ti/Zr	40.6	38.8	37.7	14.8	86.3	96.6	27.4

SDT: Sally Downs Tonalite, a sample 51706 is a host of enclave, 51702.

Fe₂O₃*: Total Fe as Fe₂O₃, LOI: Loss on ignition

N.D.: Not determined, A/CNK: Mol(Al₂O₃/(CaO+Na₂O+K₂O))

Fig. 4-21. Major element variation diagram of Mabel Hill Tonalite, a sample from the main body of the Mable Downs Granitoid, and mafic microgranular enclaves in the Sally Downs Tonalite

- A. $\text{Al}_2\text{O}_3\text{-SiO}_2$
- B. $\text{Fe}_2\text{O}_3^*\text{-SiO}_2$
- C. MgO-SiO_2
- D. CaO-SiO_2
- E. $\text{Na}_2\text{O-SiO}_2$
- F. $\text{K}_2\text{O-SiO}_2$
- G. $\text{TiO}_2\text{-SiO}_2$
- H. $\text{P}_2\text{O}_5\text{-SiO}_2$

Open square: Mabel Hill Tonalite.

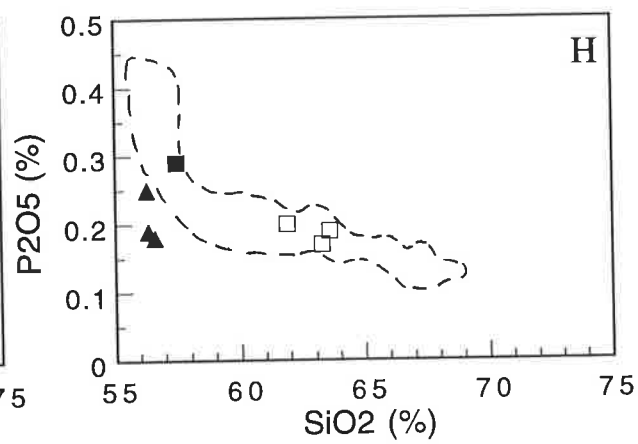
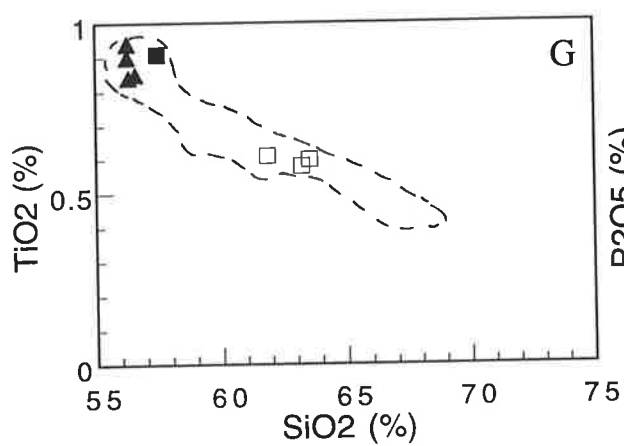
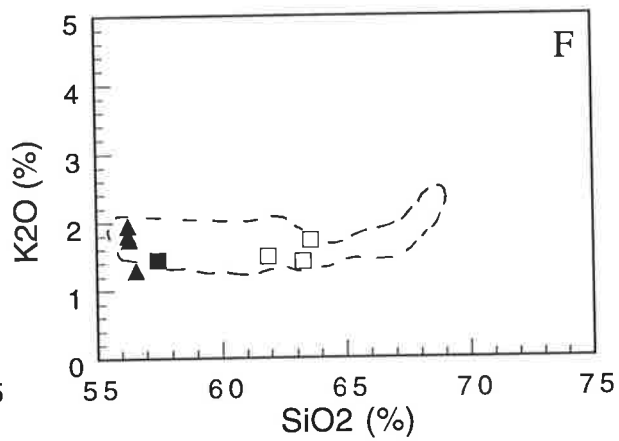
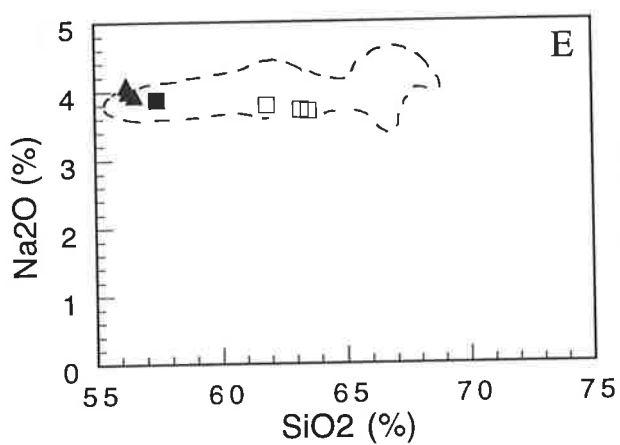
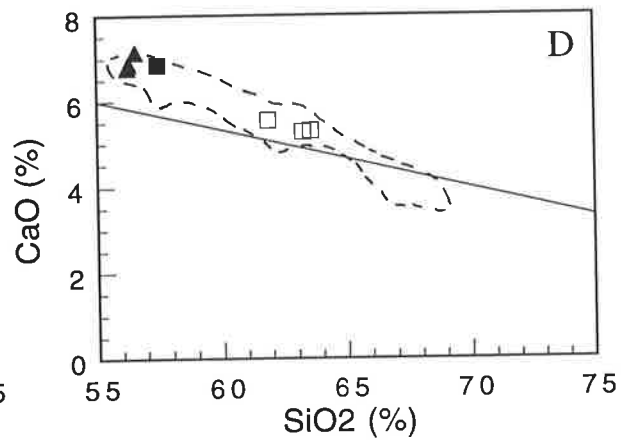
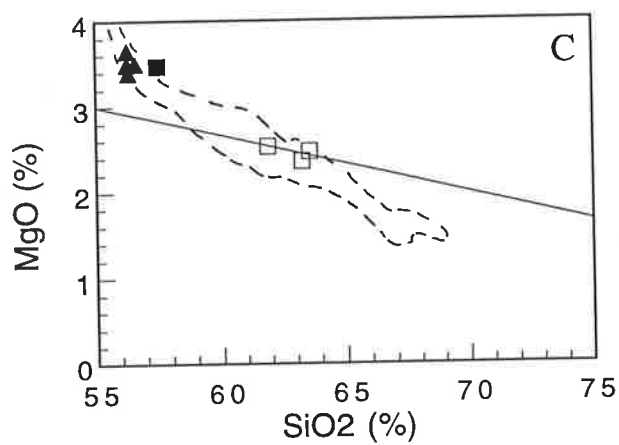
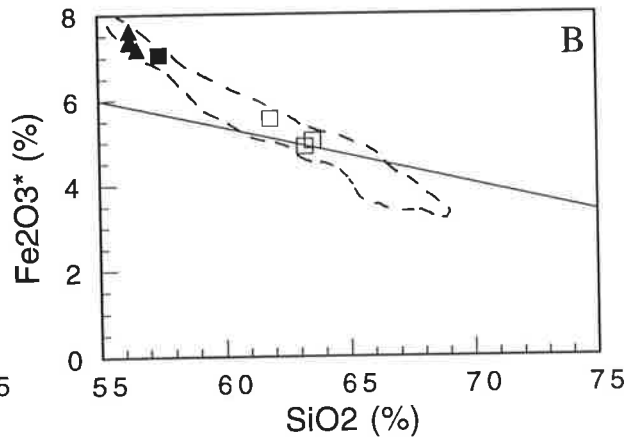
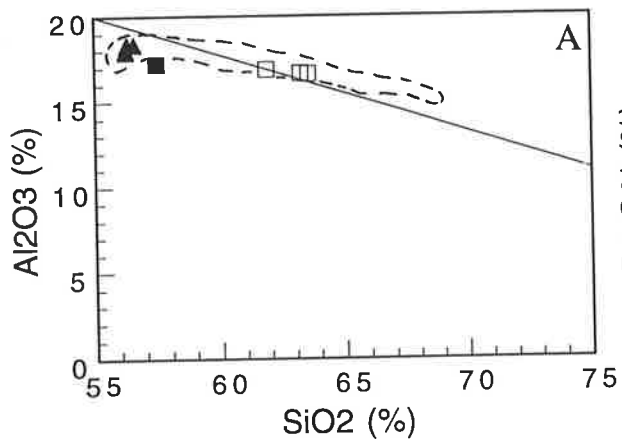
Solid square: a sample (52006) from the main body of the Mabel Downs Granitoid.

Solid triangle: samples from the mafic microgranular enclaves in the Sally Downs Tonalite.

Field marked by broken line is the compositional range found in the Sally Downs Tonalite

Reference lines in the diagrams A., B., C., and D., show effect of constant sum, and are drawn from a point representing 100% SiO_2 and 0% of the other element extrapolated into the diagram. See section 3.4.3 for detail discussion of the lines.

Fe_2O_3^* : total Fe as Fe_2O_3



microgranular enclaves is less fractionated than that of the host tonalite. A slight negative Eu anomaly ($\text{Eu}/\text{Eu}^* = 0.948$) suggests the influence of residual or crystallizing feldspar, or, most likely, of cumulate hornblende incorporated in the mafic microgranular enclaves.

Syn-plutonic basic dyke

High Cr contents are found in samples from the syn-plutonic basic dyke, viz. 496 and 624ppm (Table 4-9). Similarly, Ni contents are high, viz. 216 and 235ppm. As indicated already by the Mg-values, these high Cr and Ni contents further support the conclusion that the samples have not experienced extensive crystal fractionation.

Average concentrations of Ba, Rb, and Sr are 254, 24 and 389ppm, respectively, for the syn-plutonic basic dyke. The values are about half of those of the Sally Downs Tonalite, but are significantly higher than those of the meta-dolerite (Table 3-10). Because these elements are relatively mobile, they could have been modified by the host tonalite as the tonalite was supposedly to be still hot when the basic magma was intruded.

Ti/Zr ratios (86 and 97) are slightly lower than the chondritic Ti/Zr ratio of 110 (Sun and Nesbitt, 1977). Y contents are 13 and 13.9ppm in the syn-plutonic basic dyke samples, indicating that HREE's are about 6 times chondritic value. The chondrite normalized Ce/Y ratios of 7.8 and 9.6, manifest a LREE enriched composition.

4.6.4. Origin of Mafic Microgranular Enclaves in the Sally Downs Tonalite

Based on field observations and petrological data, the origin of the mafic microgranular enclaves in the Sally Downs Tonalite, discussed in this section, provides some constraint concerning the petrogenetic model of the tonalite.

Granitoids often contain pieces of exotic material, and the term "enclave" is commonly used to describe them (Didier and Barbarin, 1991). Classification and terminology of various different enclaves are given in Chapter 1. The origin of enclaves in granitoids is discussed by many workers, e.g. Vernon (1984) and Barbarin and Didier (1991). Vernon (1984) showed that enclaves could originate in a variety of ways, e.g. as cumulate material, restite, the marginal part of the granitoid pluton, and accidental xenoliths. Any of these mechanisms may explain the origin of the mafic microgranular enclaves. Vernon (1984) maintained that the fine grain size of mafic microgranular enclaves is in accord with the likelihood that such material is derived from the quenched marginal part of a host granitoid pluton, since this would be expected to have a finer grain than the more central parts of the pluton. Vernon (1984) also presented an alternative model for the origin of the mafic microgranular enclaves, viz. the enclaves represent globules of mafic magma that have mingled and quenched in the granitoid host magma. More recent investigations further suggest (following Vernon) that mafic microgranular enclaves may be produced by hybridization of a mafic magma by a felsic magma, accompanied by various processes such as quenching, mingling, and mixing of the magmas (e.g. Dorais et al., 1990, Poli and Tommasini, 1991, Barbarin and Didier, 1991).

The chemical composition of the mafic microgranular enclaves in the Sally Downs Tonalite is similar to that of the basic part of the host tonalite, but the indications of hybridization of a mafic magma by a tonalitic magma in the Sally Downs Tonalite body are not clear. The similar chemical composition of hornblende in the mafic microgranular enclaves to that of hornblende in the host tonalite indicates reequilibration and modification of the mafic microgranular enclaves by the tonalite melt. The reequilibration and modification of the enclaves is thus likely

to obscure the origin of the enclaves. On the other hand, the occurrence of the syn-plutonic basic dyke in the Sally Downs Tonalite indicates clearly the presence of a coeval mafic magma. The granitoid magma can be generated by partial melting of lower crustal material by the heat derived from the injection of mafic magma into the lower crust. In assuming this type of magma generation model for the Sally Downs Tonalite, hybridization of the mafic magma by the tonalitic magma is a likely process for the origin of the mafic microgranular enclaves. It is difficult to accept an unequivocal origin for the enclaves but the following two models explain most of the field occurrences and petrological characteristics of the mafic microgranular enclaves in the Sally Downs Tonalite.

(1) the mafic microgranular enclaves are originated from the fine grained marginal part of the plutonic body.

(2) the mafic microgranular enclaves have produced by the hybridization of mafic magma by granitoid magma.

4.7. Petrology of Tonalites from Mabel Hill and the Main Body of the Mabel Downs Granitoid Suite

4.7.1. Petrography

Tonalite from the main body of the Mabel Downs Granitoid Suite (sample location in Fig. 2-20) consists largely of plagioclase, quartz, blue green hornblende, biotite (α = straw yellow, β = γ = yellowish brown), and epidote. Accessory minerals are sphene apatite, zircon, allanite, and opaque minerals. It is coarse grained, and has hypidiomorphic granular texture. Since no K-feldspar is found in the rock, it is classified as a tonalite. Chemical compositions of hornblende and biotite are presented in Table A8-1. The amphibole is magnesio-hornblende or edenitic hornblende, according to Leake (1968).

The Mabel Hill Tonalite is a coarse grained hypidiomorphic granular rock, and is composed of plagioclase, quartz, biotite (α = pale yellow, β = γ = greenish yellow brown), blue green hornblende, and epidote. Accessory minerals include zircon, apatite, opaque minerals, and rare allanite. Plagioclase is subhedral and typically shows oscillatory zoning.

4.7.2. Geochemistry

Three samples of Mabel Hill Tonalite and a sample from the main body of the Mabel Downs Tonalite are examined. Major and trace element data are presented in Table A4-7.

Mol ($\text{Al}_2\text{O}_3/(\text{CaO} + \text{Na}_2\text{O} + \text{K}_2\text{O})$) ratios in the Mabel Hill Tonalite range from 0.940 to 0.965, and are similar to those in the Sally Downs Tonalite. The ratio in the tonalite from the main body is 0.844, thus slightly lower than the ratios in the Sally Downs Tonalite. All four tonalites are within the range of the I-type granitoids in terms of mol ($\text{Al}_2\text{O}_3/(\text{CaO} + \text{Na}_2\text{O} + \text{K}_2\text{O})$). Furthermore, high $\text{Na}_2\text{O}/\text{K}_2\text{O}$ ratios in the tonalites, ranging from 2.14 to 2.69, are similar to those of the I-type granitoids. Thus, the chemical characteristics suggest that the tonalites are not derived from the partial melting of sedimentary rocks.

The SiO_2 contents of the Mabel Hill Tonalite range from 61.87 to 63.55%. The range is slightly higher than the mean value (about 61.2%) of the Sally Downs Tonalite. This fact could indicate that only the acidic part of the Mabel Hill Tonalite pluton is now exposed, and may have the more basic part of the pluton underneath, thus accounting for the smaller size of the pluton compared with the main body and Sally Downs Tonalite of the Mabel Downs Granitoid Suite.

Major element variation diagrams are shown in Fig. 4-21. Most of the data occur within the range depicted by the Sally Downs Tonalite, indicating that a similar petrogenesis to that of the Sally Downs Tonalite

could be applied to the above tonalites. A slightly lower Al_2O_3 content in the tonalite from the main body of the Mabel Downs Suite accounts for the lower mol ($\text{Al}_2\text{O}_3/(\text{CaO} + \text{Na}_2\text{O} + \text{K}_2\text{O})$) ratio.

Similar trace element compositions to that of the Sally Downs Tonalite also are found (Table A4-7). There is no significant difference between the Rb and Sr contents (Rb = 44ppm, Sr = 575ppm) analyzed by Bofinger (1967) and values from sample 52006 (Rb = 44.2ppm, Sr = 588ppm) which was collected from the same locality.

K/Rb ratios range from 270 to 296, and Rb/Sr ratios 0.069 to 0.075. The ratios are similar to those of the Sally Downs Tonalite.

The similarity of major and trace element compositions among the Mabel Hill Tonalite, the tonalite from the main body of the Mabel Downs Granitoid, and the Sally Downs Tonalite supports that those can be grouped together in a same granitoid suite

CHAPTER 5. PETROLOGY (PART 3): PETROLOGY OF THE SOPHIE DOWNS GRANITOID, BOW RIVER GRANITOID, GRANITOIDS FROM THE KING LEOPOLD MOBILE ZONE, AND WHITEWATER VOLCANICS

5.1. Introduction

This chapter mainly describes the petrology of the Sophie Downs Granitoid and Bow River Granitoid. Although the Bow River Granitoid is the largest granitoid body in the Halls Creek Mobile Zone, only four samples are geochemically examined in this thesis. Previous petrological investigation of the Bow River Granitoid made by Gemuts (1971) presented only major element data of whole rock analyses, therefore it is important to have trace and additional major element data of the granitoid for petrogenetic interpretation. In addition to the descriptions of these granitoids, the petrology of granitoids from the King Leopold Mobile Zone and Whitewater Volcanics from the Halls Creek Mobile Zone are included in this chapter.

5.2. Sophie Downs Granitoid

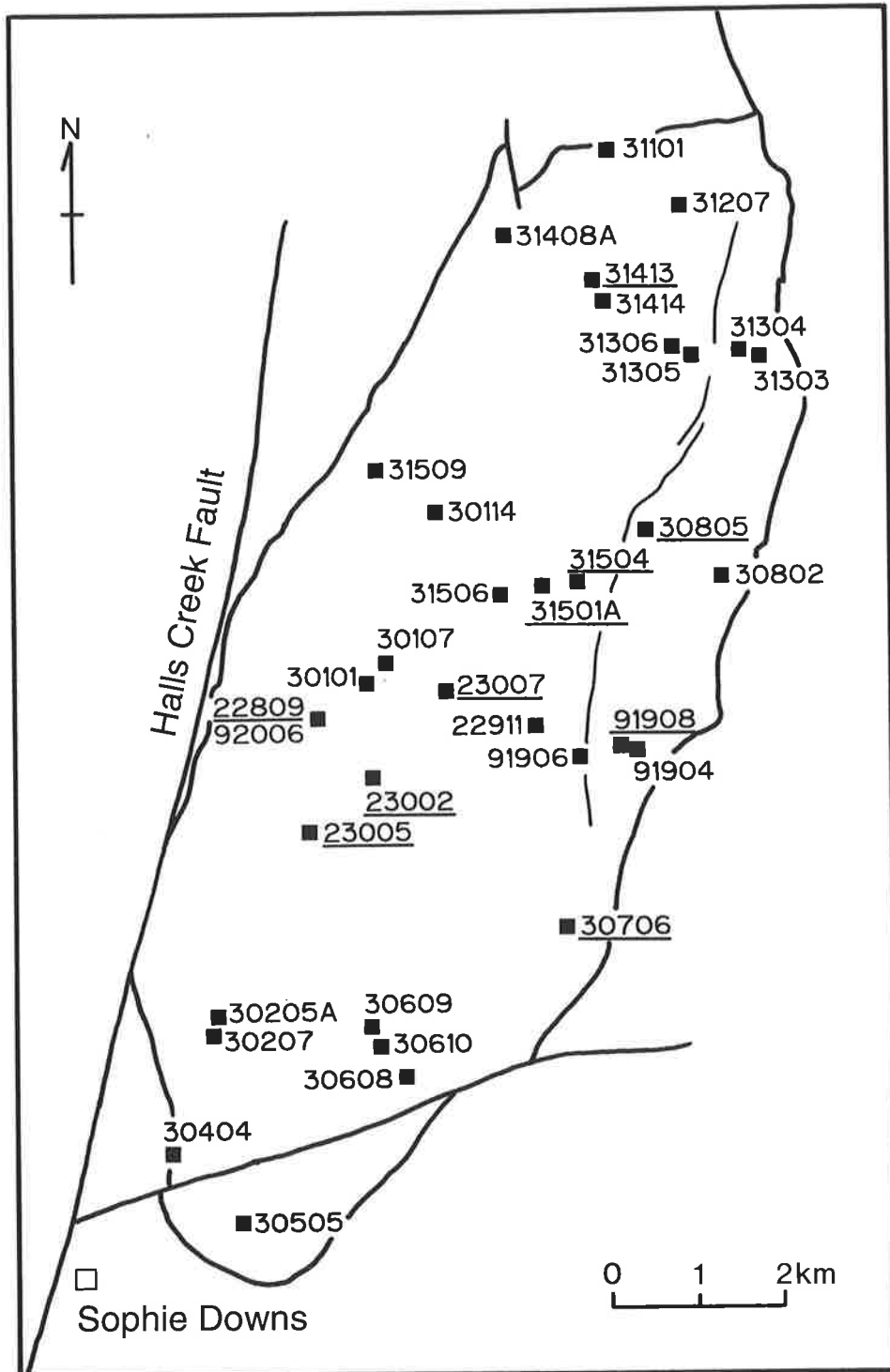
5.2.1. Petrography and Mineral Chemistry

35 samples were collected from the Sophie Downs Granitoid pluton for detailed petrographic and geochemical examinations (Fig. 5-1). One of these, 91906, is possibly an example of the granitoid metasomatised by quartz vein material, collected near the large quartz vein in the eastern part of the pluton.

The Sophie Downs Granitoid is an alkali-feldspar granite according to Streckeisen's classification (1976), consisting largely of quartz, K-feldspar, and plagioclase (Albite). It is very felsic, these minerals comprising more than 95% of the rock. The granitoid is texturally

Fig. 5-1. Sample locality map of the Sophie Downs Granitoid

Outline of the Sophie Downs Granitoid body is shown. See geology in Fig. 2-17. Sample number with underline indicates that the sample contains fluorite.



variable, but can be largely classified into four types, viz. coarse grained hypidiomorphic-granular rocks, granophyric rocks, fine grained inequigranular rocks, and strongly foliated fine grained rocks (Fig. 5-2).

Plagioclase is present as subhedral grains, commonly twinned according to the albite laws, and its An content is very low, ranging from 0.0 to 2.1 (Fig. 5-3A), thus placing the plagioclase in the field of albite.

K-feldspar occurs as small subhedral or anhedral grains of microcline, or large phenocrysts of perthite, or intergrowths with quartz. Rapakivi texture is seen rarely. Or content of the K-feldspar is generally between 90 and 97 (Fig. 5-3A).

Quartz is typically anhedral, but small rounded phenocrysts (about 1mm in diameter) are found in the fine grained inequigranular granitoids. Granophyric texture is characteristically present in samples from the eastern part of the pluton. In the granophyric rocks, quartz shows a plumose or radiating arrangement of vermicular blebs (Fig. 5-2D). These granophyric intergrowths may be the product of rapid crystallization from a few nuclei, or the result of devitrification (Barker, 1970).

Biotite (α = pale yellow, β = γ = greenish brown) is the only mafic silicate mineral in the granitoid, and occurs as small subhedral grains. Chemical analyses of the biotite (Table 5-1 and Table A8-1) show that it is low in Al_2O_3 (about 13.5%), close to that of annite-phlogopite (Fig. 5-3B). Fluorine contents of the biotite range from 1.72 to 2.67%, averaging 2.31%. These values are significantly higher than those of biotite from granitoids from northeast Japan (Kanisawa, 1979), and are comparable with those of biotite from Sn-bearing granitic rocks of Nigeria (Imeokparia, 1981).

More than accessory amounts of muscovite (up to 3%) are present. Irregularly shaped grains indicate secondary origin, but it is not clear

Fig. 5-2. Photomicrographs of the Sophie Downs Granitoid

A. Coarse grained variety of the Sophie Downs Granitoid

Sample: 30802. Qz: quartz

Plane polarized light. Scale bar is 5 mm.

B. Same as A, but under crossed polarized light.

Pl: plagioclase (albite), KF: K-feldspar

C. Medium grained variety of the Sophie Downs Granitoid with granophyric texture

Sample: 31303.

Plane polarized light. Scale bar is 5 mm.

D. Same as C, but under crossed polarized light.

Pl: plagioclase, Qz: quartz

E. Fine to medium grained variety of the Sophie Downs Granitoid

Sample: 23002. Bi: biotite, Opq: opaque mineral

Plane polarized light. Scale bar is 5 mm.

F. Same as E, but under crossed polarized light.

Pl: plagioclase, KF: K-feldspar, Qz: quartz

G. Fine grained variety of the Sophie Downs Granitoid

Sample: 30114.

Plane polarized light. Scale bar is 1 mm.

H. Same as G, but under crossed polarized light.

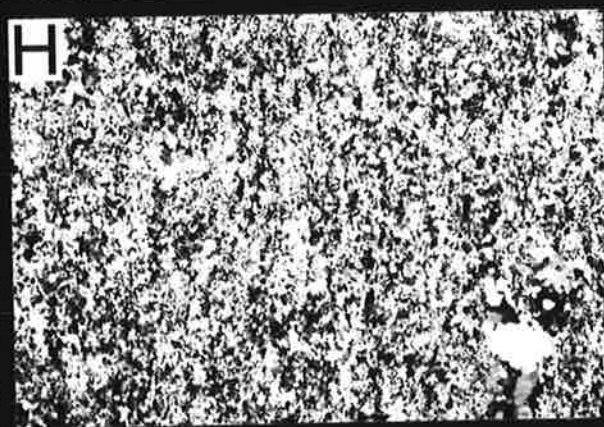
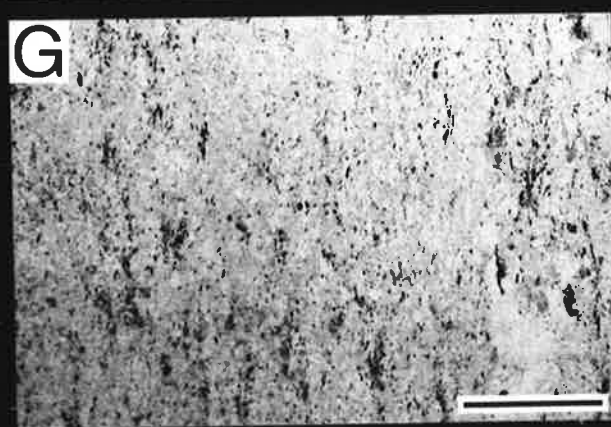
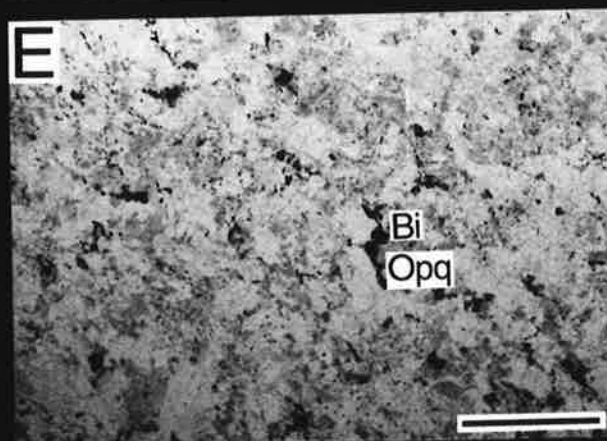
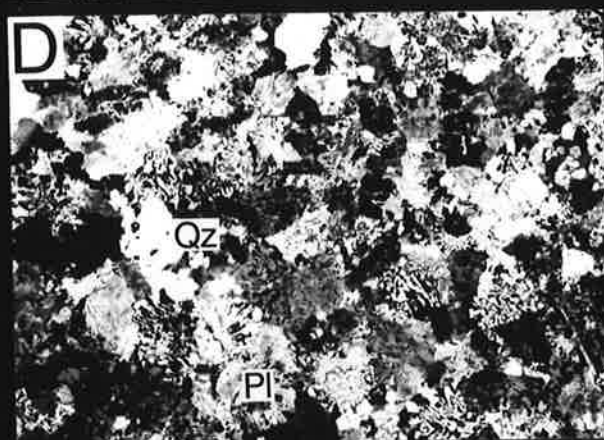
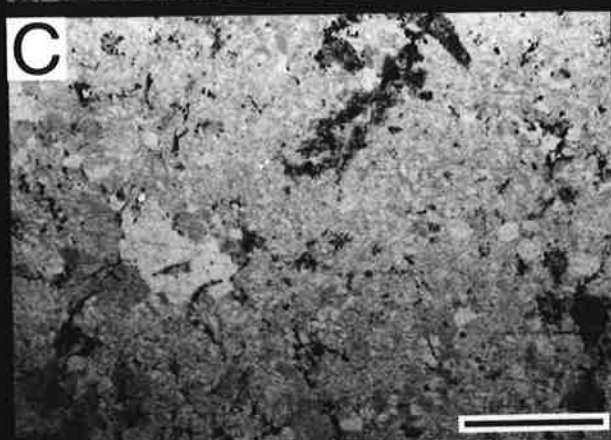
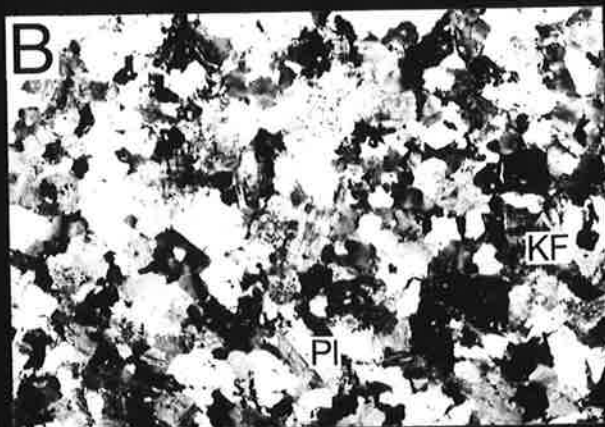
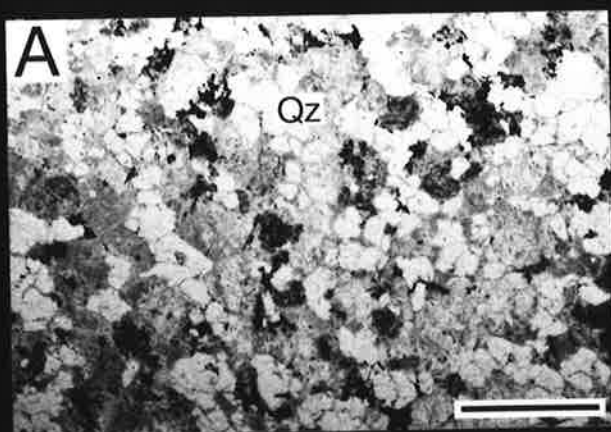


Table 5-1. Representative chemical compositions of biotite from Sample 30706 of the Sophie Downs Granitoid

Analysis	1	2	3	4	5	6	7	8
(wt%)								
SiO ₂	38.66	37.45	39.00	38.58	38.59	38.40	38.39	39.57
TiO ₂	1.50	1.52	1.52	1.68	1.57	1.29	1.28	1.23
Al ₂ O ₃	13.27	13.32	13.59	13.74	13.91	12.90	13.76	13.80
FeO*	19.15	18.78	19.69	19.21	19.67	17.00	18.43	18.85
MnO	0.23	0.14	0.26	0.25	0.26	0.27	0.31	0.29
MgO	12.34	12.03	12.77	12.22	12.33	13.55	12.88	13.31
CaO	0.00	0.00	0.00	0.00	0.00	0.00	0.00	0.00
Na ₂ O	0.00	0.09	0.05	0.00	0.07	0.06	0.00	0.00
K ₂ O	9.62	9.87	9.83	9.82	9.68	9.90	9.84	9.70
F	1.72	2.10	2.13	2.51	2.60	2.52	2.67	2.39
Total	96.49	95.30	98.84	98.01	98.68	95.89	97.56	99.14
Structural Formula (Number of oxygens = 22)								
Si	5.915	5.848	5.862	5.864	5.838	5.926	5.858	5.905
Al iv	2.085	2.152	2.138	2.136	2.162	2.074	2.142	2.095
Al vi	0.309	0.301	0.271	0.326	0.319	0.272	0.333	0.333
Ti	0.173	0.179	0.172	0.192	0.179	0.150	0.147	0.138
Fe	2.451	2.453	2.475	2.442	2.489	2.194	2.352	2.352
Mn	0.030	0.019	0.033	0.032	0.033	0.035	0.040	0.037
Mg	2.814	2.800	2.861	2.768	2.780	3.116	2.929	2.960
Ca	0.000	0.000	0.000	0.000	0.000	0.000	0.000	0.000
Na	0.000	0.027	0.015	0.000	0.021	0.018	0.000	0.000
K	1.878	1.966	1.885	1.904	1.868	1.949	1.915	1.847
Total	15.654	15.744	15.711	15.665	15.688	15.735	15.716	15.667
Mg/Mg+Fe	0.535	0.533	0.536	0.531	0.528	0.587	0.555	0.557

FeO*: Total Fe as FeO

Fig. 5-3. Compositions of feldspar and biotite from the Sophie Downs
Granitoid

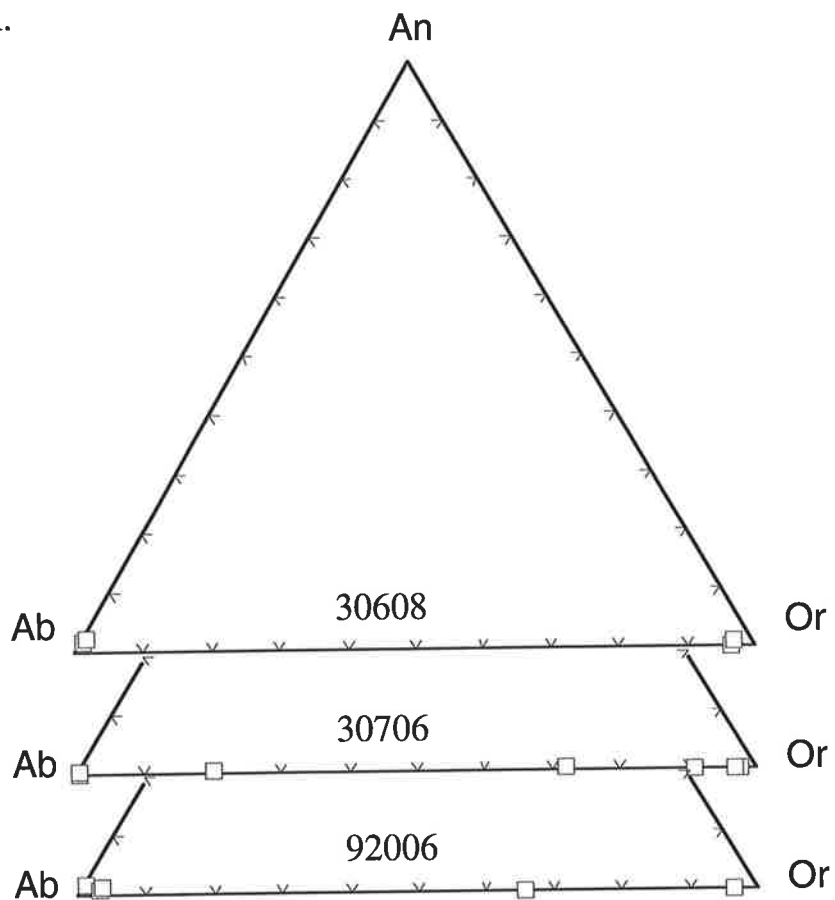
A. An-Ab-Or ternary plot of feldspar

B. biotite composition

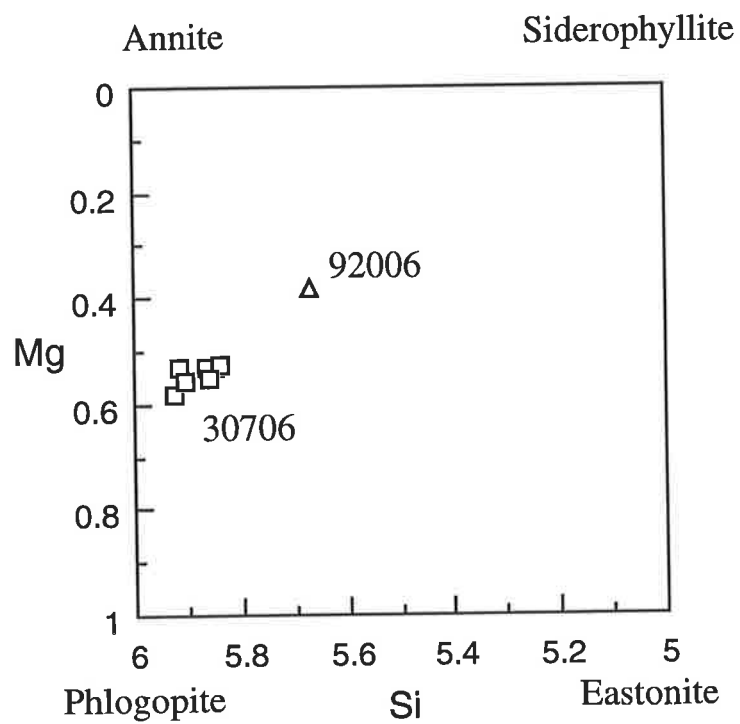
Si: Si value in the structural formula of 22 oxygens.

Mg: $Mg/Mg+Fe+Mn$

A.



B.



whether all the muscovite grains are secondary. Primary muscovite would not be stable at temperatures and pressures of the granite solidus compatible with the shallow crustal depth of emplacement of the granitoid, as discussed in section 2.4.2.

Accessory minerals include zircon, fluorite, opaques, and apatite. Fluorite is anhedral and typically interstitial. Carbonate, chlorite, and epidote are present as secondary phases.

Most of the fluorite bearing granitoids are found in the central part of the pluton (Fig. 5-1). This could indicate a residual enrichment of fluorine associated with inward crystallization of granitoid magma; in any case, initial fluorine contents of the magma must have been high.

5.2.2. Geochemistry

Major and trace element data are presented in Table A4-8. An average chemical composition of the Sophie Downs Granitoid (Table 5-2) is calculated from chemical compositions of 34 samples, excluding one metasomatized example (91906). In the following sections, geochemical descriptions of sample 91906 are not included.

A. Major elements

SiO₂ content of the Sophie Downs Granitoid is very high, ranging from 72.36 to 77.68% (Fig. 5-4) with average of 76.15% (Table 5-2).

On the Na₂O + K₂O vs. SiO₂ diagram (Fig. 5-4G), 29 out of 34 samples analyzed are plotted in the field of alkalic rock as defined by Miyashiro (1978).

The granitoids have high mol ((Na₂O + K₂O)/Al₂O₃) ratios, ranging from 0.886 to 1.018, and 7 out of 34 samples analyzed are slightly peralkaline (Table A4-8 and Fig. 5-5A). Only two samples are slightly peraluminous. These chemical characteristics are comparable

Table 5-2. Average chemical composition of the Sophie Downs Granitoid

	Average	S.D.	Max.	Min.	R.S.D.(%)
(wt%)					
SiO ₂	76.15	0.93	77.68	72.36	1.22
Al ₂ O ₃	11.90	0.41	13.63	11.21	3.45
Fe ₂ O ₃ *	1.55	0.29	2.22	1.07	18.90
MnO	0.02	0.01	0.07	0.00	61.70
MgO	0.25	0.13	0.64	0.08	53.90
CaO	0.49	0.21	1.21	0.10	43.70
Na ₂ O	3.85	0.26	4.30	3.34	6.70
K ₂ O	4.80	0.37	5.72	4.34	7.79
TiO ₂	0.16	0.03	0.23	0.09	20.50
P ₂ O ₅	0.01	0.01	0.04	0.00	100.00
LOI	0.59	0.20	1.10	0.27	33.89
Total	99.76	0.33	100.28	98.99	-
(ppm)					
Ba	955	159	1206	349	16.6
Rb	114.1	15.9	148	89	13.9
Sr	41.3	16.3	103	16	39.4
Zr	205.9	54.8	308	141	26.6
Nb	31	8.4	48.2	13.8	27
Y	64	18.3	103	26.4	28.6
Ce	124.7	36	246	60	28.9
Nd	53.9	18.5	106	22	34.4
Sc	2.3	0.8	3.7	1	35
V	3.4	3.6	20	0	102
Cr	0.1	0.5	2	0	-
Ni	2.3	1	4.1	0	43.4
Cu	9.5	5.6	25	3	59
Zn	58.9	22.1	108	20	37.4
Ga	16.6	1.9	20.2	12.8	11.31
A/CNK	0.959	0.028	1.018	0.886	-

Average: Average of 34 samples, excluding a metasomatized sample (91906)

S.D.: Standard deviation

R.S.D.: Relative standard deviation (100XS.D./Average)

Fe₂O₃*: Total Fe as Fe₂O₃

A/CNK: Mol.(Al₂O₃/(CaO+Na₂O+K₂O))

Fig. 5-4. Major element variation diagram of the Sophie Downs Granitoid

- A. $\text{Al}_2\text{O}_3\text{-SiO}_2$
- B. $\text{Fe}_2\text{O}_3^*\text{-SiO}_2$
- C. MgO-SiO_2
- D. CaO-SiO_2
- E. $\text{Na}_2\text{O-SiO}_2$
- F. $\text{K}_2\text{O-SiO}_2$
- G. $\text{TiO}_2\text{-SiO}_2$
- H. $\text{Na}_2\text{O+K}_2\text{O-SiO}_2$

Solid square: Sophie Downs Granitoid.

Open circle: metasomatized granite (91906) of the Sophie Downs Granitoid.

Reference lines in the diagrams A., B., C., and D., show effect of constant sum, and are drawn from a point representing 100% SiO_2 and 0% of the other element extrapolated into the diagram. See section 3.4.3 for detailed discussion of the lines.

Fe_2O_3^* : total Fe as Fe_2O_3

A line in $\text{Na}_2\text{O+K}_2\text{O-SiO}_2$ plot is a boundary between alkalic and subalkalic rocks defined by Miyashiro (1978).

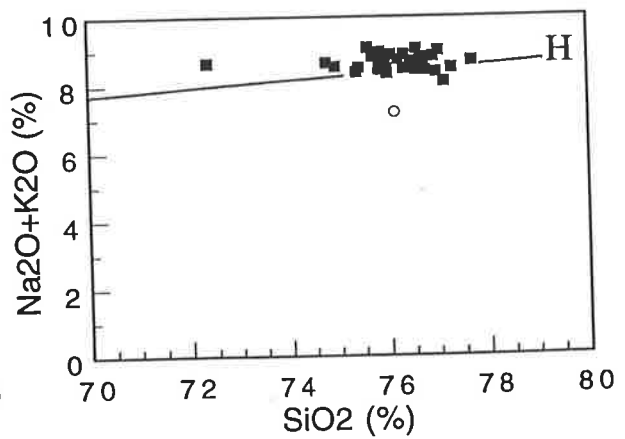
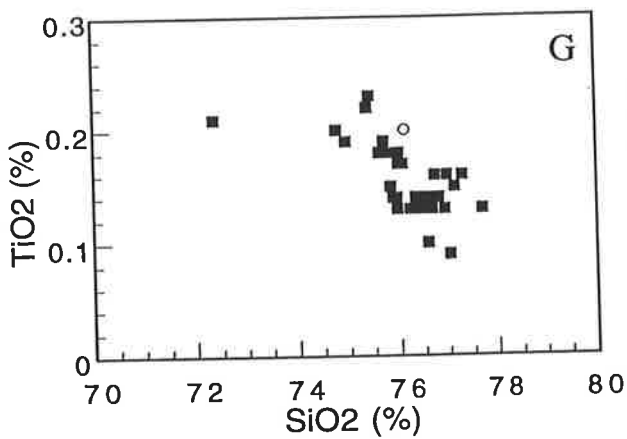
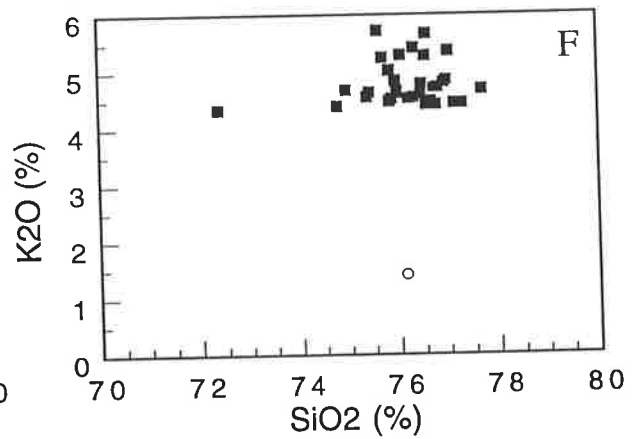
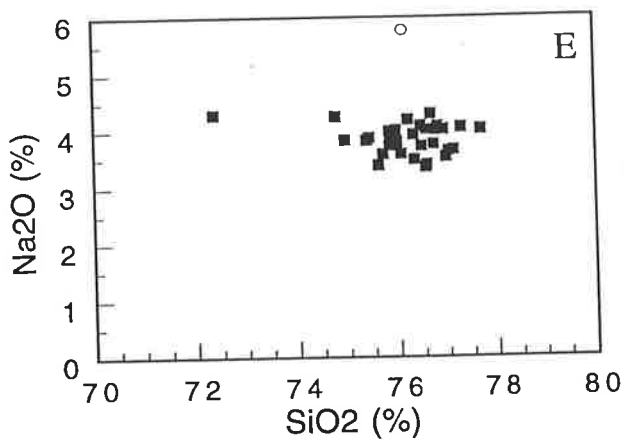
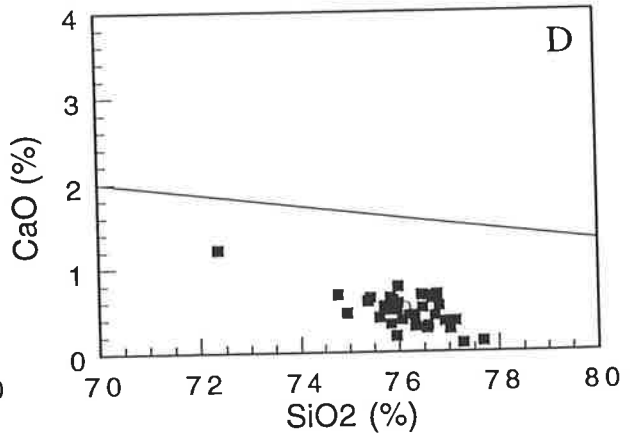
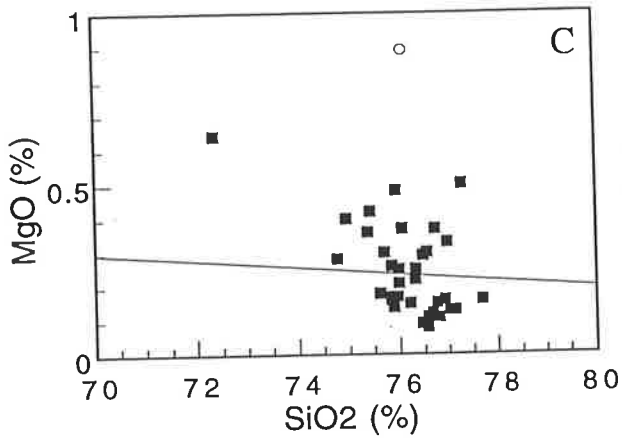
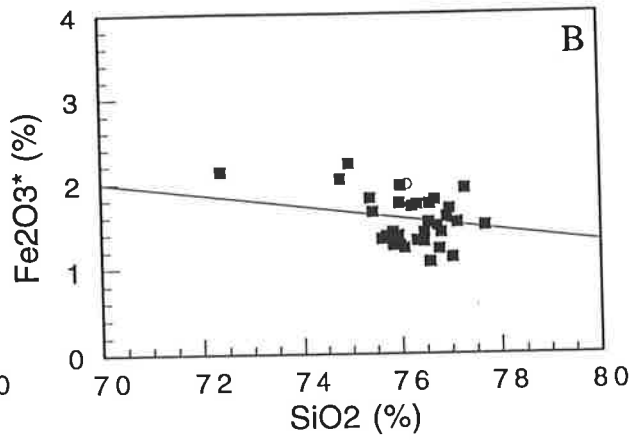
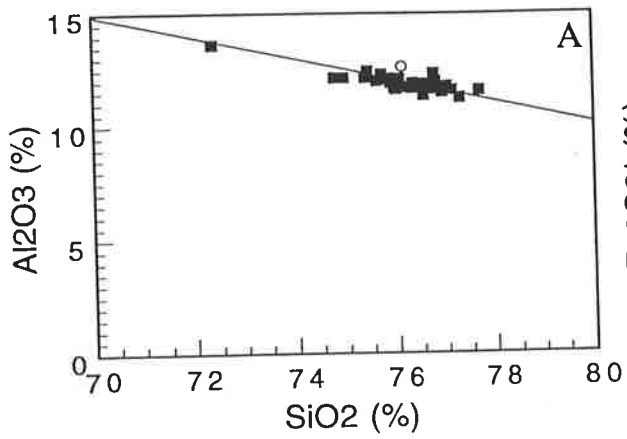


Fig. 5-5. Mol. $\text{Na}_2\text{O}+\text{K}_2\text{O}/\text{Al}_2\text{O}_3$ - Mol. $\text{Al}_2\text{O}_3/\text{CaO}+\text{Na}_2\text{O}+\text{K}_2\text{O}$ plot
and $\text{Na}_2\text{O}-\text{K}_2\text{O}$ plot of the Sophie Downs Granitoid

A. Mol. $\text{Na}_2\text{O}+\text{K}_2\text{O}/\text{Al}_2\text{O}_3$ - Mol. $\text{Al}_2\text{O}_3/\text{CaO}+\text{Na}_2\text{O}+\text{K}_2\text{O}$ plot

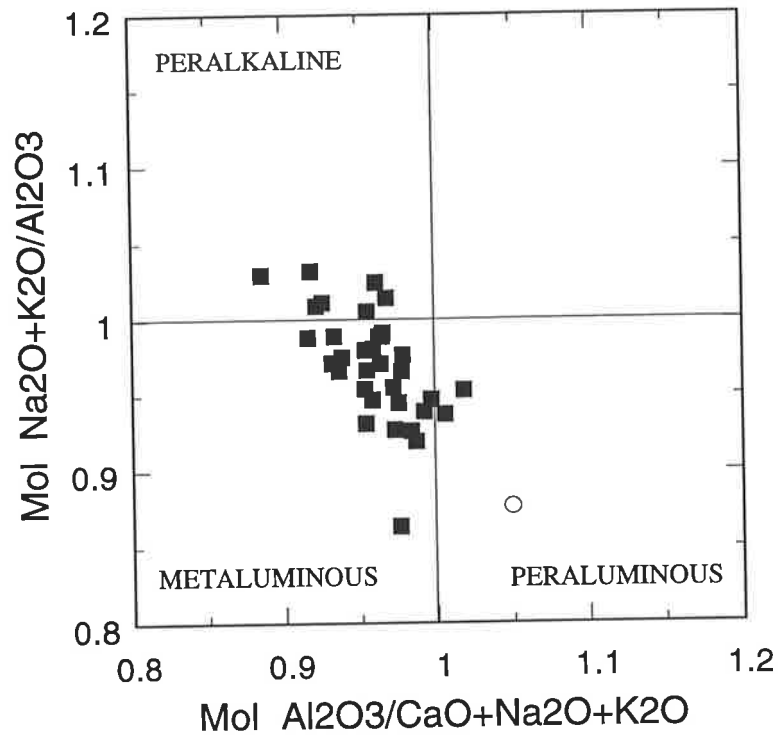
Peralkaline, metaluminous, and peraluminous fields are shown.

Most samples fall in the peralkaline and metaluminous field.

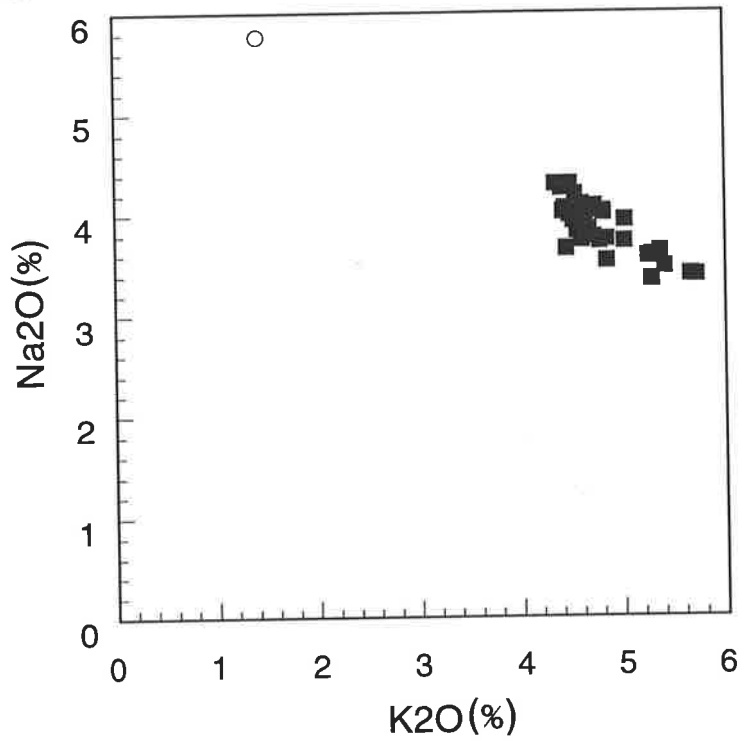
B. $\text{Na}_2\text{O}-\text{K}_2\text{O}$ plot

Symbols are the same as those in Fig. 5-4.

A.



B.



with those of the A-type granitoids of southeastern Australia (Collins et al., 1982). The A-type category was originally proposed by Loiseller and Wones (1979) for granitoids found in an anorogenic environment, such as rift zones and within stable continental blocks, and having the following chemical characteristics: mildly alkaline, low CaO and Al₂O₃ contents, high Fe/Fe + Mg, and high K₂O/Na₂O. Granitoids with these chemical characteristics can be called A-type even if they are not found in an anorogenic environment, but generally they are last in a sequence of granitic intrusions (Collins et al., 1982).

Na₂O/K₂O ratios of the Sophie Downs Granitoids are less than 0.968, indicating K₂O dominance over Na₂O (Fig. 5-5B). Although the ratios vary from 0.593 to 0.968, the total alkali (Na₂O + K₂O) contents are fairly constant (Fig. 5-5B).

As shown in Fig. 5-4A, Al₂O₃ content decreases steeply with increasing SiO₂. Thus the constant (Na₂O + K₂O) values and decreasing Al₂O₃ shifts the rocks from metaaluminous to peralkaline with increasing SiO₂ (Fig. 5-6A). On the Al₂O₃ versus SiO₂ plot (Fig. 5-4A), the data are plotted along the line indicating the effect of the constant total sum. Therefore, the decrease of Al₂O₃ with increasing SiO₂ must be largely a result of the effect of the constant total sum or in other words, the Al₂O₃ decreases proportionally with the sum of the concentrations of the elements other than Al₂O₃ and SiO₂.

The low CaO (Fig. 5-4D) is reflected in the low An content of plagioclase in the granitoids.

On the normative Qz-Ab-Or diagram (Fig. 5-6B), most of the Sophie Downs Granitoids plot near the minimum melt composition at PH₂O = 1kb.

B. Trace elements

Fig. 5-6. Mol $\text{Na}_2\text{O}+\text{K}_2\text{O}/\text{Al}_2\text{O}_3$ - SiO_2 plot and normative Q-Ab-Or diagram of the Sophie Downs Granitoid

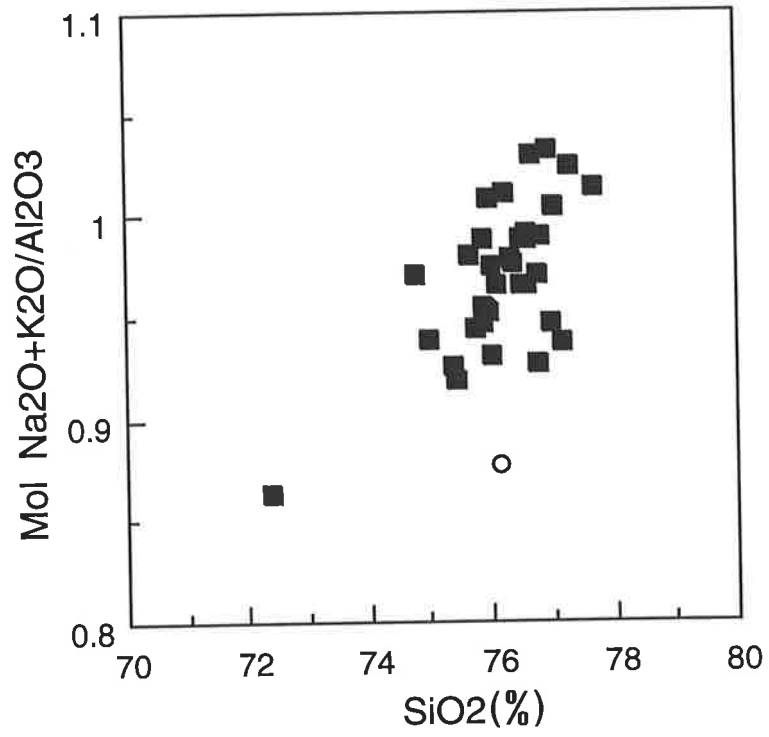
A. Mol $\text{Na}_2\text{O}+\text{K}_2\text{O}/\text{Al}_2\text{O}_3$ - SiO_2 plot

B. Normative Q-Ab-Or diagram

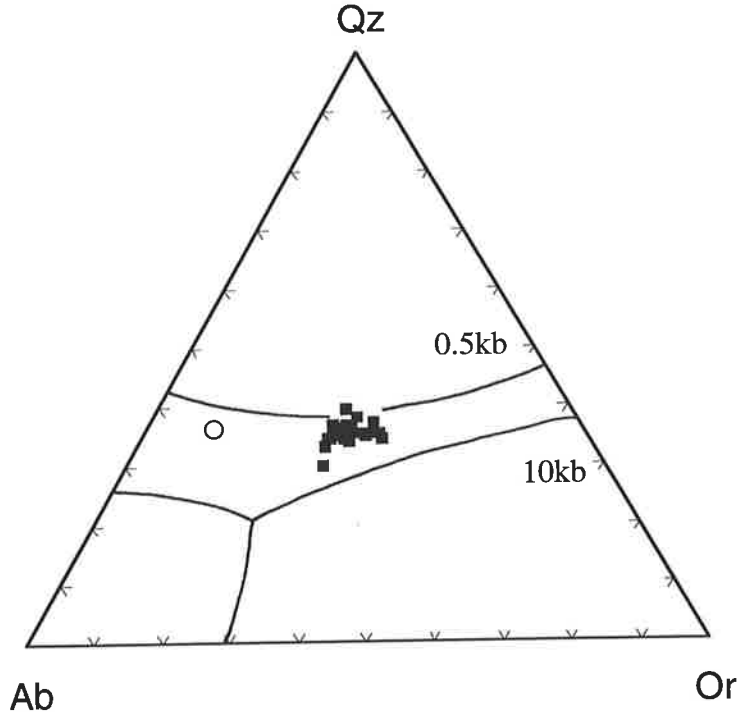
Phase boundaries of the granitic system for water pressure 0.5 kb and 10 kb are shown. Data from Tuttle and Bowen (1958) and Luth et al. (1964).

Symbols are the same as those in Fig. 5-4.

A.



B.



The granitoid is characterized by high Ba, ranging from 735 to 1206ppm, except for one sample having 349ppm (Table 5-2). No systematic change of Ba content with SiO₂ is found (Fig. 5-7A).

Rb (89 - 148ppm) and Sr (16 - 103ppm) in general decrease with increasing SiO₂ (Fig. 5-7B and C). Rb/Sr ratios range from 1.233 to 8.000 (Fig. 5-7D).

High abundances of Zr (141 - 308ppm) and Nb (13.8 - 48.2ppm) are comparable with those in A-type granitoids of southeastern Australia (Collins et al., 1982). Ce and Y contents are also notably high, ranging from 60 to 246ppm and 26.4 to 103ppm, respectively (Table 5-2). Chondrite normalized REE patterns (Fig. 5-8) from two samples (31207 and 92006) of Sophie Downs Granitoid illustrate LREE enrichment and a large negative Eu anomaly. Eu/Eu* values of the samples are 0.333 and 0.488 (Table A5-2). Although absolute concentrations of REE in sample 92006 are about 2 to 2.5 times that in sample 31207, the patterns remain basically parallel to each other. The patterns in the HREE region are flat in both samples, precluding the presence of garnet in a partial melt residue. The large negative Eu anomaly suggests the likelihood of plagioclase in the residue of partial melting to generate the granitoid magma.

Transition metals are generally low in the granitoid. Zn (20 - 108ppm) is an exception (Table 5-2). High Zn contents are found also in A-type granitoids from southeastern Australia (Collins et al., 1982).

Ga contents range from 12.8 to 20.2ppm (Table 5-2). High Ga relative to Al₂O₃ is considered by Collins et al. (1982) to be diagnostic of the A-type granitoids. Although the range found in the Sophie Downs Granitoid (Fig. 5-9A) is slightly lower than that in the A-type granitoids in the southeastern Australia (Collins et al., 1982), half of the analyzed samples are plotted near the A-type field. On a discrimination diagram

Fig. 5-7. Trace element variation diagram of the Sophie Downs
Granitoid

A. Ba-SiO₂

B. Rb-SiO₂

C. Sr-SiO₂

D. Rb-Sr

E. Zr-SiO₂

F. Nb-SiO₂

G. Y-SiO₂

H. Ce-SiO₂

Symbols are the same as those in Fig. 5-4.

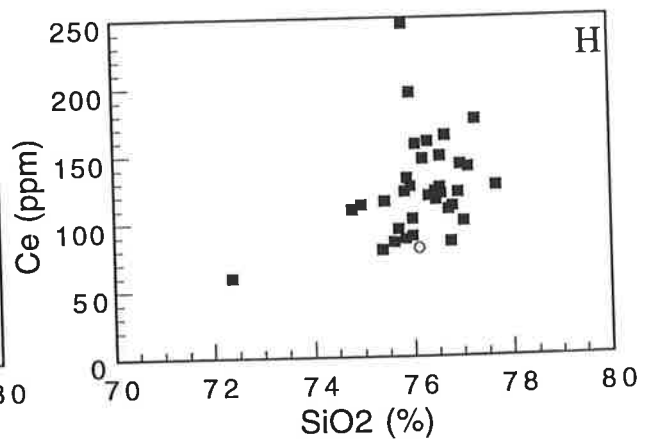
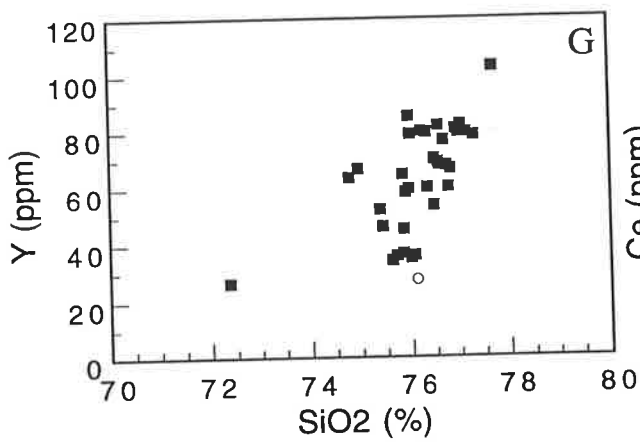
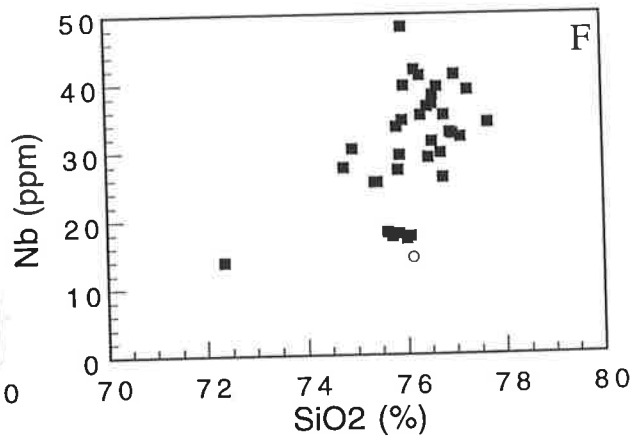
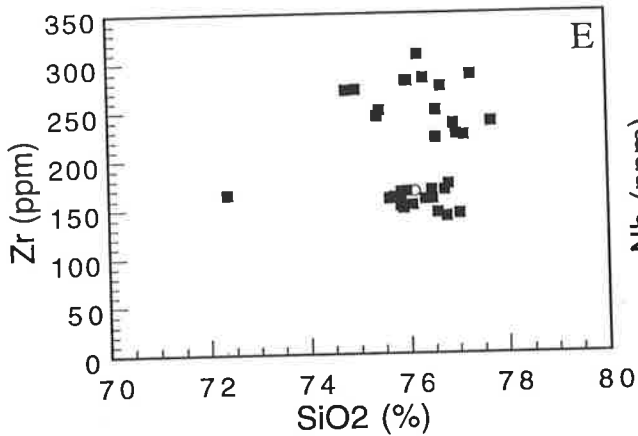
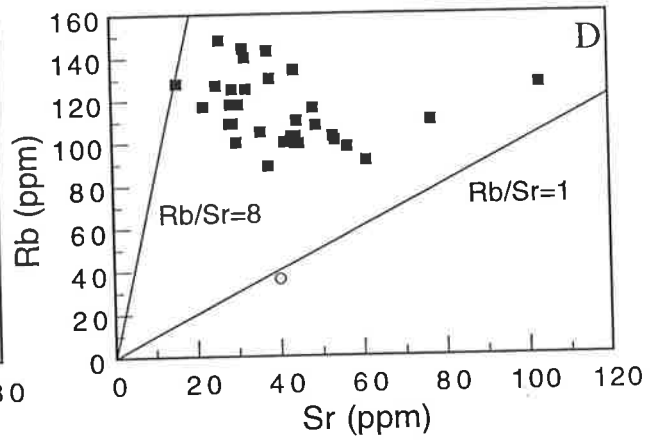
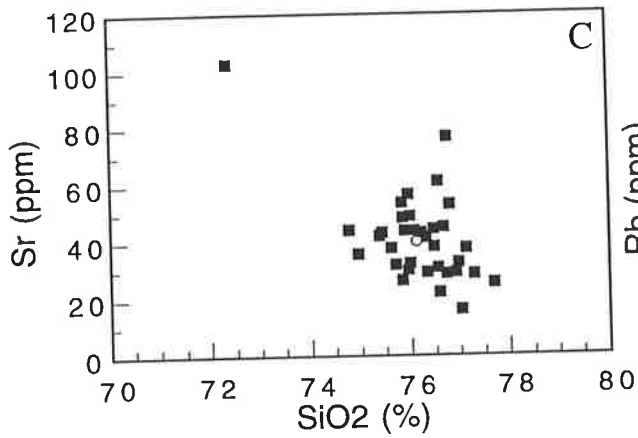
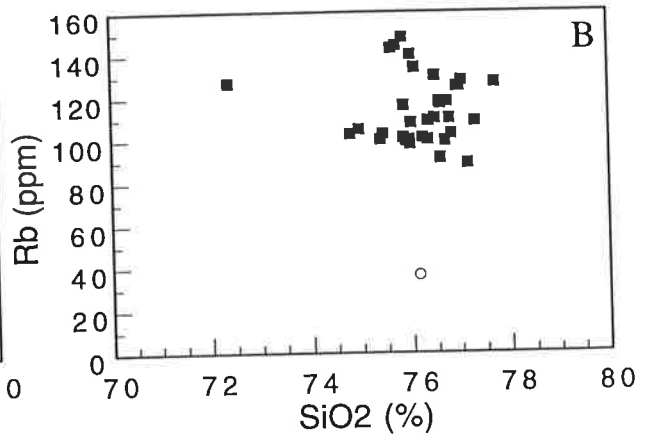
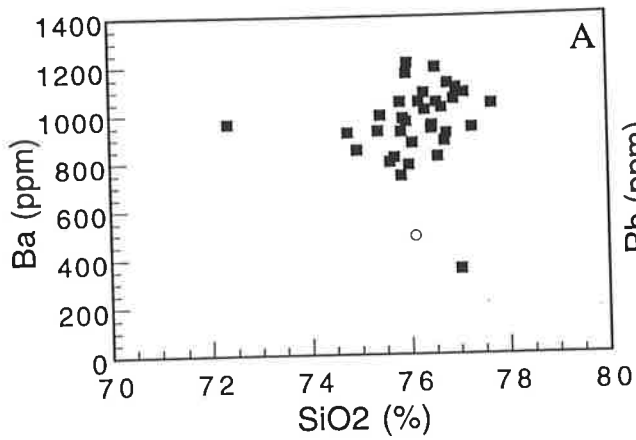


Fig. 5-8. Chondrite normalized REE patterns of the Sophie Downs
Granitoid

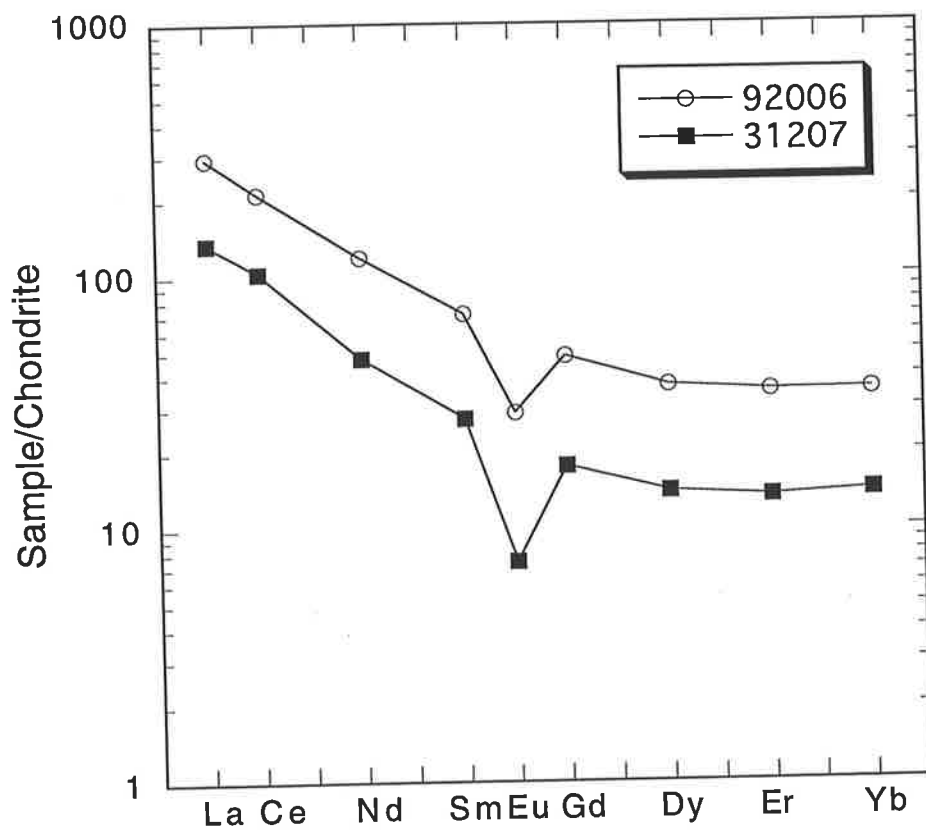


Fig. 5-9. Ga-Al₂O₃ and (Zr+Nb+Ce+Y) - (10000*Ga/Al) plots of the Sophie Downs Granitoid

A. Ga-Al₂O₃ plot

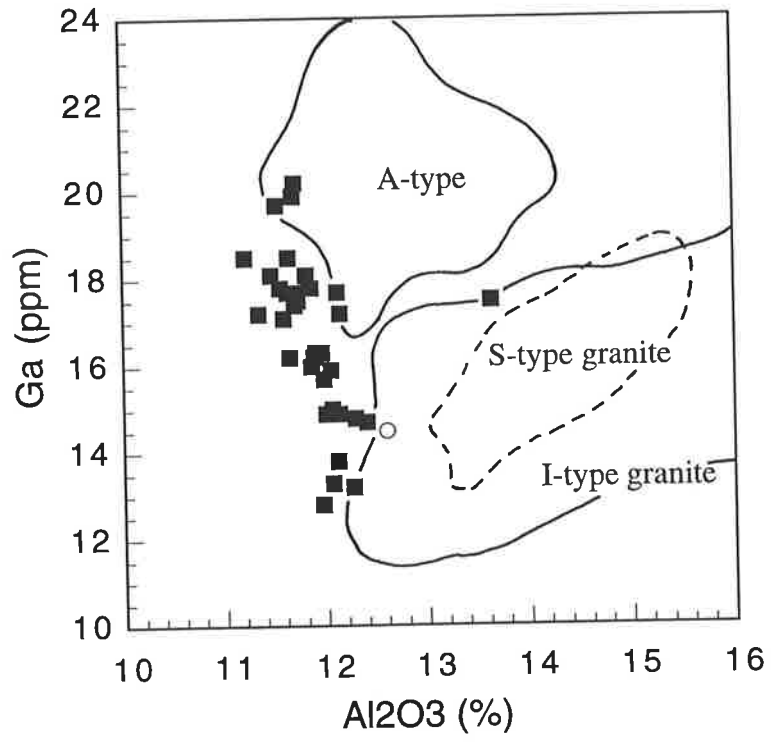
A-, S-, and I-type fields are from Collins et al. (1982).

B. (Zr+Nb+Ce+Y) - (10000*Ga/Al) plot

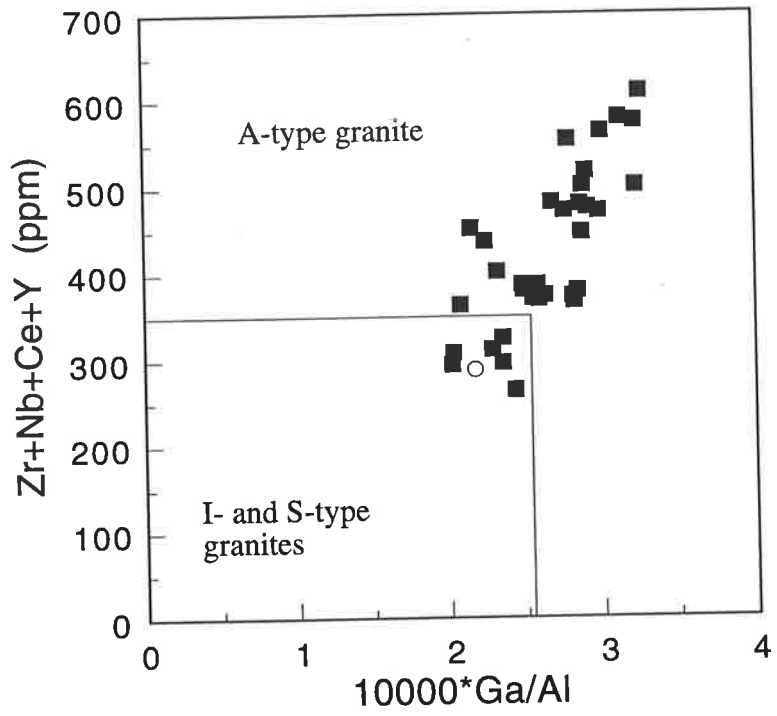
A discrimination diagram for granitoids types proposed by Whalen et al. (1987)

Symbols are the same as those in Fig. 5-4.

A.



B.



for A-type granitoids proposed by Whalen et al. (1987), samples of the Sophie Downs Granitoid are mostly plotted in the field of the A-type.

Thus all the petrological and geochemical characteristics indicate that Sophie Downs Granitoid is assigned to the A-type category.

Fluorine contents of Sophie Downs Granitoid (Table A3-4) are fairly high. Two samples (30706 and 31501A) which contain fluorite show more than 1500ppm fluorine. The high fluorine content is another chemical characteristic of the A-type granitoids (Collins et al., 1982).

5.2.3. Areal Chemical Variation in the Sophie Downs Granitoid

Areal variations of SiO₂, Al₂O₃, Fe₂O₃, Na₂O, K₂O, Rb, Sr, and Zr within the Sophie Downs Granitoid pluton are presented in Fig. 5-10. As the variation of the major elements of the granitoid is small, the areal variation of most elements also is not pronounced.

The SiO₂ value is low near the northern margin of the pluton, and generally high in the eastern part of the central zone (Table 5-10A). This high-SiO₂ zone may represent the last portion of the granitoid magma to solidify, an interpretation supported by the coarse grain size of the granitoid in the eastern part of pluton, as coarse grain size generally manifests slow cooling of magma. If the hydrothermal solution to form quartz veins was supplied from the residual magma, the presence of a large quartz vein in the eastern part of the granitoid pluton adds further weight to this interpretation. However, the high-SiO₂ zone in the eastern part could be also explained by silicification from the hydrothermal solution. A small high-SiO₂ zone in the western central part may indicate another concentration of late stage solidification of the magma. On the contrary, Al₂O₃ is high in the northern and western parts (Fig. 5-10B). Fe₂O₃ is low in the central part of the pluton (Fig. 5-10C), possibly indicating depletion of iron associated with late stage crystallization of the

Fig. 5-10. Areal geochemical variation in the Sophie Downs Granitoid

A. SiO_2

B. Al_2O_3

C. Fe_2O_3^* (Fe_2O_3^* : total Fe as Fe_2O_3)

D. Na_2O

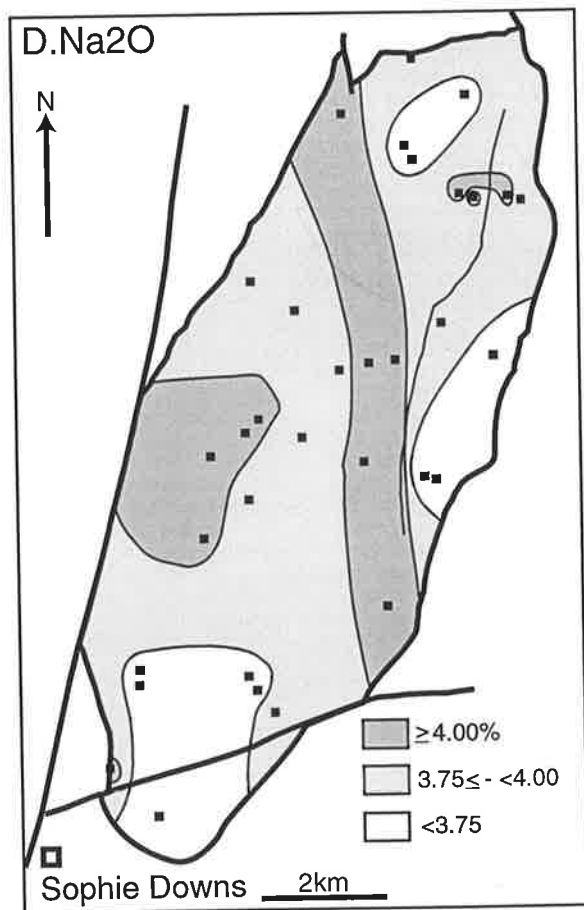
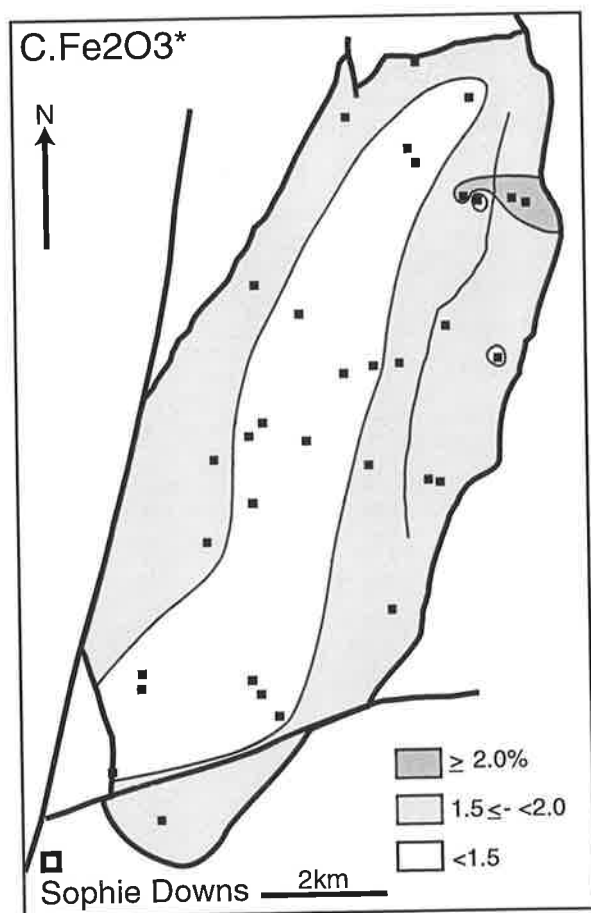
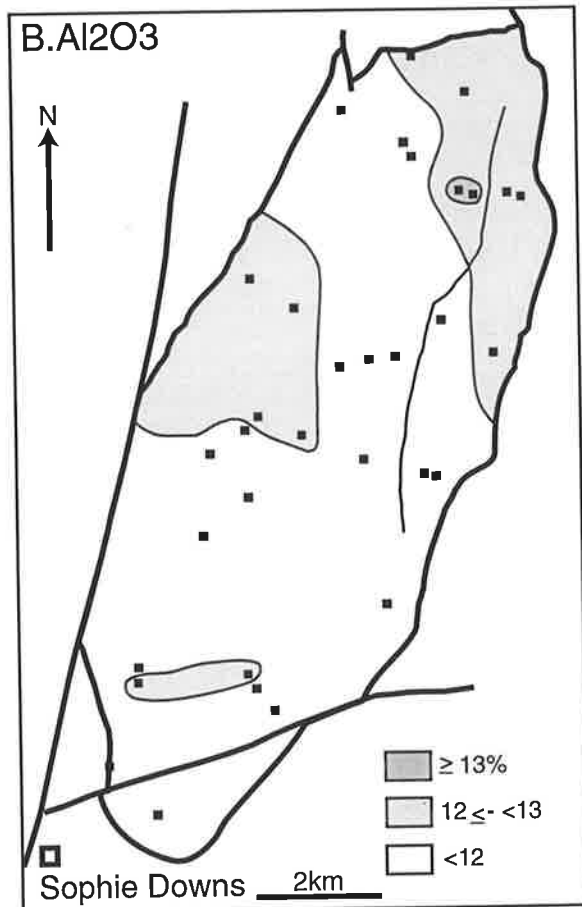
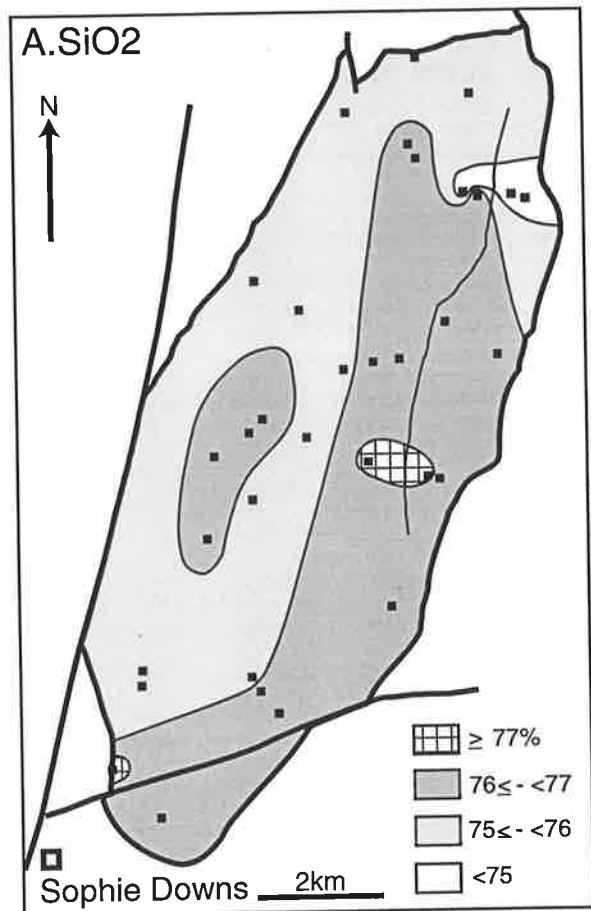


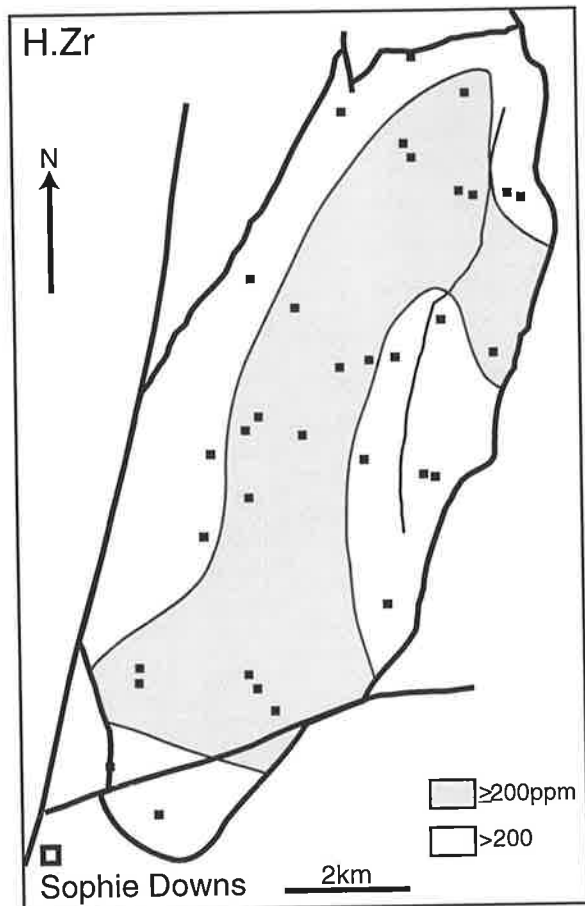
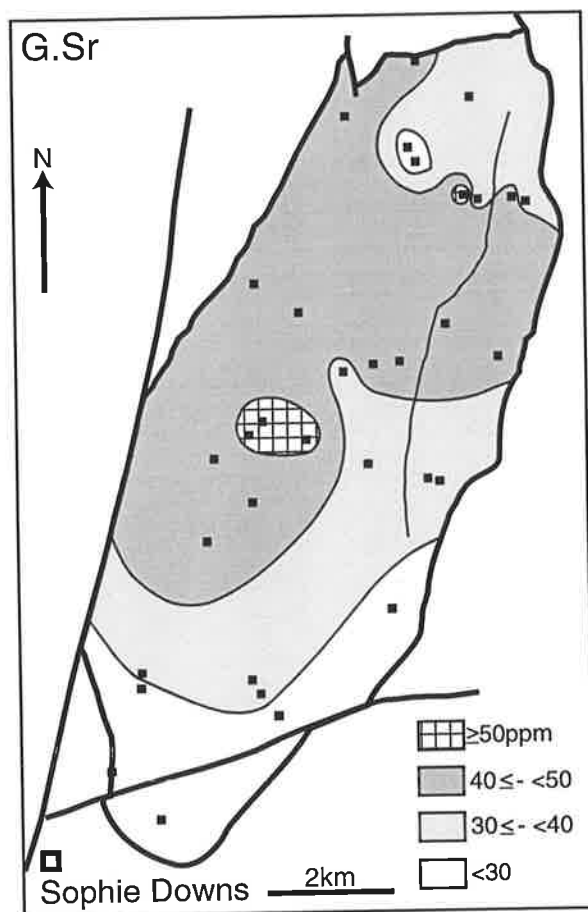
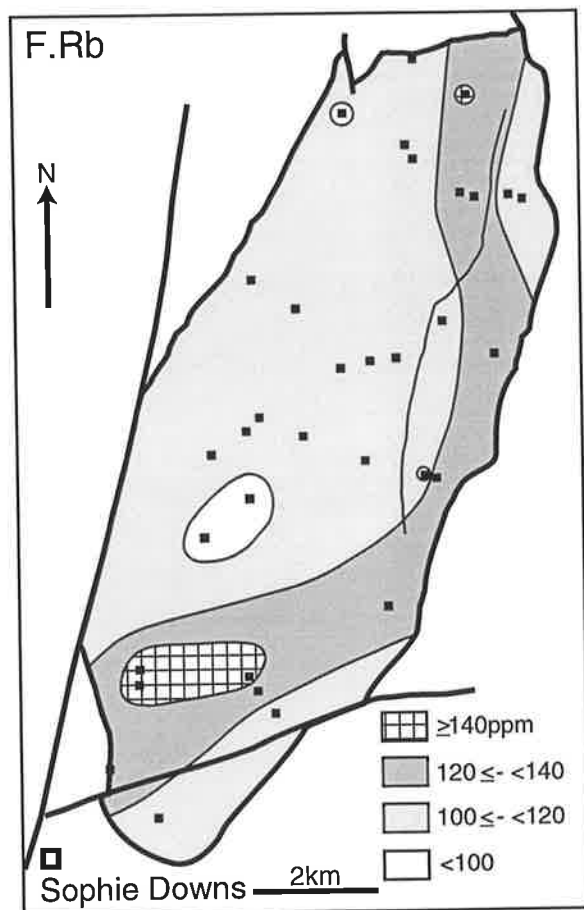
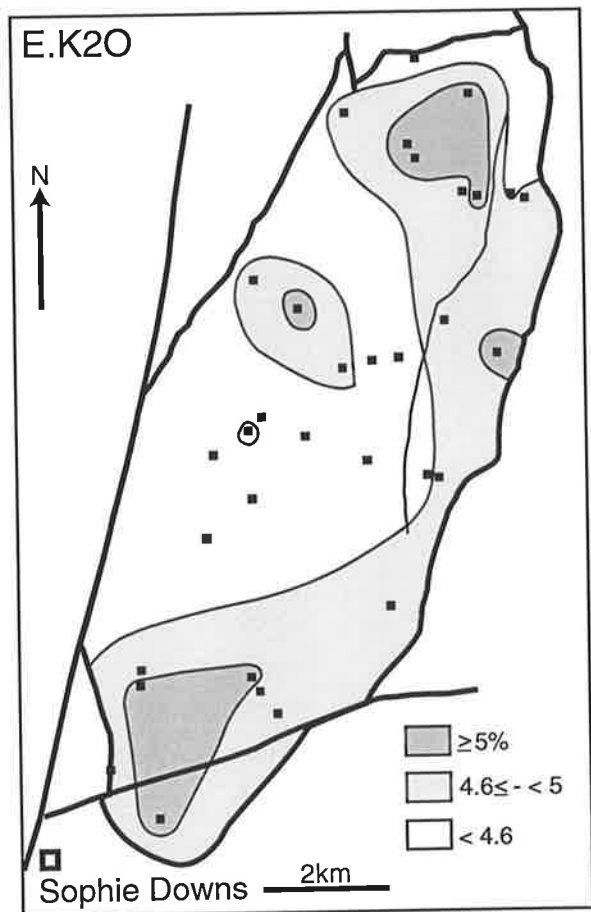
Fig. 5-10 (2). Areal geochemical variation in the Sophie Downs
Granitoid

E. K_2O

F. Rb

G. Sr

H. Zr



granitoid magma towards the centre of the pluton. Variation in the areal distribution of MnO and MgO (not shown) is similar to that of the Fe₂O₃. High Na₂O is found in the western central part (Fig. 5-10D). K₂O is generally high in the eastern part (Fig. 5-10E).

Rb is high in the eastern part (Fig. 5-10F), showing a similar areal distribution pattern to that of K₂O. Sr is high in the western part of the granitoid pluton (Fig. 5-10G). The Zr value shows a broadly concentric pattern, being high (more than 200 ppm) in the marginal zone. Two distinct concentrations of Zr apparent on the variation diagram of Fig. 5-7E are also expressed in its areal distribution. Depletion of Zr in the central part of the pluton may indicate a fractionation of zircon associated with "inward crystallization" of the granitoid magma.

In summary, regional chemical distributions of Zr and Fe₂O₃ show clear concentric patterns, decreasing from the margin to the center of the granitoid pluton. There is a tendency for Na₂O and Sr to increase from the margin to the center. The slightly complicated areal distribution found for SiO₂, K₂O, and Rb, may be due to hydrothermal activity in the late stages of magma intrusion, or more likely is related to the original shape of the pluton. As the Sophie Downs Granitoid is unconformably overlain by the Saunders Creek Formation on the northern margin and has sheared contact to the Biscay Formation along the eastern margin, the original shape of the pluton must have been modified. The high SiO₂ and coarse grain size in the eastern part of the pluton may indicate location of the center of the original pluton in the eastern part. This interpretation indicates the pluton was originally extended further to east.

5.3. Bow River Granitoid and Granitoids from the King Leopold Mobile Zone

Petrography and geochemistry of the Bow River Granitoid from the East Kimberleys and granitoids from the King Leopold Mobile Zone, West Kimberleys are presented here. Chemical compositions of minerals in the studied rocks from the granitoids are presented in Appendix 8.

5.3.1. Petrography

A. Bow River Granitoid

Modal composition (Table A2-1) of the Bow River Granitoid (52009) from Mount Nyulasy (Fig. 2-20) indicates that K-feldspar is the most dominant mineral, and the rock is a granite according to the terminology of Streckeisen (1976).

The K-feldspar megacrysts up to 8mm long (Fig. 5-11A and B), are euhedral to subhedral, and are perthitic. Or content of the K-feldspar ranges from 66 to 93 (a broad electron beam for the electron probe analysis was used to obtain average chemical composition of perthitic K-feldspar).

Plagioclase is extensively altered to fine grained epidote and sericite; limited microprobe analyses on relatively fresh plagioclase indicate that the An content ranges from 4.4 to 16.4.

Quartz phenocrysts are generally rounded and embayed.

Biotite is extensively altered to chlorite and opaque minerals. Muscovite occurs interstitially and may be secondary. Accessory minerals are zircon and opaques.

Type I Bow River Granitoid (91508) from north of Springvale (see section 2.5.3.C) has a porphyritic texture. The average grain size of phenocrysts is 1cm. The modal composition (Table A2-1) shows that the sample has more abundant plagioclase than the granite from Mount Nyulasy. K-feldspar (Or 80 - 97) is microcline perthite, and subhedral. Plagioclase shows oscillatory zoning; composition from microprobe

Fig. 5-11. Photomicrographs of the Bow River Granitoid, granitoids from the King Leopold Mobile Zone, and Whitewater Volcanics

A. Bow River Granitoid from Mount Nyulasy

Typical texture of the Bow River Granitoid. Large crystals of K-feldspar and quartz are present.

Sample: 52009 . Bi: biotite, KF: K-feldspar, Qz: quartz

Plane polarized light. Scale bar is 5 mm.

B. Same as A, but under crossed polarized light.

Pl: plagioclase

C. Bow River Granitoid from Springvale area.

Sample: 91504. Bi: biotite

Plane polarized light. Scale bar is 5 mm.

D. Same as C, but under crossed polarized light.

Large crystals of K-feldspar are present in fine grained matrix.

Pl: plagioclase, KF: K-feldspar, Qz: quartz

E. Richenda Granodiorite

Sample: 20201. Bi: biotite, Pl: plagioclase, Qz: quartz

Crossed polarized light. Scale bar is 5 mm.

F. McSherrys Granodiorite

Sample: 13104. Ho: hornblende, Bi: biotite, Pl: plagioclase,

KF: K-feldspar, Qz: quartz

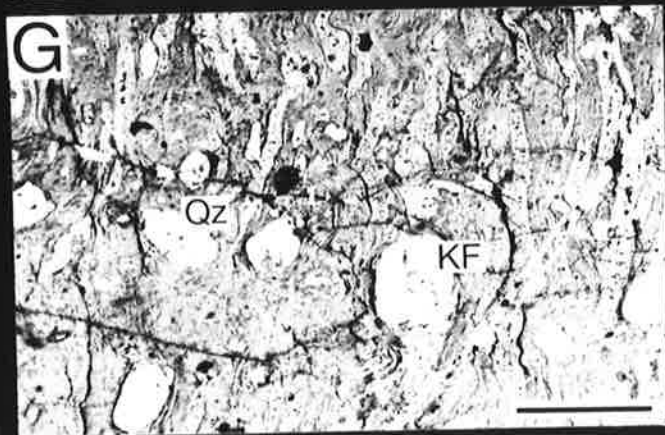
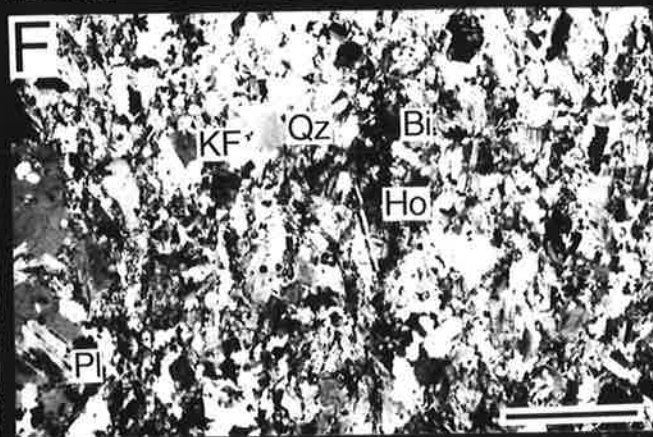
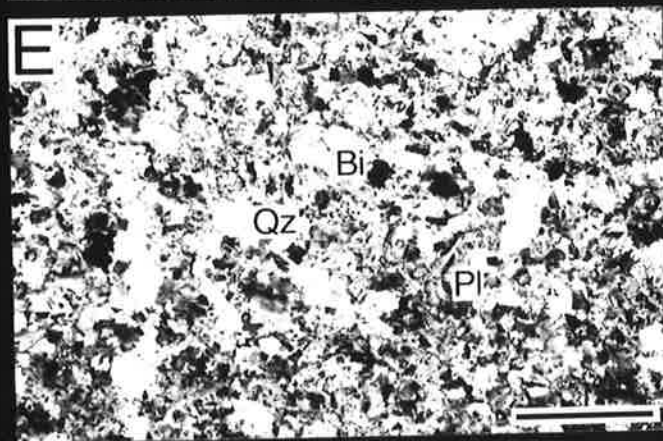
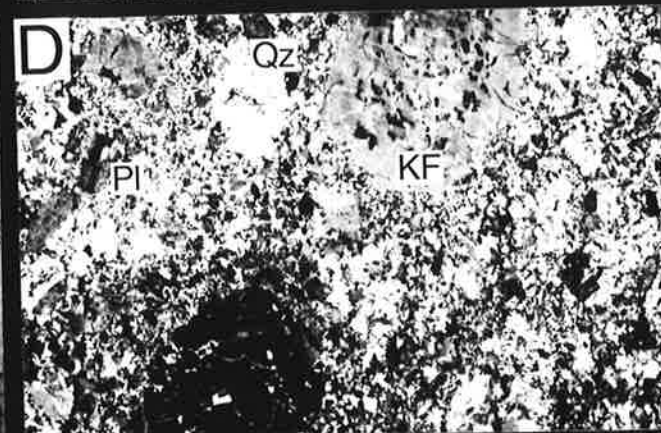
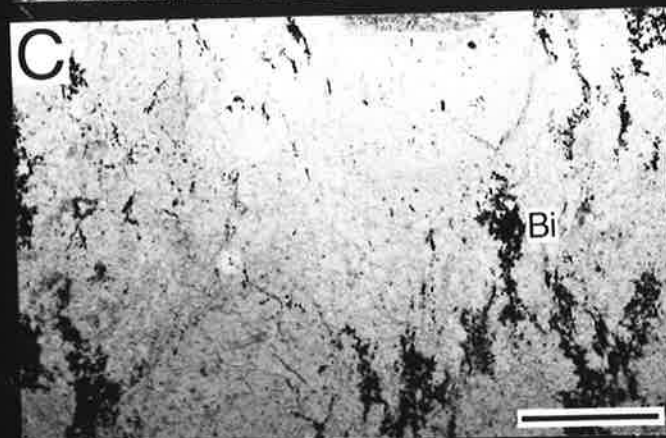
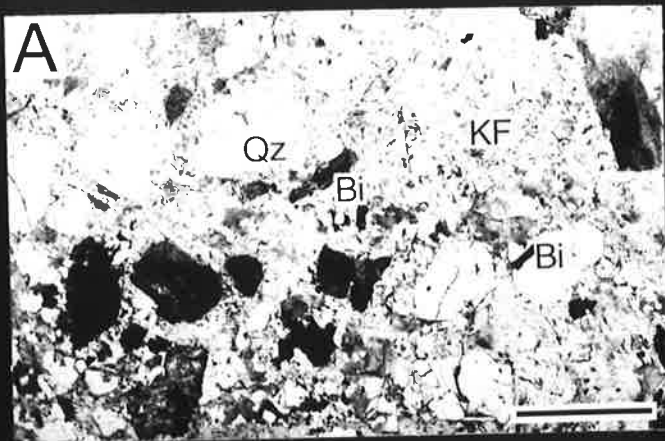
Crossed polarized light. Scale bar is 5 mm.

G. Whitewater Volcanics

Ashflow tuff of the volcanics consists of phenocrysts of quartz, K-feldspar, and plagioclase and a strongly welded and devitrified matrix.

Sample: 91603. Plane polarized light. Scale bar is 5 mm.

H. Same as G, but under crossed polarized light.



analysis, of two plagioclase grains, is An 46 and An 41. Biotite (α = yellow, β = γ = brown) is subhedral and medium grained. Small amounts of muscovite and accessory zircon and opaque minerals are present.

Type II Bow River Granitoid from north of Springvale also is a medium grained porphyritic granite (Fig. 5-11C and D). Plagioclase is extensively altered to aggregates of epidote and sericite. K-feldspar phenocrysts are perthitic; the matrix K-feldspar is mostly non perthitic microcline. Biotite is generally altered to chlorite, but where fresh, shows the following pleochroism: α = pale yellow, β = γ = reddish brown. Accessory minerals are zircon, apatite, and opaque minerals.

Another sample (91507) of Bow River Granitoid from north of Springvale (Fig. 2-21) is composed largely of K-feldspar (34%), quartz (30%), plagioclase (20%), green to blue-green hornblende (8%), and yellow brown biotite (8%). The presence of hornblende is notable. The rock is rather coarse grained and has inequigranular texture. Accessory minerals include zircon, apatite, allanite, and opaques.

B. Granitoids from the King Leopold Mobile Zone

Richenda Granodiorite

Modal composition of a sample of the Richenda Granodiorite is presented in Table A2-1. The granodiorite has a hypidiomorphic-granular texture (Fig. 5-11E). Plagioclase is euhedral and with strong oscillatory zoning. Subhedral or anhedral K-feldspar is microcline perthite. Biotite (α = pale yellow, β = γ = reddish brown) is the only mafic mineral in the granodiorite. Accessory minerals are zircon and opaques. Secondary muscovite and epidote are common.

The rhyolitic part of the Richenda Granodiorite has phenocrysts of embayed quartz, plagioclase, and fine grained biotite in a cryptocrystalline matrix. Plagioclase is extensively sericitized.

McSherrys Granodiorite

Two samples of the McSherrys Granodiorite have been examined. Modal composition of one sample is presented in Table A2-1. It is granodiorite as classified by Streckeisen (1976).

Plagioclase (An 39 - 54) is subhedral, and coarse to fine grained (Fig. 5-11F). Weak zoning is present. K-feldspar (Or 89 - 90) is mostly untwinned. Some occurs as large phenocrysts up to 1cm long, poikilitically enclosing biotite, plagioclase, and quartz. Biotite (α = pale yellow, β = γ = brown) is typically medium or fine grained, and subhedral. Blue-green hornblende is subhedral and medium grained and some, e.g. 13104, has a clinopyroxene core. The clinopyroxene is augite (Table A8-1). Accessory minerals are zircon, apatite, sphene, and opaque minerals.

Dyasons Granite

Dyasons Granite consists largely of quartz, and equal amounts of plagioclase and K-feldspar. Biotite (α = pale yellow, β = γ = brown) is the only mafic mineral. The texture is inequigranular, with average grain size of the matrix 1mm. Large lenticular plagioclase phenocrysts have dimensions up to 4mm. Epidote and secondary muscovite are present. Other accessory minerals are zircon, apatite, sphene, and opaques.

5.3.2. Geochemistry

A. Bow River Granitoid

Major and trace element data are listed in Table A4-9. The data show that SiO₂ ranges from 71.1 to 74.3%, sample (52009) having highest SiO₂ of the samples analyzed. Except for sample 91507, the granitoids are peraluminous, having mol (Al₂O₃/(CaO + Na₂O + K₂O)) ratio more than 1.065. Low Na₂O/K₂O ratios are found in all of the analyzed samples. One analysis of the Bow River Granitoid reported by Gemuts (1971) also has a high mol (Al₂O₃/(CaO + Na₂O + K₂O)) ratio

(1.095) and low Na₂O/K₂O ratio (0.390). These values are comparable with those of S-type granitoids (Chappell and White, 1974).

Variation diagrams (Fig. 5-12) illustrate that most of the major element contents are similar to those of S-type granitoids from the Kosciusko Batholith of southeastern Australia (Hine et al., 1978), though, some differences are found, for example the lower MgO and higher K₂O contents of the Bow River Granitoid. A sample (Cu-2) of Cummins Range Granite which has been grouped with the Sophie Downs Granitoid by Gemuts (1971), has similar chemical characteristics to those of the Bow River Granitoid (Table A4-9 and Fig. 5-12), suggesting that it should be grouped with the Bow River Granitoid rather than with the Sophie Downs Granitoid which has typical A-type characteristics.

The Bow River Granitoid has low K/Rb (143 - 243), high Rb/Sr (1.38 - 5.19) ratios and relatively high Rb contents (166 - 337 ppm) (Fig. 5-13B). These values are not consistent with a model of fractionation from basaltic magma or of partial melting of basaltic rocks. However, since the gabbroic rocks are present between the Bow River Granitoid in the Springvale area, possible genetic links between the granitoid and the gabbroic rocks are examined here. The high Rb contents in the granitoids would require about 26 to 53-fold enrichment of the Rb from the gabbroic rocks (assuming Rb = 6.3ppm in the gabbro, equal to an average value of Rb in hornblendite and mela-gabbro from the Sally Downs Bore area). Such enrichment necessitates an approximate maximum of 3.8% partial melting of the gabbro, or a minimum 96.2% fractional crystallization from the gabbroic magma, assuming that the bulk distribution coefficient of Rb between mineral and melt is zero. Obviously, such extremely small amounts of melt product are not reconcilable with the large volume of Bow River Granitoid. Thus the granitoids could not be derived directly from the gabbroic rocks.

Fig. 5-12. Major element variation diagram of Bow River Granitoid, granitoids from the King Leopold Mobile Zone, and Whitewater Volcanics

- A. $\text{Al}_2\text{O}_3\text{-SiO}_2$
- B. $\text{Fe}_2\text{O}_3^*\text{-SiO}_2$
- C. MgO-SiO_2
- D. CaO-SiO_2
- E. $\text{Na}_2\text{O-SiO}_2$
- F. $\text{K}_2\text{O-SiO}_2$
- G. $\text{TiO}_2\text{-SiO}_2$
- H. $\text{P}_2\text{O}_5\text{-SiO}_2$

Open square: Bow River Granitoid

Open circle: granitoid from Cummins Range.

Solid circle: Richenda Granodiorite from the King Leopold Mobile Zone.

Solid square: two samples of McSherrys Granodiorite and one sample of Dyasons Granite from the King Leopold Mobile Zone.

Open triangle: Whitewater Volcanics

Fe_2O_3^* : total Fe as Fe_2O_3

Dashed and solid lines indicate fields of S-type and I-type granitoids, respectively, of Kosciusko Batholith of southeastern Australia (Hine et al., 1978).

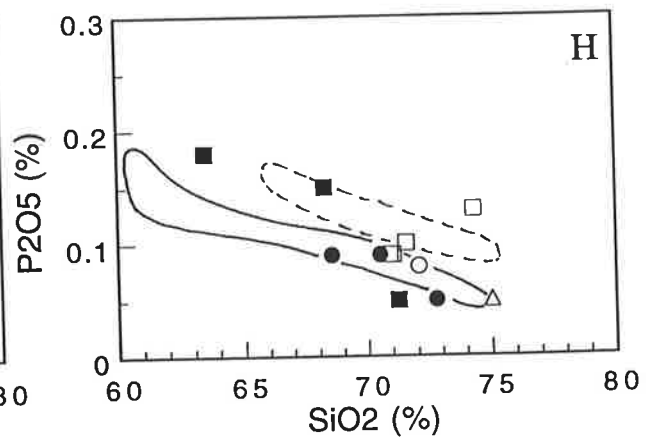
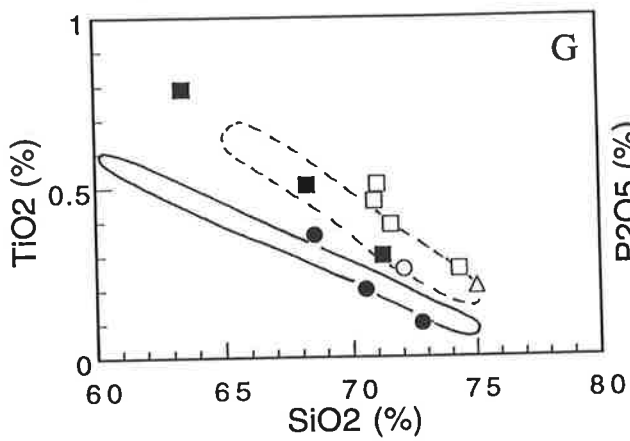
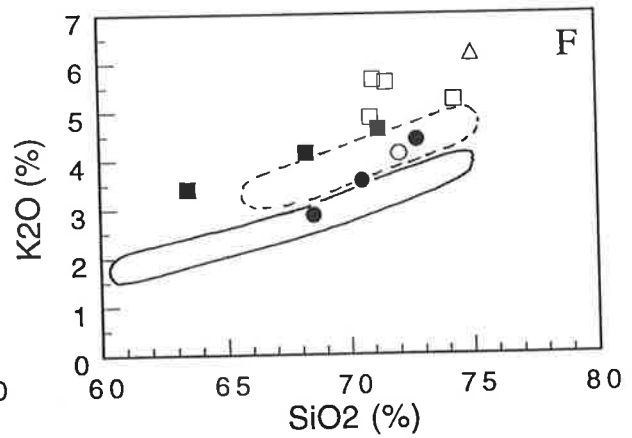
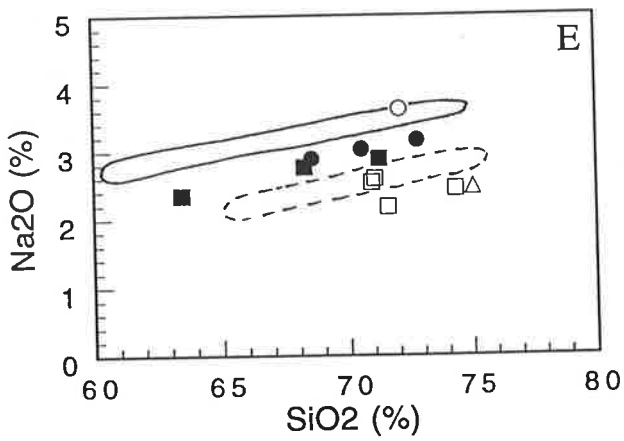
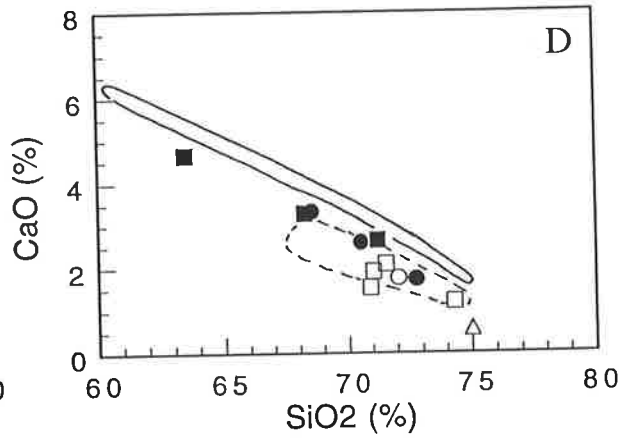
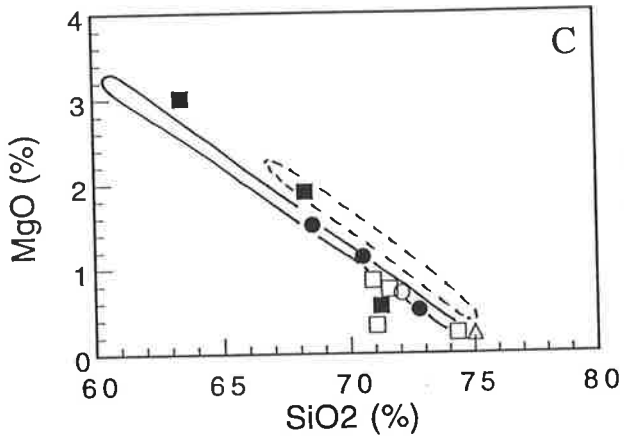
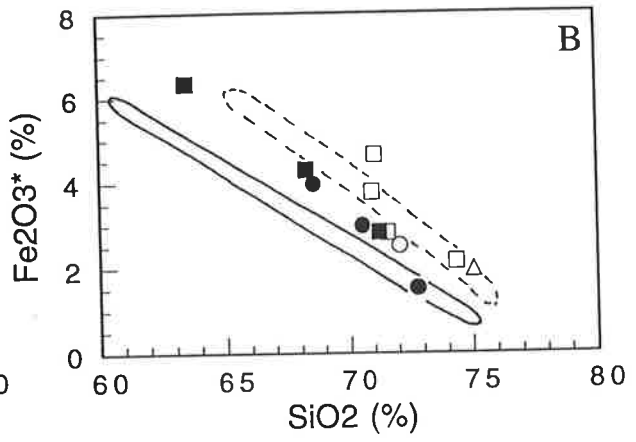
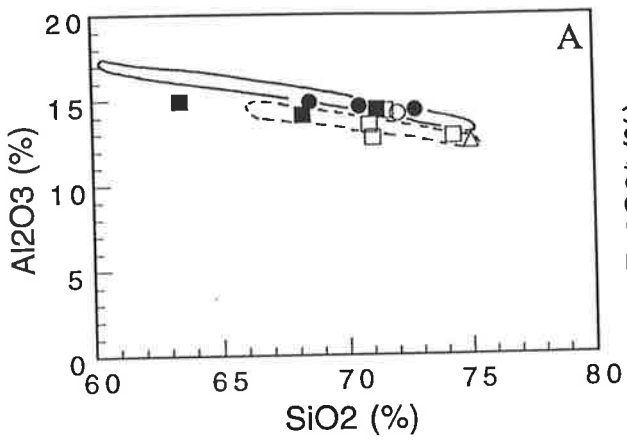
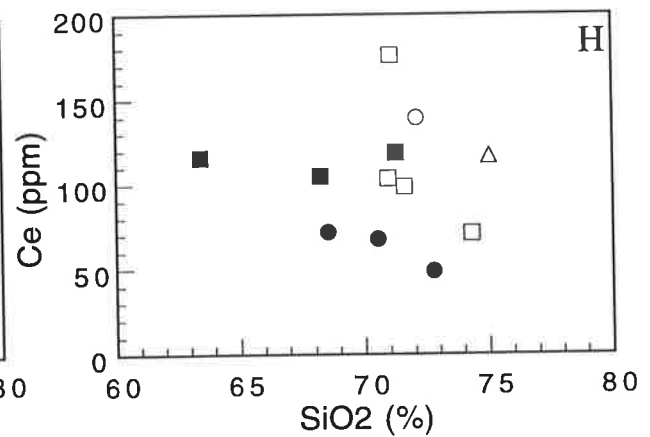
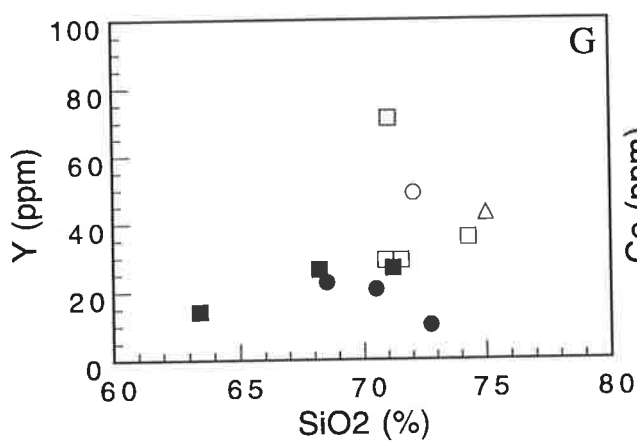
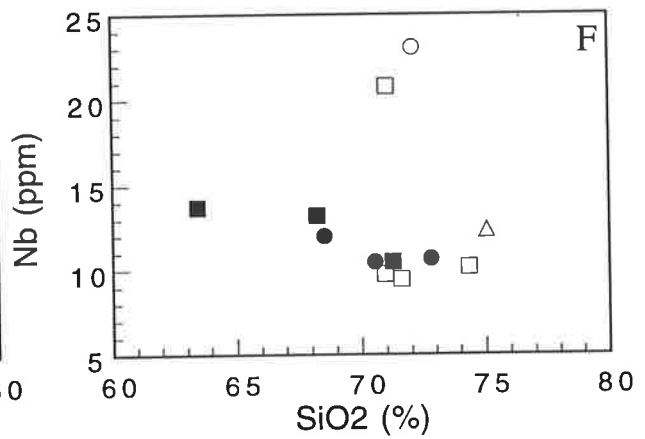
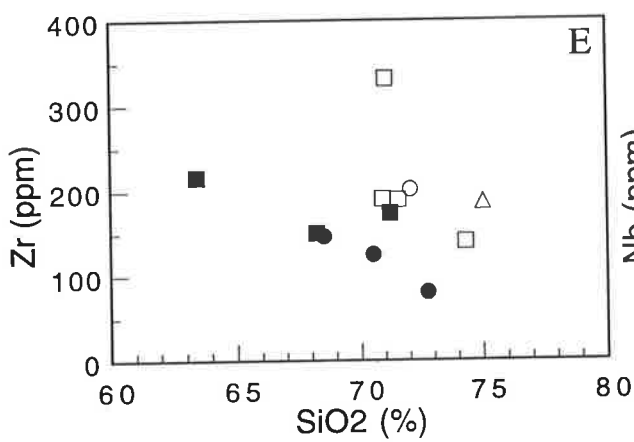
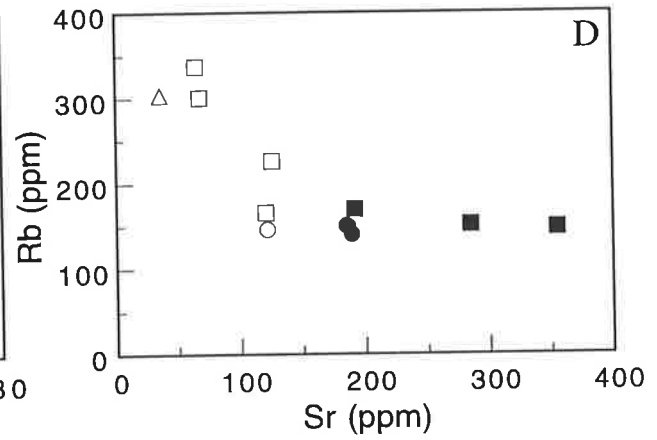
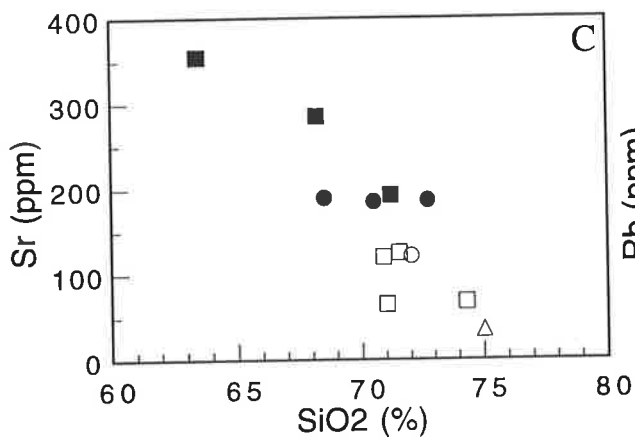
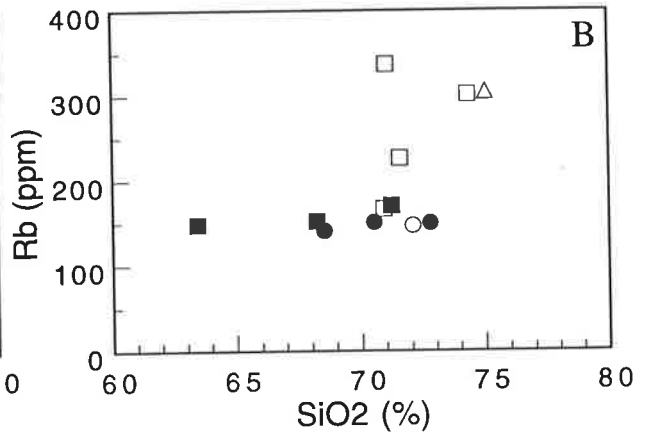
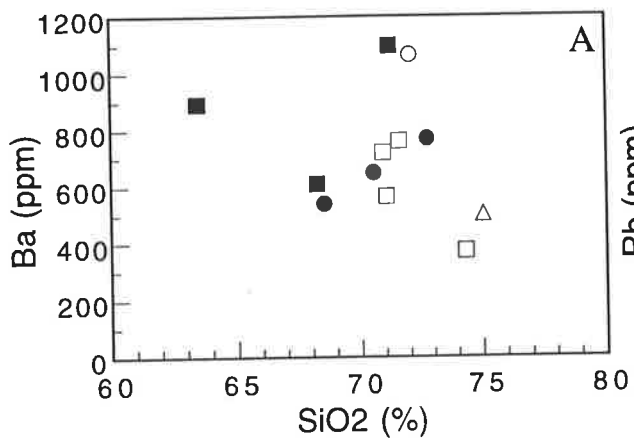


Fig. 5-13. Trace element variation diagram of Bow River Granitoid, granitoids from the King Leopold Mobile Zone, and Whitewater Volcanics

- A. Ba-SiO₂
- B. Rb-SiO₂
- C. Sr-SiO₂
- D. Rb-Sr
- E. Zr-SiO₂
- F. Nb-SiO₂
- G. Y-SiO₂
- H. Ce-SiO₂

Symbols are the same as those in Fig. 5-12.



However, the gabbroic rocks might have provided heat to generate granitic magma. As major element data are similar to those of S-type granitoids, source rocks of the Bow River Granitoid are, as inferred above, more likely to be sedimentary rocks with high K₂O and Rb contents and peraluminous character.

Zr contents range from 140 to 190ppm (Fig. 5-13), except sample 91507. Sample 91507 has a high concentration of highly-charged cations, viz. Zr (332ppm), Nb (20.8ppm), Y (71ppm), Ce (177ppm), and Nd (72ppm). The high level of these elements and metaaluminous character are more representative of an A-type granitoid. High Zn (67ppm) and Ga (19.3ppm) contents tend to support this. Further study of this granitoid is required.

REE data are listed in Table A5-2. Chondrite normalized REE patterns of the Bow River Granitoid are presented in Fig. 5-14. Two samples have basically similar LREE enriched patterns and negative Eu anomaly ($Eu/Eu^* = 0.640$ and 0.347). The patterns are different from those of the Sophie Downs Granitoid the HREE region of which is typically flat. The large Eu anomaly indicates the role of plagioclase in reducing the Eu level relative to the other REE either during partial melting or fractional crystallization.

B. Granitoids from West Kimberleys

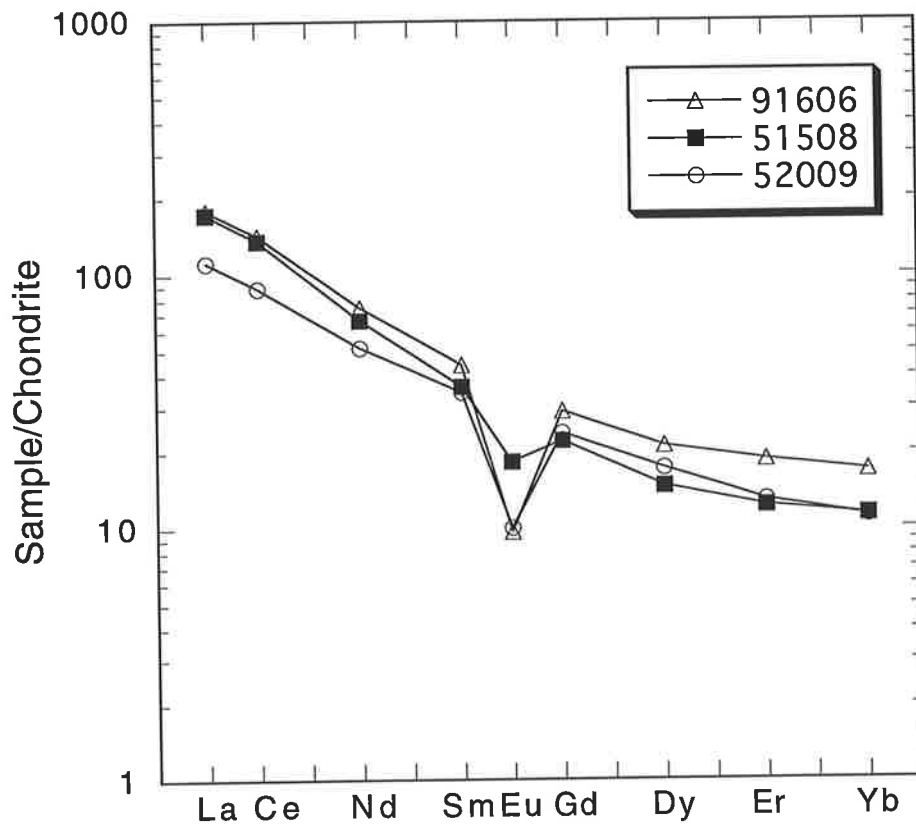
Richenda Granodiorite

Two granodiorites (20201 and 20208) and one sample (20209) from the rhyolitic part are geochemically examined (Table A4-10). SiO₂ ranges from 68.5 to 72.8%. The sample with lowest SiO₂ content is collected near the margin of the pluton. The sample from the rhyolitic part has the highest SiO₂ content. The variation between samples could be explained by fractional crystallization. Mol (Al₂O₃/(CaO + Na₂O +

Fig. 5-14. Chondrite normalized REE pattern of Bow River Granitoid
and Whitewater Volcanics

Bow River Granitoid: samples, 51508 and 52009.

Whitewater Volcanics: sample 91606.



K_2O) ratios vary from 1.069 to 1.094 with increasing SiO_2 . The increase of the ratio is largely due to a decrease in CaO contents from 3.34 to 1.74%. Na_2O/K_2O ratios decrease from about unity to 0.717 with increasing SiO_2 . Thus S-type characteristics are more evident in the rhyolitic rock than the granodiorite.

On the variation diagram (Fig. 5-12), three samples clearly define a trend, and it is considered to be a fractionation trend. The variation diagram illustrates that some major element data of the granodiorite are actually located in the field of I-type granitoids from the Kosciusko Batholith (Hine et al., 1978). The evidence may indicate that the granodiorite is transitional between S- and I-type granitoid.

Trace elements of the granodiorite also have a regular trend (Fig. 5-13). Ba increases from 539 to 767ppm with increasing SiO_2 , and the enrichment excludes the possibility of extensive biotite or K-feldspar fractionation, as these minerals have high Ba mineral/melt distribution coefficients. Rb and Sr do not change significantly, the average contents being 146ppm and 187ppm, respectively. The moderately high Rb contents eliminate direct derivation of magma by partial melting from a basaltic source. Ce and Y decrease with increasing SiO_2 , and chondrite normalized (Ce/Y) ratios range from 8.5 to 13.1, indicating a steep REE pattern. Since most of major silicate minerals have low mineral/melt distribution coefficient for the LREE, the depletion of the LREE may be due to fractionation of accessory minerals (Miller and Mittlefehldt, 1982) such as monazite and allanite, though no other evidence of fractionation of these minerals is found in the rocks.

McSherrys Granodiorite

Chemical compositions of two samples (13103 and 13104) from the McSherrys Granodiorite (Table A4-10) show that it has relatively low mol ($Al_2O_3/(CaO + Na_2O + K_2O)$) ratios (0.940 and 0.930), suggesting

I-type characteristics. However the variation diagrams (Fig. 5-12), for most of the elements of the granodiorite, indicate similarity to those of S-type granitoids. The low $\text{Na}_2\text{O}/\text{K}_2\text{O}$ ratios (0.667, 0.691) of the granodiorite are different from the typical I-type granitoids. Thus the granodiorite is not readily classified in the S- versus I-type scheme.

Rb is high, about 150ppm. High K_2O and Rb eliminate direct derivation of the granodiorite from a basaltic rock, either by fractionation or partial melting. High Ce is found in the samples, and Y is moderate, indicating a steep LREE enriched chondrite normalized pattern.

Ga content is not significantly high, thus excluding classification of the rock as an A-type granitoid.

Dyasons Granite

A sample (13105) from this granite (Table A4-10) is metaluminous ($\text{mol}(\text{Al}_2\text{O}_3/(\text{CaO} + \text{Na}_2\text{O} + \text{K}_2\text{O})) = 0.989$), and has a low $\text{Na}_2\text{O}/\text{K}_2\text{O}$ ratio, similar to the McSherrys Granodiorite. Rb (170ppm) and Ce (119ppm) are high.

In summary, the following observations characterize granitoids from the West Kimberleys:

- (1) The Richenda Granodiorite has S-type geochemical characteristics.
- (2) The McSherrys Granodiorite and Dyasons Granite have low $\text{mol}(\text{Al}_2\text{O}_3/(\text{CaO} + \text{Na}_2\text{O} + \text{K}_2\text{O}))$ ratios and $\text{Na}_2\text{O}/\text{K}_2\text{O}$ ratios, and can not be readily classified in the S- versus I-type scheme.

5.4. Whitewater Volcanics

5.4.1. Petrography

Ashflow tuffs of the Whitewater Volcanics consist of phenocrysts and a strongly welded and devitrified matrix (Fig. 5-11). The phenocrysts, up to 10% of the volume, are embayed quartz, altered plagioclase and K-feldspar. The average grain size of the phenocrysts is about 2mm. No fresh mafic mineral is found; though small aggregates of chlorite indicate the former presence of such, it is not possible to identify the original minerals.

5.4.2. Geochemistry

Only one sample (91606) has been examined. Major and trace element data are presented in Table 5-3, and are plotted on Fig. 5-12 and Fig. 5-13. REE data are listed in Table A5-2.

The sample has high SiO₂ (75.01%) and K₂O (6.19%) contents. Thus the rock can be classified as a high-K rhyolite (Peccerillo and Taylor, 1976). The chondrite normalized REE pattern (Fig. 5-14) depicts LREE enrichment and a strong negative Eu anomaly. Absolute concentrations of REE in the volcanic rock are higher than in the Bow River Granitoid; it has a similar overall pattern to that of the granitoid, though HREE are not as depleted as in the granitoid.

Table 5-3. Chemical composition of Whitewater Volcanics

Sample	91606
Unit	WV
Major elements (%)	
SiO ₂	75.01
Al ₂ O ₃	12.52
Fe ₂ O ₃ *	1.96
MnO	0.03
MgO	0.23
CaO	0.57
Na ₂ O	2.47
K ₂ O	6.19
TiO ₂	0.21
P ₂ O ₅	0.05
LOI	0.99
Total	100.23
Trace elements (ppm)	
Ba	500
Rb	304
Sr	35.5
Zr	188
Nb	12.4
Y	43.2
Ce	117
Nd	49
Sc	5.5
V	11
Cr	4
Ni	4
Cu	6
Zn	31
Ga	15.2
A/CNK	1.061

Fe₂O₃*: Total Fe as Fe₂O₃

LOI: Loss on ignition

A/CNK: Mol Al₂O₃/CaO+Na₂O+K₂O

CHAPTER 6. GEOCHRONOLOGY AND ISOTOPE GEOCHEMISTRY

6.1. Introduction

New Rb-Sr isotopic datings have been made on several igneous bodies and metamorphic rocks from the studied area, and they provide details of the geological history of the area during the Early Proterozoic. Furthermore, initial Sr isotopic ratios of the igneous and metamorphic rocks act as constraints on their petrogenesis. Examination of pre-existing Rb-Sr data is also included.

All the Rb-Sr ages measured and referred to here are calculated and adjusted using the $1.42 \times 10^{-11} \text{y}^{-1}$ decay constant recommended by the IUGS Subcommittee on Geochronology (Steiger and Jager, 1977).

The previous isotopic dating studies in the east Kimberley region are those of Bofinger (1967) and Page and Hancock (1988). Bofinger (1967) presented Rb-Sr and some K-Ar dating results, and established a framework for the geological history of the region. Bofinger (1967) summarized important Early Proterozoic events as follows :

- (1) The main metamorphism (granulite facies) took place at $1920 \pm 27 \text{ Ma}$, associated with the emplacement of the Mabel Downs Granitoid.
- (2) Intrusion of the Bow River and Sophie Downs Granitoids took place at $1815 \pm 14 \text{ Ma}$.
- (3) Intrusion and extrusion of acid porphyry and volcanics, viz. the Whitewater Volcanics and Castlereagh Hill Porphyry, were dated at $1784 \pm 17 \text{ Ma}$.

However, as it is now clear that the Mabel Downs Granitoid Suite was emplaced after the main metamorphism, the isochron based on the regression of data from both metamorphics and the granitoid would not yield a meaningful age. Thus, it is a prime objective of the present study

to obtain an isotopic date based on the Mabel Downs Granitoid Suite alone. Furthermore, since the Sophie Downs Granitoid, a typical A-type granitoid, is distinctly different from the Bow River Granitoid, a combination of these two granitoids on the same isochron is illogical. Thus, in the present study, new Sr isotope data are given also for the Sophie Downs Granitoid.

Page and Hancock (1988) determined three U-Pb zircon ages from the east Kimberley region. These are summarized as follows:

- (1) Biscay Formation (felsic volcanics or high level intrusive)

1856 ± 5 Ma

- (2) Tickalara Metamorphics (pegmatite)

1854 ± 6 Ma

- (3) Whitewater Volcanics (porphyritic dacite volcanics)

1850 ± 5 Ma

Furthermore, Page and Sun (1994) summarized new ion-probe zircon ages for a variety of igneous rocks and metasediments in the east Kimberley region. The results indicate following ages.

- (1) Crystallization ages of felsic volcanics and microgranites (Sophie Downs Granitoid)

1910-1920Ma

- (2) Crystallization age of felsic pyroclastic sequence in the Olympio Formation of the Halls Creek Group

1857±5Ma

- (3) Crystallization ages of the Whitewater Volcanics and Bow River Granitoid

1850-1865Ma

- (4) Emplacement ages of various granitic bodies that were formerly assigned to the Bow River Granite and other suites

1800-1820Ma

In addition to these published ages, the Rb-Sr dating results of present study have been examined to establish a time framework of the Early Proterozoic igneous and tectonic events in the Halls Creek Mobile Zone.

Rb, Sr, and isotopic Sr values have been determined for 42 total rock samples. Analytical techniques are presented in Appendix 6. The results are listed in Table 6-1. Isochron regressions (Table 6-2) were carried out following the method of McIntyre et al. (1966).

6.2. Sally Downs Tonalite

Eleven samples from the Sally Downs Tonalite pluton, of which five were collected from a relatively small area near the locality of sample 51706, were used in the Rb-Sr isotopic study (Table 6-1). Sample 51702 is a mafic microgranular enclave in the tonalite, and is considered from major and trace element chemistry to be comagmatic with the host tonalite. Six of the analyzed samples were primarily selected to provide as wide a range of $^{87}\text{Rb}/^{86}\text{Sr}$ ratios as possible. Despite this, the samples provided only a limited range (0.0985 - 0.3683).

Regression of the analytical data (Fig. 6-1) generates a Model 1 isochron of McIntyre et al. (1966) with mean square of weighted deviates (MSWD) of 1.47. The result indicates an age of 1834 ± 43 Ma and an initial $^{87}\text{Sr}/^{86}\text{Sr}$ ratio of 0.70292 ± 0.00015 .

Bofinger (1967) measured a sample (GA5150) from the Sally Downs Tonalite near the locality of specimen 51706, and the sample was included in the regression of 22 measurements of Mabel Downs Granitoid and country rock metamorphics, giving an age of 1922 ± 46 Ma with very low initial $^{87}\text{Sr}/^{86}\text{Sr}$ ratio of 0.7017 ± 0.0016 . Bofinger's (1967) recommended result, however, is 1920 ± 27 Ma with initial $^{87}\text{Sr}/^{86}\text{Sr}$ of

Table 6-1. Rb-Sr isotopic results

Sample	Rb (ppm)	Sr (ppm)	$^{87}\text{Rb}/^{86}\text{Sr}$	$^{87}\text{Sr}/^{86}\text{Sr}$
Sally Downs Tonalite				
32505A	61.68	483.8	0.36827	0.71255
32802A	56.64	521.5	0.31369	0.71132
40301	30.33	888.7	0.098516	0.70551
40505A	48.30	514.3	0.27121	0.71004
40802	37.37	754.6	0.14297	0.70682
50202	44.93	397.4	0.32656	0.71160
51702	28.81	565.8	0.1470	0.70668
51705A	36.61	567.6	0.18623	0.70783
51706	40.05	564.8	0.20475	0.70832
51710	41.41	559.3	0.21379	0.70863
51713	47.72	526.1	0.26194	0.70975
Sophie Downs Granitoid				
22809	97.96	42.54	6.7613	0.88087
22911	105.08	29.46	10.5639	0.97117
30608	116.37	29.67	11.6558	1.00708
30706	120.11	29.32	12.1929	1.02340
30802	132.65	42.82	9.1435	0.93542
31306	130.32	102.19	3.7148	0.79875
31408	95.51	56.05	4.9833	0.83933
31414	108.19	29.56	10.8513	0.98236
Dougalls Granitoid Suite				
12703	34.70	331.0	0.30276	0.71047
20907	27.41	305.3	0.25925	0.70905
21901	20.29	344.5	0.17004	0.70709
22107	23.45	346.7	0.19528	0.70738
51604	52.46	488.5	0.31016	0.71086
Ord River Tonalite Suite				
11203	65.0	357	0.5262	0.71700
11204	70.0	362	0.5588	0.71767
51302	51.2	430	0.3439	0.71140
51303	69.7	425	0.4738	0.71501
51304	53.6	417	0.3713	0.71205
51305	53.1	425	0.3609	0.71189
51306	51.1	439	0.3362	0.71122
51309	53.0	405	0.378	0.71232
51310	41.7	558	0.2158	0.70824
Tickalara Metamorphics				
51902	166	247	1.9498	0.75738
51904	88	334	0.7619	0.72388
51905	167	266	1.8207	0.75317
51907	93	276	0.9751	0.73088
Eastern Leucocratic Granitoid				
40306	59.34	89.87	1.9149	0.75308
41702	45.69	83.20	1.5913	0.74447
Western Porphyritic Granite				
51918	142	146	2.8271	0.77680
52103	173	128	3.9392	0.80444
Hornblendite				
11309	7.1	230	0.08911	0.70518

Table 6-2. Regression of Rb-Sr data

Regression Data Set	No.	Age (Ma)	Initial Ratio	MSWD	Model
Sally Downs Tonalite-1	11	1834±43	0.70292±0.00015	1.47	1
Sally Downs Tonalite-2	12	1833±42	0.70292±0.00015	1.38	1
Sophie Downs Granitoid-1	8	1776±92	0.7067±0.0118	69.8	4
Sophie Downs Granitoid-2	7	1799±64	0.7029±0.0065	28.4	2
Sophie Downs Granitoid-3	11	1811±48	0.7022±0.0052	23.1	2
Dougalls Granitoid Suite	5	1890±427	0.7022±0.0015	10.9	3
Ord River Tonalite Suite-1	9	1889±128	0.70219±0.00065	9.1	2
Ord River Tonalite Suite-2	5	1923±159	0.70187±0.00085	0.74	1
Tickalara Metamorphics	4	1917±194	0.7033±0.0040	34	3
Eastern Leucocratic Granitoid	2	1849	0.70214	----	-
Western Porphyritic Granite	2	1729	0.7065	----	-

Isochron regressions were carried out following the method of McIntyre et al. (1966).

No.: Number of samples in the regression

MSWD: Mean square of weighted deviates

Model: Isochron model types of McIntyre et al. (1966)

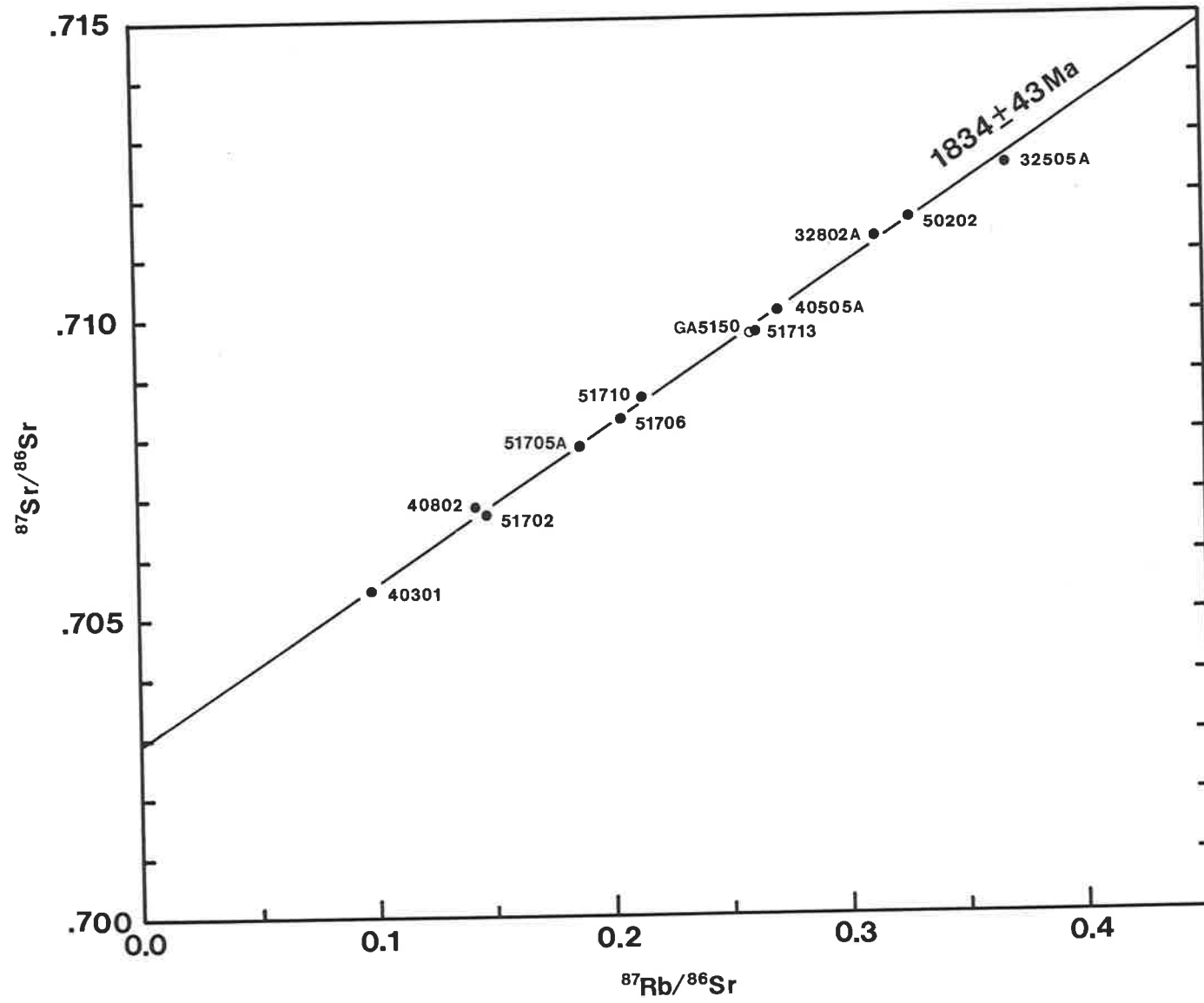
Sally Downs Tonalite-2: 11 samples of the present study and a sample (GA5150) from Bofinger (1967).

Sophie Downs Granitoid-3: 8 samples from the present study and 3 from Bofinger (1967).

Fig. 6-1. Rb-Sr isochron for the Sally Downs Tonalite

Solid circles: present study

Open circle: data by Bofinger (1967) on sample collected from the Sally
Downs Tonalite.



0.7010 ± 0.0006 based on 14 samples, after omitting 8, including GA5150, from the regression, in order to reduce the MSWD.

However, sample (GA5150) plots perfectly on the isochron of the present study (Fig. 6-1). In fact, regression of the 12 measurements (Table 6-2), 11 from the present study and one of the sample (GA5150), produce an age of 1833 ± 42 Ma and initial $^{87}\text{Sr}/^{86}\text{Sr}$ ratio (0.70292 ± 0.00015) which is not significantly different from the result obtained using 11 measurements only (see above). The new regression even slightly reduces the MSWD to 1.38.

The result is significantly different, however, from Bofinger's (1967) result, reducing as it does the age of emplacement of the Mabel Downs Granitoid Suite by 90 Ma from 1922 Ma to 1834 Ma. Bofinger's isochron is considered anomalous and to be a mixing line, the low $^{87}\text{Rb}/^{86}\text{Sr}$ region of the isochron being largely controlled by the Mabel Downs Granitoid and high $^{87}\text{Rb}/^{86}\text{Sr}$ by the metamorphics. The low initial $^{87}\text{Sr}/^{86}\text{Sr}$ has in the past presented problems of interpretation. Bofinger (1967) considered that the ratio was due to complete loss of radiogenic Sr from the metamorphics and Mabel Downs Granitoid at 1920 Ma. Page (1976) interpreted the evidence as indicating that the metamorphics and the granitoid had little or no crustal prehistory. Initial $^{87}\text{Sr}/^{86}\text{Sr}$ of 0.70292 ± 0.00015 resulting from the present study, however, does not invite such a drastic explanation.

Griffin et al. (1994) obtained ion probe U-Pb ages of 1820 Ma for zircons from the Sally Downs Tonalite. The ages are comparable to the Rb-Sr age of the present study within the analytical uncertainty.

6.3. Sophie Downs Granitoid

Eight total rock samples of the Sophie Downs Granitoid show (Table 6-1) a fair spread of $^{87}\text{Rb}/^{86}\text{Sr}$ values (3.715 - 12.193). Regression of

all eight samples results in a Model 4 isochron (MSWD = 69.8) with an age of 1776 ± 92 Ma and initial $^{87}\text{Sr}/^{86}\text{Sr}$ of 0.7067 ± 0.0118 (Table 6-2). The Model 4 isochron fit (McIntyre et al., 1966) indicates both variation in initial $^{87}\text{Sr}/^{86}\text{Sr}$ values and post-emplacement isotopic or elemental redistribution.

The MSWD may be reduced to 28.4 by omitting sample 31408A which was collected near the northwestern margin of the Sophie Downs Granitoid pluton (Fig. 5-1), and may have been the most susceptible of the samples to contamination from country rock and post-crystallization alteration. Regression yields a Model 2 isochron with an age of 1799 ± 64 Ma and an initial $^{87}\text{Sr}/^{86}\text{Sr}$ of 0.7029 ± 0.0065 (Fig. 6-2). The Model 2 isochron (McIntyre et al., 1966) suggests that the samples have undergone slight redistribution of Rb and/or Sr after crystallization. Since biotite in the samples is commonly chloritized and plagioclase is partly sericitized, the samples may have undergone a post-crystallization alteration, examples of which are common in high-level intrusive bodies.

Bofinger (1967) analyzed three samples from the Sophie Downs Granitoid pluton. Regression of 11 measurements, 8 from the present study and the 3 from Bofinger (1967), again results in a Model 2 isochron, but with MSWD slightly reduced to 23.1. The resultant age is 1811 ± 48 Ma with an initial $^{87}\text{Sr}/^{86}\text{Sr}$ of 0.7022 ± 0.0052 (Table 6-2). Ages given by both Model 2 isochrons, i.e. with and without Bofinger's (1967) data, are identical within statistical limits.

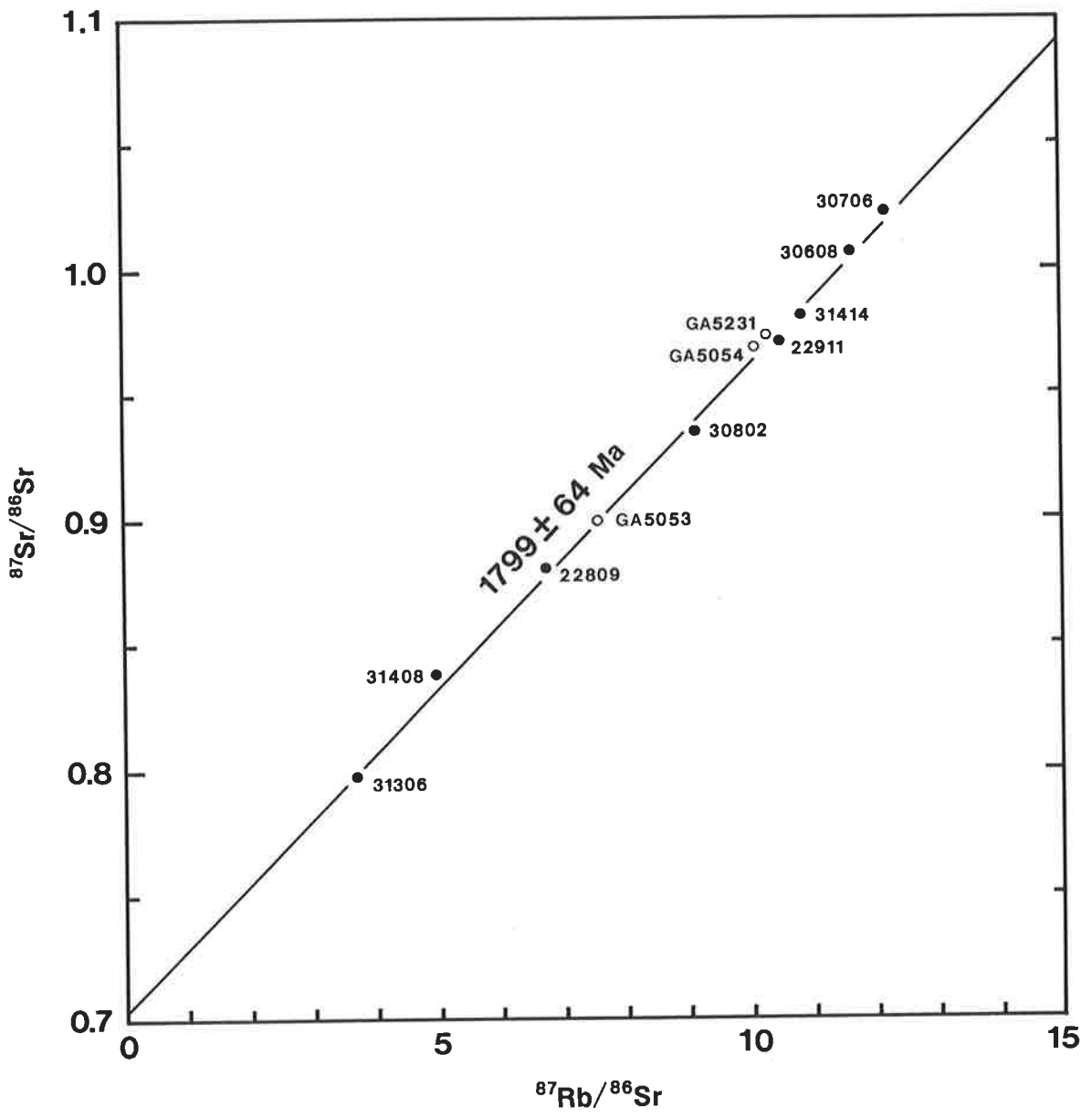
As the Sophie Downs Granitoid gives U-Pb ages from zircons of 1910Ma (Page and Sun, 1994), the Rb-Sr age of the granitoid obtained by present study may reflect a later tectono-thermal event.

6.4. Dougalls Granitoid Suite

Fig. 6-2. Rb-Sr isochron for the Sophie Downs Granitoid

Solid circles: present study

Open circles: data by Bofinger (1967) on sample collected from the
Sophie Downs Granitoid



Five total rock samples from the Dougalls Granitoid Suite were analyzed isotopically (Table 6-1); one sample (21901) is trondhjemite, and other four samples are orthopyroxene-bearing tonalite. Regression of the data results in a Model 3 isochron (Fig. 6-3), with MSWD of 10.9, which indicates an age of 1890 ± 427 Ma and an initial $^{87}\text{Sr}/^{86}\text{Sr}$ of 0.7022 ± 0.0015 (Table 6-2). A Model 3 isochron suggests variation of initial $^{87}\text{Sr}/^{86}\text{Sr}$ in the samples (McIntyre et al., 1966). Large error in the estimation of the age is partly due to the small spread of $^{87}\text{Rb}/^{86}\text{Sr}$ (0.1700 - 0.3102) in the samples. Although suggested variation of initial $^{87}\text{Sr}/^{86}\text{Sr}$ is large, all the Dougalls Granitoid Suite data are plotted on the lower $^{87}\text{Sr}/^{86}\text{Sr}$ side of the Sally Downs Tonalite isochron (compare Fig. 6-1 and Fig. 6-3), indicating clearly the lower initial $^{87}\text{Sr}/^{86}\text{Sr}$ of the Dougalls Granitoid Suite than that of the Sally Downs Tonalite.

6.5. Ord River Tonalite Suite

Nine samples of the Ord River Tonalite Suite from three localities were analyzed (Table 6-1). Five of the samples were collected from a small outcrop along the Ord River (Fig. 3-24).

Regression of the nine samples (Fig. 6-4) yields a Model 2 isochron with MSWD = 9.1, and an age of 1889 ± 128 Ma with initial $^{87}\text{Sr}/^{86}\text{Sr}$ of 0.70219 ± 0.00065 (Table 6-2). Two samples, 11203 and 11204, plot above the isochron, and contribute to the large limit of error. A second regression of five samples, from the small outcrop along the Ord River, yields a Model 1 isochron with MSWD 0.74, and indicates an age of 1923 ± 159 Ma and initial $^{87}\text{Sr}/^{86}\text{Sr}$ of 0.70187 ± 0.00085 . Large uncertainty in the age is a result of a small spread (0.3362 - 0.4738) in $^{87}\text{Rb}/^{86}\text{Sr}$ ratios. The initial $^{87}\text{Sr}/^{86}\text{Sr}$ ratio is significantly lower than that of the Sally Downs Tonalite.

Fig. 6-3. Rb-Sr isochron for the Dougalls Granitoid

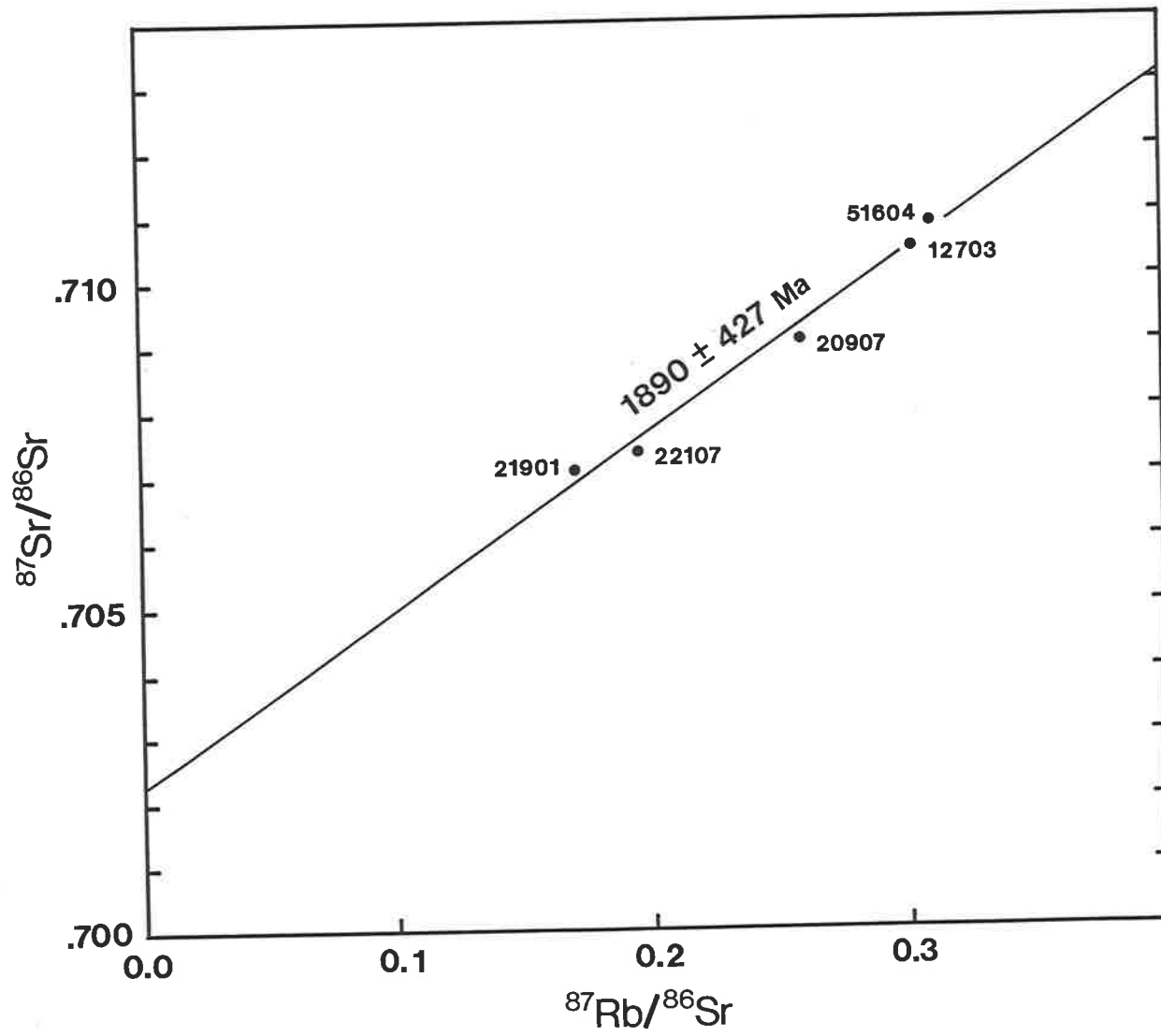
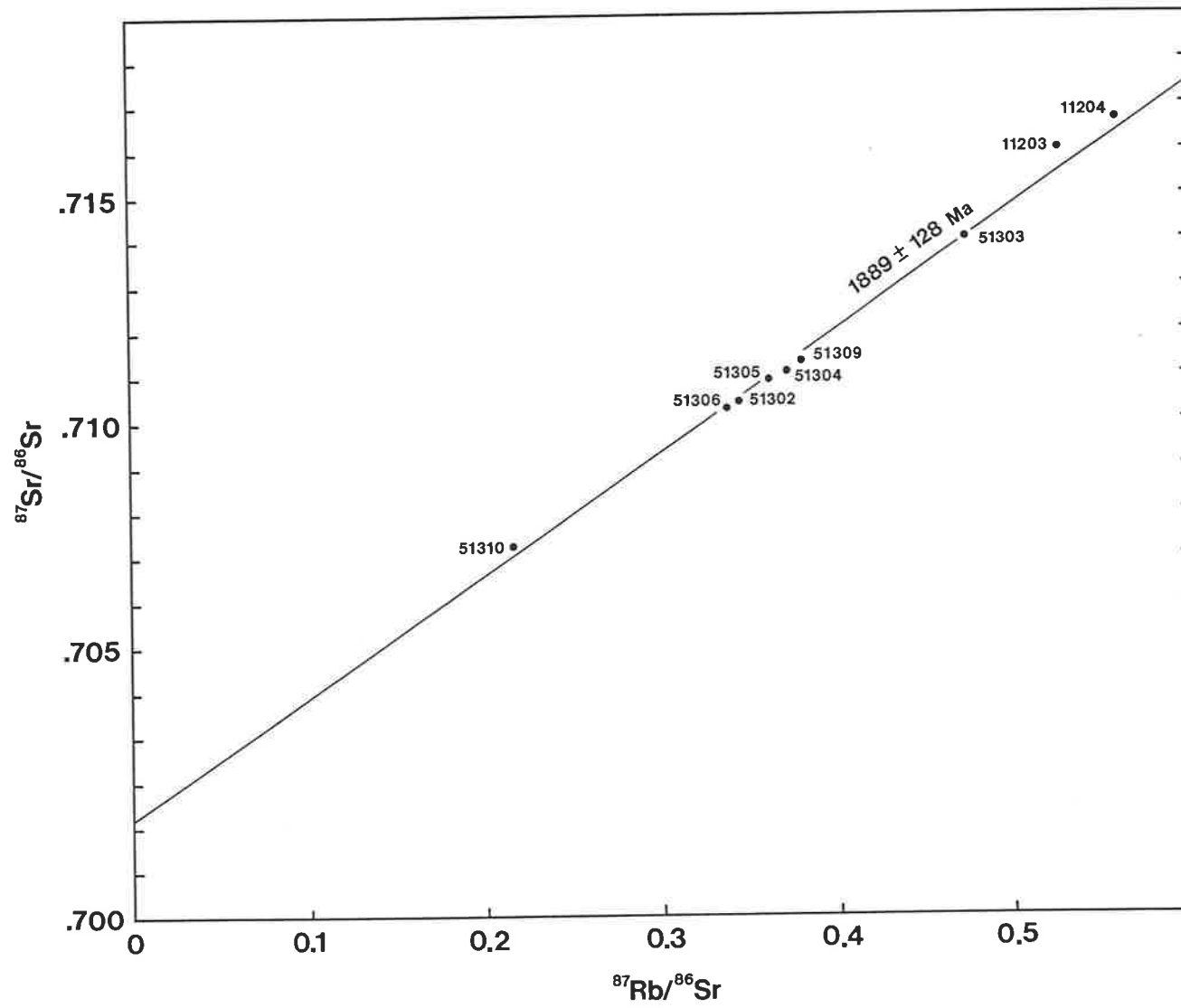


Fig. 6-4. Rb-Sr isochron for the Ord River Tonalite



Field evidence indicates that the Ord River Tonalite is different from the Sally Downs Tonalite though some acidic members of the Sally Downs Tonalite, under the microscope, resemble the Ord River Tonalite. However, the different initial $^{87}\text{Sr}/^{86}\text{Sr}$ ratios indicate that they were not derived from a common magma. Furthermore, though the indicated age of the Ord River Tonalite has a large limit of error, the result could support an interpretation that the Ord River Tonalite is older than the Sally Downs Tonalite.

6.6. Eastern Leucocratic Granitoid

Only two samples of the Eastern Leucocratic Granitoid were measured (Table 6-1). The two points yield an isochron with an age of 1849 Ma and an initial $^{87}\text{Sr}/^{86}\text{Sr}$ of 0.70214. The low initial $^{87}\text{Sr}/^{86}\text{Sr}$ ratio is noteworthy and would provide a constraint for its petrogenesis. Its age in relationship to that of the other granitoids is uncertain.

6.7. Western Porphyritic Granite

Two samples of the Western Porphyritic Granite were analyzed isotopically (Table 6-1). An isochron using the two points gives a young age (1729 Ma) with an initial $^{87}\text{Sr}/^{86}\text{Sr}$ of 0.7065. The age is difficult to interpret, since field evidence indicates that the granite was emplaced before or during D₃ deformation and before the emplacement of the Sally Downs Tonalite (1834 ± 43 Ma). Thus the granite may have undergone redistribution of radiogenic Sr after emplacement.

6.8. Tickalara Metamorphics

Four samples of pelitic biotite gneiss mapped as Tickalara Metamorphics have been collected from an outcrop about 3km northeast of the Sally Downs Bore. The results of isotope analyses are given in

Table 6-1 and plotted on Fig. 6-5. Regression of the four data points results in a Model 3 isochron fit with MSWD 34, and indicates an age of 1917 ± 194 Ma and initial $^{87}\text{Sr}/^{86}\text{Sr}$ 0.7033 ± 0.0040 . The resultant Model 3 regression suggest that there is some variation in the initial $^{87}\text{Sr}/^{86}\text{Sr}$ of the samples. The variation could be due to incomplete homogenization of Sr isotopes during the metamorphism.

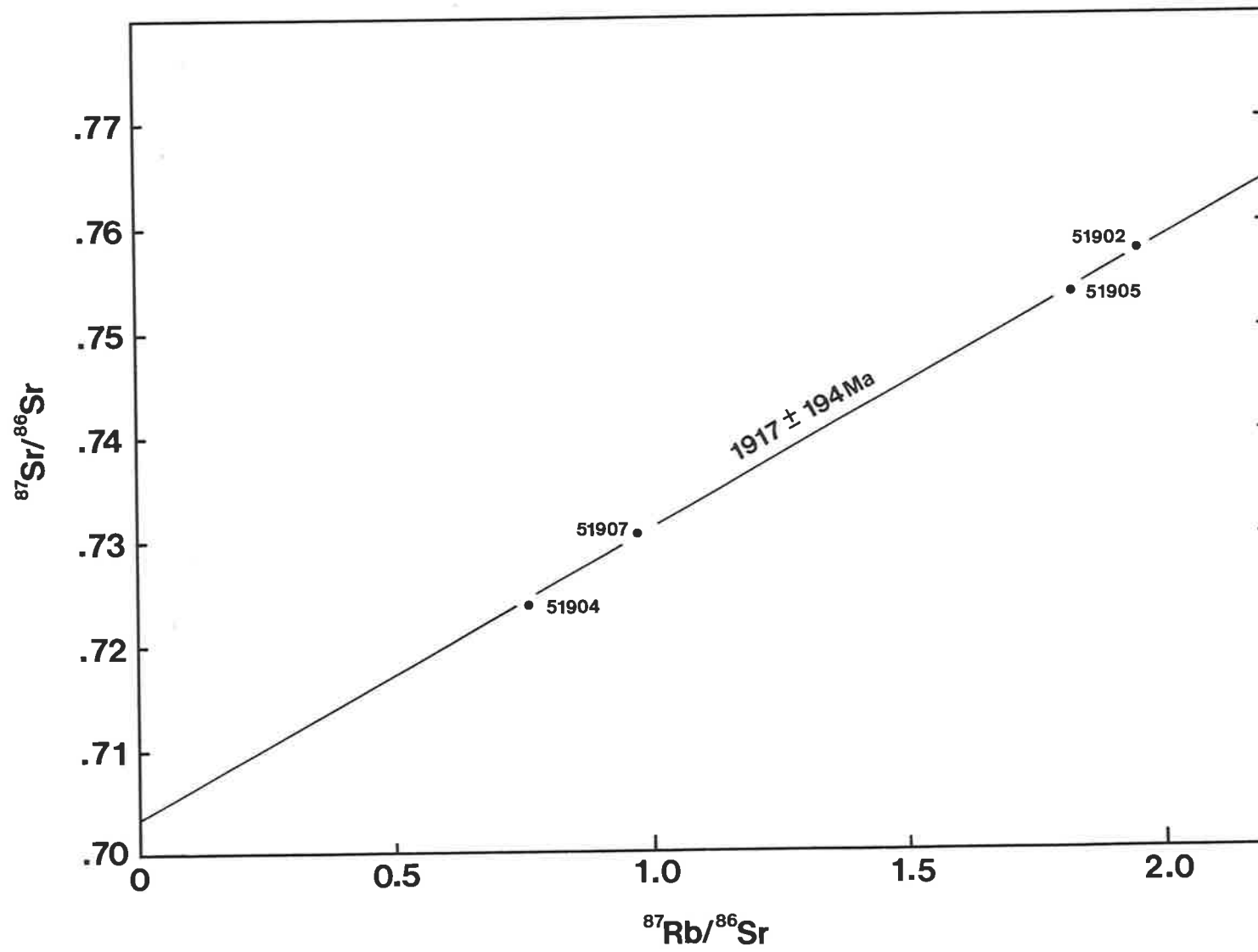
6.9. Hornblendite

One sample of the hornblendite was analyzed (Table 6-1). Since the sample has a very low Rb/Sr ratio, the initial $^{87}\text{Sr}/^{86}\text{Sr}$ could be estimated reasonably well. If the hornblendite has a similar age to the Sally Downs Tonalite (1834 ± 43 Ma), the initial $^{87}\text{Sr}/^{86}\text{Sr}$ of the hornblendite is 0.70283 ± 0.00006 . Even if it has an age of 1900 Ma, the initial $^{87}\text{Sr}/^{86}\text{Sr}$ is still 0.70274. Thus the initial $^{87}\text{Sr}/^{86}\text{Sr}$ of the hornblendite can be approximated to 0.7028. The value is significant as it is identical within the statistical limits of the initial $^{87}\text{Sr}/^{86}\text{Sr}$ of the Sally Downs Tonalite.

6.10. Discussion of the Geochronological Results

The Rb-Sr data from the Sally Downs Tonalite indicate an age of 1834 ± 43 Ma, which is significantly younger than the Rb-Sr age of the Tickalara Metamorphics and Mabel Downs Granitoid (1922 ± 46 Ma or 1920 ± 27 Ma) determined by Bofinger (1967). In the Sally Downs Bore area, the Sally Downs Tonalite was emplaced after the D₃ deformation, and thus the all regional deformation D₁ to D₃ took place before the age of 1834 ± 43 Ma. The Rb-Sr data of the Dougalls Granitoid Suite which was emplaced during or before D₁, associated with granulite facies metamorphism, indicate an imprecise age of 1890 ± 427 Ma, which could represent the approximate time of D₁ deformation and the

Fig. 6-5. Rb-Sr isochron for the Tickalara Metamorphics



metamorphism. Similar, but again imprecise, ages were obtained from the Ord River Tonalite Suite (1889 ± 128 Ma or 1923 ± 159 Ma) and from the gneisses of the Tickalara Metamorphics (1917 ± 194 Ma) from the Sally Downs Bore area. These results are similar to that of Bofinger's (1967) analysis of the Tickalara Metamorphics and Mabel Downs Granitoid. If Bofinger's (1967) age is largely controlled by data from the Tickalara Metamorphics which generally have high $^{87}\text{Rb}/^{86}\text{Sr}$, the figure could represent an approximate age of the metamorphism, though this age is slightly greater than it should be because of the positioning of a too low initial $^{87}\text{Sr}/^{86}\text{Sr}$ due to the inclusion of the Mabel Downs Granitoid data. Thus, 1890 Ma, indicated by the age of the Dougalls Granitoids Suite, is assumed to be the age of the D₁ deformation and granulite facies metamorphism, younger than Bofinger's (1967) age.

The age of high grade metamorphic event in the Tickalara Metamorphics is considered to be 1854 ± 6 Ma by Page and Hancock (1988), based on the U-Pb zircon age determination of a pegmatite found in the metamorphics. They assumed that the pegmatite was formed by the anatexis of the metamorphic rock during the high grade metamorphism. Therefore, they considered that the age of the pegmatite represents that of the high grade metamorphism. The U-Pb zircon age is 20 Ma older than the Rb-Sr isochron age of the Sally Downs Tonalite (1834 ± 43 Ma), but it is statistically indistinguishable from the Rb-Sr age of the tonalite because the Rb-Sr age of the tonalite has a large uncertainty. However, it is 40 Ma younger than the age of granulite facies metamorphism (about 1890 Ma), which is assumed from the Rb-Sr isochron data from the Dougalls Granitoid Suite. Page and Hancock (1988) stated that most of analyzed zircon grains show $^{207}\text{Pb}/^{206}\text{Pb}$ ages of about 1851 Ma, one grain having a slightly older age of 1887 Ma. The zircon $^{207}\text{Pb}/^{206}\text{Pb}$ age might indicate the age of an older igneous event in the area at about

1890 Ma. It is necessary to obtain precise U-Pb zircon ages of the older granitoids to establish timing of the igneous activity in the Halls Creek Mobile Zone.

Page and Hancock (1988) determined a U-Pb zircon age of the Whitewater Volcanics from the Halls Creek Mobile Zone of 1850 ± 5 Ma. The age is not significantly different from U-Pb ages for the Biscay Formation sill and high grade metamorphic event in the Tickalara Metamorphics also determined by Page and Hancock (1988), viz. 1856 ± 5 Ma and 1854 ± 6 Ma, respectively. Based on these results, Page and Hancock (1988) emphasised the rapid tectonic transition in the Halls Creek Mobile Zone from the deposition of the Halls Creek Group (represented by the age of the Biscay Formation sill), through high grade metamorphism, to felsic volcanism. However, it should be appreciated that the age of the pegmatite in the Tickalara Metamorphics may not be the same as that of the high grade metamorphism, and the age of the Biscay Formation sill may not signify the deposition age of the Biscay Formation. Page and Sun (1994) indicated that felsic volcanics within the Olympio Formation have crystallization ages of 1870 ± 4 Ma and 1868 ± 3 Ma. These ages may provide upper limit of the age of the deposition of the Halls Creek Group. Nevertheless, it is necessary to have more detailed geological interpretations and/or further determinations of the U-Pb age of the suitable specimens to establish the timing of the deposition of the Halls Creek Group and of the metamorphism. However, at this stage, it can be accepted that the U-Pb age of the Whitewater Volcanics indicates a zircon crystallization age and hence the extrusive and depositional age of the volcanics (Page and Hancock, 1988). Thus the U-Pb dating provides the most reliable absolute minimum age for the tectonism in the Halls Creek Mobile Zone.

6.11. Sr Isotope Geochemistry

A Rb-Sr geochronological study provides not only the age of rocks but also an initial $^{87}\text{Sr}/^{86}\text{Sr}$ ratio which sets important constraints on the petrogenesis of those rocks.

The Sally Downs Tonalite has a low initial $^{87}\text{Sr}/^{86}\text{Sr}$ of 0.70292 ± 0.00015 (Table 6-2), which is slightly higher than the Sr isotope composition ($^{87}\text{Sr}/^{86}\text{Sr} = 0.7023$) of the unfractionated mantle at 1834 Ma, calculated from the present value of $^{87}\text{Sr}/^{86}\text{Sr} = 0.7045$ and $^{87}\text{Rb}/^{86}\text{Sr} = 0.0827$ in the unfractionated mantle (DePaolo and Wasserburg, 1976). The low initial $^{87}\text{Sr}/^{86}\text{Sr}$ ratio precludes a significant contribution of older crustal materials with high Rb/Sr ratio at any stage of its evolution. If the source rock has a Rb/Sr ratio of 0.314, which is an estimated value for the post Archaean upper continental crust (Taylor and McLennan, 1981), only 53 Ma would be required to evolve an Sr isotope composition to the value of the Sally Downs Tonalite (0.70292). And because the metasediments of the Tickalara Metamorphics have a Rb/Sr ratio (0.54-0.82, from Rb and Sr data in Table 2-1) greater than 0.314, the metasediments are unlikely to have been a significant constituent of the source rock. Indeed, if the crustal residence time of the source rock of the Sally Downs Tonalite was considerable, the source rock must have had a low Rb/Sr ratio.

Hornblendite, the parental magma of which is considered to be derived directly by partial melting of mantle, has a similar initial $^{87}\text{Sr}/^{86}\text{Sr}$ ratio (0.7028) to that of the Sally Downs Tonalite; this may indicate that the mantle under the Halls Creek Orogenic Zone about 1834 Ma ago had a slightly higher $^{87}\text{Sr}/^{86}\text{Sr}$ ratio than the unfractionated mantle. If so, magma with the initial $^{87}\text{Sr}/^{86}\text{Sr}$ of 0.70292 could have been obtained directly from the mantle. The situation is compatible with a model whereby the Sally Downs Tonalite was produced by fractional

crystallization of basic magma which was directly derived from the mantle.

The initial $^{87}\text{Sr}/^{86}\text{Sr}$ of the main body of the Mabel Downs Granitoid can be estimated from sample (GA 957) which has been measured by Bofinger (1967). This has a $^{87}\text{Rb}/^{86}\text{Sr}$ ratio of 0.220, and $^{87}\text{Sr}/^{86}\text{Sr}$ of 0.7082. Assuming the age of the rocks as 1834 Ma, similar to Rb-Sr isochron age of the Sally Downs Tonalite, the calculated initial $^{87}\text{Sr}/^{86}\text{Sr}$ is 0.7024. This is lower than that of the Sally Downs Tonalite. However it is still slightly higher than the value (0.7023) of unfractionated mantle at 1834 Ma. The difference in initial $^{87}\text{Sr}/^{86}\text{Sr}$ between the main body and the Sally Downs Tonalite could be due to heterogeneity of the Sr isotope composition in the source region of the Mabel Downs Granitoid Suite. The location of the sample (GA 957) is 50km north of the Sally Downs Tonalite, and a difference in Sr isotope composition over that distance is not unlikely.

On the other hand, because the Sally Downs Tonalite is considerably smaller than the main body, and contains a number of xenoliths of country rock, it is also possible that the Sally Downs Tonalite was contaminated by country rock, and has a slightly higher initial $^{87}\text{Sr}/^{86}\text{Sr}$ ratio as a consequence of this. However, the Model 1 isochron fit for the Sally Downs Tonalite indicates complete homogenization of the Sr isotope composition, and country rock contamination of the Sr isotope composition is unlikely to have taken place.

Peterman (1979) discussed initial $^{87}\text{Sr}/^{86}\text{Sr}$ ratios of tonalites and trondhjemites throughout the earth's history, and found a simple linear trend of the initial $^{87}\text{Sr}/^{86}\text{Sr}$ ratios with time. The trend is defined as a line connecting the Sr isotope composition of meteorites at 4500 Ma with a value of 0.7039 ± 0.0004 at the present time. The initial $^{87}\text{Sr}/^{86}\text{Sr}$ of the Sally Downs Tonalite is higher than the $^{87}\text{Sr}/^{86}\text{Sr}$ of the trend at

1834 Ma (0.7020), and is even beyond the 95% confidence limit of uncertainty for the trend, indicating that the source rock of the Sally Downs Tonalite may differ slightly from the source rocks of the average tonalite and trondhjemite.

6.12. Nd Isotope Geochemistry

In the previous sections, Sr isotope data have provided new Rb-Sr isochron ages and petrogenetic information concerning the studied rocks; further constraints on the petrogenesis can be obtained from a consideration of Sm-Nd isotopes. Because Sm and Nd have slightly different chemical properties and fractionate systematically, and because they are relatively immobile during low grade metamorphism and weathering, a study of the Sm-Nd isotopes offers valuable information about the nature of the source of a granitoid (e.g. DePaolo, 1981; McCulloch and Chappell, 1982).

Sm-Nd and Rb-Sr isotopic data from the Sally Downs Tonalite and Sophie Downs Granitoid are presented in Table 6-3. Sm-Nd isotopic data are provided by McCulloch (1987). Also isotopic parameters and notations are given in Table 6-3.

The initial Nd and Sr isotopic ratios in the ϵ -notation are plotted in Fig. 6-6. The Sally Downs Tonalite and Sophie Downs Granitoid have negative ϵ_{Nd} values, -1.2 and -3.9, respectively. However, the value of the former is closer to the chondritic mantle value, indicating the absence of any significant amount of older crustal material in the source of the tonalite. The ϵ_{Sr} value of the Sophie Downs Granitoid, calculated from the initial $^{87}Sr/^{86}Sr$ ratio from the isochron regression result, is similar to that of the Sally Downs Tonalite. However, when the crystallization age of 1910Ma of the Sophie Downs Granitoid (Page and Sun, 1994) is used for the calculation, extremely low initial $^{87}Sr/^{86}Sr$ ratio and

Table 6-3. Sm-Nd and Rb-Sr isotopic parameters

Sample	Unit	Sm(ppm)	Nd(ppm)	Rb(ppm)	Sr(ppm)	$^{147}\text{Sm}/^{144}\text{Nd}$	$^{143}\text{Nd}/^{144}\text{Nd}$	$^{87}\text{Rb}/^{86}\text{Sr}$	$^{87}\text{Sr}/^{86}\text{Sr}$
51706	Sally Downs Tonalite	3.9	21.7	40.1	565	0.1083	0.51071±2	0.20475	0.70832
30802	Sophie Downs Granitoid	5.7	32.1	133.	42.8	0.1075	0.51058±2	9.1435	0.93542

Sample	Unit	$^{143}\text{Nd}/^{144}\text{Nd}(\text{I})$	$^{87}\text{Sr}/^{86}\text{Sr}(\text{I})$	ϵNd	ϵSr	T_{CHUR}	T_{DM}	T_{UR}	T
51706	Sally Downs Tonalite	0.50940	0.70292	-1.2	8.6	1940Ma	2130Ma	2170Ma	1834Ma
30802	Sophie Downs Granitoid	0.50931	0.7029	-3.9	7.7	2140Ma	2290Ma	1772Ma	1799Ma
30802*	Sophie Downs Granitoid	0.50922	0.6840	-2.7	-260	-----	-----	-----	1910Ma

30802*: Isotopic parameters are calculated using zircon U-Pb age of the Sophie Downs Granitoid (Page and Sun, 1994). Initial $^{87}\text{Sr}/^{86}\text{Sr}$ ratio is extremely low, indicating loss of radiogenic Sr after the crystallization.

Sm and Nd concentrations and Nd isotope data were measured by M.T. McCulloch, Australian National University (McCulloch, 1987); the experimental technique has been described by McCulloch and Chappell (1982). Sm and Nd concentrations of the sample, 51706, have been also determined by isotope dilution mass spectrometry in this study at the Adelaide University as a part of the REE analysis (Table A5-1), and are 3.98ppm and 22.2ppm respectively. The results of the two analyses are in good agreement.

The initial $^{143}\text{Nd}/^{144}\text{Nd}$ values are given as the deviation, ϵNd , from the value of $^{143}\text{Nd}/^{144}\text{Nd}$ in a reference reservoir (CHUR: chondritic mantle reservoir) as follows:

$$\epsilon\text{Nd} = \left(\frac{^{143}\text{Nd}/^{144}\text{Nd}}{^{143}\text{Nd}/^{144}\text{Nd}} \right)_{\text{INIT}} / \left(\frac{^{143}\text{Nd}/^{144}\text{Nd}}{^{143}\text{Nd}/^{144}\text{Nd}} \right)_{\text{CHUR}}^T - 1 \times 10^4$$

$$\text{and } \left(\frac{^{143}\text{Nd}/^{144}\text{Nd}}{^{143}\text{Nd}/^{144}\text{Nd}} \right)_{\text{CHUR}}^T = \left(\frac{^{143}\text{Nd}/^{144}\text{Nd}}{^{143}\text{Nd}/^{144}\text{Nd}} \right)_{\text{CHUR}}^0 - \left(\frac{^{147}\text{Sm}/^{144}\text{Nd}}{^{147}\text{Sm}/^{144}\text{Nd}} \right)_{\text{CHUR}}^0 (\epsilon(\lambda_{\text{Sm}}T) - 1)$$

where present-day values of the reference reservoir are

$$\left(\frac{^{143}\text{Nd}/^{144}\text{Nd}}{^{143}\text{Nd}/^{144}\text{Nd}} \right)_{\text{CHUR}}^0 = 0.511836 \text{ and } \left(\frac{^{147}\text{Sm}/^{144}\text{Nd}}{^{147}\text{Sm}/^{144}\text{Nd}} \right)_{\text{CHUR}}^0 = 0.1967 \text{ (Jacobsen and Wasserburg, 1980). } \lambda_{\text{Sm}} = 6.54 \times 10^{-12} \text{ y}^{-1}.$$

A similar notation is derived for Sr, viz. $(^{87}\text{Sr}/^{86}\text{Sr})_{\text{UR}}^0 = 0.7045$, $(^{87}\text{Rb}/^{86}\text{Sr})_{\text{UR}}^0 = 0.0827$ (DePaolo and Wasserburg, 1976) and $\lambda_{\text{Rb}} = 1.42 \times 10^{-11} \text{ y}^{-1}$.

Nd model ages have been calculated using the common formulation, which yields the time at which each sample differentiated, in an assumed single event, from mantle. T_{CHUR} and T_{DM} are model ages derived from chondritic and depleted mantle composition, respectively. The model ages are given by the following equations:

$$T_{\text{CHUR}} = 1/\lambda_{\text{Sm}} \times \ln \left(1 + \left(\frac{^{143}\text{Nd}/^{144}\text{Nd}}{^{143}\text{Nd}/^{144}\text{Nd}} \right)_{\text{meas}} - \left(\frac{^{143}\text{Nd}/^{144}\text{Nd}}{^{143}\text{Nd}/^{144}\text{Nd}} \right)_{\text{CHUR}}^0 \right) / \left(\left(\frac{^{147}\text{Sm}/^{144}\text{Nd}}{^{147}\text{Sm}/^{144}\text{Nd}} \right)_{\text{meas}} - \left(\frac{^{147}\text{Sm}/^{144}\text{Nd}}{^{147}\text{Sm}/^{144}\text{Nd}} \right)_{\text{CHUR}}^0 \right)$$

where $(^{143}\text{Nd}/^{144}\text{Nd})_{\text{meas}}$ and $(^{147}\text{Sm}/^{144}\text{Nd})_{\text{meas}}$ are measured values of the sample. T_{DM} is given similarly with $(^{143}\text{Nd}/^{144}\text{Nd})_{\text{DM}}^0 = 0.51235$ and $(^{147}\text{Sm}/^{144}\text{Nd})_{\text{DM}}^0 = 0.225$.

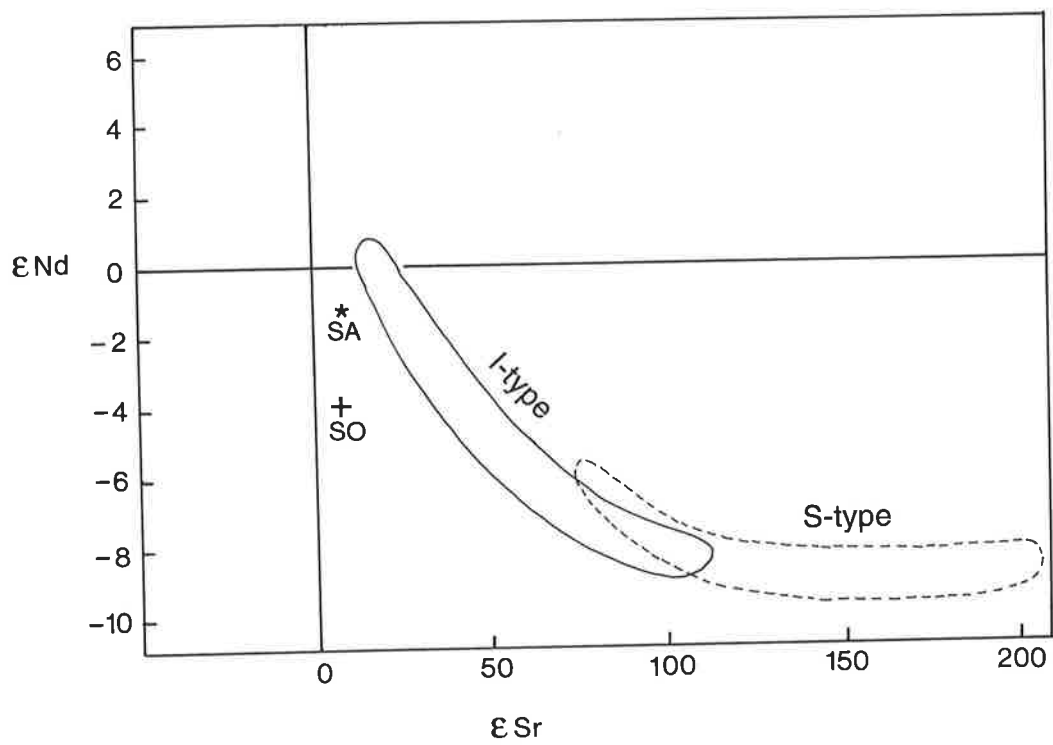
Fig. 6-6. ϵNd - ϵSr diagram

Data from McCulloch (1987).

SA: sample, 51706, from the Sally Downs Tonalite

SO: sample, 30802, from the Sophie Downs Granitoid

I- and S-type fields from McCulloch and Chappell (1982).



negative ϵSr are obtained (Table 6-3), indicating loss of radiogenic Sr after the crystallization.

Phanerozoic granitoids have a large range of ϵNd values, from -16 to +6 (Allegre and Ben Othman, 1980; McCulloch and Chappell, 1982), whereas the range of ϵNd exhibited by most Precambrian granitoids is more limited between +5 and -5 (Allegre and Ben Othman, 1980). The ϵNd values of the two granitoids from the Halls Creek Orogenic Province fall in the range and support this general view.

The Nd model ages are also presented in Table 6-3. The TCHUR is a model age which represents the time when a rock would have had the same value of $^{143}\text{Nd}/^{144}\text{Nd}$ as the chondritic mantle, and is thus an estimate of a differentiation age of the sample from the chondritic mantle in an assumed single event. Similarly TDM is a model age representing the time when a sample differentiated from a depleted mantle reservoir. McCulloch and Chappell (1982) indicated that the change in Sm/Nd during partial melting to produce a granitic magma is small, thus the model age provides a reasonable approximation of the source rock age. In general, the TCHUR age is a minimum estimate, whereas for samples which have not suffered substantial secondary changes, TDM values more closely approximate maximum age limits (Black and McCulloch, 1984).

Sm-Nd model ages (TCHUR and TDM) of the samples are between 1940 and 2290 Ma (Table 6-3), indicating the absence of a major Archaean crustal component in the source of the granitoids (McCulloch, 1987).

Differences between Sr isochron ages and Nd model ages are small compared with most of the southeastern Australian Paleozoic granitoids (McCulloch and Chappell, 1982), suggesting a less significant contribution of older rocks to the source of the Precambrian granitoids. Similar results are generally found in most Precambrian granitoids

(Allegre and Ben Othman, 1980), and these observations are interpreted as evidence of a quasi-continuous continental growth through geological time.

The model age, TCHUR, of the Sophie Downs Granitoid (30802) is 200 m.y. older than the TCHUR age of the Sally Downs Tonalite. This may indicate that the source material of the Sophie Downs Granitoid is older than that of the Sally Downs Tonalite. However, it is also likely that the source materials of the granitoids have a similar age but different Sm/Nd composition. In this case, the source of the Sally Downs Tonalite must have had a higher Sm/Nd ratio than the source of the Sophie Downs Granitoid. As a high Sm/Nd ratio is typically found in mafic rocks, this interpretation is in accordance with geochemical data.

The Nd model ages from other Early Proterozoic orogenic provinces in Australia are similar to those from the Halls Creek Orogenic Zone. The former have a narrow range of TDM model ages of from 2130 to 2290 Ma (McCulloch, 1987). TCHUR model ages from the Arunta Inlier and Tennant Creek Inlier range from 2120 to 2340 Ma, excluding two slightly older ages from the basement orthogneiss from the Tennant Creek Inlier (Black and McCulloch, 1984), and such ages are also reported from the Mount Isa Inlier (McCulloch and Hansel, 1984) and from the Gascoyne Inlier (Fletcher et al., 1983b). The Nimbuwah Complex of the Pine Creek Inlier, the Georgetown Inlier, Broken Hill Inlier, and the Olary Block also have model ages from 2100 to 2300 Ma (McCulloch and Hansel, 1984).

Younger model ages of from 1700 to 2000Ma are found in the Mid Proterozoic orogenic provinces, e.g., Albany - Fraser Province (Fletcher et al., 1983a; McCulloch and Hansel, 1984), the Musgrave Inlier, and the Mt. Painter Inlier (McCulloch and Hansel, 1984).

If the Nd model age is considered to approximate the time of differentiation of source material (protolith) from the mantle, most of the Australian Proterozoic orogenic provinces thus consist of material newly differentiated from the mantle during the Proterozoic (McCulloch and Hansel, 1984 and McCulloch, 1987), and certainly the Halls Creek Orogenic Province has this signature.

However, Arndt and Goldstein (1987) critically examined the significance of the Nd model age, and suggested another possibility, namely that it is giving the average age of a mixed source. As one of the good examples, they referred to the interpretation made by Patchett and Kouvo (1986) on the 1870 - 1900 Ma trondhjemites, diorites, and gabbros of Svecokarelian terrane in southern Finland. Patchett and Kouvo (1986) concluded that the 2000 - 2100 Ma model ages of these rocks were derived from a mixture of about 90% mantle-derived material and 10% reworked Archean crust. Nd isotopic values of the Sally Downs Tonalite and Sophie Downs Granitoid can be applied to a similar model viz. that the granitoids comprise a mixture of newly differentiated magma from the mantle and small amounts of reworked Archean crust which may be present deep in the Halls Creek Mobile Zone.

In addition to the mixing model and the simple two stage process using the model ages, a slightly more complicated two stage model is examined. The different Sm/Nd value of the source material from that of the present granitoids is considered here. The possible $^{147}\text{Sm}/^{144}\text{Nd}$ values of the source material can be calculated if the age of differentiation of source material from the mantle is known, or vice versa. Fig. 6-7 indicates the relationship between $^{147}\text{Sm}/^{144}\text{Nd}$ values and the age of the source material. As the two granitoids have negative ϵNd values, the source materials for the granitoids must have had lower $^{147}\text{Sm}/^{144}\text{Nd}$

Fig. 6-7. $^{147}\text{Sm}/^{144}\text{Nd}$ versus age of source material

See text for discussion.

DM: depleted mantle

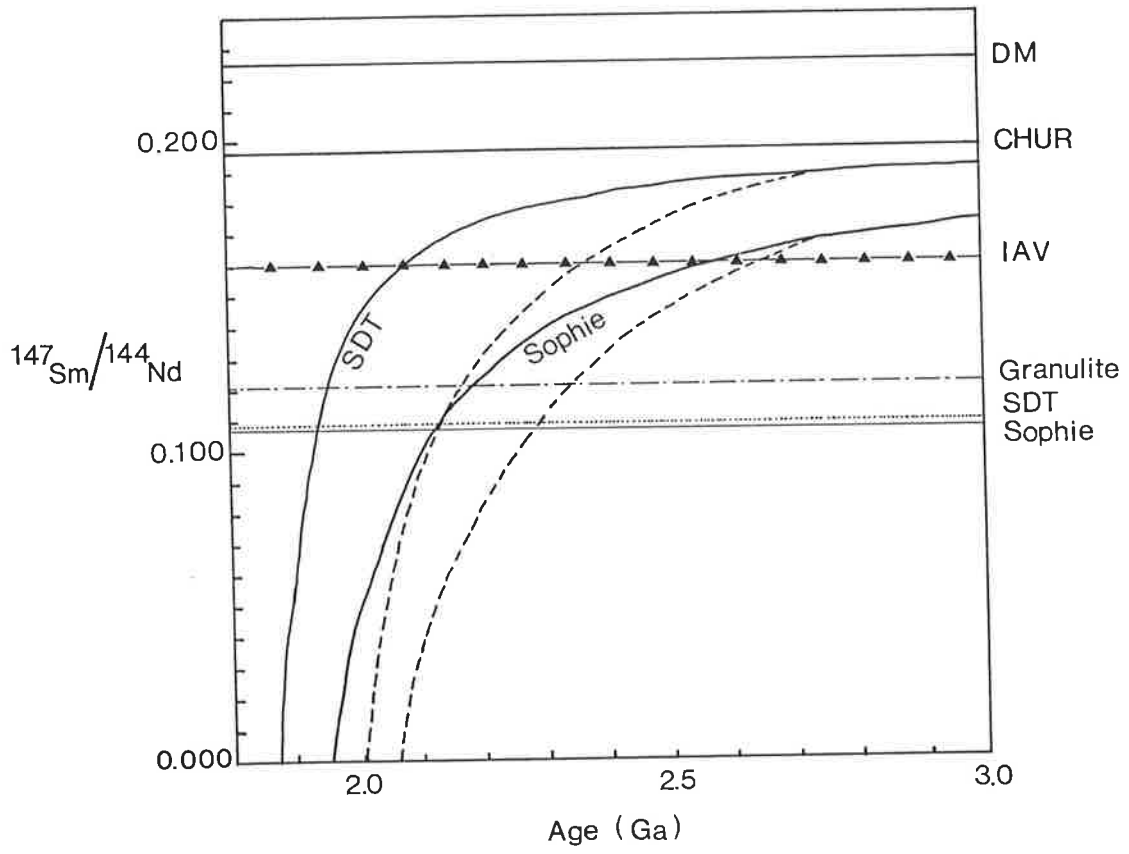
CHUR: chondritic uniform mantle reservoir

SDT: Sally Downs Tonalite, $^{147}\text{Sm}/^{144}\text{Nd}$ is 0.1083.

Sophie: Sophie Downs Granitoid $^{147}\text{Sm}/^{144}\text{Nd}$ is 0.1075

IAV: island arc volcanics, $^{147}\text{Sm}/^{144}\text{Nd}$ of IAV is assumed to be 0.160
from the data by White and Patchett (1984).

Granulite: average $^{147}\text{Sm}/^{144}\text{Nd}$ of granulite, calculated by Ben Othman
et al. (1984), is 0.121.



than did the chondritic mantle, assuming that the source material for the granitoids had been differentiated from the mantle in an assumed single event. The age at which $^{147}\text{Sm}/^{144}\text{Nd}$ equals zero provides a minimum estimate of the differentiation age of the source from the mantle, since the $^{143}\text{Nd}/^{144}\text{Nd}$ isotopic ratio is no different with $^{147}\text{Sm}/^{144}\text{Nd}$ equal to zero. Model ages, corresponding to the measured $^{147}\text{Sm}/^{144}\text{Nd}$ value of each granitoid, are given in Fig. 6-7.

The source rocks of the granitoids must have had a $^{147}\text{Sm}/^{144}\text{Nd}$ value less than 0.1967 (which is the chondritic value), and probably less than 0.1900 (Fig. 6-7). If the source material for the Sally Downs Tonalite is basaltic, then depleted-type basalts, such as the normal mid-ocean ridge basalt (Sun et al., 1979) are eliminated from the possible source material, as the depleted-type basalts generally have a $^{147}\text{Sm}/^{144}\text{Nd}$ ratio more than 0.1967. Thus the Nd isotopic values of the Sally Downs Tonalite suggest that the source material for the tonalite would have had an enriched character, similar to the modern enriched type of mid-ocean ridge basalt, or ocean island basalt, or island arc basalt.

If the source material of the Sally Downs Tonalite was of similar composition to that of the modern island arc basalt, in an oceanic environment without being influenced by the continental crust, and assuming 0.160 for the mean $^{147}\text{Sm}/^{144}\text{Nd}$ value of the basalt as derived from REE data by White and Patchett(1984), the age of differentiation of the basalt from the chondritic and depleted mantle would be 2070 Ma and 2360 Ma, respectively. Therefore, Early Proterozoic basalts having a chemistry suggesting affinity with island arc basalts would be satisfactory source material of the Sally Downs Tonalite.

Archaean basalts would be another possible source of the Sally Downs Tonalite. However, the mean $^{147}\text{Sm}/^{144}\text{Nd}$ ratio of 0.1786 for Archaean basalts derived by Claeu-Long et al. (1984) and McCulloch and

Compston (1981) provides calculated source rock ages less than 2500Ma, and therefore, does not agree with this possibility, as most Archaean basalts have an age greater than 2700Ma (Claue-Long et al., 1984 and McCulloch and Compston, 1981). But Archaean basalts with much higher $^{147}\text{Sm}/^{144}\text{Nd}$, e.g. close to 0.19, would be possible source material of the tonalite. Fig. 6-7, however, indicates that the Sophie Downs Granitoid would not be derived from Archaean basaltic rocks with the possible exception of late Archaean (about 2600Ma) basalt possessing island arc characteristics.

The average $^{147}\text{Sm}/^{144}\text{Nd}$ value of granulite, calculated by Ben Othman et al. (1984), is 0.121. If the source rocks of the granitoid are granulitic rocks having $^{147}\text{Sm}/^{144}\text{Nd} = 0.121$, the source rock differentiation age is not greater than 2350Ma.

As discussed above, the three models which are presented in this section can explain the Nd isotopic values of the Sally Downs Tonalite and Sophie Downs Granitoid. These models are summarized as follows,

- (1) Source rocks of the Sally Downs Tonalite and Sophie Downs Granitoid were differentiated from the mantle at about 2200Ma, as indicated from Nd model ages (TDM) of 2130 and 2290Ma, respectively.
- (2) Granitoid magma or source rocks for the granitoid magma originated from a mixture of newly differentiated magma from the mantle and small amounts of Archean rocks.
- (3) The Sally Downs Tonalite could have been derived by the partial melting of basaltic rocks of late Archean to Early Proterozoic age (possibly older than 2000 Ma). The Sophie Downs Granitoids could have been derived from a late Archean to Early Proterozoic protolith (older than 2140 Ma), depending on the nature of the protolith.

6.13. Comparison of Geochronological Data of Early Proterozoic Rocks in Northern Australia

Age relationships of tectonic events in northern Australia are outlined by Plumb et al. (1981). Page (1976) attempted to compare available isotopic ages of the Halls Creek Inlier with those of The Granites-Tanami Inlier. Page (1988) reviewed the geochronology of the Early to Middle Proterozoic rocks in northern Australia, and established a time framework of the orogenic history of the area. A number of U-Pb zircon ages offer firm chronological benchmarks in the review. Although U-Pb zircon data are not provided in the present study, new Rb-Sr geochronological results obtained in this work are correlated with the other isotopic ages of the Early Proterozoic rocks in northern Australia.

Before discussing this geochronology of the Early Proterozoic rocks, geochronological data of the Archaean basements in the northern Australia are first summarized. The Rum Jungle Complex and Waterhouse Complex in the western part of the Pine Creek Inlier are considered to be Archaean or at least 2400 Ma old (Richards et al., 1966). McCulloch (1987) supported this interpretation from the Nd model ages of the gneisses and granitoids of the Rum Jungle Complex, ranging from 3300 to 2710 Ma. The Nunambu Complex in the eastern Pine Creek Inlier has a zircon U-Pb age of 2470 Ma and Rb-Sr isochron age of 2468 ± 26 Ma (Page et al., 1980) and Nd model age of 2620 Ma (McCulloch, 1987), suggesting the initial formation of the complex in the Archaean. Sm-Nd data from the orthogneiss in the Tennant Creek Inlier give late Archaean ages (McCulloch, 1987), suggesting the presence of possible Archaean basement. Those data indicate that the Archaean rocks have a limited occurrence in northern Australia, and may be present as small

basement complex within the Early Proterozoic orogenic domains. Areal extent of the Archaean basement rocks is not well documented.

Concerning the Proterozoic rocks, Page et al. (1980) indicated that the Pine Creek Geosyncline sequences have a maximum depositional age between 2200 and 2000 Ma. Preliminary U-Pb zircon study of a Biscay Formation tuff from the Halls Creek Group by Page (1988) suggests that the depositional age of the Biscay Formation might be close to 1880 Ma. The Tanami Complex in The Granites-Tanami Inlier is correlated with the Halls Creek Group by Page et al. (1976). Although the isotopic data indicating the depositional age of the Early Proterozoic orogenic domains in the northern Australia are limited, available data suggest that the deposition of sediments took place between 2200 and 1880 Ma. Page (1988) examined the U-Pb data and estimated the deposition age to extend over a very narrow range, from 1890 to 1880 Ma.

1890 Ma granulite facies metamorphism and plutonism (Tickalara Metamorphics and Dougalls Granitoid Suite) in the Halls Creek Orogenic Zone can be correlated with a metamorphic event (1920 ± 60 Ma) of high grade (amphibolite facies) metamorphism in the Tennant Creek Inlier (Black, 1977). A 1886 ± 5 Ma zircon age of granulite facies rocks from the Nimbuwah Complex in the Pine Creek Inlier has been reported by Page et al. (1980). If the zircon age indicates an age of emplacement of orthopyroxene bearing granitoid at depth (Page et al., 1980), it could also imply a granulite facies metamorphic environment around the granitoid. Thus, the age is aptly correlated with the 1890 Ma event which involves granulite facies metamorphism and emplacement of the Dougalls Granitoid Suite which includes an orthopyroxene bearing tonalite. These ages indicate the time of the Barramundi Orogeny defined by Etheridge et al. (1987) to describe deformation and metamorphism in the Early Proterozoic terranes. Although Page (1988) suggested a slightly younger

age of 1854 ± 6 Ma for the orogenic event in the Halls Creek Mobile Zone, he considered a broadly synchronous age to encompass the orogenic events in this and other domains in northern Australia, viz. the Mount Isa Inlier (1885 ± 10 Ma), the Pine Creek Inlier (1885-1870 Ma), and the Tennant Creek Inlier (1920-1870 Ma).

Within the Barramundi Orogeny, extensive felsic volcanism and granitoid emplacement occurred after the major deformation and metamorphism, towards the end of the orogeny (Wyborn, 1988). The felsic volcano-plutonic rocks are described as the Barramundi igneous association by Etheridge et al. (1987). The igneous rocks of the association have distinctively high levels of K_2O , Rb, Zr, La, and low MgO and CaO contents. The age of the felsic magmatism was indicated by Etheridge et al. (1987) as 1840-1870 Ma, by Wyborn et al. (1987) as 1820-1870 Ma, by Page (1988) as 1850-1870 Ma, and Wyborn (1988) 1840-1880 Ma. The igneous association includes the following major rock units (Wyborn, 1988).

(1) Kalkadoon Granodiorite, Ewen Granite and Leichhardt Volcanics in the Mount Isa Inlier.

(2) Nimbuwah Granite, and El Sherana and Edith River Groups in the Pine Creek Inlier.

(3) Tennant Creek Granite, Cabbage Gum Granite, and Bernborough Formation in the Tennant Creek Inlier.

The Bow River Granitoid is correlated with the Kalkadoon and Ewen granitoids by Wyborn and Page (1983), and included in the Barramundi igneous association by Wyborn et al. (1987). Although no U-Pb zircon age is available from the Bow River Granitoid, emplacement age of the granitoid is likely to be in the time range of the association. The Whitewater Volcanics have a U-Pb zircon age of 1850 ± 5 Ma, and also may be grouped with the association. The Whitewater Volcanics are

correlated with the Winnecke Formation in The Granites-Tanami Inlier (Page et al., 1976), though the no precise age data of the Winnecke Formation is available.

Although chemical characteristics of the Sally Downs Tonalite of the Mabel Downs Granitoid Suite are somewhat different from those of the typical granitoids of the Barrumandi association, the Rb-Sr total rock isochron age of the tonalite indicates that the tonalite could be a member of the Barrumundi igneous association.

In summary, geochronological data from several inliers in northern Australia suggest general contemporaneity of tectonic events and igneous activities.

CHAPTER 7. GENERAL RESUME AND COMPARISON WITH OTHER EARLY PROTEROZOIC GRANITOIDS

7.1. Introduction

Petrological and geochemical characteristics of the granitoids which have already been described in previous chapters are summarized in Table 7-1. It is notable that a considerable amount of low K₂O tonalite is found in the Sally Downs Bore area of the central part of the Halls Creek Mobile Zone. The Bow River Granitoid is characterized by high K₂O. The different concentrations of K₂O between the granitoid suites are shown in Fig. 7-1. A-type characteristics of the Sophie Downs Granitoid are clearly demonstrated by the petrological and geochemical data of the present study. It is the prime objective of this chapter to summarize the petrological and geochemical characteristics of the Early Proterozoic granitoids in the Halls Creek Inlier and to compare the characteristics with those of granitoids from other Early Proterozoic inliers in these northern Australia. Comparisons of the petrological and geochemical characteristics with those of Early Proterozoic granitoids from the other continents are also presented.

Considerable petrological data are available on the granitoids from the Pine Creek Inlier (Ferguson et al., 1980; Page et al., 1980), from "The Granites-Tanami Inlier" (Blake et al., 1979), from the Arunta Inlier (Zhao and Cooper, 1992) and from the Mount Isa Inlier (Wyborn and Page, 1983). Wyborn (1988) summarized petrological and geochemical characteristics of the Early Proterozoic granitoids from northern Australia, and pointed out that most of the granitoids are compositionally uniform over a large area and characterized by high levels of K₂O, Rb, La, Ce, Th, and U. Etheridge et al. (1987) introduced the term Barramundi igneous association to describe those granitoids and related volcanics in northern Australia. Using multi-element primordial-mantle

Table 7-1. Summary of petrological and geochemical characteristics of granitoids in the Halls Creek Mobile Zone

Unit	ELG	Dougalls	Ord River	WPG	CLG	Sally Downs	Bow River	Sophie Downs
Rock	Leuco- granite	tonalite and trondhjemite	tonalite	granite	granite	tonalite	granite	Alkali-feldspar- granite
Grain size	F-C	M	M-C	C	F-M	M-C	C	F-M
Mineralogy								
Opx	-	xx or -	-	-	-	-	-	-
Cpx	-	-	-	-	-	-	-	-
Hbl	-	xxx	xxx	-	-	xxx	-	-
Bt	xx	xxx	xxx	xxx	xxx	xxx	xxx	xx
Ms	-	-	-	-	xx	-	x	x
Kfs	xxx	-	-	xxx	xxx	-	xxx	xxx
Pl	xx	xxx	xxx	xx	xxx	xxx	xx	xxx
M.M.E.	-	xx	xx	-	-	xxx	-	-
Xenoliths	x	x	xx	xx	xx	xxx	x	xxx
Geochemistry								
SiO ₂ (%)	76.0	68.2	64.8	70.7	74.6	61.2(55.7-68.8)	72.0	76.2(72.4-77.7)
CaO (%)	1.77	4.50	4.96	2.26	1.57	5.75	1.69	0.49
Na ₂ O (%)	4.31	4.36	3.86	2.80	3.25	3.96	2.44	3.85
K ₂ O (%)	2.60	0.99	1.61	4.46	4.44	1.60	5.33	4.80
A/CNK	0.992	0.983	0.970	1.035	1.041	0.930	1.040	0.960
Rb (ppm)	39	27.4	53	143	86	46	258	114
Sr (ppm)	121	380	430	159	248	604	94.5	41
Y (ppm)	31	5.1	11.8	23.8	11.1	12.6	41.4	64
Zr (ppm)	100	136	136	222	74.8	135	213	206
Rb/Sr	0.322	0.072	0.123	0.899	0.347	0.077	2.73	2.76
(La/Yb) _n	0.56	36.40	15.59	16.32	21.73	23.81	12.85	8.75
Eu/Eu*	2.34	2.06	1.18	0.58	0.70	1.03	0.50	0.41
ISr	0.70214	0.7022	0.70219	0.7065		0.70292		0.7029

ELG: Eastern Leucocratic Granitoid, Dougalls: Dougalls Granitoid Suite, Ord River: Ord River Granitoid Suite, WPG: Western Porphyritic Granite
 CLG: Central Leucocratic Granite, Sally Downs: Sally Downs Tonalite, Bow River: Bow River Granitoid, Sophie Downs: Sophie Downs Granitoid
 Grain size, F: fine grained, M: medium grained, C: coarse grained

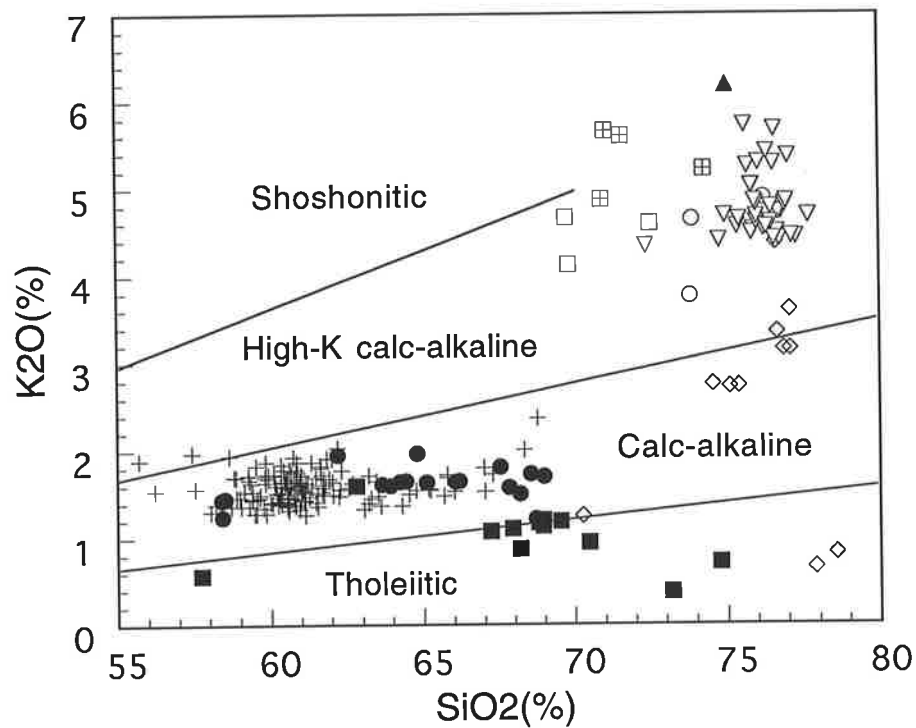
Opx: orthopyroxene, Cpx: clinopyroxene, Hbl: hornblende, Bt: biotite, Ms: muscovite, Kfs: K-feldspar, Pl: plagioclase

M.M.E.: mafic microgranular enclave, xxx: abundant, xx: common, x: minor, -: absent

A/CNK: mol Al₂O₃/(CaO+Na₂O+K₂O), ISr: initial Sr isotopic ratio

(La/Yb)_n: chondrite normalized (La/Yb), Eu/Eu*: degree of Eu anomaly $= (Eu/0.0722) / (\sqrt{(Sm/0.192) \times (Gd/0.259)})$

Fig. 7-1. SiO₂-K₂O plot of granitoids from the Halls Creek Mobile Zone
Field boundaries are from Peccerillo and Taylor (1976) and Rickwood
(1989).



- ◇ Eastern Leucocratic Granitoid
- Dougalls Granitoid Suite
- Ord River Tonalite Suite
- Western Porphyritic Granite
- Central Leucocratic Granite
- + Sally Downs Tonalite
- ▽ Sophie Downs Granitoid
- ⊞ Bow River Granitoid
- ▲ Whitewater Volcanics

normalized abundance diagrams and various petrological characteristics, Wyborn et al. (1992) subdivided Australian Proterozoic granitoids into five groups, as follows;

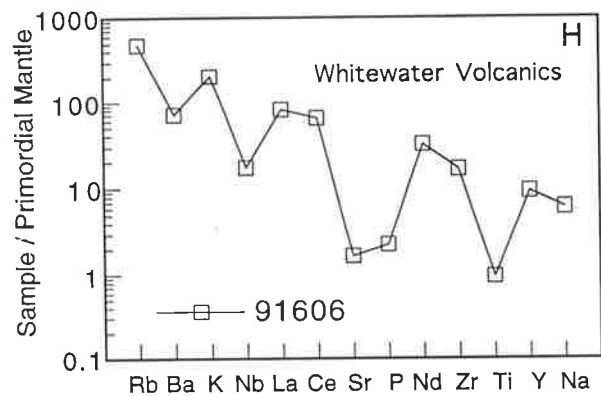
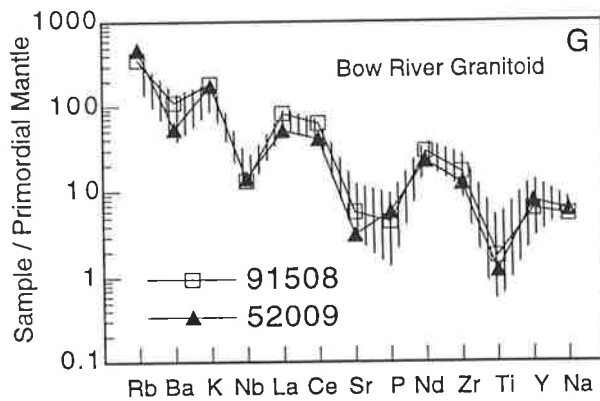
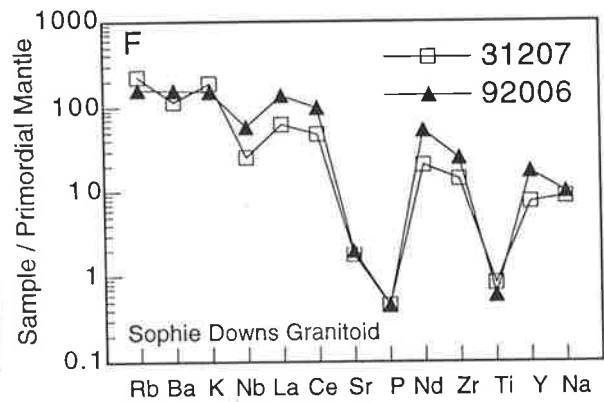
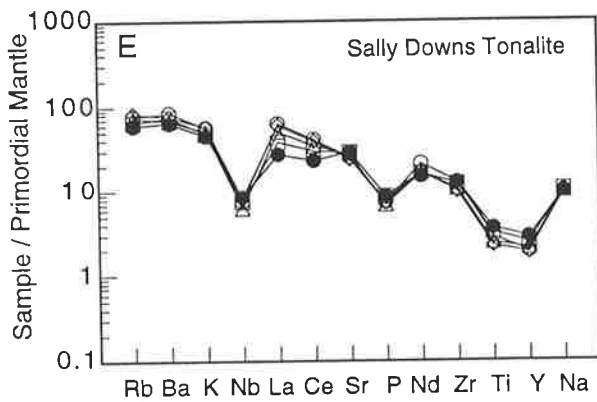
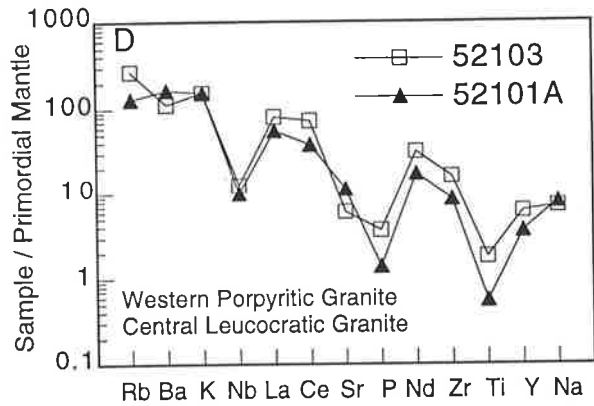
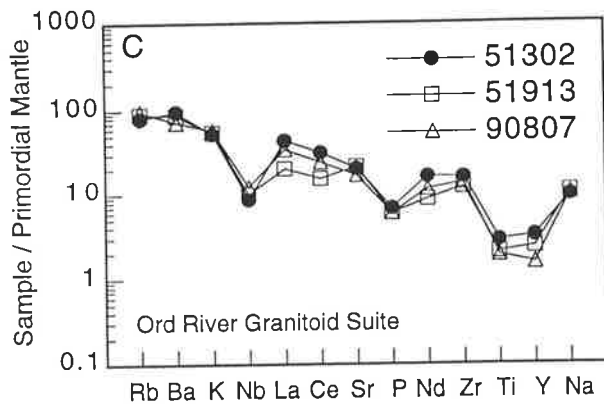
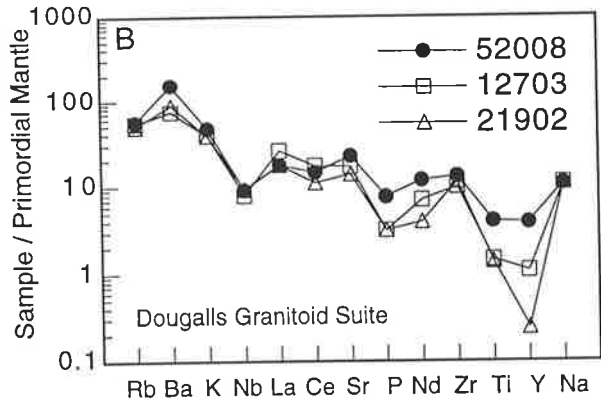
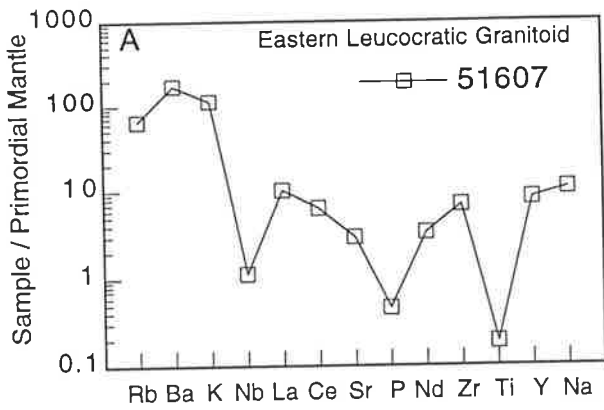
- (1) I-type, Sr-depleted, Y-undepleted, restite-dominated group
- (2) I-type, Sr-depleted, Y-undepleted, fractionated, low in incompatible elements group
- (3) I-type, Sr-depleted, Y-undepleted, enriched in incompatible elements (anorogenic) group
- (4) I-type, Sr-undepleted, Y-depleted group
- (5) S-type, Sr-depleted, Y-undepleted group

Similar primordial-mantle normalized diagrams of the granitoids from the Halls Creek Mobile Zone are shown in Fig. 7-2. In the diagram, the elements are ordered in increasing compatibility with respect to the mantle material. The primordial-mantle normalized diagrams are utilized mostly for basaltic rock studies; however, they also provide useful information for granitoids as the mantle is the ultimate source of the all crustal material. As mentioned by Wyborn et al. (1992), the diagrams represent the integrated effects of all the episodes of melting, fractionation of magma, and other processes that have contributed to the chemistry of the granitoids.

In the following sections, the discussion and comparison of the petrological characteristics of the granitoids are presented in three separate groups, viz. tonalite-trondhjemite, the A-type granitoid, and high K₂O granitoids and volcanics. As geochemical characteristics of the Eastern Leucocratic Granitoid differ significantly from the characteristics of the other Early Proterozoic granitoids in the northern Australia, discussion of the Eastern Leucocratic Granitoid is not included here.

Fig. 7-2. Primordial mantle normalized plot of granitoids from the Halls
Creek Mobile Zone

Primordial mantle values are from Sun and McDonough (1989).



7.2. Tonalite-trondhjemite

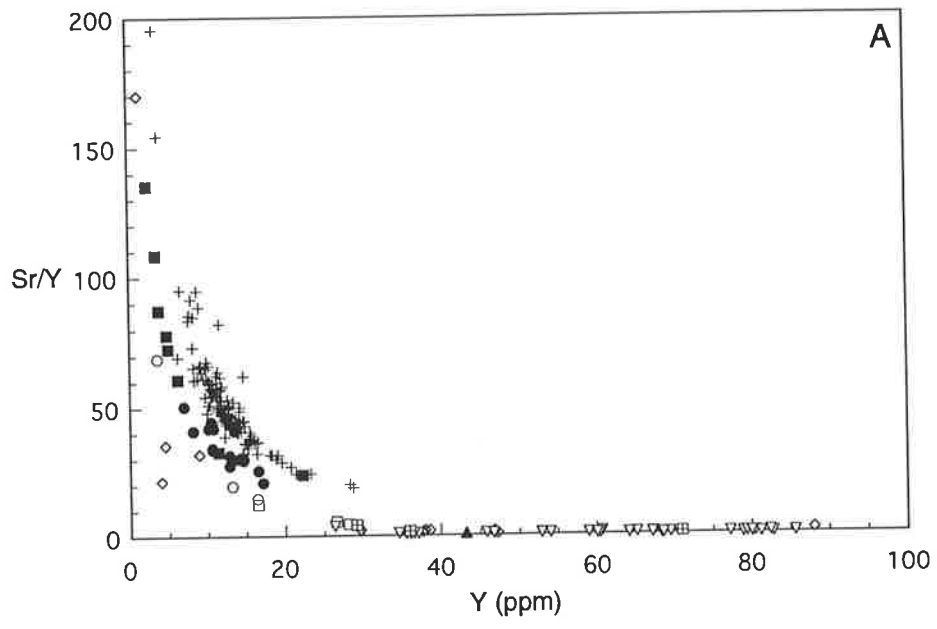
Barker (1979) defined geochemically two distinct subgroups of tonalite-trondhjemite, viz. high Al type and low Al type. The high Al tonalite-trondhjemite contains more than 15 wt% Al_2O_3 at the 70 wt% SiO_2 level, and the low Al type contains less than 15 wt% Al_2O_3 at 70 wt% SiO_2 . Drummond and Defant (1990) presented additional geochemical characteristics of the two types. The low Al type has low Sr (<200ppm), slightly enriched LREE, a negative Eu anomaly, and flat HREE pattern. On the other hand, the high Al type typically has the following geochemical characteristics: (1) high Sr (>300ppm), very low Rb/Sr ratios of <0.15, (2) enriched LREE, depleted HREE, and no Eu anomaly or only a slightly positive or negative one, (3) low Y (<15ppm), (4) low Nb (<11ppm), and (5) low to moderate K/Rb (Drummond and Defant, 1990). Tonalite and trondhjemite of the Dougalls Suite and tonalites of the Ord River Suite, and Mabel Downs Suite have geochemical characteristics of the high Al type.

The primordial mantle normalized diagrams of tonalites from the Dougalls Granitoid Suite, Ord River Tonalite Suite, and Sally Downs Tonalite of the Mabel Downs Suite are shown in Fig. 7-2. The diagrams indicate relative depletion of Nb, P, Ti, and Y compared with other elements in the tonalites. As Nb and P depletions are commonly found in the granitoids, though magnitude of the depletions may change, the significance of the depletions is not discussed in detail here. The diagrams suggest that the tonalites can be classified into the I-type, Sr-undepleted and Y-depleted group of Wyborn et al. (1992). The depletion of Y is more significant in the tonalites of the Dougalls Suite than other suites (Fig. 7-2 and 7-3), and an extremely low Y abundance is observed in trondhjemites of the Dougalls Suite (Table A4-3).

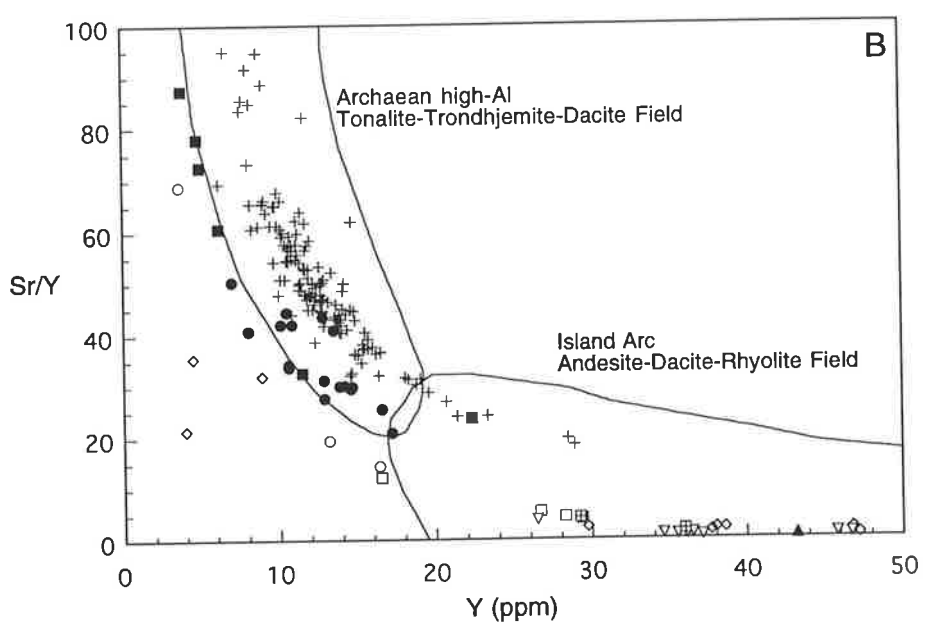
Fig. 7-3. Y-Sr/Y plot of granitoids from the Halls Creek Mobile Zone

A. Y-Sr/Y plot.

B. Portion of plot A, showing detail of plot. Archaean high-Al tonalite-trondhjemite-dacite field and island arc andesite-dacite-rhyolite field are from Atherton and Petford (1993). Adakite (Defant and Drummond, 1990) has similar field to the Archaean high-Al tonalite-trondhjemite-dacite field.



- ◇ Eastern Leucocratic Granitoid
- Dougalls Granitoid Suite
- Ord River Tonalite Suite
- Western Porphyritic Granite
- Central Leucocratic Granite
- + Sally Downs Tonalite
- ▽ Sophie Downs Granitoid
- ▣ Bow River Granitoid
- ▲ Whitewater Volcanics



From the Proterozoic granitoids in northern Australia, Wyborn et al. (1992) allotted the Marraungee Granite (Mount Isa Inlier), the Huckitta Tonalite, Alice Springs Granite and the Atnarpa Igneous Complex (Arunta Inlier) to the Sr-undepleted and Y-depleted group. Geochemical characteristics of the Huckitta Tonalite of 1767 Ma, presented by Foden et al. (1988), are largely similar to those of the tonalites from the Halls Creek Mobile Zone. However, at the same SiO₂ level, K₂O and Rb contents of the former are slightly higher than those of the latter. Zhao and Cooper (1992) identified three distinct igneous suites from the Atnarpa Igneous Complex, the characteristics of which are as follows,

(1) The 1879Ma gabbro-tonalite-trondhjemite (GTT) suite of the complex shows depletions of K, Rb, Y, Nb, and Ti.

(2) The 1873 Ma low Al tonalite-trondhjemite-granodiorite suite is also depleted in K and Rb. However, it has lower Al₂O₃ and Sr than the 1879 Ma GTT suite at comparable SiO₂ levels and displays flat HREE and negative Eu anomaly.

(3) The 1751 Ma younger tonalite suite is high in Sr and Al₂O₃, and low in Y, Nb, and Ti, and displays a strongly fractionated REE pattern with HREE depletion, typical of high Al tonalite-trondhjemite suites.

The chemical composition of the 1751 Ma younger tonalite from the Atnarpa Igneous Complex shows overall similarity to that of the Sally Downs Tonalite at comparable SiO₂ levels, though some small differences are observed, viz. lower Fe₂O₃* and Sr and higher Rb in the 1751 Ma tonalite than in the Sally Downs Tonalite. The Alice Springs Granite suite of 1751 Ma, of similar age to the younger Atnarpa tonalite suite, is a high Al tonalite-trondhjemite-granodiorite type (Zhao and McCulloch, 1995).

The occurrence of orthopyroxene bearing granitoids among the granulite facies rocks of the Nimbuwah Complex has been recorded by

Page et al. (1980). From their petrographical characteristics, these orthopyroxene bearing granitoids may be correlated with the orthopyroxene bearing tonalite of the Dougalls Granitoid Suite. The granitoids of the Dougalls Suite are characterized by low K₂O and Rb, typical of granitoids in the granulite facies (Rollinson and Windley, 1980a, 1980b). However, the Rb content of the granulite facies rocks from the Nimbuwah Complex ranges from 58 to 177 ppm (except for one sample with 11ppm Rb) -see Page et al.(1980)- values which are thus considerably higher than those of the Dougalls Suite (Table 7-1). Unfortunately, Page et al. (1980) did not present major element data, but only Rb and Sr data and if the K/Rb ratio is similar in both rocks, the high Rb values in the granulite facies might indicate higher K₂O contents in the rocks than those of the Dougalls Granitoids. Therefore, most of the granulite facies granitoids of the Nimbuwah Complex may consist of neither tonalite nor trondhjemite. Further petrological and geochemical data of the complex are necessary, especially concerning the low Rb sample.

Although tonalites and trondhjemites with Sr-undepleted and Y-depleted geochemical characteristics, have been described from the Halls Creek Inlier in the present study and from the Arunta Inlier by Foden et al. (1988) and Zhao and McCulloch (1995), such tonalites and trondhjemites may not be a common rock type in other Early Proterozoic inliers of northern Australia as suggested by Wyborn et al. (1992). It is noteworthy that the Halls Creek Inlier and Arunta Inlier are situated along the western and southern margin respectively of the North Australian craton (Plumb, 1979a). Substantial tonalite and trondhjemite may be restricted to the margins of the North Australian craton.

Early Proterozoic tonalites and trondhjemites showing similar geochemical characteristics to those from the Halls Creek Mobile Zone

can be found in other continents, e.g., the gabbro-diorite-tonalite-trondhjemite (GDTT) suite (1893-1820Ma) of southwest Finland (Arth et al. 1978), and tonalites in the Penokean Orogen(1890-1820Ma), North America (Anderson and Cullers, 1987).

The gabbro of the GDTT suite of southwest Finland described by Arth et al. (1978) is a hornblendite and hornblende mela-gabbro. Similar mafic rocks are found also around and within the Sally Downs Tonalite body. In previous chapters (chapter 3, 4, and 6), a possible genetic link between the hornblendite/mela-gabbro and the Sally Downs Tonalite has been examined. The results did not reject a possible petrogenetic relationship between the tonalite and the hornblendite/mela-gabbro. Some mafic components of the GDTT suite of the Atnarpa Igneous Complex contain hornblendite with cumulate features (Zhao and Cooper, 1992). Most gabbroic rocks of a gabbro-diorite-tonalite-trondhjemite suite might be expected to contain hornblendite, as a typical member of the suite.

Tonalites and trondhjemites are common granitoids in the Archaean terrain (Glikson, 1979), and are typically high Al type. They have Y-depleted and Sr-undepleted characteristics, similar to those of the Early Proterozoic. Tonalites and trondhjemites are also found in the modern continental arc or island arc environment (Drummond and Defant, 1990). Tonalites and trondhjemites from oceanic arc environments are characterized by extremely low abundances of K, Rb, and LREE (Chivas et al. 1982; Whalen, 1985). Chivas et al. (1982) indicated that the K/Rb ratio can be used to separate tonalites and trondhjemites of the oceanic arc environment (K/Rb more than 400) from those of the continental arc environment (K/Rb less than 400). Tonalites and trondhjemites from the Halls Creek Mobile Zone have K/Rb characteristic of the continental arc environment, i.e. less than 400. Various models have been presented for

Archaean to modern tonalite and trondhjemite petrogenesis (e.g., Drummond and Defant, 1990). A review of these and the detail petrogenetic discussion of the tonalites and trondhjemites from the Halls Creek Mobile Zone will be presented in next chapter.

7.3. A-type granitoid

Petrological and geochemical characteristics of the Sophie Downs Granitoid clearly indicate that it is a typical A-type granite. Petrographically, it is an alkali-feldspar granite. Fine grain-size of the granitoid suggests emplacement at a high level in the crust, typical of the A-type granites (Eby, 1990). The primordial mantle normalized diagrams of the Sophie Downs Granitoid (Fig. 7-2) show strong depletions of Sr, P, and Ti relative to the other elements. Magnitude of the Sr and P depletions of the Sophie Downs Granitoid is greatest among the granitoids from the Halls Creek Mobile Zone. As described in chapter 5, the granitoid has very high Zr, Nb, Y contents (Fig. 7-2).

Sample 91507 from the Bow River Granitoid Suite has a high concentration of Zr, Y, Nb, Ce, and Nd (Table A4-9 and Table 7-2), and its possible classification as A-type is suggested in chapter 5. The data indicate that the Bow River Granitoids Batholith (mostly K₂O rich I-type) may contain small bodies of the A-type granite. It is necessary to make a further detailed study of the Bow River Granitoid Batholith.

Felsic intrusives and extrusives of the Biscay Formation of the Halls Creek Group are considered to be derived from magma with A-type characteristics (Page and Hancock, 1988). The felsic rocks of the Biscay Formation have SiO₂ contents ranging from 72.65 to 76.07%, and are extremely enriched in Zr, Nb, Y, Ce and Nd. Major and trace element data from a typical example in Page and Hancock (1988) are listed in Table 7-2. Levels of Zr, Nb, Y, Ce, and Nd in the felsic rocks are higher

Table 7-2. Summary of geochemical data for A-type granites and related volcanics

	Halls Creek Inlier			Mount Isa Inlier*2		A-type*3
	Sophie D.	91507	608BG*1	Argylla F.	Bottletree F.	Average
No. of Data	46	1	1	13	19	148
(wt%)						
SiO ₂	76.15	71.05	74.03	69.03	70.00	73.81
Al ₂ O ₃	11.90	12.74	11.24	12.82	11.93	12.40
Fe ₂ O ₃ *	1.55	4.64	4.66	5.32	6.26	3.00
MnO	0.02	0.07	0.17	0.04	0.06	0.06
MgO	0.25	0.33	0.08	0.56	0.45	0.20
CaO	0.49	1.91	0.65	1.68	2.43	0.75
Na ₂ O	3.85	2.59	3.56	2.55	2.10	4.07
K ₂ O	4.80	5.65	4.35	5.52	4.76	4.65
TiO ₂	0.16	0.51	0.28	0.62	0.64	0.26
P ₂ O ₅	0.01	0.09	0.00	0.15	0.14	0.04
LOI	0.59	0.38	0.47			
Total	99.76	99.96				
(ppm)						
Ba	955	564	79	856	1483	352
Rb	114	337	176	190	175	169
Sr	41	65	31	89	180	48
Zr	206	332	1445	607	566	528
Nb	31	20.8	170	41	27	37
Y	64	71	167	77	52	75
Ce	125	177	428	172	175	137
Nd	53.9	72	211			
Sc	2.3	10.7	0.4			4
V	3.4	20	2.4			6
Cr	0.1	5				
Ni	2.3	7.7				<1
Cu	9.5	10				2
Zn	58.9	67				120
Ga	16.6	19.3				24.6
A/CNK	0.958	0.920	0.957	0.969	0.916	0.947
NK/A	0.969	0.814	0.940	0.793	0.721	0.946
Y/Nb	2.06	3.41	0.98	1.88	1.93	2.03
Ce/Nb	4.03	8.51	2.52	4.20	6.48	3.70
Rb/Sr	2.78	5.18	5.68	2.13	0.97	3.52
K/Rb	350	139	205	241	226	228
(Ce/Y) _n	5.3	6.8	7.0	6.1	9.2	5.0

Sophie D.: Sophie Downs Granitoid

91507: granite in the Bow River Granitoid Batholith

*1: rhyolite sill in the Biscay Formation, data from Page and Hancock (1988)

*2: Baltitude and Wyborn (1982), *3: Whalen et al. (1987)

A/CNK: Mol. Al₂O₃/CaO+Na₂O+K₂O, NK/A: Mol. Na₂O+K₂O/Al₂O₃

(Ce/Y)_n: chondrite normalized Ce/Y

than those of the Sophie Downs Granitoid. However, a lower Ba content of the former than that of the latter is generally observed. Although the felsic volcanics have A-type characteristics, the difference of the chemical compositions between the felsic volcanics and the Sophie Downs Granitoid is apparent. The felsic rocks may be related to a trachytic tuff of the Brockman Volcanics in the upper portion of the Biscay Formation, which contains a Zr, Nb, Y, and REE enriched ash-flow tuff horizon (Ramsden et al., 1993).

In the classification scheme of Wyborn et al. (1992), the A-type granites and volcanics are classified into the anorogenic granite group which has geochemical characteristics of the I-type, Sr-depleted, Y-undepleted group, enriched in incompatible elements. Wyborn et al. (1992) indicated that Proterozoic granites and volcanics of this group are widely distributed throughout Australia in both space and time. For example, the early Middle Proterozoic volcanics from the Mount Isa Inlier, viz. the Argilla Formation and Bottletree Formation (1800-1780 Ma), are classified as A-type (Table 7-2). However, in northern Australia, Early Proterozoic (before 1800 Ma) A-type granitoids and volcanics are found only in the Halls Creek Inlier, which is thus a unique tectonic setting for the A-type magma during the Early Proterozoic.

7.4. High K₂O granitoids and volcanics

This section is a general resume and comparative study of the geochemical characteristics of the high K₂O granitoids and volcanics, which include the Western Porphyritic Granite and Central Leucocratic Granite from the Sally Downs Bore area, the Bow River Granitoid, and Whitewater Volcanics. Samples of this group are plotted in the fields of high K calc-alkaline and shoshonitic series (Rickwood, 1989) on the K₂O versus SiO₂ plot (Fig. 7-1).

In chapter 3, a possible correlation of the Western Porphyritic Granite with the Bow River Granitoid suite is indicated, although there is a small geochemical difference between the two granitoids, e.g., slightly lower K₂O in the former compared with the latter (Fig. 7-1). However, primordial mantle normalized patterns of the two granitoid units (Fig. 7-2) portray overall similarity of geochemical characteristics, viz. high abundance of LILE elements with Nb, Sr, P, and Ti depletions and without significant Y depletion. The primordial mantle normalized pattern of the Central Leucocratic Granite shows depletions of Nb, P, and Ti. It should be noted that the Sr level of this granite is not extremely depleted as is the Western Porphyritic Granite and the Bow River Granitoid. The level of Y in the Central Leucocratic Granite indicates a small degree of depletion relative to Na.

The Bow River Granitoid is considered to be a member of the Barramundi igneous association by Wyborn (1988), and this is confirmed by the similarity of the primordial mantle normalized diagrams of the granitoid (Fig. 7-2) and those of the Barramundi igneous association (see Wyborn et al., 1992). Table 7-3 shows the average chemical composition of the Kalkadoon and Ewen Batholiths from the Mount Isa Inlier (Wyborn and Page, 1983), the former is a typical example of the Barramundi igneous association, with mol. Al₂O₃/CaO+Na₂O+K₂O averaging 1.033. This suggests that the granites of the association in the Mount Isa Inlier are mostly peraluminous but within the range of I-type granites. The ratios of the Bow River Granitoid are slightly higher than that of the granites from the Mount Isa Inlier, approaching to 1.1. Indeed, one sample (91501) from the Bow River Granitoid has a ratio of 1.102 (Table A4-9), within the S-type range. Although most of the Bow River Granitoids are grouped into the I-type category, some S-type characteristics of the granitoid are indicated in chapter 5. It is necessary

Table 7-3. Chemical characteristics of high K granites and volcanics from selected examples

Unit Sample	Early Proterozoic			Palaeozoic		Creta.	Miocene
	BR 91508	Mount Isa Average	Wopmay HY28-74	I-type Average	S-type Average	H.K. 8734	Snake R. Tjl-2
No. of Sp.	1	68	1	1074	704	1	1
Major elements (%)							
SiO ₂	71.58	69.32	68.40	69.50	70.91	70.79	73.85
Al ₂ O ₃	14.32	15.03	14.60	14.21	14.00	13.47	12.97
Fe ₂ O ₃ *	2.82	3.72	3.35	3.48	3.40	3.00	2.77
MnO	0.03	0.05	0.07	0.07	0.06	0.08	0.03
MgO	0.75	0.93	1.26	1.38	1.24	0.39	0.13
CaO	2.10	2.91	2.19	3.07	1.88	1.64	0.92
Na ₂ O	2.18	2.82	3.06	3.16	2.51	3.40	3.17
K ₂ O	5.59	4.27	4.25	3.48	4.09	5.74	5.29
TiO ₂	0.39	0.43	0.39	0.41	0.44	0.40	0.40
P ₂ O ₅	0.10	0.11	0.10	0.11	0.15	0.09	0.05
LOI	0.40					0.73	0.59
Total	100.26						
Trace elements (ppm)							
Ba	760	817	890	519	440	678	1088
Rb	226	180	170	164	245	224	193
Sr	125	241	320	235	112	167	65
Zr	190	204	190	150	157	246	408
Nb	9.5	11	12	11	13	20	
Y	29.2	25	19	31	32	41	35
Ce	99	110		66	61	140	114
Nd	44	48				53	50.4
Sc	7.3	6		13	11		4.3
V	32	33	48	57	49		15
Cr	10	16	46	20	30		10
Ni	9.4	5	35	8	11		5
Cu	9	11	18	9	9		
Zn	34	43	77	48	59		
Ga	17.6	17		16	18	16	
A/CNK	1.064	1.033	1.072	0.977	1.169	0.911	1.028
Rb/Sr	1.81	0.75	0.53	0.70	2.19	1.34	2.97

BR: Bow River Granitoid Suite, a sample (91508) from present study

Average values of 68 samples from the Kalkadoon and Ewen Batholiths of the Mount Isa Inlier.

Data from Wyborn and Page (1983).

Great Bear Batholith of the Wopmay Orogen, Canada. Data from Hildebrand et al. (1987).

Palaeozoic I-type and S-type of the Lachlan Fold Belt, southeast Australia.

Data from Chappell and White (1992).

H.K.: Cretaceous granites from Hong Kong. Data from Sewell et al. (1992)

Snake R.: Miocene rhyolite from the Snake River Plain, USA. Data from Norman et al. (1992).

Fe₂O₃*: Total Fe as Fe₂O₃

LOI: Loss on Ignition

A/CNK: Mol. Al₂O₃/CaO+Na₂O+K₂O

to make a further detailed study of the Bow River Granitoid Batholith, as it may consist of a variety of granitoids.

The primordial mantle normalized diagram of the Whitewater Volcanics is similar to that of the Bow River Granitoid, though, depletions of Ba, Sr, P, and Ti are somewhat greater in the volcanics than in the granitoid.

Wyborn et al. (1992) classified the Whitewater Volcanics and comagmatic granites of the King Leopold Mobile Zone and the Halls Creek Mobile Zone with their I-type, Sr-depleted, Y-undepleted, restite-dominated group. In their grouping, the Bow River Granitoid was included in this group. However, the presence of restite in the Bow River Granitoid is not clearly demonstrated in the present study. As described at the beginning of this chapter, Wyborn et al. (1992) defined the second type of Australian Proterozoic granitoid as an I-type, Sr-depleted, Y-undepleted, fractionated granite. They based the differences between the groups on the chemical characteristics of the each suites. Their classification requires a relatively large data set for each granite suite, and, furthermore, Wyborn et al. (1992) indicated that the geochemical characteristics of the fractionated granites are not very different from the restite-dominated group on the primordial mantle normalized diagram. Discrimination of granites into restite-dominated or fractionated types may not always be easy, and its significance is not so clear. Therefore the discrimination is not made in the present study. However, it is important to note that voluminous high K₂O granites and related volcanics of 1880-1840 Ma with the above geochemical characteristics are present in the Early Proterozoic terrain of northern Australia (Wyborn et al., 1987; Wyborn, 1988). Zhao and McCulloch (1995) reported similar high K₂O granites of 1780-1750 Ma in the Arunta Inlier, and 1730-1710 Ma granites extremely enriched in K₂O, Rb, Th, and U. Based on the many

other occurrences of high K₂O granites in Australian Proterozoic terrains, Wyborn et al. (1992) concluded that the majority of Australian Proterozoic granites are Sr-depleted, Y-undepleted and characteristically have high levels of K, Th and U.

High K₂O granites with Sr-depleted and Y-undepleted characters can be found in other Early Proterozoic orogenic zones. The Great Bear magmatic zone of 1875-1840 Ma in the Wopmay Orogen, northwestern Canada, contains high K₂O granites and volcanics (Hildebrand et al., 1987). Major and trace element data of a typical example from the granite of the zone (Hildebrand, et al., 1987) is listed in Table 7-3, showing analogous geochemical features to the Bow River Granitoid and Early Proterozoic granites from the Mount Isa Inlier.

Average compositions of Palaeozoic I-type and S-type granites of the Lachlan fold Belt, southeast Australia (Table 7-3), indicate similar chemical characteristics to the Proterozoic granites. These granites have Sr depleted and Y undepleted signatures. However, K₂O contents of the granites are slightly lower than those of the Early Proterozoic granites. Wyborn et al. (1992) indicated that the Palaeozoic granites of southeast Australia are not as enriched in K, Th and U as the Proterozoic granites.

Two other examples of High K₂O granites are presented in Table 7-3. First is a Cretaceous example from the Yenshan Orogeny in southeast China. The Yenshanian granites of 135-80 Ma from the Hong Kong area are mainly I-type and characterized by high K₂O, typically more than 4.5 wt% (Sewell et al., 1992). The Yenshanian granites comprise a large batholith, exposed over an area of 400 x 1000 km. Limited geochemical data indicate that the granites show Sr-depleted and Y-undepleted characters. A continental margin tectonic setting is assumed for the Yenshanian granites. The Early Proterozoic high K₂O granitic magma which was the source of high K₂O granites in northern Australia may

have been generated in a similar tectonic setting to that of the voluminous Yenshanian granites. The other example is Miocene rhyolites from the Snake River Plain, northwestern USA (Norman et al., 1992). The rhyolites are exposed over an area more than 400 x 600 km. A representative example of the rhyolites (Table 7-3) has high K₂O, an I-type signature with Sr-depleted and Y-undepleted. Although, the enrichment or depletion of elements is more marked in the Miocene rhyolites than in the Early Proterozoic granitoids from northern Australia, overall geochemical features of the rhyolites are analogous to the Proterozoic high K₂O granitoids. The rhyolites are considered to have been generated in an extensional environment. The two examples above show that high K₂O granites are not restricted to the Proterozoic, and are also found in different tectonic settings.

CHAPTER 8. PETROGENESIS OF GRANITOIDS IN THE HALLS CREEK MOBILE ZONE

8.1. Introduction

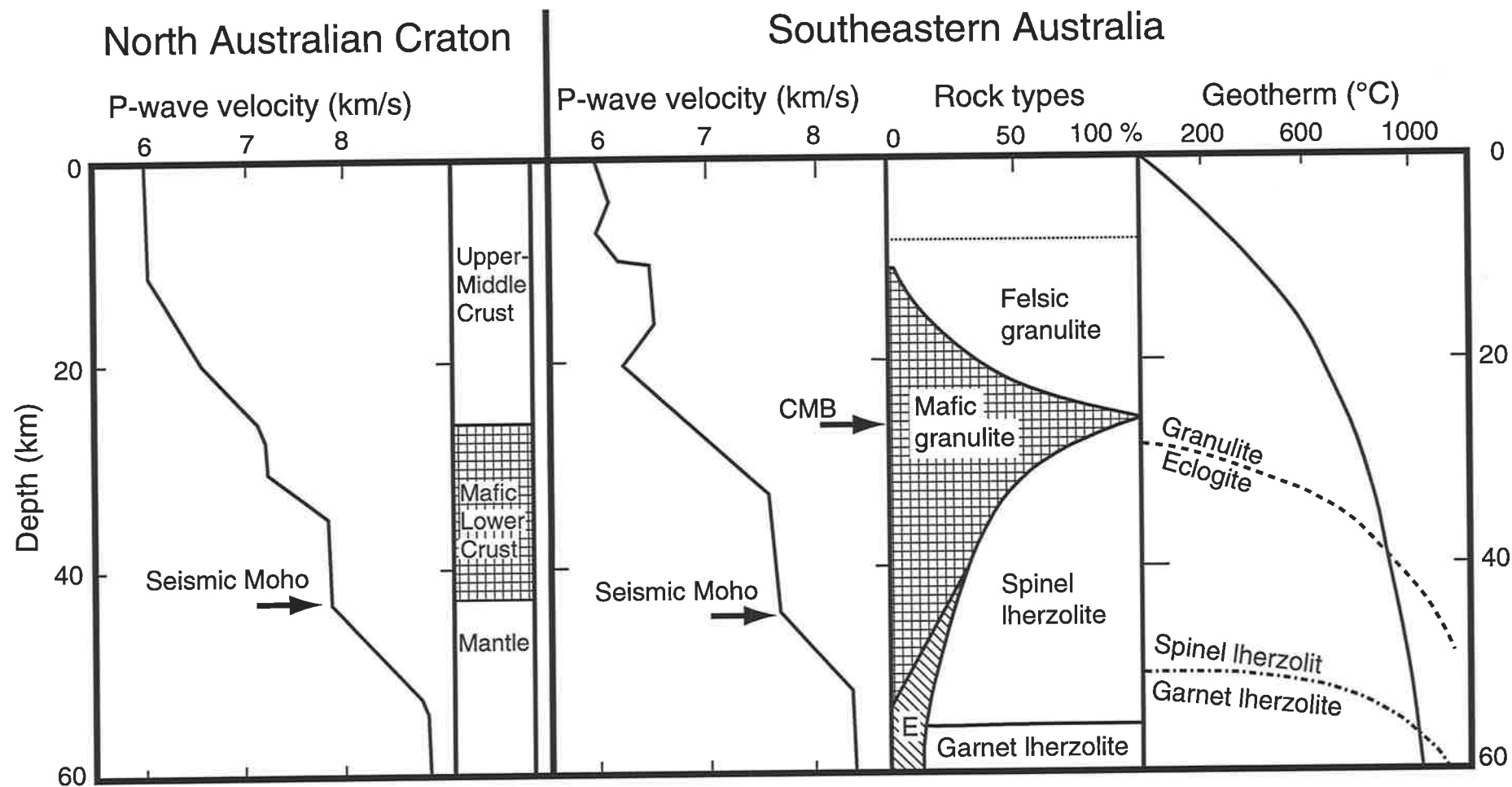
Petrogenesis of the granitoids in the Halls Creek Mobile Zone is discussed in this chapter. The petrogenetic discussions are presented separately in four groups, viz. the Eastern Leucocratic Granitoid Suite, tonalite-trondhjemite suites, Sophie Downs Granitoid, and high K₂O granitoids. The first two groups contain granitoids mainly from the Sally Downs Bore area. The high K₂O granitoids include the Bow River Granitoid and other high K₂O granitoids from the Halls Creek Mobile Zone. Before the granitoid petrogenesis is discussed, however, available information concerning the present crustal structure of the North Australian Craton is reviewed. This review is aimed to provide basic constraints on the nature of the possible source of the granitoid magmas.

8.2. Constraints on granitoid petrogenesis provided by the present crustal structure of North Australian Province

Crustal thickness of the East Kimberley region, calculated from gravity data and from the results of refraction seismic survey, has been briefly reviewed in section 2.7.2. An additional review of the crustal structure of the whole North Australian Craton as determined by refraction seismic survey is now presented. The seismic P-wave velocity/depth profiles of the North Australian Craton (Drummond and Collins, 1986; Finlayson, 1987) indicate a depth of 40-55km for the crust/mantle boundary (see Fig. 8-1). As also shown in Fig. 8-1, Drummond and Collins (1986) interpret the high (> 7km/sec) P-wave velocity in the lower crust (deeper than 25km) as an indication that the lower crust consists of underplated mafic igneous rocks in the granulite stability field. The presence of high-velocity lower crust is indicated in

Fig. 8-1. P-wave velocity models of North Australian Craton and southeastern Australia

P-wave velocity models of North Australian Craton and southeastern Australia, plus interpretation of the velocity model of the North Australian Craton (Drummond and Collins, 1986). Rock type profile and geotherm of southeastern Australia are from Griffin and O'Reilly (1987).



CMB: crust/mantle boundary suggested by Griffin and O'Reilly (1987), E: eclogite

other Proterozoic provinces in Australia and other continents (Drummond and Collins, 1986; Durrheim and Mooney, 1991). On the other hand, the crust in Archaean provinces is relatively thin and lacks a substantial high-velocity lower crust when compared with that of the Proterozoic provinces (Durrheim and Mooney, 1991).

Lithology of lower crust and upper mantle is well established in the southeastern Australia from the presence of high pressure xenoliths in Mesozoic and Cenozoic volcanic rocks (Griffin and O'Reilly, 1987). Characteristics of the P-wave velocity/depth profile of southeastern Australia (which is considered to have a Proterozoic basement), are rather similar to those of Proterozoic provinces, both having a high-velocity lower crust (Fig. 8-1). Lower crustal materials in southeastern Australia are predominantly mafic granulite and ultramafic rocks (Griffin and O'Reilly, 1987), suggesting that the high P-wave velocity in the lower crust is resulted from those rocks. Griffin and O'Reilly (1987) indicated a depth profile of the relative proportion of rock types in the area (Fig. 8-1), and defined a crust/mantle boundary (CMB; the boundary or transition between felsic-mafic crustal rocks and a dominantly ultramafic upper mantle) at a depth of 25-30km, which is much shallower than the crust/mantle boundary defined by the seismic velocity/depth profile (seismic Moho). Their interpretation suggests that material between 25 and 45 km depth is in the upper mantle, and consists largely of mafic granulite and ultramafic rocks. The proportion of mafic granulite decreases with depth, and only small amounts are present below the seismic Moho. Although the definition of crust/mantle boundary is different from the geophysical interpretation, it is significant that mafic granulite and ultramafic rocks are abundant between 25 and 45 km depth (Fig. 8-1).

In this study, the seismic Moho is considered to represent the crust/mantle boundary. Thus the high velocity portion at depth about between 25 and 45 km is in the lower crust. It is considered that the high velocity layer in the North Australian Craton is composed largely of mafic granulite.

Thornett (1981) deduced a maximum pressure of 6 kb for the granulite facies portion of the Tickalara Metamorphics in the Sally Malay area, central part of the Halls Creek Mobile Zone, and 10 km north of the Sally Downs Bore. The estimated metamorphic pressure adds another 15-20 km of upper crust in the area. However, in the western part of the mobile zone, the occurrence of the Whitewater Volcanics which are largely pyroclastic, suggests that the location of an Early Proterozoic surface during deposition of the pyroclastics is not different from the present level. Therefore the thickness of the crust in the Early Proterozoic was probably not different from the present crustal thickness in the western part of the mobile zone. Although high pressure rocks are exposed on the surface in the central part of the mobile zone, the thickness of the crust during the Early Proterozoic is not likely to be more than 55 km, including 15-20 km of crust which has been uplifted and lost by erosion. The estimated Early Proterozoic crust thickness in the Halls Creek Mobile Zone is thus within the range of crustal thickness found in the North Australian Craton.

Density of mafic magma and density of mantle and crustal rocks have been calculated by Glazner (1994), and he indicated that mafic magma can be trapped at the crust/mantle boundary or deep in the crust when the mafic magma has a neutral buoyancy relative to the crustal rocks. This indicates that underplating by mafic magma is physically possible. The high velocity lower crust may be due to underplating by mafic magma.

Wyborn et al. (1988) assumed this high velocity lower crust to be the source region for the majority of Proterozoic I-type granites.

8.3. Eastern Leucocratic Granitoid

Distinct petrological and geochemical characteristics of the Eastern Leucocratic Granitoid are presented in this study. The granitoid intruded the Tickalara Metamorphics in the early stage of the granitoid activities in the Sally Downs Bore area. It is typically leucocratic and contains small garnets. Geochemical characteristics of the granitoid can be summarized as follows,

- (1) high SiO₂ contents, ranging from 70.27 to 78.55 wt%.
- (2) metaluminous to mildly peraluminous.
- (3) high Na₂O contents, ranging from 3.25 to 4.93 wt%.
- (4) variable K₂O contents, from 0.66 to 4.38 wt%.
- (5) low concentrations of Rb, Sr, Zr, Nb, LREE, and transitional metals.
- (6) high concentrations of Y, HREE, and Ga.
- (7) low initial ⁸⁷Sr/⁸⁶Sr ratio (0.7021).

Some of the characteristics (e.g., variation of SiO₂ and Na₂O contents) are the result of fractionation of granitoid magma and some (e.g., low initial ⁸⁷Sr/⁸⁶Sr ratio) are due to mobilization of elements during metamorphism. The large variation of K₂O in the Eastern Leucocratic Granitoid (Table A4-2) is notable. Similar large variations of K₂O are found in granite-pegmatite systems from various locations in the world, e.g., the granite-pegmatite system of the Calamity Peak Pluton, South Dakota (Duke et al., 1992). In the high SiO₂ granite-pegmatite system, the dominant fractionation of K-feldspar can result in a marked depletion of K₂O. Low K₂O granitoids (trondhjemite) of the type III Eastern Leucocratic Granitoid thus may be derived by fractionation of an

assumed K-feldspar rich phase from the type I granitoid which has an intermediate SiO₂ content in the Eastern Leucocratic Granitoid Suite (Fig. 8-2A). Furthermore, the type I granitoid may be obtained from the type II granitoid (low SiO₂ granitoid in the suite) by fractionation of a group of phases which largely comprises plagioclase and mafic minerals(Fig. 8-2A). Thus most of the variations found in the Eastern Leucocratic Granitoid can be explained by a crystal fractionation model. The fractionation model indicates a sequence of crystallization from tonalite of type II, leucocratic granite of type II and I, and finally to trondhjemite (originally pegmatitic) of type III (see section 3.4 for detail petrological and geochemical descriptions). The lowest SiO₂ sample of the Eastern Leucocratic Granitoid, 42708 (Table A4-2), is considered to represent the least fractionated magma in the fractionation sequence of the granitoids.

Fig. 8-2B shows a possible model to explain Y concentration in the granitoids. It is assumed that the fractionation reduced the Y concentration from about 90ppm in the least fractionated sample 42708 to 10ppm in high SiO₂ samples. The Y concentration can be decreased by the fractionation of hornblende. Although the hornblende rich phase or hornblende crystals are not found in the Eastern Leucocratic Granitoid, such may be present in the unexposed lower portion of the granitoid body as a fractionated material. The hornblende fractionation may control overall variations of some elements in the Eastern Lucocratic Granitoid, e.g., decreasing Fe₂O₃, MgO, Y, MREE, and HREE concentrations in the magma with increasing of SiO₂. Positive Eu anomaly (see Fig. 3-14) may be developed by the hornblende fractionation.

In chapter 3, the role of garnet crystals is indicated for the some of the trace element abundances in the Eastern Leucocratic Granitoid. Spessartine rich garnets (12-34 mol.% spessartine in the Eastern

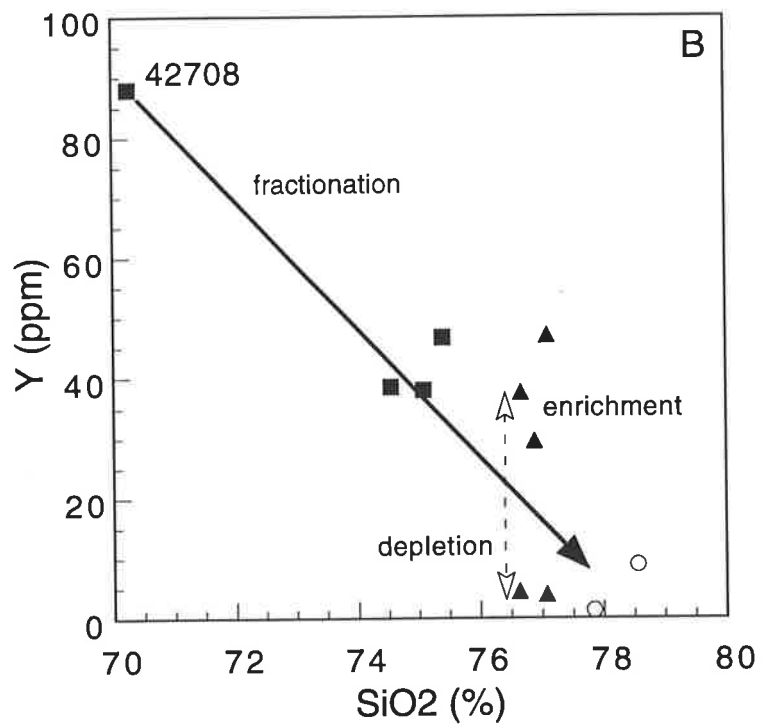
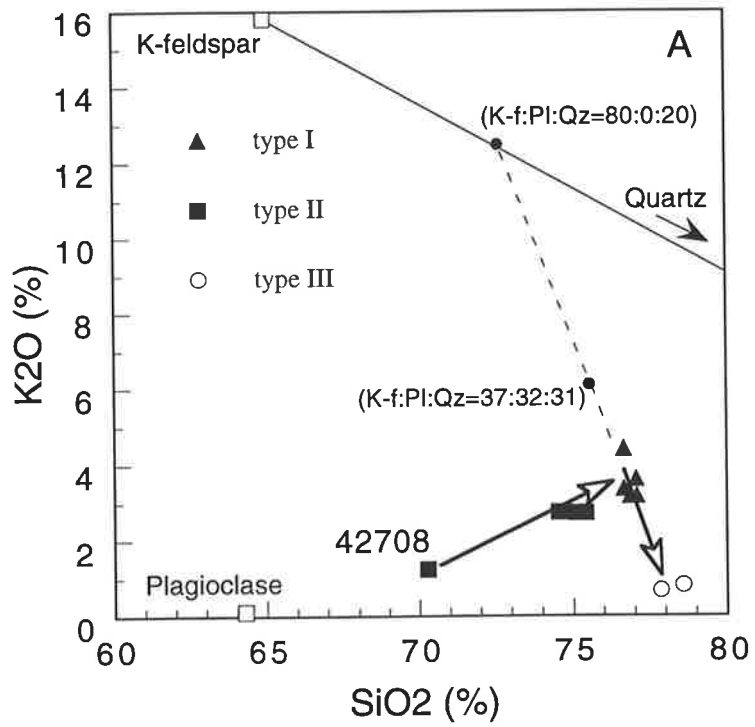
Fig. 8-2. Fractional crystallization models for the Eastern Leucocratic Granitoid

A. Fractionation model on the K_2O-SiO_2 diagram showing K-feldspar dominated fractionation from type I to type III.

Compositions of K-feldspar (Or 93.5) and plagioclase (An 18) are from results of electron microprobe analysis on a sample 51607. Large arrows indicate fractionation trend. Solid line is a tie line connecting K-feldspar and quartz. Broken line indicates range of possible fractionated phases. Compositions of two examples of the fractionated phase on the broken line are given as feldspars and quartz ratios.

B. Fractionation model on the $Y-SiO_2$ diagram.

Solid arrow indicates fractionation mainly controlled by hornblende. Small open arrows show enrichment or depletion by the incorporation or removal of garnets.



Leucocratic Granitoid) are able to crystallize directly from the granitic magma at low pressure (Green, 1977), and these are likely to contain high levels of Y and HREE. Thus the removal of garnets from the granitic magma would locally reduce the Y and HREE contents. On the other hand, accumulation of the garnets would enrich the Y and HREE content (Fig. 8-2B). Magnitude of the Y enrichment can be calculated as follows. Assuming a Y garnet/melt distribution coefficient of 35 (estimated from that of Dy and Er (Arth and Hanson, 1975)), garnets crystallizing from a magma containing 20ppm of Y at $\text{SiO}_2=76.5\%$ would contain 700ppm of Y. Incorporation of 3 wt% of these garnets in part of the granite increases Y by 21ppm in that part. Thus the total Y concentration of that part becomes 41ppm. As the behavior of HREE is considered to be similar to that of Y, the HREE would be similarly enriched in the garnet bearing granitoid. The garnets would concentrate HREE, but not much MREE. Depletion of MREE and HREE by the fractionation of crystals, mainly hornblende, and final enrichment of HREE by the garnets, would result in the distinct MREE depleted chondrite normalized pattern found in the type I granitoid of the Eastern Leucocratic Granitoid Suite. Although, detailed numerical indication of the fractionation using a least squares mixing program and other trace element modelings are not presented, the qualitative consideration of the fractionation accounts for most of the geochemical variation and characteristics of the granitoid. As mentioned above, and as shown in Fig. 8-2A, sample 42708 represents the least fractionated granitoid of the suite. Therefore, sample 42708 is selected for further petrogenetic discussion.

The least fractionated sample, 42708, is a metaluminous tonalite. Other samples of the Eastern Leucocratic Granitoid are also metaluminous or only mildly peraluminous. The low alumina saturation

of the granitoid eliminates any significant contribution of metasedimentary rocks to the source of the granitoid magma. The tonalite, 42708, is classified as a low Al type tonalite-trondhjemite, based on geochemical characteristics (Drummond and Defant, 1990), e.g., less than 15 wt% Al₂O₃ at 70 wt% SiO₂, low Sr content, and high Y content. The low Sr content implies that plagioclase was stable in the source region of the magma generation. High Y and HREE contents exclude garnet or hornblende in the source. As suggested by Drummond and Defant (1990), these characteristics indicate that the magma was generated by low pressure partial melting of basalt with a plagioclase + pyroxene residue as exemplified by the Proterozoic trondhjemite and metadacite of northern New Mexico and southwestern Colorado (Barker et al., 1976). This petrogenetic model would be applied to that of the Eastern Leucocratic Granitoid.

Low levels of K₂O and Rb suggest that the source of the granitoid magma is not enriched in these elements. Thus the high to moderately high K₂O igneous rocks of calc-alkaline andesitic or shoshonitic composition are not possible source rocks. Tholeiitic or calc-alkaline basalts, however, would be a possible source rock for the granitoid magma.

Experimental results of partial melting of tholeiitic basalt indicate that garnet is stable at pressure above 8kb (Green, 1982). Under such low pressure condition, plagioclase is stable in the partial melt (see next section for a detailed review of the experimental results). Therefore, partial melting of tholeiitic or calc-alkaline basalts under pressure less than 8kb within middle to lower crust would generate low Al type tonalitic magma, and subsequent fractionation of the low Al type tonalitic magma produces the geochemical characteristic of the Eastern Leucocratic Granitoid.

8.4. Tonalite and Trondhjemite

Petrogenetic discussions of the Dougalls Granitoid Suite, the Ord River Tonalite Suite, and the Sally Downs Tonalite of the Mabel Downs Granitoid Suite are presented in this section. Firstly, crystallization processes of tonalitic and andesitic magma under various pressures and temperatures, are examined based on available experimental data. Hornblende is considered to control the variation from tonalite to trondhjemite in the Dougalls Granitoid Suite. Similarly, hornblende plays a role in the fractionated phase of the Sally Downs Tonalite. However, fractionation models to obtain tonalites from mafic magma are not supported by the absence of a direct connection between tonalites and mafic magma. As the lowest SiO₂ contents of the Dougalls Suite, the Ord River Suite, and the Sally Downs Tonalite are 58.11%, 58.42%, and 55.72%, respectively, it is considered that primary magmas for the suites are tonalitic. Petrogenetic models for the tonalitic magmas are discussed below.

Crystallization conditions of tonalitic magmas

A P-T diagram for water-saturated andesitic compositions constructed by Green (1982) is shown in Fig. 8-3. The major element compositions of andesitic rocks used in the experiments are largely similar to those of the tonalites from the present study, thus use of the diagram here is considered justified. Green (1982) presented andesite P-T diagrams for the extremes of dry and water-saturated condition, and for intermediate, water undersaturated condition with 5 % by weight of H₂O. As biotite appears above solidus only in the water-saturated condition, the P-T diagram of water-saturated condition is shown and examined. Although the tonalitic magma may not be saturated in water at

Fig. 8-3. Composite P-T diagram for water-saturated andesitic composition, showing crystallization paths of tonalites.

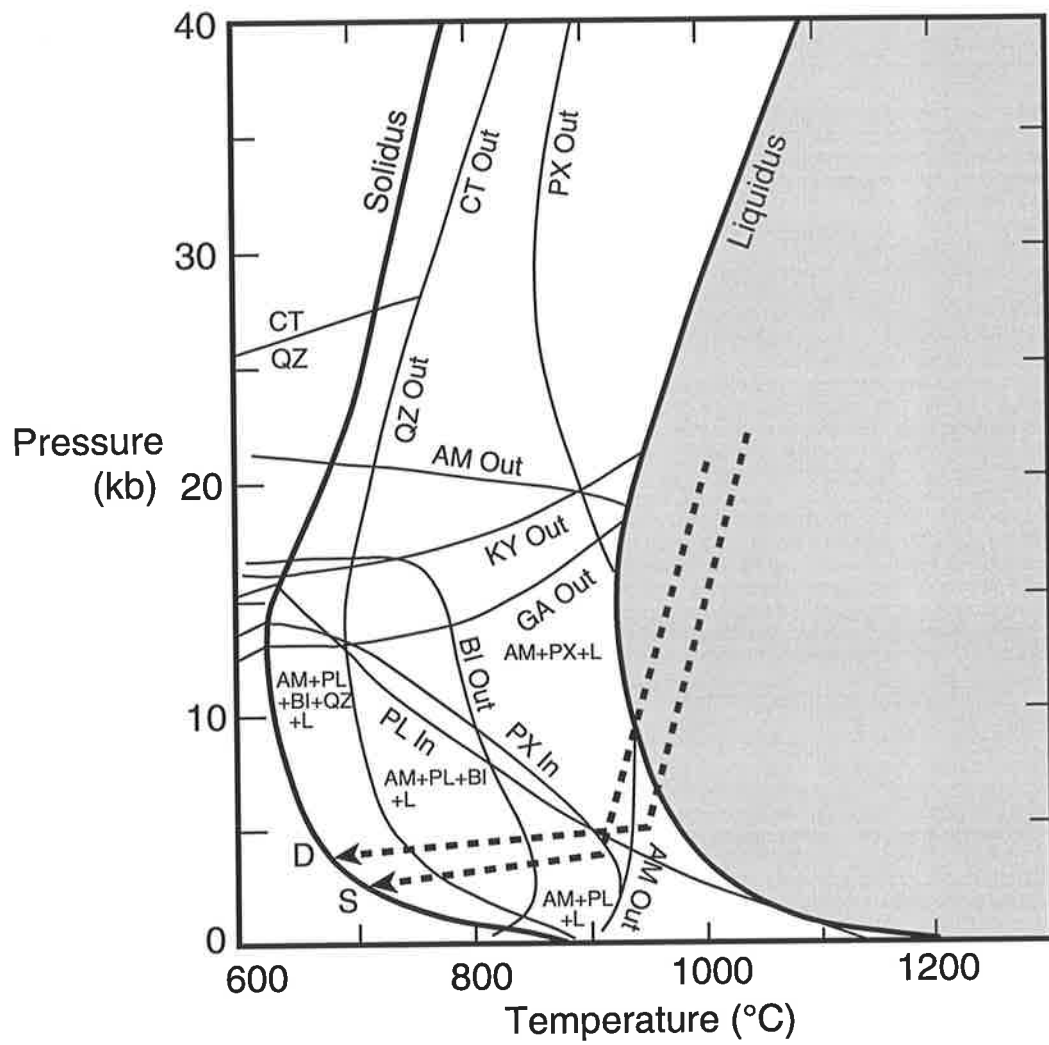
Diagram from Green (1982). Arrows indicate crystallization paths.

D: Dougalls Granitoid Suite

S: Sally Downs Tonalite

AM: amphibole, PX: pyroxenes, BI: biotite, GA: garnet

QZ: quartz, CT: coesite, L: liquid



the beginning of the crystallization sequence, the magma would become saturated in water by the initial crystallization of anhydrous minerals.

Fig. 8-3 suggests near liquidus minerals are amphibole and pyroxene. At a pressure less than 13 kb, amphibole, plagioclase, biotite, quartz, plus melt coexist near the solidus. The arrows in Fig. 8-3 show possible crystallization conditions for the tonalites. The crystallization condition for the Dougalls Suite is assumed to be slightly higher pressure to explain the presence of orthopyroxene in the suite. As indicated by crystallization path of the Dougalls Granitoid Suite in Fig. 8-3, a near liquidus mineral is pyroxene. After the initial crystallization of pyroxene, it is assumed that magma solidified with isobaric cooling. The crystallization path explains preservation of pyroxene in the tonalites.

In the case of the Sally Downs Tonalite, the tonalitic magma may rise to a level corresponding to less than 5 kb to enter into the amphibole+plagioclase+melt field, and begin to solidified. Near liquidus crystals of pyroxene must be lost during ascent of the magma. The crystallization of the tonalitic magma continued the amphibole+plagioclase+biotite field, and was completed in the field of amphibole+plagioclase+biotite+quartz. The suggested crystallisation path for the Sally Downs Tonalite clearly explains most of the petrological and geochemical characteristics found in the tonalite. The crystallization conditions for the Ord River Tonalite Suite may be similar to those of the Sally Downs Tonalite.

Generation of tonalitic magmas

Several models for the derivation of tonalitic magma are presented by many authors. They can be summarized as follows,

- (1) derivation of tonalitic magma by fractional crystallization from basaltic magma

- (2) generation of tonalitic magma from partial melting of ultramafic mantle
- (3) generation of tonalitic magma from partial melting of mafic rocks
 - (3)-1 partial melting of subducted mafic oceanic crust
 - (3)-2 partial melting of mafic rocks in the lower continental crust

The derivation of tonalitic magma by fractional crystallization from basaltic magma is generally considered likely for tonalites which are associated with more mafic rocks, e.g., in the gabbro-diorite-tonalite-trondhjemite suite of southwestern Finland (Arth et al., 1978) and in the similar suite of the Atnarpa Igneous Complex in the Arunta Inlier (Zhao and Cooper, 1992). However tonalites in the Halls Creek Mobile Zone do not have intermediate members associated with gabbro and tonalites. As already discussed at the beginning of the section (8.4), this model is considered unlikely to derive tonalitic magmas in the Halls Creek Mobile Zone.

Partial melting of metasomatically altered mantle above the descending slab in a subduction zone is considered a possibility for the formation of andesite by various authors, e.g., reviews in Mysen (1982). As the major element composition of andesite is largely similar to that of mafic tonalite, the same model can be applied to the generation of tonalitic magma. However, estimated presences of garnet and/or amphibole in the residue of the partial melt indicated by HREE and Y depleted characteristics of the high Al tonalites, do not support direct derivation of tonalitic magma by the partial melting of mantle consisting largely of olivine and pyroxenes.

Therefore, the third model listed above, viz. the generation of tonalites by the partial melting of mafic rocks, is left as a possible

mechanism for the generation of the tonalitic magmas in the Halls Creek Mobile Zone. Melting experiments with the mafic rocks have been summarized in Green (1982). In addition to the andesite melting P-T diagram discussed above, Green (1982) presented P-T diagrams of tholeiitic basalt for the extremes of dry and water-saturated condition, and for intermediate, water undersaturated condition with 5 % by weight of H₂O (Fig. 8-4A and B). The diagrams show the position of phase boundaries under pressure from 0 to 40 kb and at temperature from 600 to 1400°C, ranges of pressure and temperature applicable to a consideration of tonalite petrogenesis.

The diagram of water undersaturated conditions with 5 % H₂O (Fig. 8-4A) is frequently used in discussions of tonalitic magma genesis (e.g., Martin, 1986; Tsuchiya and Kanisawa, 1994). It shows a large field of partial melting, with a temperature interval of 500°C between solidus (650°C) and liquidus (1150°C). Clinopyroxene is present in most of the fields in Fig. 8-4A. The high Al type characteristics for the tonalites in the Hall Creek Mobile Zone have been indicated in chapter 7. The tonalites of this type typically show low HREE and Y contents with high La/Yb ratio, indicating residual garnets and/or hornblende. High Sr concentration without any significant negative Eu anomaly found in the tonalites suggests that plagioclase is not present in the residue of the partial melting. On the basis of these geochemical characteristics of the high Al tonalites, and phase boundaries shown in Fig. 8-4A, Martin (1986) indicated a liquid+garnet+hornblende coexisting field representing a possible P-T condition of partial melting as part of the tonalitic magma genesis. It is bounded by solidus, garnet out boundary, and amphibole out boundary. Tsuchiya and Kanisawa (1994) excluded plagioclase stability field from Martin's (1986) possible partial melting field. The field represents a potential partial melting condition for the formation of

Fig. 8-4. Petrogenetic examination of tonalitic rocks on composite P-T diagrams for tholeiitic composition with 5 % of added water and for dehydration melting of amphibolite.

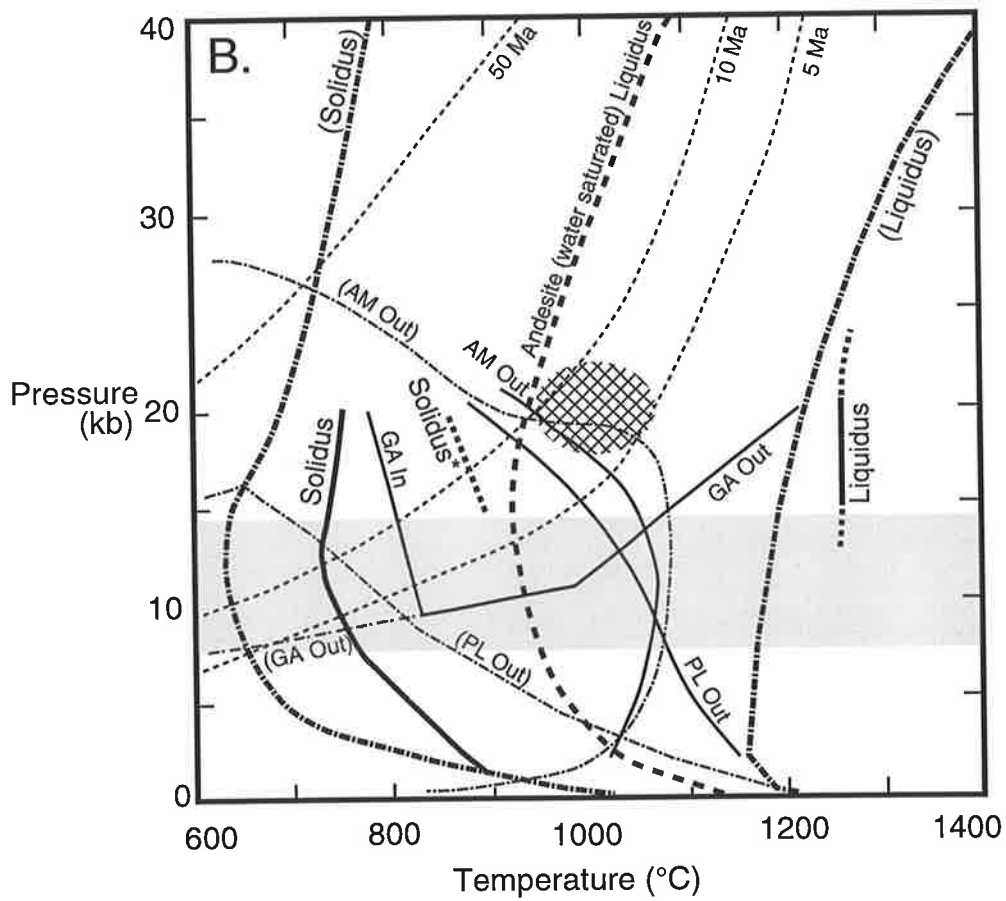
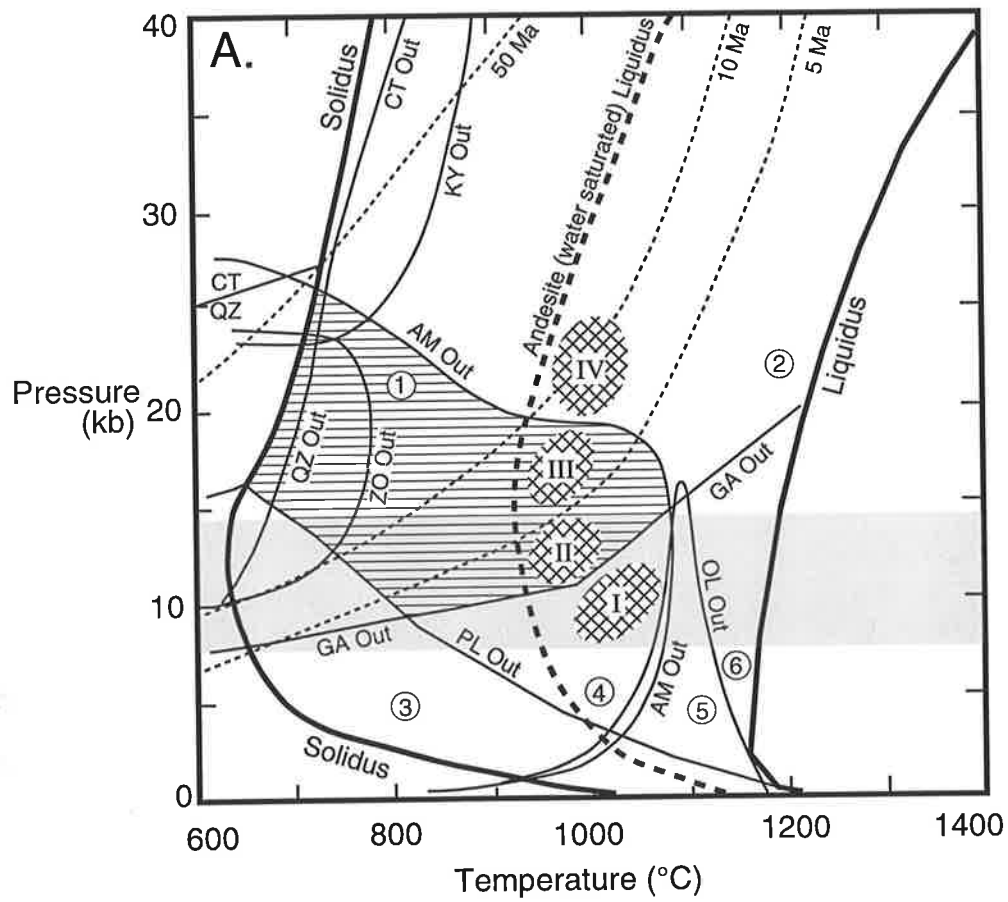
A. Composite P-T diagram, modified from Green (1982), for tholeiitic composition with 5 % of added water.

Shaded area indicates depth of mafic lower crust in the Halls Creek Mobile Zone. Andesite liquidus of water saturated condition is indicated with heavy dash. P-T-t paths of subducted slabs of three different ages at the point of subduction (Peacock, 1990) are shown with light dash. Lined area is potential partial melting field of a generating tonalitic magma, as indicated by Tsuchiya and Kanisawa (1994). Areas I, II, III, and IV are possible P-T fields of generating tonalitic magma discussed in this study (see text for detail).

AM: amphibole, PX: pyroxene, BI: biotite, GA: garnet OL: olivine, QZ: quartz, CT: coesite, L: liquid KY: kyanite, ZO: zoisite
Field 1: AM+CPX+GA+L, Field 2: GA+CPX+L,
Field 3: AM+CPX+PL+L, Field 4: AM+CPX+L,
Field 5: OL+PX+L, Field 6: PX+L

B. Composite P-T diagram for dehydration melting of amphibolite (Sen and Dunn, 1994).

Solid lines indicate phase boundaries for the dehydration of amphibolite (Sen and Dunn, 1994). Solidus* is the effective solidus (where melting exceeds more than 1%) inferred by Sen and Dunn (1994). Phase boundaries for tholeiite with 5% added water are also indicated for reference (heavy and light dash-dot). Mesh indicates estimated PT of partial melting for generation of tonalitic magmas in the Halls Creek Mobile Zone.



tonalitic magma, when limited free water (about 5% in weight) is available. When the tonalitic magma is separated from the residue in the partial melting region to move up higher level, the tonalitic magma must be largely liquid. Thus the tonalitic magma should have a temperature above the liquidus. During partial melting, available water must be incorporated in the liquid; the magma may be water saturated. The water saturated andesite liquidus is shown in Fig. 8-4A. The andesite liquidus should be the lower temperature limit of the tholeiite partial melting condition for the generation of tonalitic magma. Therefore, the initial temperature of the tonalitic magma is considered to be above 920°C.

Four possible fields of partial melting of mafic rocks to form tonalitic magmas in the Halls Creek Mobile Zone are shown in Fig. 8-4A. The fields I and II are considered to represent conditions for partial melting of mafic lower crust. The depth range (equivalent in kb) of the mafic lower crust in the Halls Creek Mobile Zone is indicated in Fig. 8-4A. Field I suggests partial melting of mafic lower crust leaving a residue consisting of primarily amphibole and clinopyroxene but not garnet. On the other hand, garnet, amphibole, and clinopyroxene are present in the residue of partial melting for field II. Melt generated from field II would show larger HREE and Y depletion than that from the field I. The formation of tonalitic magmas in the mafic lower crust requires high temperature and excess water indicated by the position of the two fields. The temperature required ranges from 950 to 1050°C at pressures of 8-14kb. This implies a necessary geothermal gradient of 25-35°C/km. Geothermal gradients calculated for shield regions and young continental regions by Ringwood (1975) are 11.5°C/km and 15°C/km, respectively. Thus the formation of tonalitic magma in the lower crust requires a temperature in the lower crust above the typical continental crust geotherm. Griffin and O'Reilly (1987) suggested a high geothermal

gradient (30°/km) in southeastern Australia based on mineral equilibria (Fig. 8-1), such temperatures being attained due to underplating by mafic magma of the lower crust. It is accepted that high temperatures, ranging from 950 to 1050°C in the lower crust, require a heat input from mafic magma intruded in to the crust. Temperature and pressure conditions for partial melting of the mafic lower crust may be obtained with this model; however, the formation of tonalitic magma requires to be satisfied with another condition, viz. availability of excess water. As the mafic lower crust consists largely of granulite facies rocks, sufficient water for the formation tonalitic magma would not be available in the lower crust. Therefore, the formation of tonalitic magma in fields I and II is not accepted.

Fields III and IV implies partial melting of mafic rocks in the subducting oceanic slab or possibly delaminated and sinking mafic lower crust into the mantle. From the examination of the thermal structure of the subducting plate, it is apparent that partial melting of mafic rocks in the subducting slab is only possible in a warm subducting slab (Wyllie, 1982; Peacock, 1990). For instance, Archaean tonalites, typically the high Al type, are considered to be derived by slab melting in conformity with the Achaean thermal evolution which indicates a dominance of young and warm subducting slabs (e.g., Martin, 1986; Arkani-Hamed and Jolly, 1989). High Al tonalites, including both Archaean and post-Archaean, are considered to be derived by slab melting by Drummond and Defant (1990) and Tsuchiya and Kanisawa (1994). Derivation of magma by slab melting is manifested by some andesitic or dacitic rocks (Defant and Drummond, 1990; Defant et al, 1991; Defant and Drummond, 1993; Sajona et al., 1993), and these are termed adakite. Adakite is characterized by low HREE and Y contents together with high Sr/Y ratios, and is considered to be the result of the melting of young

subducted oceanic crust, which leaves an eclogite residue (Defant and Drummond, 1990). The adakites are considered to be the volcanic equivalents of tonalites and trondhjemites (Defant and Drummond, 1990). In a modern subduction zone, adakites are found where the subducting slab is younger than 25Ma. Fig. 8-4A shows calculated subduction pressure-temperature-time (P-T-t) paths of Peacock (1990). In the modern thermal structure, a subducting slab with the age of 5-10 Ma at the point of subduction may reach the condition of partial melting fields III and IV. The time necessary for the slab to reach the melting field is about 40-50Ma for a subduction plate dipping angle of 27° with a convergence rate of 3cm/year. In an Early Proterozoic subduction, a possible difference of thermal structure of the slab and mantle wedge from that in the modern subduction would change the P-T-t paths of the slab. The dipping angle of the subducting slab and the convergence rate also affect the P-T-t paths. Although the above factors could change the subduction P-T-t paths, when assuming slab melting to generate tonalitic magma, a relatively young, therefore hot, slab must generally be considered.

Partial melting in field III leaves a residue consisting of amphibole, garnet, and clinopyroxene. The residue of partial melting in the field IV contains garnet and clinopyroxene, i.e., eclogitic. Thus the two fields are separated by the amphibole stability boundary (Fig. 8-4A).

The P-T diagram shown in Fig. 8-4A was constructed by Green(1982) based on the results of melting experiments of tholeiite with added water. However, basaltic rocks in the oceanic crust have been typically altered, and these are transformed to amphibolite before crossing the solidus in the subduction zone. Therefore, experiments involving dehydration melting of amphibolite would provide valuable information on conditions of slab melting. A limited number of results

of amphibolite dehydration melting experimentation is available (Beard and Lofgren, 1991; Rapp et al., 1991; Rushmer, 1991; Wolf and Wyllie, 1991; Sen and Dunn, 1994, Wolf and Wyllie, 1994; Douce and Beard, 1995; Rapp and Watson, 1995). A composite phase diagram for amphibolite dehydration melting constructed by Sen and Dunn (1994) is shown in Fig. 8-4B. Although the phase diagram does not cover the complete P-T range, it provides data for a possible slab melting. The H₂O content of the amphibolite used in experiment by Sen and Dunn (1994) is 1.5 wt%. The solidus of amphibolite dehydration melting is 100°C higher than that of tholeiite with 5% water. Different solidus curves for amphibolite dehydration melting were produced in different experiments by Wyllie and Wolf (1993). Garnet and amphibole stability fields of Sen and Dunn (1994) are not changed from those of Green (1982). However, a significant expansion of the plagioclase stability field is indicated in the diagram of Sen and Dunn (1994). Limited water availability in the dehydration melting experiments clearly increases temperature of plagioclase stability (Fig. 8-4B). Fig. 8-4B indicates that the residue of dehydration melting of amphibolite in the lower crust contains plagioclase. Therefore, a high Al type tonalitic magma, which has a high Sr content without negative Eu anomaly, is not generated by dehydration melting of amphibolite in the lower crust.

The melt composition determined in experiments indicates that it shifts from trondhjemitic to tonalitic with increasing temperature. Tonalitic melt is generated only at temperatures above 1025°C (Sen and Dunn, 1994; Rapp et al., 1991). Considering available data, it is concluded that the tonalitic magma can be generated at pressure from 20 to 22 kb and temperatures from 1000 to 1050°C. The temperature range is 50°C higher than that of Rapp et al. (1991) and Tsuchiya and Kanisawa (1994).

In a region with exceptionally thick crust, this condition may be attained if the mafic lower crust receives heat from an underplated mafic intrusion. Thus high Al type tonalitic magma may be generated in the lower crust (Kay and Kay, 1991; Atherton and Petford, 1993). However an examination of crustal thickness of the Halls Creek Mobile Zone (see section 8.2) excludes this model for the generation of tonalitic magma. The above outlined petrogenetic condition implies that the tonalitic magma in the Halls Creek Mobile Zone must be derived from slab melting.

Although the melt composition generated by this latter process is tonalitic, Sen and Dunn (1994) indicated that MgO and CaO contents of the melt derived by experiments are lower than those of natural high Al tonalites. MgO and CaO may be enriched by interaction of the magma with overlying mantle, as suggested by Johnston and Wyllie (1989) and Sen and Dunn (1994).

The Early Proterozoic tonalites in the Halls Creek Mobile Zone are considered to be derived from magma generated by slab melting. The magma may undergo some interaction with mantle during ascent to crust. Although the petrogenesis of the three tonalite suites in the Halls Creek Mobile Zone can be established with this model in general, the small geochemical and Sr isotopic differences between the three suites may indicate slightly different source compositions or conditions of melting. The differences depicted in the Sr/Y versus Y diagram (Fig. 7-3) could be due to small differences in the melting condition. On the diagram, the Sally Downs Tonalite shows a higher Y value at a particular Sr/Y ratio than does the older Dougalls Suite and Ord River Suite. The higher Y value may be derived from a smaller modal content of garnet in the partial melting residue, which may be resulted by melting in slightly lower pressure. The slab melting model is also applicable to the

petrogenesis of other high Al tonalites in the Mabel Downs Granitoid Suite.

8.5. High K₂O Granitoids

Petrogenesis of high K₂O granitoids in the Halls Creek Mobile Zone is discussed in this section. The high K₂O Granitoids include the Western Porphyritic Granite and the Central Leucocratic Granite from the Sally Downs Bore area and the Bow River Granitoids. These granitoids are characterized by a high concentration of K₂O, more than 4 wt%, and are mildly peraluminous. The petrogenesis of the Whitewater Volcanics is grouped with that of the Bow River Granitoids. Although, the Central Leucocratic Granite shows a high level of K₂O content, the trace element characteristics of the granite differ from those of other high K₂O granitoids. Thus the high K₂O granitoids are grouped into two types, type I and II, and the petrogenetic discussions are separately presented for the two types. The type I includes the Western Porphyritic Granite, the Bow River Granitoids, and the Whitewater Volcanics. The type II contains the Central Leucocratic Granite.

A. High K₂O Granitoids (Type I)

As discussed in chapter 7, the Bow River Granitoid and the Whitewater Volcanics are included as members of the Barramundi igneous association by Wyborn (1988). Wyborn et al. (1987) considered a mafic lower crust (high seismic velocity layer in the lower crust) to be the source region for the majority of Proterozoic I-type granites. Furthermore, Wyborn et al. (1992) suggested that magma of the Barramundi igneous association is derived from enriched tholeiitic underplates that were added successively to the base of the crust. Igneous rocks of the Barramundi association show Sr depleted and Y undepleted

characteristics. In chapter 7, the same characteristics were indicated for the member of the high K₂O granitoids (type I) in the Halls Creek Mobile Zone. Those characteristics are thought to indicate that a partial melting residue contains plagioclase but not garnet (Wyborn et al., 1992).

Although the high K₂O granitoids (type I) are mildly peraluminous, mol. (Al₂O₃/CaO+Na₂O+K₂O) ratios of granitoids are not as high as the ratios of the typical S-type. Therefore, the high K₂O granitoids (type I) are unlikely to be derived from a sedimentary rock source. Some S-type characteristics of granitoids may be acquired by incorporation of small amounts of sedimentary rocks in the source of the granitoid magma. However, the relatively uniform geochemical characteristics of the granitoids would require a large volume of homogeneous source material. Therefore, a heterogeneous source of igneous and sedimentary rocks is considered to be unlikely for the granitoids. Enriched igneous source material suggested by Wyborn et al. (1992) would be a possible source for the granitoids of type I. Granitoids derived from igneous source material enriched in LIL, LREE, and Zr would show some geochemical similarities to the S-type granitoids which typically contain high concentration of those elements.

Unless total melting of source rocks is assumed, the SiO₂ content of a melt is higher than that of the source rocks. Thus the source rocks for the high K₂O granitoids (type I) must be of mafic or intermediate composition, as the minimum SiO₂ content of the granitoids is about 70%. Based on the discussion presented above, it is assumed that the source material for the high K₂O granitoids (type I) is enriched mafic or intermediate igneous rocks.

Partial melting of the enriched mafic or intermediate igneous rocks leaving a residue containing plagioclase but not garnet would provide granitoid magma with geochemical characteristics of the high K₂O

granitoids (type I). However, intermediate igneous rocks with low Y and HREE concentrations, such as high Al tonalitic rocks, are not suitable source material.

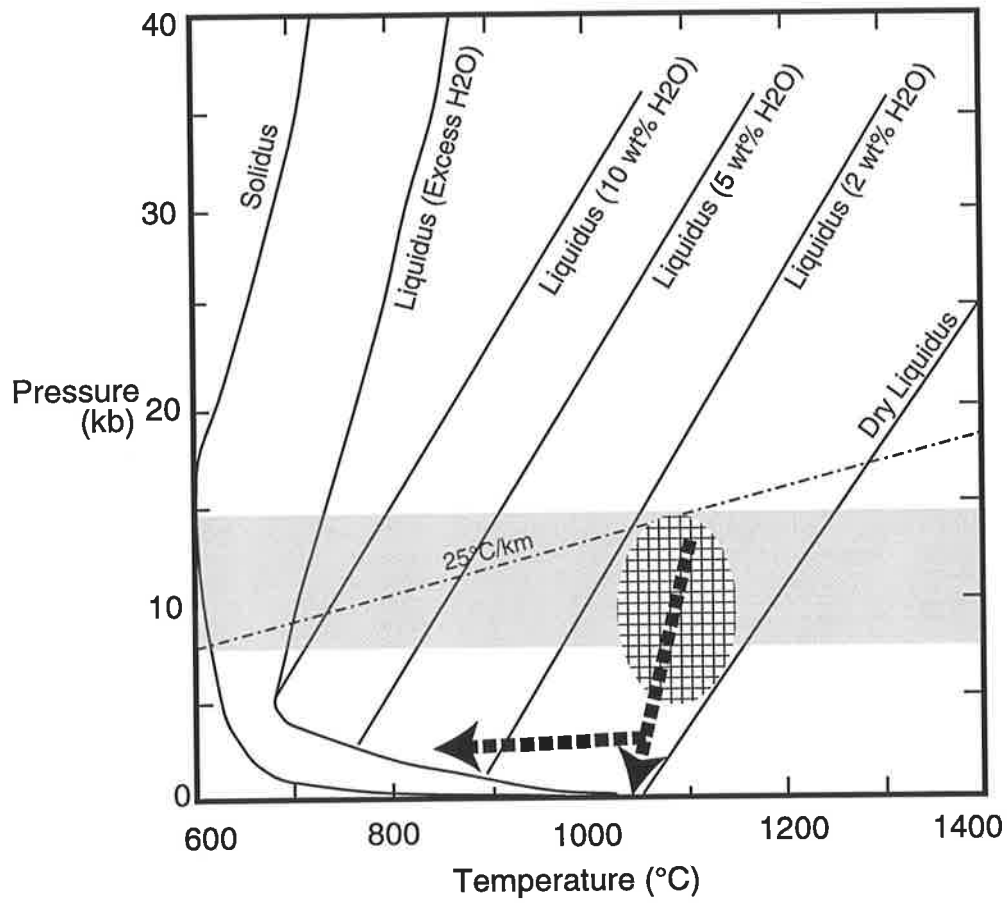
Concerning the limiting condition under which partial melting took place to form the granitoid magma, the initial temperature of the granitoid magma is estimated here with the P-T diagram for an I-type granite, experimentally constructed by Stern and Wyllie (1981), is shown in Fig. 8-5. The SiO₂ content of the granite used in the experiment is 75.4 %, which is similar to that of the Whitewater Volcanics but is slightly higher than that of the high K₂O granitoids of present study. Stern and Wyllie (1981) indicated a solidus temperature of 680°C and liquidus temperature of 715°C at 2kb for H₂O saturated condition. The solidus and liquidus temperatures increase to about 1000°C with decreasing pressure to 1bar (atmospheric pressure). As the Whitewater Volcanics were erupted to the surface, the temperature of the magma must be above solidus at 1 bar. Thus the initial temperatures of the high K₂O granitic magmas are assumed to be above 1000°C. Hildreth (1981) indicated magma temperatures in the range 700-1060°C for rhyolites based on his review from available data; the assumed magma temperature here corresponds to the higher portion of the temperature range.

The experimental H₂O saturated magma contains more than 10 wt% H₂O (Stern and Wyllie, 1981), but such high H₂O in the magmas is considered to be unlikely for high K₂O granitoids in the Halls Creek Mobile Zone. The granitic magma must have been undersaturated in H₂O when it formed. The H₂O-undersaturated liquidus are shown in Fig. 8-5. The liquidus temperature of magma with 2 wt% H₂O is about 1000°C at the pressure equivalent to the lower crust. Fig. 8-5 indicates that the temperature of granitic magma assumed from H₂O saturated solidus is likely to be above or near this liquidus. Thus it is possible for

Fig. 8-5. Cooling paths of the high K₂O granitoid (type I) magmas

The water-undersaturated granite liquidus surface extending from the dry liquidus to the water-saturated liquidus and water-saturated granite solidus is from Stern and Wyllie (1981).

Possible cooling paths of the high K₂O granitoid magmas are shown with arrows. The arrow which directly points to 0 kb is the possible cooling path of the Whitewater Volcanics. The mesh indicates the suggested region of generation of the magmas (see Fig. 8-6 for further discussion). The shaded area indicated the depth of mafic lower crust in the Halls Creek Mobile Zone at that time.



the granitic magmas to rise from the lower crust to the upper crust largely as melt. Arrows in Fig. 8-5 indicate the possible cooling path for magma of the high K₂O granitoids and the Whitewater Volcanics.

Generation of high K₂O granitoid (type I) magma by partial melting is examined with reference to the results of experiments involving mafic and intermediate igneous rocks by Green (1982). Fig. 8-6A shows a P-T diagram for tholeiitic composition with 5 wt% H₂O. This is similar to the P-T diagram of andesite with 5 wt% H₂O (Fig. 8-3), though olivine is not present in the andesite diagram and quartz appears stable over a wider temperature range in the andesite diagram than in that depicting tholeiitic composition.

Fig. 8-6A shows a potential field for partial melting with residue consisting of plagioclase but not garnet. The field is limited to a low pressure part of the diagram. Only the upper part of the lower crust would generate melt under relatively low temperature conditions, ranging from 650 to 850°C. Such a low temperature melt would not effectively be separated from the source and would not reach the surface or near surface level. Phase boundaries of plagioclase and garnet in the water saturated tholeiite melting phase diagram (not shown) are largely similar to those of tholeiite with 5 wt% of H₂O (Fig. 8-6A).

Fig. 8-6B shows plagioclase phase boundaries for anhydrous melting of tholeiite (Green, 1982) and for dehydration melting of an amphibolite (Sen and Dunn, 1994). The H₂O content of the amphibolite used in the experiment of Sen and Dunn (1994) is 1.5 wt%. Fig. 8-6B indicates that the stability field of plagioclase increases with decrease of availability of H₂O. Therefore, high K₂O granitoid magmas would be generated from a mafic rock source with relatively low H₂O content.

The lower crust is considered to comprise largely mafic granulite, the amount of water in the lower crust must therefore be low. H₂O

Fig. 8-6. Composite P-T diagrams for tholeiite composition showing possible source condition of high K₂O granitoid (type I) magmas.

A. Composite P-T diagram for tholeiitic composition with 5 % of added water (Green, 1982).

Dashed lines indicate anhydrous tholeiitic phase boundaries (Green, 1982). Shaded area indicates partial melting field with residue consisting of amphibole, clinopyroxene, and plagioclase, but not garnet.

AM: amphibole, PX: pyroxene, BI: biotite, GA: garnet

OL: olivine, QZ: quartz, CT: coesite, L: liquid

KY: kyanite, ZO: zoisite

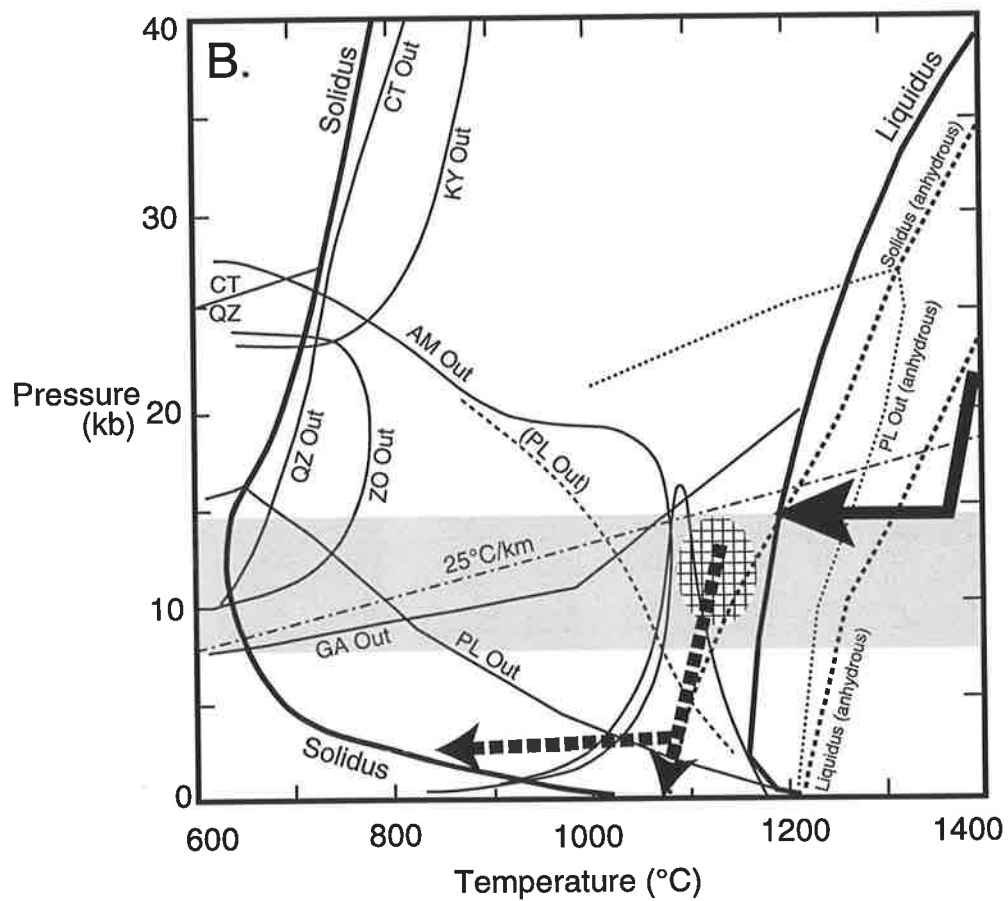
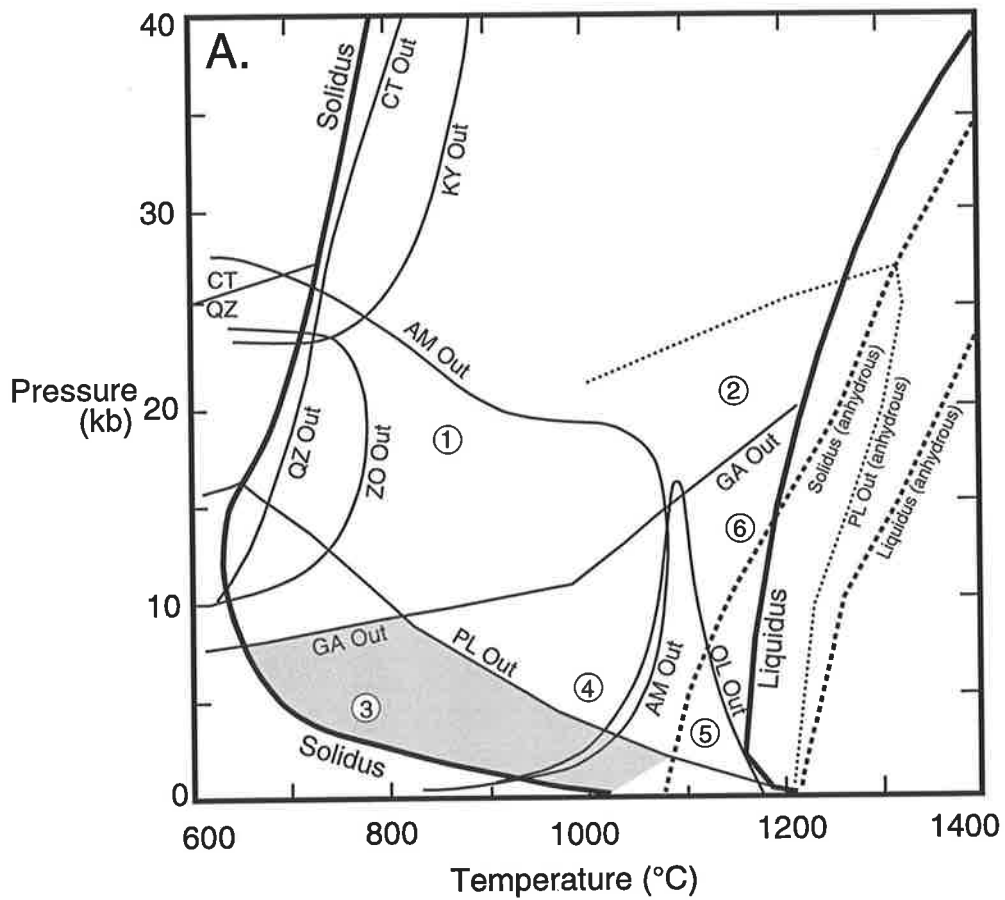
Field 1: AM+CPX+GA+L, Field 2: GA+CPX+L,

Field 3: AM+CPX+PL+L, Field 4: AM+CPX+L,

Field 5: OL+PX+L, Field 6: PX+L

B. Possible source condition of high K₂O granitoid (type I) magmas shown on composite P-T diagram for tholeiitic composition with 5% of added water and for anhydrous tholeiite.

Phase boundaries are the same as above. Extra Pl out curve is from Sen and Dunn (1994). Mesh suggests possible source condition. Dashed arrows indicate possible cooling path of the granitoid magmas. Solid arrow shows possible temperature of mafic intrusion which supplies heat to melt lower mafic crust. Shaded area indicates depth of lower crust in the Halls Creek Mobile Zone.



content in the lower crust would be lower than that of amphibolite. Therefore, with partial melting of the mafic lower crust, the plagioclase phase boundary would shift to a higher temperature than that associated with amphibolite dehydration melting. Thus the residue of partial melting of mafic lower crust should contain plagioclase. Possible P-T conditions for the partial melting of the mafic lower crust are indicated in Fig. 8-6B. As it is considered that residue of partial melting has not contained garnet, the garnet stability boundary marks higher pressure limit of the melting condition. Temperature of melting would be in range 1000-1150°C (Fig. 8-6B). The residue of the partial melting may contain amphibole with melting below 1070°C. However, a lack of HREE depletion in the high K₂O granitoids of type I may indicate that amphibole in addition to garnet is absent in the residue. At temperature above 1070°C, the residue must consist largely of plagioclase and pyroxenes, but not amphibole. The partial melting of mafic lower crust requires a high geothermal gradient, viz. about 30°C/km. It is considered that a high temperature in the lower crust must be the result of heat input from mafic intrusion into the lower crust or from underplated mafic emplacement at the crust/mantle boundary.

High K₂O and Rb contents in the type I granitoids (Table 7-1) suggest that the granitoid magmas are not derived from partial melting of mafic rocks with composition similar to N-type MORB (Mid Ocean Ridge Basalt), as the N-type MORB has a very low level of K₂O and Rb, e.g., 0.1% and 1.26ppm, respectively (Hofmann, 1988). It is necessary to invoke enriched mafic source rocks for the high K₂O granitoids as suggested by Wyborn et al. (1992). Although Wyborn et al. (1992) regarded enriched mafic source rocks as uniquely Proterozoic, occurrences of high K₂O granitoids of Phanerozoic age (see section 7-4) do not support this. Roberts and Clemens (1993) considered calc-alkaline

to high K calc-alkaline mafic rocks to be the source of high K₂O I-type granitoids. Calc-alkaline mafic rocks are regarded as a likely source of the high K₂O granitoids (type I) in the Halls Creek Mobile Zone. Calc-alkaline mafic rocks generated in a subduction environment must show Nb and Ti depletion, and these characteristics should be inherited by granitoid magma formed from partial melting of such rocks. Nb and Ti depletion in the granitoids (see Fig. 7-2) is thus accounted for.

It is concluded that the high K₂O granitoids (type I) are derived from partial melting of calc-alkaline mafic rocks present in the lower crust. Temperature of the partial melting is considered to be in the range 1000-1150°C. Such a high temperature in the lower crust must be the result of heat input from contemporaneous mafic magma intrusions in the lower crust or crust/mantle boundary.

B. High K₂O Granitoid (type II)

The Central Leucocratic Granite classified as the high K₂O granitoid (type II) shows a high concentration of K₂O and depletion of Nb, P, Ti, and Y. Although Sr in the granite is not depleted as much as in the high K₂O granitoids (type I), it is relatively low. Furthermore, the chondrite normalized REE pattern of the granite has a small negative Eu anomaly. These properties indicate that the residue of partial melting could have included plagioclase. On the Sr/Y versus Y diagram (Fig. 7-3) the granite plots near the field of tonalite-trondhjemite-dacite. These geochemical characteristics could have resulted from either of the following two models:

- (1). Partial melting of enriched mafic lower crust with residue containing plagioclase and garnet.
- (2) Partial melting of Y depleted tonalite (high Al type) with residue containing plagioclase.

The P-T condition for model (1) is indicated in Fig. 8-7A. The presence of garnet in the residue suggests a lower crustal or greater depth for the generation of the magma. The amount of melt generated in the low temperature region (less than 800°C) must be low -insufficient to become segregated to form granitoid magma. It is thus considered that model I granitic magma, with temperature more than 800°C, was derived from the lower part of mafic lower crust.

If sufficient temperature is attained, granitoid magma with the geochemical characteristic of high K₂O granitoid (type II) is generated according to model (2) at any pressure within the crust. Partial melting experiment results of tonalites and trondhjemites under pressure between 10 and 17kb are presented in Rutter and Wyllie (1988), Johnston and Wyllie (1988), Carroll and Wyllie (1990), van der Laan and Wyllie (1992), and Skjerlie and Johnston (1992). Availability of free water during partial melting within the crust may be limited. Thus dehydration of biotite and amphibole would be an important source of water for the melting. Rutter and Wyllie (1988) and Skjerlie and Johnston (1992) described details of vapor-absent dehydration melting of tonalites. Fig 8-7B shows estimated solidus, hornblende phase boundary, and liquidus for dehydration melting of the tonalites. Although experimental data at pressures less than 10 kb are not available, the estimated boundary lines in the field at pressures less than 10 kb are presented. Temperature of biotite phase boundary may be either higher or lower than that of hornblende depending on the composition of initial materials used in the experiments. Rutter and Wyllie (1988) indicated 900°C for the breakdown temperature of biotite. A higher break down temperature of biotite (more than 975°C) was deduced by Skjerlie and Johnston (1992) from their study of a tonalitic rocks with 20 % biotite. On the basis of their melting experiments at 10kb, Rutter and Wyllie (1988) suggested

Fig. 8-7. Petrogenetic model for high K₂O granite (type II)

A. Composite P-T diagram for tholeiitic composition with 5 % of added water (Green, 1982).

PL OUT (D) is the plagioclase boundary in experimental dehydration melting of amphibolite (Sen and Dunn, 1994). Shaded area indicates depth of mafic lower crust in the Halls Creek Mobile Zone. Mesh indicates partial melting field of mafic lower crust with a residue consisting of garnet, amphibole, clinopyroxene, and plagioclase.

AM: amphibole, PX: pyroxene, BI: biotite, GA: garnet

OL: olivine, QZ: quartz, CT: coesite, L: liquid

KY: kyanite, ZO: zoisite

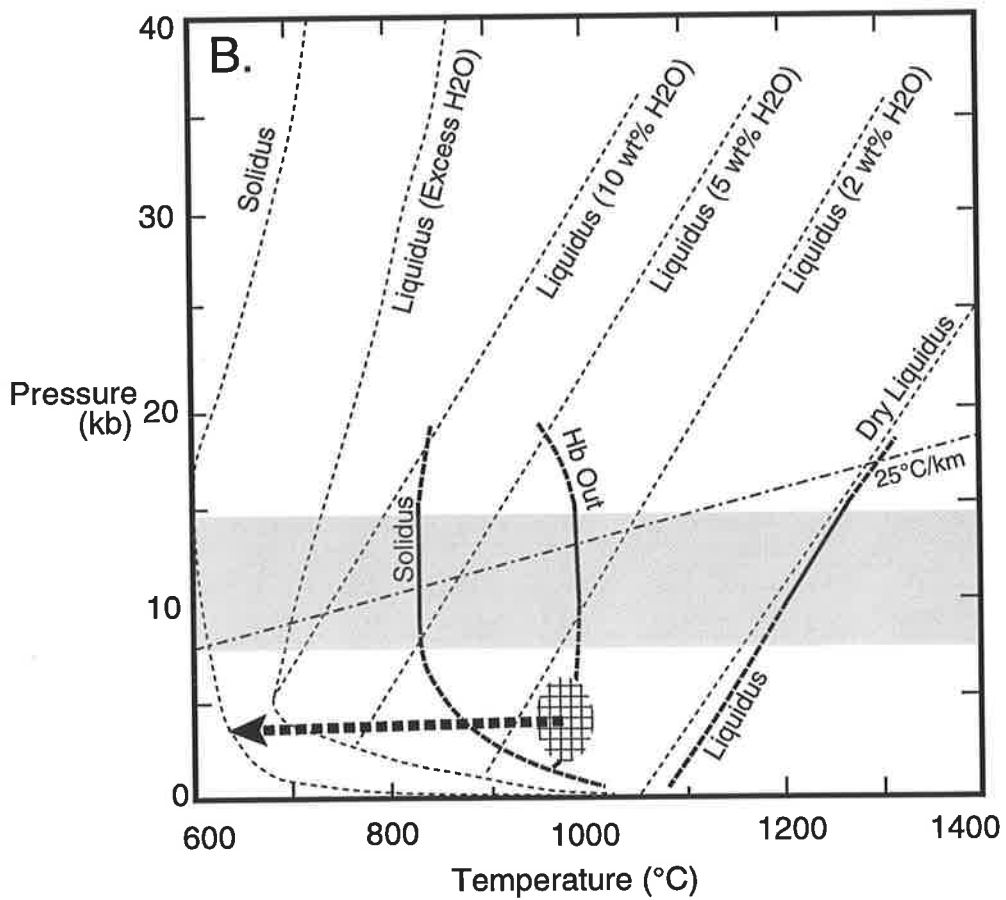
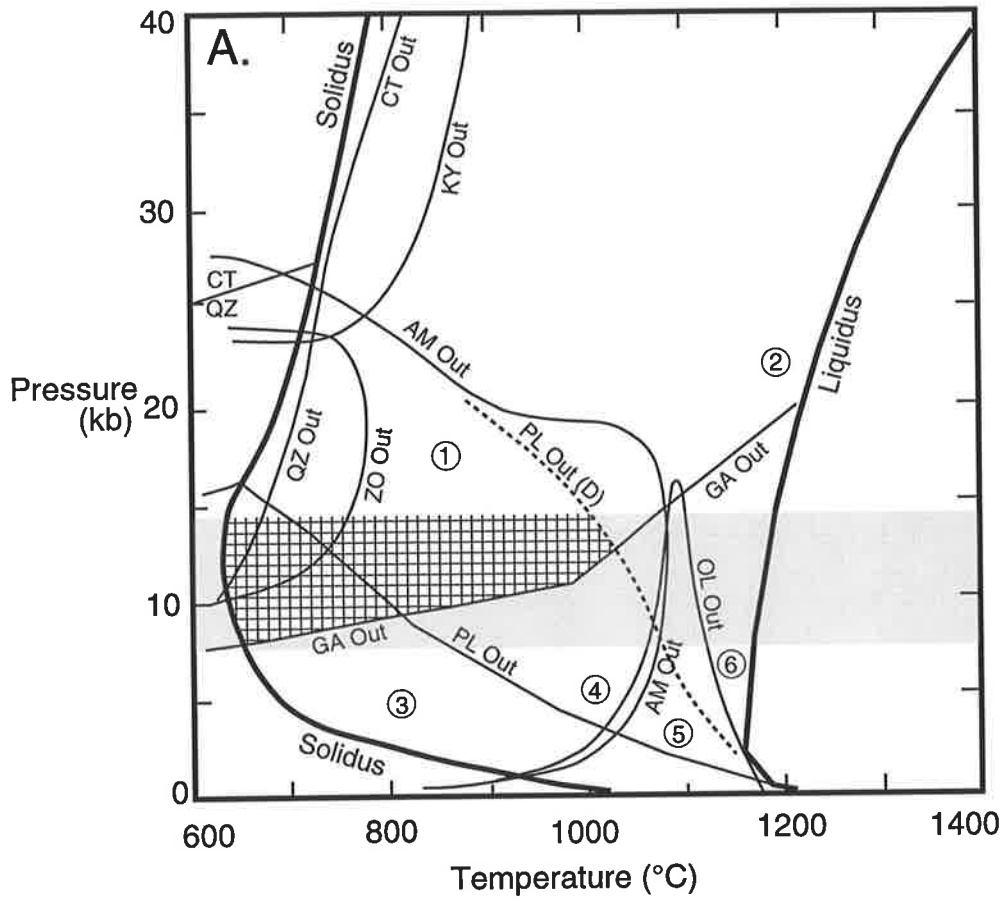
Field 1: AM+CPX+GA+L, Field 2: GA+CPX+L,

Field 3: AM+CPX+PL+L, Field 4: AM+CPX+L,

Field 5: OL+PX+L, Field 6: PX+L

B. P-T diagram for melting of tonalite

Thick solid and dashed lines are from Rutter and Wyllie (1988). Thin dashed lines are solidus and liquidus for granite after Stern and Wyllie (1981). Mesh indicates partial melting condition of tonalitic rocks to generate high K₂O granite (type II) magma. Dashed arrow shows estimated cooling path of the magma.



that granitoid magma (with about 2.3 wt% H₂O) could be segregated from a source by means of dehydration melting only at temperatures between 950 and 1000°C. The suggestion is supported by the liquidus temperature of I-type granite with 2 wt% H₂O. As shown in Fig. 8-7B, the melt, formed at temperatures between 950 and 1000°C, would be above or near the liquidus 2 wt % H₂O, and the melt would be effectively mobilized to segregate.

The Central Leucocratic Granite is present as sheet-like bodies in the central and western parts of the Sally Downs Bore area together with the Tickalara Metamorphics, the Ord River Tonalite, and the meta-dolerite. The thickness of the sheets is small, ranging from several meters to 200 meters. The granite has not formed large magma bodies, suggesting that a limited volume of melts was segregated. Therefore, it is inferred that the granite magma was not transported a great distance from the source. Model (1) indicated that magma genesis took place in the lower part of mafic lower crust, but the field evidence does not support this. The field evidence suggests model (2) for the petrogenesis of the Central Leucocratic Granite.

The source tonalite must have high Al type characteristics. It could be the Ord River Tonalite or tonalites which are not exposed at the present surface. Possible P-T conditions for partial melting to form the granitic magma is indicated in Fig. 8-7B. Meta-dolerite with close spatial relationships to the Central Leucocratic Granite may be a source of heat to melt the tonalites. Mafic intrusion as the source of heat to form the migmatite in the Halls Creek Mobile Zone was suggested by Blake and Hoatson (1993); could migmatite formation and the generation of granite magma under appropriate condition be related?

8.6. The Sophie Downs Granitoid

As described in chapter 5 and chapter 7, petrological and geochemical characteristics of the Sophie Downs Granitoid lead to its classification as an A-type granite. Metaluminous or peralkaline characteristics and high SiO₂ (average 76.15 wt%) and K₂O (average 4.8 wt%) are exhibited by the major element data. Trace element data show high concentrations of Ba, Rb, Zr, Nb, Y, REE, Ga, and F which are typical characteristics of an A-type granite.

The Sophie Downs Granitoid intruded the Ding Dong Downs Volcanics of the Halls Creek Group at about 1920 Ma (Page and Sun, 1994). The timing of intrusion of the granitoid in the Halls Creek Mobile Zone suggests that it is not a post-orogenic granitoid. The Ding Dong Downs Volcanics are considered to represent bimodal volcanism. The Sophie Downs Granitoid may be related to the felsic phase of the bimodal volcanism. The tectonic setting of both the volcanics and the Sophie Downs Granitoid is considered to be an initial rifting stage of the early Proterozoic orogeny in the region.

Since its introduction by Loiselle and Wones (1979), the A-type granite category has been popularly used in addition to I- and S-type (and M-type). The occurrence and petrological and geochemical characteristics of the A-type granites have been extensively reviewed (Collins et al., 1982; Whalen et al., 1987; Sylvester, 1989; Eby, 1990; Turner et al., 1992). Various petrogenetic models and possible source materials have been proposed for them. These models have been primarily proposed to explain the high absolute abundances of a number of incompatible and high field strength elements and the generally H₂O-poor, but often F-rich, character of the magmas (Eby, 1990). The classification into I- (igneous or infracrustal source) or S-type (sedimentary or supracrustal source) granitoids provides implications for the source material, even it is not the final answer. However, the various

petrogenetic models for the origin of A-type granites do not directly imply the nature of source material. The various models can be grouped into six types:

- (1) Residual-source model (or melt-depleted granulite model)
(Collins et al., 1982; Whalen et al., 1987; Sylvester, 1989)
- (2) Partial melting of intermediate igneous rocks
(Creaser et al., 1991; Skjerlie and Johnston, 1992)
- (3) Metasomatic model
(Taylor et al., 1980)
- (4) Partial melting induced by mantle derived halogen-rich volatiles
(Harris and Marriner, 1980)
- (5) Fractionation from I- or S-type granitoid magma
(Currie, 1976)
- (6) Fractionation from mafic magma
(Loiselle and Wones, 1979; Kleemann and Twist, 1989; Turner et al. 1992)

Eby (1990, 1992) subdivided the A-type granites into two chemical groups, A₁ and A₂, and suggested two different petrogenetic models. A₁ is characterized by element ratios similar to those in oceanic-island basalts, and is considered to represent differentiates of magma derived from sources like those of oceanic-island basalts. Therefore, group A₁ is equivalent to model (4) presented above. Group A₂ is characterized by the ratios that range from those observed in continental crust to those observed in island-arc basalts. Granites of this group can be derived according to any of the models (1), (2), and (3). Eby (1992) presented several discrimination diagrams for the grouping, including that based on the Y/Nb ratio. On this, the A₁ group has Y/Nb less than 2, and the A₂ group has more than 2. The Y/Nb ratios of the Sophie Downs Granitoid vary from 1.93 to 2.1, averaging 2.06. As the Sophie Downs Granitoid

thus shows characteristics between A1 and A2, an unequivocal petrogenetic conclusion for the granitoid is not obtained from the above discrimination.

The residual-source model (melt-depleted granulite model), proposed by Collins et al. (1982), suggests that the A-type granites may be derived from a residual felsic granulite that had previously generated an I-type granite. Although the model has been accepted by many workers (e.g., Clemens et al., 1986, Whalen et al., 1987), there are many arguments against the model (Wormald and Price, 1988; Creaser et al., 1991, Turner et al., 1992; Skjerlie and Johnston, 1992). Collins et al. (1982) suggested that a residual source from which A-type granites may be derived would contain quartz, plagioclase, alkali feldspar, and some biotite and amphibole. The biotite and amphibole are considered to be F-rich and H₂O depleted, due to previous production of I-type granitic melt. Clemens et al. (1986) also stated that during partial melting of a residual source, breakdown of mica and residual calcic plagioclase may contribute to the high (K + Na)/Ca ratio of A-type granites. However, experimental results of dehydration melting of mafic to intermediate igneous rocks to generate I-type granitoids suggest that the residue would consist of plagioclase and pyroxenes. On the basis of available experimental data, alkali feldspar and biotite are unlikely residual minerals (Creaser et al., 1991). The residual source will show depletion in incompatible trace elements (Turner et al., 1992). Therefore, partial melting of a residual source consisting mainly of plagioclase and pyroxenes can not generate A-type granite magma. It is considered that the residual-source model is unlikely to explain the origin of the A-type granite magma.

Partial melting of intermediate igneous rocks (tonalitic or granodioritic rocks) has been suggested for the origin of A-type granites

by several workers (e.g., Creaser et al., 1991; Skjerlie and Johnston, 1992). However, experiments of Rutter and Wyllie (1988) suggest that dehydration melting of tonalite will produce granodioritic melts rather than A-type melts. As Turner et al. (1992) indicated, to reach A-type compositions would require 10-20% fractionation or a small degree of partial melting. However, fractionation increases the H₂O content of the magma, and thus does not support the relatively anhydrous character of the A-type granites. Furthermore, the small degree of partial melting is unlikely to separate melt from the source region (Turner et al., 1992). Experiments of Skjerlie and Johnston (1992) on dehydration melting of tonalitic gneiss generated melts with some characteristics similar to the A-type magmas. However, the melts are peraluminous and even considering Na loss during electron microprobe analysis of melt produced, alumina-alkali element ratios of the melts are different from those of A-types. As stated by Turner et al. (1992), the model, involving partial melting of intermediate igneous rocks, would be unlikely to generate A-type magmas.

Taylor et al. (1980) suggested that the peralkaline character of anorogenic granites resulted from metasomatism by CO₂- and halogen-rich volatile phase during and after emplacement. However the anhydrous and CO₂-free characters of the A-type granites refute this model (Whalen et al., 1987). Furthermore, as the metasomatism is regarded as typically local and structurally controlled, homogeneous and large scale A-type characteristics may be difficult to develop. Therefore the metasomatic model for the origin of the A-type is considered unlikely.

Harris and Marriner (1980) invoked a high flux of mantle-derived halogen-rich volatiles to induce melting of lower crustal rocks and provide the high concentration of alkalis and high field strength elements

in anorogenic granites. This model assumes a contribution of halogen-rich volatiles similar to the metasomatic model to produce A-type characteristics, in this case homogeneous, but the anhydrous and high temperature features of the A-type granites could not be obtained by this model.

Production of the A-type granite by fractional crystallization of I- or S-type magmas can be ruled out by the hotter and more anhydrous mineralogy of the A-type granites since continued fractionation would involve decreasing temperature accompanied by increasing H₂O (Turner et al., 1992). Although Whalen et al. (1987) suggested that fractionation would be possible to produce a minor volume of granite with a partial A-type signature, they did not consider that fractionation alone could produce the distinctive chemistry of A-type granites. The role of fractional crystallization in producing alkaline to peralkaline compositions, however, has been suggested by some workers (e.g., Currie, 1976). In the Sophie Downs Granitoid pluton, the variation from metaluminous to peralkaline characteristics is indicated by increase of mol. Na₂O+K₂O / Al₂O₃ with increase of SiO₂ (Fig. 5-6 and see section 5.2.2 for discussion). The increase of the peralkaline characteristics would have resulted by fractionation within the granitoid pluton. However, most of distinct A-type geochemical characteristics of the Sophie Downs Granitoid could not have been produced by the fractionation alone.

Turner et al. (1992) suggested that the Padthaway A-type granites and volcanics in South Australia were derived by fractionation of basaltic magma. They considered that approximately 90% fractionation of tholeiitic magma took place resulted to form A-type melt. This model indicates that extensive fractional crystallization of basaltic magma could generate high silica A-type magmas enriched in alkalis and high field

strength elements. They postulated a quartz dioritic intermediate composition in the model calculation to have more than 30% fractionated magma in each step of fractionations. However, the general lack of intermediate compositions connecting basaltic composition to high silica A-type composition has presented a problem for the fractionation from the basaltic magmas. Turner et al. (1992) suggested as an alternative that segregation of interstitial melts in the mafic intrusion could be a mechanism to generate A-type melts by-passing intermediate compositions. Existence of such interstitial material is described in the Black Hill complex in South Australia (Turner et al., 1992) and in the Columbia River Basalts (Lambert et al., 1989). Major and trace elements concentration in the interstitial melts in the Columbia River Basalts determined by Lambert et al. (1989) are similar to those in A-type granites. They suggested that separation of the interstitial melt would explain the formation of bimodal tholeiitic suites. High concentration of F could be a manifestation of residual enrichment in the melt. Fractionation of basaltic magmas to form A-type magmas from interstitial separation of melt implies the presence of a large mafic intrusion. During the initial stage of an orogeny, with rifting, a large volume of mafic magma may be emplaced as an intrusion in the lower crust or as volcanics on the surface. The high gravity anomaly in the Halls Creek Mobile Zone could indicate the presence of a mafic intrusion under the surface, though the center of the high gravity anomaly would be expected to not coincide with low density Sophie Downs Granitoid.

On the basis of above discussion, the Sophie Downs Granitoid is considered to be derived by fractionation of basaltic magma. It is suggested that generation of an A-type high SiO₂ melt without the development of a phase of intermediate composition has resulted from the separation of interstitial melt from basaltic intrusive. Stability fields of

basalt under dry conditions constructed by Green (1982) are shown in Fig. 8-8. In the fractionation model presented by Turner et al. (1992), fractionated phases are mainly plagioclase, clinopyroxene, and olivine. Because olivine is stable at low pressures, the basaltic intrusive which generated the A-type magma must have solidified in the middle to upper crust, and as shown in Fig. 8-8, this is also a possible P-T condition for the separation of interstitial melt. The basaltic magma begins to crystallize at about 1200°C (dry liquidus in Fig. 8-8). During subsequent cooling, plagioclase, olivine and pyroxenes crystallize from the magma. Segregation and separation of interstitial melt could generate A-type melt before complete solidification of the basaltic magma. According to this model, the A-type granite has a high magmatic temperature. It would be possible for this magma to reach the near surface (Fig. 8-8) or even become a surface volcanic. The model accounts for the high level intrusive characteristics of the Sophie Downs Granitoid. Some of the acidic members of the Ding Dong Downs Volcanics may be similarly derived from the fractionation of basaltic magmas.

8.7. Summary of Petrogenesis of Granitoids in the Halls Creek Mobile Zone

Petrogenetic discussion of the granitoids in the Halls Creek Mobile Zone has been presented in previous sections. These include consideration of the nature of the source material, pressure and temperature for the generation of granitoid magmas, and crystallization conditions of the granitoid magmas. The pressures and temperatures of the source regions of the granitoid magmas are summarized in Fig. 8-9. Petrogenetic models are summarized as follows,

- (1) The Sophie Downs Granitoid which has A-type characteristics is considered to be derived by crystal fractionation from basaltic magma

Fig. 8-8. P-T conditions for the formation of the A-type Sophie Downs Granitoid magma by fractionation from a basaltic magma

Mesh indicates P-T condition for the separation of A-type granitoid magma from the basaltic magma. Solid lines are boundaries of fields for anhydrous tholeiitic basaltic compositions after Green (1982). Dashed lines are water saturated granite solidus and liquidus, water undersaturated liquidus (2 wt% water), and dry liquidus from Stern and Wyllie (1981). Dashed arrow is cooling path of basaltic magma. Solid arrow is cooling path of the A-type magma (the Sophie Downs Granitoid). Shaded area indicates depth of mafic lower crust in the Halls Creek Mobile Zone.

Field 1: PL+PX+OL+L, Field 2: PL+OL+L,

Field 3: PL+L, Field 4: CPX+PL+L,

Field 5: CPX+L, Field 6: CPX+GA+PL+L

Field 7: CPX+GA+L

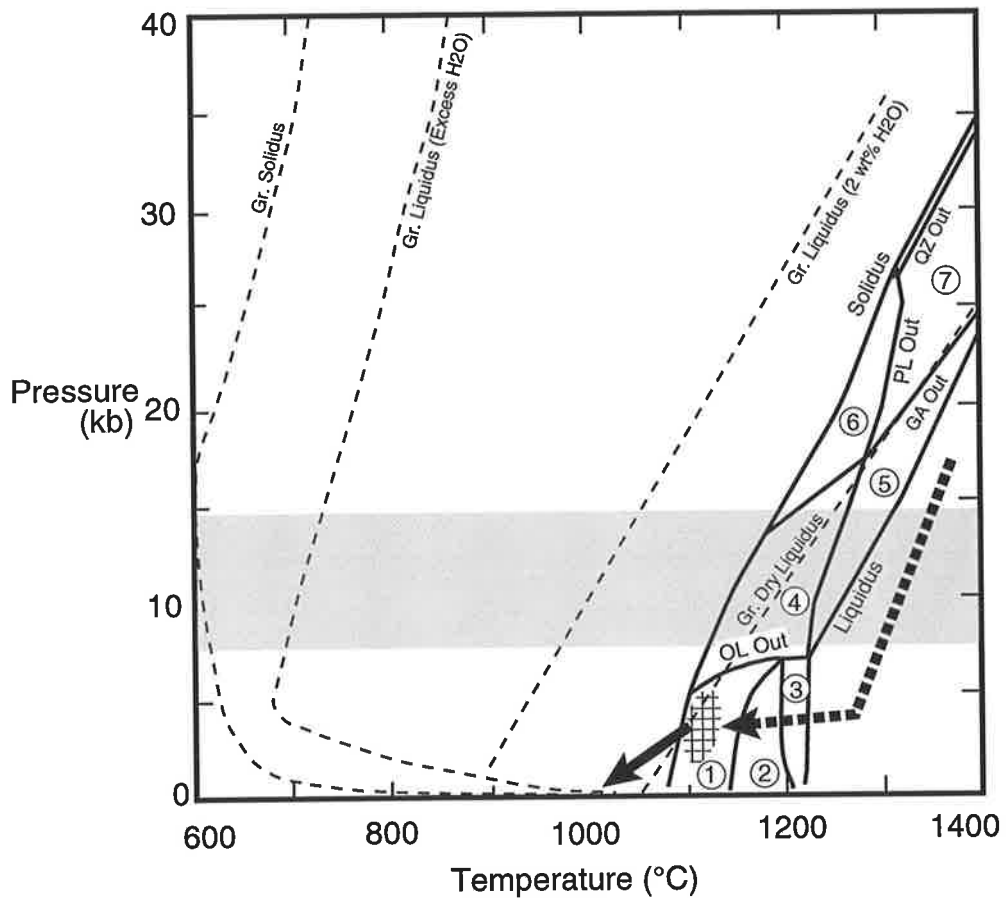
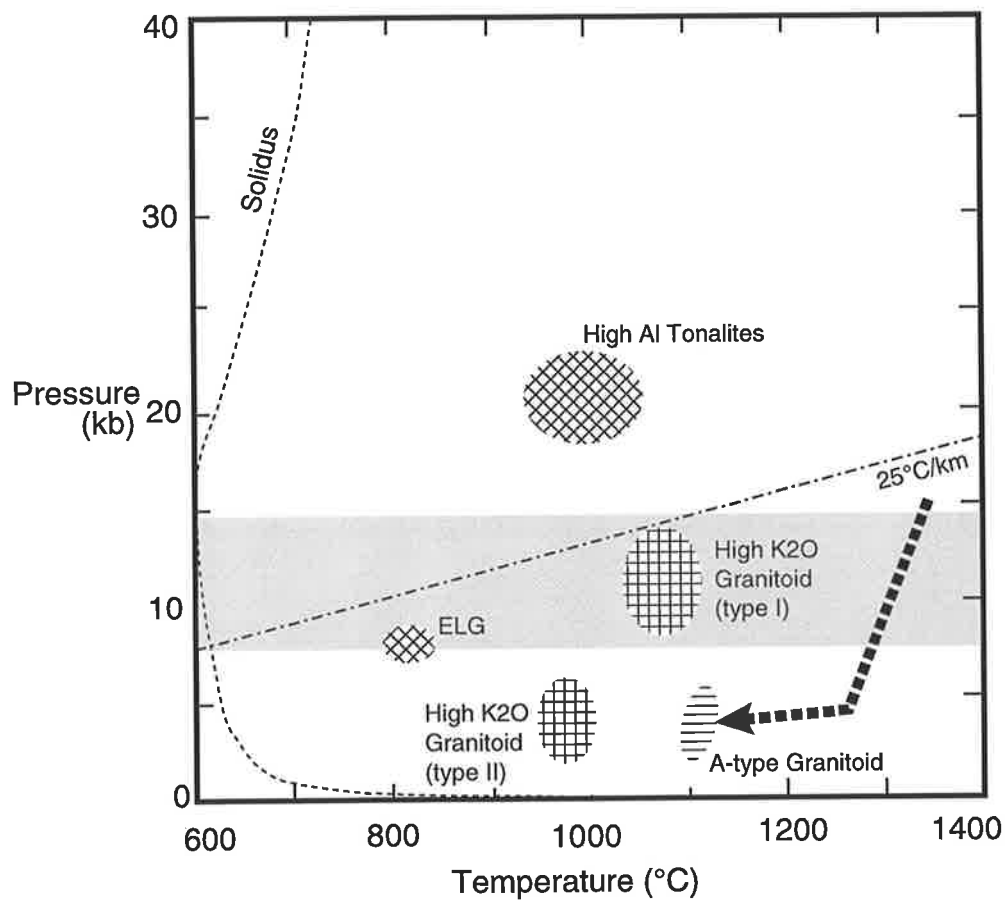


Fig. 8-9. P-T of source regions of the Early Proterozoic granitoid magmas of the Halls Creek Mobile Zone.

Solidus is water saturated granite solidus from Stern and Wyllie (1981). Dot-dash is 25°C/km geotherm. Dashed arrow indicates possible cooling path of basaltic magma before separation of the A-type Sophie Downs granitic magma.

ELG: Eastern Leucocratic Granitoid



(Fig. 8-9). The fractionated granitoid magma would represent separated interstitial melt in the mafic intrusion without the development of an intermediate composition (bimodal igneous activity). It is considered that the basaltic magma is an enriched type. The separation of granitoid magma from the mafic intrusion has taken place at middle or upper crustal levels. The initial temperature of the separated granitoid magma was high, possibly about 1100°C.

(2) Primary magma (low Al type tonalitic) of the Eastern Leucocratic Granitoid is considered to be derived by partial melting of mafic igneous rocks in the middle or upper most part of lower crust (Fig. 8-9), where garnet is not present in the partial melt residue. The garnet bearing leucocratic granite is derived by extensive fractionation from primary magma.

(3) Three tonalitic units of high Al type, the Dougalls suite, the Ord River suite, and the Sally Downs Tonalite, are considered to be derived from the partial melting of mafic rocks, leaving a residue consisting of garnet and pyroxenes. High partial melting pressures (Fig. 8-9) suggest that the tonalitic magmas have been generated by the dehydration melting of subducted oceanic crust, i.e., slab melting. The recognition of early tonalites (Dougalls suite and Ord River suite) and late tonalite (Sally Downs Tonalite) indicates two stages of slab melting event.

(4) High K₂O granitoids of type I (the Western Porphyritic Granite and Bow River Granitoid) and related volcanics (Whitewater Volcanics) were derived by partial melting of mafic lower crust (Fig. 8-9), leaving a residue consisting of plagioclase and pyroxenes (granulitic residue), but not garnet. The mafic source in the lower crust is considered to have enriched characteristics. Partial melting of the mafic lower crust must have been induced by heat from intrusions of mafic magma in the lower crust.

(5) The Central Leucocratic Granite, which is a type II high K₂O granite, was derived by the partial melting of high Al type tonalites. The partial melting of the tonalites took place at a shallow depth in the crust, not far from the present outcrop level (Fig. 8-9). Heat to melt tonalites is thought to have been supplied by mafic intrusions in the upper crust.

CHAPTER 9. IMPLICATIONS OF THE GRANITOIDS PETROGENESIS FOR THE EARLY PROTEROZOIC OROGENY IN THE HALLS CREEK MOBILE ZONE

9.1. Tectonic models for Proterozoic Orogenies

Various tectonic models for the Proterozoic Orogenies have been presented by researchers. Orogenies resulting from subduction of oceanic plates or from collision of continental blocks, similar to those related to modern plate tectonics, have been proposed by many workers (e.g., Windley, 1992). However, some workers have postulated fundamentally different tectonic styles of Proterozoic orogens from those of modern plate tectonics, such as ensialic orogeny (or intracontinental ensialic orogeny). Ensialic orogeny invokes rifting, heating, and stretching of the crust as a result of lithospheric thinning over a mantle plume. This mechanism leads to a geosynclinal basin entirely floored by continental crust. No wet oceanic crust is generated during basin formation and none is consumed during the orogeny (Kröner, 1983).

Etheridge et al. (1987) and Wyborn (1988) proposed ensialic orogeny to account for the evolution of deformed sedimentary basins during the widespread 1.88-1.85 Ga Barramundi orogeny in the North Australian Craton. The Barramundi orogeny was immediately preceded by a basin-forming episode that resulted from local extension of the pre-existing Archaean continental crust. These basins contain three separate sequences. A lower rift sequence is overlain by a laterally extensive, shallow water succession ascribed to post-rift thermal subsidence. A rapid increase in subsidence gave rise to a thick flysch sequence, which was interpreted to herald the main orogenic phase. The Barramundi orogeny is characterized by an extensive and uniform suite of I-type granitoids and comagmatic volcanics. Etheridge et al. (1987) and Wyborn (1988) considered that these igneous rocks show significant

petrological and chemical differences from those due to modern subduction related magmatism. On the basis of the character of the Barramundi orogeny, together with the absence of ophiolites, paired metamorphic belts and other diagnostic features of modern orogeny, Etheridge et al. (1987) considered that it was essentially ensialic. They proposed a model in which a polygonal array of contemporaneous upwelling convection zones triggered mantle melting, underplating and continental extension. Heat loss led to the termination of convection, thermal subsidence of the stretched regions and cooling of the lithosphere. Cooling of enriched mantle below the early Proterozoic basins is suggested to have triggered crust-mantle delamination and A-subduction (subduction of continental crust according to Kröner (1983)). Delamination provided the driving force for the compressional orogeny and the enhanced heat flow to produce the Barramundi igneous association from the previously underplated layer (Etheridge et al., 1987).

However, Windley (1992) indicated that a similar orogenic style to that of the Barramundi orogeny is found in the Jurassic-Palaeocene thrust basins in the Tien Shan range of Central Asia, situated approximately 2000 km from its deformation front in the Himalayas of Pakistan. Because the Barramundi type orogenic style is found in a modern plate tectonic setting, Windley (1992) did not support a non-actualistic model of the ensialic orogeny to explain development of the Barramundi orogeny and the Proterozoic orogens in general.

Hancock and Rutland (1984) suggested an ensialic orogeny to explain the evolution of the Halls Creek Inlier on the basis of similar criteria to those indicated by Etheridge et al. (1987). However, as suggested by Windley (1992), it is clear that the criteria do not fully support the ensialic orogeny model. Furthermore, the occurrence of high Al tonalitic

rocks in the Halls Creek Mobile Zone suggests subduction of wet oceanic crust (see petrogenetic discussions in chapter 8). Therefore, the ensialic orogeny model is unlikely to apply to the evolution of the Early Proterozoic orogeny in the Halls Creek Mobile Zone. The tectonic model for the evolution of the Halls Creek Mobile Zone is discussed in section 9.3.

Windley (1992) distinguished two types of orogenesis which operated during the Proterozoic. One involved the collision of two or more continental blocks (collisional orogen), and associated with little or no crustal growth as it formed mainly by reworking of older crust. The second type of orogenesis (accretionary orogen) involved the growth and amalgamation of many juvenile island arcs and slices of oceanic crust or oceanic plateaus, which were in places mutually sealed by intervening accretionary wedges (Windley, 1992). However, it is considered that some of accretionary orogens could be immediately incorporated within a continental block during the collisional orogen. Therefore, the classification of orogens into the above two categories is not fully satisfactory. The classification, however, is retained to account for the two types of orogenic activities.

A similar classification of orogenies has been proposed by Murphy and Nance (1991) based on the examination of characteristics of Late Proterozoic orogenic belts. They subdivided orogenies into two types, viz. interior orogenies and peripheral orogenies. The interior orogenies are the product of continent-continent collisions and hence lie within the supercontinent after its amalgamation. The peripheral orogenies occur at the exterior margins of the supercontinent. The interior orogenies and peripheral orogenies could correspond to the collisional orogens and accretionary orogens, respectively, of Windley (1992). Murphy and Nance (1991 and 1992) suggested a supercontinent cycle to conform with

the two contrasting styles of orogenies. Their model proposes an evolution of continents as follows (Murphy and Nance, 1992):

(1) The breakup of a supercontinent results in the birth of interior oceans like the present Atlantic. Inward-facing margins of the separating continents are tectonically stable.

(2) Maximum dispersal of the continents occurs when the interior oceans are about 200 million years old. Then the oldest parts of the interior oceans begin to sink, or subduct, into the mantle.

(3) Continental collisions occur after the interior oceans are consumed. The collisions create interior mountain belts and broad areas of intense deformation, uplift and erosion (interior orogenies). A new supercontinent is formed by the continental collisions. Subduction zones occur around the margin of the supercontinent, leading to widespread peripheral volcanism. Island arcs may be swept in from the exterior ocean and accreted onto the edges of the supercontinent (peripheral orogenies).

Thus, the one supercontinent cycle of this model (Murphy and Nance, 1992) includes the breakup of a supercontinent, opening of interior oceans, closure of the oceans, and continental collisions. In other words, the one cycle is characterized by the opening and closure of the interior oceans (open-close type). On the other hand, Hoffman (1991) proposed an inside-out supercontinent cycle (inside-out type). In the process of fragmentation, rifts originating in the interior of the first supercontinent became the external margins of the second supercontinent; exterior margins of the former became landlocked within the interior of the second supercontinent. Thus in Hoffman's model, a tectonic transition from peripheral orogenies to interior orogenies is possible.

The change of orogenic styles in the supercontinent cycle is diagrammatically shown in Fig. 9-1. The difference of the inside-out

Fig. 9-1. Simplified model of supercontinental cycle.

Orogenic types are indicated in relation to the supercontinental cycles.

Large ovals indicate simplified supercontinents.

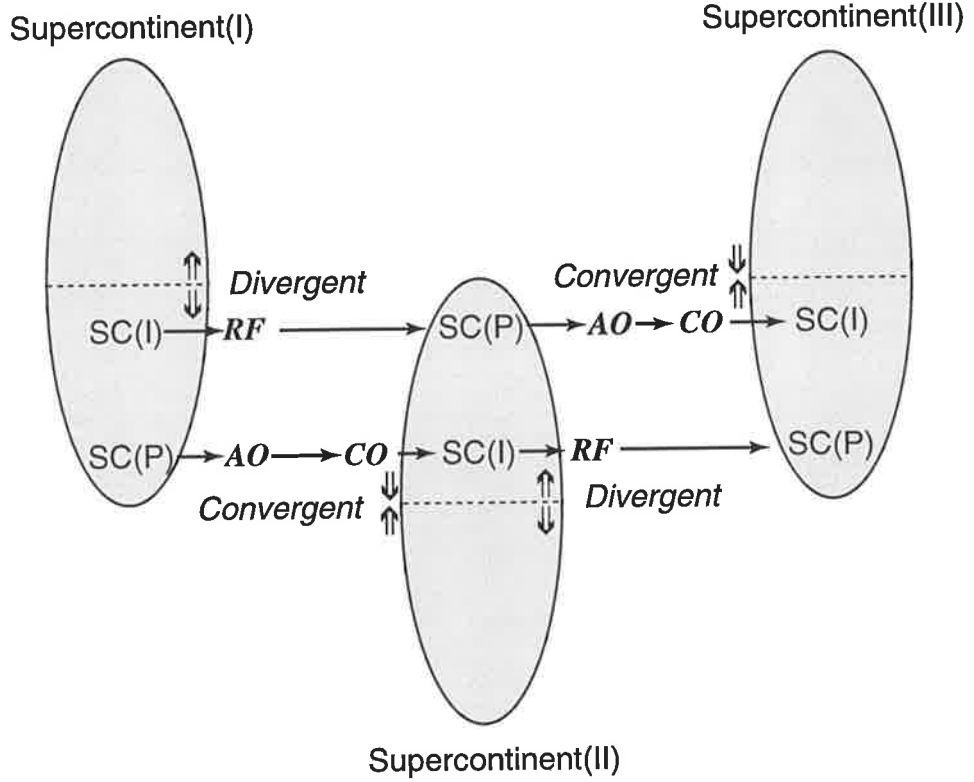
SC(I): interior of supercontinent

SC(P): periphery of supercontinent

RF: rifting

AO: accretionary orogen

CO: collisional orogen



← One Supercontinent Cycle (Open-Close type) →

← One Supercontinent Cycle (Inside-Out type) →

→ Time

type from the open-close type is the assumption in the former, of a second or other supercontinent at the other side of the globe. Two supercontinent cycles of the inside-out type roughly correspond to one supercontinent cycle of the open-close type. In the supercontinent model of inside-out type, a rifting in the interior of the supercontinent breaks up it. Then, peripherals of the supercontinent become a location of the accretionary orogen. Subsequent collisions of the continental blocks form a second supercontinent. Peripheral parts of the previous supercontinent become interior of the second supercontinent. Rifted margin of the previous interior of the supercontinent becomes peripheral to the second supercontinent. In the second supercontinent cycle of the inside-out type, the peripheral margin of the second supercontinent may become location of an interior orogen in the third supercontinent (Fig. 9-1). This model suggests a transition of tectonism from the peripheral to interior orogenies and also from the accretionary orogen to the collisional orogen. It is considered that the supercontinental cycle of the inside-out type (Hoffman, 1991) would account for tectonic evolution of the Middle to Late Proterozoic and Phanerozoic orogenies more satisfactorily than that of the open-close type (Murphy and Nance, 1992).

The duration of one supercontinent cycle would be several hundred million years. Assuming a 5cm/year for the spreading rate of an oceanic ridge (i.e., the velocity of the plate motion), a fragment of the supercontinent moves one-quarter of circumference of the earth in 200 million years. Therefore, the ocean generated at the rift located originally interior of the supercontinent would cover nearly half the circumference of the earth in 200 million years (assuming the spreading rates of 5cm/year for both sides of the rift). In the model (Fig. 9-1), typical rifting activities and accretionary orogenies would continue for up

to several hundred million years. However, collisional orogenies may have limited duration, of the order of several tens of million years.

Although some of rifting activity may have a short life-time or fragments of the supercontinent may obliquely collide with other continental blocks soon after the fragmentation, the evolution of typical orogenies could be interpreted within the frame work of this model (Fig. 9-1).

In the modern plate tectonic model, three types of plate boundary have been recognized. These are divergent boundaries (spreading zone), convergent boundaries (subduction or collision zones), and transform fault boundaries. In Hoffman's (1991) supercontinent cycle, the location of the divergent boundaries changes from within the supercontinent to its periphery (Fig. 9-1). On the other hand, the future convergent boundaries are initially peripheral to the supercontinent and terminate their role as plate boundaries when they are incorporated within the new supercontinent by the collisional orogeny. The accretionary orogen and collisional orogen are present at convergent plate boundaries.

Windley (1995) subdivided the convergent plate boundaries into four types.

1. Oceanic-oceanic plates along island arcs.
2. Oceanic-continental plates along island arcs.
3. Oceanic-continental plates along active continental margins.
4. Continental-continental plates.

The accretionary orogenies are located along the plate boundaries of the first three types, which are characterized by the subduction of oceanic plates. The collisional orogenies are found along the inter-continental plate boundaries. Windley (1993) suggested that the types of orogen that formed throughout the Proterozoic are fundamentally similar to those of the Phanerozoic. Therefore, it is important to examine the characteristics

of the Early Proterozoic orogeny and compare these with the orogenic styles of the modern plate tectonic model.

9.2. Supercontinents and the Early Proterozoic orogens

A simplified model of a supercontinent cycle for the Proterozoic and Phanerozoic is presented in Fig. 9-2. Four supercontinents are shown. In addition to the four supercontinents, a future supercontinent which would be centered on Eurasia is also indicated. The existence of an Archaean supercontinent is not apparent. Supercontinent I (tentatively named Laurentia Supercontinent in this thesis, as the Laurentia block constituted the major part of the supercontinent) may have been the first to appear in the earth's history. Williams et al. (1991) termed the Hudsonland Supercontinent for a part of the Early Proterozoic Laurentia. Configurations of continental blocks within the Pangaea and Gondwana Supercontinents are proposed by various workers (e.g., Hoffman, 1991).

Recent advances in the correlation of the Proterozoic geological features have established a configuration of continental blocks in a Late Proterozoic Rodinia Supercontinent (Fig. 9-3). The suggestion of a Late Proterozoic fit of western North America with the East Antarctic-Australia block (southwest U.S. and East Antarctic (SWEAT) connection) added significantly to the construction of the Rodinia Supercontinent (Moors, 1991; Dalziel, 1991; Dalziel, 1995) following Hoffman's (1991) configuration. Detailed support for the Rodinia Supercontinent concept is derived from geochronological and isotopic data (Ross et al., 1992; Borg and DePaolo, 1994), stratigraphic data (Young, 1992; Brookfield, 1993; Powell et al., 1994; Li et al., 1995), and paleomagnetic data (Powell et al., 1993; Idnurm and Giddings, 1995). Amalgamation of continental blocks to form the Rodinia Supercontinent is thought to have taken place during the world wide Grenville orogeny (e.g., Hoffman, 1991).

Fig. 9-2. Proterozoic and Phanerozoic supercontinents and orogenies

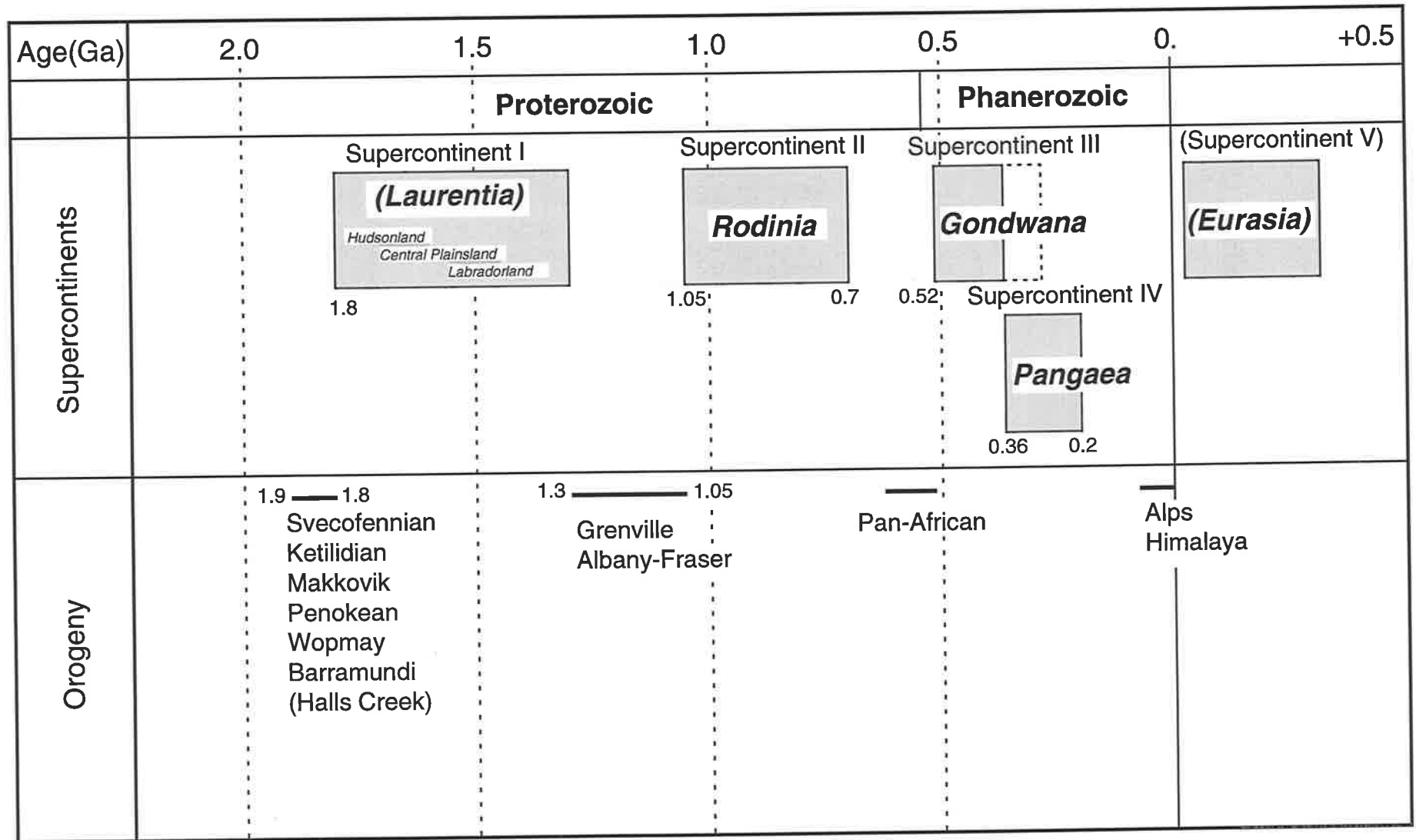


Fig. 9-3. Configuration of early Late Proterozoic supercontinent Rodinia and location of Early Proterozoic orogens.

Configuration of Rodinia is after Hoffman (1991).

Names of continental blocks are shown in the figure.

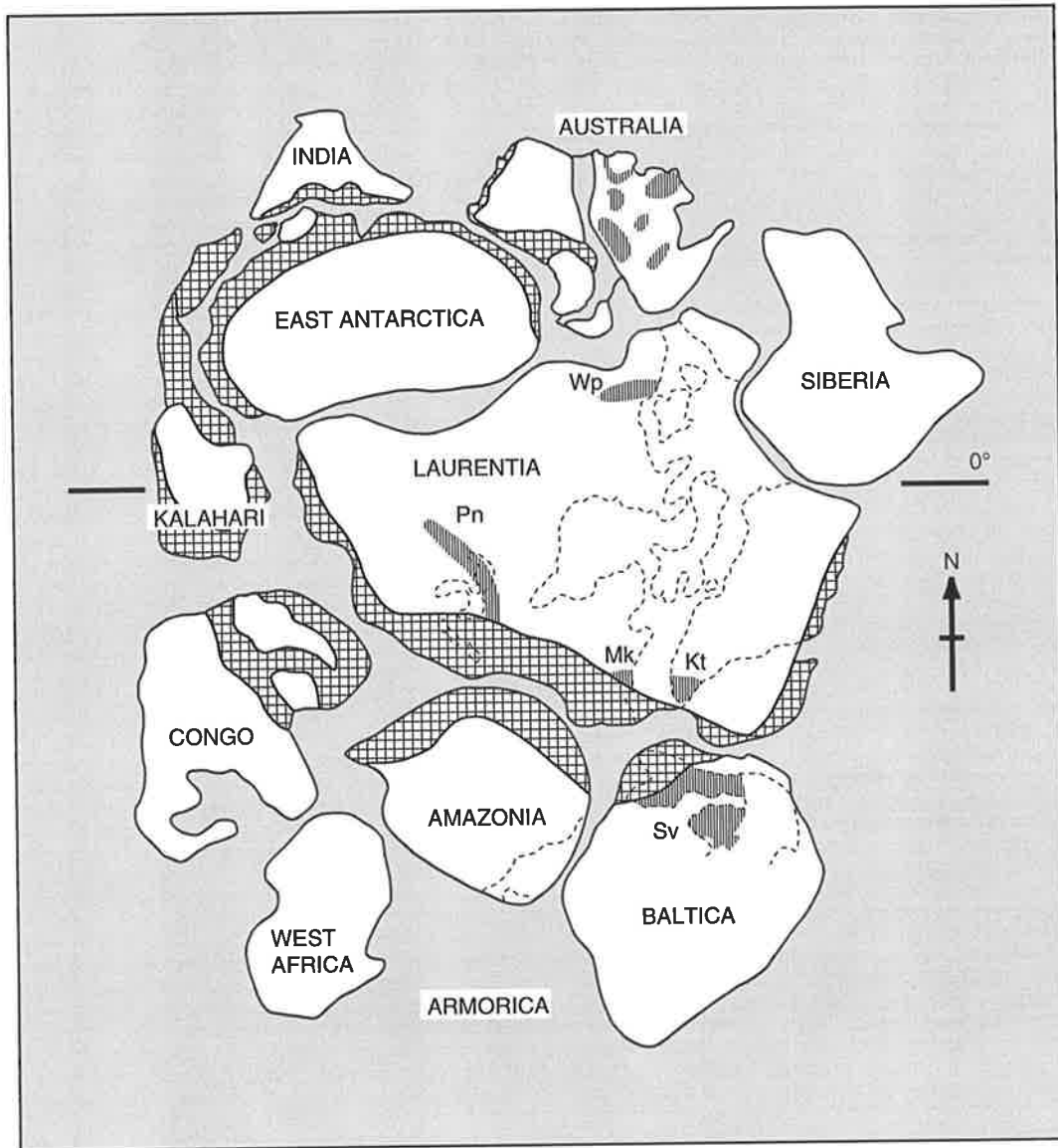
Pn: Penokean orogeny





Mk: Makkovik orogeny

Wp: Wopmay orogeny

Kt: Ketilidian orogeny

Sv: Svecofennian orogeny



- | | | | |
|---|------------------------------|---|---------------------------|
|  | early Late Proterozoic ocean |  | Grenvillian belts |
|  | pre-Grenvillian cratons |  | 1.9-1.8 Ga orogenic belts |

The extensive orogenic events of 1.9-1.8 Ga in various parts of the world correspond to the timing of formation of Supercontinent I (Fig. 9-2). The Early Proterozoic orogenesis in the Halls Creek Mobile Zone may be correlated with those events. Reconstruction of part of the supercontinent was made by Park (1991), Park (1995), and Van Kranendonk et al. (1993), fitting together Early Proterozoic orogenic belts in North America, Greenland, and northern Europe. However, a full reconstruction of Supercontinent I has not been made with data available. Fig. 9-3 depicts location of the 1.9-1.8 Ga orogens in the Late Proterozoic Rodinia reconstruction. Splitting of the Rodinia Supercontinent along the 1.3-1.05 Ga orogenic belts into continental fragments and the refitting of the opposite sides of the continental fragments may produce a possible configuration of Supercontinent I.

The following are typical 1.9-1.8 Ga orogens,

- 1) Svecofennian orogen of the Baltic Shield
- 2) Ketilidian orogen of the South Greenland
- 3) Makkovik orogen of Labrador
- 4) Penokian orogen in the Lake Superior region
- 5) Wopmay orogen in NW Canada
- 6) Trans-Hudson orogen in north-central North America
- 7) Barramundi Orogen of north Australia

Pine Creek Inlier

Mt. Isa Inlier

Halls Creek Inlier

The Svecofennian, Ketilidian, Makkovik, and Penokian orogens are classified as accretionary orogens (AO) by Windley (1992). Patchett and Arndt (1986) showed from Nd isotopes that these consist of >80% newly differentiated, subduction related material. McCulloch (1987) indicated from Nd isotopes that the Barramundi Orogen does not contain any

significant amount of older crustal component. The geochemical similarity of the gabbro-diorite-tonalite-trondhjemite (GDTT) suite from the Svecofennian orogen in southwest Finland to the similar suite in the Halls Creek Mobile Zone was indicated in section 7.2. Those data suggest that the Barramundi Orogen is classified as an accretionary orogen (AO).

The Wopmay orogen is classified as a collisional orogen (CO) by Windley (1992). However, it contains an accreted arc and a continental shelf sediment complex. The 1.88-1.86 Ga Great Bear calc-alkaline batholith in the central part of the Wopmay orogen was generated by east-dipping subduction. Before the terminal collision at about 1.8 Ga, the Wopmay orogen developed in a continental arc environment.

The Trans-Hudson orogen includes mainly juvenile, arc-related Early Proterozoic domains. It developed through (1) 1.91-1.88 Ga felsic volcanism, (2) 1.88-1.86 Ga deformation and metamorphism possibly related to the early arc-continent collision, (3) 1.86-1.84 Ga emplacement of Wathaman batholith and arc plutons, and (4) 1.83-1.80 Ga major deformation related to continent-continent collision (Bickford et al., 1990).

The occurrence of the extremely large batholiths in the Wopmay and Trans-Hudson orogens is similar to that of the Bow River Batholith in the Halls Creek Mobile Zone.

The comparison of the magmatism and structural styles between the 1.9-1.8 Ga orogens from the various parts of the world suggests a similarity of tectonic evolution of the orogens. Such synchronous tectonic evolutions would imply a major orogenic event in the earth's history.

It is significant that most of the 1.9-1.8 Ga orogens indicate subduction related magmatism, and terminal continent-continent collision

at around 1.8 Ga. Some of the orogens recorded the early arc-continent collision before the terminal continent-continent collision.

9.3. Model for the evolution of the Halls Creek Mobile Zone

Although an ensialic orogeny model is favored by some workers (e.g., Hancock and Rutland, 1984) for the Early Proterozoic evolution of the Halls Creek Mobile Zone, the petrogenetic models for granitoids from the Halls Creek Mobile Zone established by this study do not support the ensialic model. The occurrence of high Al tonalites in the Halls Creek Mobile Zone strongly suggests subduction of wet oceanic crust during the Early Proterozoic which can not be easily explained by the ensialic model. Detailed petrogenetic discussion of the granitoids in the Halls Creek Mobile Zone has been presented in Chapter 8. It provides basic constraints for constructing a model for the Early Proterozoic evolution of the Halls Creek Mobile Zone. The model incorporates the petrogenesis of the granitoids and other data obtained in this study, plus available published data. The constructed model is presented herewith.

(1) Initial rifting of continental crust (composed of the Kimberley block and an unknown continental block) at about 1920 Ma (Page and Sun, 1994) instigated the Ding Dong Downs volcanism and an intrusion of the A-type Sophie Downs Granitoid (Griffin and Tyler, 1992). The A-type magma is considered to be derived by crystal fractionation from basaltic magma generated in a rift environment (Fig. 9-4A and B). Occurrences of rift related bimodal volcanism and the A-type granitoid in the eastern part of the Halls Creek Mobile Zone are considered to indicate that an oceanic crust was generated to the east of the Halls Creek Mobile Zone. Thus, it is assumed that the Halls Creek Mobile Zone was situated

Fig. 9-4. Schematic illustration of evolution of Halls Creek Mobile Zone.

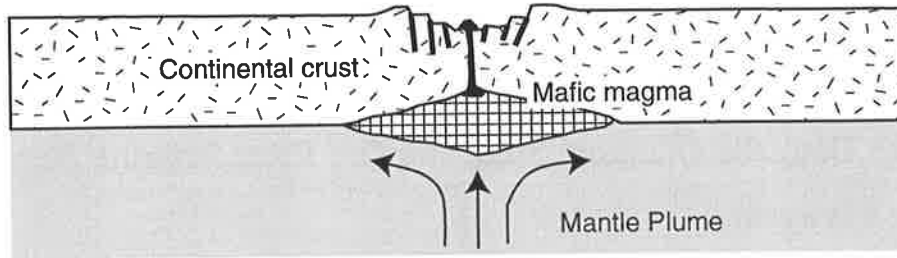
A. Initiation of rifting of a continental crust at the location above mantle plume at about 1920 Ma (Page and Sun, 1994) facilitated a bimodal volcanism of the Ding Dong Down Volcanics. A large mafic magma chamber (hatched) was formed below the continental crust, and became a mafic lower crust. The A-type magma which was the source of the Sophie Downs Granitoid, is considered to have been derived by crystal fractionation from basaltic magma in the rift environment.

B. Further rifting generated oceanic crust and a mid-ocean ridge was formed. The Kimberley block was separated from an unknown continental block. Extensive magmatism resulting from initial rifting formed a rifted volcanic continental margin, consisting of mafic lower crust and volcanic and clastic cover rocks. A small pluton in the rifted volcanic continental margin around the Kimberley Block is the Sophie Downs Granitoid. The Saunders Creek Formation was deposited in a shallow water environment.

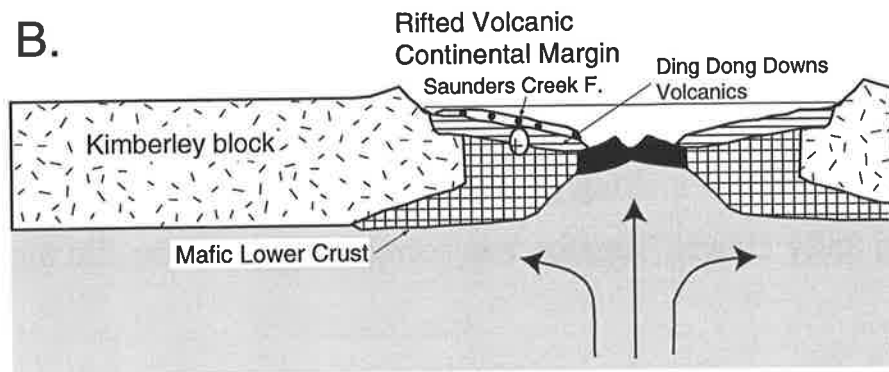
C. Oceanic crust was generated from the mid-ocean ridge for several tens of millions of years. The Biscay Formation was deposited in a slightly deeper water environment.

D. Tectonic transition from divergent to convergent tectonism resulted in westward subduction of the oceanic plate. Subduction-related volcanism was present. Part of the Biscay Formation and the Olympio Formation were deposited in this environment.

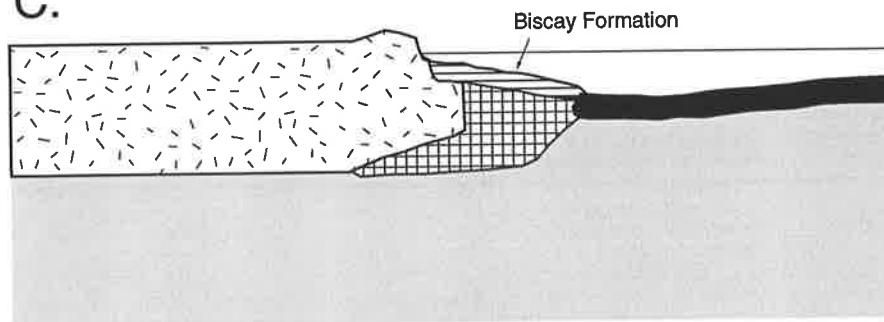
A. Rifting of continental crust



B.



C.



D.

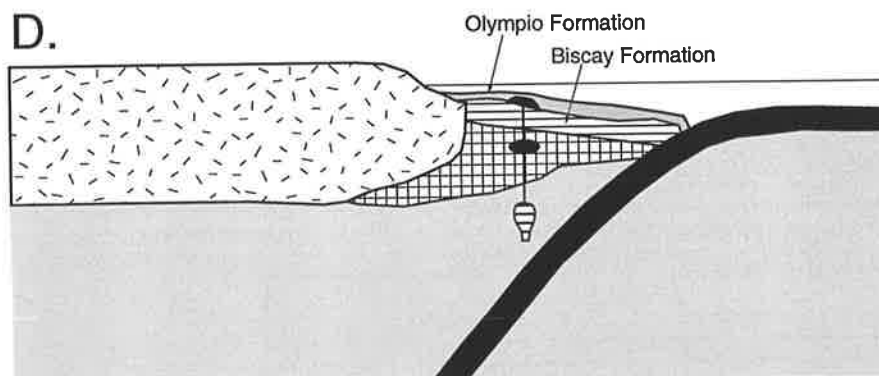


Fig. 9-4 (2). Schematic illustration of evolution of Halls Creek Mobile Zone.

E. Slab melting generated the first stage of tonalitic magmas.

The Dougalls Granitoid Suite and Ord River Tonalite Suite were formed by this event.

F. Possible ridge subduction have been responsible for the generation of voluminous high K₂O granitoids by partial melting of mafic lower crust.

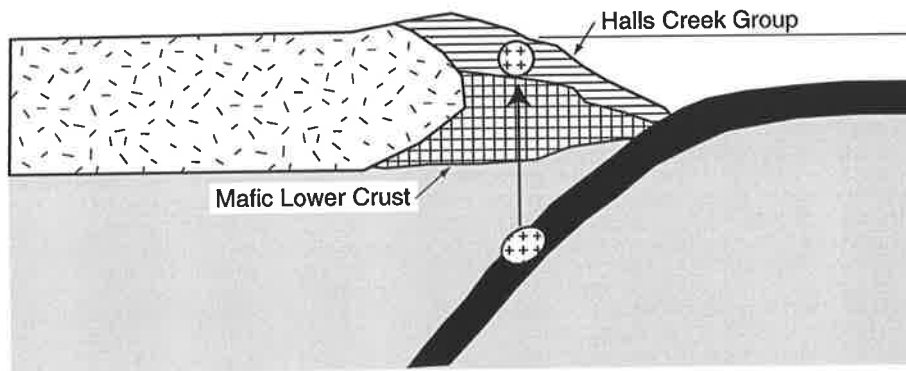
G. Further slab melting generated a second stage of tonalitic magma.

The Sally Downs Tonalite was formed from this tonalitic magma.

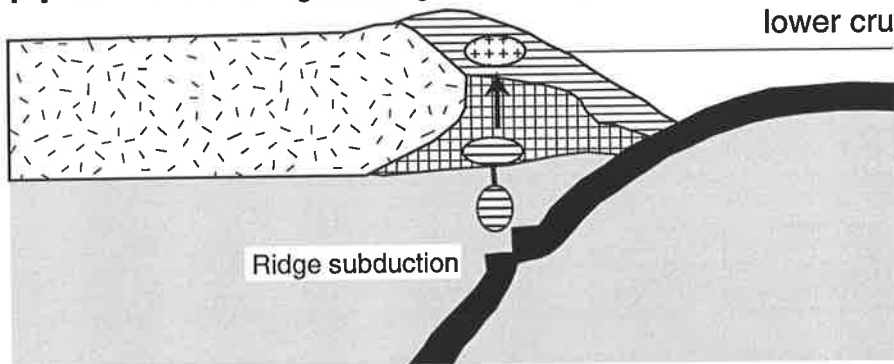
H. Collision of continental blocks

Collision of continental blocks is assumed. Location of the suture is not clear, but it is assumed to be present to the east of the present exposure of the Halls Creek Mobile Zone.

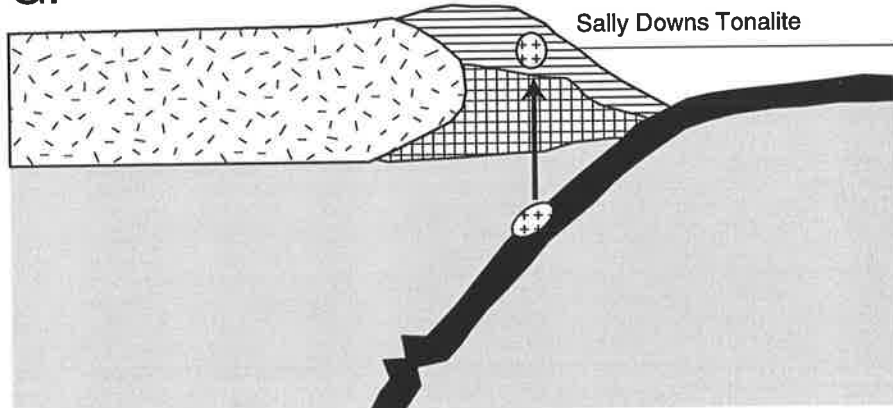
E. Generation of tonalitic magma by slab melting



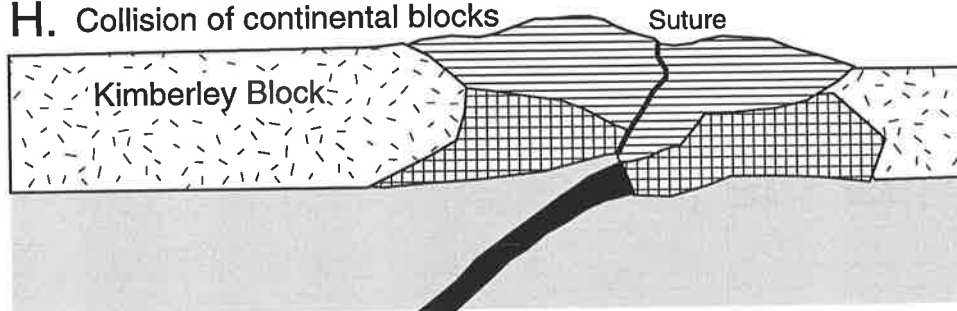
F. Generation of high K₂O granitoids by partial melting of mafic lower crust



G. Generation of tonalitic magma by slab melting



H. Collision of continental blocks



at the eastern margin of the Kimberley continental block which was rifted away from the unknown continental block from the east.

It is known that breaking up and rifting of continents to form new ocean basins, is sometimes accompanied by massive igneous activity (e.g., White and McKenzie, 1989). Volcanic continental margins generated by initial rifting are described around the North Atlantic Ocean, on the west Australian continental margin, and in other locations (White and McKenzie, 1989). Volcanism at rifted continental margins is indicated by the presence of extensive extrusive basalts. Thickness of the crust at rifted volcanic continental margins ranges from 15 to 25 km with the lower crust characterized by a relatively high (>7 km/sec) P-wave velocity (White and McKenzie, 1989), suggesting a mafic lithology. On the other hand, the thickness of an oceanic crust generated at a mid-ocean ridge is typically less than 7 km. Thus, the crustal structure of the rifted volcanic continental margins differs significantly from the typical oceanic crust and also from continental crust.

Drummond and Collins (1986) suggested that high P-wave velocity in the lower crust of the North Australian Craton indicates the presence of underplated mafic igneous rocks in the granulite stability field (see section 8.2). As inferred above, mafic lower crust is also considered to be present in the Halls Creek Mobile Zone, developed on the rifted volcanic continental margin (Fig. 9-4A and B). The mafic lower crust generated during the initial rifting would be a possible source of the Bow River Granitoid (see further discussion below).

A likely source of the large volume of mafic magma associated with the initial rifting is a mantle plume. The mafic magma may be emplaced into the lower continental crust for a considerable lateral distance from the rifted margin. Thus it is considered that underplating of mafic magma would have occurred not only in the rifted volcanic continental

margins, but also in the lower continental crust of a large area around the mantle plume. The mafic lower crust under the continental crust would be the source of most of the high K₂O I-type granitoids of the Barramundi association in the central part of the North Australian Craton, some distance away from the assumed rifted volcanic continental margin. As Etheridge et al. (1987) suggested, the high K₂O I-type granitoids of the Barramundi association were derived by the partial melting of mafic lower crust, and this mafic lower crust must have been generated as described above. The underplating mafic magma is thought to have been an enriched type derived as it was from a mantle plume, and its would explain the enriched characteristics of the mafic source of the granitoids.

(2) The Saunders Creek Formation was deposited on the Ding Dong Downs Volcanics in a the shallow water environment, possibly along the passive margin (rifted volcanic continental margin) of the separating continent (Fig. 9-4B).

(3) Following the initial rifting of the continent at about 1920 Ma (Sun and Page, 1994), oceanic crust was generated from the developed mid-ocean ridge for several tens of million years, but not more than one hundred million years. Ocean was situated to the east of the Halls Creek Mobile Zone (Fig. 9-4C). However, it is considered that this rifting and generation of oceanic crust were not sufficient to form a supercontinent at the other side of the globe.

Sedimentary rocks of the Biscay Formation were deposited in a moderately deep water environment (Fig. 9-4C). As described in section 3.2.2, the amphibolite of the Tickalara Metamorphics, which is correlated with the Biscay Formation, has geochemical characteristics of an island

arc tholeiite. This interpretation implies that the subduction of an oceanic plate was initiated before or during the deposition of the Biscay Formation (Fig. 9-4D). It should be emphasized that the divergent tectonism, viz. rifting of the continental crust and generation of oceanic crust, had a limited duration.

(4) Westward subduction of the oceanic plate from east of the Halls Creek Mobile Zone is assumed. The Olympio Formation, typical flysch facies, was deposited in association with the subduction of the oceanic plate, possibly in a fore-arc basin (Fig. 9-4D).

(5) Mafic magma was generated by the subduction. Intrusion of mafic magma into the mafic lower crust induced partial melting of the mafic lower crust and generated primary magma (low Al tonalitic) of the Eastern Leucocratic Granitoids.

(6) Subduction of relatively young, therefore hot, oceanic plate led to generation of the first stage of high Al tonalitic magma, viz. the Dougalls Granitoid and Ord River Tonalite Suites (Fig. 9-4E).

(7) High K₂O granitoids of type I (the Western Porphyritic Granite and Bow River Granitoid, see section 8.5.) and related Whitewater Volcanics were derived by partial melting of mafic lower crust which was formed during initial rifting as a part of rifted volcanic continental margin. The extremely large volume of the Bow River Granitoid suggests extensive partial melting of the mafic lower crust. It is considered that the extensive partial melting was induced by heat from new intrusions of mafic magma generated by subduction. Extensive

generation of the new mafic magma may be related a ridge subduction (Fig. 9-4F).

(8) Intrusion of mafic magma to a high crustal level induced a partial melting of tonalitic rocks (possibly the Ord River Tonalite) to generate the Central Leucocratic Granite.

(9) The second stage of the tonalitic suite, viz. the Sally Downs Tonalite and other members of the Mabel Downs Granitoid Suite, were formed by subduction of another relatively young, therefore hot, oceanic plate, which may be on the proximal side of the plate relative to the subducted ridge (Fig. 9-4G). The linear distribution of the granitoid plutons of the Mabel Downs Granitoid Suite in the Halls Creek Mobile Zone would manifest the trend of the arc.

(10) Collision of the Kimberley block with the central part of the North Australian Craton terminated the major Early Proterozoic orogenic events in the Halls Creek Mobile Zone (Fig. 9-4H). Suture of the two continental plates is not clear, however, it is considered to be present to the east of the Halls Creek Mobile Zone, under the younger cover rocks.

(11) The basic crustal structure was formed through the tectonic evolution described above before 1.8Ga. Further deformations of the crust in the Halls Creek Mobile Zone, however, took place even in the Phanerozoic.

The Early Proterozoic tectonic evolution model of the Halls Creek Mobile Zone presented here was constructed with the aid of new

petrogenetic models for the granitoids in the Halls Creek Mobile Zone. The presence of high Al tonalites, which are considered to be derived by dehydration melting of oceanic crust, implies subduction of the oceanic plate beneath the Halls Creek Mobile Zone during the Early Proterozoic. The presence and importance of oceanic crust during the Early Proterozoic orogeny is thus indicated. The model differs principally from the ensialic orogeny model (e.g., Hancock and Rutland, 1984; Etheridge et al., 1987) which, as outlined above, does not imply the generation of oceanic crust. The model presented here is basically similar to the modern plate tectonic model.

The Early Proterozoic orogenies of 1.9-1.8 Ga found in various areas of the world typically show a similar tectonic evolution to that found in the Halls Creek Mobile Zone. The existence of these global synchronous orogenic activities at the end of the Early Proterozoic would imply, as a cause, development of major mantle plume activity at this time. The typical Early Proterozoic orogenies, as exemplified by the Halls Creek Mobile Zone, include tectonisms such as the initial rifting of continental crust, the generation of ocean, the subduction and accretion of oceanic crust, and the final collision of continental blocks. The style of orogeny indicates that it contains one supercontinent cycle of the open-close type or two supercontinent cycles of inside-out type. However, it is not considered that two supercontinent cycles of the inside-out type took place during the 1.9-1.8 Ga orogeny, as there is no evidence of a supercontinent at around 1.87 Ga before the beginning of the closure of the ocean generated from 1.92 Ga. Moreover, it is significant that the Early Proterozoic orogenies were completed (from initial rifting to terminal collision) within about one hundred million years. The duration of the orogenic activities differs from the Late Proterozoic and Phanerozoic supercontinent cycles which extend for several hundred

million years. Rapid tectonic transition of the Early Proterozoic orogeny in the Halls Creek Mobile Zone is maintained also by Page and Hancock (1988). The short time from initial rifting to the beginning of the subduction would indicate that oceans generated by the Early Proterozoic rifts were not large compared to the oceans developed during the Late Proterozoic and Phanerozoic supercontinental cycles. The interpretation suggests that a subducted oceanic crust was young at the time of subduction. The model is also supported by the petrogenesis of the tonalites, viz. the generation of tonalitic magma by partial melting of young, therefore warm, subducted oceanic crust.

Although oceans generated by the Early Proterozoic rifts were small, the global synchronous occurrence of the Early Proterozoic orogenies would suggest that there was a considerable areal extent of ocean generated at that time. This implies that Early Proterozoic ridge lengths were greater than those associated with Phanerozoic oceans. It is assumed that small size but large number of mantle plumes were characteristic of the Early Proterozoic orogenies. Etheridge et al. (1987) and Wyborn (1988) suggested a small scale mantle convection model to account for the Early Proterozoic orogenies. However, they did not include the generation of oceanic crust in the model. This is the major difference between the model presented in this thesis and those of Etheridge et al. (1987) and Wyborn (1988). The model presented in this thesis suggests that a continental block was rifted, and that the rifted continental blocks may have collided again to form a new large continent, resembling the opening and closure of a back-arc basin. If this assumption is valid for the Halls Creek Mobile Zone, the unknown continental block rifted away from the Kimberley block was indeed part of the North Australian Craton. However, it is necessary to make further detailed comparisons of the Early Proterozoic tectonisms of various regions.

The central part of the North Australian Craton, e.g., the Pine Creek Inlier, may not reflect any direct involvement of the subducting oceanic crust during the Early Proterozoic. The central part of the craton was not rifted to form ocean, but was present as a continental block during the Early Proterozoic. However, the central part is considered to have been affected by a mantle plume which caused the initial rifting event at around 1920 Ma in the Halls Creek Mobile Zone (western margin of the North Australian Craton) and other provinces in the world. Mafic magma was emplaced by mantle plume activity in the lower crust of the Pine Creek Inlier. The mafic lower crust thus generated was the source of the high K₂O I-type granitoids in the central part of the North Australian Craton. The partial melting of the mafic lower crust is considered to have been induced by the subduction of an oceanic plate peripheral to this continental block, even at considerable distance from an assumed subduction zone. It may be necessary to consider magmatism related to ridge subduction or a special thermal structure in the back-arc setting to explain the Early Proterozoic igneous activities in the central part of the North Australian Craton. However, an A-subduction of thin continental crust (Kröner, 1983), which was assumed to taken place in the ensialic orogeny model (e.g., Hancock and Rutland, 1984), is unlikely to cause partial melting of the mafic lower crust to generate the high K₂O I-type magma.

The peripheral zones of the North Australian Craton, e.g., the Halls Creek Mobile Zone and Arunta Inlier (e.g., Foden et al., 1988), show clearly orogenies related to subduction of oceanic crust. The tectonic evolution model established in this thesis for the Early Proterozoic orogeny in the Halls Creek Mobile Zone can be applied to other orogenic zones peripheral to the continental blocks during the Early Proterozoic.

CHAPTER 10. CONCLUSIONS

The Halls Creek Mobile Zone in the Kimberley region, Western Australia, contains various types of Early Proterozoic granitoids. The petrogenesis of the granitoids is examined to provide constraints on the nature and style of the Early Proterozoic orogeny in the area.

Integrated field, petrographic, geochemical, and Sr isotopic studies of the granitoids have been performed in four areas in the Halls Creek Mobile Zone. The areas have been primarily selected to study the Mabel Downs Granitoid (Sally Downs Bore area and Turkey Creek area in the central part of the mobile zone), the Bow River Granitoid (Springvale area in the western part of the mobile zone), and the Sophie Downs Granite (Sophie Downs area in the southeastern part of the mobile zone). As it has become clear that the Sally Downs Bore area contains varieties of granitoid in addition to the Mabel Downs Granitoid, a particularly detailed study has been conducted in the Sally Downs Bore area with the view of establishing a frame work of the granitoid activity overall in the Halls Creek Mobile Zone.

Six granitoid suites have been recognized in the Sally Downs Bore area.

(1) The Eastern Leucocratic Granite is a garnet bearing leucocratic granite and is interpreted as a highly fractionated granitoid derived from a low Al tonalite. The granitoid is characterized by high SiO₂ (average 76.0%).

(2) The Dougalls Granitoids Suite contains tonalite and trondhjemite. Orthopyroxene is found in some of the tonalite.

(3) The Ord River Tonalite Suite contains biotite tonalite. Only minor relict hornblende crystals are found.

(4) The Western Porphyritic Granite is a coarse grained, porphyritic augen-textured biotite granite. It is mildly peraluminous, and is characterized by a high concentration of K₂O, Rb, Zr.

(5) The Central Leucocratic Granite is a fine to medium grained biotite granite and is mildly peraluminous. It has a moderate level of Sr and a negative Eu anomaly, indicating a role of plagioclase in the magma residue or in the fractionated phase. Although the granite is characterized by high K₂O (3.77-4.89 %), it has a low Y concentration (3.6-16.4 ppm) and high Sr/Y ratio.

(6) The Sally Downs Tonalite is the youngest granitoid in the area, and is a part of the Mabel Downs Granitoid Suite. Geochemical variation within the tonalite pluton is mainly ascribed to crystal fractionation during intrusion. Hornblende and plagioclase fractionation explains most of the chemical variation found in the tonalite pluton. Rb-Sr whole rock data suggest an emplacement age of 1833 ± 43 Ma with an initial Sr ratio of 0.70292 ± 0.00015 .

The tonalites and trondhjemite of suites 2, 3, and 6 above, have low K₂O, Rb, and Y contents and high Sr contents. Geochemical features suggest that tonalites and trondhjemite can be classified as high Al types.

The Bow River Granitoid is a mildly peraluminous and K₂O rich granitoid, and is enriched in Rb and Y, similar to typical granitoids of the Barramundi igneous association of the North Australian block.

The Sophie Downs Granitoid is an alkali-feldspar granite, intruded into a high crustal level, before deposition of the Saunders Creek Formation of the Halls Creek Group (Griffin and Tyler, 1992). It is the oldest granitoid in the Halls Creek Mobile Zone. It has A-type characteristics, showing a high Ga/Al ratio, and a high concentration of Rb, Ce, Y, Zr, Nb, and F.

Petrogenetic discussion of the above granitoids, presented in this thesis, include consideration of the nature of the source material, pressure and temperature for the generation of granitoid magmas, and crystallization conditions of the granitoid magmas. Suggested petrogenetic models are as follows,

(1) The Sophie Downs Granitoid which has A-type characteristics is considered to be derived by crystal fractionation from basaltic magma. The fractionated granitoid magma would be in the form of separated interstitial melt in the mafic intrusion without the development of a magma of intermediate composition (bimodal igneous activity). It is considered that the basaltic magma is an enriched type. The separation of granitoid magma from the mafic intrusion took place at middle or upper crustal levels. The initial temperature of the separated granitoid magma was high, possibly about 1100°C.

(2) Primary magma (low Al type tonalitic) of the Eastern Leucocratic Granitoid is considered to be derived by partial melting of mafic igneous rocks in the middle or upper most part of lower crust, where garnet is not present in the partial melt residue. The garnet bearing leucocratic granite is derived by extensive fractionation from primary magma.

(3) Three tonalitic units of high Al type, the Dougalls suite, the Ord River suite, and the Sally Downs Tonalite, are considered to be derived from the partial melting of mafic rocks, leaving a residue consisting of garnet and pyroxenes. High partial melting pressures suggest that the tonalitic magmas have been generated by the dehydration melting of subducted oceanic crust, i.e., slab melting. The recognition of early tonalites (Dougalls suite and Ord River suite) and late tonalite (Sally Downs Tonalite) indicates two stages of slab melting. It is inferred that a subducted oceanic slab, situated between what are now the Kimberley

block and North Australian block, was presumably young at the time of the subduction and sufficiently hot to be able to generate tonalitic magma by dehydration melting.

(4) High K₂O granitoids of type I (the Western Porphyritic Granite and Bow River Granitoid) and related volcanics (Whitewater Volcanics) were derived by partial melting of mafic lower crust, leaving a residue consisting of plagioclase and pyroxenes (granulitic residue), but not garnet. The mafic source in the lower crust is considered to have enriched characteristics. Partial melting of the mafic lower crust must have been induced by heat from intrusions of mafic magma in the lower crust.

(5) The Central Leucocratic Granite, which is a type II high K₂O granite, was derived by the partial melting of high Al type tonalites. The partial melting of the tonalites took place at a shallow depth in the crust, not far from the present outcrop level. Heat to melt tonalites is thought to have been supplied by mafic intrusions in the upper crust.

A further summary of the Early Proterozoic tectonic evolution of the Halls Creek Mobile Zone is as follows,

(1) initial rifting of continental crust and generation of A-type Sophie Downs Granitoid magma, followed by:

(2) subduction of oceanic crust resulting in partial melting of the oceanic crust to generate the first stage of tonalitic magmas.

(3) generation of a large volume of K₂O rich granitoid magma in the lower crust leaving a residue of plagioclase and pyroxene. The heat to induce the partial melting of the mafic lower crust may have been derived from underplated mafic magma in the lower crust.

(4) subduction of oceanic crust resulting in partial melting of the oceanic crust to generate a second stage of tonalitic magmas.

Although ensialic orogeny is postulated by a majority of workers for most of the Early Proterozoic provinces in the North Australian block, including the Halls Creek Mobile Zone, the results of the present study strongly suggest that tectonics relating initial rifting and subsequent subduction of oceanic crust have operated in the Halls Creek Mobile Zone during the Early Proterozoic.

REFERENCES

- Abbott, R.N., Jr. and Clarke, D.B., 1979. Hypothetical liquidus relations in the subsystem $\text{Al}_2\text{O}_3\text{-FeO-MgO}$ projected from quartz, alkali feldspar and plagioclase for a $(\text{H}_2\text{O}) \leq 1$. *Can. Mineral.*, 17, 549-560.
- Akaad, M.K., 1956. The Ardara granitic diapir of county Donegal, Ireland. *Q. J. Geol. Soc. London*, 112, 263-290.
- Allegre, C.J. and Ben Othman, D., 1980. Nd-Sr isotopic relationship in granitoid rocks and continental crust development: a chemical approach to orogenesis. *Nature*, 286, 335-346.
- Anderson, J.L. and Cullers, R.L., 1987. Crust-enriched, mantle-derived tonalites in the early Proterozoic Penokean orogen of Wisconsin. *Jour. Geol.*, 95, 139-154.
- Ando, A., Mita, N. and Terashima, S., 1987. 1986 values for fifteen GSI rock reference samples, "Igneous Rock Series". *Geostandards Newsletter*, 11, 159-166.
- Arculus, R.J., and Wills, K.J.A., 1980. The petrology of plutonic blocks and inclusions from the Lesser Antilles island arc. *J. Petrol.*, 21, 743-799.
- Arkani-Hamed, J. and Jolly, W.T., 1989. Generation of Archean tonalites. *Geology*, 17, 307-310.
- Arndt, N. and Goldstein, S., 1987. Use and abuse of crust-formation ages. *Geology*, 15, 893-895.
- Arth, J.G. and Barker, F., 1976. Rare-earth partitioning between hornblende and dacitic liquid and implications for the genesis of trondhjemitic-tonalitic magmas. *Geology*, 4, 534-536.
- Arth, J.G. and Hanson, G.N., 1972. Quartz diorites derived by partial melting of eclogite or amphibolite at mantle depths. *Contrib. Mineral. Petrol.*, 37, 161-174.

- Arth, J.G. and Hanson, G.N., 1975. Geochemistry and origin of the early Precambrian crust of northern Minnesota. *Geochim. Cosmochim. Acta.*, 39, 325-362.
- Arth, J.G., Barker, F., Peterman, Z.E. and Friedman, I., 1978. Geochemistry of the gabbro-diorite-tonalite-trondhjemite suite of southwest Finland and its implication for the origin of tonalitic and trondhjemitic magmas. *J. Petrol.*, 19, 289-316.
- Atherton, M.P. and Petford, N., 1993. Generation of sodium-rich magmas from newly underplated basaltic crust. *Nature*, 362, 144-146.
- Balk, R., 1937. Structural behaviour of igneous rocks. *Geol. Soc. Am., Mem.*, 5, 177pp.
- Barbarin, B. and Didier, J., 1991. Review of the main hypotheses proposed for the genesis and evolution of mafic microgranular enclaves. In: Didier, J. and Barbarin, B. (eds.) *Enclaves and granite petrology*. Elsevier, Amsterdam, 367-373.
- Barker, D.S., 1970. Compositions of granophyre, myrmekite, and graphic granite. *Bull. Geol. Soc. Am.*, 81, 3339-3350.
- Barker, F., 1979. Trondhjemite: definition, environment and hypotheses of origin. In Barker, F. (ed.) *Trondhjemites, dacites, and related rocks*. Elsevier, Amsterdam, 1-12.
- Barker, F. and Arth, J.G., 1976. Generation of trondhjemitic-tonalitic liquids and Archean bimodal trondhjemite-basalt suites. *Geology*, 4, 596-600.
- Bateman, P.C. and Chappell, B.W., 1979. Crystallization, fractionation, and solidification of the Toulumne Intrusive Series, Yosemite National Park, California. *Bull. Geol. Soc. Am.*, 90, 465-482.

- Beard, J.S. and Lofgren, G.E., 1991. Dehydration melting and water-saturated melting of basaltic and andesitic greenstones and amphibolites at 1, 3, 6.9 kb. *J. Petrol.*, 32, 365-401.
- Bennett, R. and Gellatly, D.C., 1970. Rb-Sr age determinations of some west Kimberley rocks. *Bur. Mineral Resour. Aust., Rec.*, 1970/20 (unpubl.).
- Ben Othman, D., Polve, M., and Allegre, C.J., 1984. Nd-Sm isotopic composition of granulites and constraints on the evolution of the lower continental crust. *Nature*, 307, 510-515.
- Berger, A.R. and Pitcher, W.S., 1970. Structures in granitic rocks: a commentary and a critique on granite tectonics. *Prc. Geologist Assoc. London*, 81, 441-461.
- Bickford, M.E., Collerson, K.D., Lewry, J.F., Van Schmus, W.R., and Chiarenzelli, J.R., 1990. Proterozoic collisional tectonism in the Trans-Hudson orogen, Saskatchewan. *Geology*, 18, 14-18.
- Birch, W.D. and Gleadow, A.J., 1974. The genesis of garnet and cordierite in acid volcanic rocks: evidence from the Cerberean cauldron, central Victoria, Australia. *Contrib. Mineral. Petrol.*, 45, 1-13.
- Black, L.P., 1977. A Rb-Sr geochronological study in the Proterozoic Tennant Creek Block, central Australia. *BMR J. Aust. Geol. Geophys.*, 2, 111-122.
- Black, L.P., 1981. Age of the Warramunga Group, Tennant Creek Block, Northern Territory. *BMR J. Aust. Geol. Geophys.*, 6, 254-257.
- Black, L.P., 1984. U-Pb zircon ages and a revised chronology for the Tennant Creek Inlier, Northern Territory. *Aust. J. Earth Sci.*, 31, 123-131.

- Black, L.P., Shaw, R.D., and Stewart, A.J., 1983. Rb-Sr geochronology of Proterozoic events in the Arunta Inlier, central Australia. *BMR J. Aust. Geol. Geophys.*, 8, 129-137.
- Black, L.P. and McCulloch, M.T., 1984. Sm-Nd ages of the Arunta, Tennant Creek, and Georgetown Inliers of northern Australia. *Aust. J. Earth Sci.*, 31, 49-60.
- Blake, D.H. and Hoatson, D.M., 1993. Granite, gabbro, and migmatite field relationships in the Proterozoic Lamboo Complex of the East Kimberley region, Western Australia. *AGSO J. Aust. Geol. Geophys.*, 14, 319-330.
- Blake, D.H., Hodgson, I.M., and Muhling, P.C., 1979. Geology of The Granites-Tanami region, Northern Territory and Western Australia. *Bur. Mineral Resour. Aust., Bull.*, 197.
- Blake, D.H., Hodgson, I.M., and Smith, P.A., 1975. Geology of the Birrindudu and Tanami 1:250000 sheet areas, Northern Territory. *Bur. Mineral. Resour. Aust., Rep.*, 174.
- Bofinger, V.M., 1967. Geochronology in the East Kimberley area of Western Australia. Ph.D. Thesis, Aust. National. Univ., Canberra, Australia, 167pp.(unpubl.).
- Borg, S.G. and DePaolo, D.J., 1994. Laurentia, Australia, and Antarctica as a Late Proterozoic supercontinent: constraints from isotopic mapping. *Geology*, 22, 307-310.
- Brookfield, M.E., 1993. Neoproterozoic Laurentia-Australia fit. *Geology*, 21, 683-686.
- Brooks, C.K., Henderson, P., and Ronsbo, J.G., 1981. Rare-earth partition between allanite and glass in the obsidian of Sandy Braes, Northern Ireland. *Mineral. Mag.*, 44, 157-160.

- Bureau of Mineral Resources, 1967. Geological Map of East Kimberley Region, Western Australia, 1:500000. Bureau of Mineral Resources, Canberra.
- Bureau of Mineral Resources, 1976. Geology of Kimberley Region, Western Australia, West Kimberley, 1:500000. Bureau of Mineral Resources, Canberra.
- Bureau of Mineral Resources, 1979. Major structural elements: BMR Earth Science Atlas. Bureau of Mineral Resources, Canberra.
- Bureau of Mineral Resources, 1977. Bouguer Anomalies, Lansdowne, WA, 1:500000. Bureau of Mineral Resources, Canberra.
- Bureau of Mineral Resources, 1977. Bouguer Anomalies, Lissadell, WA, 1:500000. Bureau of Mineral Resources, Canberra.
- Bureau of Mineral Resources, 1977. Bouguer Anomalies, Mount Elizabeth, WA, 1:500000. Bureau of Mineral Resources, Canberra.
- Bureau of Mineral Resources, 1978. Bouguer Anomalies, Dixon Range, WA, 1:500000. Bureau of Mineral Resources, Canberra.
- Bureau of Mineral Resources, 1978. Bouguer Anomalies, Gordon Downs, WA, 1:500000. Bureau of Mineral Resources, Canberra.
- Bureau of Mineral Resources, 1978. Bouguer Anomalies, Mount Ramsay, WA, 1:500000. Bureau of Mineral Resources, Canberra.
- Burnham, C.W. and Ohmoto, H., 1980. Late-stage processes of felsic magmatism. *Mining Geol., Spec. Issue*, 8, 1-11.
- Carroll, M.R. and Wyllie, P.J., 1990. The system tonalite-H₂O at 15 kbar and the genesis of calc-alkaline magmas. *Am. Mineral.*, 75, 345-357.
- Cawthorn R.G. and Brown, P.A., 1976. A model for the formation and crystallization of corundum-normative cala-alkaline magmas through amphibole fractionation. *J. Geol.*, 84, 467-476.

- Chappell, B.W. and White, A.J.R., 1974. Two contrasting granite types. *Pacific Geol.*, 8, 173-174.
- Chappell, B.W. and White, A.J.R., 1992. I- and S-type granites in the Lachlan Fold Belt. *Trans. Roy. Soc. Edinb.*, 83, 1-26.
- Chauvel, C. Arndt, N.T., Kielinzcuk, S. and Thom, A., 1987. Formation of Canadian 1.9 Ga old continental crust. I: Nd isotopic data. *Can. J. Earth Sci.*, 24, 396-406.
- Chivas, A.R., Andrew, A.S., Sinha, A.K., and O'Neil, J.R., 1982. Geochemistry of a Pliocene-Pleistocene oceanic-arc plutonic complex, Guadalcanal. *Nature*, 300, 139-143.
- Claoue-Long, J.C., Thirlwall, M.F., and Nesbitt, R.W., 1984. Revised Sm-Nd systematics of Kambalda greenstones, Western Australia. *Nature*, 307, 697-701.
- Clarke, F.W., 1924. Data of geochemistry. U.S. Geol. Surv., Bull., 770.
- Clemens, J.D., Holloway, J.R., and White, A.J.R., 1986. Origin of an A-type granite: experimental constraints. *Am. Mineral.*, 71, 317-324.
- Cloos, E., 1932. Structural survey of the granodiorite south of Mariposa, California. *Am. J. Sci.*, 23, 291-304.
- Collins, W.J., Beams, S.D., White, A.J.R., and Chappell, B.W., 1982. Nature and origine of A-type granites with particular reference to southeastern Australia. *Contrib. Mineral. Petrol.*, 80, 189-200.
- Compston, W. and Arriens, P.A., 1968. The Precambrian geochronology of Australia. *Can. J. Earth Sci.*, 5, 561-583.
- Compton, P., 1978. Rare earth evidence for the origin of the Nuk Gneisses, Buksefjorden Region, southern West Greenland. *Contrib. Mineral. Petrol.*, 66, 283-293.
- Compton, R.R., 1955. Trondhjemite batholith near Bidwell Bar, California. *Bull. Geol. Soc. Am.*, 66, 9-44.

- Condie, K.C., 1976. Trace-element geochemistry of Archean Greenstone belts. *Earth Sci. Rev.*, 12, 393-417.
- Creaser, R.A., Price, R.C., and Wormald, R.J., 1991. A-type granites revisited: assessment of a residural-source model. *Geology*, 19, 163-166.
- Currie, K.L., 1976. The alkaline rocks of Canada. *Geol. Surv. Can. Bull.* 239.
- Dalziel, I.W.D., 1991. Pacific margins of Laurentia and East Antarctica-Australia as a conjugate rift pair: evidence and implications for an Eocambrian supercontinent. *Geology*, 19, 598-601.
- Dalziel, I.W.D., 1995. Earth before Pangea. *Scientific American*, 272, 58-63.
- Daniels, J.L. and Horwitz, R.C., 1969. Precambrian tectonic units of Western Australia. *Ann. Rep. Geol. Surv. West. Aust.*, 1968, 37-38.
- Davis, G.A., 1963. Structure and mode of emplacement of Caribou Mountain Pluton, Klamath Mountains, California. *Bull. Geol. Soc. Am.*, 74, 331-348.
- Defant, M.J. and Drummond, M.S., 1990. Derivation of some modern arc magmas by melting of young subducted lithosphere. *Nature*, 347, 662-665.
- Defant, M.J. and Drummond, M.S., 1993. Mount St. Helens: potential example of the partial melting of the subducted lithosphere in a volcanic arc. *Geology*, 21, 547-550.
- Defant, M.J., Richerson, P.M., De Boer, J.Z., Stewart, R.H., Maury, R.C., Bellon, H., Drummond, M.S., Feigenson, M.D., and Jackson, T.E., 1991. Dacite genesis via both slab melting and differentiation: petrogenesis of La Yeguada Volcanic Complex, Panama. *J. Petrol.*, 32, 1101-1142.

- DePaolo, D.J., 1981. Neodymium isotopes in the Colorado Front Range and crust-mantle evolution in the Proterozoic. *Nature*, 291, 193-196.
- DePaolo, D.J., 1981. Trace element and isotopic effects of combined wallrock assimilation and fractional crystallization. *Earth Planet. Sci. Lett.*, 53, 189-202.
- DePaolo, D.J., and Wasserburg, G.J., 1976. Inferences about magma sources and mantle structure from variations of $^{143}\text{Nd}/^{144}\text{Nd}$. *Geophys. Res. Lett.*, 3, 743-746.
- Derrick, G.M. and Playford, P.E., 1973. Lennard River, Western Australia - 1:250000 Geological Series. Bur. Mineral. Resour. Aust., Explan. Notes, SE/58-8.
- Dickinson, Jr., J.E. and Hess, P.C., 1982. Zircon saturation in lunar basalts and granites. *Earth Planet. Sci. Lett.*, 57, 336-344.
- Didier, J., 1973. *Granites and their enclaves*. Amsterdam, Elsevier, 1-393.
- Didier, J. and Barbarin, B., 1991. The different types of enclaves in granites - Nomenclature. In Didier, J. and Barbarin, B. (eds.) *Enclaves and granite petrology*. Elsevier, 19-23.
- Dooley, J.C., 1976. Variation of crustal mass over the Australian region. *BMR J. Aust. Geol. Geophys.*, 1, 291-296.
- Dorais, M.J., Whitney, J.A., and Roden, M.F., 1990. Origin of mafic enclaves in the Dinkey Creek Pluton, central Sierra Nevada Batholith, California. *J. Petrol.*, 31, 853-881.
- Douce, A.E.P. and Beard, J.S., 1995. Dehydration-melting of biotite gneiss and quartz amphibolite from 3 to 15 kbar. *Jour. Petrol.*, 36, 707-738.

- Dow, D.B. and Gemuts, I., 1967. Dixon Range, Western Australia - 1:250000 Geological Series. Bur. Mineral Resour. Aust., Explan. Notes, SE/52-6.
- Dow, D.B. and Gemuts, I., 1969. Geology of the Kimberley Region, Western Australia: the east Kimberley. Bur. Mineral Resour. Aust., Bull., 116.
- Dow, D.B., Gemuts, I., Plumb, K.A., and Dunnett, D., 1964. The geology of the Ord River region, Western Australia. Bur. Mineral Resour. Aust., Rec., 1964/104 (unpubl.).
- Drake, M.J. and Weill, D.F., 1972. New rare earth element standards for electron microprobe analysis. *Chem. Geol.*, 10, 179-181.
- Drummond, B.J. and Collins, C.D.N., 1986. Seismic evidence for underplating of the lower continental crust of Australia. *Earth Planet. Sci. Lett.*, 79, 361-372.
- Drummond, M.S. and Defant, M.J., 1990. A model for trondhjemite-tonalite-dacite genesis and crustal growth via slab melting: Archean to modern comparisons. *Jour. Geophys. Res.*, 95, 21503-21521.
- Duke, E.F., Papike, J.J., and Laul, J.C., 1992. Geochemistry of a boron-rich peraluminous granite pluton: the Calamity Peak layered granite-pegmatite complex, Black Hills, South Dakota. *Canadian Mineral.*, 30, 811-833.
- Durrheim, R.J. and Mooney, W.D., 1991. Archean and Proterozoic crustal evolution: evidence from crustal seismology. *Geology*, 19, 606-609.
- Eby, G.N., 1990. The A-type granitoids: a review of their occurrence and chemical characteristics and speculations on their etrogenesis. *Lithos*, 26, 115-134.
- Eby, G.N., 1992. Chemical subdivision of the A-type granitoids: petrogenetic and tectonic implications. *Geology*, 20, 641-644.

- Eskola, P., 1949. The problem of mantled gneiss domes. *Quart. J. Geol. Soc.*, 104, 461-476.
- Etheridge, M.A., Rutland, R.W.R. and Wyborn, L.A.I., 1987. Orogenesis and tectonic process in the early to middle Proterozoic of northern Australia. In Kroner, A. (ed.) *Proterozoic lithospheric evolution.*, Geodynamic Series, 17, Am. Geophys. Union, Washington, D.C., 131-147.
- Exley, R.A., 1980. Microprobe studies of REE-rich accessory minerals: implications for Skye granite petrogenesis and REE mobility in hydrothermal systems. *Earth Planet. Sci. Lett.*, 48, 97-110.
- Ferguson, A.K. and Sewell, D.K.B., 1978. An overlay program for the on-line operation of a JEOL JXA-5A electron microprobe using a modified Mason et al ZAF correction program. *Geology Department, Univ. Melbourne, Publication 5*, p.115.
- Ferguson, A.K. and Sewell, D.K.B., 1980. A peak integration method for acquiring X-ray data for on-line microprobe analysis. *X-ray Spectrometry*, 9, 48-51.
- Ferguson, J., Chappell, B.W., and Goleby, A.B., 1980. Granitoids in the Pine Creek Geosyncline. In: Ferguson, J. and Goleby, A.B. (eds.) *Uranium in the Pine Creek Geosyncline*. International Atomic Energy Agency, Vienna, 73-90.
- Ferry, J.M. and Spear, F.S., 1978. Experimental calibration of the partitioning of Fe and Mg between biotite and garnet. *Contrib. Mineral. Petrol.*, 66, 113-117.
- Finlayson, D.M., 1987. Seismic features of Proterozoic crust in Northern Australia and their evolution. In Kroner, A. (ed.) *Proterozoic lithospheric evolution.*, Geodynamic Series, 17, Am. Geophys. Union, Washington, D.C., 99-113.

- Fitton, J.G., 1972. The genetic significance of Almandine-Pyrope phenocrysts in the calc-alkaline Borrowdale volcanic group, northern England. *Contrib. Mineral. Petrol.*, 36, 231-248.
- Fleisher, M., 1983. Distribution of the lanthanides and yttrium in apatites from iron ores and its bearing on the genesis of ores of the Kiruna type. *Econ. Geol.*, 78, 1007-1010.
- Fletcher, I.R., Wilde, S.A., Libby, W.G., and Rosman, K.J.R., 1983a. Sm-Nd model ages across the margins of the Archaean Yilgarn Block, Western Australia-II; southwest transect into the Proterozoic Albany-Fraser Province. *J. Geol. Soc. Aust.*, 30, 333-340.
- Fletcher, I.R., Williams, S.J., Gee, R.D., and Rosman, K.J.R., 1983b. Sm-Nd model ages across the margins of the Archaean Yilgarn Block, Western Australia; northwest transect into the Proterozoic Gascoyne Province. *J. Geol. Soc. Aust.*, 30, 167-174.
- Foden, J.D., Buick, I.S., and Mortimer, G.E., 1988. The petrology and geochemistry of granitic gneisses from the East Arunta Inlier, central Australia: implications for Proterozoic crustal development. *Precamb. Res.*, 40/41, 233-259.
- Fourcade, S. and Allegre, C.J., 1981. Trace elements behavior in granite genesis: a case study of the calc-alkaline plutonic association from the Querigut Complex (Pyrenees, France). *Contrib. Mineral. Petrol.*, 76, 177-195.
- Fraser, A.R., 1976. Gravity provinces and their nomenclature. *BMR J. Aust. Geol. Geophys.*, 1, 350-352.
- Frey, F.A., Chappell, B.W., and Roy, S.D., 1978. Fractionation of rare-earth elements in the Toulumne Intrusive Series, Sierra Nevada batholith, California. *Geology*, 6, 239-242.
- Gastil, R.G., 1979. A conceptual hypothesis for the relation of differing tectonic terranes to plutonic emplacement. *Geology*, 7, 542-544.

- Gellatly, D.C., 1971. Possible Archaean rocks of the Kimberley region, Western Australia. *Geol. Soc. Aust., Spec. Publ.*, 3, 93-101.
- Gellatly, D.C. and Derrick, G.M., 1967. Lansdowne, Western Australia - 1:250000 Geological Series. *Bur. Mineral Resour. Aust., Explan. Notes*, SE/52-5.
- Gellatly, D.C., Derrick, G.M., and Plumb, K.A., 1975. The geology of the Lansdowne 1:250000 Sheet area, Western Australia. *Bur. Mineral Resour. Aust., Rep.*, 152.
- Gellatly, D.C., Sofoulis, J., Derrick, G.M., and Morgan, C.M., 1974. The older Precambrian geology of the Lennard River 1:250000 Sheet area, Western Australia. *Bur. Mineral Resour. Aust., Rep.*, 153.
- Gemuts, I., 1971. Metamorphic and igneous rocks of the Lamboo Complex, east Kimberley region, Western Australia. *Bur. Mineral Resour. Aust., Bull.*, 107.
- Gemuts, I. and Smith, J.W., 1968. Gordon Downs, Western Australia - 1:250000 Geological Series. *Bur. Mineral Resour. Aust., Explan. Notes*, SE/52-10.
- Glazner, A.F., 1994. Foundering of mafic plutons and density stratification of continental crust. *Geology*, 22, 435-438.
- Glikson, A.Y., 1979. Early Precambrian tonalite-trondhjemite sialic nuclei. *Earth Sci. Rev.*, 15, 1-73.
- Govindaraju, K., 1989. 1989 compilation of working values and sample description for 272 geostandards. *Geostandards Newsletter*, 13, 1-113.
- Green, D.H., 1971. Composition of basaltic magmas as indicators of conditions of origin: application to oceanic volcanism. *Phil. Trans. Roy. Soc. London, A*, 268, 707-725.

- Green, T.H., 1977. Garnet in silicic liquids and its possible use as a P-T indicator. *Contrib. Mineral. Petrol.*, 65, 59-67.
- Green, T.H., 1982. Anatexis of mafic crust and high pressure crystallization of andesite. In Thorpe, R.S. (ed.) *Andesite*, 465-487.
- Green, T.H. and Ringwood, A.E., 1968. Origin of garnet phenocrysts in cala-alkaline rocks. *Contrib. Mineral. Petrol.*, 18, 163-174.
- Green, T.H. and Ringwood, A.E., 1972. Crystallization of garnet-bearing rhyodacite under high-pressure hydrous condition. *J. Geol. Soc. Aust.*, 19, 203-212.
- Griffin, T.J., 1989. A major thrust between the Gibb River and Hooper Terranes in the King Leopold Orogen, West Kimberley region. *Prof. Pap. West. Aust. Geol. Surv. Rep.*, 26, 69-81.
- Griffin, T.J. and Grey, K., 1990a. King Leopold and Halls Creek Orogens. In: *Geology and Mineral Resources of Western Australia. Mem. West. Aust. Geol. Surv.*, 3, 293-304.
- Griffin, T.J. and Grey, K., 1990b. Kimberley Basin. In: *Geology and Mineral Resources of Western Australia. Mem. West. Aust. Geol. Surv.*, 3, 293-304.
- Griffin, T.J. and Myers, J.S., 1988. A Proterozoic terrane boundary in the King Leopold Orogen, Western Australia. *Aust. J. Earth Sci.*, 35, 131-132.
- Griffin, T.J. and Tyler, I.M., 1992. Geology of the southern Halls Creek orogen- a summary of field work in 1992. *Record Geol. Surv. West. Aust.*, 1922/17, 1-28.
- Griffin, T.J. and Tyler, I.M., 1994. Geochemical constraints on the tectonic evolution of the Early Proterozoic orogens in the Kimberley region of Western Australia. 12th Aust. Geol. Convention, Abst. 37, 151-152.

- Griffin, T.J., White, A.J.R., and Chappell, B.W., 1978. The Moruya batholith and geochemical contrasts between the Moruya and Jindabyne suites. *J. Geol. Soc. Aust.*, 25, 235-247.
- Griffin, W.L. and O'Reilly, S.Y., 1987. Is the continental Moho the crust-mantle boundary? *Geology*, 15, 241-244.
- Gromet, L.P. and Silver, L.T., 1983. Rare earth element distributions among minerals in a granodiorite and their petrogenetic implications. *Geochim. Cosmochim. Acta*, 47, 925-939.
- G.S.A. (Geological Society of Australia), 1971. Tectonic map of Australia and New Guinea 1:5000000. Geol. Soc. Aust., Sydney.
- Hall, A., 1965. The origin of accessory garnet in the Donegal Granite. *Mineral. Mag.*, 35, 628-633.
- Hamilton, W. and Myers, W.B., 1967. The nature of batholiths. U. S. Geol. Surv., Prof. Pap., 554-C, 30 pp.
- Hamlyn, P.R., 1975. Chromite alteration in the Panton Sill, East Kimberley Region, Western Australia. *Mineral. Mag.*, 40, 181-192.
- Hamlyn, P.R., 1977. Petrology of the Panton and McIntosh layered intrusions, Western Australia, with particular reference to the genesis of the Panton chromite deposits. Ph.D. Thesis, Univ. Melbourne, Melbourne, Australia, 389pp.(unpubl.).
- Hamlyn, P.R., 1980. Equilibration history and phase chemistry of the Panton Sill, Western Australia. *Am. J. Sci.*, 280, 631-668.
- Hamlyn, P.R. and Keays, R.R., 1979. Origin of chromite compositional variation in the Panton Sill, Western Australia. *Contrib. Mineral. Petrol.*, 69, 75-82.
- Hancock, S.L. and Rutland, R.W.R., 1984. Tectonics of an early Proterozoic geosuture: the Halls Creek orogenic sub-province, northern Australia. *J. Geodynamics*, 1, 387-432.

- Hanson, G.N., 1978. The application of trace elements to the petrogenesis of igneous rocks of granitic composition. *Earth Planet. Sci. Lett.*, 38, 26-43.
- Hanson, G.N., 1980. Rare earth elements in petrogenetic studies of igneous systems. *Ann. Rev. Earth Planet. Sci.*, 8, 371-406.
- Hardman, E.T., 1884. Report on the geology of the Kimberley district. *West. Aust. Parl. Pap.*, 31.
- Hardman, E.T., 1885. Report on the geology of the Kimberley district, Western Australia. *West. Aust. Parl. Pap.*, 34.
- Harris, N.B.W. and Marriner, G.F., 1980. Geochemistry and petrogenesis of a peralkaline granite complex from the Midian Mountains, Saudi Arabia. *Lithos*, 13, 325-337.
- Hart, S.R. and Allegre, C.J., 1980. Trace-element constraints on magma genesis. In: Hargraves, R.B. (ed.) *Physics of magmatic processes*. Princeton Univ. Press, Princeton, New Jersey, 121-159.
- Henderson, P., 1980. Rare earth element partition between sphene, apatite and other coexisting minerals of the Kangerdlugssuaq intrusion, E. Greenland. *Contrib. Mineral. Petrol.*, 72, 81-85.
- Hibbard, M.J., 1986. Deformation of incompletely crystalized magma systems: granitic gneisses and their tectonic implications. *Jour. Geol.*, 95, 543-561.
- Hildebrand, R.S. and Bowring, S.A., 1984. Continental intra-arc depressions: a nonextensional model for their origin, with a Proterozoic example from Wopmay orogen. *Geology*, 12, 73-77.
- Hildebrand, R.S., Hoffman, P.F. and Bowring, S.A., 1987. Tecton-magmatic evolution of the 1.9-Ga Great Bear magmatic zone, Wopmay orogen, northwestern Canada. *J. Volc. Geotherm. Res.*, 32, 99-118.

- Hildreth, W., 1981. Gradients in silicic magma chambers: implications for lithospheric magmatism. *Jour. Geophys. Res.*, 86, 10153-10192.
- Hine, R., Williams, I.S., Chappell, B.W., and White, A.J.R., 1978. Contrasts between I- and S-type granitoids of the Kosciusko batholith. *J. Geol. Soc. Aust.*, 25, 219-234.
- Hoffman, P.F., 1987. Early Proterozoic foredeeps, foredeep magmatism, and Superior-type iron-formations of the Canadian shield. In: Kröner, A. (ed.) *Proterozoic lithospheric evolution.*, Geodynamic Series, 17, Am. Geophys. Union, Washington, D.C., 85-98.
- Hoffman, P.F., 1989. Speculations on Laurentia's first gigayear (2.0 to 1.0 Ga). *Geology*, 17, 135-138.
- Hoffman, P.F., 1991. Did the breakout of Laurentia turn Gondwanaland inside-out? *Science*, 252, 1409-1412.
- Hoffman, P.F. and Bowring, S.A., 1984. Short-lived 1.9 Ga continental margin and its destruction, Wopmay orogen, northwest Canada. *Geology*, 12, 68-72.
- Holder, M.T., 1979. An emplacement mechanism for post-tectonic granites and its implications for their geochemical features. In: Atherton, M.P. and Tarney, J. (eds.) *Origin of granite batholiths.* Shiva Pub. Ltd., Orpington, Kent, 116-128.
- Howie, R.A., 1967. Charnockites and their colour. *J. Geol. Soc. India.*, 8, 1-7.
- Idnurm, M. and Giddings, J.W., 1995. Paleoproterozoic-Neoproterozoic North America-Australia link: new evidence from paleomagnetism. *Geology*, 23, 149-152.
- Imeokparia, E.G., 1981. Fluorine in biotites from the Afu younger granite complex (Central Nigeria). *Chem. Geol.*, 32, 247-254.

- Jacobsen, S.B. and Wasserburg, G.J., 1980. Sm-Nd isotopic evolution of chondrites. *Earth Planet. Sci. Lett.*, 50, 139-155.
- Jahn, B., Vidal, P., and Kroner, A., 1984. Multi-chronometric ages and origin of Archaean tonalitic gneisses in Finnish Lapland: a case for long crustal residence time. *Contrib. Mineral. Petrol.*, 86, 398-408.
- Jakes, P. and Gill, J., 1970. Rare earth elements and the island arc tholeiitic series. *Earth Planet. Sci. Lett.*, 9, 17-28.
- Jakes, P. and White, A.J.R., 1970. K/Rb ratios of rocks from island arcs. *Geochim. Cosmochim. Acta*, 34, 849-856.
- Jakes, P. and White, A.J.R., 1972. Major and trace element abundances in volcanic rocks of orogenic areas. *Bull. Geol. Soc. Am.*, 83, 29-40.
- Jaques, A.L., Lewis, J.D., and Smith, C.B., 1986. The Kimberlites and lamproites of Western Australia. *Bull. West. Aust. Geol. Surv.*, p.268.
- Jaques, A.L., O'Neill, H.St.C., Smith, C.B., Moon, J., and Chappell, B.W., 1990. Diamondiferous peridotite xenoliths from the Argyle (AK1) lamproite pipe, Western Australia. *Contrib. Mineral. Petrol.*, 104, 255-276.
- Jaques, A.L., Webb, A.W., Fanning, C.M., Black, L.P., Pidgeon, R.T., Ferguson, J., Smith, C.B. and Gregory, G.P., 1984. The age of the diamond-bearing pipes and associated leucite lamproites of the West Kimberley region, Western Australia. *BMR Jour. Aust. Geol. Geophys.*, 9, 1-7.
- Johnston, A.D. and Wyllie, P.J., 1988. Constraints on the origin of Archean trondhjemites based on phase relationships of Nuk gneiss with H₂O at 15 kbar. *Contrib. Mineral. Petrol.*, 100, 35-46.

- Johnston, A.D. and Wyllie, P.J., 1989. The system tonalite-peridotite-H₂O at 30 kbar, with applications to hybridization in subduction zone magmatism. *Contrib. Mineral. Petrol.*, 102, 257-264.
- Joyce, A.S., 1973. Chemistry of the minerals of the granitic Murrumbidgee batholith, Australian Capital Territory. *Chemical Geol.*, 11, 271-296.
- Kanisawa, S., 1979. Content and behavior of fluorine in granitic rocks, Kitakami Mountains, northeast Japan. *Chem. Geol.* 24, 57-67.
- Kay, R.W. and Kay, S.Mahlburg, 1991. Creation and destruction of lower crust. *Geol. Rundschau*, 80, 259-278.
- Kleemann, G.J. and Twist, D., 1989. The compositionally-zoned sheet-like granite pluton of the Bushveld Complex: evidence bearing on the nature of A-type magmatism. *Jour. Petrol.*, 30, 1383-1414.
- Kosiewicz, S.T., Schomberg, P.J., and Haskin, L.A., 1974. Rare earth analysis of U.S.G.S. rocks SCo-1 and STM-1: evaluation of standards for homogeneity and of the precision and accuracy of a procedure for neutron activation analyses. *J. Radioanal. Chem.*, 20, 619-626.
- Kröner, A., 1983. Proterozoic mobile belts compatible with the plate tectonic concept. *Geol. Soc. Am. Mem.*, 161, 59-74.
- Lambert, R.St J., Marsh, I.K., and Chamberlain, V.E., 1989. The occurrence of interstitial granite-glass in all formations of the Columbia River Basalt Group and its petrogenetic implications. *Geol. Soc. Am. Spec. Pap.*, 239, 321-332.
- Leake, B.E., 1968. A catalog of analyzed calciferous and subcalciferous amphiboles together with their nomenclature and associated minerals. *Geol. Soc. Am., Spec. Pap.*, 98.

- Li, Z.X., Zhang, L., and Powell, C.McA., 1995. South China in Rodinia: part of the missing link between Australia-East Antarctica and Laurentia? *Geology*, 23, 407-410.
- Lipman, P.W., 1963. Gibson Peak pluton: a discordant composite intrusion in the southeastern Trinity Alps, northern California. *Bull. Geol. Soc. Am.*, 74, 1259-1280.
- Loiseller, M.C. and Wones, D.R., 1979. Characteristics and origin of anorogenic granites. *Geol. Soc. Am., Abstr. with Progr.*, 11, 468.
- Lopez-Escobar, L. and Frey, F.A., and Oyarzum, J., 1979. Geochemical characteristics of central Chile (33 -34 S) granitoids. *Cotrib. Mineral. Petrol.*, 70, 439-450.
- Luth, W.C., Jahns, R.H., and Tuttle, O.F., 1964. The granite system at pressure of 4 to 10 kilobars. *J. Geophys. Res.*, 69, 759-773.
- Maaloe, S. and Wyllie, P.J., 1975. Water content of a granite magma deduced from the sequence of crystallization determined experimentally with water-undersaturated conditions. *Contrib. Mineral. Petrol.*, 52, 175-191.
- MacColl, R.S., 1964. Geochemical and structural studies in batholithic rocks of southern California : part 1, structural geology of Rattlesnake Mountain pluton. *Bull. Geol. Soc. Am.*, 75, 805-822.
- Macdonald, G.A. and Katsura, T., 1964. Chemical composition of Hawaiian lavas. *J. Petrol.*, 5, 82-133.
- Martin, H., 1986. Effect of steeper Archean geothermal gradient on geochemistry of subduction-zone magmas. *Geology*, 14, 753-756.
- Martin, N.R., 1953. The structure of the granite massif of Flamanville, Manche, north-west France. *Q. J. Geol. Soc. London*, 108, 311-342.
- Matheson, R.S. and Guppy, D.P., 1949. Geological reconnaissance in the Mount Ramsay area, Kimberley Division, Western Australia. *Bur. Mineral Resour. Aust., Rec.*, 1949/48 (unpubl.).

- Mathison, C.I. and Hamlyn, P.R., 1987. The McIntosh layered troctolite-olivine gabbro intrusion, East Kimberley, Western Australia. *J. Petrol.*, 28, 211-234.
- McCarthy, T.S. and Cawthorn, R.G., 1980. Changes in initial $^{87}\text{Sr}/^{86}\text{Sr}$ ratio during protracted fractionation in igneous complexes. *J. Petrol.*, 21, 245-264.
- McCulloch, M.T., 1987. Sm-Nd isotopic constraints on the evolution of Precambrian crust in the Australian continent. In Kröner, A. (ed.) *Proterozoic lithospheric evolution.*, Geodynamic Series, 17, Am. Geophys. Union, Washington, D.C., 115-130.
- McCulloch, M.T. and Chappell, B.W., 1982. Nd isotopic characteristics of S- and I-type granites. *Earth Planet. Sci. Lett.*, 58, 51-64.
- McCulloch, M.T. and Compston, W., 1981. Sm-Nd age of Kambalda and Kanowna greenstones and heterogeneity in the Archaean mantle. *Nature*, 294, 322-327.
- McCulloch, M.T. and Hensel, H.D., 1984. Sm-Nd isotopic evidence for a major Early to Mid-Proterozoic episode of crustal growth in the Australian continent. 27th Int. Geol. Congr., Moscow, Abstract, 2, 351-352.
- McCulloch, M.T. and Wasserburg, G.J., 1978. Sm-Nd and Rb-Sr chronology of continental crust formation. *Science*, 200, 1003-1011.
- McIntyre, G.A., Brooks, C., Compston, W., and Turek, A., 1966. The statistical assessment of Rb-Sr isochrons. *J. Geophys. Res.*, 71, 5459-5468.
- McLennan, S.M. and Taylor, S.R., 1980. Geochemical standards for sedimentary rocks: trace element data for U.S.G.S. standards SCo-1, MAG-1 and SGR-1. *Chem. Geol.*, 29, 333-343.
- Miller, C.F. and Mittlefehldt, D.W., 1982. Depletion of light rare-earth elements in felsic magmas. *Geology*, 10, 129-133.

- Miller, C.F. and Stoddard, E.F., 1981. The role of manganese in the paragenesis of magmatic garnet: an example from the old Woman-Piute Range, California. *J. Geol.*, 89, 233-246.
- Miyashiro, A., 1955. Pyralspite garnets in volcanic rocks. *J. Geol. Soc. Japan*, 61, 463-470.
- Miyashiro, A., 1974. Volcanic rocks series in island arcs and active continental margins. *Am. J. Sci.*, 274, 321-355.
- Miyashiro, A., 1975. Classification, characteristics, and origin of ophiolites. *J. Geol.*, 83, 249-281.
- Miyashiro, A., 1978. Nature of alkalic volcanic rock series. *Contrib. Mineral. Petrol.*, 66, 91-104.
- Miyashiro, A. and Shido, F., 1975. Tholeiitic and calc-alkalic series in relation to the behaviors of titanium, vanadium, chromium, and nickel. *Am. J. Sci.*, 275, 265-277.
- Moore, E.M., 1991. Southwest U.S.-East Antarctic (SWEAT) connection: a hypothesis. *Geology*, 19, 425-428.
- Murphy, J.B. and Nance, R.D., 1991. Supercontinent model for the contrasting character of Late Proterozoic orogenic belts. *Geology*, 19, 469-472.
- Murphy, J.B. and Nance, R.D., 1992. Mountain belts and the supercontinent cycle. *Scientific American*, 34-41.
- Mysen, B.O., 1982. The role of mantle anatexis. In Thorpe, R.S. (ed.) *Andesite*, 489-522.
- Nagasawa, H., 1970. Rare earth concentration in zircon and apatite and their host dacites and granites. *Earth Planet. Sci. Lett.*, 5, 377-381.
- Naney, M.T. and Swanson, S.E., 1980. The effect of Fe and Mg on crystallization in granitic systems. *Am. Mineral.*, 65, 639-653.
- Nelson, B.K. and DePaolo, D.J., 1985. Rapid production of continental crust 1.7 to 1.9 b.y. ago: Nd isotopic evidence from the basement of

- the North American mid-continent. *Geol. Soc. Am. Bull.*, 96, 746-754.
- Nelson, C.A. and Sylvester, A.G., 1971. Wall rock decarbonation and forcible emplacement of Birch Creek pluton, Southern White Mountains, California. *Bull. Geol. Soc. Am.*, 82, 2891-2904.
- Nelson, D.R., McCulloch, M.T. and Sun, S.S., 1986. The origins of ultrapotassic rocks as inferred from Sr, Nd and Pb isotopes. *Geochim. Cosmochim. Acta.*, 50, 231-245.
- Nesbitt, R.W. and Stanley, J., 1980. Compilation of analytical geochemistry reports. Centre for Precambrian Research, Res. Rep., 3, University of Adelaide.
- Nesbitt, R.W., Sun, S.S., and Purvis, A.C., 1979. Komatiites: geochemistry and genesis. *Can. Mineral.*, 17, 165-186.
- Nicholls, I.A. and Harris, K.L., 1980. Experimental rare earth element partition coefficients for garnet, clinopyroxene and amphibole coexisting with andesitic and basaltic liquids. *Geochim. Cosmochim. Acta*, 44, 287-308.
- Norman, M.D., Leeman, W.P. and Mertzman, S.A., 1992. Granites and rhyolites from the northwestern U.S.A.: temporal variation in magmatic processes and relations to tectonic setting. *Trans. Roy. Soc. Edinb.*, 83, 71-81.
- Norrish, K. and Hutton, J.T., 1969. An accurate X-ray spectrographic method for the analysis of a wide range of geological samples. *Geochim. Cosmochim. Acta*, 33, 431-453.
- Norrish, K. and Chappell, B.W., 1977. X-ray fluorescence spectrometry. In: Zussman, J. (ed.) *Physical methods in determinative mineralogy*. 2nd ed., Academic Press, London, 201-272.

- Ogasawara, M., 1988. Geochemistry of the Early Proterozoic granitoids in the Halls Creek Orogenic Subprovince, northern Australia. *Precambrian Res.*, 40/41, 469-486.
- Oliver, R.L., 1956. The origin of garnets in the Borrowdale volcanic series and associated rocks, English Lake District. *Geol. Mag.*, 93, 121-139.
- Oliver, R.L. and Schultz, P.K., 1968. Colour in charnockites. *Mineral. Mag.*, 36, 1135-1138.
- Page, R.W., 1976. Reinterpretation of isotopic ages from the Halls Creek Mobile Zone, northwestern Australia. *BMR J. Aust. Geol. Geophys.*, 1, 79-81.
- Page, R.W., 1988. Geochronology of early to middle Proterozoic fold belts in northern Australia: a review. *Precambrian Res.*, 40/41, 1-19.
- Page, R.W., Blake, D.H., and Mahon, M.W., 1976. Geochronology and related aspects of acid volcanics, associated granites, and other Proterozoic rocks in The Granites-Tanami region, northwestern Australia. *BMR J. Aust. Geol. Geophys.*, 1, 1-13.
- Page, R.W., Bower, M.J. and Guy, D.B., 1985. An isotopic study of granitoids in the Litchfield Block, Northern Territory. *BMR Jour. Aust. Geol. Geophys.*, 9, 219-223.
- Page, R.W., Compston, W., and Needham, R.S., 1980. Geochronology and evolution of the late-Archaean basement and Proterozoic rocks in the Alligator Rivers Uranium Field, Northern Territory, Australia. In: Ferguson, J. and Goleby, A.B. (eds.) *Uranium in the Pine Creek Geosyncline*. International Atomic Energy Agency, Vienna, 39-68.

- Page, R.W. and Hancock, S.L., 1988. Geochronology of a rapid 1.85-1.86 Ga tectonic transition: Halls Creek orogen, northern Australia. *Precambrian Res.*, 40/41, 447-467.
- Page, R.W., McCulloch, M.T. and Black, L.P., 1984. Isotopic record of major Precambrian events in Australia. *Proceedings 27th International Geol. Congress, Precambrian Geology*, 5. VNU Science Press, Amsterdam, 25-72.
- Page, R. and Sun, S.S., 1994. Evolution of the Kimberley region, W.A. and adjacent Proterozoic inliers - new geochronological constraints. *12th Aust. Geol. Convention, Abst.*, 332-333.
- Page, R.W. and Williams, I.S., 1988. Age of the Barramundi Orogeny in northern Australia by means of ion microprobe and conventional U-Pb zircon studies. *Precambrian Res.*, 40/41, 21-36.
- Park, A.F., 1991. Continental growth by accretion: a tectonostratigraphic terrane analysis of the evolution of the western and central Baltic Shield, 2.50 to 1.75 Ga. *Geol. Soc. Am. Bull.*, 103, 522-537.
- Park, R.G., 1995. Palaeoproterozoic Laurentia-Baltica relationships: a view from the Lewisian. *Geol. Soc. Spec. Pub.* 95, 211-224.
- Patchett, P.J. and Arndt, N.T., 1986. Nd isotopes and tectonics of 1.9-1.7 Ga crustal genesis. *Earth Planet. Sci. Lett.*, 78, 329-338.
- Patchett, P.J. and Kouvo, O., 1986. Origin of continental crust of 1.9-1.7 Ga age: Nd isotopes and U-Pb zircon ages in the Svecokarelian terrain of south Finland. *Contrib. Mineral. Petrol.*, 92, 1-12.
- Paterson, S.R., Vernon, R.H. and Fowler, T.K.Jr., 1991. Aureole tectonics. In: Kerrick, D.M. (ed.) *Contact Metamorphism. Reviews Mineral.*, 26, 673-722.

- Paterson, S.R., Vernon, R.H. and Tobisch, O., 1989. A review of criteria for the identification of magmatic and tectonic foliations in granitoids. *Jour. Struc. Geol.*, 11, 349-363.
- Pattison, D.R.M., Carmichael, D.M., and St-Onge, M.R., 1982. Geothermometry and geobarometry applied to early Proterozoic S-type granitoid plutons, Wopmay Orogen, Northwest Territories, Canada. *Contrib. Mineral. Petrol.*, 79, 394-404.
- Peacock, S.M., 1990. Fluid processes in subduction zones. *Science*, 248, 329-337.
- Pearce, J.A., 1975. Basalt geochemistry used to investigate past tectonic environments on Cyprus. *Tectonophysics*, 25, 41-67.
- Pearce, J.A. and Cann, J.R., 1971. Ophiolite origin investigated by discriminant analysis using Ti, Zr and Y. *Earth Planet. Sci. Lett.*, 12, 339-349.
- Pearce, T.H., Gorman, B.E., and Birkett, T.C., 1975. The TiO_2 - K_2O - P_2O_5 diagram: a method of discriminating between oceanic and non-oceanic basalt. *Earth Planet. Sci. Lett.*, 24, 419-426.
- Pearce, T.H., Gorman, B.E., and Birkett, T.C., 1977. The relationship between major element chemistry and tectonic environment of basic and intermediate volcanic rocks. *Earth Planet. Sci. Lett.*, 36, 121-132.
- Peccerillo, A. and Taylor, S.R., 1976. Geochemistry of Eocene calc-alkaline volcanic rocks from the Kastamonu area, northern Turkey. *Contrib. Mineral. Petrol.*, 58, 63-81.
- Perfit, M.R., Brueckner, H., Lawrence, J.R., and Kay, R.W., 1980a. Trace element and isotopic variations in a zoned pluton and associated volcanic rocks, Unalaska Island, Alaska: a model for fractionation in the Aleutian calcalkaline suite. *Contrib. Mineral. Petrol.*, 73, 69-87.

- Perfit, M.R., Gust, D.A., Bence, A.E., Arculus, R.J., and Taylor, S.R., 1980b. Chemical characteristics of island-arc basalts: implications for mantle sources. *Chem. Geol.*, 30, 227-256.
- Peterman, Z.E., 1979. Strontium isotope geochemistry of Late Archean to Late Cretaceous tonalites and trondhjemites. In: Barker, F. (ed.) *Trondhjemites, dacites, and related rocks*. Elsevier Sci. Pub. Co., Amsterdam, 133-147.
- Pettijohn, F.J., 1957. *Sedimentary rocks*. Harper, New York. p.
- Pettingill, H.S. and Patchett, P.J., 1981. Lu-Hf total-rock age for the Amitsoq gneisses, West Greenland. *Earth Planet. Sci. Lett.*, 55, 150-156.
- Pietsch, B.A. and Edgoose, C.J., 1988. The stratigraphy, metamorphism and tectonics of the Early Proterozoic Litchfield Province and western Pine Creek Geosyncline, Northern Territory. *Precambrian Res.*, 40/41, 565-588.
- Pitcher, W.S., 1970. Ghost stratigraphy in intrusive granites: a review. In: Newall, G. and Rast, N. (eds.) *Mechanisms of igneous intrusion*. *Geol. J., Spec. Issue*, 2, 123-140.
- Pitcher, W.S., 1979. The nature, ascent and emplacement of granitic magmas. *J. Geol. Soc. London*, 136, 627-662.
- Pitcher, W.S. and Berger, A.R., 1972. *The geology of Donegal: a study of granite emplacement and unroofing*. Wiley Interscience, London, 435pp.
- Piwinskii, A.J. and Wyllie, P.J., 1968. Experimental studies of igneous rock series: a zoned pluton in the Wallowa batholith, Oregon. *J. Geol.*, 76, 205-234.
- Plumb, K.A., 1968. Lissadell, Western Australia - 1:250000 Geological Series, Bur. Mineral Resour. Aust., Explan. Notes, SE/52-2.

- Plumb, K.A., 1979a. Structure and tectonic style of the Precambrian shields and platforms of northern Australia. *Tectonophysics*, 58, 291-325.
- Plumb, K.A., 1979b. The tectonic evolution of Australia. *Earth Sci. Rev.*, 14, 205-249.
- Plumb, K.A. and Derrick, G.M., 1975. Geology of the Proterozoic rocks of the Kimberley to Mount Isa region. In: Knight, C.L. (ed.) *Economic Geology of Australia and Papua New Guinea*. 1. Metals. Australas. Inst. Min. Metall. Monogr., 5, 217-252.
- Plumb, K.A. and Gemuts, I., 1976. Precambrian geology of the Kimberley region, Western Australia. 25th Int. Geol. Congr., Sydney, Excursion Guide 44C.
- Plumb, K.A., Derrick, G.M., Needham, R.S., and Shaw, R.D., 1981. The Proterozoic of northern Australia. In: Hunter, D.R. (ed.) *Precambrian of the southern hemisphere*. Elsevier Sci. Pub. Co., Amsterdam, 205-307.
- Plumb, K.A., Allen, R. and Hancock, S.L., 1985. Proterozoic evolution of the Halls Creek Province, Western Australia. *Aust. Bur. Miner. Resour. Geol. Geophys. Rec.*, 1985/25.
- Poli, G.E. and Tommasini, S., 1991. Model for the origin and significance of microgranular enclaves in calc-alkaline granitoids. *J. Petrol.*, 32, 657-666.
- Powell, C.McA., Li, Z.X., McElhinny, M.W., Meert, J.G., and Park, J.K., 1993. Paleomagnetic constraints on timing of the Neoproterozoic breakup of Rodinia and the Cambrian formation of Gondwana. *Geology*, 21, 889-892.
- Powell, C.McA., Preiss, W.V., Gatehouse, C.G., Krapez, B., and Li, Z.X., 1994. South Australia record of a Rodinian epicontinental

- basin and its mid-Neoproterozoic breakup (-700Ma) to form the Palaeo-Pacific Ocean. *Tectonophys.*, 237, 113-140.
- Pride, C. and Muecke, G.K., 1980. Rare earth element geochemistry of the Scourian complex N.W. Scotland - evidence for the granite-granulite link. *Contrib. Mineral. Petrol.* 73, 403-412.
- Raase, P., 1974. Al and Ti contents of hornblende, indicators of pressure and temperature of regional metamorphism. *Contrib. Mineral. Petrol.*, 45, 231-236.
- Ramsden, A.R., French, D.H. and Chalmers, D.J., 1993. Volcanic-hosted rare-metals deposit at Brockman, Western Australia, mineralogy and geochemistry of the Niobium Tuff. *Mineral Deposita*, 28, 1-12.
- Rapp, R.P. and Watson, E.B., 1995. Dehydration melting of metabasalt at 8-32 kbar: implications for continental growth and crust-mantle recycling. *Jour. Petrol.*, 36, 891-931.
- Rapp, R.P., Watson, E.B., and Miller, C.F., 1991. Partial melting of amphibolite/eclogite and the origin of Archean trondhjemites and tonalites. *Precamb. Res.*, 51, 1-25.
- Richards, J.R., Berry, H., and Rhodes, J.M., 1966. Isotopic and lead-alpha ages of some Australian zircons. *Jour. Geol. Soc. Aust.*, 13, 69-96.
- Rickwood, P.C., 1989. Boundary lines within petrologic diagrams which use oxides of major and minor elements. *Lithos*, 22, 247-263.
- Ringwood, A.E., 1975. *Composition and petrology of the Earth's mantle.* McGraw Hill, New York, 618 pp.
- Roberts, H.G., Halligan, R., and Playford, P.E., 1968. Mount Ramsay, Western Australia - 1:250000 Geological Series. *Bur. Mineral Resour. Aust., Explan. Notes, SE/52-5.*
- Roberts, M.P. and Clemens, J.D., 1993. Origin of high-potassium, calc-alkaline, I-type granitoids. *Geology*, 21, 825-828.

- Rod, E., 1966. Clues to ancient Australian geosutures. *Eclogae Geol. Helv.*, 59, 849-883.
- Rollinson, H.R. and Windley, B.F., 1980a. Selective elemental depletion during metamorphism of Archaean granulites, Scourie, NW Scotland. *Contrib. Mineral. Petrol.*, 72, 257-263.
- Rollinson, H.R. and Windley, B.F., 1980b. An Archaean granulite-grade tonalite-trondhjemite-granite suite from Scourie, NW Scotland: geochemistry and origin. *Contrib. Mineral. Petrol.*, 72, 265-281.
- Ross, G.M., Parrish, R.R., and Winston, D., 1992. Provenance and U-Pb geochronology of the Mesozoic Belt Supergroup (northwestern United States): implications for age of deposition and pre-Panthalassa plate reconstructions. *Earth Planet. Sci. Lett.*, 113, 57-76.
- Rushmer, T., 1991. Partial melting of two amphibolites: contrasting experimental results under fluid-absent conditions. *Contrib. Mineral. Petrol.*, 107, 41-59.
- Rutland, R.W.R., 1976. Orogenic evolution of Australia. *Earth Sci. Rev.*, 12, 161-196.
- Rutland, R.W.R., 1981. Structural framework of the Australian Precambrian. In: Hunter, D.R. (ed.) *Precambrian of the southern hemisphere*. Elsevier Sci. Pub. Co., Amsterdam, 1-32.
- Rutter, M.J. and Wyllie, P.J., 1988. Melting of vapour-absent tonalite at 10 kbar to simulate dehydration-melting in the deep crust. *Nature*, 331, 159-160.
- Sajona, F.G., Maury, R.C., Bellon, H., Cotten, J., Defant, M.J., and Pubellier, M., 1993. Initiation of subduction and the generation of slab melts in western and eastern Mindanao, Philippines. *Geology*, 21, 1007-1010.

- Sakai, C., Higashino, T., and Enami, M., 1984. REE-bearing epidote from Sanbagawa pelitic schists, central Shikoku, Japan. *Geochem. J.*, 18, 45-53.
- Sawka, W.N., Chappell, B.W., and Norrish, K., 1984. Light-rare-earth-element zoning in shene and allanite during granitoid fractionation. *Geology*, 12, 131-134.
- Sen, C. and Dunn, T., 1994. Dehydration melting of a basaltic composition amphibolite at 1.5 and 2.0 GPa: implications for the origin of adakites. *Contrib. Mineral. Petrol.*, 117, 394-409.
- Sewell, R.J., Darbyshire, D.P.F., Langford, R.L. and Strange, P.J., 1992. Geochemistry and Rb-Sr geochronology of Mesozoic granites from Hong Kong. *Trans. Roy. Soc. Edinb.*, 83, 269-280.
- Sheppard, S., Griffin, T.J., and Tyler, I.M., 1995. Geochemistry of felsic igneous rocks from the southern Halls Creek Orogen. *Geol. Surv. West. Aust. Record*, 1995/4, 81pp.
- Shervais, J.W., 1982. Ti-V plots and the petrogenesis of modern and ophiolitic lavas. *Earth Planet. Sci. Lett.*, 59, 101-118.
- Skjerlie, K.P. and Johnston, A.D., 1992. Vapor-absent melting at 10 kbar of a biotite- and amphibole-bearing tonalitic gneiss: implications for the generation of A-type granites. *Geology*, 20, 263-266.
- Steiger, R.H. and Jager, E., 1977. Subcommittee on geochronology: convention on the use of decay constants in geo- and cosmochronology. *Earth Planet. Sci. Lett.*, 36, 359-362.
- Stephens, W.E. and Halliday, A.N., 1980. Discontinuities in the composition surface of a zoned pluton, Criffell, Scotland. *Bull. Geol. Soc. Am.*, 91, 165-170.

- Stern, C.R. and Wyllie, P.J., 1981. Phase relationships of I-type granite with H₂O to 35 kilobars: the Dinkey Lakes biotite-granite from the Sierra Nevada batholith. *Jour. Geophys. Res.*, 86, 10412-10422.
- Streckeisen, A., 1976. To each plutonic rock its proper name. *Earth Sci. Rev.*, 12, 1-33.
- Sun, S.S., 1982. Chemical composition and origin of the earth's primitive mantle. *Geochim. Cosmochim. Acta*, 46, 179-192.
- Sun, S.S. and Hanson, G.N., 1975. Origin of Ross Island basanitoids and limitations upon the heterogeneity of mantle sources for alkali basalts and nephelinites. *Contrib. Mineral. Petrol.*, 52, 77-106.
- Sun, S.S. and McDonough, W.F., 1989. Chemical and isotopic systematics of oceanic basalts: implications for mantle composition and processes. In Saunders, A.D and Norry, M.J. (eds) *Magmatism in the ocean basins*, *Geol. Soc. Spec. Pub.*, 42, 313-345.
- Sun, S.S. and Nesbitt, R.W., 1977. Chemical heterogeneity of the Archaean mantle, composition of the earth and mantle evolution. *Earth Planet. Sci. Lett.*, 35, 429-448.
- Sun, S.S. and Nesbitt, R.W., 1978. Petrogenesis of Archaean ultrabasic and basic volcanics: evidence from rare earth elements. *Contrib. Mineral. Petrol.*, 65, 301-325.
- Sun, S.S., Nesbitt, R.W., and Sharaskin, A.Y., 1979. Geochemical characteristics of mid-ocean ridge basalts. *Earth Planet. Sci. Lett.*, 44, 119-138.
- Sun, S.S., Jaques, A.L. and McCulloch, M.T., 1986. Isotopic evolution of the Kimberley Block, Western Australia. 4th Int. Kimberlite Conf., *Geol. Soc. Aust. (Abs.)*, 16, 346-348.
- Sun, S.S., Wallace, D.A., Hoatson, D.M., Glikson, A.Y. and Keays, R.R., 1991. Use of geochemistry as a guide to platinum group element potential of mafic-ultramafic rocks: examples from the west Pilbara

- Block and Halls Creek Mobile Zone, Western Australia. *Precambrian Res.*, 50, 1-35.
- Sweet, I.P., Mendum, J.R., Morgan, C.M., and Pontifex, I.P., 1974. The geology of the northern Victoria River region, Northern Territory. *Bur. Mineral Resour. Aust., Rep.*, 166.
- Sylvester, P.J., 1989. Post-collisional alkaline granites. *Jour. Geol.*, 97, 261-280.
- Tarney, J., Weaver, B., and Drury, S.A., 1979. Geochemistry of Archean trondhjemitic and tonalitic gneisses from Scotland and East Greenland. In: Barker, F. (ed.) *Trondhjemites, dacites, and related rocks*. Elsevier Sci. Pub. Co., Amsterdam, 275-299.
- Taylor, S.R. and McLennan, S.M., 1981. The rare earth element evidence Precambrian sedimentary rocks: implications for crustal evolution. In: Kröner, A. (ed.) *Precambrian plate tectonics*, Elsevier Sci. Pub. Co., Amsterdam, 527-548.
- Taylor, R.P., Strong, D.F., and Kean, B.F., 1980. The Topsails igneous complex: Silurian-Devonian peralkaline magmatism in western Newfoundland. *Can. Jour. Earth Sci.*, 17, 425-439.
- Thom, J.H., 1975. Kimberley region. In: *Geology of Western Australia*. West. Aust. Geol. Survey, Mem., 2, 160-193.
- Thornett, J.R., 1981. The Sally Malay deposit: gabbroid-associated nickel-copper sulfide mineralization in the Halls Creek Mobile Zone, Western Australia. *Econ. Geol.*, 76, 1565-1580.
- Tindle, A.G. and Pearce, J.A., 1981. Petrogenetic modelling of in situ fractional crystallization in the zoned Loch Doon pluton, Scotland. *Contrib. Mineral. Petrol.*, 78, 196-207.
- Traves, D.M., 1955. The geology of the Ord-Victoria region, northern Australia. *Bur. Mineral Resour. Aust., Bull.*, 27.

- Troll, G., Farzaneh, A., and Cammann, K., 1977. Rapid determination of fluoride in mineral and rock samples using ion-selective electrode. *Chem. Geol.*, 20, 295-305.
- Tsuchiya, N. and Kanisawa, S., 1994. Early Cretaceous Sr-rich silicic magmatism by slab melting in the Kitakami Mountains, northeast Japan. *Jour. Geophys. Res.*, 99, 22205-22220.
- Turnbull, K.R., 1980. Analysis for rare earth elements by stable isotope dilution mass spectrometry. In: Nesbitt, R.W. and Stanley, J., (Ed.). *Compilation of analytical geochemistry reports. Centre for Precambrian Research, University of Adelaide, Res. Rep.*, 3, 168-177.
- Turner, S.P., Forden, J.D., and Morrison, R.S., 1992. Derivation of some A-type magmas by fractionation of basaltic magma: an example from the Padthaway Ridge, South Australia. *Lithos*, 28, 151-179.
- Tuttle, O.F. and Bowen, N.L., 1958. Origin of granite in the light of experimental studies in the system $\text{NaAlSi}_3\text{O}_8\text{-KAlSi}_3\text{O}_8\text{-SiO}_2\text{-H}_2\text{O}$. *Geol. Soc. Am., Mem.*, 74.
- Tyler, I.M. and Griffin, T.J., 1990. Structural development of the King Leopold Orogen, Kimberley region, Western Australia. *Jour. Struct. Geol.*, 12, 703-714.
- van der Laan, S.R. and Wyllie, P.J., 1992. Constraints on Archean trondhjemite genesis from hydrous crystallization experiments on Nuk gneiss at 10-17 kbar. *Jour. Geol.*, 100, 57-68.
- Van Kranendonk, M.J., St-Onge, M.R., and Henderson, J.R., 1993. Paleoproterozoic tectonic assembly of Northeast Laurentia through multiple indentations. *Precam. Res.*, 63, 325-347.

- Vennum, W.R. and Meyer, C.E., 1979. Plutonic garnets from the Werner batholith, Lassiter Coast, Antarctic Peninsula. *Am. Mineral.*, 64, 268-273.
- Vernon, R.H., 1984. Microgranitoid enclaves in granites - globules of hybrid magma quenched in a plutonic environment. *Nature*, 309, 438- 439.
- Walsh, J.N., Beckinsale, R.D., Skelhorn, R.P., and Thorpe, R.S., 1979. Geochemistry and petrogenesis of Tertiary granitic rocks from the Island of Mull, northwest Scotland. *Contrib. Mineral. Petrol.*, 71, 99-116.
- Watson, E.B., 1979. Zircon saturation in felsic liquids: experimental results and applications to trace element geochemistry. *Contrib. Mineral. Petrol.*, 70, 407-419.
- Weaver, B.L., 1980. Rare-earth element geochemistry of Madras granulites. *Contrib. Mineral. Petrol.*, 71, 271-279.
- Weaver, B.L. and Tarney, J., 1980. Rare earth geochemistry of Lewisian granulite-facies gneisses, northwest Scotland: implications for the petrogenesis of the Archaean lower continental crust. *Earth Planet. Sci. Lett.*, 51, 279-296.
- Weaver, B.L. and Tarney, J., 1981a. The Scourie dyke suite: petrogenesis and geochemical nature of the Proterozoic sub-continental mantle. *Contrib. Mineral. Petrol.*, 78, 175-188.
- Weaver, B.L. and Tarney, J., 1981b. Lewisian gneiss geochemistry and Archaean crustal development models. *Earth Planet. Sci. Lett.*, 55, 171-180.
- Weaver, B.L., Tarney, J., Windley, B.F., and Leake, B.E., 1982. Geochemistry and petrogenesis of Archaean metavolcanic amphibolites from Fiskenaasset, S.W. Greenland. *Geochim. Cosmochim. Acta*, 46, 2203-2215.

- Welin, E., 1987. The depositional evolution of the Svecofennian supracrustal sequence in Finland and Sweden. *Precambrian Res.*, 35, 95-113.
- Wellman, P., 1976a. Gravity trends and the growth of Australia: a tentative correlation. *J. Geol. Soc. Aust.*, 23, 11-14.
- Wellman, P., 1976b. Regional variation of gravity, and isostatic equilibrium of the Australian crust. *BMR J. Aust. Geol. Geophys.*, 1, 297-302.
- Wellman, P., 1978. Gravity evidence for abrupt changes in mean crustal density at the junction of Australian crustal blocks. *BMR J. Aust. Geol. Geophys.*, 3, 153-162.
- Wellman, P., 1979. On the isostatic compensation of Australian topography. *BMR J. Aust. Geol. Geophys.*, 4, 373-382.
- Wells, P.R.A., 1977. Pyroxene thermometry in simple and complex systems. *Contrib. Mineral. Petrol.*, 62, 129-139.
- Whalen, J.B., 1985. Geochemistry of an island-arc plutonic suite: the Uasilau-Yau Yau intrusive complex, New Britain, P.N.G. *Jour. Petrol.*, 26, 603-632.
- Whalen, J.B., Currie, K.L., and Chappell, B.W., 1987. A-type granites: geochemical characteristics, discrimination and petrogenesis. *Contrib. Mineral. Petrol.*, 95, 407-419.
- White, A.J.R. and Chappell, B.W., 1977. Ultrametamorphism and granitoid genesis. *Tectonophysics*, 43, 7-22.
- White, A.J.R. and Chappell, B.W., 1983. Granitoid types and their distribution in the Lachlan Fold Belt, southeastern Australia. *Geol. Soc. Am., Mem.*, 159, 21-34.
- White, A.J.R., Chappell, B.W., and Cleary, J.R., 1974. Geologic setting and emplacement of some Australian Paleozoic batholiths and implications for intrusive mechanisms. *Pacific Geol.*, 8, 159-171.

- White, R. and McKenzie, D., 1989. Magmatism at rift zones: the generation of volcanic continental margins and flood basalts. *Jour. Geophys. Res.*, 94, 7685-7729.
- White, S.H. and Muir, M.D., 1989. Multiple reactivation of coupled orthogonal fault systems: an example from the Kimberley region in north Western Australia. *Geology*, 17, 618-621.
- White, W.H., 1973. Flow structure and form of the Deep Creek stock, Southern Seven Devils Mountains, Idaho. *Bull. Geol. Soc. Am.*, 84, 199-210.
- White, W.M. and Patchett, J., 1984. Hf-Nd-Sr isotopes and incompatible element abundances in island arcs: implications for magma origins and crust-mantle evolution. *Earth Planet. Sci. Lett.*, 67, 167-185.
- Whitney, J.A. and Stormer, J.C., Jr., 1977. Two-feldspar geothermometry, geobarometry in mesozonal granitic intrusions: three examples from the Piedmont of Georgia. *Contrib. Mineral. Petrol.*, 63, 51-64.
- Wilkinson, J.F.G., Duggan, M.B., Herbert, H.K., and Kalocsai, G.I.Z., 1975. The Salt Lick Creek layered intrusion, east Kimberley region, Western Australia. *Contrib. Mineral. Petrol.*, 50, 1-23.
- Williams, H., Hoffman, P.F., Lewry, J.F., Monger, J.W.H., and Rivers, T., 1991. Anatomy of North America: thematic geological portrayals of the continent. *Tectonophysics*, 187, 117-134.
- Wilson, M.R., Hamilton, P.J., Fallick, A.E., Aftalion, M. and Michard, A., 1985. Granites and early Proterozoic crustal evolution in Sweden: evidence from Sm-Nd, U-Pb and O isotope systematics. *Earth Planet. Sci. Lett.*, 72, 376-388.
- Windley, B.F., 1992. Proterozoic collisional and accretionary orogens. In Condie, K.C. (ed.) *Proterozoic Crustal Evolution*. Elsevier, Amsterdam, 419-446.

- Windley, B.F., 1993. Uniformitarianism today: plate tectonics is the key to the past. *Jour. Geol. Soc. Lond.*, 150, 7-19.
- Windley, B.F., 1995. *The Evolving Continents*, 3rd ed., John Wiley, Chichester, 526pp.
- Windrim, D.P., McCulloch, M.T., Chappell, B.W., and Cameron, W.E., 1984. Nd isotopic systematics and chemistry of central Australian sapphirine granulites: an example of rare earth element mobility. *Earth Planet. Sci. Lett.*, 70, 27-39.
- Wolf, M.B. and Wyllie, P.J., 1991. Dehydration-melting of solid amphibolite at 10 kbar: textural development, liquid interconnectivity and applications to the segregation of magmas. *Mineral. Petrol.*, 44, 151-179.
- Wolf, M.B. and Wyllie, P.J., 1994. Dehydration-melting of amphibolite at 10 kbar: the effects of temperature and time. *Contrib. Mineral. Petrol.*, 115, 369-383.
- Wood, B.J. and Banno, S., 1973. Garnet-orthopyroxene and garnet-clinopyroxene relationships in simple and complex systems. *Contrib. Mineral. Petrol.*, 42, 109-124.
- Wood, C.P., 1973. Petrogenesis of garnet-bearing rhyolites from Canterbury, New Zealand. *N.Z. J. Geol. Geophys.*, 17, 759-787.
- Wormald, R.J. and Price, R.C., 1988. Peralkaline granites near Temora, southern New South Wales: tectonic and petrological implications. *Aust. Jour. Earth Sci.*, 35, 209-221.
- Wright, T.L. and Doherty, P.C., 1970. A linear programming and least squares computer method for solving petrologic mixing problems. *Bull. Geol. Soc. Am.*, 81, 1995-2008.
- Wyborn, L.A.I., 1988. Petrology, geochemistry and origin of a major Australian 1880-1840 Ma felsic volcano-plutonic suite: a model for

- intracontinental felsic magma generation. *Precambrian Res.*, 40/41, 37-60.
- Wyborn, L.A.I. and Page, R.W., 1983. The Proterozoic Kalkadoon and Ewen batholiths, Mount Isa inlier, Queensland: source, chemistry, age, and, metamorphism. *BMR J. Aust. Geol. Geophys.*, 8, 53-69.
- Wyborn, L.A.I., Page, R.W. and Paker, A.J., 1987, Geochemical and geochronological signatures in Australian Proterozoic igneous rocks. *Geol. Soc. Spec. Pub.*, 33, 377-394.
- Wyborn, L.A.I., Wyborn, D., Warren, R.G., and Drummond, B.J., 1992. Proterozoic granite types in Australia: implications for lower crust composition, structure and evolution. *Trans. Royal Soc. Edinb.: Earth Sci.*, 83, 201-209.
- Wyllie, P.J., 1984. Sources of granitoid magmas at convergent plate boundaries. *Phys. Earth Planet. Inter.*, 35, 12-18.
- Wyllie, P.J. and Wolf, M.B., 1993. Amphibolite dehydration-melting: sorting out the solidus. *Geol. Soc. Spec. Pub.*, 76, 405-416.
- Young, G.M., 1992. Late Proterozoic stratigraphy and the Canada-Australia connection. *Geology*, 20, 215-218.
- Yurimoto, H., Duke, E.F., Papike, J.J., and Shearer, C.K., 1990. Are discontinuous chondrite-normalized REE patterns in pegmatitic granite systems the results of monazite fractionation? *Geochim. Cosmochim. Acta*, 54, 2141-2145.
- Zhao, J.-X. and Cooper, J.A., 1992. The Atnarpa Igneous Complex, southeast Arunta Inlier, central Australia: implications for subduction at an Early-Mid Proterozoic continental margin. *Precam. Res.*, 56, 227-253.
- Zhao, J.-X. and Cooper, J.A., 1993. Fractionation of monazite in the development of V-shaped REE patterns in leucogranite systems:

evidence from a muscovite leucogranite body in central Australia.
Lithos, 30, 23-32.

Zhao, J.-X. and McCulloch T., 1995. Geochemical and Nd isotopic systematics of granites from the Arunta Inlier, central Australia: implications for Proterozoic crustal evolution. *Precam. Res.*, 71, 265-299.

APPENDIX 1. SAMPLE CATALOGUE

Samples studied and in this thesis are listed in Table A1-1. Table provides sample locations given as grid reference value based on the Australian map grid. Most of sample locations are plotted on figures. Figure numbers on which sample locations are plotted, are also given.

Types of analytical work are indicated for each sample. Samples are listed in ascending order of sample numbers in Table A1-1. Formal sample numbers for this project in the Geology Department contain prefix of A534/. Although it is omitted in this thesis, it should be included in the departmental collection. For example, sample number 51706 should read as A534/51706 in department.

Table A1-1. Sample catalogue

Notes for a sample list

1. Unit: Rock Unit

TM: Tickarala Metamorphics
AM: Amphibolite
FT: Fine grained tonalitic rocks
MG: Meta-gabbro
EG: Eastern Leucocratic Granitoid
DU: Dugalls Granitoid Suite
OR: Ord River Tonalite Suite
WG: Western Porphyritic Granitoid
MD: Meta-dolerite
CG: Central Leucocratic Granitoid
UM: Hornblendite and Mela-gabbro
SA: Sally Downs Tonalite
ME: Mafic microgranular enclaves in the Sally Downs Tonalite
SY: Syn-plutonic dyke in the Sally Downs Tonalite
SG: Granite dyke within the Sally Downs Tonalite
MA: Mabel Downs Granitoid
SO: Sophie Downs Granitoid
BR: Bow River Granitoid
KL: Granitoids from the King Leopold Mobile Zone
WV: Whitewater Volcanics
UD: Undifferentiated rocks

2. Sample location

2.1. Sample location with grid reference values

Sample locations are given as grid reference value based on Australian map grid. Last two digits of 1000 meter grid and additional one digit of 100 meter scale within the grid were read on the each 1/100,000 topographic map. Name of the map and grid reference value of three digits are listed here. East-west direction reading and North-South direction reading are given in X and Y values, respectively.

Abbreviations for name of the 1/100,000 map.

BW: Bow
DX: Dixon
HC: Halls Creek
LD: Leopold Downs
MC: McIntosh
MR: Mount Remarkable
RD: Richenda
TC: Turkey Creek

2.2. Sample locations on figure

Fig.: figure number in which sample location is plotted.

3. Analytical methods

TS: Thin section examination
EP: Electron microprobe analysis
MD: Modal analysis
WR: Whole rock chemical analysis (major and trace elements)
RE: Rare earth element determination with isotope dilution technique.
SR: Sr isotopic analysis

Table A1-1 (1)

	Sample	Unit	Map	X	Y	Fig.	TS	EP	MD	WR	RE	SR
1	11005	OR	MR	921	678	3-24	o			o		
2	11110	FT	TC	935	664	3-2	o	o	o	o		
3	11203	OR	MR	935	668	3-24	o	o	o	o		o
4	11204	OR	MR	935	668	3-24	o			o		o
5	11301	FT	MR	925	674	3-2	o	o		o		
6	11303	UD	MR	924	673	3-2	o			o		
7	11305	OR	MR	924	672	3-24	o			o		
8	11309	UM	MR	924	669	3-5	o	o		o	o	o
9	12702	DU	TC	967	661	3-17	o	o				
10	12703	DU	TC	955	664	3-17	o	o	o	o	o	o
11	13103	KL	LD	547	512	2-25	o		o	o		
12	13104	KL	LD	558	540	2-25	o	o		o		
13	13105	KL	LD	560	560	2-25	o			o		
14	20201	KL	RD	490	640	2-25	o			o		
15	20208	KL	RD	468	642	2-25	o		o	o		
16	20209	KL	RD	469	638	2-25	o			o		
17	20606	MD	TC	939	651	3-5	o	o		o	o	
18	20904	AM	TC	954	650	3-5	o	o				
19	20907	DU	DX	955	647	3-17	o	o		o		o
20	21502	DU	DX	949	609	3-17	o	o		o		
21	21503	DU	DX	948	609	3-17	o		o	o		
22	21602	AM	DX	948	601	3-5	o			o		
23	21603	AM	DX	942	598	3-5	o	o		o		
24	21901	DU	DX	938	610	3-17	o			o		o
25	21902	DU	MC	936	612	3-17	o	o	o	o	o	
26	22101	MG	TC	961	680	3-5	o	o		o		
27	22102	MG	TC	959	679	3-5	o	o				
28	22103	MG	TC	961	681	3-5	o					
29	22105	AM	TC	963	683	3-5	o	o				
30	22107	DU	TC	971	683	3-17	o			o		o
31	22809	SO	HC	776	940	5-1	o			o		o
32	22911	SO	HC	801	937	5-1	o			o		o
33	23002	SO	HC	782	932	5-1	o			o		
34	23005	SO	HC	775	927	5-1	o			o		
35	23007	SO	HC	791	942	5-1	o			o		
36	30101	SO	HC	782	942	5-1	o			o		
37	30107	SO	HC	784	945	5-1	o			o		
38	30114	SO	HC	791	962	5-1	o			o		
39	30205A	SO	HC	762	906	5-1	o			o		
40	30207	SO	HC	761	904	5-1	o			o		
41	30404	SO	HC	755	889	5-1	o			o		
42	30505	SO	HC	767	883	5-1	o			o		
43	30608	SO	HC	784	896	5-1	o	o		o		o
44	30609	SO	HC	780	903	5-1	o			o		
45	30610	SO	HC	781	900	5-1	o			o		

Table A1-1 (2)

	Sample	Unit	Map	X	Y	Fig.	TS	EP	MD	WR	RE	SR
46	30706	SO	HC	803	913	5-1	o	o		o		o
47	30802	SO	HC	823	953	5-1	o	o		o		o
48	30805	SO	HC	815	959	5-1	o			o		
49	31101	SO	HC	812	1004	5-1	o			o		
50	31207	SO	HC	819	980	5-1	o		o	o	o	
51	31303	SO	HC	829	979	5-1	o			o		
52	31304	SO	HC	827	980	5-1	o			o		
53	31305	SO	HC	821	979	5-1	o			o		
54	31306	SO	HC	819	981	5-1	o			o		o
55	31408A	SO	HC	800	994	5-1	o			o		o
56	31413	SO	HC	809	988	5-1	o			o		
57	31414	SO	HC	811	986	5-1	o			o		o
58	31501A	SO	HC	802	953	5-1	o	o		o		
59	31504	SO	HC	801	953	5-1	o			o		
60	31506	SO	HC	798	953	5-1	o			o		
61	31509	SO	HC	784	968	5-1	o			o		
62	32505A	SA	MC	872	624	4-1	o			o		o
63	32506A	SA	MC	874	619	4-1	o			o		
64	32601	SA	MC	897	626	4-1	o			o		
65	32602	SA	MC	898	619	4-1	o			o		
66	32603	SA	MC	898	612	4-1	o			o		
67	32604	SA	MC	904	632	4-1	o			o		
68	32702	MD	MC	895	608	3-5	o			o		
69	32704	SA	MC	892	606	4-1	o			o		
70	32705	SA	MC	898	605	4-1	o			o		
71	32801	SA	MC	891	625	4-1	o			o		
72	32802A	SA	MC	892	619	4-1	o			o		o
73	32809	SA	MC	892	612	4-1	o			o		
74	32810A	SA	MC	891	632	4-1	o			o		
75	32901A	SA	MC	904	626	4-1	o			o		
76	32902A	SA	MC	904	619	4-1	o			o		
77	32903A	SA	MC	904	612	4-1	o	o		o		
78	32904	OR	MC	905	614	3-24	o			o		
79	32907	SA	MC	898	631	4-1	o			o		
80	40201	MD	MC	909	618	3-5	o	o		o		
81	40204	TM	MC	908	620	3-2	o	o				
82	40206	UM	MC	912	616	3-5	o	o		o	o	
83	40301	SA	MC	903	606	4-1	o			o		o
84	40302	SA	MC	906	606	4-1	o			o		
85	40306	EG	MC	920	607	3-10	o	o		o		o
86	40307C	SA	MC	916	639	4-1	o			o		
87	40307F	SA	MC	916	639	4-1	o			o		
88	40402	SA	MC	885	619	4-1	o			o		
89	40403	SA	MC	887	618	4-1	o			o		
90	40404	SA	MC	886	613	4-1	o			o		

Table A1-1 (3)

	Sample	Unit	Map	X	Y	Fig.	TS	EP	MD	WR	RE	SR
91	40406	SA	MC	885	608	4-1	o	o		o	o	
92	40407A	SA	MC	887	626	4-1	o			o		
93	40501A	SA	MC	879	625	4-1	o			o		
94	40502	SA	MC	879	619	4-1	o			o		
95	40503	SA	MC	879	613	4-1	o			o		
96	40505A	SA	MC	880	607	4-1	o			o		o
97	40801A	SA	MC	929	646	4-1	o			o		
98	40802	SA	MC	928	640	4-1	o			o		o
99	40902	SA	MC	866	625	4-1	o			o		
100	40905	SA	MC	866	618	4-1	o			o		
101	40908	SA	MC	867	612	4-1	o			o		
102	40909	SA	MC	867	606	4-1	o			o		
103	41001A	SA	MC	924	640	4-1	o			o		
104	41001B	UD	MC	924	640	4-1	o			o		
105	41002A	SA	MC	910	639	4-1	o			o		
106	41003A	SA	MC	909	633	4-1	o			o		
107	41004	SA	MC	909	626	4-1	o			o		
108	41005	SA	MC	908	633	4-1	o			o		
109	41006A	SA	MC	904	639	4-1	o			o		
110	41008	SA	MC	897	638	4-1	o			o		
111	41009B	SA	MC	885	632	4-1	o			o		
112	41101A	SA	MC	873	613	4-1	o			o		
113	41104	SA	MC	873	606	4-1	o			o		
114	41105	SA	MC	873	601	4-1	o			o		
115	41106A	SA	MC	867	600	4-1	o			o		
116	41202	SA	MC	860	618	4-1	o			o		
117	41203	SA	MC	860	613	4-1	o			o		
118	41204A	SA	MC	861	606	4-1	o			o		
119	41301	SA	MC	854	618	4-1	o			o		
120	41302	SA	MC	855	612	4-1	o			o		
121	41307	SA	MC	853	606	4-1	o			o		
122	41601A	SA	MC	900	588	4-1	o			o		
123	41602	SA	MC	893	588	4-1	o			o		
124	41603	SA	MC	887	588	4-1	o			o		
125	41604	SA	MC	880	588	4-1	o			o		
126	41605	SA	MC	874	588	4-1	o			o		
127	41702	EG	MC	915	592	3-10	o	o		o		o
128	41702B	EG	MC	915	592	3-10	o			o		
129	41705	SA	MC	898	595	4-1	o			o		
130	41706	SA	MC	892	595	4-1	o			o		
131	41802	SA	MC	905	601	4-1	o			o		
132	41803	UM	MC	904	602	3-5	o	o		o		
133	41804	SA	MC	903	601	4-1	o			o		
134	41805	SA	MC	899	601	4-1	o			o		
135	41806	SA	MC	892	600	4-1	o			o		

Table A1-1 (4)

	Sample	Unit	Map	X	Y	Fig.	TS	EP	MD	WR	RE	SR
136	41901	SA	MC	886	601	4-1	o	o		o		
137	41902	SA	MC	881	600	4-1	o			o		
138	41903	SA	MC	880	594	4-1	o			o		
139	41904	SA	MC	875	595	4-1	o			o		
140	41905	SA	MC	886	594	4-1	o			o		
141	42201	SA	MC	898	582	4-1	o			o		
142	42202	SA	MC	893	582	4-1	o			o		
143	42203A	SA	MC	887	582	4-1	o			o		
144	42204	SA	MC	880	582	4-1	o			o		
145	42205A	SA	MC	875	582	4-1	o			o		
146	42301	SA	MC	893	577	4-1	o			o		
147	42302	SG	MC	892	576	4-20	o			o		
148	42303	SA	MC	887	576	4-1	o			o		
149	42304A	SA	MC	880	575	4-1	o			o		
150	42305	SA	MC	876	576	4-1	o			o		
151	42401	SA	MC	887	569	4-1	o			o		
152	42402	SA	MC	881	569	4-1	o	o	o	o	o	
153	42403	SA	MC	874	569	4-1	o			o		
154	42601	SA	MC	880	563	4-1	o			o		
155	42602	SA	MC	876	563	4-1	o			o		
156	42603	SA	MC	870	563	4-1	o			o		
157	42604	SA	MC	869	570	4-1	o			o		
158	42702	SA	MC	875	557	4-1	o			o		
159	42703	SA	MC	869	557	4-1	o			o		
160	42705	SA	MC	864	559	4-1	o			o		
161	42706	DU	MC	881	553	3-17	o	o		o		
162	42707	DU	MC	877	550	3-17	o			o		
163	42708	EG	MC	868	545	3-10	o			o		
164	50201A	SA	MC	850	595	4-1	o			o		
165	50202	SA	MC	849	600	4-1	o			o		o
166	50203B	SA	MC	847	605	4-1	o	o		o		
167	50302	SA	MC	856	598	4-1	o			o		
168	50303	SA	MC	861	601	4-1	o			o		
169	50305	SA	MC	863	595	4-1	o			o		
170	50306	SA	MC	857	594	4-1	o			o		
171	50501A	SA	MC	869	575	4-1	o			o		
172	50502A	SA	MC	869	581	4-1	o			o		
173	50503A	SA	MC	869	588	4-1	o			o		
174	50505	SA	MC	868	593	4-1	o			o		
175	50601A	SA	MC	859	624	4-1	o			o		
176	50602A	ME	MC	860	624	4-20	o	o		o		
177	50602B	ME	MC	860	624	4-20	o	o		o		
178	50603	SA	MC	860	624	4-1	o			o		
179	50604	SA	MC	872	631	4-1	o			o		
180	50702	SA	MC	851	587	4-1	o			o	o	

Table A1-1 (5)

	Sample	Unit	Map	X	Y	Fig.	TS	EP	MD	WR	RE	SR
181	50703	SA	MC	856	587	4-1	o			o		
182	50704	SA	MC	863	589	4-1	o			o		
183	50801	SA	MC	848	613	4-1	o	o	o	o	o	
184	51004	TM	MC	854	637	3-2	o			o		
185	51006	MD	MC	854	634	3-5	o	o		o		
186	51202	CG	MR	914	654	3-2	o			o		
187	51205	SA	MR	928	652	4-1	o			o		
188	51302	OR	MR	919	678	3-24	o	o	o	o	o	o
189	51303	OR	MR	919	678	3-24	o			o		o
190	51304	OR	MR	919	678	3-24	o			o		o
191	51305	OR	MR	919	678	3-24	o			o		o
192	51306	OR	MR	919	678	3-24	o			o		o
193	51307	OR	MR	919	678	3-24	o			o		
194	51309	OR	TC	940	664	3-24	o			o		o
195	51310	OR	TC	940	664	3-24	o			o		o
196	51401	SA	MC	897	646	4-1	o			o		
197	51408	SA	MC	904	647	4-1	o			o		
198	51409A	SA	MC	890	639	4-1	o			o		
199	51410A	SA	MC	885	639	4-1	o			o		
200	51501	SY	MC	902	622	4-20	o	o		o		
201	51502	SY	MC	902	622	4-20	o			o		
202	51504	SY	MC	902	622	4-20	o	o				
203	51505	MD	MC	902	622	3-5	o	o		o		
204	51506	UD	MC	902	622	3-5	o			o		
205	51508	UM	MC	900	625	3-5	o	o		o		
206	51510	SA	MC	911	643	4-1	o			o		
207	51512	ME	MC	911	643	4-20	o			o		
208	51513B	SA	MR	922	652	4-1	o			o		
209	51514	SA	MR	917	652	4-1	o			o		
210	51601	SA	MC	923	646	4-1	o			o		
211	51602	SA	MC	917	646	4-1	o			o		
212	51603	EG	MC	930	635	3-10	o	o		o		
213	51604	DU	TC	975	654	3-17	o	o		o		o
214	51605	DU	TC	975	654	3-17	o	o				
215	51606	DU	TC	976	666	3-17	o			o		
216	51607	EG	TC	956	676	3-10	o	o	o	o	o	
217	51608	EG	TC	956	682	3-10	o			o		
218	51701	SA	MC	880	630	4-1	o			o		
219	51702	ME	MC	880	630	4-20	o	o	o	o	o	o
220	51703	SA	MC	880	630	4-1	o			o		
221	51705A	SA	MC	880	630	4-1	o			o		o
222	51705B	SA	MC	880	630	4-1	o			o		
223	51706	SA	MC	879	629	4-1	o	o	o	o	o	o
224	51709	SA	MC	879	629	4-1	o			o		
225	51710	SA	MC	879	629	4-1	o			o		o

Table A1-1 (6)

	Sample	Unit	Map	X	Y	Fig.	TS	EP	MD	WR	RE	SR
226	51711A	SA	MC	878	629	4-1	o			o		
227	51712	SA	MC	877	630	4-1	o			o		
228	51713	SA	MC	878	630	4-1	o			o		o
229	51714	SA	MC	878	630	4-1	o			o		
230	51715	SA	MC	878	630	4-1	o			o		
231	51901	TM	MC	871	641	3-2	o			o		
232	51902	TM	MC	871	641	3-2	o			o		o
233	51903	TM	MC	871	641	3-2	o			o		
234	51904	TM	MC	871	641	3-2	o			o		o
235	51905	TM	MC	871	641	3-2	o			o		o
236	51907	TM	MC	871	641	3-2	o			o		o
237	51908	TM	MC	871	641	3-2	o			o		
238	51912	OR	MC	872	639	3-24	o			o		
239	51913	OR	MC	872	638	3-24	o	o	o	o	o	
240	51914	OR	MC	872	638	3-24	o			o		
241	51918	WG	MR	883	650	3-2	o	o		o		o
242	52003	DU	TC	192	134	2-21	o			o		
243	52006	MA	TC	196	142	2-21	o	o		o		
244	52008	DU	BW	186	244	2-21	o	o	o	o	o	
245	52009	BR	BW	235	480	2-21	o	o	o	o	o	
246	52101	CG	MC	912	623	3-2	o	o	o	o	o	
247	52103	WG	MC	865	642	3-2	o	o	o	o	o	o
248	52106	MA	MC	753	473	2-22	o			o		
249	73103	MD	MC	929	640	3-5	o	o		o		
250	80902	SA	MC	907	640	4-1	o			o		
251	81001	MD	MC	915	636	3-5	o			o		
252	81507A	SA	MC	908	632	4-1	o			o		
253	81507B	SA	MC	908	632	4-1	o			o		
254	81702	TM	MC	929	623	3-2	o			o		
255	82107	SA	MC	913	630	4-1	o			o		
256	82302	SA	MC	908	624	4-1	o			o		
257	82305	SA	MC	905	622	4-1	o			o		
258	82405	SA	MC	908	627	4-1	o			o		
259	82406	SA	MC	909	626	4-1	o			o		
260	82701	SA	MC	900	622	4-1	o			o		
261	82803	UD	MC	900	625	4-20	o			o		
262	82804	SA	MC	900	625	4-1	o			o		
263	83001	SA	MC	892	626	4-1	o			o		
264	83002	SA	MC	888	624	4-1	o			o		
265	83101	UM	MC	889	629	3-5	o			o		
266	90101	SA	MC	904	646	4-1	o			o		
267	90201	SA	MC	901	640	4-1	o			o		
268	90301	DU	DX	943	593	3-17	o			o		
269	90601	CG	MC	897	639	3-2	o	o		o		
270	90702	SA	MC	878	635	4-1	o			o		

Table A1-1 (7)

	Sample	Unit	Map	X	Y	Fig.	TS	EP	MD	WR	RE	SR
271	90703	SA	MC	877	634	4-1	o			o		
272	90805	WG	MC	872	638	3-2	o			o		
273	90806	TM	MC	872	638	3-2	o			o		
274	90807	OR	MC	872	638	3-24	o	o	o	o	o	
275	91004	OR	TC	938	663	3-24	o			o		
276	91101	EG	TC	950	675	3-10	o			o		
277	91102	EG	TC	949	673	3-10	o			o		
278	91103	EG	TC	952	676	3-10	o			o		
279	91104	EG	TC	956	674	3-10	o			o		
280	91501	BR	MC	611	405	2-23	o			o		
281	91502	DU	MC	605	409	2-23	o	o		o		
282	91507	BR	MC	610	450	2-22	o		o	o		
283	91508	BR	MC	612	404	2-23	o	o	o	o	o	
284	91606	WV	MR	515	700	2-22	o			o	o	
285	91608	WV	MR	516	687	2-22	o	o				
286	91904	SO	HC	812	934	5-1	o			o		
287	91906	SO	HC	806	933	5-1	o			o		
288	91908	SO	HC	810	934	5-1	o			o		
289	92006	SO	HC	776	940	5-1	o	o	o	o	o	
290	92401	SA	MC	919	641	4-1	o			o		
291	92402	SA	MC	874	628	4-1	o			o		
292	92403	MA	MC	752	472	2-22	o			o		
293	92404	MA	MC	750	467	2-22	o	o		o		
294	CU 2	BR				-	o			o		

APPENDIX 2. MODAL COMPOSITION OF GRANITOIDS

Modal compositions of granitoid samples were determined on the stained rock slabs or on stained thin sections. The modal composition is important not only as a constituent of the basic petrographic characteristics but also to provide an appropriate rock name based on the classification scheme recommended by the IUGS (Streckeisen, 1976).

1. Staining of samples

Rock slabs or thin sections were etched with hydrofluoric acid, then dipped in a saturated solution of sodium cobaltinitrite. This procedure results in K-feldspar being stained bright yellow. Plagioclase and quartz are easily distinguished as the former becomes white on etching with hydrofluoric acid, and the latter remains clear.

2. Point Counting

A Swift automatic point counter on a petrographic microscope was used for point counting on thin sections, points being on a 0.33 x 1mm grid.

A Leitz mechanical XY stage fitted on a wooden board under binocular microscope was used for point counting on stained rock slabs, points being on a 2 x 2 mm grid. Samples which have coarse grain size, such as the Bow River Granitoid, were analysed on stained rock slabs.

Number of counts ranged from 1000 to 1900 for each sample. 23 representative samples of granitoids from the Halls Creek Mobile Zone and King Leopold Mobile Zone were analysed.

3. Results of modal analysis

Modal compositions of granitoids are presented in Table A2-1.

Table A2-1. Modal compositions of granitoids

Rock Unit	FT	EG	DU	DU	DU	DU	OR	OR	OR
Sample	11110	51607	12703	21503	21902	52008	11203	51302	51913
Quartz	21.43	39.6	28.46	32.45	30.05	9.67	30.66	18.99	32.37
K-feldspar	0	21.54	0	0	0	0	0	0	0
Plagioclase	52.51	37.47	60.93	63.08	57.44	62.25	54.98	58.82	43.69
Biotite	11.49	0	7.93	2.92	11.69	8.73	13.96	16.96	19.36
Hornblende	13.42	0	1.5	1.55	0	4.04	0	1.16	0
Orthopyroxene	0	0	0.83	0	0	13.43	0	0	0
Muscovite	0	0.32	0	0	0	0	0.2	0.1	0
Epidote	0.19	0	0	0	0	0	0	2.81	3.77
Apatite	0.29	0	0	0	0.18	0	0	0.29	0.5
Sphene	0	0	0	0	0	0	0	0.19	0
Oxide	0.39	0.64	0.25	0	0	1.78	0.2	0.58	0.1
Zircon	0.29	0	0	0	0	0.1	0	0	0.1
Garnet	0	0.43	0	0	0	0	0	0	0
Sericite	0	0	0.08	0	0	0	0	0	0
Chlorite	0	0	0	0	0	0	0	0	0
Carbonate	0	0	0	0	0.64	0	0	0.1	0.1
Total	100.01	100.00	99.98	100.00	100.00	100.00	100.00	100.00	99.99
Qz	28.98	40.16	31.84	33.97	34.35	13.45	35.80	24.41	42.56
K-f	0.00	21.84	0.00	0.00	0.00	0.00	0.00	0.00	0.00
Pl	71.02	38.00	68.16	66.03	65.65	86.55	64.20	75.59	57.44

Rock Unit code: same as Table A1-1

Qz=100XQuartz/(Quartz+K-feldspar+Plagioclase)

K-F=100XK-feldspar/(Quartz+K-feldspar+Plagioclase)

Pl=100XPlagioclase/(Quartz+K-feldspar+Plagioclase)

APPENDIX 3. MAJOR AND TRACE ELEMENT ANALYTICAL TECHNIQUES

A3.1. Pulverising Techniques for Whole Rock Chemical Analysis

Rock samples of between 0.3 and 10 kg weight were collected from the field for chemical analysis with a geological hammer and sledge hammer. Weight of samples collected varied with grain size, viz. a large sample for coarse grain. Sample weight of typical coarse grained Bow River Granitoid was more than 5kg.

Rock samples were cleaned of all weathered surfaces initially with a hammer. A rock slab was taken from each sample with a diamond saw. Any weathered surface which was not removed by means of a hammer, was removed by means of the saw. A large sample was broken into small fragments with a screw-type rock splitter.

The sample was then reduced to fragments of 10mm or less, in a jaw crusher.

This crushed sample was then quartered on paper several times to reduce the sample to about 100-500 g for final grinding. The sample was then pulverised in a tungsten-carbide swing-mill, in maximum of 150g maximum lots. If the necessary sample weight exceeded 150g, batches of powder from each sample so produced were then recombined and thoroughly mixed in a plastic bag.

A3.2. Major Element Analytical Techniques

Major element analysis was performed using X-ray fluorescence spectrometry. Fused glass discs were prepared for the analysis using the method of Norrish and Hutton (1969).

Thus rock powders were dried at 110°C. The rock powders were then ignited at about 1000°C. Loss on ignition was determined.

Each disc was prepared from 1.5g of flux, 0.02g of sodium nitrate and 0.28g of ignited sample. The flux was prepared from a mixture comprising lithium tetraborate, lithium carbonate, and lanthanum oxide; known as the Norrish composition.

Na₂O contents were determined either by flame photometry or X-ray fluorescence spectrometry method using a boric acid-backed pressed pellet which was used for trace element analysis.

The major elements were analysed using a Siemens SRS1 automatic X-ray fluorescence spectrometer with a 10 sample holder. Instrumental settings for the spectrometer are given in Table A3-1. Matrix corrections were made on nominal percentage reading from the X-ray fluorescence spectrometer using the method of Norrish and Hutton (1969).

Monitor standard FS-11 was used for the analyses. In every batch of analyses, FS-11 was calibrated against international standards.

Analytical results of two standard samples are given in Table A3-2 to indicate the precision and accuracy of analysis.

A3.3. FeO Determination Technique and Results

FeO contents were determined on 18 samples by titration method. Sample powder of 0.25g was dissolved by 10ml of 1:1 H₂SO₄ and 5ml of HF in a platinum crucible with a close fitting lid. The crucible was placed on a hot plate at 300-350°C. Content of the crucible was transferred into a previously prepared H₂SO₄-H₃BO₄ solution. The solution was immediately titrated with ceric sulphate solution.

The results of FeO determinations are presented in Table A3-3. Fe₂O₃ values were calculated from total Fe content obtained by X-ray fluorescence spectrometer.

A3.4. Fluorine Determination Technique and Results

Fluorine contents were determined on 8 samples by the selective ion electrode method. This analytical method used is largely similar to that of Troll et al. (1977).

Sample powder of 1g was fused with Na₂CO₃ flux of 8g in a platinum crucible. The crucible was placed in a furnace at a temperature of 1000°C, then was put onto a burner to complete the melting. After cooling, the fused sample was dissolved in dilute hydrochloric acid and made up to a volume of 250ml. An aliquot of this solution (5ml) was then mixed with 50ml of buffer solution and left for one hour to ensure complete complexing of iron and aluminium. Calibration was achieved by means of a standard addition technique. Analysis blank (0.7ppm) was subtracted from the analytical results.

The results of fluorine determination are presented in Table A3-4. As the Sophie Downs Granitoid contains fluorite as an accessory mineral, three samples from the granitoid were selected for analysis. Two of the samples show a high fluorine concentration. Samples of the Bow River Granitoid and Whitewater Volcanics also show high fluorine concentration.

A3.5. Trace Element Analytical Techniques

Boric acid-backed, pressed pellets were prepared after the method of Norrish and Chappell (1977) for the analysis of trace elements and Na. Pellets were made with 3-4 g of rock powder. Norrish and Chappell (1977) suggested that a 2g sample would be infinitely thick for elements up to about atomic number 40 (Zr).

A Siemens SRS1 X-ray fluorescence spectrometer was used for trace element analysis. The instrumental settings used in this study are given in Table A3-5. The mass absorption coefficients used for matrix correction

were calculated from the major element composition, or were estimated from Compton scatter peak intensity.

Details of the analytical procedures for each trace element can be found in Nesbitt and Stanley (1980).

Precision of analysis was examined for Rb and Sr analyses. Three pellets were prepared from a sample 51706. Each of pellets was analysed three times. Statistics for a total of 9 measurements are given in Table A3-6. Relative standard deviations for 40 ppm Rb and 620 ppm Sr are 0.55% and 0.13%, respectively, indicating extremely good precision of analysis.

The accuracy of the trace element analyses was assessed by analysing 8 international standard reference samples. Their results of analysis with recommended values are given in Table A3-7.

Table A3-1. Instrumental settings of X-ray fluorescence spectrometer for major elements analysis

Element	Analytical Line	Crystal	Angle	Collimeter	Detector	Counting Time (s)
Si	K α	PET	109.000	C	FPC	100
Ti	K α	LiF200	86.232	F	FPC	20
Al	K α	PET	144.920	C	FPC	100
Fe	K α	LiF200	57.540	C	FPC	20
Mn	K α	LiF220	95.295	F	FPC	100
Mg	K α	TIAP	45.405	C	FPC	100
Ca	K α	LiF200	113.204	F	FPC	20
K	K α	PET	50.553	F	FPC	100
Na	K α	TIAP	55.250	C	FPC	200
P	K α	PET	89.340	C	FPC	100

Instrument: Simens SRS2
 60kV, 40mA on chromium anorode X-ray tube.
 Analysis under vacuum condition
 Collimeter C: coarse, F: fine
 Detector FPC: flow propotional counter

Table A3-2. Major elements analyses of standard samples by x-ray fluorescence spectrometry

A. JG-1

	A	B	A	B	C	Av.	Rec.
(wt%)							
SiO ₂	72.61	72.03	72.48	71.88	72.43	72.29	72.30
Al ₂ O ₃	14.32	14.27	14.33	14.23	14.22	14.27	14.20
Fe ₂ O ₃ *	2.11	2.08	2.10	2.10	2.10	2.10	2.14
MnO	0.06	0.06	0.06	0.05	0.06	0.06	0.06
MgO	0.69	0.76	0.71	0.68	0.86	0.74	0.74
CaO	2.17	2.14	2.17	2.15	2.17	2.16	2.18
Na ₂ O	3.28	3.28	3.28	3.28	3.28	3.28	3.39
K ₂ O	4.01	3.98	4.00	3.96	3.94	3.98	3.95
TiO ₂	0.25	0.26	0.25	0.25	0.26	0.25	0.26
P ₂ O ₅	0.08	0.08	0.08	0.08	0.10	0.08	0.10
LOI	0.49	0.49	0.49	0.49	0.49	0.49	
Total	100.07	99.43	99.95	99.15	99.91	99.70	

Duplicate analysis on glass beads of A and B and single analysis on a glass bead of C

B. JB-1

	A	B	A	B	A	B	C	Av.	Rec.
(wt%)									
SiO ₂	52.69	52.50	52.79	52.41	52.78	52.50	52.66	52.61	52.17
Al ₂ O ₃	14.85	14.81	14.81	14.75	14.81	14.64	14.74	14.77	14.53
Fe ₂ O ₃ *	8.97	8.95	8.93	8.94	8.93	8.94	9.00	8.95	8.97
MnO	0.16	0.16	0.15	0.14	0.15	0.14	0.16	0.15	0.16
MgO	7.92	7.96	8.04	7.88	7.86	7.92	8.10	7.95	7.73
CaO	9.28	9.28	9.32	9.25	9.32	9.28	9.31	9.29	9.29
Na ₂ O	2.69	2.69	2.69	2.69	2.69	2.69	2.69	2.69	2.79
K ₂ O	1.47	1.44	1.44	1.43	1.43	1.41	1.42	1.43	1.42
TiO ₂	1.30	1.30	1.32	1.30	1.32	1.30	1.31	1.31	1.34
P ₂ O ₅	0.26	0.25	0.27	0.25	0.25	0.26	0.26	0.26	0.26
LOI	0.44	0.44	0.44	0.44	0.44	0.44	0.44	0.44	
Total	100.01	99.78	100.20	99.48	99.98	99.52	100.09	99.85	

Triplicate analysis on glass beads of A and B and single analysis on a glass bead of C

Av.: Average

Rec.: Recommended value from Ando et al. (1987)

Fe₂O₃*: Total Fe as Fe₂O₃

LOI: Loss on ignition

Table A3-3. Results of FeO determination

Sample	Rock type	FeO(%)	Fe ₂ O ₃ (%)	Fe ₂ O ₃ *(%)	FeO/FeO*
90806	TM	3.83	1.90	6.01	0.68
81001	MD	7.73	2.82	11.12	0.75
80902	SA	3.9	1.96	6.15	0.68
82302	SA	3.67	2.51	6.45	0.61
82305	SA	4.2	2.64	7.15	0.63
82405	SA	2.65	2.12	4.97	0.57
83001	SA	3.55	2.25	6.06	0.63
90101	SA	3.57	1.61	5.44	0.70
92401	SA	3.68	1.58	5.53	0.71
92402	SA	3.78	1.30	5.36	0.76
92403	MA	2.81	2.53	5.55	0.54
92404	MA	2.66	2.17	5.03	0.57
91904	SO	1.43	0.15	1.69	0.91
91906	SO	1.37	0.50	1.97	0.75
91908	SO	0.92	0.54	1.53	0.65
92006	SO	0.86	0.81	1.73	0.53
91501	BR	2.86	0.70	3.77	0.81
91507	BR	3.18	1.22	4.64	0.74

Fe₂O₃*: Total Fe as Fe₂O₃ obtained by XRF analysis

FeO*: Total Fe as FeO

Table A3-4. Results of fluorine determination

Sample	Rock type	F (ppm)
50801	SA	598
51706	SA	935
30706	SO	1550
31207	SO	825
31501A	SO	1825
52009	BR	2250
91508	BR	1113
91606	WV	1575
GSP-1	Standard	4050

Recommended value of GSP-1: 3630ppm

Table A3-5. Instrumental settings of X-ray fluorescence spectrometer for trace element analysis

Element	Line	Tube	Crystal	Coll	Det	Vac	D.L.	Line Corr.	Standard	M.A.
Ba	L α	Cr	200	F	F	Yes	3.4	TiK α	VHG+Ba+Sc	W
Sc	K α	Cr	200	C	F	Yes	0.9	CaK α	VHG+Ba+Sc	W
Rb	K α	Mo/W	220	F	S	No	1.1	SrK α ,UL α 1,ThL α 1	MBM+BCC+Y	C/W
Sr	K α	Mo/W	220	F	S	No	1.0	RbK α	MBM+BCC+Y	C/W
Y	K α	Mo/W	220	F	S	No	1.1	RbK α ,ThL β 2,4	MBM+BCC+Y	C/W
Zr	K α	Au	220	F	S	No	2.0	ThL β 1,2,SrK β 1,3,UL β	Zr+Nb Spk	C
Nb	K α	Au	220	F	S	No	.5	UL β 4,ZrK α	Zr+Nb Spk	C
Ce	L β 1	W	220	C	F	Yes	7.5	NdL α 1	G2	W
Nd	L α 1	W	220	C	F	Yes	4.5	CeL β 1	G2	W
V	K α	W	220	C	F	Yes	1.9	TiK β	MDP+V	W
Ni	K α	Au	220	C	S	No	2.8		PCC-1	C
Cr	K α	Mo	200	C	S	Yes	4.3	VK β	MBM+BCC+Y+Cr	C
Zn	K α	Au	220	C	S	No	1.3		MRG-1	C
Cu	K α	Au	220	C	S	No	1.7		MRG-1	C
Ga	K α	Mo	220	C	S	No	2.9		Fe Mica	W

Crystal: 200(=LiF200) or 220(LiF220)

Coll: Collimator, F: fine, C: coarse

Det: Detector, F: Flow proportional counter, S: Scintillation counter

Vac: Vacuum

D.L.: Detection limit in ppm

Line Corr.: Lines corrected for interference

Standard: Standard used for analysis

M.A.: Mass absorption correction factors, W: calculated from whole rock analysis data, C: calculated from Compton peak

Table A3-6. X-ray fluorescence analysis of Rb and Sr on sample 51706, for the examination of precision of the analysis

Pellet No.	Analysis	Rb (ppm)	Sr (ppm)	Rb/Sr
Pellet(1)	1	41.99	621.5	0.06756
	2	42.13	623.2	0.06760
	3	41.63	624.3	0.06668
	Average	41.91	623.0	0.06728
Pellet(2)	1	41.85	622.8	0.06719
	2	41.48	624.1	0.06646
	3	42.04	622.9	0.06749
	Average	41.79	623.3	0.06705
Pellet(3)	1	41.92	622.7	0.06731
	2	41.74	622.4	0.06706
	3	41.44	622.9	0.06653
	Average	41.70	622.7	0.06697
Grand Average		41.80	623.0	0.06710
Standard Deviation		0.28	0.8	0.00042
R.S.D.		0.55(%)	0.13(%)	0.62(%)

Three pellet have been prepared from the sample 51706.

Each pellet has been analysed three times.

R.S.D.: Relative standard deviaton,

100 X (Grand Average / Standard Deviation)

Table A3-7. Trace elements analyses of standard samples by x-ray fluorescence spectrometry

	JB-1		JB-2		JA-1		JG-1		JR-1		AGV-1		BCR-1		GSP-1	
	XRF	Rec	XRF	Rec	XRF	Rec	XRF	Rec	XRF	Rec	XRF	Rec	XRF	Rec	XRF	Rec
Ba	526	490	234	208	306	307	461	462	47	40	1188	1226	688	681	1310	1310
Ce	-	-	-	-	19	13.2	-	-	-	-	73	67	-	-	315	399
Cr	458	469	20	27.4	1	7.3	54	64.6	1	2.3	13.4	10.1	18	16	13	13
Cu	58	56.3	244	227	46	42.2	5	1.5	4.2	1.4	62	60	-	-	33	33
Ga	18	18.1	17.6	17	17	17.3	18	17	16.8	17.6	20	20	-	-	22	23
Nb	37	34.5	0.7	0.8	1	1.7	12.8	12.6	14.1	15.5	14.5	15	12.5	14	26	27.6
Nd	-	-	-	-	9	11	-	-	-	-	32	33	-	-	152	196
Ni	125	139	14.7	14.2	3.1	1.8	5	6	1.4	0.66	17.4	16	14.2	13	16.3	8.8
Rb	40	41.2	6.5	6.2	11.2	11.8	177	181	257	257	67	67.3	48	47.2	250	254
Sc	24.9	27.4	57	54	31.1	28.4	9.1	6.5	5.2	5.2	15	12.2	31.4	32.6	6.2	6.2
Sr	448	435	180	178	260	266	185	184	28	30	658	662	334	330	232	234
V	208	212	598	578	111	105	32	25	6.7	9	123	121	400	407	53	53
Y	24.4	24	25.1	26	32	31.4	27.6	30	49	46	20.2	20	39.2	38	25.9	26
Zn	81	83	108	110	85	90.6	40	41.5	28	30	83	88	-	-	101	104
Zr	134	143	45.6	52	82	87	107	108	99	102	227	227	184	190	513	530

XRF: present study

Rec: recommended values from Govindaraju (1989)

APPENDIX 4. RESULTS OF MAJOR AND TRACE ELEMENT ANALYSIS OF GRANITOIDS

Results of major and trace element analyses of granitoids are presented here. Details of analytical techniques are given in Appendix 3. Results of FeO and fluorine analyses of selected samples are listed in Appendix 3. Techniques and results of complete rare earth element analyses of selected samples are listed in Appendix 5.

Results of major and trace element analysis of samples excluding granitoids are found in tables of the main text; Tables 3-1, 3-2, 3-4, 3-6, 3-11, 3-14, 4-9, 5-3. Chemical compositions of the Sally Downs Tonalite are listed in three groups based on sampling strategy (see section 4.1 for details).

Major and trace element data of granitoids are presented in the following tables,

Table A4-1. Chemical compositions of Fine Grained Tonalitic Rocks

Table A4-2. Chemical compositions of the Eastern Leucocratic Granitoid

Table A4-3. Chemical compositions of the Dougalls Granitoid Suite

Table A4-4. Chemical compositions of the Ord River Tonalite Suite

Table A4-5. Chemical compositions of the Western Porphyritic Granite and the Central Leucocratic Granite

Table A4-6(A). Chemical compositions of the Sally Downs Tonalite (grid samples)

Table A4-6(B). Chemical compositions of the Sally Downs Tonalite (samples for chemical variability assessment and geochronology)

Table A4-6(C). Chemical compositions of the Sally Downs Tonalite (samples for initial examination)

Table A4-7. Chemical compositions of the Mabel Hill Tonalite and a tonalite from the main body of the Mabel Downs Granitoid Suite

Table A4-8. Chemical compositions of the Sophie Downs Granitoid

Table A4-9. Chemical compositions of the Bow River Granitoid

Table A4-10. Chemical compositions of granitoids from the King Leopold Mobile Zone

Table A4-11. Chemical compositions of miscellaneous granitoids from the Sally Downs Bore area

Table A4-1. Chemical compositions of Fine Grained Tonalitic Rocks

Sample	11110	11301
Major elements (%)		
SiO ₂	61.79	61.92
Al ₂ O ₃	17.05	17.62
Fe ₂ O ₃ *	5.53	5.96
MnO	0.08	0.07
MgO	3.01	2.12
CaO	5.89	4.96
Na ₂ O	3.6	3.68
K ₂ O	1.47	2.01
TiO ₂	0.62	0.69
P ₂ O ₅	0.18	0.21
LOI	0.51	0.57
Total	99.73	99.81
Trace elements (ppm)		
Ba	420	829
Rb	35.3	83
Sr	511	477
Zr	105	208
Nb	5.5	9.1
Y	12	15.4
Ce	38	123
Nd	19	50
Sc	16.7	14.8
V	102	75
Cr	56	5
Ni	25.8	11.8
Cu	23	31
Zn	60	71
Ga	19	22.1
Ratio		
K/Ba	29.06	20.13
K/Rb	345.7	201.0
Rb/Sr	0.069	0.174
FeO*/MgO	1.71	2.62
Na ₂ O/K ₂ O	2.45	1.83
A/CNK	0.936	1.022

Fe₂O₃*: Total Fe as Fe₂O₃, LOI: Loss on ignition
A/CNK: Mol. Al₂O₃/CaO+Na₂O+K₂O

Table A4-2. Chemical compositions of the Eastern Leucocratic Granitoid

Sample	40306	41702	41702B	42708	51603	51607
Unit	EG	EG	EG	EG	EG	EG
Type	II (Garnet)	II (Garnet)	II (Garnet)	II -	I (Garnet)	I (Garnet)
Major elements (%)						
SiO ₂	75.40	74.55	75.09	70.27	77.08	76.65
Al ₂ O ₃	13.29	13.53	13.24	14.94	12.64	12.35
Fe ₂ O ₃ *	1.67	1.93	1.82	3.70	1.13	1.14
MnO	0.04	0.06	0.06	0.09	0.04	0.08
MgO	0.17	0.35	0.16	0.95	0.02	0.00
CaO	1.64	1.70	1.65	3.23	0.96	1.22
Na ₂ O	4.62	4.66	4.68	4.93	4.68	4.21
K ₂ O	2.73	2.75	2.72	1.25	3.16	3.35
TiO ₂	0.10	0.10	0.09	0.27	0.04	0.04
P ₂ O ₅	0.02	0.02	0.02	0.06	0.01	0.01
LOI	0.19	0.23	0.19	0.33	0.13	0.21
Total	99.87	99.88	99.72	100.02	99.89	99.26
Trace elements (ppm)						
Ba	683	672	689	333	841	1175
Rb	60	46.6	46.1	39.5	47.6	40.6
Sr	90	84.7	82	152	36.6	63
Zr	93	96	96	169	80.8	78.5
Nb	14.2	12.5	12.2	19.2	10.1	0.8
Y	46.8	38.6	38	88	47.2	37.7
Ce	28	22	17	28	29	11
Nd	11	14	9.3	14	6	5
Sc	2.4	2.6	2.1	5.3	0.9	1.4
V	5.9	5.9	4.5	29	0	0
Cr	0	2	0	0	0	0
Ni	4.6	2	3.7	7.7	2	0
Cu	3	3	5	3	5	6
Zn	68	87	85	95	65	29
Ga	22.2	22.9	22.3	N.D.	22.5	19.8
Ratios						
A/CNK	0.982	0.985	0.970	0.974	0.983	0.967
NK/A	0.794	0.787	0.804	0.633	0.880	0.854
10000Ga/Al	3.16	3.20	3.18	-	3.36	3.03
K/Ba	33.2	34.0	32.8	31.2	31.2	23.7
K/Rb	378	490	490	263	551	685
Rb/Sr	0.667	0.550	0.562	0.260	1.301	0.644

Fe₂O₃*: Total Fe as Fe₂O₃, LOI: Loss on ignition

N.D.: Not determined

A/CNK: Mol. Al₂O₃/CaO+Na₂O+K₂O, NK/A: Mol. Na₂O+K₂O/Al₂O₃

Table A4-2. (continued)

Sample	51608	91101	91102	91103	91104
Unit	EG	EG	EG	EG	EG
Type	I	III	I	I	III
	-	-	(Garnet)	-	-
Major elements (%)					
SiO ₂	77.06	78.55	76.87	76.62	77.84
Al ₂ O ₃	12.54	12.10	12.66	12.82	12.97
Fe ₂ O ₃ *	1.19	1.28	1.51	1.36	0.31
MnO	0.00	0.02	0.05	0.00	0.00
MgO	0.19	0.34	0.03	0.00	0.04
CaO	1.08	2.62	1.26	1.22	2.91
Na ₂ O	4.18	3.57	4.50	3.25	4.15
K ₂ O	3.60	0.81	3.16	4.38	0.66
TiO ₂	0.04	0.13	0.05	0.05	0.03
P ₂ O ₅	0.01	0.03	0.00	0.01	0.01
LOI	0.23	0.32	0.13	0.29	0.37
Total	100.12	99.77	100.22	100.00	99.29
Trace elements (ppm)					
Ba	1222	405	1188	2266	276
Rb	31.7	16.6	41.7	51	6.2
Sr	86	286	70	160	221
Zr	73	129	89	108	82
Nb	0.4	4.4	1.3	0.9	0
Y	4	8.9	29.7	4.5	1.3
Ce	7.2	74	22	10	8
Nd	0.9	26	8	0	4
Sc	0.8	3.1	1.1	1.2	1.6
V	0	8	0	0	2
Cr	0	0	0	0	0
Ni	1.2	2.9	2	5.8	4.5
Cu	13	23	11	8	6
Zn	16	23	36	16	10
Ga	17.6	14.2	20.9	15.4	14.9
Ratios					
A/CNK	0.985	1.051	0.965	1.042	1.011
NK/A	0.859	0.558	0.855	0.787	0.581
10000Ga/Al	2.65	2.22	3.12	2.27	2.17
K/Ba	24.5	16.6	22.1	16.0	19.9
K/Rb	943	405	629	713	884
Rb/Sr	0.369	0.058	0.596	0.319	0.028

Fe₂O₃*: Total Fe as Fe₂O₃, LOI: Loss on ignition

N.D.: Not determined

A/CNK: Mol. Al₂O₃/CaO+Na₂O+K₂O, NK/A: Mol. Na₂O+K₂O/Al₂O₃

Table A4-3. Chemical compositions of the Dougalls Granitoid Suite

Sample	12703	20907	21502	21503	21901	21902	22107	42706
Unit	DU	DU	DU	DU	DU	DU	DU	DU
Rock	P-Tn	P-Tn	Tn	Tr	P-Tn	Tn	P-Tn	Tn
Major elements (%)								
SiO ₂	68.80	68.97	57.75	73.19	68.20	69.55	67.21	67.93
Al ₂ O ₃	16.05	15.45	18.35	15.43	16.40	15.74	16.74	16.26
Fe ₂ O ₃ *	3.17	3.81	7.08	0.84	3.68	3.06	3.80	3.42
MnO	0.03	0.04	0.11	0.00	0.03	0.01	0.06	0.03
MgO	1.24	1.03	3.23	0.25	1.15	1.00	1.45	1.17
CaO	4.12	3.89	7.53	4.62	4.65	3.96	4.76	4.53
Na ₂ O	4.36	4.45	4.02	4.49	4.60	4.40	4.46	4.53
K ₂ O	1.17	1.20	0.57	0.38	0.86	1.18	1.07	1.10
TiO ₂	0.32	0.35	0.70	0.09	0.36	0.30	0.36	0.37
P ₂ O ₅	0.07	0.12	0.14	0.05	0.09	0.07	0.10	0.09
LOI	0.47	0.32	0.42	0.24	0.22	0.51	0.28	0.59
Total	99.80	99.63	99.90	99.58	100.24	99.78	100.29	100.02
Trace elements (ppm)								
Ba	519	549	221	243	469	619	533	418
Rb	34.5	28.6	13.3	9.1	21	31.4	25.1	30.9
Sr	363	332	375	390	374	294	377	379
Zr	112	132	106	95	168	130	108	162
Nb	5.7	4.4	2.9	0.7	3.6	6.7	3.6	3.8
Y	5	3.8	11.5	0	4.8	0	6.2	3.5
Ce	29	26	24	9.6	31	22	17	16
Nd	11	15	15	4	12	4	12	6
Sc	6.6	7.7	22.4	3.4	8.4	5	10	7.2
V	28	31	109	11	36	27	42	33
Cr	9	9	47	3	11	9	21	13
Ni	10	9.1	30	4.2	9.5	9	15.3	10
Cu	7	44	34	7	4	5	4	12
Zn	45	51	63	11	51	38	41	41
Ga	17.7	19.5	19.8	15.4	17.8	18.8	18.9	18.8
Ratio								
K/Ba	18.71	18.15	21.41	12.98	15.22	15.83	16.67	21.85
K/Rb	281.5	348.3	355.8	346.7	340.0	312.0	353.9	295.5
Rb/Sr	0.095	0.086	0.035	0.023	0.056	0.107	0.067	0.082
FeO*/MgO	2.38	3.44	2.04	3.13	2.98	2.85	2.44	2.72
Na ₂ O/K ₂ O	3.73	3.71	7.05	11.82	5.35	3.73	4.17	4.12
A/CNK	1.008	0.985	0.877	0.953	0.967	1.002	0.976	0.963

Rock, P-Tn: orthopyroxene-bearing tonalite, Tn: tonalite, Tr: trondhjemite

Fe₂O₃*: Total Fe as Fe₂O₃, LOI: Loss on ignition

A/CNK: Mol. Al₂O₃/CaO+Na₂O+K₂O

Table A4-3. (continued)

Sample	42707	51604	51606	52003	52008	90301	91502
Unit	DU	DU	DU	DU	DU	DU	DU
Rock	Tr	P-Tn	P-Tn	Tr	P-Tn	Tr	P-Gd
Major elements (%)							
SiO ₂	74.77	62.82	68.95	72.20	58.11	70.48	64.53
Al ₂ O ₃	13.68	17.17	16.18	14.47	18.69	15.74	15.42
Fe ₂ O ₃ *	2.47	5.77	3.07	2.21	7.92	2.45	5.76
MnO	0.02	0.08	0.03	0.02	0.10	0.04	0.08
MgO	0.38	1.67	1.23	0.83	2.39	1.11	2.94
CaO	2.99	4.75	4.52	3.46	6.20	3.65	3.76
Na ₂ O	4.37	3.98	3.93	3.77	4.25	4.77	2.21
K ₂ O	0.71	1.60	1.13	1.53	1.41	0.94	3.64
TiO ₂	0.15	0.65	0.38	0.37	0.88	0.28	0.68
P ₂ O ₅	0.04	0.28	0.11	0.06	0.17	0.08	0.20
LOI	0.30	0.58	0.32	0.56	0.09	0.25	0.46
Total	99.88	99.35	99.85	99.48	100.21	99.79	99.68
Trace elements (ppm)							
Ba	339	773	689	660	1078	634	867
Rb	16.1	55	36.2	47.6	35.3	27.9	140
Sr	324	529	357	435	478	461	316
Zr	131	211	168	105	149	114	182
Nb	3.3	11	4.2	3.9	6.6	1.8	15.3
Y	2.4	22.3	1.6	2.1	18	0.4	22.6
Ce	19	79	26	31	26	9	93
Nd	0.7	36	8.5	6	17	3.2	43
Sc	2.8	13.2	4.4	3.2	20.6	5.2	18.4
V	1	68	27	20	89	26	73
Cr	0	0	5	15	25	11	131
Ni	0	8	10.1	6	14	8.4	40
Cu	9	113	9	7	15	4	13
Zn	26	61	30	22	80	42	73
Ga	14.6	20.1	17.1	14.5	25.1	18	19.9
Ratio							
K/Ba	17.39	17.18	13.61	19.24	10.86	12.31	34.85
K/Rb	366.1	241.5	259.1	266.8	331.6	279.7	215.8
Rb/Sr	0.050	0.104	0.101	0.109	0.074	0.061	0.443
FeO*/MgO	6.05	3.22	2.32	2.48	3.08	2.05	1.82
Na ₂ O/K ₂ O	6.15	2.49	3.48	2.46	3.01	5.07	0.61
A/CNK	1.021	1.015	1.017	1.023	0.944	1.015	1.070

Rock, P-Tn: orthopyroxene-bearing tonalite, Tn: tonalite, Tr: trondhjemite

Fe₂O₃*: Total Fe as Fe₂O₃, LOI: Loss on ignition

A/CNK: Mol. Al₂O₃/CaO+Na₂O+K₂O

Table A4-4. Chemical compositions of the Ord River Tonalite Suite
(1)

Sample	11005	11203	11204	11305	32904	51302
Unit	OR	OR	OR	OR	OR	OR
Type	I	II	II	I	II	I
Major elements (%)						
SiO ₂	62.20	69.00	67.53	58.43	68.72	63.94
Al ₂ O ₃	15.89	15.42	15.99	17.74	15.53	16.59
Fe ₂ O ₃ *	6.27	3.53	3.72	6.16	2.77	5.10
MnO	0.09	0.03	0.02	0.09	0.04	0.07
MgO	3.11	1.36	1.50	3.88	1.30	2.06
CaO	5.14	3.55	3.69	7.31	4.27	5.17
Na ₂ O	3.54	3.96	4.19	3.88	3.82	3.79
K ₂ O	1.95	1.70	1.81	1.24	1.21	1.60
TiO ₂	0.79	0.40	0.43	0.57	0.37	0.61
P ₂ O ₅	0.18	0.14	0.15	0.10	0.10	0.15
LOI	0.50	0.60	0.68	0.43	0.86	0.71
Total	99.66	99.69	99.71	99.83	98.99	99.79
Trace elements (ppm)						
Ba	672	485	487	311	443	670
Rb	66	65	70	30.7	28.8	51.2
Sr	360	357	362	356	615	430
Zr	123	130	143	66	108	181
Nb	10.3	17	17.2	3.5	4.1	6.2
Y	17.2	10.6	10.6	12.9	0.7	14.6
Ce	45	35	44	16	115	56
Nd	27	17	21	12	35	22
Sc	17.5	9.5	9.1	22.1	4.9	13.4
V	97	48	50	115	36	73
Cr	89	8	10	59	9	23
Ni	38.6	9.4	8.4	41	8	17
Cu	34	5	5	10	16	6
Zn	75	44	49	57	30	62
Ga	N.D.	19.5	20.1	N.D.	N.D.	22
Ratio						
K/Ba	24.09	29.10	30.85	33.10	22.67	19.82
K/Rb	245.3	217.1	214.7	335.3	348.8	259.4
Rb/Sr	0.183	0.182	0.193	0.086	0.047	0.119
FeO*/MgO	1.88	2.42	2.31	1.48	1.98	2.30
Na ₂ O/K ₂ O	1.82	2.33	2.31	3.13	3.16	2.37
A/CNK	0.920	1.041	1.028	0.844	1.011	0.955

Fe₂O₃*: Total Fe as Fe₂O₃, LOI: Loss on ignition

N.D.: Not determined

A/CNK: Mol. Al₂O₃/CaO+Na₂O+K₂O

Table A4-4. (continued)

Sample	51303	51304	51305	51306	51307	51309
Unit	OR	OR	OR	OR	OR	OR
Type	I	I	I	I	I	II
Major elements (%)						
SiO ₂	64.82	64.24	64.44	63.66	65.12	67.82
Al ₂ O ₃	16.45	16.54	16.68	16.52	16.38	16.02
Fe ₂ O ₃ *	4.67	4.87	4.89	5.07	4.58	3.95
MnO	0.05	0.08	0.07	0.06	0.07	0.07
MgO	1.93	1.92	1.89	2.11	1.86	1.25
CaO	4.49	4.98	5.08	5.16	4.85	3.76
Na ₂ O	3.54	3.79	3.77	3.66	3.90	4.23
K ₂ O	1.97	1.64	1.65	1.61	1.63	1.57
TiO ₂	0.54	0.60	0.56	0.60	0.52	0.46
P ₂ O ₅	0.15	0.14	0.15	0.14	0.14	0.15
LOI	0.85	0.71	0.75	0.61	0.67	0.53
Total	99.46	99.51	99.93	99.20	99.72	99.81
Trace elements (ppm)						
Ba	682	648	657	641	560	412
Rb	69.7	53.6	53.1	51.1	53.7	53
Sr	425	417	425	439	428	405
Zr	160	165	137	175	152	139
Nb	8.2	6.9	7.1	6.9	7.4	7.1
Y	10.1	13.9	16.6	14.7	14.2	12.9
Ce	51	36	51	45	29	49
Nd	13	12	17	19	14	17
Sc	13	11.8	13.3	14.2	12.8	8.7
V	64	71	70	73	68	47
Cr	24	27	22	27	23	11
Ni	15	18	18	17	18	7
Cu	6	8	6	7	5	12
Zn	60	62	61	60	54	57
Ga	21.4	20.5	21.5	20.7	20.7	20.1
Ratio						
K/Ba	23.98	21.01	20.85	20.85	24.16	31.63
K/Rb	234.6	254.0	258.0	261.6	252.0	245.9
Rb/Sr	0.164	0.129	0.125	0.116	0.125	0.131
FeO*/MgO	2.25	2.36	2.41	2.24	2.29	2.94
Na ₂ O/K ₂ O	1.80	2.31	2.28	2.27	2.39	2.69
A/CNK	1.021	0.969	0.968	0.964	0.964	1.034

Fe₂O₃*: Total Fe as Fe₂O₃, LOI: Loss on ignition

N.D.: Not determined

A/CNK: Mol. Al₂O₃/CaO+Na₂O+K₂O

Table A4-4. (continued)

Sample	51310	51912	51913	51914	90807	91004
Unit	OR	OR	OR	OR	OR	OR
Type	I	I	I	II	II	I
Major elements (%)						
SiO ₂	58.42	66.06	66.18	68.19	68.54	58.51
Al ₂ O ₃	18.03	16.73	16.50	16.05	16.14	17.71
Fe ₂ O ₃ *	6.16	4.13	4.06	3.98	3.61	5.94
MnO	0.07	0.06	0.04	0.05	0.05	0.08
MgO	3.58	1.45	1.54	1.12	1.23	3.70
CaO	7.34	4.70	4.71	4.02	3.94	7.10
Na ₂ O	3.49	4.16	4.20	4.20	4.00	3.30
K ₂ O	1.43	1.64	1.65	1.50	1.73	1.45
TiO ₂	0.88	0.45	0.45	0.43	0.41	0.83
P ₂ O ₅	0.10	0.13	0.13	0.14	0.13	0.14
LOI	0.62	0.68	0.65	0.37	0.61	0.71
Total	100.12	100.19	100.11	100.05	100.39	99.47
Trace elements (ppm)						
Ba	289	602	605	610	512	284
Rb	41.7	55	57	49.8	61	42.9
Sr	558	466	454	332	353	553
Zr	97	135	137	183	153	72
Nb	5.4	6.3	7.1	5.7	8.9	4.9
Y	12.8	10.5	10.8	8.1	7	13.5
Ce	26	67	26	55	45	36
Nd	16	23	13	23	18	17
Sc	27.7	7.4	8.6	8.7	8.4	28.7
V	179	54	52	58	52	169
Cr	26	14	17	5	7	19
Ni	76	13.1	14	10	13.1	75
Cu	50	9	14	8	23	44
Zn	64	48	42	52	45	66
Ga	N.D.	N.D.	N.D.	18.3	18.7	N.D.
Ratio						
K/Ba	41.08	22.62	22.64	20.41	28.05	42.38
K/Rb	284.7	247.5	240.3	250.0	235.4	280.6
Rb/Sr	0.075	0.118	0.126	0.150	0.173	0.078
FeO*/MgO	1.60	2.65	2.45	3.31	2.73	1.49
Na ₂ O/K ₂ O	2.44	2.54	2.55	2.80	2.31	2.28
A/CNK	0.874	0.975	0.956	1.013	1.034	0.890

Fe₂O₃*: Total Fe as Fe₂O₃, LOI: Loss on ignition

N.D.: Not determined

A/CNK: Mol. Al₂O₃/CaO+Na₂O+K₂O

Table A4-5. Chemical compositions of the Western Porphyritic Granite and the Central Leucocratic Granite

Sample Unit	51918 WG	52103 WG	90805 WG	51202 CG	52101 CG	90601 CG
Major elements (%)						
SiO ₂	69.74	72.49	69.83	73.81	73.89	76.23
Al ₂ O ₃	14.43	13.32	14.29	14.01	13.59	13.01
Fe ₂ O ₃ *	4.17	2.78	3.71	1.41	1.44	1.02
MnO	0.05	0.05	0.02	0.05	0.02	0.02
MgO	1.00	0.58	0.81	0.34	0.33	0.27
CaO	2.34	1.90	2.53	1.58	1.66	1.46
Na ₂ O	2.74	2.74	2.92	3.92	3.13	2.71
K ₂ O	4.66	4.59	4.12	3.77	4.65	4.89
TiO ₂	0.56	0.39	0.53	0.13	0.12	0.09
P ₂ O ₅	0.14	0.08	0.13	0.03	0.03	0.03
LOI	0.33	0.39	0.67	0.39	0.46	0.54
Total	100.16	99.31	99.56	99.44	99.32	100.27
Trace elements (ppm)						
Ba	1014	777	1008	989	1152	732
Rb	142	173	114	105.6	81.5	72
Sr	146	128	202	258	239	248
Zr	240	179	246	78.7	96.7	49
Nb	12.9	9	8.4	10.9	7.2	1.5
Y	26.6	28.2	16.5	13.2	16.4	3.6
Ce	76	130	88	53	59	10
Nd	36	45	35	12	17	1.5
Sc	12.2	9	9.7	4	4	1.2
V	41	25	35	6	4	10
Cr	9	4	10	0	0	0
Ni	9	4	10	0	0	5.9
Cu	19	5	69	4	5	5
Zn	46	47	33	25	18	13
Ga	18	14.5	17.1	16.7	14	11.6
Ratio						
K/Ba	38.15	49.04	33.93	31.64	33.51	55.46
K/Rb	272.4	220.3	300.0	296.4	473.6	563.8
Rb/Sr	0.973	1.352	0.564	0.409	0.341	0.290
FeO*/MgO	3.88	4.46	4.26	3.86	4.06	3.52
Na ₂ O/K ₂ O	0.59	0.60	0.71	1.04	0.67	0.55
A/CNK	1.045	1.030	1.031	1.045	1.030	1.049

Fe₂O₃*: Total Fe as Fe₂O₃, LOI: Loss on ignition

A/CNK: Mol. Al₂O₃/CaO+Na₂O+K₂O

Table A4-6(A). Chemical compositions of the Sally Downs Tonalite (grid samples)
(1)

Sample	32505A	32506A	32601	32602	32603	32604	32704
(%)							
SiO ₂	60.86	60.68	61.16	59.84	59.42	59.82	59.79
Al ₂ O ₃	17.65	17.52	17.55	17.85	17.95	17.82	18.02
Fe ₂ O ₃ *	5.68	5.66	5.38	6.10	6.09	6.16	5.82
MnO	0.10	0.08	0.07	0.10	0.09	0.08	0.08
MgO	2.41	2.52	2.43	2.82	2.83	2.65	2.85
CaO	5.67	5.73	5.71	6.16	6.11	6.10	6.28
Na ₂ O	3.76	3.83	4.06	3.99	4.17	3.84	3.94
K ₂ O	1.87	1.75	1.52	1.63	1.53	1.70	1.34
TiO ₂	0.64	0.69	0.64	0.70	0.72	0.73	0.72
P ₂ O ₅	0.18	0.18	0.17	0.20	0.19	0.20	0.19
LOI	0.62	0.61	0.79	0.72	1.00	0.68	0.51
Total	99.44	99.25	99.48	100.11	100.10	99.78	99.54
(ppm)							
Ba	539	605	522	530	525	507	517
Rb	65.5	57.4	42.1	45.9	44.5	47.1	36.4
Sr	517	574	608	580	603	632	622
Y	21.4	18.3	11.1	15.5	16.5	12.7	10.8
Zr	144	149	129	136	134	163	137
Nb	7.4	7.9	5.3	5.9	5.9	5.8	4.9
Ce	39	65	75	53	55	59	53
Nd	19	26	25	22	31	22	19
Sc	14.9	12.8	14.1	16.5	17	14.4	15.8
V	91	92	86	98	98	98	95
Cr	29	30	25	35	34	29	35
Ni	20	19	17	21	21	20	22
Cu	39	31	32	37	37	50	38
Zn	67	65	64	66	69	69	65
Ga	22.3	N.D.	N.D.	N.D.	N.D.	N.D.	N.D.
Ratio							
K/Ba	28.80	24.01	24.17	25.53	24.19	27.83	21.52
K/Rb	237.0	253.1	299.7	294.8	285.4	299.6	305.6
Rb/Sr	0.127	0.100	0.069	0.079	0.074	0.075	0.059
FeO*/MgO	2.12	2.02	1.99	1.95	1.94	2.09	1.84
Na ₂ O/K ₂ O	2.01	2.19	2.67	2.45	2.73	2.26	2.94
A/CNK	0.953	0.941	0.938	0.914	0.915	0.926	0.931

Fe₂O₃*: Total Fe as Fe₂O₃

LOI: Loss on ignition

N.D.: Not determined

A/CNK: Mol. Al₂O₃/CaO+Na₂O+K₂O

Table A4-6(A). (continued)

Sample	32705	32801	32802A	32809	32810A	32901A	32902A
(%)							
SiO ₂	60.36	61.75	58.82	60.55	60.31	59.68	59.86
Al ₂ O ₃	17.71	17.55	18.15	17.73	17.65	17.44	17.76
Fe ₂ O ₃ *	5.71	5.34	6.51	5.87	5.88	5.97	6.22
MnO	0.09	0.06	0.09	0.09	0.10	0.08	0.09
MgO	2.69	2.38	2.80	2.55	2.50	2.84	2.95
CaO	5.99	5.60	6.24	5.50	5.91	6.09	6.32
Na ₂ O	3.96	3.97	3.77	3.99	4.11	3.77	3.93
K ₂ O	1.50	1.68	1.70	1.68	1.46	1.49	1.28
TiO ₂	0.70	0.65	0.63	0.64	0.69	0.70	0.75
P ₂ O ₅	0.18	0.18	0.21	0.20	0.18	0.22	0.23
LOI	0.92	0.76	0.62	0.77	0.64	1.04	0.66
Total	99.81	99.92	99.54	99.57	99.43	99.32	100.05
(ppm)							
Ba	544	510	467	603	521	577	572
Rb	42	57.6	59.4	51.3	44.7	41.5	37.1
Sr	617	601	563	567	606	662	700
Y	11.7	10.8	23.3	14	12.7	14.8	13.4
Zr	140	140	165	152	153	138	143
Nb	5.3	4.7	4.5	7	5.9	6.7	5.9
Ce	59	42	47	51	49	66	82
Nd	22	21	20	22	17	32	32
Sc	13.6	12	23.4	17.3	13.8	16.8	15.5
V	90	87	98	97	93	97	100
Cr	28	28	31	29	28	35	36
Ni	21	19	21	19	21	23	23
Cu	35	22	37	38	33	16	30
Zn	65	61	74	75	66	67	72
Ga	N.D.	N.D.	23.4	N.D.	N.D.	N.D.	N.D.
Ratio							
K/Ba	22.89	27.34	30.22	23.13	23.26	21.44	18.58
K/Rb	296.5	242.1	237.6	271.8	271.1	298.0	286.4
Rb/Sr	0.068	0.096	0.106	0.090	0.074	0.063	0.053
FeO*/MgO	1.91	2.02	2.09	2.07	2.12	1.89	1.90
Na ₂ O/K ₂ O	2.64	2.36	2.22	2.38	2.82	2.53	3.07
A/CNK	0.931	0.947	0.936	0.965	0.925	0.923	0.918

Fe₂O₃*: Total Fe as Fe₂O₃

LOI: Loss on ignition

N.D.: Not determined

A/CNK: Mol. Al₂O₃/CaO+Na₂O+K₂O

Table A4-6(A). (continued)

Sample	32903A	32907	40301	40302	40307C	40307F	40402
(%)							
SiO ₂	56.24	59.32	58.06	61.10	61.55	57.56	61.82
Al ₂ O ₃	18.38	18.16	17.99	17.58	17.12	18.17	17.08
Fe ₂ O ₃ *	7.24	6.05	6.60	5.78	5.62	6.94	5.19
MnO	0.09	0.09	0.06	0.09	0.07	0.09	0.07
MgO	3.59	2.71	3.06	2.51	2.46	3.08	2.45
CaO	6.96	6.37	6.73	5.88	5.80	6.41	5.52
Na ₂ O	3.65	4.10	3.84	3.98	4.06	4.09	3.96
K ₂ O	1.55	1.36	1.30	1.42	1.36	1.57	1.61
TiO ₂	0.88	0.71	0.76	0.66	0.62	0.76	0.55
P ₂ O ₅	0.29	0.20	0.25	0.18	0.19	0.22	0.17
LOI	0.91	0.68	0.80	0.76	0.91	0.94	0.87
Total	99.78	99.75	99.45	99.94	99.76	99.83	99.29
(ppm)							
Ba	865	438	634	593	487	542	499
Rb	38.7	38.1	32.7	41.7	38.9	41.2	50.5
Sr	913	671	954	613	594	605	528
Y	14.7	11.2	11.6	12.4	13.6	16.5	15.3
Zr	171	128	135	144	148	152	122
Nb	6.1	5.5	5.7	5.6	5.7	5.6	5
Ce	84	35	55	55	45	54	20
Nd	36	24	30	26	24	26	14
Sc	19	18.3	18.4	16.3	16	20.4	19.7
V	124	105	111	93	92	114	82
Cr	46	34	42	29	25	38	28
Ni	29	21	26	20	20	26	18
Cu	39	14	35	27	47	82	14
Zn	80	71	63	69	65	80	65
Ga	21.9	N.D.	20.8	N.D.	N.D.	N.D.	N.D.
Ratio							
K/Ba	14.87	25.77	17.02	19.88	23.18	24.05	26.78
K/Rb	332.5	296.3	330.0	282.7	290.2	316.3	264.6
Rb/Sr	0.042	0.057	0.034	0.068	0.065	0.068	0.096
FeO*/MgO	1.82	2.01	1.94	2.07	2.06	2.03	1.91
Na ₂ O/K ₂ O	2.36	3.02	2.95	2.80	2.99	2.61	2.46
A/CNK	0.904	0.917	0.901	0.936	0.916	0.905	0.934

Fe₂O₃*: Total Fe as Fe₂O₃

LOI: Loss on ignition

N.D.: Not determined

A/CNK: Mol. Al₂O₃/CaO+Na₂O+K₂O

Table A4-6(A). (continued)

(4)

Sample	40403	40404	40406	40407A	40501A	40502	40503
(%)							
SiO ₂	60.96	61.15	65.25	58.89	61.28	60.11	60.87
Al ₂ O ₃	17.31	17.57	16.29	17.87	17.46	17.90	17.39
Fe ₂ O ₃ *	5.53	5.67	4.40	6.07	5.62	5.60	5.64
MnO	0.07	0.08	0.04	0.08	0.09	0.08	0.07
MgO	2.70	2.71	1.93	2.86	2.56	2.57	2.52
CaO	5.81	5.92	4.95	6.10	5.76	5.76	5.73
Na ₂ O	3.90	3.86	3.87	3.83	3.93	3.91	4.03
K ₂ O	1.65	1.63	1.54	1.69	1.47	1.73	1.75
TiO ₂	0.61	0.67	0.53	0.69	0.67	0.70	0.62
P ₂ O ₅	0.19	0.18	0.15	0.21	0.18	0.18	0.18
LOI	0.84	0.66	0.60	0.83	0.63	0.65	0.95
Total	99.57	100.10	99.55	99.12	99.65	99.19	99.75
(ppm)							
Ba	488	451	476	534	527	560	510
Rb	51.2	51	47.1	53.4	40.7	54	54.8
Sr	590	632	583	591	600	591	542
Y	13.7	14.3	9.5	14.4	10.4	13.9	14.9
Zr	131	140	118	143	146	140	126
Nb	5.6	5.8	4.5	5.7	5.2	6.1	6.9
Ce	73	73	61	43	49	55	43
Nd	34	29	22	19	18	22	22
Sc	15.7	14.6	9.2	15	14	13.7	15.3
V	91	94	70	101	85	90	87
Cr	32	28	22	40	29	29	26
Ni	22	18	13	23	18	21	20
Cu	31	21	11	41	39	44	39
Zn	64	61	54	74	62	66	65
Ga	N.D.	N.D.	N.D.	N.D.	N.D.	N.D.	N.D.
Ratio							
K/Ba	28.07	30.00	26.86	26.27	23.15	25.64	28.48
K/Rb	267.5	265.3	271.4	262.7	299.8	265.9	265.1
Rb/Sr	0.087	0.081	0.081	0.090	0.068	0.091	0.101
FeO*/MgO	1.84	1.88	2.05	1.91	1.98	1.96	2.01
Na ₂ O/K ₂ O	2.36	2.37	2.51	2.27	2.67	2.26	2.30
A/CNK	0.922	0.931	0.956	0.930	0.942	0.953	0.918

Fe₂O₃*: Total Fe as Fe₂O₃

LOI: Loss on ignition

N.D.: Not determined

A/CNK: Mol. Al₂O₃/CaO+Na₂O+K₂O

Table A4-6(A). (continued)

(5)

Sample	40505A	40801A	40802	40902	40905	40908	40909
(%)							
SiO ₂	59.85	60.55	60.26	61.63	60.43	60.77	61.66
Al ₂ O ₃	17.62	17.79	17.68	17.03	17.42	17.70	17.31
Fe ₂ O ₃ *	5.97	5.83	5.81	5.30	5.52	5.62	5.09
MnO	0.10	0.07	0.06	0.07	0.07	0.09	0.08
MgO	2.60	2.57	2.58	2.25	2.49	2.73	2.25
CaO	5.93	6.04	6.09	5.42	5.68	5.89	5.22
Na ₂ O	4.03	3.95	4.01	3.91	4.08	4.05	4.52
K ₂ O	1.73	1.36	1.42	1.82	1.78	1.68	1.80
TiO ₂	0.62	0.72	0.70	0.62	0.67	0.68	0.60
P ₂ O ₅	0.20	0.19	0.20	0.16	0.17	0.16	0.16
LOI	0.90	0.51	0.96	1.11	0.96	0.91	1.18
Total	99.55	99.58	99.77	99.32	99.27	100.28	99.87
(ppm)							
Ba	509	487.5	631	576	556	540	447
Rb	52.8	39.4	39.2	56	53.4	52.4	45.4
Sr	564	644	798	544	566	573	478
Y	19.6	12.8	9	15.1	12.3	12.8	14.7
Zr	121	131	147	138	133	119	129
Nb	7.5	5.6	5.8	7.6	7	6.7	9
Ce	43	59	58	58	51	62	46
Nd	23	21	25	24	22	23	23
Sc	17.9	14.4	15.4	12.2	14.5	14.8	12.6
V	93	95	96	83	89	87	82
Cr	36	30	30	27	29	28	25
Ni	22	20	22	19	20	21	17
Cu	29	37	46	12	34	50	18
Zn	70	67	60	62	64	64	62
Ga	22.2	N.D.	20.5	N.D.	N.D.	N.D.	N.D.
Ratio							
K/Ba	28.21	23.16	18.68	26.23	26.58	25.83	33.43
K/Rb	272.0	286.5	300.7	269.8	276.7	266.1	329.1
Rb/Sr	0.094	0.061	0.049	0.103	0.094	0.091	0.095
FeO*/MgO	2.07	2.04	2.03	2.12	2.00	1.85	2.04
Na ₂ O/K ₂ O	2.33	2.90	2.82	2.15	2.29	2.41	2.51
A/CNK	0.914	0.939	0.921	0.933	0.919	0.922	0.917

Fe₂O₃*: Total Fe as Fe₂O₃

LOI: Loss on ignition

N.D.: Not determined

A/CNK: Mol. Al₂O₃/CaO+Na₂O+K₂O

Table A4-6(A). (continued)
(6)

Sample	41001A	41002A	41003A	41004	41005	41006A	41008
(%)							
SiO ₂	60.96	60.51	61.49	60.61	63.22	60.39	61.01
Al ₂ O ₃	17.37	17.60	17.64	17.69	16.79	17.65	17.47
Fe ₂ O ₃ *	5.84	5.71	5.38	5.91	5.05	5.92	5.60
MnO	0.08	0.08	0.08	0.07	0.07	0.07	0.08
MgO	2.90	2.67	2.34	2.70	2.32	2.61	2.55
CaO	6.08	5.87	5.58	6.14	5.18	6.09	5.77
Na ₂ O	3.93	3.88	4.11	3.97	4.04	3.80	3.79
K ₂ O	1.33	1.63	1.69	1.32	1.40	1.52	1.71
TiO ₂	0.61	0.69	0.64	0.71	0.62	0.70	0.67
P ₂ O ₅	0.23	0.18	0.17	0.19	0.16	0.20	0.17
LOI	0.62	0.78	0.77	0.70	0.77	0.62	0.79
Total	99.95	99.60	99.89	100.01	99.62	99.57	99.61
(ppm)							
Ba	576	533	552	522	564	537	465
Rb	35.7	49.9	48.5	38.3	40.4	46.7	51.2
Sr	688	588	555	622	593	613	569
Y	14.1	14	13.5	10.8	8.1	12.2	18.8
Zr	127	128	132	134	129	142	126
Nb	6.1	5.6	7.1	5.4	5	6.1	7
Ce	66	84	35	62	85	59	72
Nd	32	29	16	24	28	22	26
Sc	17.2	14.7	14	15	10.4	14.6	13.2
V	88	92	87	89	80	102	90
Cr	32	31	25	30	24	31	27
Ni	20.2	18	20	21	15	20	18
Cu	22	40	24	33	37	38	42
Zn	63	63	63	68	59	71	64
Ga	N.D.	N.D.	N.D.	N.D.	N.D.	N.D.	N.D.
Ratio							
K/Ba	19.17	25.39	25.41	20.99	20.61	23.50	30.53
K/Rb	309.3	271.2	289.3	286.1	287.7	270.2	277.2
Rb/Sr	0.052	0.085	0.087	0.062	0.068	0.076	0.090
FeO*/MgO	1.81	1.92	2.07	1.97	1.96	2.04	1.98
Na ₂ O/K ₂ O	2.96	2.38	2.43	3.01	2.89	2.50	2.22
A/CNK	0.916	0.935	0.942	0.925	0.955	0.930	0.940

Fe₂O₃*: Total Fe as Fe₂O₃

LOI: Loss on ignition

N.D.: Not determined

A/CNK: Mol. Al₂O₃/CaO+Na₂O+K₂O

Table A4-6(A). (continued)
(7)

Sample	41009B	41101A	41104	41105	41106A	41202	41203
(%)							
SiO ₂	60.14	62.05	65.79	59.52	66.01	62.33	59.93
Al ₂ O ₃	17.45	17.42	15.89	17.46	15.90	16.63	17.55
Fe ₂ O ₃ *	5.75	5.59	4.69	5.94	4.44	5.34	5.66
MnO	0.07	0.08	0.08	0.10	0.05	0.08	0.09
MgO	2.59	2.21	1.80	2.86	1.67	2.48	2.73
CaO	5.92	5.51	4.40	6.08	4.73	5.35	5.90
Na ₂ O	3.98	4.03	4.30	3.88	4.00	3.93	4.14
K ₂ O	1.63	1.64	1.69	1.82	1.53	1.77	1.68
TiO ₂	0.67	0.61	0.54	0.67	0.56	0.63	0.65
P ₂ O ₅	0.18	0.19	0.17	0.22	0.13	0.18	0.17
LOI	1.03	0.87	0.74	1.05	0.84	1.07	0.87
Total	99.41	100.20	100.09	99.60	99.86	99.79	99.37
(ppm)							
Ba	531	506	586	577	664	557	521
Rb	49.9	53.8	51.5	56.2	46.2	55.3	48.1
Sr	575	573	475	604	664	536	562
Y	12.3	15.4	12.3	16	3.4	11.9	13
Zr	138	145	149	141	122	139	125
Nb	6.3	4.2	7.6	7.7	5	6.2	8
Ce	21	46	80	68	60	49	21
Nd	15	23	29	28	19	23	18
Sc	16.1	15.2	11.2	16.3	6.3	13.4	16.6
V	95	85	66	99	69	87	97
Cr	29	31	22	38	21	31	31
Ni	20	19	19	24	15	22	22
Cu	21	38	10	35	4	27	21
Zn	66	65	56	68	50	63	65
Ga	N.D.	N.D.	N.D.	N.D.	N.D.	N.D.	N.D.
Ratio							
K/Ba	25.48	26.90	23.94	26.18	19.13	26.38	26.77
K/Rb	271.2	253.0	272.4	268.8	274.9	265.7	289.9
Rb/Sr	0.087	0.094	0.108	0.093	0.070	0.103	0.086
FeO*/MgO	2.00	2.28	2.34	1.87	2.39	1.94	1.87
Na ₂ O/K ₂ O	2.44	2.46	2.54	2.13	2.61	2.22	2.46
A/CNK	0.915	0.946	0.940	0.900	0.944	0.918	0.907

Fe₂O₃*: Total Fe as Fe₂O₃

LOI: Loss on ignition

N.D.: Not determined

A/CNK: Mol. Al₂O₃/CaO+Na₂O+K₂O

Table A4-6(A). (continued)

(8)

Sample	41204A	41301	41302	41307	41601A	41602	41603
(%)							
SiO ₂	62.21	68.34	61.06	60.48	60.23	61.70	60.83
Al ₂ O ₃	16.72	15.26	17.41	17.50	17.79	17.27	18.05
Fe ₂ O ₃ *	5.42	3.47	5.40	5.72	5.66	5.22	5.26
MnO	0.10	0.07	0.07	0.07	0.08	0.08	0.08
MgO	2.45	1.56	2.58	2.55	2.68	2.48	2.58
CaO	4.86	3.99	5.87	5.82	6.05	5.61	6.05
Na ₂ O	4.38	4.21	3.94	4.11	4.07	4.11	4.18
K ₂ O	2.03	2.01	1.55	1.65	1.51	1.52	1.37
TiO ₂	0.62	0.43	0.67	0.66	0.64	0.61	0.63
P ₂ O ₅	0.18	0.13	0.18	0.18	0.20	0.16	0.16
LOI	0.82	0.82	0.62	0.83	0.97	1.06	0.80
Total	99.79	100.29	99.35	99.57	99.88	99.82	99.99
(ppm)							
Ba	564	597	509	552	606	525	495
Rb	55.9	52.5	45.2	49.2	41	43.4	38.5
Sr	468	479	564	570	679	564	618
Y	14.6	10	13.9	12	11.8	11.3	10.3
Zr	136	98	136	131	132	132	136
Nb	10.8	6.3	6.7	6.1	6.4	6.1	4.9
Ce	48	58	52	43	47	35	67
Nd	23	22	22	22	22	17	24
Sc	14	8.8	13.4	14.9	15.6	13	12.3
V	86	50	90	96	92	82	83
Cr	28	19	32	32	32	27	25
Ni	21	19	21	22	21	17	19
Cu	14	9	22	43	34	22	32
Zn	66	43	62	67	65	58	63
Ga	N.D.	N.D.	N.D.	N.D.	N.D.	N.D.	N.D.
Ratio							
K/Ba	29.88	27.95	25.28	24.81	20.68	24.03	22.97
K/Rb	301.5	317.8	284.7	278.4	305.7	290.7	295.4
Rb/Sr	0.119	0.110	0.080	0.086	0.060	0.077	0.062
FeO*/MgO	1.99	2.00	1.88	2.02	1.90	1.89	1.83
Na ₂ O/K ₂ O	2.16	2.10	2.54	2.49	2.70	2.70	3.05
A/CNK	0.917	0.933	0.925	0.915	0.920	0.928	0.932

Fe₂O₃*: Total Fe as Fe₂O₃

LOI: Loss on ignition

N.D.: Not determined

A/CNK: Mol. Al₂O₃/CaO+Na₂O+K₂O

Table A4-6(A). (continued)

(9)

Sample	41604	41605	41705	41706	41802	41804	41805
(%)							
SiO ₂	59.29	64.78	59.54	59.05	59.48	61.16	59.44
Al ₂ O ₃	17.79	16.18	18.11	18.07	17.54	17.71	17.75
Fe ₂ O ₃ *	5.75	4.41	6.05	5.99	6.16	5.68	6.02
MnO	0.09	0.06	0.10	0.08	0.07	0.08	0.08
MgO	2.95	1.96	2.75	2.81	2.89	2.55	2.71
CaO	6.15	5.02	6.47	6.45	6.38	6.09	6.11
Na ₂ O	3.91	3.98	4.07	4.07	3.86	3.95	4.05
K ₂ O	1.66	1.54	1.28	1.36	1.28	1.26	1.45
TiO ₂	0.67	0.51	0.71	0.65	0.71	0.69	0.69
P ₂ O ₅	0.20	0.17	0.19	0.17	0.20	0.18	0.21
LOI	0.91	1.03	0.82	0.78	0.89	0.86	1.09
Total	99.37	99.64	100.09	99.48	99.46	100.21	99.60
(ppm)							
Ba	621	568	493	484	531	591	518
Rb	47.1	43.4	34.7	38.9	34.3	32.3	38.9
Sr	702	659	630	609	729	696	615
Y	12	7.7	13.7	12.9	11.4	8.2	15.7
Zr	139	99	135	122	125	135	143
Nb	6.6	3.9	5.7	4.9	4.8	4.5	5.1
Ce	44	73	50	34	63	49	61
Nd	25	23	25	22	30	22	26
Sc	16	8.7	17.1	18.4	17.6	15.4	17.2
V	91	67	100	99	104	98	98
Cr	36	24	36	35	42	31	30
Ni	21	17	24	23	28	19	21
Cu	13	20	50	41	38	27	34
Zn	67	54	68	70	66	65	68
Ga	N.D.	N.D.	N.D.	N.D.	N.D.	N.D.	N.D.
Ratio							
K/Ba	22.19	22.51	21.55	23.33	20.01	17.70	23.24
K/Rb	292.6	294.6	306.2	290.2	309.8	323.8	309.4
Rb/Sr	0.067	0.066	0.055	0.064	0.047	0.046	0.063
FeO*/MgO	1.75	2.03	1.98	1.92	1.92	2.00	2.00
Na ₂ O/K ₂ O	2.36	2.58	3.18	2.99	3.02	3.14	2.79
A/CNK	0.917	0.933	0.913	0.908	0.907	0.935	0.918

Fe₂O₃*: Total Fe as Fe₂O₃

LOI: Loss on ignition

N.D.: Not determined

A/CNK: Mol. Al₂O₃/CaO+Na₂O+K₂O

Table A4-6(A). (continued)
(10)

Sample	41806	41901	41902	41903	41904	41905	42201
(%)							
SiO ₂	60.07	59.27	60.34	60.55	60.84	58.66	61.01
Al ₂ O ₃	17.92	17.72	17.53	17.16	17.22	17.85	17.36
Fe ₂ O ₃ *	5.74	6.43	5.94	5.82	5.53	6.37	5.45
MnO	0.08	0.08	0.08	0.08	0.08	0.10	0.06
MgO	2.67	2.79	2.80	2.81	2.68	3.06	2.43
CaO	6.22	6.23	5.93	5.97	5.69	6.17	5.75
Na ₂ O	4.10	3.84	4.05	4.03	3.94	3.68	3.97
K ₂ O	1.40	1.71	1.71	1.57	1.78	1.94	1.52
TiO ₂	0.66	0.69	0.65	0.67	0.64	0.70	0.63
P ₂ O ₅	0.17	0.21	0.21	0.23	0.22	0.21	0.18
LOI	0.87	0.72	0.91	0.97	1.08	0.86	0.96
Total	99.90	99.69	100.15	99.86	99.70	99.60	99.32
(ppm)							
Ba	501	468	568	608	774	496	590
Rb	37.8	54.3	48.9	45.5	52.7	70.9	49.2
Sr	609	561	641	656	663	557	670
Y	12.7	28.4	12.7	14.6	11.7	20.7	9.9
Zr	133	140	143	154	168	141	133
Nb	5.4	4.6	6.2	5.8	7.8	5.4	5.5
Ce	38	37	58	76	86	50	46
Nd	21	25	27	35	38	25	22
Sc	15.3	17.6	16	15.8	13.6	17.1	13.4
V	94	104	97	95	88	108	90
Cr	33	42	35	37	37	40	26
Ni	22	22	24	25	23	25	22
Cu	34	54	11	25	14	60	7
Zn	66	75	70	70	65	73	58
Ga	N.D.	N.D.	N.D.	N.D.	N.D.	N.D.	N.D.
Ratio							
K/Ba	23.20	30.33	24.99	21.44	19.09	32.47	21.39
K/Rb	307.4	261.4	290.3	286.4	280.4	227.1	256.5
Rb/Sr	0.062	0.097	0.076	0.069	0.079	0.127	0.073
FeO*/MgO	1.93	2.07	1.91	1.86	1.86	1.87	2.02
Na ₂ O/K ₂ O	2.93	2.25	2.37	2.57	2.21	1.90	2.61
A/CNK	0.916	0.909	0.909	0.895	0.918	0.921	0.932

Fe₂O₃*: Total Fe as Fe₂O₃

LOI: Loss on ignition

N.D.: Not determined

A/CNK: Mol. Al₂O₃/CaO+Na₂O+K₂O

Table A4-6(A). (continued)

(11)

Sample	42202	42203A	42204	42205A	42301	42303	42304A
(%)							
SiO ₂	60.45	59.01	62.07	60.62	59.15	60.77	60.98
Al ₂ O ₃	17.44	18.05	17.40	17.13	17.72	17.58	17.57
Fe ₂ O ₃ *	5.59	6.11	5.46	5.42	6.36	5.56	5.47
MnO	0.06	0.09	0.05	0.07	0.09	0.08	0.08
MgO	2.54	2.84	2.40	2.74	2.81	2.76	2.58
CaO	5.73	6.35	5.79	5.67	6.17	6.07	5.76
Na ₂ O	4.03	4.08	4.11	4.00	3.91	3.99	3.95
K ₂ O	1.65	1.46	1.49	1.77	1.52	1.46	1.63
TiO ₂	0.63	0.71	0.62	0.63	0.70	0.69	0.65
P ₂ O ₅	0.18	0.19	0.18	0.20	0.24	0.18	0.16
LOI	1.20	0.96	0.64	1.32	0.91	1.03	0.83
Total	99.50	99.85	100.21	99.57	99.58	100.17	99.66
(ppm)							
Ba	546	532	521	598	634	484	524
Rb	53.6	39.5	44.2	49.8	44.5	40.8	46.1
Sr	572	613	577	625	672	593	555
Y	10.5	13.9	10.6	11.2	12.6	10.8	11.8
Zr	124	137	116	138	169	125	114
Nb	6.6	7	6.6	6.5	5.8	6.1	6
Ce	38	32	69	76	64	33	53
Nd	18	19	30	29	25	15	20
Sc	15.2	17.6	14.1	13.5	16.2	14.2	12.3
V	90	101	84	86	103	87	86
Cr	30	35	26	31	34	28	27
Ni	20	23	18.6	22	23	20	18
Cu	13	45	32	14	57	28	30
Zn	65	70	61	63	72	64	60
Ga	N.D.	N.D.	N.D.	N.D.	N.D.	N.D.	N.D.
Ratio							
K/Ba	25.09	22.78	23.74	24.57	19.90	25.04	25.82
K/Rb	255.5	306.8	279.8	295.0	283.5	297.0	293.5
Rb/Sr	0.094	0.064	0.077	0.080	0.066	0.069	0.083
FeO*/MgO	1.98	1.94	2.05	1.78	2.04	1.81	1.91
Na ₂ O/K ₂ O	2.44	2.80	2.76	2.26	2.57	2.73	2.42
A/CNK	0.926	0.910	0.921	0.911	0.918	0.917	0.938

Fe₂O₃*: Total Fe as Fe₂O₃

LOI: Loss on ignition

N.D.: Not determined

A/CNK: Mol. Al₂O₃/CaO+Na₂O+K₂O

Table A4-6(A). (continued)
(12)

Sample	42305	42401	42402	42403	42601	42602	42603
(%)							
SiO ₂	63.62	60.37	58.23	60.57	60.95	60.56	59.36
Al ₂ O ₃	17.05	17.73	18.20	17.77	17.44	17.61	17.89
Fe ₂ O ₃ *	4.71	5.84	6.42	5.63	5.60	5.50	6.27
MnO	0.07	0.08	0.08	0.08	0.07	0.07	0.10
MgO	2.19	2.71	3.09	2.53	2.46	2.49	2.76
CaO	5.48	5.82	6.73	5.96	5.77	5.87	6.27
Na ₂ O	3.99	4.19	3.84	4.13	3.95	4.14	4.00
K ₂ O	1.37	1.40	1.38	1.40	1.61	1.41	1.62
TiO ₂	0.60	0.68	0.78	0.68	0.68	0.68	0.76
P ₂ O ₅	0.15	0.19	0.19	0.17	0.17	0.18	0.20
LOI	0.69	0.88	0.78	0.85	1.02	0.73	0.64
Total	99.92	99.89	99.72	99.77	99.72	99.24	99.87
(ppm)							
Ba	493	519	451	514	551	555	578
Rb	40.5	37.4	38.2	38.8	44	38.5	45.8
Sr	589	610	604	602	592	638	589
Y	9	11.9	12.8	14	12.4	9.8	15.4
Zr	118	131	143	132	128	132	139
Nb	5.1	5.9	6.1	5.8	6.7	6.2	5.9
Ce	194	58	41	52	39	21	53
Nd	61	23	20	21	18	16	23
Sc	10.9	16	18	14.7	12.9	15	15.6
V	73	93	102	90	88	89	104
Cr	19	29	35	27	25	29	35
Ni	14	21	22	18	19	21	22
Cu	11	35	40	29	22	28	42
Zn	55	68	68	64	61	63	70
Ga	N.D.	N.D.	N.D.	N.D.	N.D.	N.D.	N.D.
Ratio							
K/Ba	23.07	22.39	25.40	22.61	24.26	21.09	23.27
K/Rb	280.8	310.7	299.9	299.5	303.7	304.0	293.6
Rb/Sr	0.069	0.061	0.063	0.064	0.074	0.060	0.078
FeO*/MgO	1.94	1.94	1.87	2.00	2.05	1.99	2.04
Na ₂ O/K ₂ O	2.91	2.99	2.78	2.95	2.45	2.94	2.47
A/CNK	0.947	0.934	0.908	0.928	0.931	0.926	0.907

Fe₂O₃*: Total Fe as Fe₂O₃

LOI: Loss on ignition

N.D.: Not determined

A/CNK: Mol. Al₂O₃/CaO+Na₂O+K₂O

Table A4-6(A). (continued)
(13)

Sample	42604	42702	42703	42705	50201A	50202	50203B
(%)							
SiO ₂	60.97	60.64	62.30	61.50	61.34	68.77	67.03
Al ₂ O ₃	17.27	17.56	17.38	17.55	17.25	14.99	15.74
Fe ₂ O ₃ *	5.44	5.77	5.12	5.57	5.45	3.33	3.80
MnO	0.07	0.08	0.08	0.09	0.08	0.05	0.06
MgO	2.40	2.62	2.29	2.47	2.38	1.48	1.63
CaO	5.66	5.85	5.47	5.90	5.43	3.54	4.21
Na ₂ O	3.98	4.11	4.22	3.80	3.98	4.11	4.56
K ₂ O	1.60	1.60	1.55	1.41	1.87	2.37	1.53
TiO ₂	0.61	0.66	0.63	0.66	0.64	0.42	0.50
P ₂ O ₅	0.18	0.17	0.17	0.18	0.17	0.13	0.14
LOI	1.15	0.87	0.82	0.83	0.71	0.41	0.68
Total	99.33	99.93	100.03	99.96	99.30	99.60	99.88
(ppm)							
Ba	543	548	571	568	525	562	578
Rb	43.9	44.3	43.8	40.1	53.4	49.3	47.4
Sr	604	577	581	603	539	430	514
Y	10.2	12.1	12	9.1	12.9	6.2	10.1
Zr	123	139	145	127	134	107	99
Nb	5.3	5.5	6.5	4.5	7.9	6	6.9
Ce	58	42	35	67	56	64	62
Nd	24	22	15	24	23	26	25
Sc	13.3	14.7	13.9	12.6	13.5	5.6	8.4
V	88	91	81	92	88	51	56
Cr	32	29	27	39	27	19	21
Ni	19	21	16	19	18	16.1	18
Cu	35	40	25	22	13	12	11
Zn	66	65	62	66	65	41	45
Ga	N.D.	N.D.	N.D.	N.D.	N.D.	16.6	N.D.
Ratio							
K/Ba	24.46	24.24	22.53	20.61	29.57	35.01	21.97
K/Rb	302.5	299.8	293.8	291.9	290.7	399.1	267.9
Rb/Sr	0.073	0.077	0.075	0.067	0.099	0.115	0.092
FeO*/MgO	2.04	1.98	2.01	2.03	2.06	2.03	2.10
Na ₂ O/K ₂ O	2.49	2.57	2.72	2.70	2.13	1.73	2.98
A/CNK	0.930	0.918	0.936	0.948	0.935	0.951	0.936

Fe₂O₃*: Total Fe as Fe₂O₃

LOI: Loss on ignition

N.D.: Not determined

A/CNK: Mol. Al₂O₃/CaO+Na₂O+K₂O

Table A4-6(A). (continued)
(14)

Sample	50302	50303	50305	50306	50501A	50502A	50503A
(%)							
SiO ₂	59.93	59.85	66.85	63.06	60.35	60.63	61.00
Al ₂ O ₃	17.52	17.17	15.63	17.35	17.57	17.79	17.44
Fe ₂ O ₃ *	6.15	6.17	3.70	4.88	5.85	5.82	5.38
MnO	0.10	0.08	0.06	0.05	0.09	0.08	0.05
MgO	2.57	2.81	1.55	2.15	2.61	2.49	2.48
CaO	6.04	5.98	3.69	5.93	6.02	6.01	5.88
Na ₂ O	3.89	3.92	3.42	4.20	3.89	3.91	3.86
K ₂ O	1.72	1.87	3.36	1.33	1.52	1.37	1.72
TiO ₂	0.68	0.70	0.41	0.57	0.67	0.70	0.61
P ₂ O ₅	0.22	0.23	0.11	0.22	0.21	0.18	0.20
LOI	0.69	0.94	0.52	0.65	1.00	0.62	0.96
Total	99.51	99.72	99.30	100.39	99.78	99.60	99.58
(ppm)							
Ba	566	666	2087	553	505	630	575
Rb	49.4	57	46.4	37	42.5	35.8	48.8
Sr	628	600	537	733	629	692	824
Y	15.5	19.1	8.2	8	11.9	11.1	8.7
Zr	143	154	90	122	132	141	123
Nb	6.5	7.8	5.1	5.8	5.4	5.2	4.8
Ce	73	116	52	65	63	30	52
Nd	29	46	16	27	24	12	20
Sc	15.3	13.7	8.7	10.2	13	15.7	12.8
V	101	99	53	76	91	96	90
Cr	31	38	17	28	34	30	31
Ni	21	25.4	12	18.4	20	20	19
Cu	31	29	10	33	46	33	19
Zn	72	67	45	53	65	65	61
Ga	N.D.	N.D.	N.D.	N.D.	N.D.	N.D.	N.D.
Ratio							
K/Ba	25.23	23.31	13.36	19.96	24.99	18.05	24.83
K/Rb	289.0	272.3	601.1	298.4	296.9	317.7	292.6
Rb/Sr	0.079	0.095	0.086	0.050	0.068	0.052	0.059
FeO*/MgO	2.15	1.98	2.15	2.04	2.02	2.10	1.95
Na ₂ O/K ₂ O	2.26	2.10	1.02	3.16	2.56	2.85	2.24
A/CNK	0.910	0.888	0.979	0.907	0.925	0.944	0.923

Fe₂O₃*: Total Fe as Fe₂O₃

LOI: Loss on ignition

N.D.: Not determined

A/CNK: Mol. Al₂O₃/CaO+Na₂O+K₂O

Table A4-6(A). (continued)
(15)

Sample	50505	50601A	50603	50604	50702	50703	50704
(%)							
SiO ₂	67.01	60.75	60.35	63.46	63.21	61.36	60.83
Al ₂ O ₃	15.86	17.53	17.51	16.59	16.72	17.16	17.26
Fe ₂ O ₃ *	3.53	5.70	5.79	4.67	5.03	5.42	5.57
MnO	0.05	0.09	0.09	0.08	0.08	0.08	0.08
MgO	1.43	2.42	2.60	2.41	2.32	2.48	2.64
CaO	4.41	5.64	5.86	5.19	5.12	5.74	5.82
Na ₂ O	3.84	3.82	3.83	4.20	3.83	3.95	3.88
K ₂ O	1.80	1.93	1.84	1.65	1.71	1.58	1.68
TiO ₂	0.46	0.60	0.64	0.59	0.61	0.63	0.65
P ₂ O ₅	0.11	0.19	0.20	0.18	0.16	0.18	0.20
LOI	0.85	0.89	0.81	1.14	0.80	1.13	1.05
Total	99.35	99.56	99.52	100.16	99.59	99.71	99.66
(ppm)							
Ba	781	560	588	511	591	608	661
Rb	41.4	58	54.5	49.4	48.3	45.6	47.7
Sr	586	529	539	561	533	633	668
Y	3.8	16.4	14.9	11.7	8.7	9.7	10.1
Zr	91.8	148	145	130	143	133	120
Nb	6.4	7.9	7.8	7	5.4	5.4	5.6
Ce	47	51	44	72	72	82	74
Nd	14	17	18	29	29	30	24
Sc	6.2	13.1	14.5	12.4	10.8	12.6	11.3
V	61	90	90	73	75	85	86
Cr	14	27	33	36	27	26	31
Ni	11	19	20	25	18	17	18
Cu	6	39	25	8	30	12	39
Zn	41	65	69	63	57	61	63
Ga	N.D.	N.D.	N.D.	N.D.	N.D.	N.D.	N.D.
Ratio							
K/Ba	19.13	28.61	25.98	26.80	24.02	21.57	21.10
K/Rb	360.9	276.2	280.3	277.3	293.9	287.6	292.4
Rb/Sr	0.071	0.110	0.101	0.088	0.091	0.072	0.071
FeO*/MgO	2.22	2.12	2.00	1.74	1.95	1.97	1.90
Na ₂ O/K ₂ O	2.13	1.98	2.08	2.55	2.24	2.50	2.31
A/CNK	0.974	0.941	0.924	0.915	0.958	0.920	0.919

Fe₂O₃*: Total Fe as Fe₂O₃

LOI: Loss on ignition

N.D.: Not determined

A/CNK: Mol. Al₂O₃/CaO+Na₂O+K₂O

Table A4-6(A). (continued)
(16)

Sample	50801	51205	51401	51408	51409A	51410A	51510
(%)							
SiO ₂	67.27	61.16	65.17	64.55	65.78	61.65	60.53
Al ₂ O ₃	15.66	17.53	16.02	16.32	15.61	16.69	17.36
Fe ₂ O ₃ *	4.00	5.59	4.47	5.05	4.45	5.32	5.66
MnO	0.06	0.08	0.05	0.08	0.06	0.08	0.08
MgO	1.69	2.46	1.96	2.24	1.86	2.43	2.42
CaO	4.26	5.80	4.83	5.06	4.42	5.31	5.67
Na ₂ O	4.06	3.97	4.02	4.09	4.15	4.09	3.93
K ₂ O	1.73	1.43	1.56	1.50	1.72	1.72	1.68
TiO ₂	0.48	0.68	0.58	0.58	0.55	0.64	0.65
P ₂ O ₅	0.16	0.19	0.16	0.17	0.15	0.19	0.19
LOI	0.65	0.60	0.73	0.54	0.80	0.89	0.93
Total	100.02	99.49	99.55	100.18	99.55	99.01	99.10
(ppm)							
Ba	531	593	497	592	429	514	463
Rb	53.2	43.1	46.4	44.1	53.1	52.5	53.3
Sr	504	613	529	526	476	550	574
Y	8.3	10.1	10.4	9.7	10.8	12.2	18.1
Zr	110	138	140	118	120	145	146
Nb	5.9	5.6	4.6	6	8.2	6.9	6
Ce	70	48	68	94	72	55	58
Nd	23	22	22	37	21	21	23
Sc	8.7	15.2	8	11	8.8	11.8	14.6
V	63	95	71	79	69	85	87
Cr	23	27	25	28	27	33	25
Ni	16	18	18	21.6	17	22	18
Cu	8	28	8	20	9	20	26
Zn	51	65	49	55	52	60	66
Ga	17.6	N.D.	N.D.	N.D.	20	N.D.	N.D.
Ratio							
K/Ba	27.04	20.02	26.06	21.03	33.28	27.78	30.12
K/Rb	269.9	275.4	279.1	282.3	268.9	272.0	261.6
Rb/Sr	0.106	0.070	0.088	0.084	0.112	0.095	0.093
FeO*/MgO	2.13	2.05	2.05	2.03	2.15	1.97	2.10
Na ₂ O/K ₂ O	2.35	2.78	2.58	2.73	2.41	2.38	2.34
A/CNK	0.961	0.941	0.938	0.930	0.933	0.915	0.934

Fe₂O₃*: Total Fe as Fe₂O₃

LOI: Loss on ignition

N.D.: Not determined

A/CNK: Mol. Al₂O₃/CaO+Na₂O+K₂O

Table A4-6(A). (continued)
(17)

Sample	51513B	51514	51601	51602	51706	51715
(%)						
SiO ₂	61.77	62.24	60.61	61.12	60.69	61.85
Al ₂ O ₃	17.49	17.22	17.91	17.70	17.79	17.31
Fe ₂ O ₃ *	5.63	5.35	5.63	5.71	5.84	5.35
MnO	0.07	0.06	0.06	0.09	0.07	0.07
MgO	2.40	2.41	2.58	2.47	2.67	2.25
CaO	5.81	5.58	5.99	5.84	6.08	5.55
Na ₂ O	3.99	3.96	3.92	4.01	4.03	3.85
K ₂ O	1.49	1.48	1.47	1.53	1.45	1.91
TiO ₂	0.68	0.65	0.69	0.69	0.69	0.63
P ₂ O ₅	0.18	0.17	0.18	0.19	0.19	0.18
LOI	0.55	0.68	0.70	0.52	0.58	0.73
Total	100.06	99.80	99.74	99.87	100.08	99.68
(ppm)						
Ba	552	611	505	570	528	532
Rb	42.6	44.5	42	43.4	41.6	60.4
Sr	607	608	635	602	613	563
Y	10.6	9.9	10.7	10.6	11.3	11.5
Zr	139	137	129	144.2	135	136
Nb	6.1	5.7	6.2	6.1	5.3	6.2
Ce	63	64	52	49	54	58
Nd	23	23	22	19	22	20
Sc	13.8	13.9	14.8	15	15	12.2
V	93	84	94	91	94	86
Cr	24	28	31	32	27	26
Ni	18	18	18	21	19	18
Cu	32	40	23	30	36	19
Zn	66	62	60	66	66	63
Ga	N.D.	N.D.	N.D.	N.D.	22.4	N.D.
Ratio						
K/Ba	22.41	20.11	24.16	22.28	22.80	29.80
K/Rb	290.3	276.1	290.5	292.6	289.3	262.5
Rb/Sr	0.070	0.073	0.066	0.072	0.068	0.107
FeO*/MgO	2.11	2.00	1.96	2.08	1.97	2.14
Na ₂ O/K ₂ O	2.68	2.68	2.67	2.62	2.78	2.02
A/CNK	0.933	0.943	0.946	0.938	0.924	0.936

Fe₂O₃*: Total Fe as Fe₂O₃

LOI: Loss on ignition

N.D.: Not determined

A/CNK: Mol. Al₂O₃/CaO+Na₂O+K₂O

Table A4-6(B). Chemical compositions of the Sally Downs Tonalite
(Samples for local chemical variability assessment and geochronology)

Sample	51701	51703	51705A	51705B	51709	51710	51711A
(%)							
SiO ₂	60.01	60.70	61.01	60.81	59.40	61.05	61.73
Al ₂ O ₃	17.93	17.64	17.83	17.84	17.92	17.77	17.66
Fe ₂ O ₃ *	5.90	5.87	5.82	5.84	6.13	5.76	5.61
MnO	0.06	0.07	0.07	0.08	0.09	0.08	0.08
MgO	2.64	2.59	2.54	2.61	2.79	2.51	2.43
CaO	6.08	5.88	6.00	6.03	6.11	5.98	5.82
Na ₂ O	4.00	3.82	4.00	3.99	4.07	3.93	4.00
K ₂ O	1.41	1.50	1.43	1.39	1.43	1.53	1.57
TiO ₂	0.72	0.73	0.70	0.71	0.74	0.69	0.65
P ₂ O ₅	0.20	0.20	0.20	0.20	0.20	0.19	0.18
LOI	0.62	0.60	0.43	0.56	0.66	0.44	0.55
Total	99.57	99.60	100.03	100.06	99.54	99.93	100.28
(ppm)							
Ba	551	576	528	560	502	541	535
Rb	39.4	40.2	39.1	39.6	40.3	44.7	46.5
Sr	624	610	616	620	614	610	590
Y	10.8	10.8	11.6	11.7	13.2	12.2	12.2
Zr	131	151	152	142	146	125	136
Nb	4.9	4.8	4.5	5.7	6.6	6.3	5.5
Ce	58	63	63	50	48	54	32
Nd	21	21	23	20	22	19	17
Sc	14.2	13.8	15.6	15.6	16.3	14.8	15.1
V	94	92	96	96	96	93	91
Cr	31	30	31	30	31	31	30
Ni	20	20	18	18	20	20	19
Cu	34	36	36	36	42	34	31
Zn	68	66	66	66	67	65	65
Ga	N.D.	N.D.	21.6	N.D.	N.D.	23.4	N.D.
Ratio							
K/Ba	21.24	21.62	22.48	20.60	23.65	23.48	24.36
K/Rb	297.1	309.7	303.6	291.4	294.6	284.1	280.3
Rb/Sr	0.063	0.066	0.063	0.064	0.066	0.073	0.079
FeO*/MgO	2.01	2.04	2.06	2.01	1.98	2.07	2.08
Na ₂ O/K ₂ O	2.84	2.55	2.80	2.87	2.85	2.57	2.55
A/CNK	0.936	0.948	0.937	0.937	0.926	0.936	0.936

Fe₂O₃*: Total Fe as Fe₂O₃

LOI: Loss on ignition

N.D.: Not determined

A/CNK: Mol. Al₂O₃/CaO+Na₂O+K₂O

Table A4-6(B). (continued)

Sample	51712	51713	51714
(%)			
SiO ₂	60.49	61.92	60.96
Al ₂ O ₃	17.60	17.23	17.65
Fe ₂ O ₃ *	5.83	5.64	5.67
MnO	0.09	0.08	0.09
MgO	2.66	2.51	2.55
CaO	5.93	5.63	5.75
Na ₂ O	3.96	3.84	3.93
K ₂ O	1.59	1.68	1.64
TiO ₂	0.68	0.67	0.66
P ₂ O ₅	0.18	0.19	0.18
LOI	0.71	0.56	0.66
Total	99.72	99.95	99.74
(ppm)			
Ba	540	572	566
Rb	45.9	51	49.8
Sr	596	571	591
Y	13.8	12.8	12.7
Zr	143	145	121
Nb	5.5	5.8	6.5
Ce	51	42	46
Nd	22	15	19
Sc	15	15.2	13.6
V	90	93	90
Cr	25	29	29
Ni	19	18	20
Cu	22	30	31
Zn	64	66	62
Ga	N.D.	20.7	N.D.
Ratio			
K/Ba	24.44	24.38	24.05
K/Rb	287.6	273.4	273.4
Rb/Sr	0.077	0.089	0.084
FeO*/MgO	1.97	2.02	2.00
Na ₂ O/K ₂ O	2.49	2.29	2.40
A/CNK	0.925	0.938	0.944

Fe₂O₃*: Total Fe as Fe₂O₃

LOI: Loss on ignition

N.D.: Not determined

A/CNK: Mol. Al₂O₃/CaO+Na₂O+K₂O

Table A4-6(C). Chemical compositions of the Sally Downs Tonalite
(samples for initial examination)

(1)

Sample	81507A	81507B	82107	82302	82305	82405	82406
(%)							
SiO ₂	63.29	64.32	60.27	58.73	57.45	63.52	59.65
Al ₂ O ₃	16.86	16.75	17.77	17.80	17.69	17.08	17.71
Fe ₂ O ₃ *	5.18	4.86	5.70	6.45	7.15	4.97	6.13
MnO	0.07	0.06	0.05	0.09	0.09	0.05	0.09
MgO	2.55	2.20	2.70	3.07	3.46	2.15	2.86
CaO	5.20	5.17	5.96	6.35	5.99	5.11	6.13
Na ₂ O	3.65	3.75	3.84	3.98	3.65	3.70	3.69
K ₂ O	1.45	1.37	1.38	1.36	1.97	1.48	1.46
TiO ₂	0.64	0.59	0.71	0.75	0.94	0.58	0.71
P ₂ O ₅	0.17	0.17	0.19	0.23	0.42	0.18	0.20
LOI	0.70	0.78	0.93	0.68	0.85	0.64	1.02
Total	99.76	100.02	99.50	99.49	99.66	99.46	99.65
(ppm)							
Ba	584	553	716	553	928	708	705
Rb	42.5	39.8	44.8	37.8	62	47	46.2
Sr	588	591	723	640	712	635	657
Y	9.2	9	11.7	14.9	14.2	7.6	12.9
Zr	129	118	129	140	148	126	139
Nb	6.2	5.4	6	5.9	8.8	5.3	5.9
Ce	88	71	49	111	99	60	44
Nd	29	23	17	41	39	19	19
Sc	10.5	10	13.7	16.4	14.4	12.8	15.4
V	88	82	96	106	124	76	103
Cr	29	26	29	37	40	24	35
Ni	20.2	18.8	21.9	24.8	29.6	19.7	24.8
Cu	42	38	26	46	20	14	26
Zn	63	59	65	72	83	57	75
Ga	N.D.	N.D.	21.6	N.D.	N.D.	N.D.	N.D.
Ratio							
K/Ba	20.61	20.56	16.00	20.41	17.62	17.35	17.19
K/Rb	283.2	285.7	255.7	298.7	263.8	261.4	262.3
Rb/Sr	0.072	0.067	0.062	0.059	0.087	0.074	0.070
FeO*/MgO	1.83	1.99	1.90	1.89	1.86	2.08	1.93
Na ₂ O/K ₂ O	2.52	2.74	2.78	2.93	1.85	2.50	2.53
ACNK	0.990	0.982	0.953	0.910	0.930	1.006	0.942

Fe₂O₃*: Total Fe as Fe₂O₃

LOI: Loss on ignition

N.D.: Not determined

A/CNK: Mol. Al₂O₃/CaO+Na₂O+K₂O

Table A4-6(C). (continued)

(2)

Sample	82701	82804	83001	83002	90101	90201	90702
(%)							
SiO ₂	65.68	61.55	60.88	58.90	62.56	60.19	62.69
Al ₂ O ₃	16.29	17.34	17.50	18.00	16.89	17.82	16.84
Fe ₂ O ₃ *	3.72	5.71	6.06	6.38	5.44	6.00	5.14
MnO	0.04	0.08	0.07	0.09	0.07	0.08	0.07
MgO	1.91	2.72	2.69	3.04	2.32	2.76	2.42
CaO	4.77	5.59	5.97	6.46	5.42	6.07	5.53
Na ₂ O	3.79	3.65	3.83	3.80	4.31	3.74	3.79
K ₂ O	1.48	1.50	1.56	1.46	1.57	1.60	1.62
TiO ₂	0.54	0.64	0.68	0.75	0.66	0.68	0.60
P ₂ O ₅	0.15	0.21	0.20	0.21	0.19	0.20	0.18
LOI	0.79	0.76	0.63	1.09	0.74	0.76	1.18
Total	99.16	99.75	100.07	100.18	100.17	99.90	100.06
(ppm)							
Ba	574	571	529	493	558	511	547
Rb	44.2	51	45.2	44.3	47.6	48.6	48.4
Sr	627	586	567	636	553	589	573
Y	6.6	15.7	12.7	14.1	11.3	16.2	11.4
Zr	117	137	158	130	134	125	136
Nb	4.8	6.7	6.5	6	7.5	5.8	7.9
Ce	109	80	37	39	64	75	62
Nd	33	29	21	21	23	28	23
Sc	6.5	15.7	13.5	15.4	13.4	17.3	11.7
V	54	93	97	104	89	96	98
Cr	22	30	29	42	28	30	34
Ni	20.8	23	21.6	27.9	24.1	22.7	24.4
Cu	18	45	17	35	28	34	51
Zn	45	67	62	70	67	70	60
Ga	N.D.	N.D.	N.D.	N.D.	N.D.	N.D.	N.D.
Ratio							
K/Ba	21.40	21.81	24.48	24.58	23.36	25.99	24.58
K/Rb	278.0	244.1	286.5	273.6	273.8	273.3	277.8
Rb/Sr	0.070	0.087	0.080	0.070	0.086	0.083	0.084
FeO*/MgO	1.75	1.89	2.03	1.89	2.11	1.96	1.91
Na ₂ O/K ₂ O	2.56	2.43	2.46	2.60	2.75	2.34	2.34
ACNK	0.987	0.975	0.929	0.919	0.906	0.942	0.933

Fe₂O₃*: Total Fe as Fe₂O₃

LOI: Loss on ignition

N.D.: Not determined

A/CNK: Mol. Al₂O₃/CaO+Na₂O+K₂O

Table A4-6(C). (continued)

(3)

Sample	90703	92401	92402
(%)			
SiO ₂	55.72	61.22	62.02
Al ₂ O ₃	17.26	17.64	17.50
Fe ₂ O ₃ *	7.76	5.53	5.36
MnO	0.13	0.07	0.07
MgO	3.98	2.58	2.47
CaO	6.90	5.70	5.57
Na ₂ O	3.69	4.05	3.81
K ₂ O	1.89	1.61	1.90
TiO ₂	0.86	0.68	0.64
P ₂ O ₅	0.44	0.18	0.18
LOI	1.03	0.72	0.74
Total	99.66	99.98	100.26
(ppm)			
Ba	561	540	552
Rb	55	46.5	61
Sr	531	641	580
Y	28.8	11.1	10.6
Zr	165	116	111
Nb	10.5	6.7	7.4
Ce	128	30	64
Nd	56	16	26
Sc	24.4	12.2	10.5
V	128	90	83
Cr	94	31	27
Ni	52	21.3	20.7
Cu	90	28	23
Zn	87	62	59
Ga	N.D.	N.D.	N.D.
Ratio			
K/Ba	27.97	24.75	28.57
K/Rb	285.3	287.4	258.6
Rb/Sr	0.104	0.073	0.105
FeO*/MgO	1.75	1.93	1.95
Na ₂ O/K ₂ O	1.95	2.52	2.01
ACNK	0.835	0.940	0.948

Fe₂O₃*: Total Fe as Fe₂O₃

LOI: Loss on ignition

N.D.: Not determined

A/CNK: Mol. Al₂O₃/CaO+Na₂O+K₂O

Table A4-7. Chemical compositions of the Mable Hill Tonalite and a tonalite from the main body of the Mable Downs Granitoid Suite

Sample	52106	92403	92404	52006
Unit	MA Mable Hill	MA Mable Hill	MA Mable Hill	MA Main body
Major elements (%)				
SiO ₂	63.24	61.87	63.55	57.45
Al ₂ O ₃	16.65	16.87	16.64	17.19
Fe ₂ O ₃ *	4.90	5.55	5.03	7.04
MnO	0.07	0.10	0.07	0.11
MgO	2.36	2.53	2.47	3.47
CaO	5.28	5.55	5.31	6.85
Na ₂ O	3.72	3.79	3.70	3.87
K ₂ O	1.41	1.49	1.73	1.44
TiO ₂	0.58	0.61	0.60	0.91
P ₂ O ₅	0.17	0.20	0.19	0.29
LOI	0.92	1.01	0.66	0.71
Total	99.30	99.57	99.95	99.33
Trace elements (ppm)				
Ba	622	590	713	437
Rb	43.2	43.3	48.6	44.2
Sr	612	630	666	588
Zr	152	142	131	172
Nb	5.5	6.1	7.4	9.3
Y	9.3	12.2	10.4	18.6
Ce	79	65	103	65
Nd	28	25	39	26
Sc	12.3	13.4	10.7	20.9
V	71	84	78	129
Cr	31	36	40	55
Ni	17	24.4	22.3	43
Cu	45	28	25	61
Zn	62	74	59	77
Ga	19.5	20.2	19.8	21.2
Ratio				
K/Ba	18.82	20.96	20.14	27.35
K/Rb	271.0	285.7	295.5	270.5
Rb/Sr	0.071	0.069	0.073	0.075
FeO*/MgO	1.93	2.04	1.90	1.89
Na ₂ O/K ₂ O	2.64	2.54	2.14	2.69
A/CNK	0.965	0.940	0.945	0.844

Fe₂O₃*: Total Fe as Fe₂O₃, LOI: Loss on ignition

A/CNK: Mol. Al₂O₃/CaO+Na₂O+K₂O

Table A4-8. Chemical compositions of the Sophie Downs Granitoid. (1)

Sample Unit	22809 SO	22911 SO	23002 SO	23005 SO	23007 SO	30101 SO	30107 SO
Major Elements (%)							
SiO ₂	76.22	77.29	75.89	76.67	75.84	76.80	76.76
Al ₂ O ₃	11.69	11.21	11.90	11.59	12.05	11.96	12.29
Fe ₂ O ₃ *	1.71	1.93	1.30	1.79	1.42	1.42	1.22
MnO	0.02	0.00	0.02	0.02	0.02	0.01	0.03
MgO	0.15	0.50	0.14	0.12	0.16	0.11	0.15
CaO	0.44	0.10	0.62	0.63	0.64	0.54	0.68
Na ₂ O	4.20	4.06	3.93	4.30	3.99	4.08	4.02
K ₂ O	4.54	4.44	4.52	4.49	4.48	4.73	4.42
TiO ₂	0.13	0.16	0.14	0.13	0.15	0.14	0.14
P ₂ O ₅	0.00	0.00	0.01	0.00	0.01	0.00	0.01
LOI	0.55	0.43	0.52	0.54	0.64	0.30	0.39
Total	99.65	100.12	98.99	100.28	99.40	100.09	100.11
Trace Elements (ppm)							
Ba	1046	937	977	1021	1046	1121	912
Rb	101	109	99.5	99.5	101	103	110
Sr	43.1	28.5	43.9	44.9	53.5	53	76.6
Zr	308	287	150	275	161	174	141
Nb	41.8	38.8	29.3	39.3	33.5	35.2	26
Y	80.4	78.9	58.9	77.2	65.1	67.2	60.6
Ce	146	175	132	163	122	111	85
Nd	64	91	55	73	48	59	32
Sc	1.9	1.3	2	2.1	2.5	2	2.6
V	0.2	1.8	2.5	0	3.1	2.7	3
Cr	0	0	0	0	0	0	0
Ni	1	1	2	2	2	2	3
Cu	5	3	8	11	4	10	4
Zn	84	97	55	64	46	60	38
Ga	19.9	18.5	16.3	17.1	15.9	16.3	14.8
A/CNK	0.926	0.961	0.953	0.886	0.958	0.933	0.973
NK/A	1.011	1.025	0.954	1.030	0.947	0.989	0.927

Fe₂O₃*: Total Fe as Fe₂O₃A/CNK: Mol Al₂O₃/(CaO+Na₂O+K₂O)NK/A: Mol (Na₂O+K₂O)/Al₂O₃

Table A4-8. continued. (2)

Sample	30114	30205A	30207	30404	30505	30608	30609
Unit	SO	SO	SO	SO	SO	SO	SO
Major Elements (%)							
SiO ₂	75.85	75.99	75.84	77.68	76.55	76.72	75.71
Al ₂ O ₃	12.06	11.96	12.11	11.53	11.34	11.65	12.26
Fe ₂ O ₃ *	1.27	1.27	1.29	1.49	1.53	1.49	1.37
MnO	0.03	0.03	0.03	0.02	0.03	0.02	0.02
MgO	0.26	0.25	0.17	0.16	0.30	0.37	0.30
CaO	0.33	0.77	0.49	0.12	0.28	0.43	0.54
Na ₂ O	3.94	3.74	3.73	4.03	3.36	3.77	3.59
K ₂ O	5.03	4.61	5.02	4.68	5.28	4.72	5.25
TiO ₂	0.18	0.18	0.18	0.13	0.14	0.16	0.19
P ₂ O ₅	0.01	0.02	0.01	0.00	0.00	0.00	0.01
LOI	0.35	1.04	0.83	0.41	0.49	0.61	0.60
Total	99.31	99.86	99.70	100.25	99.30	99.94	99.84
Trace Elements (ppm)							
Ba	921	782	735	1035	1188	882	813
Rb	116	140	148	127	118	118	144
Sr	48.4	32.4	26.4	25.3	30.7	28.8	31.9
Zr	166	153	152	238	222	168	161
Nb	27.1	17.2	17.9	34	31.3	29.6	17.5
Y	45.8	35.5	37.1	103	69.4	68.3	36.1
Ce	87	89	246	126	125	109	94
Nd	31	32	106	55	57	48	35
Sc	2.8	2.9	2.8	1.2	1.2	2.1	3
V	5.6	4.7	5	0.2	0.3	4.7	6.6
Cr	0	0	0	0	0	0	0
Ni	2	2	3	3	1	3	3
Cu	10	20	21	10	5	11	10
Zn	42	23	28	49	76	54	24
Ga	15	12.8	13.8	19.7	17.2	16.2	13.2
A/CNK	0.963	0.954	0.972	0.968	0.965	0.963	0.975
NK/A	0.989	0.932	0.955	1.014	0.991	0.971	0.945

Fe₂O₃*: Total Fe as Fe₂O₃A/CNK: Mol Al₂O₃/(CaO+Na₂O+K₂O)NK/A: Mol (Na₂O+K₂O)/Al₂O₃

Table A4-8. continued. (3)

Sample	30610	30706	30802	30805	31101	31207	31303
Unit	SO	SO	SO	SO	SO	SO	SO
Major Elements (%)							
SiO ₂	76.48	76.92	76.07	75.99	75.38	75.62	74.96
Al ₂ O ₃	11.70	11.47	12.06	11.63	12.13	12.00	12.14
Fe ₂ O ₃ *	1.41	1.60	1.24	1.95	1.82	1.34	2.22
MnO	0.02	0.01	0.02	0.02	0.03	0.00	0.04
MgO	0.29	0.16	0.37	0.21	0.36	0.18	0.40
CaO	0.52	0.36	0.38	0.58	0.60	0.41	0.46
Na ₂ O	3.73	4.03	3.60	3.82	3.83	3.39	3.85
K ₂ O	4.78	4.81	5.29	4.67	4.56	5.72	4.68
TiO ₂	0.14	0.13	0.17	0.17	0.22	0.18	0.19
P ₂ O ₅	0.02	0.00	0.01	0.00	0.01	0.01	0.01
LOI	0.71	0.64	0.56	0.74	0.86	0.58	0.68
Total	99.80	100.13	99.77	99.78	99.80	99.43	99.63
Trace Elements (ppm)							
Ba	948	1057	874	1206	924	794	843
Rb	130	125	134	108	100	143	105
Sr	38.2	29.2	44	48.9	42	37.8	35.8
Zr	159	237	153	281	245	160	272
Nb	28.9	32.6	17.5	39.5	25.3	18.1	30.3
Y	70.5	81.2	36.5	79.4	52.8	34.6	67.1
Ce	116	121	157	102	79	84.6	113
Nd	48	55	70	44	29	28.4	52
Sc	1.8	1.3	3.1	2.3	3.6	3.4	3.3
V	4.1	0.4	5.2	2.8	5.7	5.6	4.8
Cr	0	0	0	0	0	0	0
Ni	3	2	3	3	2	2	2
Cu	4	8	3	9	25	5	16
Zn	48	85	25	87	61	20	48
Ga	17.4	18.1	13.3	17.7	14.9	14.9	17.2
A/CNK	0.955	0.918	0.977	0.938	0.984	0.959	0.992
NK/A	0.967	1.032	0.966	0.975	0.926	0.981	0.939

Fe₂O₃*: Total Fe as Fe₂O₃

A/CNK: Mol Al₂O₃/(CaO+Na₂O+K₂O)

NK/A: Mol (Na₂O+K₂O)/Al₂O₃

Table A4-8. continued. (4)

Sample Unit	31304 SO	31305 SO	31306 SO	31408A SO	31413 SO	31414 SO	31501A SO
Major Elements (%)							
SiO ₂	74.77	77.02	72.36	75.97	76.58	76.33	76.47
Al ₂ O ₃	12.12	11.73	13.63	11.71	11.86	11.88	11.86
Fe ₂ O ₃ *	2.04	1.12	2.13	1.75	1.07	1.32	1.31
MnO	0.02	0.01	0.02	0.02	0.01	0.01	0.01
MgO	0.28	0.13	0.64	0.17	0.11	0.25	0.09
CaO	0.68	0.27	1.21	0.49	0.31	0.30	0.67
Na ₂ O	4.26	3.64	4.30	4.01	3.40	3.49	4.10
K ₂ O	4.40	5.36	4.34	4.82	5.67	5.41	4.60
TiO ₂	0.20	0.09	0.21	0.13	0.10	0.14	0.13
P ₂ O ₅	0.02	0.00	0.04	0.01	0.00	0.00	0.00
LOI	0.57	0.53	1.10	0.45	0.59	0.57	0.90
Total	99.36	99.90	99.98	99.53	99.70	99.70	100.14
Trace Elements (ppm)							
Ba	918	349	960	1163	815	1013	935
Rb	103	128	127	98.1	117	109	110
Sr	44.2	16	103	56.5	22.2	29.2	44.4
Zr	271	144	165	281	145	159	168
Nb	27.5	41.1	13.8	48.2	38.1	35.2	36.4
Y	64.1	82.8	26.4	85.6	68.5	60.3	54
Ce	110	100	60	195	120	119	122
Nd	50	45	22	90	50	51	53
Sc	3.5	1.2	3.7	1.5	1.8	2.5	2.8
V	4.8	0	20	0.4	0	2.4	1.4
Cr	0	0	0	0	0	0	0
Ni	3	1	4	2	2	1	4
Cu	8	9	6	6	8	16	21
Zn	59	63	75	108	50	68	59
Ga	17.7	17.5	17.5	20.2	16	16.2	17.8
A/CNK	0.932	0.955	0.976	0.922	0.965	0.978	0.916
NK/A	0.971	1.005	0.864	1.009	0.989	0.976	0.989

Fe₂O₃*: Total Fe as Fe₂O₃A/CNK: Mol Al₂O₃/(CaO+Na₂O+K₂O)NK/A: Mol (Na₂O+K₂O)/Al₂O₃

Table A4-8. continued. (5)

Sample Unit	31504 SO	31506 SO	31509 SO	91904 SO	91906 SO	91908 SO	92006 SO
Major Elements (%)							
SiO ₂	76.57	75.95	75.43	76.97	76.12	77.13	76.32
Al ₂ O ₃	11.81	11.98	12.40	11.69	12.60	11.56	11.64
Fe ₂ O ₃ *	1.74	1.38	1.66	1.69	1.97	1.53	1.73
MnO	0.02	0.00	0.03	0.03	0.03	0.02	0.07
MgO	0.08	0.48	0.42	0.33	0.89	0.13	0.22
CaO	0.66	0.19	0.64	0.36	0.53	0.36	0.44
Na ₂ O	4.03	3.75	3.88	3.54	5.78	3.66	3.94
K ₂ O	4.42	4.85	4.64	4.85	1.42	4.45	4.55
TiO ₂	0.14	0.14	0.23	0.16	0.20	0.15	0.13
P ₂ O ₅	0.00	0.00	0.02	0.01	0.04	0.02	0.01
LOI	0.49	0.48	0.85	0.36	0.64	0.27	0.57
Total	99.96	99.20	100.20	99.99	100.22	99.28	99.62
Trace Elements (ppm)							
Ba	1042	964	990	1102	483	1083	1081
Rb	91.4	100	102.9	125	36.2	89	100
Sr	61	30.1	43.2	32.6	40	37.5	41.4
Zr	251	167	251	226	167	225	284
Nb	36.7	34.4	25.3	32.4	14.3	31.9	41
Y	82.4	60	46.7	80	27.6	80	80
Ce	148	126	115	142	80	140	159
Nd	70	52	46	62	28	59	71
Sc	2.3	1.7	2.9	1.5	2.3	1.4	1
V	1	3.8	7	5	12	5	1
Cr	0	2	2	0	4	0	0
Ni	2	1	0	4	6.5	3.3	4.1
Cu	12	5	8	8	6	10	4
Zn	81	50	53	75	24	57	92
Ga	18.1	15.7	14.7	17.7	14.5	17.8	18.5
A/CNK	0.936	1.018	0.987	0.997	1.049	1.006	0.954
NK/A	0.966	0.953	0.920	0.947	0.877	0.937	0.980

Fe₂O₃*: Total Fe as Fe₂O₃A/CNK: Mol Al₂O₃/(CaO+Na₂O+K₂O)NK/A: Mol (Na₂O+K₂O)/Al₂O₃

Table A4-9. Chemical compositions of the Bow River Granitoid

Sample Unit	52009 BR	91501 BR	91507 BR	91508 BR	CU 2 BR
Major elements (%)					
SiO ₂	74.30	70.93	71.05	71.58	72.06
Al ₂ O ₃	12.82	13.48	12.74	14.32	14.18
Fe ₂ O ₃ *	2.15	3.77	4.64	2.82	2.52
MnO	0.01	0.04	0.07	0.03	0.05
MgO	0.24	0.86	0.33	0.75	0.71
CaO	1.20	1.54	1.91	2.10	1.77
Na ₂ O	2.44	2.53	2.59	2.18	3.62
K ₂ O	5.22	4.87	5.65	5.59	4.12
TiO ₂	0.26	0.46	0.51	0.39	0.26
P ₂ O ₅	0.13	0.09	0.09	0.10	0.08
LOI	0.90	1.30	0.38	0.40	0.72
Total	99.67	99.87	99.96	100.26	100.09
Trace elements (ppm)					
Ba	371	720	564	760	1063
Rb	301	166	337	226	146
Sr	68	120	65	125	121
Zr	140	191	332	190	202
Nb	10.2	9.8	20.8	9.5	23.1
Y	36	29.3	71	29.2	49.2
Ce	71	104	177	99	140
Nd	27	44	72	44	25
Sc	3.8	8.7	10.7	7.3	5.3
V	11	37	20	32	20
Cr	0	21	5	10	0
Ni	3	9.6	7.7	9.4	5.9
Cu	11	4	10	9	15
Zn	41	26	67	34	45
Ga	18	16	19.3	17.6	17.8
Ratio					
K/Ba	116.80	56.15	83.16	61.06	32.18
K/Rb	144.0	243.5	139.2	205.3	234.3
Rb/Sr	4.426	1.383	5.185	1.808	1.207
FeO*/MgO	8.34	4.08	13.09	3.50	3.30
Na ₂ O/K ₂ O	0.47	0.52	0.46	0.39	0.88
A/CNK	1.082	1.102	0.920	1.064	1.040

Fe₂O₃*: Total Fe as Fe₂O₃, LOI: Loss on ignitionA/CNK: Mol. Al₂O₃/CaO+Na₂O+K₂O

Table A4-10. Chemical compositions of granitoids from the King Leopold Mobile Zone

Sample Unit	13103 KL McSherrys	13104 KL McSherrys	13105 KL Dyasons	20201 KL Richenda	20208 KL Richenda	20209 KL Richenda
Major elements (%)						
SiO ₂	68.23	63.44	71.22	68.52	70.52	72.78
Al ₂ O ₃	14.09	14.89	14.41	14.86	14.60	14.37
Fe ₂ O ₃ *	4.30	6.33	2.84	3.96	2.98	1.53
MnO	0.06	0.09	0.03	0.04	0.04	0.02
MgO	1.91	3.01	0.56	1.52	1.14	0.51
CaO	3.28	4.66	2.65	3.34	2.61	1.74
Na ₂ O	2.76	2.35	2.88	2.88	3.03	3.16
K ₂ O	4.14	3.40	4.63	2.86	3.57	4.41
TiO ₂	0.51	0.79	0.30	0.36	0.20	0.10
P ₂ O ₅	0.15	0.18	0.05	0.09	0.09	0.05
LOI	0.56	0.55	0.39	1.23	1.05	1.20
Total	99.99	99.69	99.96	99.66	99.83	99.87
Trace elements (ppm)						
Ba	608	893	1094	539	647	767
Rb	152	148	170	140	150	149
Sr	285	355	192	189	185	186
Zr	151	216	174	147	125	81
Nb	13.2	13.7	10.5	12	10.5	10.7
Y	26.6	14.4	26.9	22.8	20.8	10.2
Ce	105	116	119	72	68	49
Nd	51	49	49	33	32	22
Sc	12.1	19.1	6.1	12.6	9.7	5.3
V	62	108	18.5	30	18.6	5.5
Cr	72	153	9	67	49	11
Ni	19.2	34.4	3.2	13.4	11.2	3.7
Cu	5	23	8	9	5	5
Zn	49	67	39	33	37	17
Ga	16.7	19.1	18.2	19.6	16.2	17.3
Ratio						
K/Ba	56.53	31.61	35.13	44.05	45.81	47.73
K/Rb	226.1	190.7	226.1	169.6	197.6	245.7
Rb/Sr	0.533	0.417	0.885	0.741	0.811	0.801
FeO*/MgO	2.10	1.96	4.72	2.43	2.43	2.79
Na ₂ O/K ₂ O	0.67	0.69	0.62	1.01	0.85	0.72
A/CNK	0.940	0.930	0.989	1.069	1.074	1.094

Fe₂O₃*: Total Fe as Fe₂O₃, LOI: Loss on ignition

A/CNK: Mol. Al₂O₃/CaO+Na₂O+K₂O

Table A4-11. Chemical compositions of miscellaneous granitoids from the Sally Downs Bore area

Sample Unit	42302 SG	11303 UD	41001B UD	51506 UD	82803 UD
Major elements (%)					
SiO ₂	74.68	52.50	54.40	59.47	59.15
Al ₂ O ₃	12.93	17.49	18.85	17.33	17.45
Fe ₂ O ₃ *	0.79	11.03	7.73	6.34	6.56
MnO	0.00	0.11	0.13	0.08	0.10
MgO	0.16	3.57	3.70	3.56	3.83
CaO	1.26	8.24	8.00	6.04	6.16
Na ₂ O	3.05	3.44	4.02	3.55	3.67
K ₂ O	5.62	0.96	1.10	1.64	1.67
TiO ₂	0.05	1.80	0.64	0.76	0.75
P ₂ O ₅	0.01	0.13	0.30	0.16	0.17
LOI	0.77	0.57	0.78	0.76	0.71
Total	99.32	99.84	99.65	99.69	100.22
Trace elements (ppm)					
Ba	1192	275	452	486	487
Rb	122	23.9	24.6	44.6	47.1
Sr	178	467	733	520	519
Zr	72	70	155	106	103
Nb	5.2	7.7	6	5.6	6.7
Y	11.9	15.8	28.2	12.3	12.2
Ce	40	31	106	38	35
Nd	14	19	49	14	19
Sc	3	28	35.3	17.4	18.2
V	2.1	311	118	99	103
Cr	0	10	47	77	77
Ni	4	15.6	26	54	55
Cu	6	82	39	39	32
Zn	9	81	81	70	72
Ga	14.8	N.D.	N.D.	N.D.	N.D.
Ratios					
A/CNK	0.966	0.807	0.843	0.932	0.916
Rb/Sr	0.685	0.051	0.034	0.086	0.091
(Ce/Y) _n	9.15	5.34	10.23	8.41	7.81

Fe₂O₃*: Total Fe as Fe₂O₃, LOI: Loss on ignition

N.D.: Not determined, A/CNK: Mol.Al₂O₃/CaO+Na₂O+K₂O

(Ce/Y)_n: Chondrite normalized Ce/Y

APPENDIX 5. EXPERIMENTAL TECHNIQUE AND RESULTS OF RARE EARTH ELEMENT ANALYSIS

Whole rock rare earth element (REE) concentrations have been determined by an isotope dilution mass spectrometric technique. The analytical technique is based on procedures described by Sun and Nesbitt (1978) and Turnbull (1980). All but four of the naturally occurring REE can be analysed by the isotope dilution technique. Pr, Tb, Ho and Tm have only one stable isotope each and as consequence cannot be analysed by the isotope dilution technique. Pm has no stable isotopes and does not occur in nature. In this thesis, Lu was not analysed.

Sm and Nd are not interfered with by other elements or oxides. If Ba is separated from the sample, Eu is easily analysed. All other REE, however, interfere with each others or with oxides, and therefore good chemical separation is necessary for their analysis (Turnbull, 1980). If Lu is not analysed, it is sufficient to separate the REE into four fractions,

- 1) a heavy REE fraction
- 2) a light REE fraction
- 3) a Ce fraction free of Nd
- 4) a La fraction free of Ce and Ba.

1. Sample Dissolution

Between 0.65 and 1.4 g of powder samples were mixed with a composite REE spike, and dissolved in Teflon beakers on a hotplate with 15ml of HF, 4ml of 6N HNO₃, and 15 drops of HClO₄. When dry, after evaporation, a further 2ml Hf and 1ml of HClO₄ were added, and the sample reheated and evaporate again to dryness. The dry residue was transferred to a Teflon bomb container for pressure digestion. A few ml of Hf and few drops of HClO₄ were then added to the container. The Teflon bomb was heated in oven overnight at 200°C.

2. Ion Exchange Column Separation

After pressure digestion, the samples were passed successively through two cation exchange columns to obtain REE fractions.

The cation exchange resin BIO RAD AG50W-8X, 100-200 mesh, was used in both columns. Column (1), the Nitric Acid Column, was 20cm long with 1cm internal diameter. Column (2), the Hydrochloric Acid Column, was 27cm long with 1cm internal diameter.

The samples from the bomb were first taken up in 2N HNO₃ and put into column (1). The whole REE fraction was collected with 6N HNO₃. The fraction was taken up with 2N HCl and put into column (2). Four fractions of REE were collected with 3N HCl.

3. Mass Spectrometry

Samples were loaded onto Re triple filament beads which were previously degassed. Isotopic measurements were performed on a 30 cm-radius, 90°-sector, Thomson mass spectrometer.

4. Result of REE analysis

The analysis of USGS standard rock SCo-1 is presented in Table A5-1. It shows good agreement with reference values. The results of REE analysis of samples from the Halls Creek Mobile Zone are presented in Table A5-2.

Table A5-1. Rare earth element analysis of USGS standard sample SCo-1

(ppm)	Present work	McLennan & Taylor (1980)	Kosiewicz et al. (1974)	Difference(%) *1
La	29.8	29.7	29.2	-0.3
Ce	63	63.4	54.4	0.6
Nd	26.1	27.9	27.3	6.9
Sm	5.05	5.07	5.13	1.4
Eu	1.1	1.03	1.02	-6.4
Gd	4.47	4	4.2	-10.5
Dy	3.96	3.79	4.21	-4.3
Er	2.36	2.39	2.5	1.3
Yb	2.32	2.25	2.33	-3
Method	ID*2	SSMS*2	RNAA*2	

*1 Relative difference between the result of this work and that of McLennan and Taylor (1980).

*2 Abbreviations for method of analysis:

ID: Isotope dilution mass spectrometry

SSMS: Spark source mass spectrometry

RNAA: Radiochemical neutron activation analysis.

Table A5-2. Results of rare earth element analysis by isotope dilution mass spectrometry

	ELG	Dougalls Granitoid			Ord River Tonalite			WPG	MetDol
	51607	52008	12703	21902	51302	51913	90807	52103	20606
La (ppm)	6.99	12.3	17.9	12.2	30.2	14	23.8	55.6	12.6
Ce	11.3	26.3	30.9	19.8	55.5	27.5	43.1	130	27.5
Nd	4.59	16.1	9.69	5.44	22.1	11.9	15.6	42.4	13.9
Sm	1.03	3.74	1.6	0.737	4.01	2.4	2.57	7.34	3.54
Eu	0.937	1.45	0.637	0.552	1.19	0.859	1.07	1.27	1.19
Gd	1.48	3.77	1.32	0.514	3.6	2.24	2.07	6.2	4.66
Dy	4.31	3.48	0.957	0.245	2.89	1.88	1.41	4.98	5.93
Er	5.99	1.95	0.497	0.117	1.55	1.05	0.667	2.72	4.01
Yb	8.18	1.86	0.428	0.118	1.39	0.97	0.52	2.25	3.86
Eu/Eu*	2.344	1.193	1.354	2.770	0.967	1.144	1.433	0.581	0.905
SiO ₂ (%)	76.65	58.11	68.80	69.55	63.94	66.18	68.54	72.49	49.38

	CLG	Hornblendite		Sally Downs Tonalite					MME
	52101A	11309	40206	42402	51706	50702	40406	50801	51702
La (ppm)	38.5	14.3	5.02	19	26	43.5	34.3	41.2	11.2
Ce	67.8	34.9	16.5	41.2	53.7	72.4	61	69.5	29.7
Nd	23.1	21.2	13.7	20.2	22.2	28.8	22.3	23.2	21.6
Sm	3.89	4.45	3.31	3.97	3.98	4.13	3.56	3.26	5.08
Eu	0.797	1.23	0.911	1.22	1.19	1.1	0.99	1.01	1.5
Gd	3.14	3.55	2.82	3.29	3.25	2.93	2.72	2.39	4.58
Dy	2.55	2.18	1.91	2.52	2.49	1.97	2	1.63	3.45
Er	1.32	0.925	0.885	1.31	1.3	0.937	0.996	0.808	1.81
Yb	1.17	0.653	0.748	1.11	1.04	0.895	0.809	0.694	1.62
Eu/Eu*	0.704	0.956	0.921	1.043	1.022	0.977	0.983	1.118	0.960
SiO ₂ (%)	73.89	48.15	48.70	58.23	60.69	63.21	65.25	67.27	56.56

	Sophie Downs G.		Bow River G.		WWV
	31207	92006	91508	52009	91606
La (ppm)	42.5	92.5	54.8	35.3	56.7
Ce	84.6	174	111	72	116
Nd	28.4	71.4	39.5	30.7	44.5
Sm	5.23	13.63	6.91	6.59	8.47
Eu	0.532	2.08	1.32	0.722	0.696
Gd	4.55	12.4	5.72	6.13	7.5
Dy	4.52	11.9	4.75	5.58	6.86
Er	2.84	7.44	2.6	2.74	3.94
Yb	2.9	7.29	2.33	2.3	3.5
Eu/Eu*	0.337	0.494	0.648	0.351	0.270
SiO ₂ (%)	75.62	76.32	71.58	74.30	75.01

ELG: Eastern Leucocratic Granitoid, WLG: Western Porphyritic Granite, MetDol: Meta-dolerite

CLG: Central Leucocratic Granite, MME: Mafic microgranular enclave, WWV: Whitewater Volcanics

Eu/Eu*: Degree of Eu anomaly(= (Eu/0.0722)/SQRT((Sm/0.192)x(Gd/0.259))

APPENDIX 6. EXPERIMENTAL TECHNIQUE OF SR ISOTOPE ANALYSIS

Rb, Sr, and isotopic Sr values have been determined for 42 total rock samples. Isotopic measurements were performed at the BMR isotope laboratory in the Research School of Earth Science, Australian National University. Rb and Sr contents of 25 samples were obtained by the isotope dilution technique described by Page et al. (1976). Rb and Sr values of the remaining 17 samples were determined at Adelaide University by the X-ray fluorescence technique which is described in Appendix 3.

In preparation of the isotope measurements, between 0.025 and 0.1 g of powder samples were spiked with a mixed Rb/Sr spike, dissolved in Teflon beakers with 3ml of HF, 0.5ml of 2.5N HCl, and 3 drops of HClO₄, and homogenized in 6N HCl. The samples were then taken up in 1N HCl and passed through cation exchange columns to obtain Rb and Sr fractions.

Rb isotopic measurements were performed on a 15.25cm-radius, 90°-sector, mass spectrometer (MSX) and Sr isotopic compositions were analyzed by a Nuclide Analysis Associates 30.5cm-radius, 60°-sector, mass spectrometer with rhenium triple-filament sources.

Sr isotope compositions of the 17 samples, of which Rb and Sr concentrations were determined by X-ray fluorescence spectrometry, were measured on unspiked samples. Approximately 0.5g of unspiked powder samples were dissolved by the procedure similar to that of the spiked samples. Sr isotope measurements were normalized to an $^{88}\text{Sr}/^{86}\text{Sr}$ value of 8.3752. All the results were adjusted to a value of 0.71014 for the standard NBS 987 strontium carbonate. The actual value observed for the NBS 987 was 0.70999. Regression of the Rb-Sr isochron was carried out using the computer program of McIntyre et al. (1966).

The coefficients of variation for $^{87}\text{Rb}/^{86}\text{Sr}$ and $^{87}\text{Sr}/^{86}\text{Sr}$ have been taken as 0.5 and 0.01 percent, respectively. All errors are quoted at the 95 percent confidence level.

Results of Rb-Sr isotoic analysis are presented in Table 6-1. Regression results of Rb-Sr isochron are listed in Table 6-2.

APPENDIX 7. EXPERIMENTAL TECHNIQUE OF ELECTRON MICROPROBE ANALYSIS

Chemical compositions of minerals were obtained using electron microprobe analysis technique. Most of analyses were carried out on the JEOL Superprobe 733 instrument in the former Electron Optical Center at the University of Adelaide (now Center for Electron Microscopy and Microstructure Analysis (CEMMSA)); some were done on the JEOL JXA-5A probe at Melbourne University.

The JEOL Superprobe 733 instrument at the University of Adelaide had three crystal spectrometers (wavelength dispersive spectrometers). Instrumental conditions of the electron probe analysis are listed in Table A7-1. The standard Z (atomic number), A (absorption), F (fluorescence) corrections were applied for the analyses.

The JEOL JXA-5A probe at Melbourne University has three crystal spectrometers. Instrumental conditions of the electron probe analysis are presented in Table A7-1. The modified ZAF correction (Ferguson and Sewell, 1978) was applied for the analyses.

Analyses were performed on polished thin sections which were coated with carbon.

Some feldspar compositions were obtained by measurements of three elements, i.e. Ca, Na, K, with JXA-5A probe at Melbourne University. Other elements in the feldspars were numerically calculated on the basis of their stoichiometry to check accuracy of the analytical result.

Rare earth element contents in the accessory minerals were determined using the JEOL Superprobe 733. Analytical conditions are presented in Table A7-2. Analytical procedure was largely similar to that of Exley (1980). In addition to rare earth elements, Y, Sr, and Th were analysed. Standards used were REE glass standards prepared by Drake and Weill (1972). Two separate analyses on a spot were performed.

Initial analysis was as described above to obtain major composition of mineral. A analysis determined the REE compositions, using higher accelerating voltage (25kV) and higher probe current (150nA). Typical lower detection limits for the REE were about 80ppm.

Precision and accuracy of the electron probe REE analyses were assessed by analysing an apatite standard. REE concentration in the apatite standard was determined using isotope dilution mass spectrometry. Results of the electron probe REE analyses (Table A7-3) show a good agreement with the value obtained by the isotope dilution mass spectrometry.

Table A7-1. Instrumental conditions of electron microprobe analysis

Equipment	JEOL JXA-5A Melbourne University		JEOL 733 Adelaide University	
H.V.	15kV		15kV	
Probe current	300nA		100nA	
Probe diameter	5-10 μ m		5-10 μ m	
Element	Crystal	Standard	Crystal	Standard
Si	RAP	Wollastonite	TAP	Wollastonite
Ti	LIF	TiO ₂	PET	Metal
Al	RAP	Al ₂ O ₃	TAP	Al ₂ O ₃
Fe	LIF	Fe ₂ O ₃	LIF	Metal
Mn	PET	Metal	LIF	Metal
Mg	RAP	MgO	TAP	MgO
Ca	PET	Wollastonite	PET	Wollastonite
Na	RAP	Jadite	TAP	Albite
K	PET	Katantalite	PET	Orthoclase
Cr	LIF	Metal	LIF	Metal
F			TAP	SrF ₂
Counting time	Peak 30sec. Bgd 12sec.		Peak 15sec. Bgd 10sec.	

Table A7-2. Instrumental conditions of electron microprobe for rare earth element analysis

1) Instrumental conditions for rare earth elements, Y, Sr, and Th

Equipment	JEOL 733
Accelerating voltage	25kV
Probe current	150nA
Probe diameter	20 μ m
Counting time on peak	60 sec.
Counting time on background	30 sec.
Analytical Lines	
La	L α
Ce	L α
Pr	L β 1
Nd	L β 1
Sm	L β 1
Gd	L β 1
Dy	L β 1
Y	K α
Sr	K α
Th	L α

2) Analytical conditions for other elements are same as those shown in Table A7-1 for JEOL 733.

Two separate analyses of rare earth and major elements on a single spot have been performed with off-line ZAF correction.

Table A7-3. Electron probe analysis of rare earth elements on Durango Apatite Standard

Counting*1	IDMS	Probe Results			
		50sec.			75sec.
ProbeD.*2		10	20	40	40
(ppm)					
La ₂ O ₃	3980	4500	4365	4518	4468
Ce ₂ O ₃	5491	5204	5102	5218	5317
Pr ₂ O ₃	(419.)*3	507	343	380	387
Nd ₂ O ₃	1285	1206	1329	1242	1260
Sm ₂ O ₃	183.4	N.D.	157	113	124
Eu ₂ O ₃	18.78	N.A.	N.A.	N.A.	N.A.
Gd ₂ O ₃	164.1	N.D.	61	168	158
Dy ₂ O ₃	114.6	N.D.	133	N.D.	N.D.
Er ₂ O ₃	61.75	240	101	N.D.	N.D.
Yb ₂ O ₃	44.3	N.D.	N.D.	60	N.D.

*1: Counting time on peak in seconds.

*2: Probe diameter in micron.

*3: Pr concentration was interpolated from the Ce and Nd values.

N.D.: Not detected

N.A.: Not analysed.

Durango apatite was supplied by Dr. B.J. Griffin from the museum collection of the Geology Department, the University of Tasmania. IDMS values are from the present study.

Major element composition

P ₂ O ₅ (%)	41.12
CaO	54.7
F	3.23
Cl	0.46
MnO	0.01
FeO	0.08
MgO	0.02

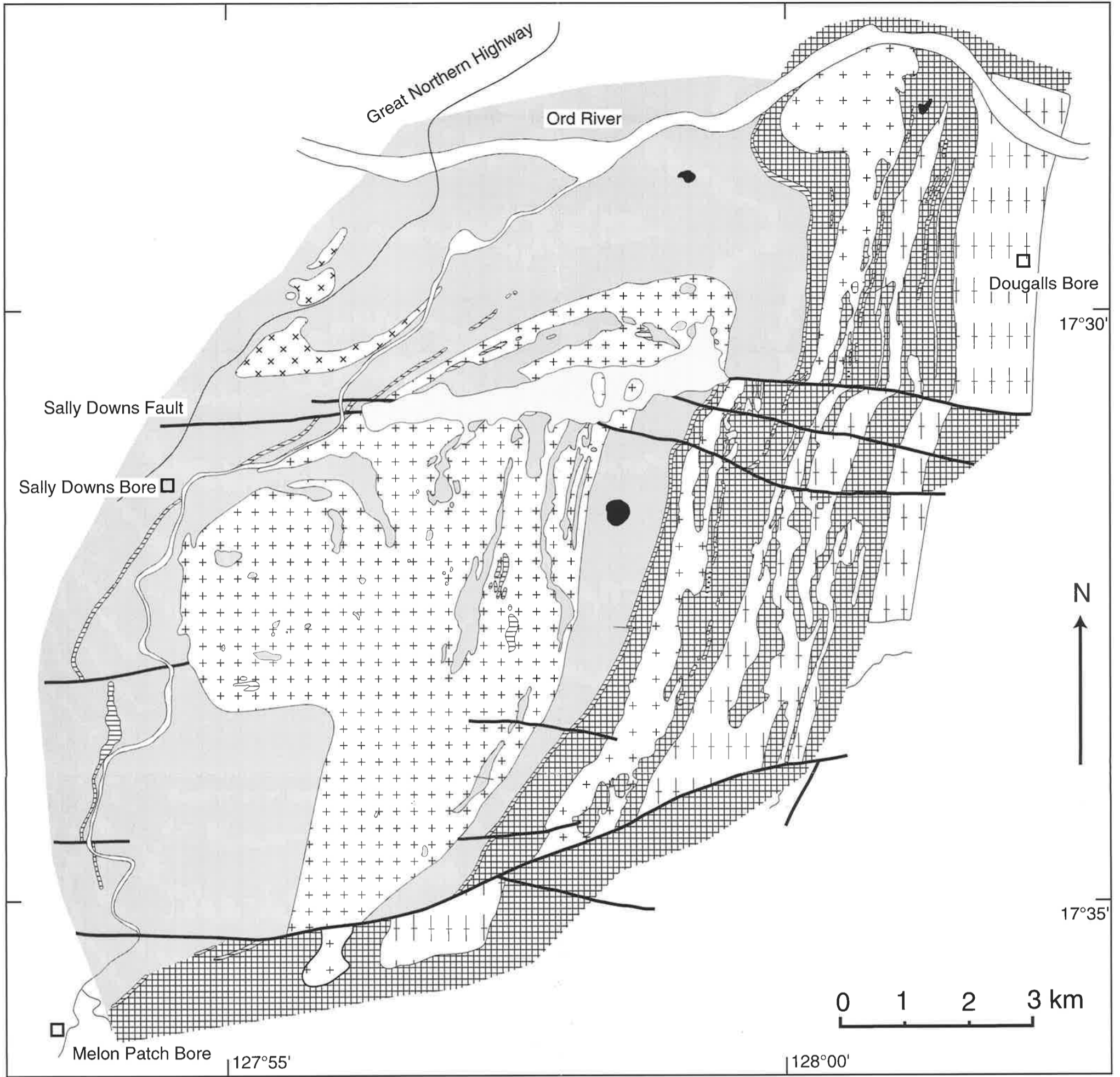
Major element composition was determined by P. Robinson (Geology Department, the University of Tasmania).

APPENDIX 8. CHEMICAL COMPOSITION OF MINERALS

The chemical compositions of minerals obtained with the electron microprobe are listed in Table A8-1 as microfiches. These are placed in a pocket inside the back cover. Representative data are presented in tables of the main text.

034
02

Plate 1. Geological Map of the Sally Downs Bore Area



□ Cenozoic sand, soil, and gravel

+++ Sally Downs Tonalite

xxx Western Porphyritic Granite

+ + + Eastern Leucocratic Granite

□□□□□ Tickalara Metamorphics

Undifferentiated rocks (Tickalara Metamorphics, Ord River Tonalite, Meta-dolerite, and Central Leucocratic Granite)

■ Gabbroic rocks

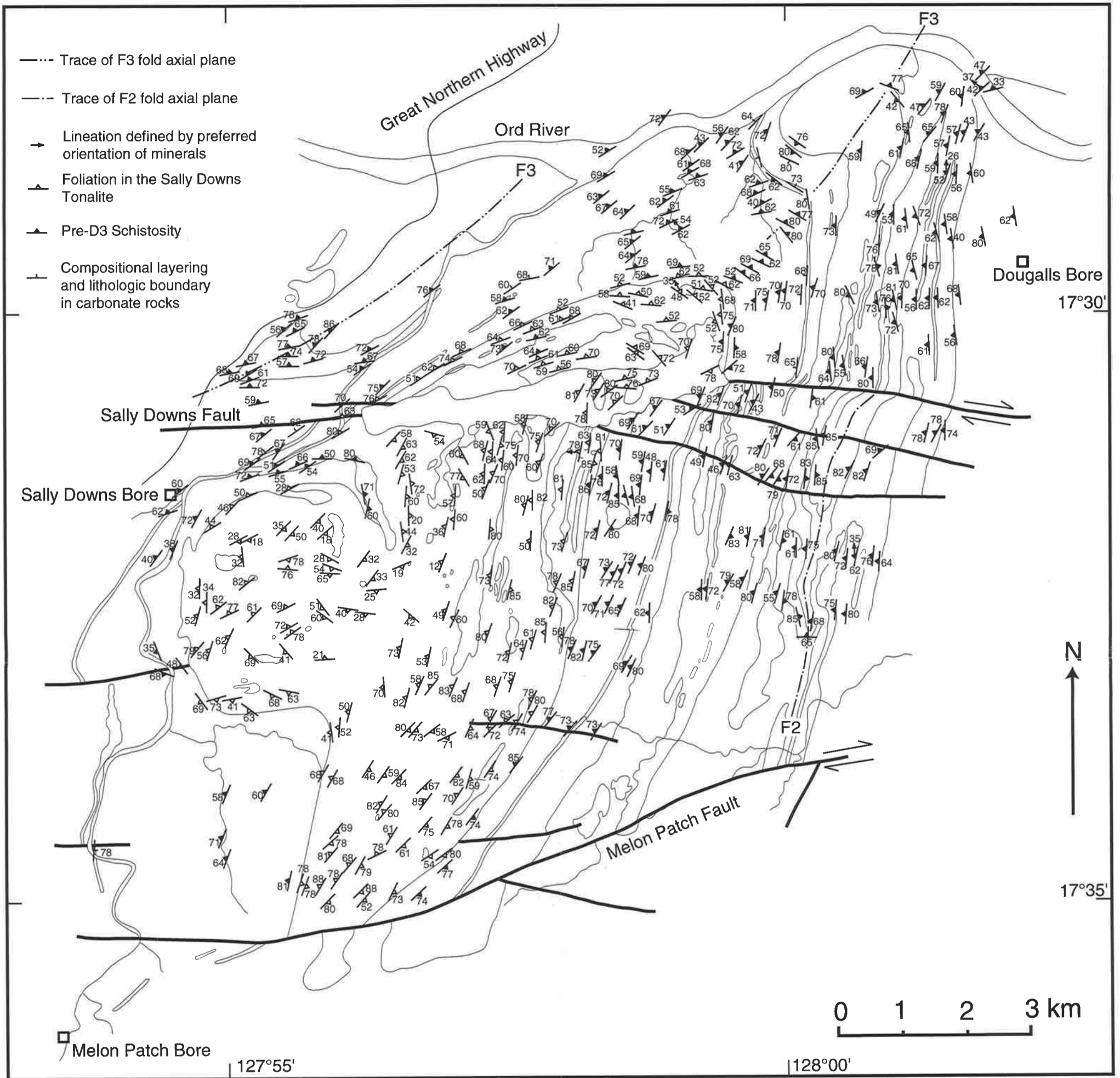
||| Dougalls Granitoid Suite

||| Carbonate rocks of Tickalara Metamorphics

M. Ogasawara (1996)
 Petrology of Early Proterozoic Granitoids in the Halls Creek Mobile Zone, Northern Australia.
 University of Adelaide

09PH
034
c.2

Plate 2. Structural Map of the Sally Downs Bore Area



M. Ogasawara (1996)
Petrology of Early Proterozoic Granitoids in the Halls Creek Mobile Zone, Northern Australia.
University of Adelaide